Université catholique de Louvain

de Duve Institute

CELL biology unit

How cytoskeletal impairment in hereditary elliptocytosis and spherocytosis affects erythrocyte membrane composition, organization and deformation

Hélène POLLET

Promotor: Donatienne TYTECA

Thesis for the degree of PhD in Biomedical and Pharmaceutical Sciences

Members of the jury

Prof. Jean-François COLLET (President)
Université catholique de Louvain

Prof. Donatienne TYTECA (Promotor)
Université catholique de Louvain

Prof. Marie-Paule MINGEOT
Université catholique de Louvain

Prof. Philippe GAILLY
Université catholique de Louvain

Prof. Mark RIDER
Université catholique de Louvain

Prof. Yves POUMAY
Université de Namur

Prof. Anna Yu. BOGDANOVA
University of Zürich

Remerciements

Après plus de six ans à travailler dans le laboratoire de l'unité CELL, dont deux ans de mémoire et plus de quatre ans de thèse, me voici aux termes de cet épisode de ma vie.

Je vais commencer par remercier la personne la plus importante de cette thèse, ma promotrice, Donatienne Tyteca. Je tiens d'abord à te remercier de m'avoir permis d'intégrer ton groupe pour mon mémoire et de m'avoir proposé de rester en thèse ensuite. C'est une grande chance d'apprendre la recherche à ton contact, grâce à ton implication et ton optimisme. Je salue particulièrement ton intuition scientifique, rarement prise en défaut. C'était aussi très enrichissant d'observer et de participer à l'agrandissement du groupe LiDo de ces dernières années : de deux à trois personnes, nous sommes à présent 6 (et bientôt plus !). Merci pour tout.

Je tiens également à remercier les membres permanents de mon comité d'encadrement, les Professeurs Jean-François Collet, Marie-Paule Mingeot, Philippe Gailly et Mark Rider pour vos conseils avisés, vos questions pertinentes, votre compréhension, les corrections d'anglais plus que nécessaires et globalement le temps consacré à mon travail. Merci également au Professeur Yves Poumay d'avoir accepté de faire partie de mon jury de thèse, pour votre intérêt et bienveillance lors de la défense privée. Enfin, merci au Professeure Anna Bogdanova d'avoir accepté de faire partie de mon jury de thèse, pour ses conseils d'expert concernant l'étude des globules rouges, ses corrections pointues et son enthousiasme.

Je remercie aussi les Docteurs Christiane Vermylen et Benedicte Brichard pour leur contribution qui nous a permis de recruter les patients nécessaires à nos études. Un tout grand merci à Angélique Pontikas, la personne de contact au service d'hématologie pédiatrique, avec qui j'ai passé beaucoup de temps au téléphone pour trouver des solutions (et se plaindre un peu) lorsque les patients ne venaient pas à leur rendez-vous.

La collaboration avec le laboratoire du Professeur Miikka Vikkula, dans le cadre du séquençage du génome des patients, m'a beaucoup ouvert sur ce sujet fascinant qu'est la génétique. Je remercie plus particulièrement Pascal Brouillard, Audrey Debue et Dominique Cottem. Votre gentillesse, votre souci du détail et votre disponibilité ont rendu cette collaboration très enrichissante pour moi, malgré les quelques difficultés rencontrées !

Merci au Professeur Giulio Muccoli et son doctorant Adrien Paquot pour leur travail sur les lipides des globules rouges ! Vous avez été d'une efficacité à toute épreuve lors de cette fructueuse collaboration !

Je voudrai également remercier les trois autres chefs de groupe de l'unité : Christophe Pierreux, Patrick Henriet et Etienne Marbaix. Merci à Christophe Pierreux pour son professionnalisme teinté d'une bonne dose d'enthousiasme (surtout visible lors des team-buildings). Au-delà du professionnel, j'ai grandement apprécié le souci discret mais bien réel pour les gens qui travaillent avec lui. A Patrick Henriet, je voudrais exprimer ma reconnaissance pour ses bons conseils concernant la biomol, son indignation lorsque les firmes font du mauvais boulot (ces foutues amorces !!), son humour toujours présent et son fameux lait de poule.

Je remercie aussi Patrick Van Der Smissen, Monsieur Microscope, toujours isolé dans sa tour d'ivoire, proche de ses précieuses machines et dont je comprends l'humour une fois sur deux. En revanche, je ne remercie pas les microscopes confocaux et électronique qui ont eu le chic de tomber en panne aux moments les plus inopportuns.

Le groupe du LiDo est probablement le meilleur du monde, et il faut encore que je remercie Donatienne d'avoir réuni une si fine équipe, non seulement de scientifiques rigoureux mais aussi de personnes généreuses, travailleuses et drôles, qui rendent le travail bien plus facile ! Je dois commencer par remercier absolument tous les gens qui sont passés par le groupe d'avoir toujours participé au projet maladie lorsque les patients se présentaient ! Ce projet était vraiment un gros travail de groupe et sans votre bonne volonté jamais il n'aurait été possible de rassembler autant de données !!! Je peux difficilement commencer ces remerciements sans parler de **Mélanie Carquin**, qui n'est certes plus là mais qui a marqué mon arrivée au labo. Véritable légende de notre groupe, on se raconte encore aujourd'hui au pied du feu (autour de la machine à café) ses aventures à base de toxines, de levures et de sport en tout genre. Elle reste un exemple, un phare à suivre dans la tourmente, car son acharnement, sa rigueur scientifique et son ardeur au travail n'ont jamais faibli lorsqu'elle était au labo. Après quelques temps est venue s'ajouter à ce groupe **Louise Conrard**. Tout d'abord je te remercie de rire à toutes les bêtises que je raconte. Travailler avec toi a été un tel plaisir ! J'ai beaucoup appris personnellement à ton contact, car, moi qui suis une vraie drama-queen, ta manière simple et souriante de gérer les aléas professionnels et personnels force mon respect. J'ai toujours aussi grandement apprécié nos discussions et ta propension à t'intéresser à des choses très éloignées (régime, cuisine, k-pop, mais aussi féminisme) avec beaucoup de bienveillance et d'enthousiasme. Je te souhaite beaucoup de bonheur pour cette nouvelle page de ta vie qui s'annonce. Merci bien sûr à **Anne-Sophie Cloos**, cette petite souris qui parait bien timide et inoffensive au début mais qui révèle des trésors d'humour décapant, de gentillesse et de facéties à qui prend le temps de la découvrir. Je n'oublie pas non plus ta rouerie lorsqu'il s'agit de cacher

à tes doctorantes adorées l'existence d'une nouvelle machine à chocolat chaud ! Merci à **Amaury Stommen**, enthousiaste inébranlable (sauf lorsque tu es stressé), tu es toujours le premier à vouloir aider au labo, participer à des soirées voire carrément à les organiser ! Bonne chance pour ta future thèse, et n'oublie pas « Blackpink » est le meilleur groupe de K-pop ! A **Mauriane Maja**, la martyre officielle du labo (et surtout d'Anne-Sophie), migrante du labo de Patrick Henriet que nous avons accueilli par bonté de cœur, merci pour ta bonne humeur ces derniers mois, malgré les petits soucis de manips et n'hésite pas à frapper Anne-Sophie quand elle t'embête. Merci à **Sandrine Verstraeten**, doctorante de Donatienne à temps partiel, pour ta franchise, ton humour rentre-dedans et ta bienveillance ! Merci à **Maxime Lingurski**, j'ai pris beaucoup de plaisir à maniper avec toi sur cette fin de thèse, ce qui a été grandement enrichis par nos petites histoires de western-blot (et tout ce qui peut mal se passer). Finalement, à **Marine Ghodsi** que je n'ai malheureusement pas assez côtoyée, j'espère que tu t'épanouiras au labo et bonne chance pour ton mémoire.

Ces remerciements seraient incomplets si je n'adressais pas un grand merci à l'ensemble des membres de l'Unité CELL. A Charlotte Heymans et Catherine Spourquet, l'indissociable duo, dont l'enthousiasme à rendre la vie du labo la plus efficace et agréable possible n'a jamais démérité, merci pour ce travail de chaque instant et pour l'organisation des team-buildings ! Merci à Virginie pour le sourire en coin à chaque fois que tu sens que je vais dire une connerie. Tu es une personne drôle, entière et extrêmement forte, dont la discussion est soit enrichissante soit drôle (ou les deux). Je ne te souhaite que le meilleur pour ta fin de thèse ! A Charlotte Thieffry, pour tes innombrables anecdotes complètement folles et pour ton amour de la mayonnaise. A Pascale Lemoine, discrète mais toujours prête à aider. Merci à Freddy pour toutes nos discussions passionnantes à propos de la pop-culture et les films de super héros. A Aimée-Lys, pour ta gentillesse et nos conversations. Merci aussi à tous les nouveaux que je ne cite pas, qui contribuent grandement à la bonne humeur et entente du labo.

Pour les personnes déjà parties mais que je n'oublie pas. Merci à Manuel Guthmann, mon premier mémorant, qui est une des personnes les plus chill de la planète, dont la bonne humeur a su compenser mes premières difficultés d'encadrante. A Jasmine Sik, une stagiaire du tonnerre ! A Catherine Leonard, la bio-physicienne du groupe pour un temps. A Antoine Cominelli, aide biomol des premiers mois, grand farceur et épicurien.

Ma reconnaissance et mes remerciements vont finalement à ceux qui assuré le soutien affectif ces dernières années en me rassurant constamment, en m'écoutant beaucoup et en me nourrissant (littérairement et littéralement parfois), ma famille et mes amis. Ma famille avec surtout ma mère qui m'a perpétuellement soutenue et écoutée durant toutes ces années et qui a été très présente aussi lors de l'écriture finale ; et ma

sœur qui est la personne la plus incroyable et badass de l'univers, la meilleure jumelle qui existe. Merci à Dio pour les relectures et le soutien continu ; A Amandine et Khanh pour les midis discussions. Enfin j'aimerais remercier Cyril, dont je partage la vie (à distance) depuis plus de 8 ans. Ou 9, franchement je ne sais plus, ça fait trop longtemps. Mais peu importe les années car avec toi tout est toujours nouveau, excitant et drôle. A nos prochaines aventures parisiennes !

Finalement je voudrais adresser mes excuses à la personne que j'ai enfermée un vendredi soir dans les pièces microscopes.

Contents

LIST OF ABBREVIATIONS

2,3-BPG, 2,3-biphosphoglyceric acid
AA, ascorbic acid
AE1, anion exchanger 1
AFM, atomic force microscopy
aSMase, acid sphingomyelinase
BODIPY, 4,4-difluoro-5.7-dimethyl-4-bora-3a,4a-diaza-s-indacene-3-pentanoic
BSA, bovine serum albumin
CalA, calyculin A
Cer, ceramide
CFTR, cystic fibrosis transmembrane regulator
CH, calponin homology
CTxB, cholera toxin B subunit
DAG, diacylglycerol
DHE, dehydroergosterol
EV, extracellular vesicle
FERM, 4.1 ezrin radixin moexin
GAPDH, glyceraldehyde 3-phosphate dehydrogenase
GP, generalized polarization
GPA, glycophorin A
GPC, glycophorin C
GPI, glycosylphosphatidylinositol
GSH, reduced glutathione
GSL, glycosphingolipid
GSSG, oxidized glutathione
H2DCFDA, 2', 7'-dichlorodihydrofluorescein diacetate
H_2O_2, hydrogen peroxide
HC, high curvature
HE, hereditary elliptocytosis
HS, hereditary spherocytosis
L_d, liquid-disordered
L_o, liquid-ordered
LC, low curvature
lysoPL, lysophospholipid
mβCD, methyl-β-cyclodextrin
MV, microvesicle
NBD, 7-nitrobenz-2-oxa-1,3-diazol-4yl
NMDA, N-methyl-D aspartate

NO, nitric oxide
PC, phosphatidylcholine
PDMS, polydimethylsiloxane
PE, phosphatidylethanolamine
PH, pleckstrin homology
PI, phosphatidylinositol
PIP, phosphoinositides
PIP_2, phosphatidylinositol-4,5-bisphospate
PKA, protein kinase A
PKC, protein kinase C
PLA, phospholipase A
PLC, phospholipase C
PLL, poly-L-Lysine
PMA, phorbol 12-myristate 13-acetate
PMCA, plasma membrane calcium ATPase
PS, phosphatidylserine
RBC, red blood cell
Rh, Rhesus
ROS, reactive oxygen species
S_o, solid-ordered
S1P, sphingosine-1-phosphate
SDS-PAGE, sodium dodecyl sulfate polyacrylamide gel electrophoresis
SEM, scanning electron microscopy
SIRPα, signal regulatory protein α
SL, sphingolipid
SM, sphingomyelin
SMase, sphingomyelinase
SOD1, superoxide dismutase
SPHK, sphingosine kinase
Tm, melting temperature
TRPC, transient receptor potential cation channels
VDAC, voltage-dependent anion-selective channel

ABSTRACT

During the last decade, the host laboratory has explored the contribution of the plasma membrane lateral heterogeneity in red blood cell (RBC) deformation. According to their current model, three types of lipid domains coexist at the RBC surface: (i) the cholesterol-enriched domains, which gather in high curvature areas upon RBC deformation; (ii) the GM1/phosphatidylcholine (PC)/cholesterol-enriched domains, whose abundance increases with calcium entry upon RBC deformation; and (iii) the sphingomyelin (SM)/PC/cholesterol-enriched domains, whose abundance increases with calcium efflux after deformation. During my thesis, I evaluated whether those lipid domains could be modified in abundance, composition and dynamics in two RBC fragility diseases caused by impairment of the cytoskeleton, hereditary elliptocytosis and spherocytosis.

The RBCs from the patient suffering from hereditary elliptocytosis were more circular and more fragile. Spectrin tetramerization was perturbed due to the exclusive expression of the Pro260 variant of α-spectrin. The impairment of cytoskeletal protein distribution was accompanied by a rise in the intracellular calcium content and the alteration of calcium exchanges at the RBC surface. Moreover, both GM1/PC/chol- and SM/PC/chol-enriched domains were altered in abundance, cholesterol enrichment and response to calcium exchange stimulation. The intracellular calcium overload led to phosphatidylserine exposure at the external plasma membrane leaflet and reactive oxygen species overproduction, resulting into increased lipid peroxidation and activation of the plasmatic acid sphingomyelinase. All those membrane lipid alterations contributed to membrane lipid domain reorganization and dysfunction in elliptocytosis. Inhibition of the plasmatic acid sphingomyelinase by amitriptyline increased the abundance of SM/PC/cholesterol-enriched domains and partially restored the calcium content and the RBC circularity and deformability.

The spherocytosis study included ten splenectomised patients from seven families exhibiting *SPTB* or *ANK1* mutations. In all patients, the mRNA of the allele carrying the mutation was degraded by the nonsense-mediated mRNA decay mechanism. Three groups of patients were defined based on clinical parameters and RBC morphology and deformability features. Although β-spectrin and ankyrin mutations led to differential RBC morphology, cytoskeletal organization defect and rigidity, cholesterol and total phospholipid content loss as well as microvesicle release, none of these features did correlate with the disease severity. Instead, the rise in intracellular calcium and ATP levels represented two factors to consider upon evaluation of the disease severity. On one hand, the intracellular calcium accumulation contributed to spherocytosis through the increased exposition of phosphatidylserine at the RBC surface but not through increased oxidative stress. Such calcium accumulation could result from the decreased abundance of the mechanosensitive cation channel PIEZO1 and its activity through the impaired response of the ganglioside GM1/PC/cholesterol-enriched domains to calcium influx stimulation by Yoda1. On the other hand, the rise in intracellular ATP content lowered the disease severity by limiting the intracellular calcium content increase, possibly through direct stimulation of the calcium efflux pump PMCA activity and/or maintenance of the membrane asymmetry

and the functionality of the SM/PC/cholesterol-enriched domains. Based on the integration of the intracellular calcium and ATP content modifications and the resulting alterations of membrane transversal and lateral heterogeneity in lipid domains, the ten patients were classified into three groups that perfectly matched with the disease severity score defined by clinical parameters and RBC morphology and fragility.

In conclusion, this work uncovered the importance of calcium accumulation and the resulting alterations of membrane transversal and lateral heterogeneity in both elliptocytosis and spherocytosis. Hence, it indicated that clinical heterogeneity in spherocytosis can be reflected in the calcium-dependent membrane defects. Finally, the plasmatic acid sphingomyelinase could represent a possible target for the development of new therapeutics in elliptocytosis.

CHAPTER 1. INTRODUCTION

1. Plasma membrane lipid composition, biophysical properties and organization

Plasma membranes are indispensable for life as they allow cells to maintain their internal composition. In nucleated cells, membranes also separate the cytoplasm from subcellular organelles which need to adapt their internal composition to their specialized activities. Basically, membranes are lipid bilayers in which lipid tails from both leaflets face up while lipid polar head-groups are oriented through the cytoplasm or the exterior of the cell and in which proteins are embedded.

1.1. Membrane lipid composition and turn-over

Approximatively 5% of the eukaryotic cell genes are used to generate thousands of different lipids [1]. Except for sterols, lipids possess a hydrophobic portion (the tail) made of fatty acyl chains and a polar head-group. Diversity of head-groups, fatty acyl chain length and saturation explain the enormous variety of lipids found in membranes. This large diversity is nevertheless classified in three main groups: glycerophospholipids, sphingolipids and cholesterol.

1.1.1. Membrane lipid composition

Glycerophospholipids are the principal components of the membrane bilayer. Their basic structure is composed of two esterified fatty acyl chains attached to one glycerol (Figure 1.1.). Generally fatty acids at the C1 are saturated or monosaturated while fatty acids at the C2 are polyunsaturated. Predominant cell fatty acids contain 14-20 carbon atoms (Table 1.1.). Every double bond drives a stable curvature to the acyl chain. The polar head is attached to the C3 of the glycerol via a phosphoester bond and could be an ethanolamine, a choline, a serine or an inositol, among others.

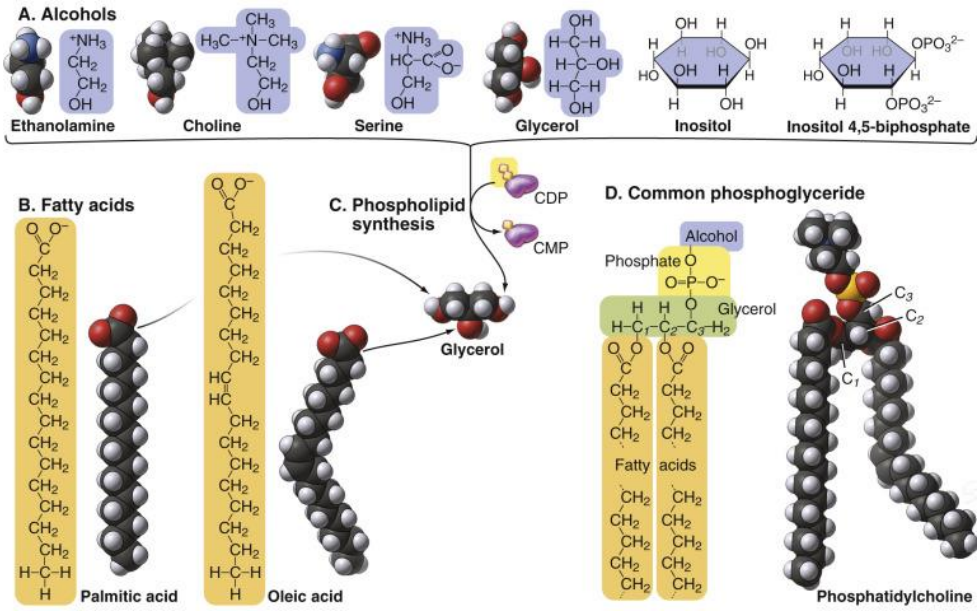

Figure 1.1. Glycerophospholipids. A. Stick figures and space-filling models of the alcohol head-groups. B. Stick figures and space-filling models of two fatty acids. C. An alcohol (the head-group), phosphate, glycerol and two fatty acids combined to make a glycerophospholipid. D. Stick figure of a glycerophospholipid and the space-filling model of phosphatidylcholine [2].

Name	Carbons	Double Bonds (Positions)
Myristate	14	0
Palmitate	16	0
Palmitoleate	16	1 (Δ9)
Stearate	18	0
Oleate	18	1 (Δ9)
Linoleate	18	2 (Δ9, Δ12)
Linolenate	18	3 (Δ9, Δ12, Δ15)
Arachidonate	20	4 (Δ5, Δ8, Δ11, Δ14)

Table 1.1. Common fatty acids of membrane lipids. From [2].

Every polar head presents different electric charges, bestowing distinct properties to the lipid. For instance, phosphatidylethanolamine (PE) and phosphatidylcholine (PC) are neutral whereas phosphatidylinositol (PI) can be modified by esterification of the hydroxyl functions of the inositol with one to five phosphates, creating heavily charged polyphosphoinositides [2]. Another factor to consider is the lipid global shape depending on the size of the head and the saturation and length of the tail. For instance, PC possesses

a nearly cylindrical molecular geometry, leading to self-organisation as a planar bilayer, while PE assumes a conical molecular geometry because of the relatively small size of its polar head-group, imposing a curvature to the membrane [1].

Sphingolipids, the second major lipid class, are named based of the sphingosine, a nitrogenous base with an unsaturated fatty acid chain (Figure 1.2.). A second fatty acid is attached by an amide bond to the C2, forming a ceramide while the polar head is attached to the hydroxyl function of C1. The polar head-group can be i) a phosphocholine, forming SM, the major sphingolipid; or ii) carbohydrates, forming the less abundant but highly diversified glycosphingolipids (GSLs). Among these, glucosylceramide represents the simplest, with one glucose as polar head. Gangliosides, which include the GM1, are GSLs with terminal sialic acids. Sphingolipids generally have saturated (or trans-unsaturated) tails, thereby forming taller, narrower cylinders than PCs of the same chain length.

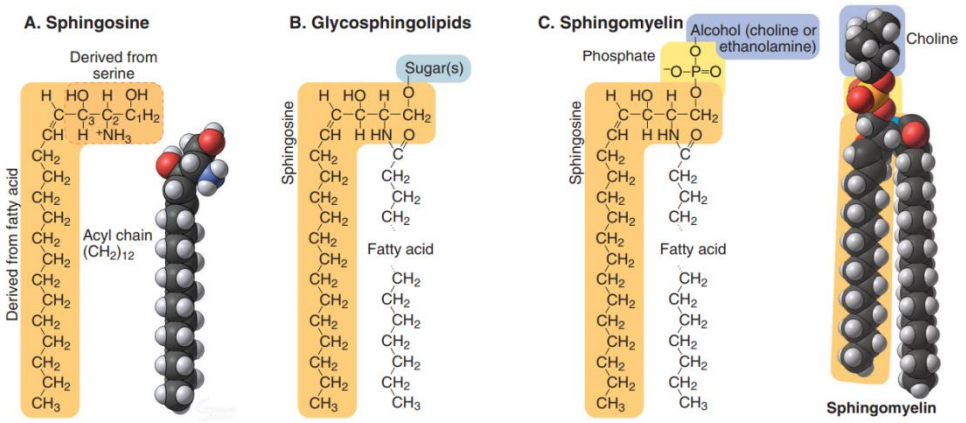

Figure 1.2. Sphingolipids. A. Stick figure and space-filling model of sphingosine. B. Diagram of the parts of a glycosphingolipids. C. Stick figure and space-filling model of sphingomyelin [2].

Sterols are the least polar membrane components. Cholesterol, the sterol found in mammalian cells, is composed of four carbon cycles forming a rigid hydrophobic core linked to a short hydrocarbon tail and to a polar hydroxyl group, responsible for the slightly amphipathic character of the molecule (Figure 1.3.).

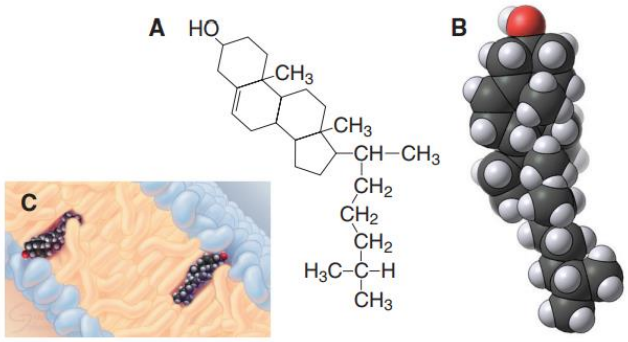

Figure 1.3. Cholesterol. A. Stick figure. B. Space-filling model. C. Disposition of cholesterol in a lipid bilayer with the hydroxyl (red) oriented toward the surface [2].

Huge differences in membrane composition can be found between prokaryotes and eukaryotes, but also within eukaryotes. These differences are presented in table 1.2. (adapted from [3]). Notice the higher enrichment in cholesterol in the human red blood cell (RBC) membrane as compared to other membranes. Since cholesterol plays a dominant role in the regulation of membrane organization, changes in cholesterol levels should have differential consequences in different cell types.

Molar %	Polar lipids								Sterols[a]	Other	Ref.
	PC	PE	PI	PS	PA	PG	CL	SLs[a]			
E. coli		82		Tr.		6	12				[4, 5]
S. cerevisiae	25	10	9	3	5		2	10-20 *MIPC*	30-40 *erg*		[5-7]
Human RBCs	24	6	tr.	3	Tr.			19 *SM*	48 *chol*	Tr.	[5, 8]
Human platelets	18	20	1	12				16 *SM*	32 *chol*		[9, 10]
Fibroblast cell line (NIH 3T3)	43	16	8	6.5	1.5			12 *SM*	13 *chol*		[11]
Chinese hamster ovary cells (CHO)	25	21	n.d.	7				12 *SM*	35 *chol*		[12]
Schwann cell line (NF1T)	27	9	6	2				18 *SM*	38 *chol*		[13]
Undifferentiated L6 myoblasts	24	9	2	6				16 *SM*	42 *chol*		[14]
Human alveolar macrophages	30	21		21				7 *SM*	8 *chol*	13	[5, 15]

Table 1.2. Lipid composition of the plasma membrane in different cells. PC, phosphatidylcholine; PE, phosphatidylethanolamine; PI, phosphatidylinositol; PS, phosphatidylserine; PA, phosphatidic acid; PG, phosphatidylglycerol; CL, cardiolipin; SLs, sphingolipids; MIPC, mannosyl-inositol phosphorylceramide; SM, sphingomyelin; erg, ergosterol; chol, cholesterol. The most abundant lipid of these categories is indicated in italics. n.d., not detected. Tr., traces. From [3].

1.1.2. Membrane lipid metabolism

Living cells are to regulate and remodel their membrane lipid composition thanks to specialized enzymes [16, 17]. This underlines the fact that phospholipids are not only membrane components but also cellular intermediates playing multiple roles in cell development, metabolism and signalling [18]. For example, even though the concentration of phosphatidic acid (PA, the common precursor of glycerophospholipids) is maintained at very low intracellular levels, it contributes to membrane curvature maintenance and acts as signalling lipid regulating glycerophospholipid biosynthesis [16]. Due to its negative charge, it also contributes to the activation or the recruitment of proteins with polybasic regions [19]. Sphingolipids also control many membrane-associated cellular processes including endocytosis and signal transduction [20-23].

Phospholipases comprise four major classes based on the type of catalysed reaction [18]. Phospholipase A cleaves either the *sn-1* acyl chain (PLA_1) or the *sn-2* acyl chain (PLA_2) of phospholipids, releasing a free fatty acid and a lysophospholipid (LPL). Based on their primary structure, enzymatic and subcellular localization properties, PLA_2 can be subdivided into 3 categories: i) calcium dependent cytosolic PLA_2 ($cPLA_2$); ii) calcium dependent secretory PLA_2 ($sPLA_2$); and iii) calcium independent intracellular PLA_2 [18]. $cPLA_2$ is

activated in response to an increase in intracellular calcium and releases arachidonic acid, the precursor for eicosanoids. On the other hand, lysoPLs present an inverted conical shape and support membrane vesiculation and vesicle fusion [19]. Phospholipase B cumulates the enzymatic activities of PLA_1 and PLA_2 as it can release indifferently the fatty acyl chain in *sn-1* or *sn-2* [18]. Phospholipase C (PLC) catalyses the hydrolysis of PIP_2, producing two second messengers: inositol 1,4,5-triphosphate (IP_3, known to induce calcium release from intracellular calcium stores) and diacylglycerol (DAG, able to bind calcium dependent C2 domains and activates protein kinase C). DAG kinase and lipase can then convert DAG into potent bioactive messengers such as PA and arachidonic acid, respectively [19]. Phospholipase D (PLD) hydrolyses the phosphodiester bond of phospholipids, in particular PC, resulting in the production of a free choline and PA.

Ceramides are synthesized *de novo* in the endoplasmic reticulum but can also be produced directly at the membrane by hydrolysis of SM into ceramide and phosphocholine. This reaction is catalysed by **sphingomyelinases** (SMases) which include neutral and acid SMases depending on the pH at which their enzymatic activity is optimal. Acid SMases (aSMases) are either lysosomal or secreted. Ceramide can then be de-acylated by ceramidases to sphingosine. The generation of ceramide and sphingosine mediate cell death, senescence and/or cell cycle arrest [24]. Secreted aSMases are found in synovial, salivary and cerebrospinal fluids, as well as in tears, urine and blood [25]. Outside an acidic environment, the membrane lipid composition could alter the Km of aSMase, allowing enzyme activity at higher pH [26]. The biological functions of aSMases have been extensively studied, although mostly in pathological conditions, and are associated with acute and/or chronic inflammation [25]. Thus, increased secreted aSMase in plasma is suggested to be proinflammatory [27].

Lipids can also be phosphorylated by **kinases** which can change the reactivity and localization of the lipid and can be used in signal transmission. Phosphatidylinositol kinases phosphorylate phosphatidylinositol species, generating phosphatidylinositol 3,4-biphosphate ($PI(3,4)P_2$), phosphatidylinositol 3,4,5-triphosphate ($PI(3,4,5)P_3$) and phosphatidylinositol 3-phosphate (PI_3P) among others. The phosphorylation state of phosphatidylinositol plays a major role in cellular signalling [28]. Another example is the metabolic conversion of sphingosine to sphingosine-1-phosphate (S1P) by the sphingosine kinase (SPHK) [29]. SPHK1 is found in the cytosol and is translocated to the membrane upon activation while sphingosine kinase 2 (SPHK2) is located mainly in the nucleus. A small portion of SPHK1 is secreted constitutively into the extracellular space. S1P acts not only intracellularly as a second messenger, but also extracellularly as a ligand for its membrane receptors [29]. Circulating S1P serves as key regulator of lymphocyte trafficking, endothelial barrier function and vascular tone [29].

1.1.3. Membrane lipid organization: a brief history

In 1926, Gorter and Grendel proposed that cell membranes are organized in a lipid bilayer (Figure 1.4.A). It was proved by determining RBC membrane surface area by electron microscopy and comparing it to extracted RBC membrane lipids spread out at an air-water interface. Comparison of both measurements revealed that the surface area of the lipid monolayer was approximately twice that occupied by the RBC membrane, in perfect agreement with their lipid bilayer prediction [30]. Yet, lipid bilayers alone could not explain plasma membrane mechanical properties and the role of proteins. As proteins are more hydrophilic than phospholipid head-groups, Davson and Danielli proposed that proteins coat the bilayer to reinforce its resistance (Figure 1.4.B) [31]. In the 1950s improved resolution of electron microscopy was enough to study membrane structure, revealing that membranes present two hard lines (assimilated as proteins) separated by a soft space (assimilated as lipid bilayer) [32]. However, this model seemed contradictory with the large diversity of membranes in term of constituents that was being discovered at the time [33]. Moreover, membrane proteins are not very soluble in water, contesting the point of view of hydrophilic proteins protecting the bilayer [2].

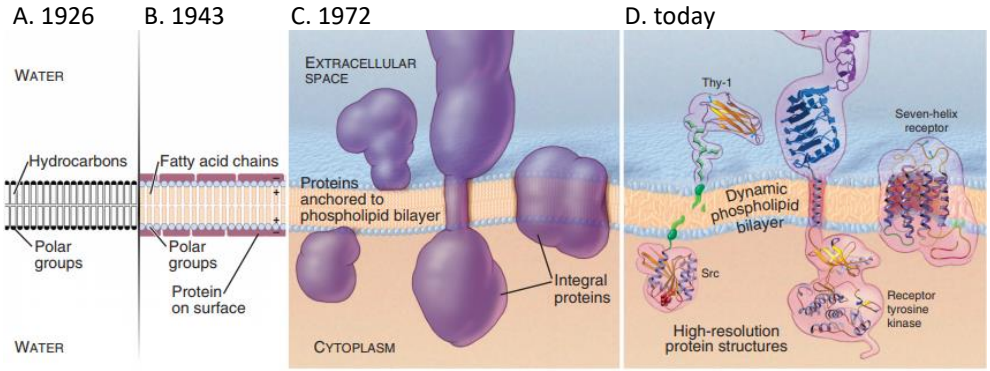

Figure 1.4. Evolution of the concepts of membrane structure and organization. A. Basic bilayer with double hydrophobic-hydrophilic interface (model of Gorter & Grendel). B. Multilayer model of the bilayer coated with hydrophilic proteins (model of Davson & Danielli). C. Peripheral *vs* integral membrane proteins (Singer & Nicolson fluid mosaic model, 1972). D. Contemporary model with peripheral and integral membrane proteins embedded in a dynamic phospholipid bilayer. Adapted from [2].

Later, electron microscopy images of membranes cleaved by cryofracture showed the presence of proteins inside the lipid bilayer [34]. Chemical labelling of membrane proteins indicated that numerous proteins span the bilayer, exposing different parts of the polypeptide to the aqueous phase located on both sides of the membrane. This disposition maximizes the contact between hydrophilic part of proteins and phospholipids with water, at the same time furnishing a hydrophobic part away from water. Labelling experiments, x-

ray diffraction and calorimetry indicated that membrane proteins diffuse into the bilayer, the rate of which depend on viscosity. Based on these results, Singer and Nicolson presented in 1972 their fluid mosaic model of cell membrane structure in which proteins are embedded in a homogenous lipid bilayer and free to diffuse laterally (Figure 1.4.C) [35]. In this model, lipids only play a passive structural role. However, abundant evidence indicates that lipids do not homogeneously distribute in the membrane but present multilevel of heterogeneity (Figure 1.4.C). Transversal asymmetry, which corresponds to differential composition between both leaflets (section 1.3.), and lateral asymmetry inside one leaflet (section 1.4.), can be distinguished. Both heterogeneities influence biophysical membrane properties (see below).

1.2. Membrane biophysical properties

Biophysical membrane properties depend on lipid and protein membrane composition and on the strength of membrane anchorage to the underlying cytoskeleton. Three properties are described i) fluidity (section 1.2.1.), ii) curvature (section 1.2.2.) and iii) thickness (section 1.2.3.).

1.2.1. Membrane lipid phase behaviour and fluidity

Lipid bilayer phase behaviour is the response of the lipid bilayer to the relative mobility of the individual lipid molecules (*i.e.* fluidity). These phases have specific properties depending on the presence of cholesterol and the length of lipid tails and their degree of unsaturation. At physiological temperature, fatty acids with 18 or more carbons form a solid phase (S_o) unless they contain double bonds that create a permanent bend and promote a disordered liquid state (L_d) by creating free space within the bilayer (Figure 1.5.). Tight packing of saturated acyl chains in the S_o state limits lateral diffusion while disruption of packing allows additional flexibility. On the other hand, short acyl chains favour liquid state [1, 36]. Cholesterol seems to have a differential effect, favouring an ordered liquid phase (L_o) by disrupting the order of the gel state (S_o) while increasing the mechanical rigidity and decreasing the lateral diffusion coefficient if added to a L_d phase [37]. As a consequence of phase behaviour, a membrane that contains mostly SM with or without cholesterol is thicker (≈4-5nm) than a membrane composed of PC and cholesterol (≈4nm), itself thicker than a membrane of short PC alone (≈3nm) [38]. Sphingolipids like SM are appropriate for the formation of L_o phases as saturation is prevalent in their acyl chains and because the stabilizing effect of their hydroxyl function allows the formation of hydrogen bonding between their head-groups [39]

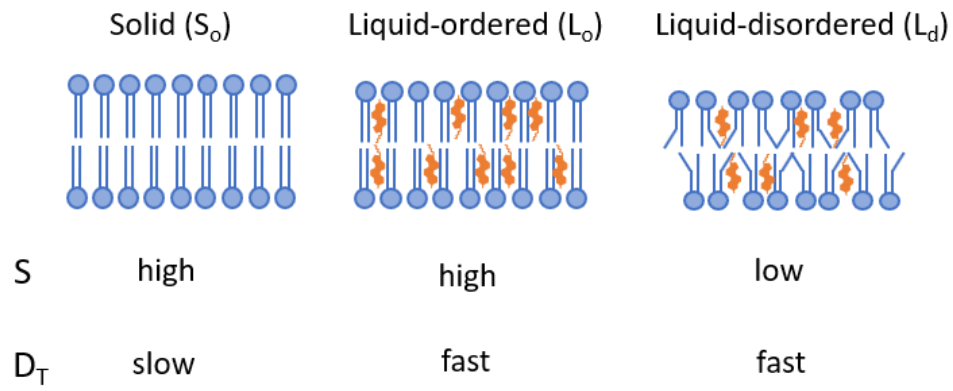

Figure 1.5. Simplified schematic representation of membrane lipid phases. S, order parameter of a segment of acyl chain; D_T, translational diffusion coefficient.

When phases coexist, an interface is created in between. As both phases present different properties (e.g. thickness), it generates an energy per unit length at the interface (i.e. the line tension). Line tension plays a central role in the regulation of lipid domain size. Domain size and mismatch in bilayer thickness at the phase boundary are directly correlated [40]. Moreover, external perturbation of lipid domain shape is shortly followed by a return to its initial circular phase [41], minimizing the boundary length and the energy lost. Furthermore, alteration cholesterol from the bilayer by treatment with cholesterol oxidase leads to irregular domain shape followed by domain disappearance [41].

To probe membrane order in living cells, a classical method consists of inserting into the membrane the fluorescent probe Laurdan. Its spectroscopic properties are influenced by both the composition and dynamics of its surrounding environment. Its emission spectrum is ≈440nm in ordered membranes but switches to ≈490nm in disordered membranes. On images generated by bi-photon microscopy, "generalized polarization" (GP=$\frac{I440-I490}{I440+I490}$) can be measured for each pixel based on both fluorescence intensities [42]. A high GP value reflects high lipid ordering and therefore low membrane fluidity.

Atomic force microscopy (AFM) can be used to measure the elasticity of the cells. AFM consists of a cantilever with a sharp tip (probe) at its end taping the sample surface. The interaction force between the tip and the sample surface changes the amplitude of the cantilever's oscillation. The vertical and lateral deflection, vibration phase and amplitude of the AFM probe upon interaction with the sample are used to determine surface topography, friction and elastic property imaging [43, 44]. By this method, Young's modulus can be calculated, reflecting elastic deformation at the surface, *i.e.* stiffness. The higher the modulus, the stiffer the membrane [44].

1.2.2. Membrane curvature

The ability of cellular membranes to bend and adapt their shape is critical for a variety of cellular functions including membrane trafficking, fission, fusion, differentiation, motility and signal transduction [45]. Passive and active curvature generation mechanisms can be described based on i) membrane composition and asymmetry, ii) partitioning of shaped transmembrane proteins, iii) reversible insertion of hydrophobic protein motifs, iv) scaffolding by oligomerized hydrophilic protein domains and, v) scaffolding by the cytoskeleton with forces generated by polymerization and by molecular motors (Figure 1.6.) [46].

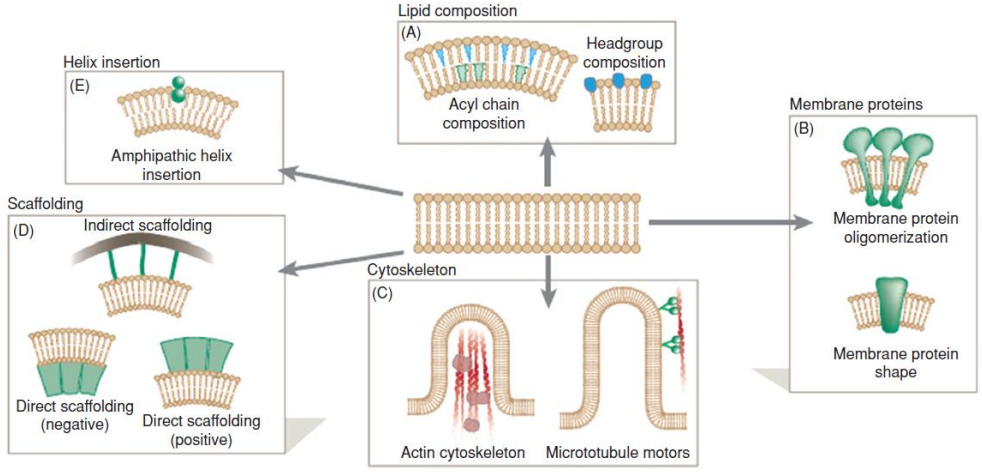

Figure 1.6. Mechanisms underlying membrane curvature. Curvature can be generated by (a) asymmetric lipid distribution; (b) intrinsic shape of transmembrane proteins or their complexes; (c) pushing or pulling the membrane by polymerisation of cytoskeletal filaments or by cytoskeletal motors; (d) scaffolding; and (e) insertion of amphipathic helices [47].

The intrinsic shapes of membrane phospholipids define the global curvature of the bilayer. As already mentioned, depending on head-group, length and saturation, lipids present cylindrical (PC and PS), conical (PE and PA) or inverted-conical (LPL and PI) shapes [1, 17]. Curvature is generated by the creation of lipid asymmetry between the two membrane leaflets (by the action of flippases; see section 1.3.), by the application of forces or mechanical constraints to the membrane forcing the lipids to reorganize [48, 49] or through the effect of lipases which generate lipids with distinct intrinsic shape (see section 1.1.2.).

Transmembrane proteins with conical shapes promote membrane curving. For example, the nicotinic acetylcholine receptors are not uniformly distributed throughout the depth of the junctional folds of axons but are concentrated at the upper surface near the

axonal membrane, at least partly resulting from the inverted-conical shape of the receptor [50]. In addition, many integral membrane proteins oligomerize, resulting in induction of membrane curvature by a crowding mechanism [51]. Another example is the bacterial potassium channel KvAP. Using a micropipette to induce artificial curvature to protein-enriched giant unilamellar vesicles, it was shown that KvAP is heterogeneously distributed with greater enrichment in more highly curved membrane areas [52].

Insertion of amphipathic helices into the bilayer can also induce curvature. The best example is the endocytic protein Epsin which contains an Epsin N-terminal homology (ENTH) domain possessing an α-helical superstructure and a PIP_2-binding region [47]. PIP_2 binding is the first step in membrane bending. Upon binding, the N-terminal domain forms an amphipathic α-helix which inserts in the inner leaflet, inducing membrane curvature [53]. Similar amphipathic helices are present in many proteins but vary in length and in affinity for charged lipids [54]

Nanoscopic proteins might also assemble into larger structures with an intrinsic shape affecting membrane curvature at the microscopic level. Coat proteins such as clathrin, COPI and COPII stabilize membrane curvature during vesicle budding. Caveolins constitute another important set of curvature-related scaffold proteins that are necessary for the formation of flask-shaped, cholesterol-rich invaginations of the plasma membrane called caveolae [55].

Finally, the cytoskeleton can be a direct inducer of membrane curvature. The polymerization of cytoskeleton subunits into filaments can push or pull the membrane into filopodia or lamellipodia [46].

1.2.3. Membrane thickness

To minimize energy loss, the hydrophobic thickness of the protein should be equal to that of the lipid bilayer [56, 57]. Most of the time, the protein tends to localize in a part of the bilayer where the hydrophobic thickness is favorable. If, for some reason, the protein does not find a match, the annulus lipids surrounding it could adjust to the protein, as lipid bilayers are dynamic and smooth structures. The protein can also be forced to alter conformation or tilt to hide the hydrophobic part of its transmembrane domain in the hydrophobic part of the bilayer. If the mismatch is too important, the protein can aggregate to decrease the energy loss [57, 58]. The hydrophobic mismatch could be used as a way to sort the protein as a function of the length of its hydrophobic part and then address it to different compartments and parts of the membrane. Van Galen and collaborators showed that changes in the trans-Golgi network bilayer thickness by disruption of the SM homeostasis leads to a different functional enzymatic domain organization and different sorting of transmembrane proteins [59]. Also x-ray diffraction studies of membrane-embedded crystals of the plasma membrane calcium ATPase

(PMCA) revealed that variations in membrane thickness of about 2.5Å allow large tilting movements of the protein transmembrane helices [60, 61].

The bilayer thickness can also modulate the activity of transporters or receptors. For instance, the calcium ATPase exhibits the highest activity in membranes containing phospholipids with a chain length of about 18 carbons [62]. The chain length dependence of the activity of the plasma membrane Na^+,K^+-ATPase is quite different as the optimal chain length is C22 in the absence of cholesterol but C18 in the presence of cholesterol [62]. However, this difference could also be linked to the charges of the bilayer and not only to the membrane thickness [63, 64].

1.3. Membrane transversal asymmetry

The composition of lipids in the two plasma membrane leaflets is not identical. This transversal asymmetry was first found during the 1970's in RBCs by several methods including enzymatic or chemical modifications of lipids [65, 66] and by sodium dodecyl sulfate-digested freeze-fracture replica labelling (SDS-FRL) [67]. SM and GSLs are mainly found in the external leaflet while PS, PE, PI or PA are present in the cytosolic leaflet (Figure 1.7.) [68], leading to a neutrally charged outer leaflet vs a negatively charged inner leaflet. Moreover, the fatty acyl chains in the outer leaflet are somewhat more saturated than those in the inner leaflet [69]. As consequences of differential lipid composition, the cytoplasmic leaflet of human RBC is more fluid than the extracellular leaflet, as indicated by electron spin resonance with spin-labelled lipids and lateral diffusion measurements by photobleaching with fluorescent lipids [70-72].

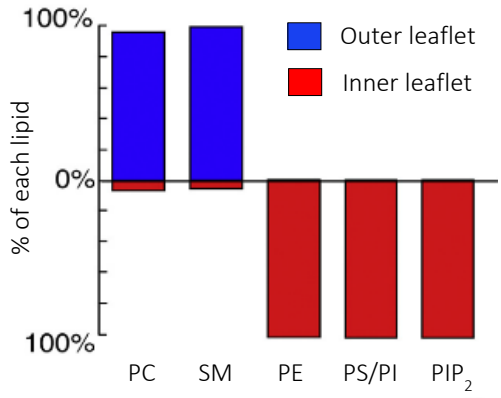

Figure 1.7. Asymmetric transbilayer phospholipid distribution in human RBC. Determination by freeze-fracture replica-labelling immunoelectron microscopy in combination with lipid-binding proteins to examine transbilayer distribution of various phospholipids in RBCs. PC, phosphatidylcholine; SM, sphingomyelin; PE, phosphatidylethanolamine; PS, phosphatidylserine; PI, phosphatidylinositol; PIP_2, phosphatidylinositol-4.5-bisphosphate [67].

The difference in composition could not be explained by spontaneous translocation across the leaflets. Indeed, this process, named "flip-flop", is governed by the size, the

charge and the polarity of the lipid. The high energy barrier imposed by resistance to the passage of polar head-groups through the hydrophobic core of the bilayer could explain the difficulty for the lipids to cross it. For instance, the transbilayer movement of a GSL would take one day (10^{-15} s^{-1}) as compared to seconds for DAG, ceramide and cholesterol [1, 73]. For sphingolipids, the difference in composition between leaflets takes place during their biosynthesis. Sphingolipids are synthetized in the luminal leaflet of the Golgi apparatus and brought by vesicular traffic to the outer leaflet [1, 74]. Glycerophospholipids such as PE, PC and PS are synthetized in the endoplasmic reticulum where they are homogeneously distributed between the two leaflets. Their reorganization takes place at the membrane via ATP-dependent transbilayer lipid translocators, confining them to the plasma membrane inner leaflet. Among these enzymes, flippases and floppases can be distinguished (Figure 1.8.). Flippases transport lipids of the outer leaflet to the inner one while floppases do the opposite. Phospholipid transfer may lead to local or extended cell shape changes through bending of the lipid bilayer. The steady-state asymmetry can be disrupted by the activation of phospholipid scramblases, a group of homologous ATP-independent calcium-dependent bidirectional lipid translocators [73].

Physiologically, PS translocation to the outer leaflet, normally restricted to the inner one, plays a role in RBCs upon aging and stress, inducing their phagocytosis and degradation by spleen macrophages [75]. In addition, premature PS exposure by sickle and thalassaemic RBCs results in a shortened RBC life span and is associated with hemolytic anaemia (see sections 4 and 5).

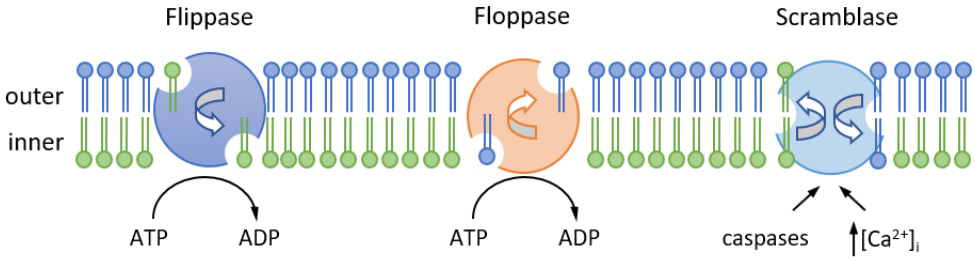

Figure 1.8. Simplified schematic representation of the maintenance of the asymmetric distribution of phospholipids in the membrane. ATP-dependent flippases and floppases move lipids only in one direction and they are lipid-specific while scramblases move lipids bidirectionally.

Currently, the repartition of cholesterol between leaflets is still a matter of debate [69]. Cholesterol flip-flop between leaflets is fast due to its low polarity and small size which could suggest a homogeneous distribution between leaflets [76]. However, it is not possible to conclude that the repartition is homogeneous as interactions with other confined lipids/proteins could promote preferential segregation of cholesterol into one of the leaflets [69, 77]. On one hand, SLs and cholesterol are enriched in lipid rafts present in the outer

leaflet [20] and monolayer freeze-fracture autoradiography on RBCs labelled with radioiodinated concanavalin A indicated that ~60% of cholesterol is present in the outer leaflet [69, 78]. On the other hand, the preferential accumulation of cholesterol (up to 75%) in the inner leaflet was seen in RBCs by quenching of dehydroergosterol fluorescence and fluorescence photobleaching of NBD-cholesterol [79]. It was also suggested that some cholesterol may also occupy the inter-leaflet midplane of the bilayer [69]. Interestingly, cholesterol has been shown to inhibit phospholipid scrambling, an unsuspected function which could be critical for cell deformation [80].

1.4. Membrane lateral heterogeneity

As protein-to-lipid ratio of purified stripped membranes is close to the unity on a mass basis, their large difference in molecular weight makes ≈50 lipid molecules per membrane protein a reasonable general estimate, underlining that membrane lipids actually cover most of the plasma membrane [81, 82]. It seems reasonable that due to intrinsic lipid complexity, cell membranes are arranged in far more intricate structures than simple homogenous fluid bilayers. Lateral heterogeneity was, however, for a long time a matter of intense debate. Limited availability of reliable fluorescent probes, poor lipid fixation, imaging artefacts due to membrane protrusions/projections and utilization of highly disruptive methods of isolation were criticized. Moreover, lipid domains have sometimes been reported under non-physiological conditions, potentially explaining the discrepancies between the results obtained by different research groups. Two types of lipid domains, transient nanometric domains (section 1.4.1) and stable submicrometric lipid domains (section 1.4.2) will be briefly discussed here.

1.4.1. Transient nanometric domains

In 1987, Kai Simons and Gerrit Van Meer discovered that GSLs are enriched in the apical membrane, making it thick and robust. Lipid segregation between apical and basolateral membranes is maintained due to tight junctions [83]. Sorting is made possible by the clustering of GSLs in the Golgi apparatus before being conveyed to the apical surface. Strikingly glycosylphosphatidylinositol (GPI)-anchored proteins are also sorted exclusively to the apical membrane in polarized cells [84]. Moreover, it was already known that GPI-linked proteins are resistant to solubilization with non-ionic detergents such as Triton X-100, along with GSLs and SM [85]. Whether the GPI-linked proteins and GSLs are indeed associated in the detergent insoluble-material was addressed experimentally by Brown and Rose, as the reference method for the isolation of lipid rafts as detergent resistant membranes (DRMs) [39, 86]. Then, Simons and van Meer proposed that GPI-linked proteins and GSLs follow the same sorting pathway to apical domains, associating to form “patches” in the Golgi apparatus. The term of “lipid rafts” was introduced and defined later [87]. However, the raft concept has been extensively criticized due to their artificial isolation as

"DRMs" as possible sources of artefacts. For instance, the use of detergents may reorganize membrane components, as proved for Triton (known to promote formation of ordered domains in model membranes [88]). Moreover, visualization of lipid rafts by microscopy was lacking due to their nanometric size, instability and heterogeneity.

To eliminate any misinterpretations, lipid rafts were redefined during the Keystone Symposium of 2006 as "small (20-100nm), heterogenous, highly dynamic, sterol- and SLs-enriched domains that compartmentalize cellular processes. Small rafts can sometimes be stabilized to form larger platforms through protein-protein and protein-lipid interactions" (Figure 1.9.) [89, 90]. These domains create a thicker L_o phase inside a L_d phase. This membrane thickening could help the recruitment of specific proteins with the same hydrophobic length [63].

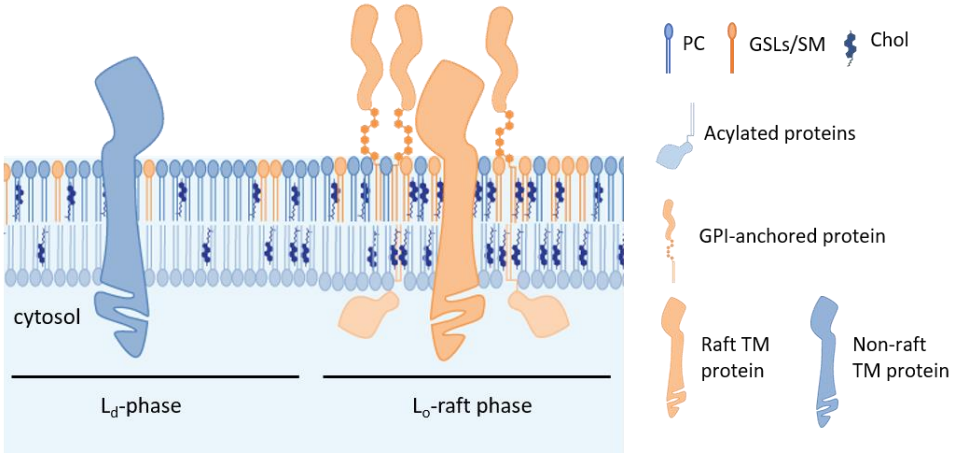

Figure 1.9. The lipid raft hypothesis. Rafts are enriched in sphingolipids (GSLs and SM), cholesterol (Chol), lipid-anchored proteins and some transmembrane proteins. TM, transmembrane; GPI, glycosylphosphatidylinositol; GSLs, glycosphingolipids; SM, sphingomyelin; PC, phosphatidylcholine; L_o, ordered phase; L_d, disordered phase.

Recently several emerging biochemical and biophysical techniques using natural systems such as giant plasma membrane vesicles derived from cells have provided support for the presence of these domains in cells, [91]. Also, the conservation of lipid rafts between prokaryotes and eukaryotes has also been shown [91, 92]. Moreover, super-resolution microscopy allowed the visualization of lipid-mediated protein clustering [91]. Very recently, using single molecule localization microscopy that achieves remarkable spatial resolution of ≈10nm, Yan et al were able to observe the formation of raft-like nanodomains in the membrane of living mammalian cells [93]. More information about recent techniques to study membrane organization can be found in [91, 94, 95] or by consulting our review [3] (Abstract in Annex 3).

In addition to rafts, other nanoscale domains (i.e. <100nm in diameter) have been described in the plasma membrane of eukaryotes such as caveolae [55] and tetraspanin-rich domains [96]. Caveolae are specialized nanodomains able to form stable membrane invaginations of 60-80nm enriched in sphingolipids and cholesterol. Two protein families are essential to their formation and function, caveolins and cavins. Caveolae are numerous in endothelial cells and adipocytes but are absent in RBCs. Tetraspanins are structural proteins bearing four transmembrane domains, which control the formation of membrane tubules. As they oligomerize, they can recruit various proteins to establish functional domains.

1.4.2. Stable submicrometric domains

Besides nanosized lipid domains, morphological evidence for stable (min *vs* sec) submicrometric (i.e. >200nm in diameter *vs* 20-100nm) lipid domains was first suggested by dynamic studies. For instance, by fluorescence recovery after photobleaching, Edidin et al pointed out a restriction to lateral diffusion of a fluorescent PC analog inserted in the fibroblast plasma membrane [97]. Also Kusumi et al showed that phospholipids diffuse more slowly in the fibroblast membranes than in artificial bilayers as they are confined for ≈11ms in a defined area before hopping to adjacent compartments [98]. In the past decades, several groups have provided evidence for submicrometric domains in a variety of living cells, from prokaryotes, to yeast and animal cells (Figure 1.10.). For more information, see [3] (Abstract in Annex 3).

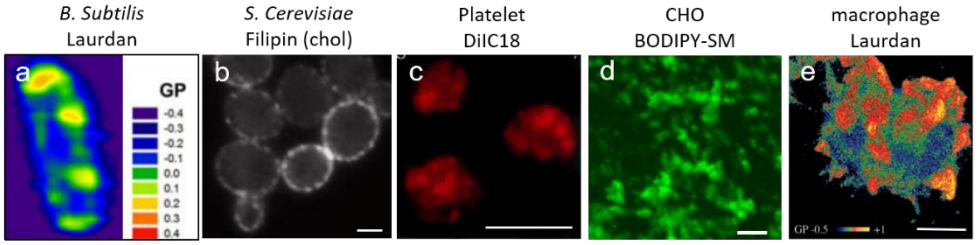

Figure 1.10. Visualization of plasma membrane submicrometric lipid domains by fluorescence/confocal imaging. (a) *B. Subtilis* labelled with Laurdan at 37°C [99]. (b) *S. Cerevisiae* stained with filipin (ergosterol) [100]. (c) Platelets labelled with DilC18 and examined at 15°C [101]. (d) CHO cell labelled with BODIPY-SM, pretreated with latrunculin B and examined at 4°C (to prevent both endocytosis and membrane protrusions) [102]. (e) Living RAW264.7 macrophage labelled with Laurdan and examined at 37°C, then reconstructed to a 3D image from 50-100 images [103]. All scale bars, 2µm. Adapted from [3].

2. Red blood cell life cycle

RBCs are the most abundant cell type in the blood (4-6x10^6 RBCs/µL). Their principal function is the oxygen transport which is optimized by their small size and biconcavity allowing a greater surface for rapid diffusion. In mammals, RBCs lose their nucleus and organelles. The space liberated by the nucleus is occupied by hemoglobin responsible for oxygen transport due to four heme groups.

2.1. Erythropoiesis

2.1.1. Erythroid differentiation stages

Erythropoiesis (from the Greek *erythros*: red and *poiesis*: to make) is the process by which RBCs are produced. During adult life, erythropoiesis -and hematopoiesis in general- mostly takes place in the bone marrow, a semi-solid tissue found within the central cavities of axial and long bones.

Bone marrow consists of hematopoietic cells, adipose tissue and supportive stromal cells (Figure 2.1.) [104]. The marrow is served by numerous blood arteries opening up into venous sinuses near the bone, which lead back to a central longitudinal vein. The hematopoietic microenvironment consists of a reticulin skeleton and adventitial reticular cells which furnish a proper environment for cell differentiation [104]. Erythroid progenitors are organized in a hematopoietic subcompartment called “erythroid island”. Each island is made up of a central iron-containing macrophage surrounded by maturing erythroid precursors at various stages of development [105].

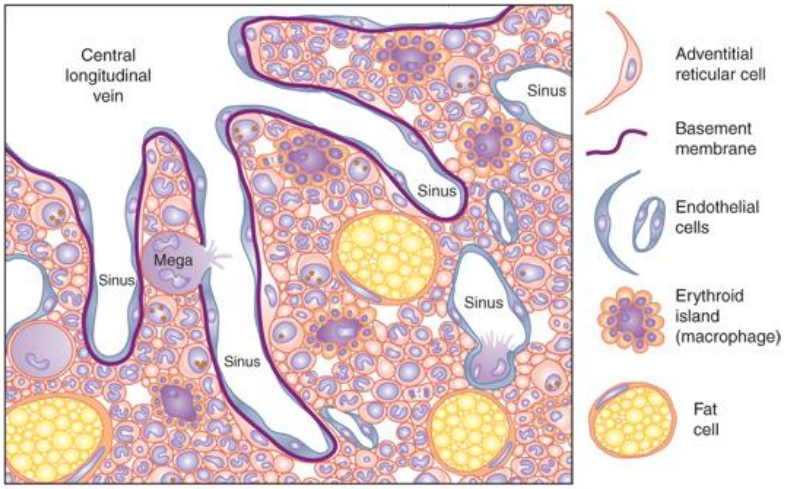

Figure 2.1. Bone marrow structure [106].

The central macrophage extends cytoplasmic protrusions and its function is to regulate erythroid proliferation, differentiation, enucleation and to clear the pyrenocytes resulting from the enucleation process [107].

Hematopoietic stem cells are a self-renewing population, common ancestors of all blood cells. The most immature lineage-committed erythroid progenitors are termed burst-forming unit erythroid (BFU-E) which then differentiate into colony-forming unit-erythroid (CFU-E) (Figure 2.2.). These progenitors are defined by their ability to form colonies of mature erythroid cells in semi-solid media [108].

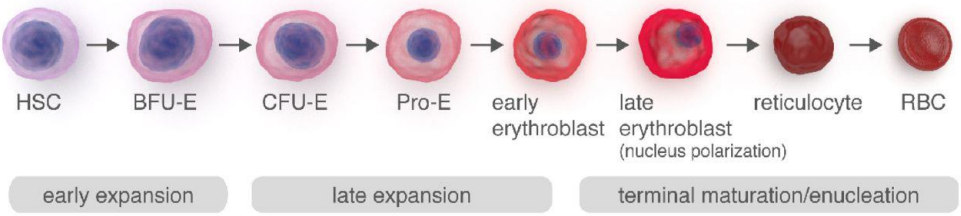

Figure 2.2. Schematic representation of erythroid differentiation. HSC, hematopoietic stem cell; BFU-E, burst-forming unit erythroid: CFU-E, colony-forming unit erythroid; Pro-E, proerythroblast [109].

The proerythroblast is the earliest recognizable erythroid precursor, arising directly from the CFU-E under the influence of erythropoietin (EPO). As the maturation process advances to erythroblasts and reticulocytes, cells divide and accumulate iron and hemoglobin while decreasing in size due to decreased RNA content and progressive nuclear condensation. The degree of hemoglobin and RNA content is reflected by cytoplasmic staining which progressively switches from basophilia (blue; acidic cytoplasm due to the nucleic acids) to polychromatophilia [108].

Enucleation is the final step of maturation and results in the formation of two cell types. The first population consists of reticulocytes, that contain most of the cytoplasm and hemoglobin as well as the proteins needed to form the cytoskeletal network. The second population consists of pyrenocytes (“extruded nuclei”) that contain the condensed nucleus surrounded by a lipid bilayer and a thin layer of cytoplasm. Pyrenocytes expose PS at their surface, providing an “eat me” signal, and are rapidly ingested by surrounding macrophages [108]. Enucleation is a complex process involving multiple steps including i) nuclear and chromatin condensation, dependent on the acetylation status of histones H3 and H4; ii) establishment of cell polarity through microtubule action; iii) formation of a contractile actomyosin ring, in as in cytokinesis but in an asymmetric way; and iv) coalescence of lipid rafts between reticulocytes and pyrenocytes [108, 110]. During this process, erythroid membrane and cytoskeletal proteins and other cellular machineries are selectively sorted between reticulocytes and pyrenocytes. For instance, Band3, ankyrin, 4.1R, glycophorin A

(GPA), glycophorin C (GPC), RhAG and spectrins segregate to the nascent reticulocyte while β1 integrin, fibronectin receptor and transferrin receptor are selectively lost [111, 112]. Although, the mechanisms of protein sorting are still largely unknown, they appear to be involve the spectrin/ankyrin/4.1R cytoskeleton, as revealed by the aberrant protein sorting in mice lacking ankyrin or 4.1R [113].

Once enucleation is complete, the reticulocytes join the circulation and finish their maturation (for 1-2 days) by losing 20-30% of their cell surface, adopting a biconcave morphology with improved viscoelasticity [114] and eliminating any remaining membrane-bound cytosolic organelles through an autophagy/exosome-combined pathway [108, 110] [115, 116]. Maturation is also accompanied by intense membrane remodelling. Indeed, cytosolic actin and tubulin are lost and other proteins such as GLUT4, Na^+/K^+ ATPase, GPA and CD47 are reduced in abundance [114, 117].

2.1.2. Regulation

As the primary stimulus, a low O_2 level into the blood flow stimulates the kidneys - and to a lesser extent the liver- to secrete the hormone erythropoietin (EPO) via the binding of hypoxia-inducible transcription factor 2 (HIF2) to hormone response element (HRE) sequences on the EPO promoter. This hormone in a domino effect stimulates the bone marrow to produce erythrocytes. EPO seems less important for the terminal stages of differentiation of the mature erythroblast but is essential for BFU-E maturation into CFU-E. Indeed, EPO receptor expression is tightly restricted to cells between the late BFU-E and CFU-E cell stages [118, 119].

Other factors that positively regulate erythropoiesis include insulin, insulin-like growth factor, activin and angiotensin II. By contrast, transforming growth factor β, inflammatory cytokines such as γ-interferon and tumour necrosis factor α among others, all have negative effects on erythropoiesis [119, 120]. The precise relevance of these pathways for *in vivo* erythropoiesis remains to be established. A recent study highlights the importance of S1P signalling to modulate terminal erythroid differentiation. Indeed, sphingosine kinase activity regulates key mitophagy genes and SPHK1 inhibition disrupts the clearance of mitochondria in late erythroblasts. Moreover, supplementation of S1P *in vitro* promotes erythroid differentiation [121].

2.2. Energy supply

During its intravascular lifespan, the erythrocyte requires energy to maintain a number of vital functions. These include: i) maintenance of glycolysis (see below); ii) maintenance of the electrolyte gradient between plasma and red cell cytoplasm through the activity of ATP-driven membrane pumps (see section 2.4.); iii) synthesis of glutathione and other metabolites (see section 3.1.2.); iv) maintenance of hemoglobin iron in its

functional reduced ferrous state (see section 2.3.); v) protection of metabolic enzymes, hemoglobin and membrane lipids and proteins from oxidative damage (see section 3); and vi) preservation of phospholipid asymmetry (see section 1.3.) [122].

RBCs are devoid of mitochondria and are thus unable to use fats and generate energy from Krebs cycle. Production of ATP is via anaerobic glycolysis. As normal erythrocytes do not have glycogen, ATP production depends only on a continuous supply of glucose freely entering the cell by facilitated diffusion through the glucose transporter GLUT1 (~200 000/cell; ~10% of the total protein mass [123]).

RBC metabolism requires ATP as a source of energy and NADH and NADPH as cofactors. Approximately 90% of glucose is catabolized anaerobically to pyruvate or lactate by glycolysis. The net gain is two ATP molecules and two NADH molecules for one glucose. NADH produced can be used to reduce methemoglobin to hemoglobin by the NADH-dependent enzyme methemoglobin reductase (see section 3). As RBCs are subjected to a high degree of oxidative stress from oxygen transport, the cells use glutathione to scavenge reactive oxygen species. Glutathione reductase regenerates functional glutathione by using NADPH as electron donor. The only non-mitochondrial source of NADPH is the pentose phosphate shunt which produces two molecules of NADPH. The pentose phosphate pathway catabolizes about 10% of the entered glucose.

To ensure an effective production of energetic molecules, a metabolic complex is assembled next to the membrane. In summary, the RBC uses a membrane-associated glycolytic complex to create a localized pool of metabolites (glucose, ATP and protons). Glucose enters the RBCs via GLUT1 glucose transporter and is metabolized via the neighbouring membrane-bound glycolytic complex. The protein Band3, also known as anion exchanger 1 (AE1), has turned out to be a multipurpose protein around which cytoskeleton (section 2.4.3.) and metabolic enzymes are gathered, adding to its primary role of chloride/bicarbonate exchange (section 2.3.1.). It possesses three functional domains: i) the N-terminal cytoplasmic domain which is the key attachment site for the membrane skeleton, glycolytic enzymes and deoxyhemoglobin; ii) the transmembrane domain which forms the red cell anion-exchange channel; and iii) the cytoplasmic C-terminal domain which has a binding site for carbonic anhydrase II [124]. The enzymes associated with the metabolic complex include phosphofructokinase, aldolase, glyceraldehyde-3-phosphate dehydrogenase (GAPDH) and enolase. They stay inactive when bound but are activated when displaced either by hemoglobin binding to the N-terminal segment or by phosphorylation of 2 tyrosines within the binding sites [125]. Interestingly, ATP is sequestered within the cytoskeletal-membrane complex, probably due to β-spectrin, ankyrin, Band3 and GAPDH [126]. When formation of the metabolon complex is impeded, glycolytic flux increased up to 45% compared with untreated cells [127]. Lactate produced

by glycolysis is removed from the cell by the monocarboxylate transporter 1 (MCT1) in a proton-dependent manner. The ATP produced can be used locally by ATP-driven pumps such as the Na^+/K^+-ATPase [128].

2.3. Functions

2.3.1. Oxygen and carbon dioxide transport

The low solubility of O_2 in water, and by consequence in the blood, is bypassed by the production of specialized proteins –hemoglobins- which transport ≈98% of total O_2 present in blood.

Hemoglobin is composed of four subunits, each with a globin chain associated with a heme group (Figure 2.3.A). The heme group is a porphyrin ring –a heterocyclic ring-containing the Fe in the +2 redox state (ferrous) which can reversibly bind oxygen. If the iron ion is in Fe(III) state, the product –methemoglobin- cannot bind oxygen. In adult, hemoglobin A is predominant (≈97%) and is a tetramer of 2 α-chains and 2 β-chains ($\alpha_2\beta_2$). These subunits are structurally very similar, with a molecular mass of ≈16kDa (≈64kDa for the complete protein), and are encoded by *HBA1*, *HBA2* and *HBB* genes [119].

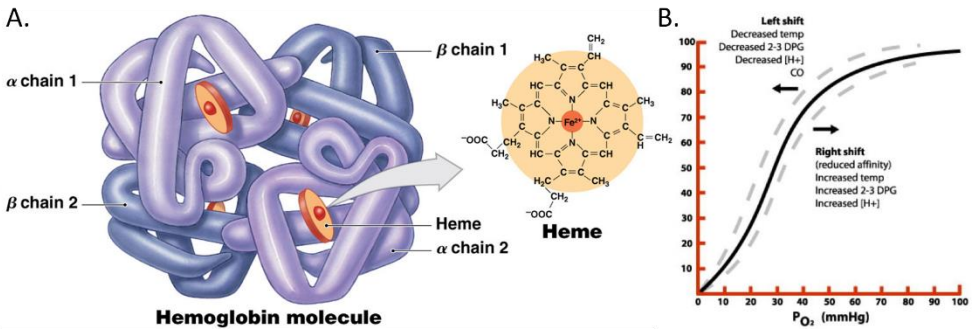

Figure 2.3. Hemoglobin, heme and interaction with oxygen. A. Hemoglobin and heme structures [129]. B. Standard human oxygen-hemoglobin dissociation curve. pO_2: oxygen pressure. Left shift: increase affinity of O_2 for hemoglobin; Right shift: reduction of the affinity [130].

The binding of oxygen is a cooperative process. Deoxygenated hemoglobin has T or tense conformation which has a weak affinity for oxygen and tends to liberate it. As O_2 binds to one globin, the tetramer conformation shifts from the T state to the R state –relaxed state- promoting the binding of oxygen to the remaining three heme-globin chains. Therefore, the oxygen binding curve of oxygen to hemoglobin is sigmoidal (Figure 2.3.B).

R state is favoured in high pH, low pCO_2 and low 2,3-BPG (2,3-biphosphoglyceric acid, a derived from glycolysis) concentrations which promote the fixation of O_2 when the blood circulates in the pulmonary alveoli. The T state is favoured by an acidic pH (Bohr effect),

high CO_2 concentration (Haldane effect) and high concentration of 2,3-BPG, favouring the liberation of O_2 when the blood circulates throughout the tissues. Moreover, increasing temperature lowers the affinity of hemoglobin for O_2 and shifts the oxygen dissociation curve to the right.

Besides oxygen, hemoglobin ligands also include competitive inhibitors (CO) and allosteric ligands (CO_2 or NO). Carbon monoxide (CO; from smoking or exhaust gas) competes with oxygen at the heme binding site with a high affinity, forming a carboxyhemoglobin. CO_2 is bound to amino groups of the globin chains, forming carbaminohemoglobin. Nitric oxide (NO) can also be transported by hemoglobin by a specific thiol group in the globin protein, forming a S-nitrosothiol. S-nitrosothiol dissociates into free NO and thiol again when hemoglobin releases O_2.

When RBCs are hemolyzed in the circulation, hemoglobin binds to haptoglobin and free heme is fixed by hemopexin to restrict the oxidant effect. The degradation of heme forms biliverdin, then the yellow bilirubin. Insoluble, it is bound in the blood by albumin and transported to the liver where it is processed in glucuronic acid and secreted by the intestine with bile [109].

CO_2 is twenty times more soluble in plasma than O_2. This property explains why CO_2 diffuses effectively despite weak variations of the partial pressure. CO_2 is transported in three ways: i) 7% dissolved in the blood; ii) 23% bond to free hemoglobin on exposed amino groups, forming carbaminohemoglobin (see above); and iii) 70% in the RBCs converted in carbonic acid (H_2CO_3) by carbonic anhydrase present at the membrane cytoplasmic surface linked to the band3 anion transport protein. H_2CO_3 then spontaneously dissociates to form bicarbonate ions (HCO_3^-) and protons (H^+). The protons bind to the deoxygenated hemoglobin. Cell membranes are generally impermeable to charged ions but RBCs possess the anion exchanger protein Band3 which pumps out HCO_3^- in exchange for one chloride ion (Cl^-). It is known as the Hamburger phenomenon or the chloride shift. Consequently, Cl^- concentrations are lower in venous blood than in arterial blood. The opposite occurs in the pulmonary capillaries in the lungs, as pO_2 rises and pCO_2 falls, releasing the proton from hemoglobin. It increases free H^+ concentrations within RBCs and shifts the equilibrium towards CO_2 and water formation from bicarbonate [129].

2.3.2. Secondary functions

RBCs can act as a regulator of blood flow. Indeed, upon passing through the microcirculation, RBCs may sense tissue oxygen conditions via the degree of deoxygenation of hemoglobin and couple this information to the release of vasodilatory compounds, such as ATP or nitric oxide (NO) [131]. At first it may be surprising that RBCs release ATP as it is a cellular energy supply. However, a large variety of cells, including RBCs, are capable of

releasing small amounts of ATP [132]. Extracellular ATP binds and activates the purinergic P_{2Y} receptors on vascular endothelial cells and induces the synthesis and release of NO [133, 134]. NO is a well-known vasodilator, which causes relaxation of the surrounding smooth muscle cells. RBCs release ATP under a variety of external stimuli, including hypoxia and hypercapnia but also mechanical, pH and osmotic stresses [133]. Studies with erythrocytes from individuals with cystic fibrosis have suggested that ATP release requires the cystic fibrosis transmembrane conductance regulator (CFTR). However, the involvement of CFTR in RBCs has not been clearly demonstrated [135, 136]. ATP release from human RBCs may involve the gap junction protein pannexin 1, which forms an ATP-permeable channel in the RBCs [131, 137]. A recent study highlights that PIEZO1, a mechanically activated cation channel, regulates shear-induced ATP release from RBCs [138].

2.4. Red blood cell biconcavity

The RBC is a biconcave disc with a ≈8µm-diameter and a ≈2µm-thickness, adapted to a 90fL volume and a surface area of 140µm², with high and low curvature areas. The discocyte shape allows the RBC to deform, fold and squeeze against the endothelial walls of capillaries, exposing maximal surface area thus offering minimal diffusional distances for rapid O_2 and CO_2 exchanges across the capillary walls. Maintenance of the biconcavity is essential for optimal viability and functionality for an extended circulatory lifespan [139].

2.4.1. RBC shape and volume control

Under physiological conditions, the RBC biconcave discoid (discocyte) shape allows the RBC to minimize bending energy. A variety of agents can reversibly modify this shape at constant area and volume. For instance, high salts, high pH, ATP depletion and proximity to a glass surface (negatively charged) induce a series of crenated shapes, called echinocytes and characterized by convex rounded protrusions or spicules (Figure 2.4.). If the action of these agents is prolonged, the spicules become smaller and more numerous before budding off irreversibly, forming extracellular vesicles. The resulting RBC is smaller and more spherical (spherocyte). On the other hand, low salts and low pH induce concave shapes called stomatocytes [140]. Sheetz and Singer were the first to propose an explanation based on the relaxed area difference ΔA_0 between the two membrane leaflets [141]. Any effect that could expand the outer leaflet compared to the inner leaflet (and increasing the ΔA_0) would then tend to form convex structures on the cell surface (i.e. spicules) while an expansion of the inner leaflet area relative to the outer leaflet (decreasing ΔA_0) favours concavities (i.e. stomatocytic shapes) [140, 141]. However, this model does not consider the shape control by membrane-bound proteins (e.g. spectrin, ankyrin or Band3), which was reflected by RBC shape aberrations upon mutation of these proteins (see section 5).

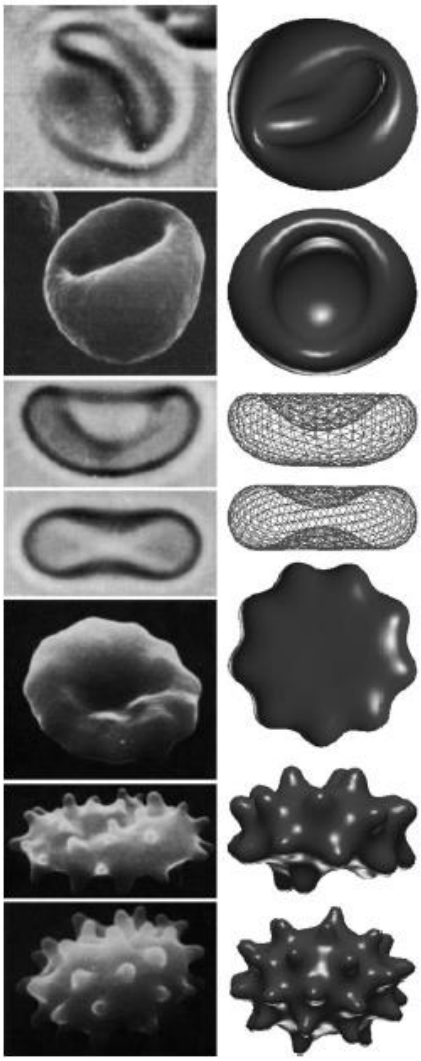

Figure 2.4. Representative shapes from the main stomatocyte-discocyte-echinocyte sequence. From top to bottom: stomatocyte III, II and I; discocyte; and echinocyte I, II, III. *Left,* scanning electron microscopy. *Right,* minimum-energy shapes with variations in ΔA_0 [140].

Combining theoretical prediction with spherical harmonic series expansions of theoretical cell surfaces and 3D imaging of live cells, it was demonstrated that the cytoskeleton is important for stabilizing the RBC shape against perturbations such as asymmetric changes in lipid bilayer composition. In the absence of a membrane skeleton, the discocyte form is the minimum energy shape only for a very small range of ΔA_0, while in the presence of cytoskeleton, this range is ≈100-fold larger [142].

Maintenance of a constant volume in the face of extracellular and intracellular osmotic perturbations is critical for RBCs. Under normal physiological conditions, the

osmolarity of the extracellular fluid is kept constant (≈285mOsm) and cell volume is most commonly perturbed by changes in intracellular, rather than extracellular, osmolarity. Water moves through the RBC membrane sufficiently fast for its volume to be established as the result of the osmotic difference between its internal and external solutions. As hemoglobin cannot cross the membrane, the cell has a tendency to swell [143]. To thwart this effect and keep a steady volume, the cytoplasmic content of K^+, Na^+ and Cl^- ions is tightly controlled [144] due to ion pumps, ion channels, symporters and antiporters (Figure 2.5.) [145, 146]. K^+ concentration in cytosol is high (≈150mM compared to ≈5mM in the extracellular liquid) whereas Na^+ concentration is low (≈15mM compared with ≈150mM in the plasma) [147]. This difference is maintained by the Na^+/K^+-ATPase which actively transports 3 Na^+ ions out of the cell and 2 K^+ into the cell. Plasma membrane Ca^{2+}-ATPase plays the same role and drives calcium out of the cells to keep low intracellular concentrations (≈30-60nM compared to ≈1.8mM in the plasma) [148]. This is especially important as calcium is a universal and ubiquitous signalling molecule and its intracellular concentration is carefully monitored.

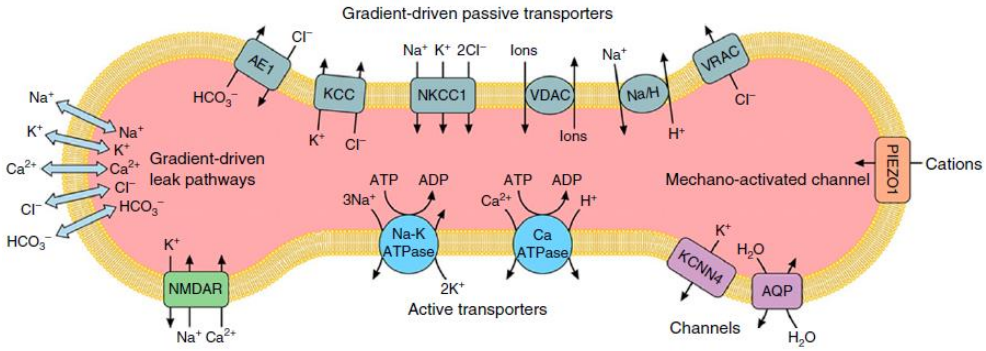

Figure 2.5. Model of ion transport pathways in the human erythrocyte. Gradient-driven transport pathways: AE1, anion exchange protein 1 (or Band3); NKCC1 $Na^+K^+Cl^-$-cotransporter 1; KCC, K^+-Cl^- cotransporter; VDAC, voltage-dependent anion channels; NHE1, Na^+-H^+ exchanger 1; VRAC, voltage-regulated anion channels. Gradient-driven leak pathways not otherwise identified and indicated by the arrows. PIEZO1 is a mechano-activated cation channel. Other erythrocyte membrane channels are the water channels aquaporins (AQP1 and AQP3) and KCNN4 (or Gardos channel), a calcium-activated K^+ channel. Active transporters: calcium-ATPase and Na^+K^+-ATPase. NMDAR, N-methyl D-aspartate receptor, participating in calcium entry. Other transport pathways (CO_2, urea, glucose) are not shown [149].

2.4.2. RBC membrane lipid organization

The RBC plasma membrane is a model of choice to study lipid lateral and transversal organization as artefacts can be ruled out. Indeed, RBCs exhibit a smooth membrane, do not have vesicular trafficking and have minimal lipid metabolism. Moreover, it is the best-characterized membrane for both lipid and protein composition. Finally, it is easily available,

abundant and rapidly isolated by centrifugation. Membrane lateral asymmetry will only be considered here as transversal asymmetry has already been explained in section 1.3.

2.4.2.1. Detergent resistant membrane-based studies

DRMs were actually first described for the RBC membrane after treatment of ghosts with cold Triton X100 followed by sucrose density gradient fractionation [85], even if DRMs had not been defined at that time. The detergent resistant fraction was enriched in SM and GSLs and associated with the spectrin skeleton. By electron microscopy, DRMs were proven to be derived from original ghosts and not simply aggregates of dispersed lipids and proteins. RBC DRMs were then shown to be enriched in stomatin and flotillins [150]. In both ghosts [151] and erythrocytes [152, 153], DRMs appear to be connected to the membrane cytoskeleton through electrostatic interactions [154]. However, most of the studies are fraught by contamination of blood granulocytes, resulting in proteolysis [39]. To overcome difficulties, leucodepletion of blood samples and utilization of carbonate supplemented medium was proposed [39].

By analysing the mesomorphic state of DRMs by electron paramagnetic resonance (EPR) spectroscopy with spin labelled lipid molecules, the lipid bilayer of DRMs isolated from human RBCs was found to display a higher ordered state compared with the RBC plasma membrane, which is compatible with the existence of L_o domains in the RBC membrane, as hypothesized for raft domains [152]. The cholesterol molar ratio is approximately ≈55mol% in DRMs *vs* ≈45mol% in the RBC plasma membrane. Moreover, DRMs obtained after cholesterol depletion are more in S_o phase, in accordance with $S_o/L_o/L_d$ phase knowledge (see section 1.2.1.) [155].

2.4.2.2. Microscopy-based studies

First evidence

Submicrometric domains at the RBC surface were first acknowledged using fluorescence microscopy after labelling with fluorescent NBD-phospholipid analogs. For instance, Rodgers and Glaser reported the existence of large lipid domains in the membrane of rabbit erythrocytes and ghosts [156]. However, the NBD-lipids used could have had their own partitioning properties as the bulky fluorochrome NBD is attached to the 2-position of the glycerol moiety [3].

Other laboratories then observed stable domains enriched in gangliosides GM1 [157, 158] or GM3 [67], SM [67] or ceramide [159]. The GM1 domains were observed by two different approaches. The first induced patches experimentally due to the use of the multivalent non-toxic pentameric B subunit of cholera toxin in fixed RBCs (Figure 2.6.a) [158]. Both multivalence of the probe and paraformaldehyde fixation can lead to artefactual lipid redistribution, and by consequence are serious limitation for lipid organization studies.

The second study circumvented the labelling and fixation methods by membrane insertion of a fluorescent lipid analog in live RBCs (Figure 2.6.b) [157]. The fluorochrome chosen was the 4,4-difluoro-5.7-dimethyl-4-bora-3a,4a-diaza-*s*-indacene (BODIPY) which, unlike NBD, has the advantage of high quantum yield and photostability, thus requiring insertion at lower concentration and imaging at lower laser power [160]. Uniform distribution of the probe was observed at room temperature and cooling at 4°C was needed to evidence domains, precluding physiological relevance of such domain [157].

Using the same family of analogs, Montes et al used BODIPY-SM to analyse hot-cold hemolysis by $PlcHR_2$, a phospholipase C/sphingomyelinase from *Pseudomonas aeruginosa*, known to hydrolyse SM to phosphocholine and ceramide. The formation of ceramide-enriched domains as a result of $PlcHR_2$ activity was observed (Figure 2.6.c), suggesting that the formation of those rigid domains leads to membrane fragility and hemolysis [159].

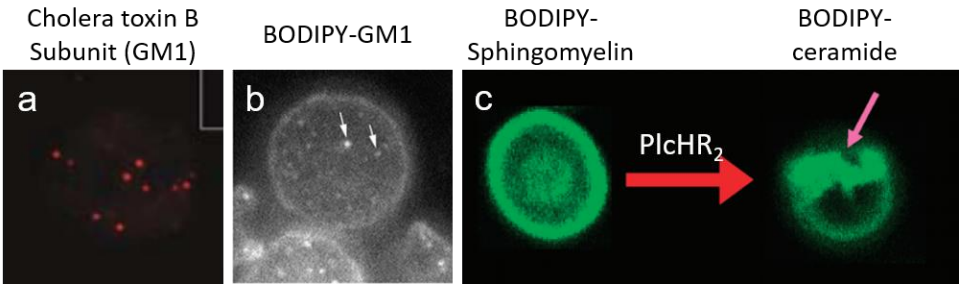

Figure 2.6. Fluorescence microscopy images of lipid domains in red blood cells. a. Human RBC treated with cholera toxin B subunit (CTB) plus anti-CTB and fixed with paraformaldehyde [158]. b. Living RBCs labelled with BODIPY-GM1 and cooled to 4°C to induce visible domains [157]. c. Human RBC stained with BODIPY-sphingomyelin before and after 10 min of treatment with $PlcHR_2$. The smaller pink arrow points to ceramide-enriched domains [159].

Development of new specific probes

As highlighted, the interpretation of results from these studies must be taken with caution as they used disruptive and/or non-physiological methods to analyse membrane lipid organization. However, stable lipid domains have been observed and characterized by our laboratory on living RBCs. They were first revealed on spread RBCs by vital fluorescence and/or confocal imaging using trace insertion at the external membrane leaflet of BODIPY-SM, PC and GM1 (Figure 2.7.) [102, 161, 162]. Since the substitution of the fatty acid chain by a fluorochrome remained a potential problem, the study was then extended to the visualization of endogenous membrane lipids by exogenous protein probes.

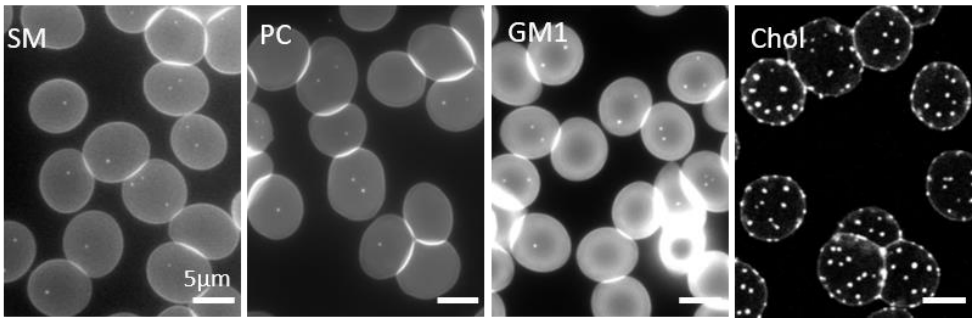

Figure 2.7. Gathering of SM, PC, GM1 and cholesterol in submicrometric domains at the RBC outer plasma membrane leaflet. Living RBCs spread onto poly-L-lysine pre-treated coverslips and labelled with either BODIPY-SM, -PC, -GM1 or mCherry-Theta-D4 to reveal endogenous cholesterol [163].

To label endogenous SM, natural toxins are available. Amongst these is Lysenin, produced by coelomic fluid of the worm *Eisenia Foetida*. However, after binding to membrane SM, Lysenin oligomerizes and forms pores in the membrane, leading to cell target lysis. Lysenin possess two distinct domains, an N-terminal domain responsible for the lytic activity and a C-terminal domain responsible for SM binding [164]. Kobayashi and colleagues validated a minimal truncated form of Lysenin, corresponding to the C-terminal domain, devoid of lytic activity but preserving the ability to specifically bind to SM. This form is called NT-Lysenin (for non-toxic Lysenin) [165, 166].

Cholesterol labeling is more challenging. Indeed, fluorescent sterols are available, but their membrane orientation and/or distribution behaviour have been found to deviate from native cholesterol [167]. Dehydroergosterol (DHE) is a natural fluorescent analog of cholesterol but is difficult to insert into membrane and is rapidly photobleached [168]. The fluorescent antibiotic filipin is sometimes used but it tends to aggregate membrane cholesterol, thereby perturbing its organization, and is toxic at high concentration [169]. Besides these probes, cholesterol-dependent cytolysins appear more promising. Those include streptolysin O of *Streptococcus pyogenes*, pneumolysin of *Streptococcus pneumoniae*, listeriolysin O of *Listeria monocytogenes* or perfringolysin O (or Theta toxin) of *Clostridium perfringens*. Their structure and pore formation mechanisms are very similar [170]. Theta toxin structure was the first to be resolved and displays 4 domains (D1-D4) rich in β-sheets [171]. The C-terminal domain of D4 possesses a motif rich in tryptophan responsible for membrane cholesterol recognition. As for Lysenin, the D4 domain as minimal segment able to recognize cholesterol without promoting cytolysis, was isolated by the group of Kobayashi [172, 173].

Upon coupling with the fluorescent protein Dronpa (suitable for super-resolution microscopy), NT-Lysenin and Theta revealed SM- and cholesterol-enriched domains on fixed Hela cells [174]. In our laboratory, we used NT-Lysenin and Theta-D4 coupled with the

fluorescent protein mCherry to label living RBCs spread on poly-L-lysine coated coverslips (Figure 2.7.) or maintained in suspension (in plastic chambers or in three-dimensional gels) and revealed submicrometric domains for both SM and cholesterol [175, 176] (see Annexes 1 and 2 for abstracts).

Combining BODIPY-lipids and toxin fragments, we were then able to map the RBC outer plasma membrane leaflet, showing the coexistence of at least three types of domains: i) those mostly enriched in cholesterol (≈8/hemi-RBC), present in RBC high curvature areas; ii) those co-enriched in GM1/PC/cholesterol, less abundant(≈1.5/hemi-RBC) and associated with RBC low curvature areas; and iii) those co-enriched in SM/PC/cholesterol, also found in RBC low curvature areas but quite less abundant (≈0.5/hemi-RBC) (Figure 2.8.) [163, 177] (see Annexes 4 and 6 for abstracts).

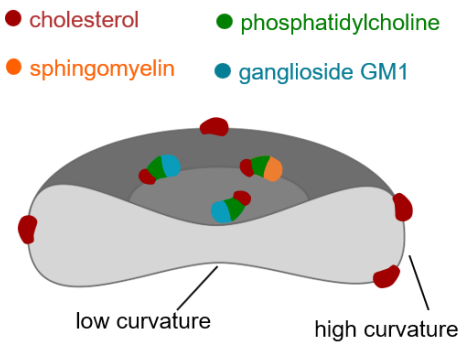

Figure 2.8. Our current model for the mapping of lipid domains at the outer plasma membrane leaflet of RBCs in the resting state.

Lipid domain biophysical properties

To analyse the lipid domain biophysical properties, the fluorescent probe Laurdan is useful (see section 1.2.1.). By RBC co-labelling with Laurdan and fluorescent lipid probes specific for SM, PC or cholesterol, we revealed that cholesterol-enriched domains in high curvature RBC areas exhibit a higher lipid order than the SM- and PC-enriched domains associated with the RBC low curvature areas. More surprisingly, all domains display a lower lipid order than the surrounding membrane. Although this observation is in opposition with the general idea that lipid domains are more ordered than the bulk membrane, it could result from the high cholesterol content and the strong membrane:cytoskeleton anchorage found in RBCs [163, 178] (Annexes 5 and 6 for abstracts). Atomic force microscopy (AFM) is also useful to study the biophysical properties of the RBC membrane. In collaboration with D. Alsteens (UCLouvain, LLN), we showed that the RBC membrane presents numerous submicrometric (≈200nm) and nanometric (<100nm) protrusions with heights ranging between 5 to 100nm. These protrusions are softer than the rest of the membrane [179], in agreement with the Laurdan studies.

2.4.3. RBC cytoskeleton organization

The first simple model of RBC membrane skeleton, proposed in 1979 [180] based on SDS-page, suggested that spectrin tetramers are connected to the membrane by ankyrin- and 4.1R-based complexes (Figure 2.9.A). The basic structure (section 2.4.3.1.) and membrane anchorage proteins were already well-identified (section 2.4.3.2.).

2.4.3.1. Spectrin network

Spectrin, first described by Marchesi and Steers in 1968 [181], is the construction block of the RBC cytoskeleton. Spectrin tetramers form a protein meshwork laminating the inner leaflet of the membrane (Figure 2.9.B). The spectrin meshwork presents a regular pentagonal or hexagonal architecture in which every side consists of spectrin tetramers of 200nm long [47] as seen in electron micrographs of purified spectrin tetramers or spectrin filaments in fully stretched skeletons. However, filaments of native, unstretched skeletons are much more compact and simple calculations show that the average distance between actin filaments (i.e., the length of a spectrin tetramer) is only 60 to 70 nm *in vivo* [182-184].

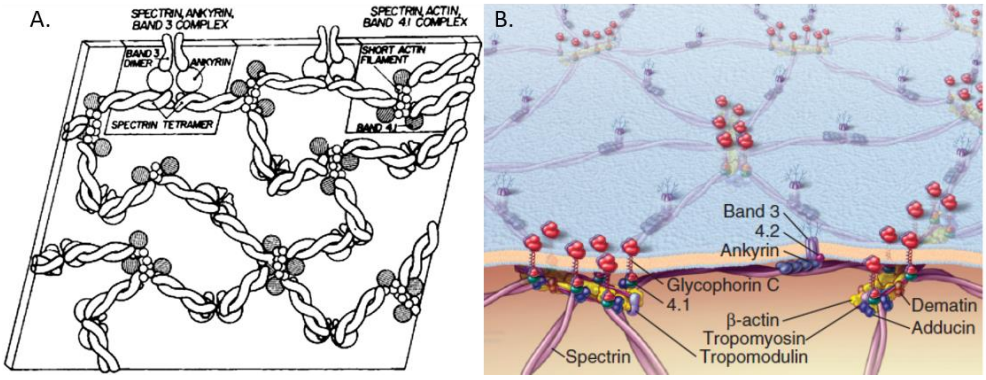

Figure 2.9. Evolution of the cytoskeleton model from the first proposal and now. The first model of the red cell membrane skeleton, published in 1979 [180]. B. Simplification of the actual model [2]. The spectrin meshwork laminates the inner leaflet forming a regular hexagonal architecture and is anchored to the membrane by two anchorage complexes, based on 4.1R and ankyrin.

A- and β-spectrins are encoded by *SPTA1* and *SPTB* genes, respectively. Both share a similar structural organization which consists of a succession of repeating units of approximately 106 amino acids. These units are now referred to as spectrin repeats and are made up of three α-helices [185]. A-spectrin contains 20 repeat units and one incomplete motif (Figure 2.10. yellow) while β-spectrin has 16 complete repeats and one partial segment (Figure 2.10. blue). Both incomplete segments interact with each other to restore the triple helical repeat structure while forming the spectrin tetramer [184, 185]. A- and β-spectrins associate in opposite directions leaving a specialized functional domain at the

"head" end for spectrin dimer-tetramer association. In spectrin αβ dimers, the longer α chain folds back on the end of β-spectrin (closed dimer) but nearly 95% of the spectrins are in the tetramer forms [186]. Tetramers dissociate and reform under physiological conditions, and this is greatly accentuated when the membrane is distorted by shear forces. This mechanism may be an evolutionary accommodation to permit the enormous distortions that the RBC undergoes in the microvasculature [182].

Spectrin tetramers are linked to i) the actin protofilament which forms a junctional complex with the ends of spectrin dimers, 4.1R and adducin proteins; and ii) the plasma membrane via two non-redundant anchorage complexes based on the peripheral proteins 4.1R and ankyrin [187]. At its N-terminus, β-spectrin contains two calponin homology (CH) domains which form an actin-binding domain (ABD) also able to link 4.1R. The CH1 domain is constitutively active but the CH2 domain is "unmasked" by PIP_2 which then promotes 4.1R binding (Figure 2.10. left and below inset) [185, 188]. Repeats 14 and 15 of β-spectrin bind ankyrin, which means that each tetramer potentially binds two ankyrins (Figure 2.10. center) [185].

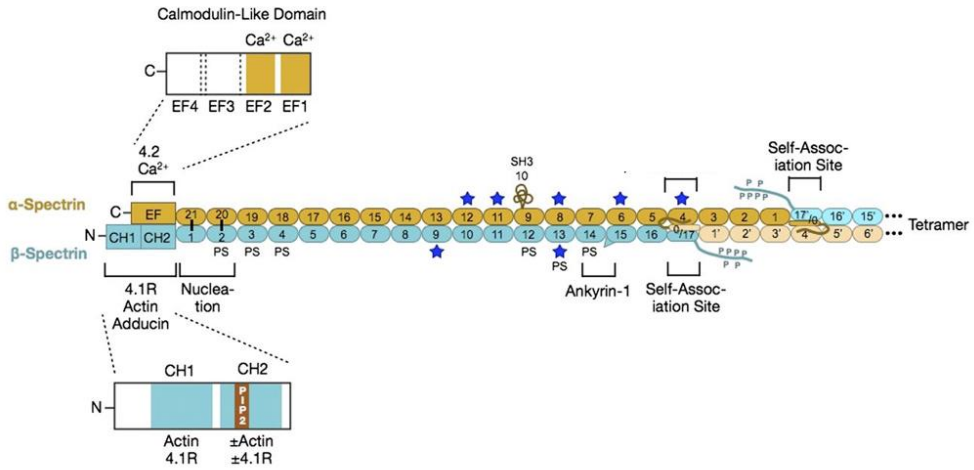

Figure 2.10. Structure of spectrin with sites of interaction for proteins and lipids. Spectrin repeats are represented by rounded rectangles. PS, phosphatidylserine; PIP_2, phosphatidylinositol 4,5-biphosphate; CH, calponin homology domain [182].

The C-terminal domain of α-spectrin consists of two EF-hand motifs (calcium-dependent and calcium-independent) related to calmodulin. The function of these calcium-binding motifs remains unknown [182]. It must be noted that the short unstructured C-terminal region of β-spectrin contains phosphorylation sites. Although the function of these

sites is not known, it could be linked to the mechanical properties of the RBC membrane [189].

2.4.3.2. Cytoskeletal anchorage

As the spectrin network is linked to the membrane through two non-redundant anchorage complexes, named ankyrin and 4.1R complexes according to their adaptors (Figure 2.11.). Links between the cytoskeleton and the membrane are based both on direct interaction with the lipid bilayer and transmembrane proteins or indirect interaction through adaptor proteins. Some cytoskeletal proteins possess more than one type of linkage, as shown above with spectrin interactions.

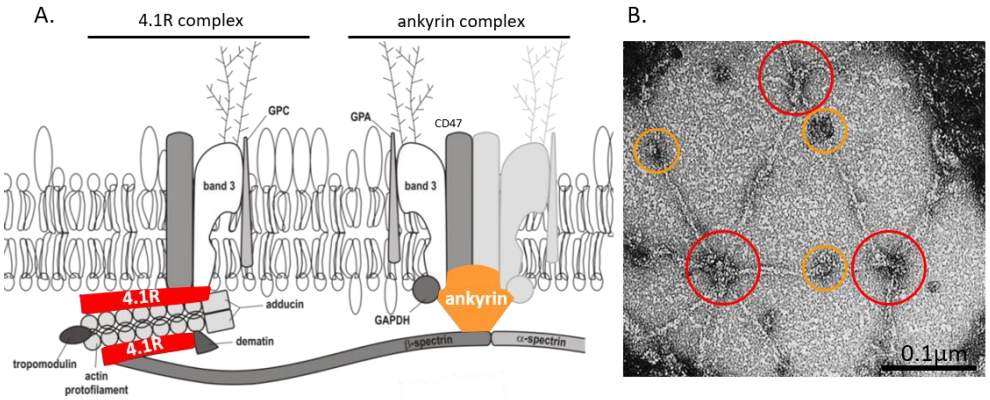

Figure 2.11. Anchorage of the membrane to the spectrin cytoskeleton by two complexes centered around protein 4.1R and ankyrin. A. Simplified representation of the complexes. GPC, glycophorin C; GPA, glycophorin A; GAPDH, glyceraldehyde-3-phosphate dehydrogenase [190]. B. Transmission electron microscopy of the spectrin network at the inner face of the membrane. Red circles, 4.1R complexes; yellow circles, ankyrin complexes [191].

Ankyrin-based complexes

Ankyrin-R (the erythroid ankyrin) is encoded by the *ANK1* gene. The protein contains three structural and functional domains. Firstly, the N-terminal domain has 24 "ankyrin" repeats, grouped functionally into 4 subdomains of 6 repeats (Figure 2.12. left) [185]. Ankyrin repeats are short helix-loop-helix structures which fold together to form an open, spiral structure that encircles and binds Band3 tetramers [182]. Secondly, the central domain contains the spectrin-binding domain with one ZU5A subdomain. ZU5A binds to the junction of the 14th and 15th spectrin repeats within β-spectrin (Figure 2.12. center). Third, the C-terminal (regulatory) domain is thought to modulate the binding functions of the other two domains (Figure 2.12. right).

Apart from the anion exchanger Band3, other proteins are present in the ankyrin complexes among which: i) glycophorin A, a type 1 transmembrane protein which has a chaperone-like activity for Band3 [185]; ii) CD47, a transmembrane protein "marker-of-self" with an extracellular IgG domain which prevents RBC clearance; and iii) protein 4.2, a peripheral membrane protein that binds to the cytoplasmic domains of Band3, Rhesus (Rh) complex and CD47 [185].

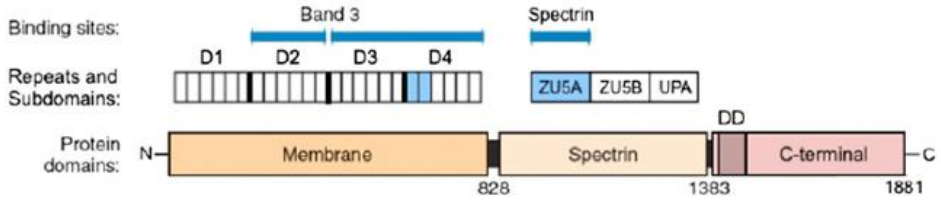

Figure 2.12. Schematic representation of the erythroid ankyrin structure. The membrane domain contains 24 ankyrin repeats with two binding sites for Band3. The spectrin domain contains three subdomains, of which ZU5A contains the binding site for spectrin. The C-terminal domain is the regulatory domain [182].

Linkage of Band3, protein 4.2, Rh complex and CD47 to ankyrin seems to be required for efficient sorting of membrane proteins during maturation of the RBCs [113]. During enucleation, if the ankyrin-attachment is absent, Band3 and the Rh complex are missorted and lost [113]. On the other hand, RBCs lacking Band3 also lack protein 4.2 and GPA [192] and RBCs lacking protein 4.2 lack CD47 [193].

4.1R-based complexes

4.1R is the most abundant form of protein 4.1 in RBCs and is encoded by *EPB41*. On SDS-PAGE, 4.1R appears at 80kDa as two closely spaced bands (known as a and b forms) due to progressive age-dependent deamidation of two asparagine residues [185]. 4.1R contains several domains (Figure 2.13.). Firstly, the FERM domain (4.1. ezrin radixin moesin) folds with three globular lobes arranged as a cloverleaf-like structure. The FERM domain has binding sites for transmembrane proteins (Band3), calmodulin, PS and PIP_2 and its activity is regulated through phosphorylation [194]. Secondly, the FERM adjacent (FA) domain is a substrate for phosphorylation by protein kinases A (PKA) and C (PKC). Thirdly, the spectrin-actin binding domain (SABD) is in the middle of the molecule. Fourthly, the C-terminal domain binds some membrane proteins. Interspersed between these domains are unconserved regions U1, U2 and U3 whose roles are not well understood. U1 has been reported to bind calcium/calmodulin.

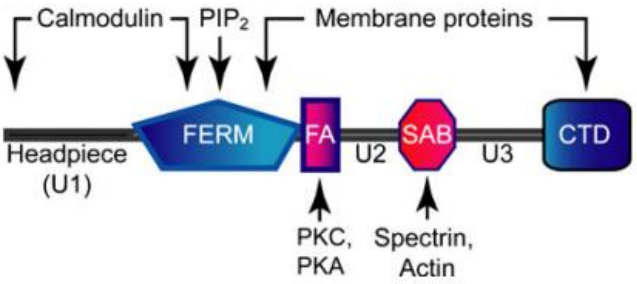

Figure 2.13. The general domain structure of protein 4.1R. FERM adjacent domain, FA; spectrin actin-binding domain, SAB; C-terminal domain, CTB [185].

Protein 4.1R binds to both spectrin and actin and generates a high-affinity ternary complex [182]. Like the ankyrin complex, the 4.1R complex is centered on the transmembrane protein Band3. Other proteins involved comprise: i) GPC; ii) glycophorin A; iii) glucose transporter 1; iv) stomatin ; v) dematin; vi) blood group proteins Kx/Kell and Duffy; and vii) F-actin and associated proteins [182].

Actin filaments are key constituents of the 4.1R complexes. RBCs contain short, double-helical filaments of nonmuscle β-actin, termed "protofilaments", with highly uniform lengths of ≈37nm [195, 196]. It is known that mice lacking proteins regulating F-actin polymerization develop hemolytic anaemias with misshaped red cells and clumped or irregular skeletons [182]. RBC actin filaments are stabilized along their lengths by two tropomyosin molecules (TM5b and TM5NM1) and capped at their ends by two tropomodulin-1 molecules and an αβ-adducin heterodimer (Figure 2.14.). RBC actin filaments provide additional sites for the spectrin-actin network to anchor to the bilayer, via their connections with 4.1R, Band3 and GPC [196].

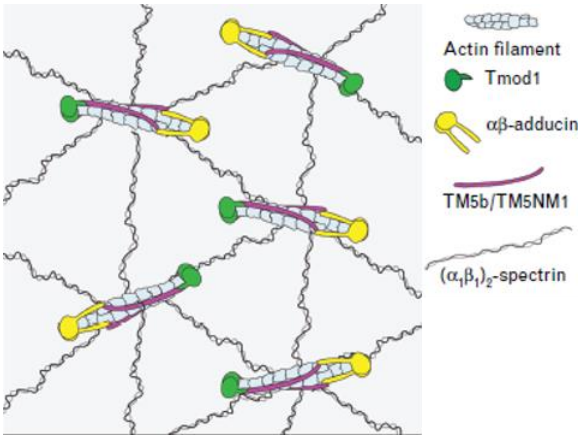

Figure 2.14. Simplified representation of the actin nodes. Spectrin tetramers ((αβ)2-spectrin) form a 2-dimensional network interconnecting short actin filament nodes, which are capped by tropomodulin 1 (Tmod1) and αβ-adducin and stabilized along their sides by TM5b and TM5NM1, two tropomyosins [196].

2.5. Red blood cell deformation

Along their journey, RBCs travel approximately 250km passing through capillaries, arteries and organs to optimally fulfil their primary function [197]. This requires a high membrane plasticity, which is tested ≈12000 times during the life of RBCs when crossing the spleen. Arterial blood arrives in splenic cords (or Billroth cords) of the red pulp of the spleen, which form an open blood system. From the cords, the RBCs pass into the venous sinuses demarcated by a discontinuous endothelium. Abnormal or old RBCs have difficulty in crossing this passage and stay blocked in the cords where they are phagocytosed (Figure 2.15.) [198].

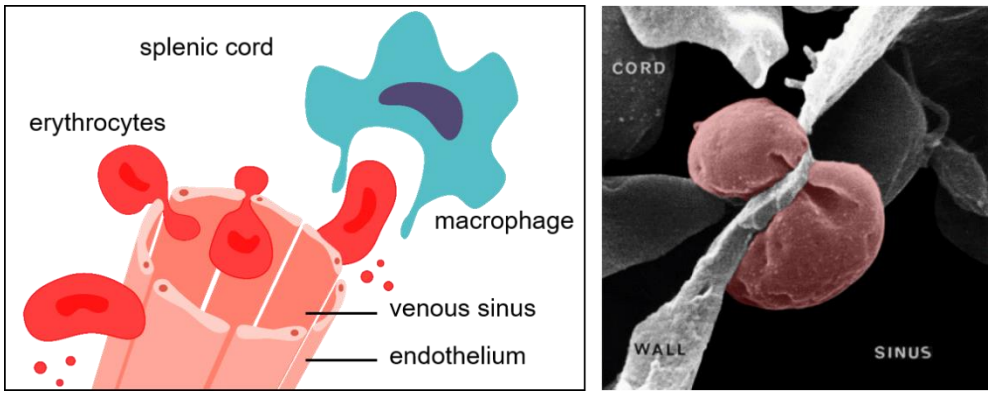

Figure 2.15. Venous sinuses in the red pulp of the spleen. Left, schematic representation of a venous sinus in the cords of the red pulp. Blood from the cords collects in the sinuses which consist of a lining of endothelial cells positioned in parallel. Ageing or abnormal RBCs that are no longer able to pass through the slits are phagocytosed. Right, scanning electron microscopy image of one RBC passing through an endothelial split of a sinus [187].

RBC deformability is made possible due to the finely controlled cytoplasmic viscosity, the unique cytoskeleton and the geometry. Firstly, the cytoplasmic viscosity is determined by the intracellular hemoglobin concentration, which is finely regulated between 30-35g/dL. By tightly regulating hemoglobin concentration, RBCs minimize cytoplasmic viscous dissipation during deformation. In RBCs with more than 37g/dL of hemoglobin, the recovery of the RBC initial shape after bending deformation is markedly decreased [187, 199]. Secondly, the RBC possesses a unique cytoskeleton of spectrin filaments attached to the membrane by two anchorage complexes (section 2.4.3.). This anchorage is particularly strong, conferring to RBCs a ≈20-fold higher adhesion energy than in typical fibroblasts [200]. Thirdly, the RBC exhibits a unique biconcave geometry characterized by a higher membrane surface:volume ratio as compared to a sphere of the same volume (membrane surface excess of ≈40%) (section 2.4.). Moreover, membrane composition and organization have been proposed to play a role in deformation (Section 2.4.2.).

The molecular basis responsible for RBC deformation (section 2.5.1) and the possible contribution of membrane organization adaptation in this process are detailed below (section 2.5.2).

2.5.1. Molecular mechanism of RBC deformation

2.5.1.1. Calcium entry

Upon mechanic stress, for instance when RBCs pass through small capillaries (<5µm of diameter) or inter-endothelial slits in the spleen (0.5-1µm in diameter), a reversible and transient calcium influx occurs [136, 201-204] (Figure 2.16.). Several possible pathways of calcium entry have been identified in RBCs, including non-selective voltage-activated cation channel [205], the P/Q voltage-dependent calcium channel $Ca_v2.1$ [206], the transient receptor potential cation channel subfamily C 6 (TRPC6) [207], voltage-dependent anion channel (VDAC) [208] or N-methyl D-aspartate receptors (NMDA-receptors) [209]. The more recent discovery of PIEZO1, a mechano-sensitive non-selective cation channel abundant in RBCs, initiated studies on the link between the channel, mechanical stress and volume changes through the Gardos channel. The first studies performed on animal models [210, 211] and in pathophysiological conditions [212] suggested that PIEZO1 is the major mechano-sensitive channel that allows calcium entry after RBC mechanical stimulation. This was confirmed in human RBCs [213] even if other mechano-sensitive transporters could not be excluded as possible secondary mechanism of calcium entry.

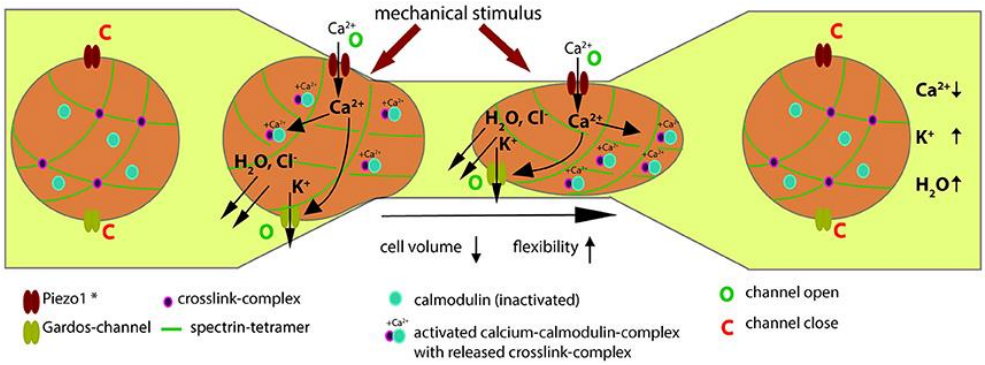

Figure 2.16. Hypothesis for the calcium-signalling mechanism when RBCs pass through thin capillaries [213].

PIEZO1 is a large homotrimeric pore-forming cation channel, allowing for influx of cations as sodium and calcium upon mechanical activation. Mechanically-induced macroscopic PIEZO1 currents are activated in the µsecond timescale and closed in the millisecond range in the continued presence of the stimulus [214]. The center “core” domain contains the C-terminal segments of each subunit and the peripheral domains form a “blade” structure [214, 215]. PIEZO1 mutations cause dehydrated stomatocytosis (or

xerocytosis), a hereditary disorder in which RBCs are characterized by increased permeability to cations and subsequent dehydration [149].

2.5.1.2. Intracellular calcium targets

The transient calcium increase induces RBC deformation by i) promoting cell transient dehydration through activation of the Gardos channels, ii) generating rapid reversible changes in the cytoskeletal flexibility and iii) promoting calcium efflux through PMCA.

The Gardos channel, also known as KCNN4, is a voltage-independent potassium channel activated by increased intracellular calcium. The activation of the channel leads to potassium loss, followed by chloride ion and water loss and transient cell dehydration [148].

There are numerous calcium-dependent proteins involved in cytoskeleton remodelling, including i) calmodulin; ii) proteins containing C2 domains (e.g. PKC, phospholipases, phosphoinositide 3-kinase); iii) flippases and scramblases; iv) μ-calpain; and iv) the C-terminal domain of α-spectrin. Calmodulin is a small protein comprising two globular EF hands which bind calcium. It is recruited to the plasma membrane upon calcium binding and regulates cytoskeletal stability. The interaction of 4.1R with calcium-calmodulin reduces the affinity of 4.1R with all interacting partners [148]. On the other hand, adducin tetramers are capping the formation of actin protofilaments. These filaments are disrupted after interaction of adducin with calcium-calmodulin [216]. Also, calcium-calmodulin induces the dissociation of Na^+/H^+ exchanger 1 (NHE1) from the ankyrin complexes and 4.1R protein, which leads to activation of the ion transporter and dysregulation of cell volume [148]. Calcium-calmodulin can also activate PMCA.

Calcium-dependent activation of PKC causes its translocation to the plasma membrane, where it phosphorylates several proteins such as i) PMCA; ii) 4.1R (in the domain flanked by the spectrin-actin binding domain and a domain for interaction with transmembrane proteins), weakening the interaction of 4.1R with β-spectrin by ≈30% [217]; and iii) α-adducin, leading to decreased affinity for F-actin among others [148].

In addition, the calcium-dependent flippase inhibition and scramblase activation promote the loss of asymmetry between the leaflets of the membrane [148] (see section 1.3.).

The calcium-dependent cysteine protease μ-calpain (calpain-1) in RBCs cleaves cytoskeletal and membrane proteins after calcium activation. Targets of activated μ-calpain are PMCA, Band3, 4.1R, 4.2 and calpain itself [218]. At normal calcium levels it should not be activated. However, a 40kDa activator protein increases its affinity for calcium.

2.5.1.3. Calcium extrusion

In RBCs, calcium efflux is mediated by PMCA, a plasma membrane P-type calcium ATPase ubiquitously expressed and considered as a housekeeping protein. It contains by ten transmembrane domains, two intracellular loops containing binding sites for ATP and phosphorylation. The C-terminal domain contains a binding domain for calcium-calmodulin, phosphorylation sites and a PDZ binding domain [148, 219]. In the absence of calcium, the C-terminal domain binds the principal domain of the pump to keep it closed and block ATP binding [219, 220]. An increase in intracellular free calcium is sensed by PMCA in response to interaction between the calcium-calmodulin complex and the C-terminal extremity [219]. Moreover, activated PKC can then phosphorylate a conserved serine residue to further activate the pump. The limiting factor to the transport capacity of PMCA is ATP availability [184, 219]. PMCA function is temperature-sensitive with ≈30-fold reduction in turnover rate for every 10°C drop [148, 221].

2.5.2. Membrane reorganization

In section 2.4.2 was summarized data supporting our current model on the coexistence of lipid domains at the RBC surface: i) domains mostly enriched in cholesterol, the most abundant (≈8/hemi-RBC) and associated with high-curvature membrane areas; ii) domains co-enriched in GM1/PC/cholesterol, les abundant (≈1.5/hemi-RBC) and found in low curvature areas; and iii) domains co-enriched in SM/PC/cholesterol, also found in the low curvature areas but less abundant (≈0.5/hemi-RBCs) [163, 177] (Annex 6).

To evaluate whether such lipid domains could contribute to RBC deformation upon mechanical stimulation, RBC deformation was stimulated while concomitantly observing the membrane lipid organization. This was achieved by analysing labelled RBCs immobilized in polymethylsiloxane (PDMS) chambers that can be stretched for one minute and then left to recover their initial shape. This approach was successful since a rapid and transient increase in intracellular calcium was observed after the stretching (Figure 2.17.B., grey symbols). Regarding lipid domains, several observations were made: i) cholesterol-enriched domains gather in high-curvature membrane areas (Figure 2.17.A), ii) GM1-enriched domains increase in abundance concomitantly to the transient increase in intracellular calcium (Figure 2.17.B., blue symbols), and iii) SM-enriched domains also increase in abundance but later, i.e. when intracellular calcium decreases (Figure 2.17.B., orange symbols).

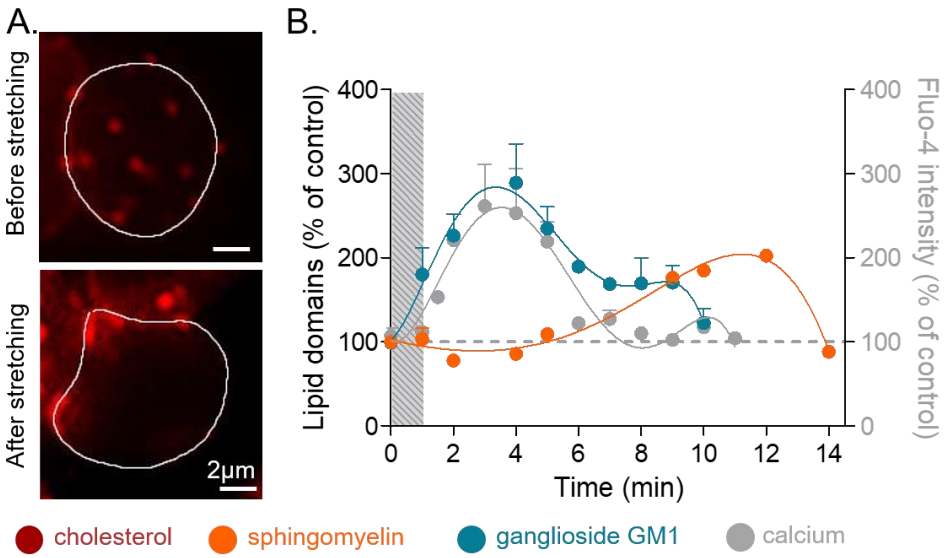

Figure 2.17. RBC mechanical stretching is accompanied by a transient calcium increase and leads to differential effects on lipid domain distribution and abundance. A. Cholesterol-enriched domain gathering in high curvature areas after stretching [177]. B. SM- and GM1-enriched domain and calcium content modifications upon RBC destretching at the indicated times [163].

We then explored the potential relationship between lipid domain reorganization upon RBC stretching and PIEZO1 and/or PMCA activation. The modulation of the abundance of GM1-enriched domains shown in PDMS chambers was confirmed upon specific PIEZO1 activation (with Yoda1) or inactivation (with GsMTx4), [163]. Moreover, SM-enriched domains increased in abundance upon forced RBCs calcium depletion (through the use of the extracellular calcium chelator EGTA) [163, 177]. Based on all these data, we suggested that the three types of lipid domains present at the RBC surface contribute to deformation by differential mechanisms, summarized in Figure 2.18.

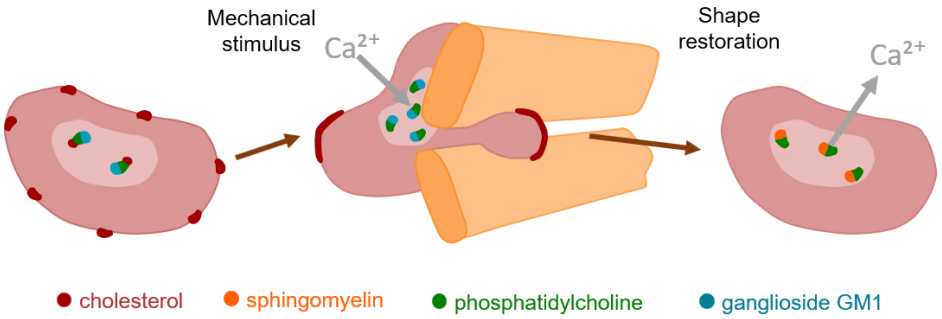

Figure 2.18. Evidence-based hypothetical model of the contribution of lipid domains to RBC deformation. Under mechanical stress, GM1/PC-enriched domains (blue/green) increase in abundance, potentially contributing to calcium influx while cholesterol-enriched domains (red) gather in the high-curvature membrane areas. At the same time, cell volume decreases via activation of the Gardos channels and RBC flexibility increases via uncoupling between membrane and the cytoskeleton at the 4.1R complexes [213]. The cell volume is restored after the end of the stress application by calcium efflux, which could require the contribution of SM/PC-enriched domains (orange/green) [163].

3. Red blood cell senescence

RBC aging is a multifactorial event accompanied by multiple processes occurring at various rates driving the circulating RBCs from adolescence to senescence within approximately 120 days [222]. The resulting "markers of senescence" are then recognized by macrophages and clearance of RBCs is promptly initiated [222, 223]. Premature clearance is a hallmark of various disorders associated with anemia, in which one or multiple markers of senescence appear prematurely [222]. Those markers include excessive oxidative stress, and cation leak followed by dehydration, decrease in RBC size and loss of RBC membrane through vesiculation and metabolic abnormalities [222]. Those multiple changes lead to increased cellular density.[182].

In the following chapters are addressed several key parameters involved in RBC senescence, among which oxidative stress (section 3.1.) and other modifications (section 3.2.). Some mechanisms of clearance are then discussed (section 3.3.). RBC vesiculation is introduced later in section 5.

3.1. Oxidative stress

Changes in the balance between production of pro-oxidants and their removal by antioxidative enzymes and scavengers is intimately related with cell aging [224]. Gradual accumulation of irreversibly oxidized and denatured proteins and lipids then leads to modification of enzyme activity, loss and reorganization of several proteins and alterations in plasma membrane lipid composition [225]. As *de novo* synthesis of both proteins and lipids is absent in mature RBCs, the antioxidative defenses in RBCs must be optimal to ensure the RBC ability to continue its function the longest time possible.

3.1.1. Reactive oxygen species sources

Reactive oxygen species (ROS) are oxygen-centered molecules that include non-radical species such as hydrogen peroxide (H_2O_2) and radical species possessing an unpaired electron, such as superoxide anion ($\bullet O_2^-$), hydroxyl radical ($\bullet OH^-$) and nitric oxide (NO). $\bullet O_2^-$ undergoes transformations depending on the availability of NO, superoxide dismutase (SOD) and H_2O_2 [224]. $\bullet O_2^-$ is transformed by superoxide dismutase 1 (SOD1; see below) to H_2O_2 while interaction of $\bullet O_2^-$ with NO leads to formation of peroxynitrite ($ONOO^-$). H_2O_2 is not especially toxic to the cell but it can pass through membranes and this feature is potentially important because the extracellular environment possesses few antioxidant defense mechanisms. Moreover, H_2O_2 can then oxidize ferrous ion (Fe(II)) to ferric ion (Fe(III)), OH^- and $\bullet OH^-$ (Fenton reaction). The latter is highly reactive with a half-life of a few nanoseconds [226]. Another way to produce $\bullet OH^-$ is via the reaction of H_2O_2 and O_2^- (Haber-Weiss reaction). This process is generally more complex and includes intermediate formation of transient metal/peroxide complex [227].

RBCs age-related oxidation is largely a membrane-localized event, because free radical generators are mostly localized within the membrane or attached to membrane proteins from the cytosolic side [224]. In RBCs, three main sources of ROS are described: i) autoxidation of hemoglobin; ii) NADPH oxidase activity; and iii) NO synthase. ROS are continuously produced in small amounts in healthy RBCs, mostly by **autoxidation of oxyhemoglobin** (HbO_2) to methemoglobin. The RBC intracellular hemoglobin concentration is high enough for a small rate of autoxidation to produce substantial levels of ROS [226]. Autoxidation of HbO_2 results from the oxidation of the ferrous ion (Fe(II)) to ferric iron (Fe(III)) by O_2 and includes the release of a superoxide anion ($\bullet O_2^-$). Iron ions are becoming accessible in the pre-membrane space during the process of oxidation and denaturation of membrane-bound haemoglobin occurring with aging of RBCs [224]. **NADPH oxidase** is a membrane enzyme complex catalysing the oxidation reaction of NADPH by O_2 to produce $NADP^+$, H^+ and $\bullet O_2^-$. In RBCs from patients suffering from sickle cell disease, ROS content is elevated due to overactivation of NADPH oxidase through PKC and Rac GTPase signalling [228]. **NO synthases** are present in endothelium and the NO produced diffuses in the endothelium into the vascular smooth muscle but also into the blood. NO participates to haemoglobin oxidation as it reacts with oxyhemoglobin to form methemoglobin and nitrate or binds with strong affinity to deoxyhemoglobin to form nitrosylhemoglobin [229].

3.1.2. Red blood cell antioxidant defenses

RBCs possess an efficient enzymatic machinery to process and detoxify reactive oxygen and nitrogen species, including specialized enzymes (SOD1, catalase, glutathione peroxidase, peroxiredoxin 2 and glutaredoxin 1) working in association with ROS scavengers (Glutathione, vitamin C, vitamin E). The activities of some of those antioxidant enzymes decline during aging (SOD1 and catalase) [224] or in RBCs from patients suffering from chronic hemolytic anemias (e.g. glutathione peroxidase in sickle cell disease [230]).

SOD1 catalyses the dismutation of $\bullet O_2^-$ to H_2O_2. The Zn^{2+} present in the protein appears to stabilize it while the Cu^{2+} is required for enzyme activity [231]. SOD1 contributes to the protection of RBCs against ROS by scavenging free radicals and preventing methemoglobin formation [226]. In addition, **catalase** breaks down H_2O_2 produced externally to form H_2O and O_2 [232]. In view of their elevated catalase activity, RBCs have been proposed to function as mobile ROS scavengers, protecting other cell types from oxidative damage [233]. RBCs also possess high levels of **peroxiredoxin 2**, a thiol-dependent peroxidase reducing H_2O_2 and other hydroperoxides [234], thereby dimerizing by forming disulfide bonds [235]. The regeneration of peroxiredoxin 2 requires thioredoxin reductase, the concentration of which is low in erythrocytes [236]. The association of peroxiredoxin 2 with the membrane preserve it from lipid peroxidation [237].

The **glutathione** is a tripeptide (γ-glutamyl-cysteinyl-glycine) that reduces disulfide bonds formed within cytoplasmic proteins to cysteines by serving as an electron donor. In the process, glutathione (GSH) is converted to its oxidized form, glutathione disulfide (GSSG). Because the direct reaction between H_2O_2 and GSH is very slow, **glutathione peroxidase** reduces H_2O_2 by oxidizing GSH to GSSG [226]. Oxidized GSSG is reduced back to GSH by the glutathione reductase using one NADPH as reducing agent. The NADPH pool is maintained by the pentose phosphate pathway (see section 2.2.). The glutathione S-transferase constitutes a second line of defense against ROS. This enzyme is involved in detoxification of xenobiotics through GSH conjugation. It can also reduce lipid peroxyl radical and detoxify lipid peroxidation end products [238]. In unstressed human RBCs, the concentration of GSH is usually more than tenfold the concentration of GSSG [236]. The GSSG to GSH ratio determines the intracellular redox potential and an increase in the ratio is indicative of oxidative stress. To prevent a major shift in the redox equilibrium when an oxidative stress arises to overcome the ability of the cell to reduce GSSG to GSH, GSSG can be actively exported out of the cell by the ATP/GTP-dependent transporter (RLIP76) and multidrug resistance protein 1 (MRP1) [239, 240].

N-acetylcysteine, the acetylated variant of the amino acid L-cysteine and precursor of GSH, is converted in the body into metabolites able to stimulate GSH synthesis, promoting detoxification. N-acetylcysteine supplementation has been proven useful to improve the quality of RBCs stored for transfusion [241] and to mitigate oxidative stress associated with neurodegenerative disorders in rat models [242] and in individuals with low levels of glutathione [243].

Apart from its role as cofactor in enzyme reactions, **vitamin C** (or ascorbic acid, AA) is another major scavenger of ROS. As for GSH, vitamin C acts as a reducing agent and is then oxidized to dehydroascorbic acid. AA is then resynthesized at the expense of GSH in a reaction catalysed by a variety of enzymes, such as **glutaredoxin** [244]. As mature RBCs do not have specific AA transporters, it is obtained by transporting dehydroascorbic acid by GLUT1 transporters and then reduced inside the cell [245]. AA is effectively used as additive in transfusion units to preserve RBCs from hemolysis and in patients with iron deficiency anaemia [246-248]. However, *in vivo* AA supplementation increased hemolysis in patients with sickle cell anemia [249].

Vitamin E (or α-tocopherol), a potent peroxyl radical scavenger in RBCs, is a chain-breaking antioxidant. Due to its lipophilicity, vitamin E accumulates in RBC membranes and plays a central role in preventing the propagation of free radicals within lipids [237, 250]. Peroxyl radicals react 1000 times faster with vitamin E than with polyunsaturated fatty acids. The vitamin E-radical created reacts with vitamin C, thereby oxidizing the latter and returning vitamin E to its reduced state [250]. Although the interaction of vitamins E and C

via this “recycling” pathway is well recognized [250], evidence in humans for the fat-soluble antioxidant function of vitamin E is limited.

3.1.3. Oxidative stress targets

The superoxide anion, H_2O_2 and hydroxyl radical can damage RBC membrane proteins and lipids. The coordinated action of all antioxidant systems makes RBCs very resistant to oxidation. Nevertheless, senescence, antioxidant defenses impairment and/or conditions increasing oxidants production lead to protein and lipid oxidation and subsequent RBC dysfunction [237].

3.1.3.1. Hemoglobin

Hemoglobin, the most abundant protein in RBCs, is the main generator of ROS, the main target of oxidative damage and also a scavenger of free radicals [224]. Detoxification of free radicals by haemoglobin is associated with the production of methemoglobin and oxidation of a cysteine residue in position 93 of the β-chain [224, 251]. Methemoglobin does not bind nor transport oxygen as the sixth coordination position of the heme iron is occupied by $\bullet OH^-$ or water [252] (Figure 3.1.).

To maintain functional hemoglobin, most of the methemoglobin is reduced back to Fe(II) hemoglobin by NADH-dependent cytochrome B5 reductase [226, 252]. The congenital deficit of NADH-dependent cytochrome B5 reductase leads to methemoglobinemia [253]. The slow denaturation of methemoglobin produces hemichrome. During this process, the H_2O at the sixth coordination site is replaced by an amino acid (typically histidine) from a distal part of the globin chain for instance [254], producing “reversible hemichromes” which can be reduced back to deoxyhemoglobin. “Irreversible hemichromes” are produced by significant distortions in the tertiary structure of hemoglobin [252]. Gradual accumulation of hemichromes in circulating erythrocytes is proposed to occur as they age and to associate with the cell membrane via the Band3 N-terminal domain (see below). Precipitates of hemichromes called Heinz bodies can be observed in RBCs from patient suffering of α-thalassemia or after administration of oxidant drugs. The release of the heme moiety can arise when the polypeptide chains is dissociated from the total hemichromes, which leads to initiation of oxidative damage to adjacent membrane components [252].

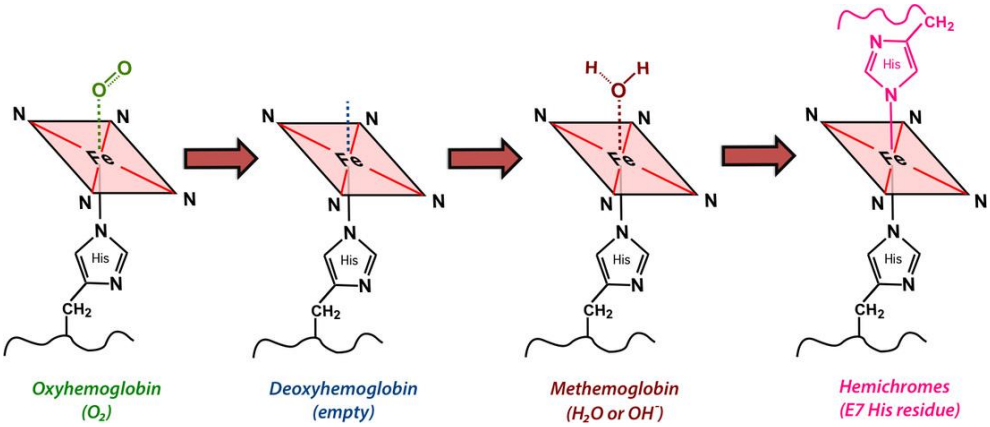

Figure 3.1. Chemical state of Fe in the center of the heme. Iron has 6 potential coordination sites, four of which are occupied by porphyrin nitrogens (N) whereas the fifth coordination site (below the plane of the ring) is occupied by N of the His in position F8 in the globin chain. The sixth coordination site (above the plane of the ring) is occupied by H_2O, $\bullet OH^-$ or His from the globin chains [254].

3.1.3.2. Polar lipids

Lipid peroxidation is the oxidative degradation of lipids. A free radical "steals" an electron from membrane lipid, usually made of polyunsaturated fatty acids as they contain multiple double bonds. The fatty acid radical formed is not stable and reacts readily with oxygen, creating a peroxyl-fatty acid radical which in turn reacts with another free fatty acid. It leads to the formation of one lipid peroxide and a new fatty acid radical able to propagate and continue the cycle. The chain reaction is stopped when the fatty acid radical reacts with another radical or a radical scavenger such as vitamin E present in the membrane [255]. The secondary or decomposition products of lipid peroxidation are reactive aldehydes such as malondialdehyde (MDA) or 4-hydroxy-2-nonenal. These end products can readily react with proteins, DNA and phospholipids which cause deleterious effects [256]. For instance, MDA can cross-link phospholipids and proteins, which causes impairment of membrane-related functions. MDA can also affect Band3 anion transport and the function of its associated enzymes, GAPDH and phosphofructokinase [226].

3.1.3.3. Cholesterol

Oxysterols are oxidized derivatives of cholesterol with one or more additional oxygen-containing functional groups (hydroxyl, carbonyl, carboxyl or epoxy). The most abundant oxysterols in the human body are 27-, 24(S)-, 7α- and 4β-hydroxycholesterol and are generated by cholesterol hydroxylases (part of the cytochrome P450) in the mitochondria or the endoplasmic reticulum. Oxysterols may also arise through a non-enzymatic pathway, due to the attack by free radical [257]. The most common oxysterols

produced during the non-enzymatic pathway, named cholesterol autoxidation, are 7β-hydroxycholesterol and 7-ketocholesterol (Figure 3.2) [255-257].

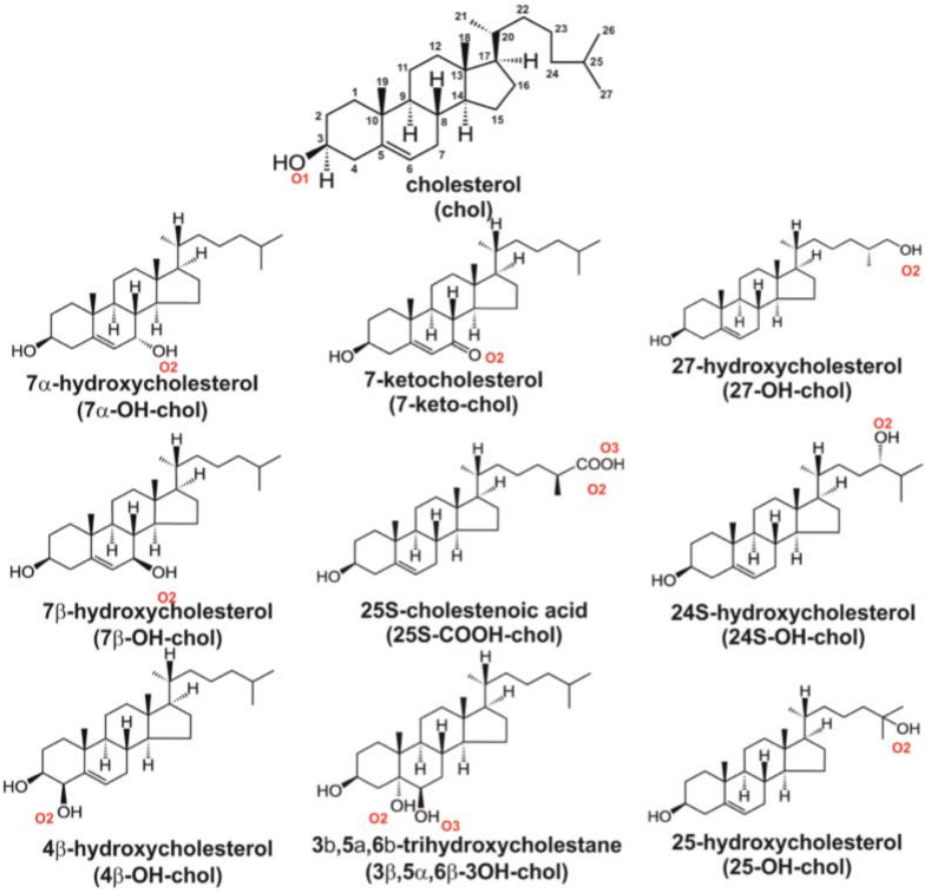

Figure 3.2. Chemical structures of cholesterol and some common oxysterols [258].

Oxysterols have a peculiar three-dimensional shape that is responsible for their poor membrane packing. Their effects on biophysical membrane properties depend on the position of the oxygen substitution [259]. Oxysterols can act as ligands for numerous receptor proteins, including liver X receptors, sterol-regulating element-binding proteins, oxysterol-binding proteins, oestrogen receptor, Niemann-Pick disease proteins and the Hedgehog system [259, 260]. Therefore, oxysterols are implicated in several pathophysiological mechanisms including atherosclerosis, lung and liver diseases, cancer and neurodegeneration [259, 261-263].

3.1.3.4. Membrane transporters

Calcium ATPase contains one or more reactive sulhydryl groups susceptible to oxidation, which leads to inactivation of the transporter and subsequent increase in intracellular calcium [264-266]. Band3 could also be a target of oxidation, especially when it has already formed complexes with oxidized and denatured hemoglobin, hemichromes [224]. Diamide, a thiol group oxidant, induces disulfide cross-linking of poorly glycosylated Band3. Oxidation seems to be a trigger for activation of Src tyrosine kinases and inhibition of tyrosine phosphatases, resulting in tyrosine hyperphosphorylation in the Band3 N-terminal domain and facilitating formation of high molecular mass Band3 aggregates [267]. Tyrosine phosphorylation reduces the affinity of Band3 for ankyrin, causing destabilization of the Band3:cytoskeleton interaction and increasing lateral mobility of the protein in the membrane [268].

3.2. Other modifications

Apart from the oxidation modifications, other mechanisms contribute to the densification seen in RBC aging. For instance, the activities of key glycolytic enzymes such as hexokinase, pyruvate kinase and glucose-6-phosphate dehydrogenase decrease progressively with red cell density, i.e. RBC age [224]. Glucose transport and metabolism also decrease [269]. Intracellular ATP levels drop in parallel [224], thereby impairing i) membrane transversal asymmetry, ii) antioxidant enzyme machinery, and iii) maintenance of the intracellular ion concentration.

Among accumulated ions upon aging is calcium. Besides distorted calcium homeostasis due to PMCA oxidation (see section 3.1.3.4), PMCA activity was shown to be reduced in dense RBCs fraction [270, 271]. Work on TRPC6 -/- RBC progenitors and in mice RBCs suggested that this channel could promote calcium entry in calcium-induced suicidal death [207]. Gradual increase in intracellular calcium leads to activation of the Gardos channel, which causes leakage of K^+ and subsequent cell dehydration [225]. At higher concentration, calcium also activates μ-calpain, transglutaminase-2 and some caspases that can degrade/cross-link cytoskeletal proteins. Calcium also inhibits phosphotyrosine phosphatases increasing Band3 phosphorylation [225]. Increased intracellular calcium was proposed to trigger apoptosis-like events in mature erythrocytes [272]. Two underlying signalling pathways have been reported: i) formation of prostaglandin E2 leading to activation of calcium-permeable cation channels, and ii) phospholipase A2-mediated release of platelet-activating factor activating a sphingomyelinase, leading to the formation of ceramide [272].

3.3. Red blood cell clearance

Despite the cumulative events of senescence (described above), the RBC removal signals do not seem to gradually accumulate in RBC. On the opposite, they appear as rapid and non-linear cascades of events at the terminal stage of the aging process, probably shortly before RBCs are removed by macrophages [223]. Since RBCs lack the ability to synthesize new proteins, signals that mark senescent RBCs for clearance must arise from proteins already present in the membrane or by the acquisition of plasma-derived opsonins directed against these markers [223, 273] as exposed below.

3.3.1. Band3-based mechanisms

Aged RBCs are cleared from circulation by macrophages from the reticuloendothelial system, which recognize senescent cells in an IgG-dependent manner. The reticuloendothelial system involves the mononuclear phagocytic cells in the spleen but also in the liver and lymph nodes. Moreover, the densest fraction of RBCs separated from whole blood has 10-fold more surface-bound IgG than younger cell fractions [274, 275]. These autoantibodies, called natural antibodies or naturally occurring (auto)antibodies, are specific for Band3 and are omnipresent in serum [275, 276]. IgGs on high-density RBCs co-localize with membrane aggregates composed of Band3, partially denatured hemoglobin (hemichromes) and the immune system protein component complement C3 [274, 277].

As explained above, the N-terminal region of Band3 competitively binds hemoglobin and a number of glycolytic enzymes [187]. Band3 exists in healthy RBC membranes as dimers and tetramers [278] and in senescent cells as aggregates associated with high concentrations of autoantibodies [274]. Hemichromes bind to the Band3 cytoplasmic domain with higher affinity than native hemoglobin [279] inducing Band3 clustering. This clustering is also promoted by lipid peroxidation [280], Band3 hyperphosphorylation and autoxidation [267]. Band3 clustering induces increased autoantibody binding and phagocytosis *in vitro* [281-283]. Current models propose protein clustering as the event preceding IgG deposition, through two molecular mechanisms in which a new antigenic site is revealed in Band3. In the first model, Band3 dimers are unable to bind senescence autoantibodies [283] and the senescence antigen is formed by association of Band3 dimers into clusters [283]. Therefore, clustering of Band3 is required for opsonization. In the second model, hemichrome induces Band3 cluster formation, which initiates autoantibody binding by exposing cryptic antigens due to conformational rearrangement of Band3 molecules after clustering [284]. How the clustering of Band3 results in exposure of this cryptic sequence is unknown [273]. Clustered Band3 and associated IgGs create a site of dense opsonization but might not be able to induce opsonisation without concomitant C3b complement deposition [285-288].

3.3.2. Phosphatidylserine exposure

In healthy RBCs, phosphatidylserine (PS) is normally restricted to the inner leaflet of the RBC membrane. The increase of PS exposure at the outer leaflet is proposed to be an "eat me" signal for phagocyte recognition, resulting in a non-inflammatory clearance of the dying cell [223]. If exposure of PS at the RBC surface is a widely accepted signal to trigger removal of senescent erythrocytes [289, 290], supporting data are lacking. Indeed, human RBCs *in vivo* have increased amounts of membrane-bound IgGs but are not enriched at all in PS-positive cells [291]. Furthermore, density separated fractions of erythrocytes labelled with the outer PS-specific probe Annexin V do not reveal increased labelling in old erythrocytes [289]. Arguments in favour of this theory are mainly based on pathological situations, including sickle cell anemia, thalassemia and spherocytosis [290]. In addition, the lower activity of aminophospholipid flippases/floppases in old RBCs [291], probably partially due to a lack of ATP, suggests a greater tendency of old RBCs to externalize PS. Moreover, calcium homeostasis perturbation (see above section 3.2.) could activate the scramblase, also contributing to PS externalization. Thus, PS exposure could represent a terminal event followed by very rapid removal [291], potentially explaining the lack of data.

3.3.3. CD47 as molecular switch for RBC phagocytosis

CD47 (integrin-associated protein) present at the surface of RBCs protects the cell from being phagocytosed. On one hand, when RBCs in the circulation encounter macrophages, CD47 actively prevents engulfment by binding to SIRPα on macrophages. It provides a "do not eat me" signal. On the other hand, loss of CD47 though vesiculation was proposed as mechanism to tag senescent RBCs for clearance. Indeed, microvesicles (MVs) isolated from blood stored for 21-31 days are enriched in CD47 while the resultant RBCs lack CD47 and are therefore removable by spleen red pulp macrophages. This hypothesis was based on data obtained from stored RBCs and may not be representative of *in vivo* aging [292].Recently, Burger et al suggested that CD47 may act like a molecular switch from suppression to promotion of phagocytosis [293]. This switch appears mediated by a CD47 conformational change that switches the molecule from an inhibitory to activating signal by adding thrombospondin-1 to the CD47-SIRPα interaction thereby prompting cell phagocytosis [293].

4. Red blood cell membrane fragility diseases

RBC hereditary diseases lead to chronic hemolytic anaemia and can be classified in two groups based on mutations in: i) globin genes (sickle cell disease and thalassemias), or ii) membrane or cytoskeletal proteins, with two sub-categories depending on whether the mutation affects RBC mechanical properties (spherocytosis, elliptocytosis) or the passive flux of cations through the membrane (stomatocytosis). Here the focus will be on spherocytosis and elliptocytosis.

4.1. Clinical management of hemolytic anemia

4.1.1. Diagnosis

Typical chronic hemolytic anaemias are physically associated with fatigue, pallor, jaundice and splenomegaly, the extent of each depending on the severity of the disease. Diagnosis is based on clinical and family history, physical examination and laboratory data [294]. The later comprise blood smear analysis, RBC morphology determination (mean corpuscular volume MCV), full blood cell count, reticulocyte count and determination of mean corpuscular hemoglobin concentration (MCHC) and bilirubin concentration. Patients with a family history of chronic anaemia or typical biological manifestations do not require additional tests. When diagnosis is not clear, the recommended supplementary tests are: i) the eosin-5'-maleimide (EMA) binding test, based on flow cytometry measurement of mean red cell fluorescence after RBC specific transmembrane protein labelling with EMA dye [295, 296]; and ii) the cryohemolysis test, easy but exhibiting low sensitivity and based on the increased susceptibility of fragile RBCs to rapid cooling from 37°C to 0°C under hypertonic conditions [296]. Finally, analysis of major RBC membrane proteins via SDS-PAGE represents invaluable support for the identification of different subsets of patients and when the clinical phenotype is more severe than predicted from the RBC morphology. However, diagnosis does not require further investigation by molecular analysis of the affected genes [294].

4.1.2. Treatment

The "routine" treatment and follow-up depend on the severity of the disease. In severe forms of anaemia (6-8g/dL hemoglobin), patients could need regular blood transfusions or EPO treatment. Moreover, folate supplementation is highly recommended [294]. A medical visit once a year is sufficient for stabilized children. Parents should be warned about the risk of parvovirus B19 infection (enhancement of pallor, asthenia, dyspnea, fever and classical skin eruption). Vaccination against hepatitis B is recommended in addition to the usually recommended vaccinations, since patients with severe anaemia may need regular transfusions [295].

Splenectomy is very effective in reducing hemolysis in hereditary spherocytosis. Indeed, less deformable RBCs are trapped in the spleen causing a mild splenomegaly. Splenectomy should be considered only after 6 years-of age and preceded with vaccination against encapsulated bacteria (such as *Neisseria meningitidis*, *streptococcus pneumonia* and *hemophilus influenza*) [295, 297].

4.1.3. Complications

Chronic hemolysis may lead to the formation of bilirubinate gallstones, which is the most frequent complication. Interval ultrasonography to detect gallstones is recommended to prevent complications in the biliary tract (biliary obstruction, cholecystitis and cholangitis) [297]. Hemolytic and aplastic crisis lead to jaundice, increased splenomegaly and decreased hematocrit, generally associated with viral infection, such as parvovirus B19 infection of erythropoietic progenitor cells [297].

4.2. Hereditary elliptocytosis

Hereditary elliptocytosis (HE) is a collection of disorders characterized by the presence of elliptical-shaped erythrocytes in a peripheral blood smear and associated with variable clinical manifestations. The worldwide incidence of HE is estimated at 1 per 2000-4000 individuals. However, prevalence could be much more as 90% of the cases are asymptomatic and are fortuitously discovered when undergoing screening for an unrelated condition. Nevertheless, where malaria is endemic, some subtypes of HE are significantly more prevalent (1:100) [298, 299]. An uncommon subtype of HE is hereditary pyropoikilocytosis in which patients present severe anaemia.

The clinical presentation of HE is heterogeneous, ranging from asymptomatic carrier to severe transfusion-dependent anaemia. Asymptomatic carriers can potentially become symptomatic during pregnancy and vitamin B12 deficiency. Symptomatology may vary among members of the same family sharing the same molecular defects and in the same individual over time [300].

Blood smear evaluation is essential both for diagnosis and classification. Peripheral blood smears classically present few to 100% elliptocytes, from elongated “bacillus-like” shapes to more oblong cells (Figure 4.1.A) [295]. Some silent carriers can show normal erythrocyte morphology [300]. HE with moderate to severe compensated hemolysis show elliptocytes, poikilocytes, spherocytes and cell fragments, which can produce a marked decrease in mean corpuscular volume (MCV). In HPP, elliptocytes, poikilocytes, RBC fragments, (micro)spherocytes, triangulocytes and other bizarre-shaped cells can be observed (Figure 4.1.B) [295, 299]. Some of the fragmented RBCs are counted as platelets by the hematology analyser and as such overestimate the platelet count. Another feature

of HPP RBCs is their increased sensitivity to thermal fragmentation at a lower temperatures (45° to 46°) than normal (49°) [295].

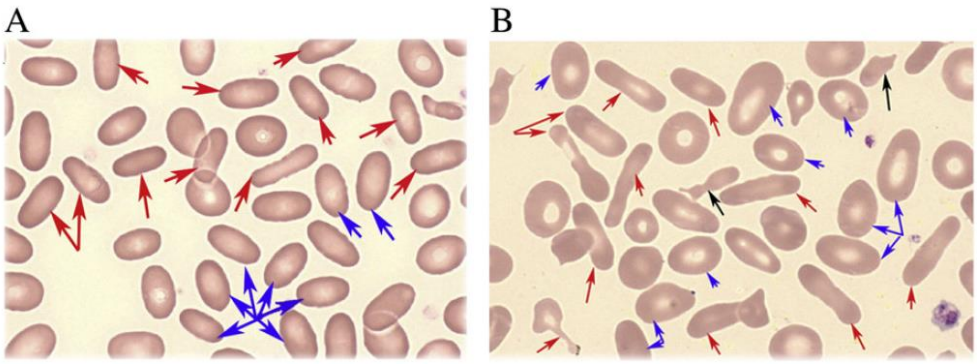

Figure 4.1. Smear of blood from patients suffering from hereditary elliptocytosis and pyropoikilocytosis. A. Elliptocytosis: classical elliptic (red arrows) and oblong cells (blue arrows). B. Pyropoikilocytosis: elliptic (red arrows), ovalocytic (blue arrows) and fragmented cells (black arrows) [295].

4.2.1. Genetic defects

HE is mainly inherited in an autosomal dominant fashion, with rare cases of *de novo* mutations, whereas HPP patients exhibit autosomal recessive inheritance. Homozygous or compound heterozygous individuals for HE variants experience mild-to-severe hemolysis with moderate-to-marked anaemia (HPP). The genes mutated in HE are *SPTA1* (α-spectrin), *SPTB* (β-spectrin) or *EPB41* (protein 4.1R) (Table 4.1.) [295, 298].

Disease symbol	Phenotype	Phenotype MIM number	Gene location	Protein name	Inheri-tance
HE1	Hereditary elliptocytosis type 1	611804	EPB41 1p35.3	Band 4.1R	AD
HE2	Hereditary elliptocytosis type 2	130600	SPTA1 1q23.1	Spectrin α	AD
HE3	Hereditary elliptocytosis type 3	-	SPTB 14q23.3	Spectrin β	AD
HPP	Hereditary pyropoikilocytosis	266140	SPTA1 1q23.1	Spectrin α	AR

Table 4.1. Classification of elliptocytosis according to the OMIM database. AD, autosomal dominant; AR, autosomal recessive. Adapted from [299].

4.2.1.1. Spectrin mutations

In **α-spectrin**, more than 25 mutations have been reported and most of them are in the first α0 incomplete repeat and α1-4 repeats (see Figure 2.10. in section 2.4.3.1.) [300]. Four mutations have been observed in codon 28 within this first incomplete repeat, suggesting that it is a hotspot for mutation [301-305]. A subset of mutations is located around the SH3 domains near repeats 8-9: spectrins Jendouba, Oran and St Claude [306-309]. Most mutations are missense mutations even if some insertions and deletions are also observed [308-313].

To note, low expression polymorphism of SPTA1 has also been described in association with HE/HPP. The most documented example is the spectrin α^{LELY} ("low expression allele, Lyon") with 42% heterozygosity and 9% homozygosity in European Caucasian populations [295], and ≈20% heterozygosity in all ethnic groups studied so far [314, 315]. A C>T substitution in an acceptor splice site 12 nucleotides before the splice junction caused exon 46 (18 nucleotides) to be skipped in 50% of the transcripts [316]. The α-chains missing the corresponding 6 amino acids are unable to dimerize [317, 318]. Spectrin α^{LELY} also carries a functionally neutral polymorphism (Leu1857Val) [319]. Spectrin α^{LELY} alone causes minimum damage in both heterozygous and homozygous states since the spectrin α chains are produced in excess (3- to 4- fold compared with β-chains). However, HE patients heterozygous for mutations in α-spectrin on one allele and α^{LELY} on the other could present a more severe phenotype than expected, i.e. HPP, or on the contrary improve the elliptocytic phenotype [295, 300].

Molecular epidemiologic studies indicated that α-spectrin defects are more prevalent in black ethnic populations than in Caucasian populations. Some mutations are widely distributed in Africa while others are characterized in Caucasians. For instance, the Leu260Pro mutation is frequent in southern Benin and Togo amongst two ethnic groups (Fon and Yoruba) and the Leu207Pro mutation is observed in ethnic groups from West Africa [320]. Certain HE mutations could give an advantage against the propagation of malaria [321] explaining the preservation of the mutations in these populations.

Concerning **β-spectrin**, fewer mutations are found and are restricted to the incomplete β17 repeat [301, 322-336]. Most of the β-spectrin abnormalities are frameshift mutations [330-333], nonsense mutations or abnormal splicing [322-325, 336] leading to premature chain termination.

4.2.1.2. 4.1R mutations

4.1R mutations are less common than spectrin mutations but quantitative and qualitative defects in protein 4.1 due to mutations have been reported. Four families exhibit

a total deficiency of the protein (Algeria, Annery, Lille and Madrid) [337-340] as the first codon is affected by the mutation leading to abolition of the initiation codon [337, 338] or destruction of the transcript by nonsense-mediated mRNA decay [339, 340]. The other mutations are all located in the exon coding for the FERM-domain [341-344].

4.2.2. Pathophysiology

The main defect in HE erythrocytes is a mechanical weakness or fragility of the erythrocyte membrane cytoskeleton due to defective connections of cytoskeletal proteins with the membrane at 4.1R junctional complexes [299]. Prolonged or repetitive cellular deformation in the circulation leads to abnormal rearrangement of skeletal proteins that prevent normal recovery of the biconcave shape [300]. This is consistent with the fact that HE erythrocyte precursors are round, progressively becoming more elliptical with aging after release into the circulation [345]. There is a great interest in HE-associated mutations, especially in spectrins, to study the organization of the spectrin meshwork in RBCs. The actual observations are summarized below.

4.2.2.1. Spectrin mutations

Mutations in the tetramerization site

The tetramerization site comprises α-spectrin partial repeat 0 (N-terminal; one helix; Figure 4.2. orange) and β-spectrin partial repeat 17 (C-terminal; two helices; Figure 4.2. blue) [346]. The N-terminal helix from α-spectrin in the first dimer associates with the two helices in β-spectrin repeat 17 to form an “atypical” complete spectrin repeat. Most of the mutations in α-spectrin and β-spectrin are found at this tetramer self-association contact site. Residues 17-20 (before partial repeat 0 of the α-spectrin N-terminal domain) and residues 46-52 (junction region between partial repeat 0 and the first repeat) undergo conformational changes upon binding to β-spectrin [347, 348]. The interface interaction is driven by the clustering of the hydrophobic side chains and is stabilized by electrostatic interactions [348]. The helix of the α-spectrin N-terminal domain consists of residues 21-45. Mutations found in this domain are all missense mutations and the mutant proteins do not show any misfolding or structural destabilization [349, 350]. Indeed, the effects of most mutations are not due to conformational perturbations of the protein but are instead due to the loss of specific interactions in which particular residues participate [347, 351]. For instance, R34 interacts by electrostatic interactions with E2022 and E2029 in helix A of partial repeat 17 of β-spectrin. R34 also forms a hydrogen bond with E2029 and the aliphatic portion of the amino acid can participate in hydrophobic interactions at the spectrin tetramerization site; the P34 mutation creates a cavity which abolishes electrostatic interactions and also disrupts the hydrogen bond and van der Waal’s forces [352]. L49 forms a hydrophobic cluster with V2041, V2044, L2047 and I2048 of the partial domain of β-spectrin to stabilize tetramers [348, 353] while R28 has been proposed to make an

electrostatic interaction with E2069 [348]. The conclusion is quite different for β-spectrin mutations. Substantial perturbation of the conformation of both partial repeat β17 and adjacent repeat β16 were reported for 3 mutations in the C-terminal repeat 17 of β-spectrin [354].

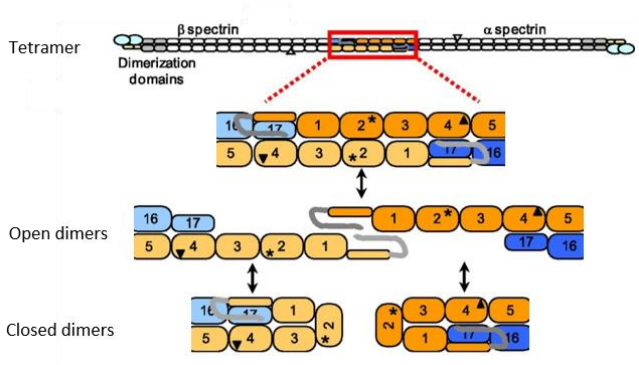

Figure 4.2. Schematic representation of erythrocyte spectrin equilibria. Full-length red cell spectrin illustrating the closed dimer ↔ open dimer ↔ tetramer equilibria. The ≈106 residues of the "spectrin repeat units" are represented by rounded rectangles. The approximate location of both Leu260Pro and Gln471Pro mutations in the proteins are shown by an asterisk and a triangle respectively [186].

Mutations next to the tetramerization site

Since the formation of spectrin tetramers appears to require progressive distortions of the spectrin molecule and since both spectrin subunits appear to contribute to its flexibility, factors that alter the flexibility of the C-terminal region of β-spectrin and the N-terminal region of α-spectrin could potentially have important effects on spectrin association [355]. Interestingly, most pathological mutations involve the putative linker regions between the spectrin repeat units by disrupting stabilizing interactions that exist between repeats [356, 357]. This highlights the importance of the interplay between repeats to stabilize the adjacent repeats and, by so doing, the whole multidomain protein. For instance, it was already shown that the Leu260Pro mutation could modify the equilibrium between spectrin "open" dimers and "closed" dimers, favouring the latter, which decreases tetramerization (Figure 4.2.) [186].

4.2.2.2. 4.1R mutations

Less is known about the alteration of cytoskeleton when a mutation of *EPB41* is present. Interestingly, loss of protein 4.1R is accompanied by loss of other proteins such as GPC, by abnormal sorting during enucleation [113]. Electron microscope studies of homozygous 4.1(-) Madrid red cell membranes, i.e. with complete deficiency of 4.1R protein, reveal a disrupted skeletal network with perturbation of the intramembrane molecules [358], suggesting that protein 4.1R plays an important role in maintenance not only of the skeletal network, but also of the integral proteins of the membrane structure.

Mutations observed in the FERM domain could disrupt the association of 4.1R with membrane proteins (such as Band3) and lipids (such as PS or PIP_2), and thereby lead to detachment of the 4.1R junctional complex from the membrane.

4.3. Hereditary spherocytosis

Hereditary spherocytosis (HS) is the most common inherited hemolytic anemia characterized by round-shaped, less deformable RBCs. The prevalence is 1:1000-5000 in the Caucasian population. The prevalence in people of other ethnic backgrounds is unknown but it is much less common, even if often described in Eastern Asia [359]. HS refers to a group of heterogeneous inherited anaemias showing a broad spectrum of clinical severity, from asymptomatic to severe transfusion-dependent forms, even within the same family [299].

The number of spherocytes present in peripheral blood smears depends on the severity of the disease: from very few in 25 to 35% of mild cases to abundant in the more severe forms [295]. Various shape abnormalities can be observed: i) "mushroom"-shaped red cells, a feature of Band3 defects (Figure 4.3.A. green arrow) [360]; ii) acanthocytes, more present in β-spectrin defective RBCs (Figure 4.3.B. red arrows); while iii) ovalocytes and stomatocytes associated with few spherocytes in 4.2 defects [361].

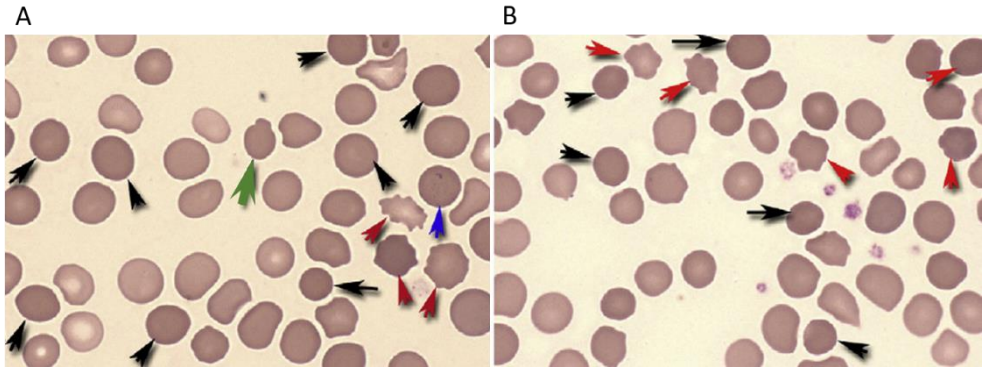

Figure 4.3. Smear of blood of patients suffering from hereditary spherocytosis. A. Band3 defect. B. β-spectrin defect. Mushroom cell, green arrow; dense and hyperchromic spherocytic red cells, black arrows; acanthocytes, red arrows; basophilic red cell due to hematopoietic stress, blue arrow [295].

4.3.1. Genetic defects

Typically, HS is inherited in an autosomal dominant fashion in 75% of cases, while the 25% remnant cases are inherited in autosomal recessive fashion or *de novo* mutations [295, 298, 299]. Autosomal dominant HS is often associated with primary mutations in the genes encoding ankyrin (*ANK1*), Band3 (*SLC4A1*) or β-spectrin (*STPB*) (Table 4.2.). Recessive mutations occur due to homozygous mutations in protein 4.2 (*EPB42*) gene or homozygous

or compound heterozygous for α-spectrin (*SPTA1*). Most of the mutations described are "private" or sporadic occurrences, i.e. they are specific to one family or a few families.

Disease symbol	Phenotype	Phenotype MIM number	Gene location	Protein name	Inheri-tance
HS1	Hereditary spherocytosis type 1	182900	ANK1 8p11.21	Ankyrin-1	AD
HS2	Hereditary spherocytosis type 2	616649	SPTB 14q23.3	Spectrin β	AD
HS3	Hereditary spherocytosis type 3	270970	SPTA1 1q23.1	Spectrin α	AR
HS4	Hereditary spherocytosis type 4	612653	SLC4A1 17q21.31	Band3	AD
HS5	Hereditary spherocytosis type 5	612690	EPB42 15q15.2	Band 4.2	AR

Table 4.2. Classification of spherocytosis according to the OMIM database. AD, autosomal dominant; AR, autosomal recessive. Adapted from [299].

In ***ANK1***, frameshift and nonsense mutations are the most common types of mutations in Caucasian patients, while promoter mutations are found mainly in Asian patients [362]. Mutation results either in unstable ankyrin transcripts, which are destroyed by nonsense-mediated mRNA decay or truncated peptides [298]. To note, frameshift mutations are mostly present in exons 1 to 26, especially in the Band3 binding domain of ankyrin 1 while nonsense mutations are mostly present at the 3'terminal side in the spectrin-binding domain and the regulatory domain [359]. Missense mutations were also described and may disrupt normal ankyrin-protein interactions [363, 364].

Monoallelic expression of β-spectrin occurs frequently in HS due to ***SPTB*** mutations in dominant inheritance forms [323, 365-368]. These mutations are private and unique to family, with the exception of β-spectrin Houston [369] which has been found in several unrelated patients. Amongst the mutations, truncated β-spectrin chains due to nonsense [329, 370, 371], missense [367, 372, 373] and frameshift mutations [329, 365, 370, 371, 374] have been identified. Some patients have missense mutations, such as spectrin Atlanta (W182G) [369] and spectrin Kissimmee (W202R) [373], which are located in the highly conserved region of β-spectrin involved in the interaction with protein 4.1 and actin. These mutations can then alter the binding of spectrin to actin and 4.1R anchorage complexes [306].

The silent polymorphic allele α^{LEPRA} ("low expression Prague") accounts for nearly 3-5% of ***SPTA1*** alleles among white people [375]. Allele α^{LEPRA} carries the C>T transition at position -99 of intron 30 causing missplicing and frameshift in about 80% in pre-mRNAs [295]. Amongst non-dominant HS, α^{LEPRA} is prevalent [376]. An individual homozygous α^{LEPRA}

allele or compound heterozygous allele (co-inheritance of α^{LEPRA} with another pathogenic HS allele) results in severe HS [377].

Many ***SLC4A1*** (Band3) mutations have been described in HS and account for 30% of HS Caucasian patients [364, 378]. Missense, frameshift and nonsense mutations are most commonly found but splicing abnormalities and nucleotide duplications have been described [316]. In the coding regions, mutations are clustered in exons 4 and 5, 9 and 10, and 17-19, which appear to be "hot spots". Missense mutations tend to be localized in the region corresponding to the C-terminal cytoplasmic domain while frameshift and nonsense mutations are densely localized in the region corresponding to the cytoplasmic domain at the N-terminus. Mutations in the cytoplasmic domains of Band3 can interfere with its binding to other proteins, resulting in a functional defect. Conserved arginine residues are frequent sites of mutation: R490C, R518C, R760Q, R808C, R808H, R870W [298, 378]. These extremely conserved sites are positioned at the integral boundaries of transmembrane segments, and substitution possibly interferes with co-translational insertion of Band3 in the membranes of the endoplasmic reticulum during synthesis of the protein [379]. HS due to Band3 mutations is generally milder than HS caused by ankyrin or spectrin mutations [295, 298].

EPB42 mutations have been mostly found in Japanese populations [380-384] and are mostly missense mutations. Most patients are homozygotes or compound heterozygotes of missense mutations. Only heterozygote missense mutations are asymptomatic with nearly normal protein 4.2 content in the RBC [385].

4.3.2. Pathophysiology

Two factors are involved in the pathophysiology of HS: intrinsic qualitative and quantitative RBC membrane defects contrasting with an intact spleen that selectively retains, damages and removes defective RBCs [361]. Although the main molecular defects are heterogeneous, the weakening of vertical linkages between the membrane skeleton and the lipid bilayer is postulated to be a common feature in all cases, which leads to destabilisation of the lipid bilayer and the release of skeleton-free lipid vesicles [386]. Two mechanisms have been proposed. The first is based on defects in spectrin, ankyrin or protein 4.2, which, by reducing skeletal density, release Band3-containing MVs. Spectrin deficiencies lead to a decreased density of the skeletal network underlying the lipid bilayer [316], suggesting that unsupported areas of the lipid bilayer are susceptible to be released in MVs. The second mechanism is based on defects in Band3, resulting in Band3-free portions of the membrane susceptible to blebbing [386]. Whatever the mechanism, the reduction in membrane surface area leads to the formation of spherocytes with reduced deformability [361]. Interestingly, decreased surface area is a feature of both the reticulocytes and mature RBCs in HS [387]. Splenic conditioning can exert additional damage

when abnormal erythrocytes are stuck in Billroth cords, in which the environment is more acid, low in glucose and ATP concentrations. The contact with high macrophages concentration and the resulting high local concentrations of oxidants contribute to reduce the RBC survival [361].

Densitometric quantification of membrane proteins separated by SDS-PAGE and western blotting analysis allows the classification of HS into different subsets: i) spectrin deficiency due to *SPTB* or *SPTA1* mutation, ii) combined deficiency of spectrin and ankyrin generally due to *ANK1* mutation, iii) deficiency of Band3 and 4.2 protein, due to *SLC4A1* mutation, and iv) deficiency of 4.2 due to 4.2 gene mutation[388]. Several other features have been observed, including lower AQP1 content [389], excessive sodium influx [390], increased activity of Na^+/K^+-ATPase [390], accelerated ATP turnover and glycolysis [316, 391], increased adhesion to laminin and thrombospondin [392] and loss of Band3 and GPA during enucleation [113].

5. Red blood cell microvesicle release

These last decades, the field of transcellular signaling was revolutionized by the emerging concept of signal transmission through extracellular vesicles (EVs). For a long time, vesicles seen in intercellular spaces by electron microscopy were thought to be artifacts or inert cellular fragments resulting from damaged cells in the vicinity. Nonetheless, all cells, from bacteria to plants and animal cells, seem to have the ability to produce EVs [393, 394]. However, there is still no real consensus regarding EV classification and nomenclature [395], probably due to the variety of EV size, composition, origin and targets but also to difficulties related to their isolation and analysis. Most reviews classify EVs in three groups: exosomes, MVs and apoptotic bodies (Figure 5.1) [396-399]. Exosomes are the smallest EVs (50–150 nm in diameter) that are released upon multivesicular bodies exocytosis. MVs are produced by direct local deformation and budding of the plasma membrane leading to vesicles of more heterogeneous and bigger size (100 nm–1 µm in diameter). It should be noted that these vesicles are often given other names, including ectosomes, microparticles, shedding vesicles or oncosomes (in the particular case of cancer cells). Apoptotic bodies (1–5 µm in diameter) are generated by blebbing of cells undergoing apoptosis. However, this classification should be taken with caution as most of the currently used techniques only allow to separate small EVs enriched in exosomes from large EVs enriched in MVs [400]. Yet, other studies have evidenced by imaging the budding from the plasma membrane of vesicles with size closer to that of exosomes [401-403]. In this review we will focus on plasma membrane-derived vesicles whatever their size.

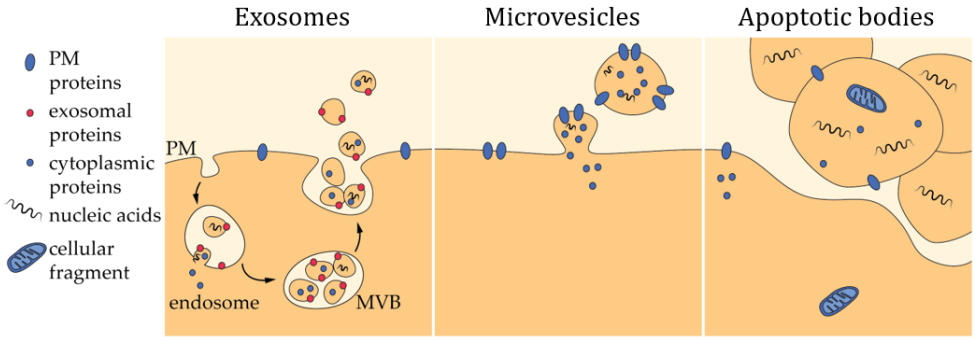

Size	50-150nm	0.1-1µm	1-5µm
Origin	endosome	plasma membrane	plasma membrane of apoptotic cells
Isolation	• differential ultracentrifugation • density gradient • size-exclusion chromatography • immune-capture		differential ultracentrifugation (standard protocol needed)
Other names	prostasomes	ectosomes microparticles shedding vesicles	

Figure 5.1. Characteristics of the three main classes of extracellular vesicles. MVB, multivesicular body; PM, plasma membrane [404].

EVs have been shown to contribute to a large variety of pathophysiological processes including red blood cell (RBC) senescence [405], coagulation [406], inflammation [406, 407], migration [408], tumorigenesis [409] and infection [410]. As they are found in body fluids (e.g., blood, urine, cerebrospinal fluid, milk), they are easily accessible and might represent useful diagnostic biomarkers and/or targets for therapeutic applications (reviewed in [411]). In this review, we will focus on vesicles derived from the plasma membrane of RBCs, platelets, immune cells, nervous cells and tumor cells. Before providing detailed information regarding their biogenesis, we here below present a short non-exhaustive overview of their pathophysiological effects.

RBCs undergo multiple changes during their 120-day lifespan in the circulation, including the decreased activity of multiple enzymes, the gradual accumulation of oxidative damages, the redistribution of ions, the loss of membrane by vesiculation as well as cell volume, density and deformability alterations (for reviews, see [224, 412, 413]). MV generation constitutes a central mechanism in the RBC homeostasis and is responsible for the loss of ~20% of the plasma membrane while the hemoglobin concentration increases by ~14% [414, 415]. MVs have been proposed to contribute to RBC senescence by two opposite mechanisms. On one hand, they protect RBCs from premature elimination via transport of molecules that could induce recognition by the reticuloendothelial system such

as non-functional hemoglobin, Band3 oxidation and aggregation and oxidized proteins [415] (Figure 5.2a). On the other hand, they appear to contain CD47, a “self-marker” that prevents the recognition and clearance of RBCs by macrophages. Elimination of CD47 from the RBC membrane through selective shedding could then promote the removal of old RBCs [292] (Figure 2b). Studies on mice suggest that MVs from RBCs are removed very fast from the circulation by the reticuloendothelial system [416] because they can have deleterious effects on other cells. For instance, MVs bear at their external leaflet PS, which acts as an “eat me” signal for macrophages but also promotes coagulation, as PS enhances prothrombinase activity and other coagulation factors (Figure 5.2a,c). Moreover, RBC-derived MVs induce an excessive production of reactive oxygen species (ROS) in neutrophils and could be responsible for exhortation of the “respiratory burst”, i.e., the rapid release of ROS necessary to answer to an infection [417] (Figure 5.2d). Finally, they contain hemoglobin, which allows them to bind nitric oxide modifying thereby its bioavailability for vascular homeostasis regulation [418] (Figure 5.2e). However, these effects have been shown with MVs isolated from blood storage. Although the biological content should reflect the functional properties of circulating MVs, further investigations in vivo are needed to confirm this hypothesis. Nevertheless, the properties described above could partly explain reduced post-transfusion efficacy and increased risk of adverse reactions in patients after transfusion [419, 420].

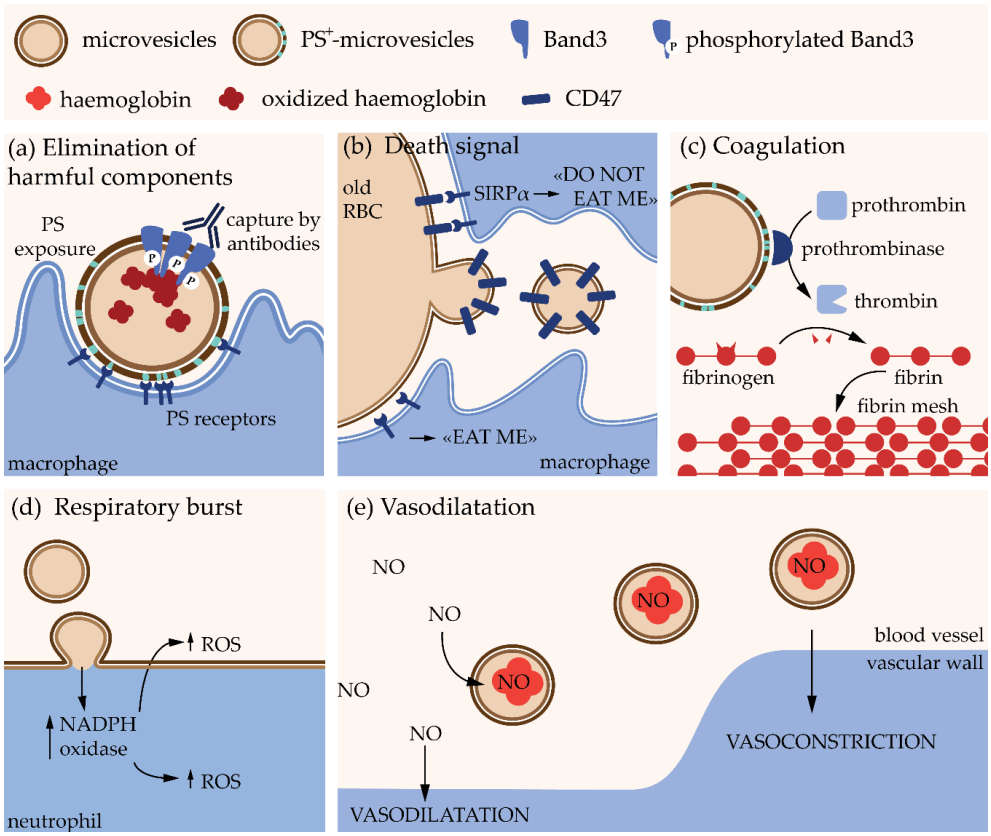

Figure 5.2. Pathophysiological effects of RBC-derived MVs. PS, phosphatidylserine; SIRPα, signal regulatory protein α; ROS, reactive oxygen species; NO, nitric oxide. For additional information, please refer to the text [404].

CHAPTER 2. AIMS AND STRATEGIES OF THE STUDY

During the last decade, the host laboratory has explored the contribution of plasma membrane lateral heterogeneity and biophysical properties for RBC deformation. To do so, the group developed and validated a series of complementary fluorescent probes compatible with confocal vital imaging (e.g. trace insertion in the plasma membrane of exogenous fluorescent lipid analogs or artificial probes and labelling of endogenous lipids with fluorescent toxin derivatives) and specific to the main outer plasma membrane lipids, i.e. sphingomyelin (SM), phosphatidylcholine (PC), ganglioside GM1 and cholesterol. The laboratory also validated several technics to mimic RBC deformation. Using these approaches, submicrometric lipid domains that differ in abundance, lipid composition, temperature dependence, lipid order, curvature association and spatial relationship were detected. The current model highlights the coexistence at the RBC surface of three types of lipid domains that play differential roles. The first type of domains is present in RBC high curvature membrane area, is enriched in cholesterol and can gather during RBC deformation. The two other types of lipid domains are associated with the RBC low curvature areas: (i) those enriched in GM1/PC/cholesterol whose abundance increases upon calcium entry during RBC deformation; and (ii) those enriched in SM/PC/cholesterol whose abundance increases upon calcium efflux and RBC shape restoration after deformation. Those findings, to which I contributed, have been published in 2018 (Conrard et al, Cell Physiol Biochem 2018; Annex 6) and suggested that the low curvature-associated lipid domains could provide platforms for the recruitment and/or activation of the mechanosensitive cation channel PIEZO1 and the plasma membrane calcium efflux pump PMCA.

At the end of their 120-days lifetime and upon storage at 4°C before transfusion, the RBCs become less deformable and lose part of their membrane by microvesiculation. The host laboratory has shown that, during the RBC storage, the high curvature-associated cholesterol-enriched domains are preferentially lost, potentially representing preferential sites for membrane microvesiculation. This observation was the starting point of a review entitled “Plasma membrane lipid domains as platforms for vesicle biogenesis and shedding?” to which I am first author (Pollet et al, Biomolecules 2018; Annex 7).

Based on the observations that lipid domains contribute to RBC deformation but are instead lost upon storage, we postulated that they could be impaired in RBC fragility diseases. The goal of my thesis was therefore to evaluate whether lipid domains could be modified in abundance, composition and dynamics in hereditary elliptocytosis (HE) and spherocytosis (HS), and by which mechanism. Those two diseases are caused by impairment

of the horizontal and vertical linkages between the membrane and the underlying cytoskeleton, respectively. HE is characterized by the progressive transformation of the RBC discoid shape into elliptic shape whereas HS exhibits small spherical less deformable RBCs.

Due to the low prevalence of symptomatic patients with HE, I was limited to one patient suffering from a severe form of elliptocytosis (pEl) and her asymptomatic mother (pElm). Two mutations in the α-spectrin-coding *SPTA1* gene were identified by NGS sequencing, the Leu260Pro (or Nigerian) variant, shared by the patient and her mother, and Arg1811*, a premature stop codon for which the mRNA is likely degraded by the nonsense-mediated mRNA decay mechanism. The patient therefore exclusively expresses the Pro260 variant of SPTA1. We analyzed the consequences of this mutation in RBCs from pEl and pElm by characterizing their morphology (scanning electron microscopy and blood smears), deformability (hemoglobin release in hypo- and hypertonic medium), cytoskeletal and membrane protein distribution (confocal and transmission electron microscopy) and content (western blotting and proteomics). We also examined the calcium exchanges at the RBC surface as well as the lipid domain abundance and response to calcium exchange stimulation (live cell confocal imaging). We found that the pEl RBC size and circularity were decreased and deformability was impaired. The cytoskeletal and membrane proteins were altered. The RBC intracellular calcium content was increased and calcium influx and efflux upon RBC deformation were both slowed down. Although the high curvature-associated cholesterol-enriched domains were not modified, the low curvature-associated GM1/PC/cholesterol- and SM/PC/cholesterol-enriched domains were altered in abundance, cholesterol-enrichment and response to calcium exchange stimulation. To address the mechanism behind, we looked whether the lipid domains could be (i) directly altered in composition or biophysical properties by SM hydrolysis into ceramide through the plasmatic acid sphingomyelinase; and/or (ii) indirectly modified by the intracellular calcium accumulation and the resulting increased activity of protein kinase C, NADPH oxidase and scramblase. We found that the reactive oxygen species accumulated in pEl RBCs and resulted into increased lipid peroxidation and overactivation of the plasmatic acid sphingomyelinase. In addition, the phosphatidylserine exposure at the RBC surface was increased, indicating perturbation of the plasma membrane transversal asymmetry. Our data revealed that alterations in membrane lipid composition and transversal and lateral heterogeneity in lipid domains through plasmatic acid sphingomyelinase, oxidative stress and lipid scramblase activation contribute to the pathophysiology of elliptocytosis. This study also suggested targets for therapeutics. This first investigation is included in a research paper as first author (Pollet et al, *In preparation*; Chapter 3, section 1).

The spherocytosis study included ten splenectomised patients from seven families exhibiting *SPTB* or *ANK1* mutations. In all patients, the mRNA of the allele carrying the mutation was degraded by the nonsense-mediated mRNA decay mechanism. Three groups

of patients were defined based on clinical parameters and RBC morphology and deformability features. Although β-spectrin and ankyrin mutations led to differential RBC morphology, cytoskeletal organization defect and rigidity, cholesterol and total phospholipid content loss as well as microvesicle release, none of those features did correlate with the disease severity. Instead, the rise in intracellular calcium and ATP content represented two factors to consider upon evaluation of the disease severity. On one hand, the intracellular calcium accumulation contributed to spherocytosis through the increased exposition of phosphatidylserine at the RBC surface but not through increased oxidative stress. Such calcium accumulation could result from the decreased abundance of the mechanosensitive cation channel PIEZO1 and its activity through the impaired response of the ganglioside GM1/PC/cholesterol-enriched domains to calcium influx stimulation by Yoda1. On the other hand, the rise in intracellular ATP lowered the disease severity by limiting the intracellular calcium rise, possibly through direct stimulation of the calcium efflux pump PMCA activity and/or maintenance of the membrane asymmetry and the functionality of the SM/PC/cholesterol-enriched domains. Based on the integration of the intracellular calcium and ATP content modifications and the resulting alterations of membrane transversal and lateral heterogeneity in lipid domains, the ten patients were classified into three groups that perfectly matched with the disease severity score defined by clinical parameters and RBC morphology and fragility. These data highlighted the importance of the interplay between lipid domains and the cytoskeleton for RBC morphology and deformability and indicated that clinical heterogeneity in HS are reflected in the calcium-dependent membrane defects. Observations are included in a second research paper as co-first author (Pollet, Cloos et al, *In preparation*; Chapter 3, section 2).

CHAPTER 3. RESULTS

1. Publication 1: Alteration of membrane composition and biophysical properties contributes to the pathophysiology of elliptocytosis- A case study

H. Pollet[1], L. Conrard[1], A.S. Cloos[1], A. Paquot[2], A. Stommen[1], M. Carquin[1], C. Léonard[1], M. Guthmann[1], M. Lingurski[1], C. Vermylen[3], S. Pyr dit Ruys[4], D. Vertommen[4], M. Vikkula[5,6], P. Brouillard[5], P. Van Der Smissen[1], G.G. Muccioli[2] and D. Tyteca[1]

Université catholique de Louvain, 1200 Brussels, Belgium

[1] CELL Unit & PICT imaging Platform, de Duve Institute

[2] Bioanalysis and Pharmacology of Bioactive Lipids Research Group, Louvain Drug Research Institute

[3] PEDI Unit, Institut de Recherche Expérimentale et Clinique & Saint-Luc Hospital

[4] PHOS Unit, de Duve Institute

[5] Human Molecular Genetics, de Duve Institute

[6] Walloon Excellence in Life Sciences and Biotechnology (WELBIO), de Duve Institute

In preparation

Keywords : red blood cell fragility, spectrin cytoskeleton, PIEZO1, PMCA, lipid domains, reactive oxygen species, oxidized lipids, polyunsaturated fatty acids, cell fragmentation, cholesterol, ascorbic acid, amitriptyline

Running title: Membrane and calcium alterations in elliptocytosis

1.1. Abstract

Hereditary elliptocytosis is a red blood cell (RBC) disease mainly caused by mutations in spectrin, leading to cytoskeletal destabilization. Although patients with heterozygous mutation in α-spectrin (SPTA1) are asymptomatic, morphological changes and hemolysis are observed upon reduced production of functional α-spectrin. The molecular mechanism is unknown. We analyzed the consequences of a α-spectrin mutation in a patient almost exclusively expressing the Pro260 variant of SPTA1 (pEl) and her asymptomatic mother. In pEl, RBC size and circularity are decreased and deformability is impaired. Membrane association and lateral distribution of cytoskeletal and membrane proteins are altered. The two populations of membrane lipid domains associated with RBC low curvature areas are modified in abundance, cholesterol content and response to calcium exchange stimulation. This results from three features. Firstly, the plasmatic acid sphingomyelinase is upregulated, leading to increased ceramide-enriched domains. Secondly, the intracellular calcium content is strongly increased, inducing downstream (i) PKC-dependent cytoskeletal and membrane protein phosphorylation; (ii) NADPH oxidase-dependent reactive oxygen species production and lipid peroxidation; and (iii) scramblase-dependent phosphatidylserine exposition at the RBC surface. Thirdly, the membrane content of long unsaturated phosphatidylserine and phosphatidylcholine species is decreased. All these features could lead to eryptosis and membrane fragmentation. This study shows that alteration of membrane lipids and lipid domains through the plasmatic acid sphingomyelinase, calcium increase and downstream oxidative stress and scramblase activation contribute to the pathophysiology of elliptocytosis. It also provides the first evidence that α-spectrin defect leads to alteration of membrane composition and transversal and lateral heterogeneity and could help develop novel therapies.

1.2. Introduction

During its lifetime, the red blood cell (RBC) undergoes high deformations needed to pass through narrow capillaries to deliver oxygen to tissues. Such exceptional deformability relies on intrinsic features, including (i) a biconcave shape due to the excess of plasma membrane (PM) surface *vs* the cytoplasmic volume, (ii) a finely regulated cytoplasmic viscosity controlled by the hemoglobin concentration, and (iii) a cytoskeleton composed of a meshwork of spectrin tetramers linked to the membrane by two anchorage complexes based on 4.1R and ankyrin proteins [185]. RBC deformation is also associated with a transient intracellular calcium increase, which activates Gardos channels, leading to cell dehydration, and favors a local membrane:cytoskeleton uncoupling [148]. RBC calcium entry is mostly operated by mechano-activated ion channels like PIEZO1 [210], whereas calcium efflux is ensured by the PM calcium ATPase (PMCA), in a tightly regulated process. RBC deformation also depends on ATP content and antioxidant system which allows to neutralize the harmful reactive oxygen species (ROS) generated through the constant exposure to variable oxygen pressures [224].

The RBC membrane exhibits a very high cholesterol/phospholipid ratio and three types of lipid domains involved in its deformation [3, 102, 161-163, 179]. The first ones, associated with high-curvature membrane areas, are mainly enriched in cholesterol and gather upon RBC deformation. The second ones, associated with RBC low-curvature areas, are enriched in ganglioside GM1, phosphatidylcholine (PC) and cholesterol. Their abundance increases upon PIEZO1 activation. The third ones, also associated with low-curvature areas, are enriched in sphingomyelin (SM), PC and cholesterol. Their abundance rises upon calcium extrusion [163, 177].

RBC deformability and lifespan are altered in inherited RBC disorders, leading to chronic hemolytic anemia [145, 187, 295]. Contrary to other hemolytic anemias, elliptocytosis is asymptomatic in 90% of cases, leading to prevalence underestimation [300]. This group of heterogeneous diseases affecting α-spectrin-, β-spectrin- or 4.1R-coding genes is inherited in an autosomal dominant manner, with rare cases of *de novo* mutations. The only treatments are folate therapy, transfusions and splenectomy [297, 421].

A recent simulation study has revealed that elliptocytotic RBCs are unable to recover their original biconcave shape after passing through splenic interendothelial slits due to impaired elasticity, leading to fragmentation when the RBC cytoskeleton connectivity is lower than 20% [422]. However, the relevance of this model remains to be tested *in vitro*. Hence, the molecular mechanism is still unknown. In this study, we explored these

questions by analyzing the morphology, deformability, cytoskeleton organization, calcium exchange and membrane composition and organization of RBCs from a female teenager diagnosed for elliptocytosis during infancy (pEl). She underwent cholecystectomy, required to eliminate the cholelithiases accumulating in the gall bladder, but no splenectomy. Throughout the study period, pEl blood samples exhibited hemolysis markers, high reticulocyte count and low RBC mean corpuscular volume. The RBC mean corpuscular hemoglobin concentration and the RBC abundance were less affected (Figure S1A-F). None of her relatives consulted for similar symptoms nor were diagnosed but her mother nevertheless appeared mildly affected (pElm).

1.3. Results

The patient pEl expresses the Pro260 variant of SPTA1. NGS sequencing of pEl unraveled two heterozygous nucleotide substitutions in *SPTA1*, the gene encoding α-spectrin, resulting in a Leucine-to-Proline change (*c.779T>C*; p.Leu260Pro) and a premature stop codon (*c.5431C>T*; p.Arg1811*) (Figure 1A, Table). The *c.779T>C* (Leu260Pro) change was inherited from the mother (pElm), as confirmed by direct RNA sequencing (Figure 1A, bottom left). In pEl, the C-allele (corresponding to proline) was predominant at position c.779, with almost complete loss of the T-allele (corresponding to leucine). This is likely due to degradation by nonsense-mediated mRNA decay of the RNA of the paternal allele carrying the premature stop codon (Figure 1A, bottom right). Reduced quantity of the paternal mRNA allele was confirmed by sequencing a common polymorphism, which was heterozygous in pEl DNA (*c.525C>*A; p.Ala1764Ala; Figure 1A, Table) but squewed in its RNA (Figure 1A, bottom center). Based on these results, the phase of the alleles was deduced (Figure 1A, bottom), showing that pEl expressed mainly the proline-mutated allele inherited from her mother. In contrast, her second allele (presumably paternal, not available for testing), carrying the premature stop codon (p.Arg1811*), as well as the A-allele of the polymorphism at position *c.5292*, was degraded. Thus, at the protein level, pEl should almost exclusively express the Pro260 variant of SPTA1. This Pro260 variant has already been described in the literature [186, 320, 423] but consequences for the RBC morphology and deformability were not evaluated.

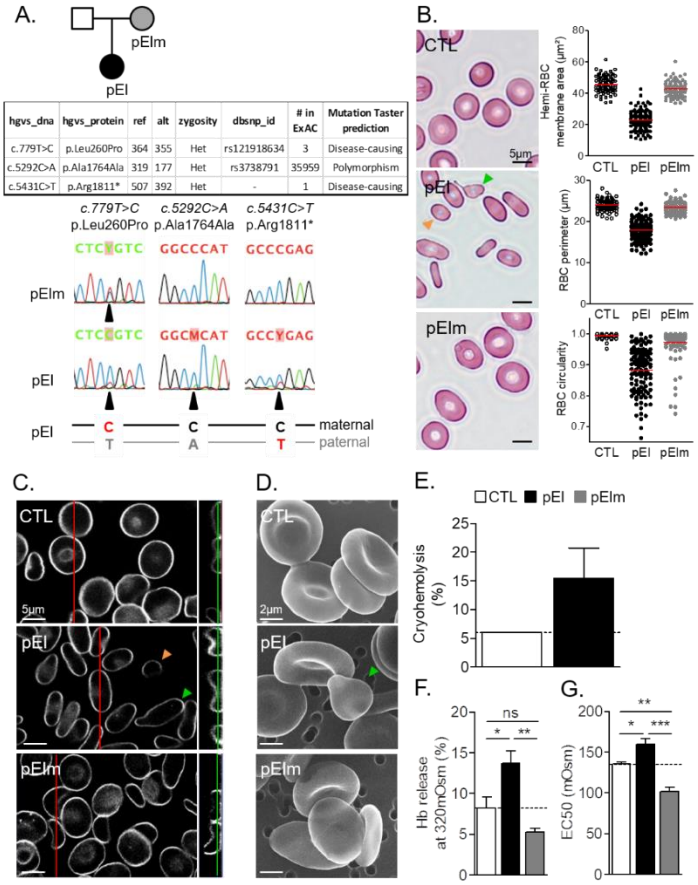

hgvs_dna	hgvs_protein	ref	alt	zygosity	dbsnp_id	# in ExAC	Mutation Taster prediction
c.779T>C	p.Leu260Pro	364	355	Het	rs121918634	3	Disease-causing
c.5292C>A	p.Ala1764Ala	319	177	Het	rs3738791	35959	Polymorphism
c.5431C>T	p.Arg1811*	507	392	Het	-	1	Disease-causing

Figure 1. Pedigree, genetic defects and RBC morphology and fragility of the family enrolled in the study. (A) Pedigree and genetic defects. Affected patient (pEl) and her mother (pElm), partially affected but not diagnosed. Table, NGS results for pEl showing coverage (ref, reads with reference allele; alt; alternative allele), zygosity, code in dbSNP, number of occurrences in control population (The Exome Aggregation Consortium) and impact prediction from Mutation Taster, for two likely mutations and one heterozygous polymorphism. Sequences, RNA sequencing showing partial loss of the allele carrying the premature Stop codon (T-allele at position 5431) in pEl. pElm is heterozygous for Leu260Pro, whereas pEl is almost homozygous for the C at position 779 (Proline) and at position 5292, due to degradation. Y = T or C; M = C or A. **(B)** RBC membrane hemi-area, perimeter and circularity determined on May-Grünwald Giemsa-stained blood smears. Left, representative images; green arrowhead, poïkilocytotic RBC; orange arrowhead, small spherical RBC. Right, quantification for one representative blood smear (n=3; CTL *vs* pEl, ***; CTL *vs* pElm, ns; pEl *vs* pElm, ***). **(C,D)** RBC biconcavity evaluated on RBCs in suspension. (C) RBCs labeled with a BODIPY-lipid, laid down in IBIDI chambers and analyzed by vital confocal microscopy. The figure shows in left panels X-Y sections (positions indicated by the green lines in the right panels) and in right panels the corresponding X-Z sections (positions indicated by the red lines in the left panels). (D) RBCs fixed in suspension, laid down on filters and analyzed by scanning electron microscopy. Images are representative of 2 independent experiments at both C and D. Green arrowheads, poïkilocytotic RBCs; orange arrowhead, small spherical RBC. **(E-G)** RBC fragility evaluated in hyper- (E), iso- (F) and hypotonic media (G). (E) Cryohemolysis (mean ± SEM of 6 independent experiments). (F,G) Hemoglobin released in isosmotic medium and half-maximal effective osmolarity (EC50) determined upon RBC incubation in decreasing osmolarity media (means ± SEM of 3-4 independent experiments). For evolution of these parameters with time, see Figure S1G-J.

pEl RBCs exhibit decreased size and circularity and increased fragility but normal biconcavity and low microvesicles release. Blood smears of pEl revealed anisocytosis dominated by small elliptic RBCs (Figure 1B, orange arrowhead). The decreased projected membrane area, perimeter and circularity of pEl RBCs were shown by quantification on blood smears (Figure 1B, right) and poly-L-lysine (PLL)-coated coverslips (Figure S2), the system used below to analyze membrane organization. Poïkilocytosis was also observed, but to a lower extent (Figure 1B, green arrowhead). At first glance, blood smears of pElm appeared normal. However, quantification revealed a larger distribution of RBC circularity, suggesting the presence of elliptic RBCs as in pEl (Figure 1B, right). The decreased surface area and circularity of pEl RBCs were maintained throughout the 4-year study and did not result from pEl young age since no difference can be seen between healthy donors whatever their age (Figure S1G,H & S3A-C).

Confocal microscopy on living suspended RBCs and scanning electron microscopy on fixed RBCs laid down on filters revealed that pEl and pElm elliptic cells preserved their biconcavity (Figure 1C,D). Moreover, the progressive appearance of echinocytes and spherocytes upon storage were delayed in pEl and pElm as compared to healthy donors. In addition, microvesicles isolated from pEl and pElm blood were less abundant than those from control blood (Figure S4A-D). These data indicated that, in contrast to RBCs upon storage at 4°C and from hemolytic anemias [187, 424], elliptocytotic RBCs appeared preserved from microvesiculation.

Cryohemolysis and hemoglobin release in iso- or hypotonic media were increased in pEl *vs* healthy donors but changed during the study period (Figure 1E-G; S1I,J & S5A). Surprisingly, pElm RBCs showed lower hemoglobin release and EC50 than healthy RBCs (Figure 1F,G). Altogether, those data indicated that pEl RBCs presented decreased size and circularity *vs* increased fragility, but preserved their biconcavity.

Cytoskeletal and membrane protein plasma membrane association and lateral segregation are decreased whereas hemoglobin membrane retention is increased in pEl. Hemoglobin was more retained in the pEl than healthy or pElm ghost membrane, as revealed both by SDS-PAGE (Figure S6A,B) and mass spectrometry (Figure S6C). In contrast, all cytoskeletal proteins, except the β-Tubulin, exhibited a two-fold decreased association with the pEl ghost membrane than in healthy donors (Figure S6D). All membrane proteins were also decreased by two-fold, except the Transferrin receptor which was slightly increased (Figure S6E).

We then assessed whether abnormal protein association with membrane could result from alteration of the spectrin cytoskeleton organization. At the microscale level,

spectrin occupancy was significantly decreased neither in pEl nor in pElm (Figure 2A,B). In contrast, the variation of the labeling intensity was greatly increased in pEl RBCs (Figure 2C), showing spectrin gathering at one cell edge in ~75% of pEl RBCs *vs* ~20% in pElm and ~5% in healthy RBCs (Figure 2A, arrowheads). Spectrin gathering was confirmed by electron microscopy in pEl (Figure S7, arrowheads) and was exacerbated upon storage of pEl and pElm RBCs (Figure S4E), suggesting microvesiculation-independent changes upon RBC storage in elliptocytosis. Moreover, at the nanoscale level, less dense areas alternating with darker ones were revealed in pEl RBCs (Figure 2D, red areas), suggesting reorganization of the cytoskeleton:membrane anchorage complexes.

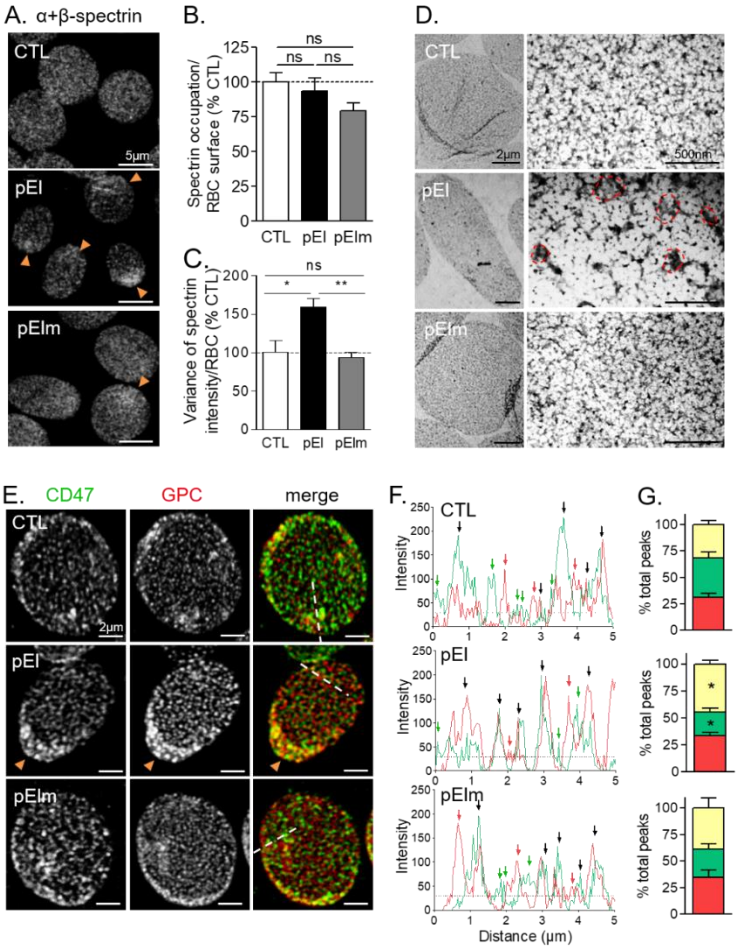

Figure 2. The organization of the spectrin network is hetereogeneous and the segregation of membrane proteins from the two anchorage complexes is decreased in pEl RBCs. (A-D) Spectrin network analyzed by confocal (A-C) and transmission electron microscopy (D). RBCs were laid down on PLL-precoated coverslips (A-C) or formvar coated grids (D), permeabilized with 0.5% Triton X-100, fixed and stained with anti-pan spectrin antibodies (A-C) or not (D). (A,D) Representative images. Orange arrowheads at A and red areas at D, increased cytoskeleton

density. (B,C) Quantification of spectrin occupation and dispersion on confocal images. Data are expressed by reference to the mean of control RBCs from the same experiment (means ± SEM from 5 independent experiments with 50-150 RBCs measured/condition). **(E-G)** Membrane protein distribution determined by confocal imaging. RBCs were laid down on PLL-precoated coverslips, fixed and stained with antibodies against CD47 (ankyrin complexes; green) and glycophorin C (GPC; 4.1R complexes; red). (E) Representative images. Orange arrowhead, high protein density. (F) Representative intensity profiles along the paths indicated at E by white dotted lines. Green arrows, CD47 only; red arrows, GPC only; black arrows, CD47/GPC overlapping. (G) Quantification of the abundance of CD47, GPC and CD47/GPC-overlapping peaks (yellow portion of the columns) determined on 30-40 profiles per condition generated from 3 independent experiments (expressed as percentage of total peaks from all the profiles; means ± SEM).

These observations were confirmed by RBC immunolabeling for glycophorin C (GPC) and CD47, respectively enriched in the 4.1R- and the ankyrin-based complexes. First, ~40% of pEl RBCs presented at one edge a stronger labeling for both CD47 and GPC *vs* only ~10% in control and pElm RBCs (Figure 2E, arrowhead; Figure S8). Second, the spatial dissociation between CD47- and GPC-enriched clusters was significantly decreased in pEl but not in pElm RBCs (Figure 2F,G). Thus, pEl exhibited defects in spectrin organization, altering membrane protein distribution and raising hemoglobin membrane association.

Lipid domains in pEl RBCs are altered in abundance and response to calcium exchange stimulation. We then asked whether alteration of cytoskeletal and membrane protein content and segregation could in turn affect membrane lipid lateral distribution into domains previously evidenced by our group both in low- and high-curvature RBC areas [163, 177]. The abundance of low curvature-associated SM- and PC-enriched domains was significantly increased in pEl RBCs as compared to healthy donors (Figure 3A, orange arrowheads; Figure 3B & S3D,E). In contrast, cholesterol-enriched domains were not visible in the pEl RBC low-curvature areas but well associated with the high-curvature ones (Figure 3A, orange *vs* green arrowheads), resulting into a slight decrease of the total cholesterol-enriched domain abundance (Figure 3B).

We next assessed whether lipid domains in pEl RBCs could also be impaired in functionality, using the PIEZO1 agonist Yoda1 to stimulate calcium influx and the extracellular calcium EGTA to deplete intracellular calcium [163, 177]. We observed that GM1-enriched domains did not increase upon Yoda1 in pEl contrasting with a 2-fold increase in controls. Moreover, SM-enriched domains increased by less than ~2-fold upon EGTA in pEl *vs* ~3-fold increase in controls (Figure 3C,D). Those data suggested that lipid domains were altered for their response to calcium exchange stimulations.

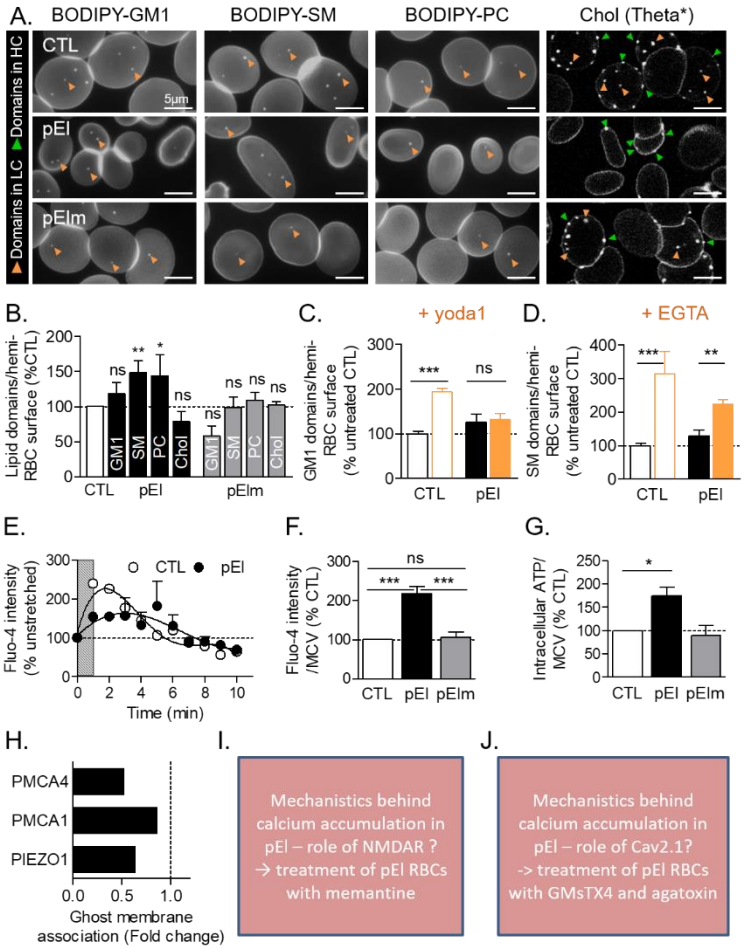

Figure 3. Lipid domains are impaired in abundance and response to calcium exchange stimulation in pEl RBCs and the intracellular calcium content is raised. (A,B) Lipid domains on RBCs at resting state. RBCs were either spread onto PLL-coated coverslips and labeled with BODIPY-GM1, -SM or -PC or labeled in suspension with Theta* and spread onto coverslips. All coverslips were directly visualized by vital fluorescence/confocal microscopy. (A) Representative images. Green arrowheads, domains in high curvature areas (HC); orange arrowheads, domains in low curvature areas (LC). (B) Quantification of lipid domain abundance per hemi-RBC area (means ± SEM from 3-19 independent experiments/lipid in which 300-600 RBCs were counted/experiment). **(C,D)** Abundance of lipid domains upon modulation of calcium influx stimulation (C, addition of Yoda1 just after labeling) or calcium depletion (D, incubation with EGTA). Data represent lipid domain abundance per hemi-RBC area (means ± SEM from 3-5 independent experiments/lipid in which 300-600 RBCs were counted per condition in each experiment). **(E)** Calcium exchange during RBC deformation on PDMS chambers. RBCs were labeled for calcium with Fluo-4 AM and measured for fluorescence intensity before (0min) and after stretching for 1min (grey stripped zone). Data are expressed as percentage of unstretched RBCs (means ± SD of 2 experiments where 150-200 RBCs were analyzed at each time). **(F)** RBC intracellular calcium content evaluated by Fluo-4 AM and expressed by reference to the mean corpuscular volume (MCV; means ± SEM of 5-9 independent experiments). **(G)** Intracellular ATP content measured by luminescence after RBC incubation with luciferase and luciferin and expressed by reference to MCV (means ± SD/SEM of 2-4 independent experiments). **(H)** Abundance of PIEZO1, PMCA1 and 4 evaluated by mass spectrometry on pEl ghost membranes. Data are expressed by reference to a healthy donor. (I,J) Contribution of NMDAR and Cav2.1 in calcium accumulation in pEl RBCs?.

To rule out aspecific effects of Yoda1 and EGTA, we then evaluated calcium exchanges upon RBC deformation in stretchable PDMS chambers [163, 178]. Control RBCs exhibited a rapid calcium raise followed by initial content restoration within 5min, whereas pEl RBCs showed a flatter calcium response with both a decrease of entry and a delay of exit (Figure 3E). We concluded that low curvature-associated lipid domains were less prone to respond to calcium exchange stimulation.

The intracellular calcium content is increased in pEl. Based on calcium exchange impairment in pEl RBCs and since an increased calcium content is often described in patients with sickle cell disease, thalassemia or spherocytosis [424], we also measured the intracellular calcium content in pEl RBCs at resting state. The calcium content was increased by ~2-fold in pEl but not in pElm as compared to the healthy donors (Figure 3F & S5B). The intracellular ATP content increase in pEl RBCs excluded the possibility that calcium accumulation resulted from ineffective extrusion due to disruption of the ATP pool fueling the PMCA (Figure 3G). In contrast, the decreased abundance of PIEZO1 and PMCA4 (one of the two PMCA isoforms found in RBCs [425]) associated with the ghost membrane in pEl RBCs (Figure 3H) could partially explain this accumulation. Indeed, upon lower PIEZO1 abundance, NMDAR and/or Cav2.1 could take over, leading to calcium accumulation (under investigation; Figure 3I,J).We concluded that elliptocytotic RBCs exhibited an increased intracellular calcium content at resting state and a decreased capacity to respond to calcium exchange upon RBC deformation. Since neither lipid domain nor calcium alterations were observed in pElm (Figure 3B,F), we focused on pEl for mechanistics. We suggested that, besides the decreased abundance of PIEZO1 and PMCA4 at the RBC surface, alterations in pEl could result from impairment of lipid domain distribution and dynamics.

Lipid domains are impaired for their cholesterol content, thereby contributing to calcium accumulation in pEl. To test the above hypothesis, we first explored whether lipid domains could be altered in composition. Double-labeling indicated that GM1- and SM-enriched domains were less colocalized with those enriched in cholesterol in pEl RBCs than in control RBCs (Figure 4A,B & S9). Hence, a ~30% cholesterol depletion by mβCD [176], which induced the disappearance of cholesterol-enriched domains and the decrease of GM1- and SM-enriched domain abundance in both pEl and control RBCs (Figure 4C), led to a ~3-fold increase of the calcium content in pEl RBCs *vs* a ~1.5-fold increase in healthy RBCs (Figure 4D), suggesting a synergistic effect between the lower cholesterol enrichment of lipid domains in pEl and cholesterol depletion by mβCD. Accordingly, mβCD decreased the resistance of pEl RBCs to hemolysis, without any modification on control RBCs (Figure 4E). Thus, alteration of calcium exchanges and decreased resistance to hemolysis of pEl RBCs could be linked to the alteration of the cholesterol enrichment in GM1- and SM-enriched domains.

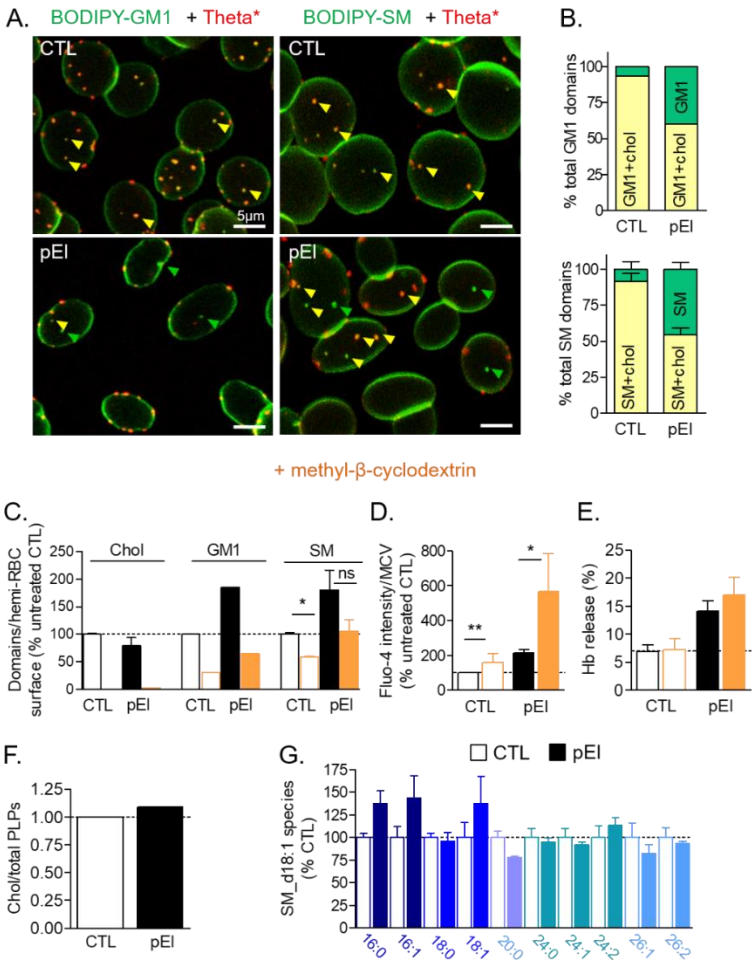

Figure 4. GM1- and SM-enriched domains are dissociated from cholesterol-enriched domains in pEI RBC low-curvature areas, contributing to the calcium accumulation. (A,B) RBCs were labeled in suspension with Theta*, spread onto coverslips and labeled with BODIPY-GM1 or -SM. (A) Representative images. Green arrowheads, BODIPY-GM1 or -SM only; yellow arrowheads, BODIPY-GM1/Theta* or BODIPY-SM/Theta* co-labelled domains. For single channel images, see Figure S9. (B) Quantification of spatial association of GM1- and SM-enriched domains with cholesterol (chol)-enriched domains (yellow parts of the columns) (means ± SD/SEM of 2 and 3 independent experiments in which 50-100 RBCs were counted). **(C-E)** Alteration of lipid domains, exacerbation of calcium accumulation and hemolysis upon cholesterol depletion. (C) Abundance of cholesterol-, GM1- and SM-enriched domains in RBCs pretreated with mβCD (means ± SD/SEM of 2-4 independent experiments). (D) Intracellular calcium content measured as in Figure 3F in RBCs incubated with Fluo-4 AM then with mβCD (means ± SEM of 5 independent experiments). (E) Hemoglobin release in the supernatant measured 2min after incubation with mβCD and expressed as percentage of total hemoglobin content in the sample (means ± SEM of 5 independent experiments). **(F,G)** Cholesterol and SM contents. RBCs were washed, lysed, extracted for lipids (only in G) and assessed either for cholesterol and total phospholipids (Cholesterol/PLPs ratio; F) or for SM species based on a d18:1 D-erythro-sphingosine backbone by lipidomics (classification based on fatty acid length and insaturation number; G). Results are expressed as cholesterol/PLP ratio in F (mean of 2-3 independent experiments) and as percentage of control RBCs in G (mean of 9 healthy women).

SM-enriched domains in pEl are affected by the plasmatic acid SMase, leading to increased ceramide-enriched domains and contributing to calcium accumulation. Alteration of SM-enriched domains for their cholesterol content did not appear to result from lower cholesterol or SM membrane content (Figure 4F,G). We therefore tested the alternative hypothesis that those domains could be the target of the plasmatic acid SMase (aSMase), an enzyme known to be activated in Sickle cell disease [426] and which hydrolyses SM into ceramide (Cer), it-self able to compete with cholesterol for the formation of domains with SM [427]. We found that the activity of aSMase was raised in pEl plasma (Figure 5A). Surprisingly, this increase was accompanied by the decrease of nearly all the RBC Cer species measured (Figure 5B). Cer decrease by metabolism into other sphingolipids was precluded, as revealed by the similar decrease of sphingosine content and sphingosine kinase activity in pEl *vs* controls (Figure S10A,B). Cer loss by vesiculation was also excluded as shown by the similar decrease of the different Cer species on vesicles/fragments (Figure S10C). Like other lipids, Cer clustered in domains. Those domains associated with both high and low membrane curvature areas and were increased in pEl (Figure 5C). We concluded that plasmatic aSMase and Cer-enriched domains were increased in elliptocytosis. It remains to be tested whether Cer could compete with cholesterol in SM-enriched domains, forming domains with altered biophysical properties (Figure 5D).

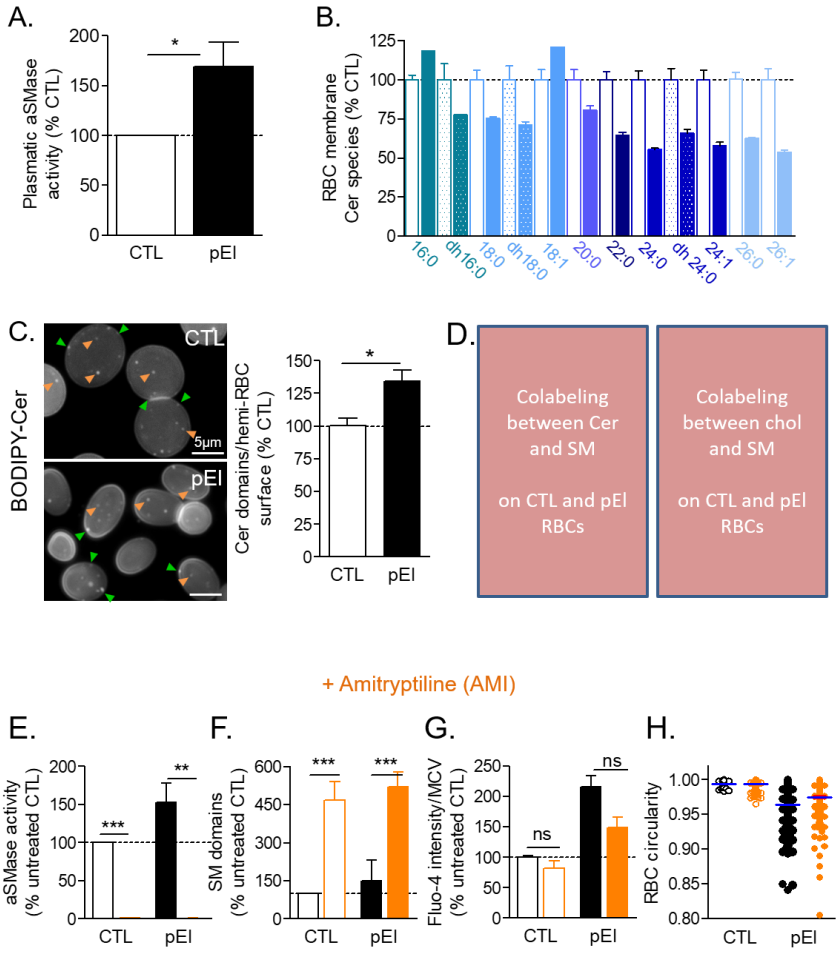

Figure 5. The plasmatic acid SMase activity and Cer-enriched domains are increased in pEI and contribute to the calcium accumulation. (A) aSMase activity determined in plasma isolated through Ficoll separation (mean ± SEM of 4 independent experiments). **(B)** RBC ceramide (Cer) content assessed by HPLC-MS on washed, lysed and lipid-extracted RBCs. Cer and dihydro (dh)-Cer species are classified based on fatty acid length and insaturation number and results are expressed as percentage of control RBCs (mean of 9 healthy women). **(C)** Abundance of Cer-enriched domains at the RBC surface. RBCs spread on coverslips were labeled with BODIPY-Cer and directly visualized by fluorescence microscopy. Left, representative images. Green arrowheads, domains in high curvature areas (HC); orange arrowheads, domains in low curvature areas (LC). Right, Cer-enriched domain quantification per hemi-RBC surface (means ± SEM of 3 independent experiments in which 200-400 RBCs were counted in each coverslip). **(D)** Spatial relationship between Cer- and SM/cholesterol (chol)-enriched domains. RBCs were labeled or not in suspension with Theta*, spread onto coverslips and labeled with BODIPY-Cer and/or -SM. **(E-H)** Effect of amitriptyline (AMI) on SM-enriched domain abundance, calcium accumulation and RBC circularity. Whole blood was incubated with AMI, washed and assessed. (E) aSMase activity determined in plasma as in Figure 5A (means ± SEM of 3 independent experiments). (F) Abundance of SM-enriched domains determined as in Figure 3 (means ± SEM of 3-4 independent experiments). (G) Intracellular calcium content measured as in Figure 3F (means ± SEM of 3-4 independent experiments). (H) RBC circularity measured on images produced in C (one representative out of 4 independent experiments; CTL vs CTL+AMI, *; pEI vs pEI+AMI, **).

To further test the implication of the plasmatic aSMase in the alteration of lipid domains and calcium exchanges, we evaluated whether SM domain abundance, calcium content and RBC circularity could be reestablished by reduction of the plasmatic aSMase activity using the tricyclic antidepressor amitriptyline (AMI; ref [426]; Figure 5E). AMI induced a ~5-fold increase of SM-enriched domain abundance and a lower calcium accumulation in both healthy and pEl RBCs (Figure 5F,G & S5H) as well as a partial restoration of RBC circularity in pEl RBCs (Figure 5H). Since the effects were only partial, we suggested that additional mechanisms might take place.

The pEl membrane is impaired by the calcium-dependent membrane and protein phosphorylation by PKC and NADPH oxidase-dependent ROS production. Because calcium was increased in pEl RBCs, we tested the possibility that lipid domains could also be altered through the upregulation of calcium-dependent enzymes, including μ-calpain (ongoing; Figure 6A) and protein kinase C (PKC) [148]. To test the contribution of the later, RBCs were incubated with phorbol esters in the presence of a phosphatase inhibitor (PMA/CalA), a treatment known to uncouple membrane:cytoskeleton at 4.1R complexes and to increase the abundance of SM-enriched domains in healthy RBCs [161]. Such increase was not observed in pEl RBCs (Figure 6B), which could suggest PKC hyperactivation. In agreement with this hypothesis, the major targets of PKCs [148] were more phosphorylated in pEl than healthy RBCs (Figure 6C).

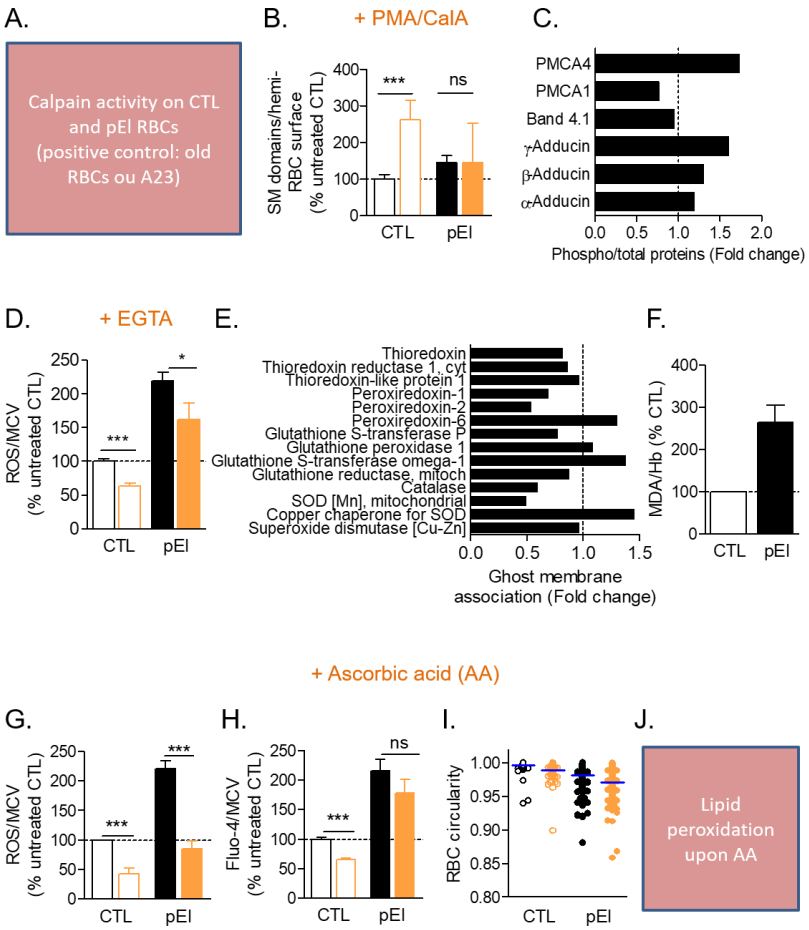

Figure 6. Calcium-dependent activation of PKC-mediated protein phosphorylation and NADPH oxidase-dependent ROS production contribute to alter the pEl membrane. **(A)** Calpain activity. **(B)** Abundance of SM-enriched domains upon modulation of membrane:cytoskeleton anchorage by PKC activation (incubation with PMA/CalA). Data represent SM-enriched domain abundance per hemi-RBC area (means ± SEM from 3-5 independent experiments/lipid and 300-600 RBCs were counted per condition in each experiment). **(C)** PKC-dependent phosphorylation of membrane and cytoskeletal proteins determined by mass spectrometry on ghost membranes. The abundance of phosphorylated proteins in pEl is expressed by reference to the corresponding total protein content and then expressed in fold changes *vs* the healthy donor. **(D)** Intracellular ROS level upon calcium depletion. Washed RBCs were incubated with 2',7'-dichlorodihydrofluorescein diacetate (H_2DCFDA) in the presence or not of EGTA to deplete intracellular calcium (means ± SEM of 3 independent experiments). **(E)** Abundance of antioxidant proteins determined by mass spectrometry on ghost membranes. Results are expressed by reference to the healthy donor. **(F)** Membrane lipid peroxidation. Washed and lysed RBCs were measured for malondialdehyde (MDA), the natural product of lipid peroxidation which forms an adduct with thiobarbituric acid (TBA). The adduct was then quantified by fluorimetry (means ± SEM of 4 independent experiments). **(G-J)** Effect of ascorbic acid (AA) on calcium accumulation, RBC circularity and membrane lipid peroxidation. Diluted blood incubated with AA was washed and assessed**.** (G) ROS measured as in D (means ± SEM of 4 independent experiments). (H) Intracellular calcium content evaluated as in Figure 3F (means ± SEM of 3-4 independent experiments). (I) RBC circularity measured on microscopy images of treated RBCs, washed and laid down on poly-L-lysine pretreated coverslip (one representative out of 4 independent experiments; CTL vs CTL+AA, **; pEl vs pEl+AA, *). (J) Membrane lipid peroxidation evaluated as in F.

In addition, pEl RBCs exhibited a more than 2-fold increase of intracellular reactive oxygen species (ROS) and this increase was partially restored by intracellular calcium depletion through EGTA treatment (Figure 6D & S5G), suggesting activation of the PKC-activated NADPH oxidase [228]. Moreover, the majority of the antioxidant enzymes exhibited a lower association with the pEl ghost membrane (Figure 6E). Increased ROS levels led to increased membrane lipid peroxidation, as revealed by the increased generation of malondialdehyde (MDA), a product of polyunsaturated fatty acid oxidation [428] (Figure 6F). All those data indicated an increase of oxidative stress in pEl RBCs.

However, reduction of oxidative stress using ascorbic acid in pEl (Figure 6G) was able to restore neither the intracellular calcium content nor the RBC circularity (Figure 6H,I). This could be due to the inability of ascorbic acid to reduce the membrane damages (ongoing; Figure 6J) and/or to additional calcium-dependent but ROS-independent enzyme activation.

The pEl membrane exhibits altered PS and lysoPS contents and higher PS surface exposure. Among those enzymes is scramblase, known to be activated by calcium increase [148] and cholesterol content decrease [80] and to induce PS exposure at the plasma membrane external leaflet, leading to PIEZO1 activity impairment as revealed in myoblasts [429]. We found an increased abundance of pEl RBCs showing PS exposure, as revealed by Annexin V. This increase was however quite modest as compared to RBCs stored for 2 weeks at 4°C (Figure 7A).

This modest effect could partially result from the decreased abundance of PS species, in particular the long and unsaturated ones (Figure 7B). Those modifications, which were similar for PC species (Figure S10D), were accompanied by the decreased membrane association of two enzymes involved in fatty acid elongation, the very long chain (3R)-3-hydroxyacyl-CoA dehydratase 3 and the elongation of very long chain fatty acids protein 2 (Figure 7D).

Besides PS exposure, incorporation of lysophosphatidylserine (lysoPS) at the outer plasma membrane leaflet is also able to decrease the PIEZO1 activity in myoblasts [429]. In pEl RBCs, six out of nine lysoPS species were increased whereas all the lysophosphatidylcholesteroline (lysoPC) species were decreased (Figure 7C, S5D,F & S10E). We concluded that (i) membrane asymmetry was impaired in pEl RBCs but could have been underestimated due to decreased total PS content; and (ii) several lysoPS species were also increased. It remains to determine whether and how those alterations could impair PIEZO1 activity (Figure 7G,J) and/or lipid domain transversal asymmetry (Figure 7E,F,H,I).

Effect of intracellular calcium decrease on pEl RBC membrane transversal and lateral heterogeneity, morphology and deformability. Altogether those data indicated that the calcium boost in pEl appears to contribute to the disease. We therefore finally tested whether a decrease of calcium could partially restore the ROS content, the extent of aSMase activation and PS externalization, the RBC circularity and the dynamics of GM1- and SM-enriched domains upon RBC stretching in PDMS chambers (ongoing; Figures 7K-O).

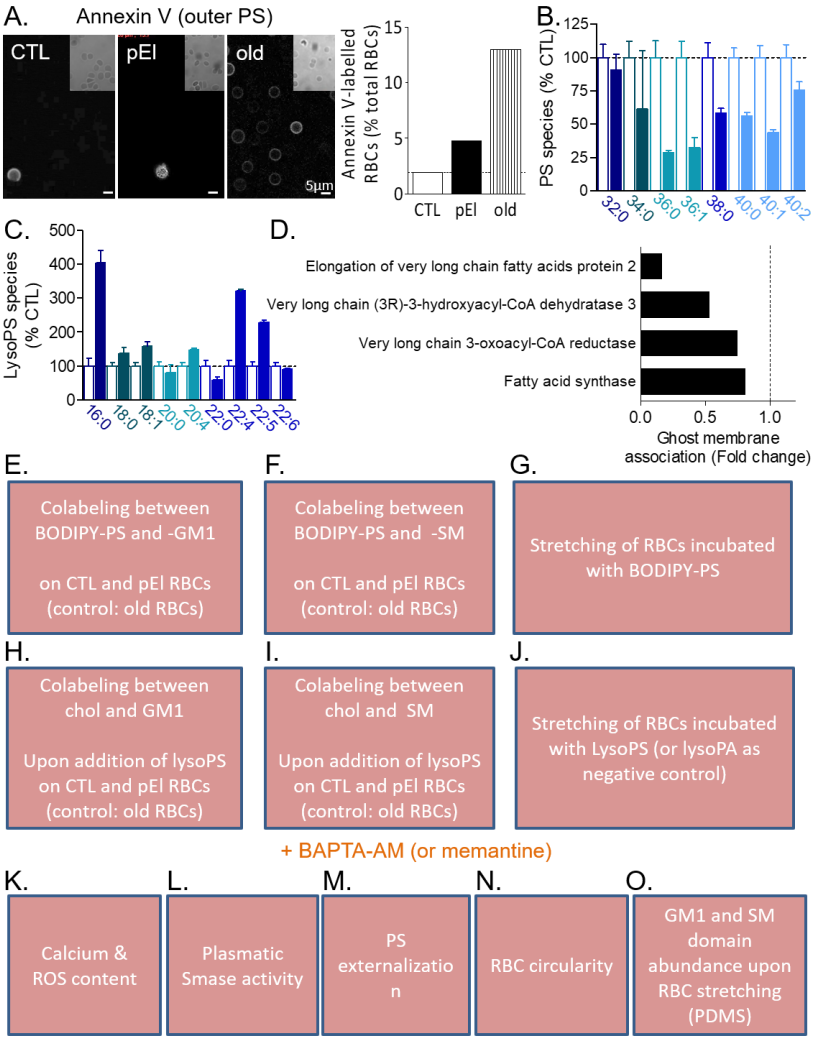

Figure 7. The calcium-dependent PS exposure at the pEl surface is accompanied by decreased PS and increased lysoPS contents. (A) Surface exposition of phosphatidylserine (PS) evaluated on RBCs labeled in suspension with Annexin V-Alexa Fluor 647 and laid down on PLL-coated coverslips. Left, representative images; right, quantification of the percentage of RBCs exposing PS at their surface (1 experiment in which 100-150 RBCs were

counted). **(B,C)** Quantification of PS and lysoPS species. RBCs were washed, lysed, extracted for lipids and assessed for PS (B) and lysoPS (C) species by lipidomics. Species are classified based on fatty acid length and unsaturation number and results are expressed as percentage of controls (mean of 9 healthy women). **(D)** Abundance of fatty acid biosynthesis enzymes associated to pEl ghost membrane and determined by mass spectrometry. Results are expressed by reference to the healthy donor. **(E,F)** Spatial relationship between GM1- or SM-enriched domains and outer PS. RBCs were spread onto coverslips and labeled with BODIPY-GM1 or -SM and -PS. **(H,I)** Effect of lysoPS addition at the outer leaflet on the spatial relation between GM1- or SM-enriched domains and cholesterol domains. RBCs were spread onto coverslips, incubated with lysoPS and labeled with Theta* and BODIPY-GM1 or -SM. **(G,J)** Effect of addition of BODIPY-PS or lysoPS at the external leaflet on RBC stretching in PDMS chambers. **(K-O)** Effect of intracellular calcium chelation by BAPTA-AM on the aSMase activity, PS externalization, RBC circularity and lipid domain abundance.

1.4. Discussion

pEl presents a severe form of elliptocytosis, resulting from compound heterozygous mutations on α-spectrin gene SPTA1. The nonsense Arg1811* mutation has not been described before. Expression of the allele carrying this mutation is strongly reduced by nonsense-mediated mRNA decay. The Leu260Pro mutation, already described [423], is located at the end of the second spectrin repeat, next to the linker between α2 and α3 repeats, *i.e.* distal to the tetramerization sites. Although the folding of the domain containing this mutation is normal, the stabilizing interactions between adjacent repeats, and thus the whole proteins, are disrupted [356]. On a mini-spectrin construct incorporating this mutation, reduced tetramer formation is observed without significant changes in the secondary structure [186]. In patients carrying this mutation only, as pElm, these effects are well-compensated by the other allele as α-spectrin is produced in large excess as compared to β-spectrin [430].

The inability of elliptocytotic RBC to recover its original biconcave shape after passage through splenic interendothelial slit was recently linked to impaired elasticity [422]. We here showed that alteration of the RBC membrane, and in particular lipid domains involved in calcium exchanges [163], could represent the molecular link between cytoskeleton and deformation impairment in elliptocytosis, as supported by the following features. Firstly, lipid domains presented lower cholesterol enrichment and cytoskeleton anchorage and calcium exchanges upon RBC stretching were decreased. Secondly, GM1-enriched domain increase upon calcium entry stimulation by Yoda1 was abolished and SM-enriched domain increase upon intracellular calcium depletion by EGTA was lowered. Thirdly, alteration of lipid domain cholesterol content by mβCD exacerbated the calcium increase and worsened the RBC fragility. Those lipid domain modifications could in turn alter PIEZO1 and PMCA activity (Figure S11). Besides, the lower PIEZO1 and PMCA contents, which could result either from aberrant membrane protein sorting during erythropoiesis [190] or a differential loss by membrane fragmentation, could also contribute to impair calcium content and exchange.

Based on chronic inflammation [27] and sickle cell disease [426], our first hypothesis to explain the alteration of lipid domains and calcium exchanges in pEl was the upregulation of the plasmatic aSMase (Figure S11). We reasoned that aSMase could form Cer-enriched domains [26, 431] and/or compete with cholesterol for the formation of domains with SM [427]. Accordingly, we observed that SM-enriched domains exhibited a lower cholesterol content and that Cer-enriched domains increased in abundance in pEl. Moreover, aSMase inhibition by amitriptyline, which has already proven effective in sickle red cells [426], partly restored the calcium content and the morphology of pEl RBCs. However, the aSMase-induced modifications were not accompanied by an increase of the total Cer content. This

unexpected observation was explained neither by Cer metabolism into sphingosine nor by Cer loss through vesiculation/fragmentation. It could alternatively result from oxidation in species like 3-ketoceramide [432] following flipping to the inner leaflet.

Although this hypothesis remains to be tested, it is supported by the fact that signaling cascades via activation of aSMase can be induced by oxidized phospholipids [433, 434]. Moreover, like in sickle cell disease and chronic inflammation, pEl RBCs showed both aSMase upregulation and oxidative stress, as shown by the following lines of evidence. Firstly, ROS strongly accumulate in pEl RBCs. These could originate from abnormal hemoglobin membrane interaction (and its possible auto-oxidation), plasma hemoglobin and free heme increases due to chronic hemolysis as well as calcium signaling via the activation of ROS-generating enzymes [266], as revealed by the ROS reduction upon EGTA. Secondly, membrane lipid peroxidation was considerably increased in pEl. Third, some lysoPS species were also enhanced. These bioactive signaling phospholipids have been shown in neutrophils to be generated following activation of the NADPH oxidase, which produces oxidized PS intermediates as potential substrates of phospholipase A_2 [435, 436] (Figure S11). Besides lipids, oxidative stress could also affect PMCA activity [437-439], hemoglobin and spectrin, thereby altering cytoskeletal protein interactions [440]. However, decrease of the intracellular ROS content by ascorbic acid was inefficient to restore calcium content in pEl and even worsened cell circularity.

Such inefficiency, which is in agreement with absence of effect in sickle cell anemia [249], could be explained by the inability of ascorbic acid to decrease lipid peroxidation. Alternatively, the intracellular calcium accumulation in pEl could have multiple consequences on membrane organization that can not be targeted by ascorbic acid. For instance, we evidenced a higher PKC-dependent phosphorylation of cytoskeletal proteins of the 4.1R complexes as well as of PMCA. Since SM/PC/cholesterol-enriched domains appear to be anchored to the cytoskeleton at 4.1R complexes [161] and are enriched in SM (a target of aSMase locally producing Cer [441] as confirmed here by the increased abundance of Cer domains upon aSMase inhibition), PC (a major source of peroxidation if they are polyunsaturated [442-444]) and cholesterol (known to compete with Cer for the formation of domains with SM [427] as confirmed by the disappearance of cholesterol from SM domains), we propose they provide platforms for the crosstalk between redox signaling and aSMase in pEl. Those domains could be less prone to remodeling upon RBC deformation, precluding formation of new domains needed for deformation and shape restoration. Our model is in agreement with the impaired formation of cholesterol-dependent nanodomains in the CHO cell PM treated with oxidized PC species due to upregulated aSMase activity [445].

Besides the increased activity of calcium-dependent PKC and NADPH oxidase, a higher exposition of PS at the cell surface was observed in pEl despite lower total PS and higher lysoPS levels. PS content modifications at least partially resulted from alterations of enzymes involved in fatty acid and phospholipid synthesis. As the mechanisms behind impaired transversal distribution, we suggested activation of the RBC scramblase PLSCR1 which is known to be activated by the increase of the intracellular calcium but also by the decrease of cholesterol [80], two features seen in pEl RBCs. Based on the recent observation that PS exposure and lysoPS surface insertion in myoblasts suppress PIEZO1 activation leading to impairment of myotube formation [429], we suggest that alteration of PS composition and distribution in pEl will in turn affect the PIEZO1 activity (Figure S11).

Downstream of the alteration of lipid domain and bulk membrane, several perturbations may act in a positive feed-back loop to drive the pathogenesis of elliptocytosis: (i) calcium accumulation and exacerbation of the cytoskeletal instability through PKC activation, (ii) hemolysis and increased ROS production, (iii) increased RBC curvature and aSMase activity [446], and (iv) membrane fragmentation. The latter event is supported by simulation studies [422] and several features provided here, including the RBC perimeter decrease and the rise of oxidative stress, Cer and calcium contents, all known to induce eryptosis and cell fragmentation.

In summary, this study paves the way towards a better understanding of the molecular mechanism behind elliptocytosis. We revealed that plasmatic aSMase and increase of intracellular calcium and oxidative stress cooperate to induce membrane damage and lipid domain impairment, leading to calcium exchange impairment and alteration of RBC curvature and deformation. Moreover, we showed that plasmatic aSMase inhibition by amitriptyline modified lipid domain abundance and partially restored calcium content and RBC circularity, opening new perspectives for treatment.

1.5. Materials and methods

Blood collection and preparation. The study was approved by the Medical Ethics Committee of the University of Louvain, Brussels, Belgium. Blood was collected by venipuncture into K^+/EDTA-coated tubes from healthy volunteers (17 adults, 1 child), the patient (pEl) and her mother (pElm) who gave written informed consent. pEl blood samples were analyzed every 3-6 months from her 14 to 18 years, while pElm came only 3 times. Before experiments blood was diluted 10-fold in glucose- and HEPES (*N*-2-hydroxyethylpiperazine-*N*'-2-ethanesulfonic acid)-containing medium (Invitrogen) and washed twice by centrifugation at 200g for 2min and resuspended. Experiments were carried out on blood maintained for < 5 days at 4°C, except for storage studies.

Chemical treatments. All treatments, except amitriptyline, were performed on diluted washed RBCs. To activate PIEZO1, RBCs were incubated with 0.5µM Yoda1 (Biotechne) for 20sec at RT. To modulate the intracellular calcium content, RBCs were preincubated at RT either in a calcium-free medium containing 1mM of the calcium-chelating agent EGTA (Sigma-Aldrich) for 10min or with 0.2µM of the calcium ionophore A23187 for 15min. To activate protein kinase C (PKC), RBCs were preincubated with 6µM phorbol 12-myristate 13-acetate (PMA; Sigma-Aldrich) and 20nM calyculin A (CalA; Sigma-Aldrich) for 20min at 37°C. For cholesterol depletion, RBCs were preincubated with 0.9mM methyl-β-cyclodextrin (mβCD; Sigma-Aldrich) for 30min at 37°C. To decrease oxidative stress, RBCs were preincubated with 1mM ascorbic acid for 1h at 37°C. For the plasmatic acid sphingomyelinase (aSMase) inhibition, whole blood was incubated with 5µM amitriptyline (Sigma-Aldrich) for 1h at 37°C, then diluted and washed as above. Only EGTA and PMA/CalA were maintained during the whole experiment.

Membrane lipid vital imaging. Endogenous cholesterol labeling (Theta* at 20°C) and BODIPY-lipid membrane insertion (BODIPY-SM, -PC and -ceramide at RT *vs* -GM1 at 37°C) were performed as in [163]. For co-labeling, RBCs were first incubated with Theta* then with BODIPY-lipids. RBCs were either spread onto poly-L-lysine (PLL)-coated coverslips and placed upside down in Lab-Tek chambers (ThermoFisher) or dropped to settle down in µ-Slide VI0.4 uncoated IBIDI chambers (Proxylab), both filled with medium. Samples were observed either with a Zeiss LSM510 confocal microscope (plan-Apochromat 63X 1.4 oil objective) or a Zeiss wide-field fluorescence microscope (Observer.Z1; plan-Apochromat 100X 1.4 oil Ph3 objective).

Calcium, ATP and reactive oxygen species measurements. Intracellular calcium was measured as previously [177]. Calcium exchanges upon RBC deformation were evaluated on RBCs spread onto a PLL-precoated polydimethylsiloxane stretchable chamber (PDMS;

Strex Inc) as in [163]. Intracellular ATP content was measured using a chemiluminescence assay kit (Abcam). Intracellular reactive oxygen species (ROS) content was determined on RBCs incubated in suspension with 15µM 2',7'-dichlorodihydrofluorescein diacetate (H_2DCFDA; Invitrogen) in Krebs-Ringer medium for 60min at 37°C. RBCs were then pelleted, resuspended and measured by spectrofluorimetry (GloMax; Promega) at $\lambda_{exc}/\lambda_{em}$ of 490nm/520nm. Data were reported on the mean corpuscular value (MCV).

Lipid measurements. Total phospholipids were evaluated by phosphorus assay after lipid extraction [447]. Cholesterol content, sphingosine kinase activity and lipid peroxidation were assessed using the following assay kits: Amplex Red cholesterol (Invitrogen) [102, 448], luminescence (Echelon) [449] and malondialdehyde (Abcam) [428]. Phospholipids, cholesterol and malondialdehyde levels were reported on the hemoglobin content. Plasmatic aSMase activity was evaluated on plasma freshly isolated after ficoll separation using the SMase kit (Abcam) [448].

Blood smears. A blood drop was spread onto a superfrost+ slide. The resulting blood smear was fixed in methanol for 5min, colored with May-Grunwald for 5min and with Giemsa (both from Merk Millipore) for 12min and finally washed with water to favor salt precipitation.

Sequencing. DNAs were extracted from whole blood using Wizard genomic DNA purification kit (Promega). SPTA1 gene was sequenced by Ion Torrent technology using a custom-designed Ampliseq panel (www.ampliseq.com) covering the coding exons and 5bp of flanking introns (= splice sites). DNA libraries for pEl were prepared using Ion AmpliSeq Library Kit according to the manufacturer protocol (Life Technologies) with 10ng of DNA for each of the two Ampliseq primer pools. Sequencing was performed on a *Personal Genome Machine* (PGM, Life Technologies), with chip 316. The sequences were aligned to the human reference genome (hg19) with the Ion Torrent Suite Server v5 (Life Technologies) in the form of *.bam* files. These files were imported in Highlander, a software developed in the DDUV Institute (http://sites.uclouvain.be/highlander/), for variant calling with the embarked Torrent variant Caller v5.2 (Life Technologies), annotation and filtering.

RNAs were extracted from whole blood using TRIzol reagent (Invitrogen) and retrotranscribed with moloney murine leukemia virus reverse transcriptase (M-MLV RT; ThermoFisher). For RT-PCR, primers were chosen in exons distant from those carrying the changes of interest (sequences and conditions available on request). Amplicons were purified using the Wizard® SV gel and PCR clean-up system from Promega, and sequenced on an ABI3130xl sequencer with the Big Dye Terminator v3.1 chemistry (Applied Biosystems). Chromatograms were analyzed using CLCbio Main Workbench.

Mass spectrometry. RBC membranes were exploded with hypotonic 5mM PBS and Ghost were generated by recircularization of the membranes in 20mM PBS. Ghost were then lysed in 50mM TEAB, pH 7.6, 150mM NaCl, 1% IGEPAL (CA-630), 0.1% SDS, 0.2% Dodecyl-B-maltoside, 50mM NaF, 5mM Sodium Orthovanadate, 0.5mM PMSF. Detergent was then removed thanks to a spin column (Thermo Fisher Scientific) to obtain proteins in 100mM TEAB. Proteins (300 µg) were then precipitated with 10% TCA and digested sequentially by RapidGest® (Waters) and trypsin. Labelling has been done on 100µg by Tandem Mass Tag (TMT), according to manufacturer's instructions. Alkylation, reduction and acidification were respectively realized with dithiothreitol, chloroacetamide and HCl. Finally phosphopeptides were enriched by $T_{itanium}$ oxide affinity and eluted in 5% ammonia. Samples were vacuum dried in a SpeedVac system before being recovered in solvent A (0.1% TFA in 3.5% ACN), directly loaded onto reversed-phase pre-column (Acclaim PepMap 100, Thermo Scientific) and eluted in backflush mode. Peptide separation was performed using a reversed-phase analytical column (Acclaim PepMap RSLC, 0.075 x 250 mm,Thermo Scientific) with a linear gradient of 4%-32% solvent B (0.1% FA in 98% ACN) for 110 min, 32%-60% solvent B for 10 min, 60%-95% solvent B for 1 min and holding at 95% for the last 10 min at a constant flow rate of 300 nl/min on an EASY-nLC 1000 UPLC system. The peptides were analyzed by an Orbitrap Fusion Lumos tribrid mass spectrometer (ThermoFisher Scientific). The peptides were subjected to NSI source followed by tandem mass spectrometry (MS/MS) in Fusion Lumos coupled online to the UPLC. Intact peptides were detected and quantified using the synchronous precursor selection (SPS)-based MS3 scan routine implemented in the Orbitrap Fusion Lumos tribrid instrument. The Orbitrap Fusion Lumos was operated at a positive ion spray voltage of 2100 V and a transfer tube temperature of 275°C. Briefly, the full scan was performed in the range 375-1500 m/z at a nominal resolution of 120 000 and AGC set to $4x10^5$, followed by selection of the most intense ions above an intensity threshold of 5000 for collision-induced dissociation (CID)-MS2 fragmentation in the linear ion trap with 35% normalized collision energy. The isolation width was set to 0.7 m/z with no offset. The top 10 fragment ions for each peptide MS2 was notched out with an isolation width of 2 m/z and co-fragmented to produce MS3 scans analysed in the Orbitrap at a nominal resolution of 30 000 after higher-energy collision dissociation (HCD) fragmentation at a normalized collision energy of 65%. Raw data files from Orbitrap Fusion Lumos were processed using Proteome Discoverer (version 2.3). MS/MS spectra were searched against the UniprotKB Human proteome reference database (87 489 total sequences). SEQUEST parameters were specified as: trypsin enzyme, two missed cleavages allowed, minimum peptide length of 6, TMT tags on lysine residues and peptide N-termini (+229.1629 Da) and carbamidomethylation of cysteines residues (+ 57.0214 Da) as fixed modifications and oxidation of methionine residues (+ 15.9949 Da) as a variable modification, precursor mass tolerance of 20 ppm, and a fragment mass tolerance of 0.6 Da. Peptide spectral match (PSM) error rates were determined using the target-decoy

strategy coupled to Percolator modeling of true and false matches. Reporter ions were quantified from MS3 scans using an integration tolerance of 20 ppm with the most confident centroid setting. An MS2 spectral assignment false discovery rate (FDR) of less than 1% was achieved. Following spectral assignment, peptides were assembled into proteins and were further filtered based on the combined probabilities of their constituent peptides to a final FDR of 1%. The mass spectrometry proteomics data have been deposited to the ProteomeXchange Consortium (http://proteomecentral.proteomexchange.org) via the PRIDE partner repository with the dataset identifier <PXD000xxx>."

Scanning electron microscopy of RBCs on filters. Washed RBCs were fixed in graded concentrations (0.1% followed by 0.5% then 1.5%) of glutaraldehyde in 0.1M cacodylate buffer for 5min each. Fixed RBCs were then filtered on 0.4µm polycarbonate (it4ip) filters using a syringe and washed by cacodylate buffer pushed gently through the syringe. Post-fixation was performed on the filters in the syringe in 1% OsO_4 in 0.1M cacodylate for 2h. Filters were then washed extensively in 0.1M cacodylate and 6 times for 10min in water. Samples were dissociated from the filter capsule and covered by a second filter in order to protect the sample during further processing, *i.e.* the dehydration and the critical point drying. Dehydration was performed in graded baths of ethanol (50, 60, 70, 80, 90, 95% for 10min each, followed by 100% 3 times for 10min) and critical point dried. Finally, samples were mounted on scanning electron microscopy stubs and sputtered with 10nm gold. All samples were observed in the CM12 electron microscope with the SED detector at 80kV.

Transmission electron microscopy of the RBC cytoskeleton. Formvar/carbon-coated grids were treated with PLL for 15min at RT and washed extensively (3x in water and 2x in medium). Grids were then seeded with washed diluted RBCs for 7min in medium, rinsed 3 times in medium and permeabilized in 0.5% Triton X-100 for 3min at RT. Grids were then washed 3 times in medium, fixed for 15min in 1% glutaraldehyde in 0.1M cacodylate, washed in buffer and post-fixated in 1% OSO_4 in 0.1M cacodylate for 60min at 4°C. Grids were again extensively washed (6x 5min in 0.1M cacodylate and 3x in water) and stained in 1% uranyl acetate for 30min at RT. Finally, samples were washed (6x 10min) in water and overnight air-dried. Samples were then observed in the CM12 electron microscope in transmission mode at 80kV.

Immunofluorescence staining of RBC membrane and cytoskeleton proteins. Diluted washed RBCs were spread onto PLL-precoated coverslips, fixed with 4% paraformaldehyde for 10min and blocked with 1% bovine serum albumin (BSA; Sigma-Aldrich) for 30min. To label membrane proteins, RBCs were then incubated for 1h with rabbit monoclonal antibodies to glycophorin C (Abcam) together with mouse monoclonal antibodies to CD47 (Invitrogen), washed 4 times in 1% BSA, incubated for 1h with the

appropriate Alexa-secondary antibodies (5µg/ml) and washed 4 times with 1% BSA. Total spectrin was revealed with antibodies against α/β-spectrins (Abcam) using the same protocol as above except that a permeabilization step with 0.5% Triton X-100 for 3min was done before the fixation. All coverslips were mounted in Mowiol in the dark for 24h and examined with a Zeiss LSM 510 confocal microscope using a plan-Apochromat 63x NA 1.4 oil immersion objective.

Lipid quantification. The quantification was achieved as previously described[450, 451]. Briefly, lipids from $250*10^6$ RBCs or fragments and microvesicles were measured after liquid/liquid extraction and SPE purification in the presence of respective internal standards. Lipid fractions were then analyzed using a LTQ Orbitrap mass spectrometer coupled to an Accela HPLC system (both from Thermo Fischer Scientific). Analyte separation was achieved using a Kinetex LC-18 column coupled to an appropriate guard column (Phenomenex). For the analyses, we used two mobile phase systems as described in Guillemot-Legris et al. for lysophospholipids, phospholipids, sphingomyelin and sphingosine[450] and in Mutemberezi et al. for oxysterols and ceramides[451]. Lipid relative quantification was based on the ratio of area under the curve (AUC) of the lipid species on the AUC of the respective internal standard. The data are normalized to the CTL red blood cells condition (expressed in %).

Coomassie blue and Western blotting. RBC ghosts were prepared using a hypo-osmotic hemolysis method at 4°C[452]. Ghosts were then analyzed using 4-15% sodium dodecysufalte-polyacrylamide gel electrophoresis (SDS-PAGE; Bio-rad) and PageBlue™ Protein staining solution (ThermoFisher) following Fairbanks et al instruction[453]. Quantification of the relative abundance of proteins in PageBlue stained gels was performed using Fiji software. Western blotting were performed using antibodies against PIEZO1 (ProteIntech), PMCA (ThermoFisher) or GAPDH (Invitrogen), followed by HRP-conjugated secondary antibodies and revelation by chemiluminescence (SuperSignal® west pico/femto chemiluminescent substrate, ThermoFisher) with the Fusion Solo S from Vilber.

RBC hemoglobin release measurements. Four types of measurements were performed. Firstly, to evaluate the effect of a chemical agent, washed RBCs were incubated with the agent as explained above in isosmotic medium (*i.e.* 320mOsm) and pelleted by centrifugation at 200g for 2min. Supernatants and pellets broken with 0.5% Triton X-100 were both assessed for hemoglobin at 450nm in 96-well plates (SpectraCountTM, Packard BioScience Co). Hemoglobin release in the supernatant was expressed as percentage of the total hemoglobin present in the sample. Secondly, to compare RBC fragility between donors, washed RBCs were incubated in isosmotic medium for 1h at 37°C under constant agitation, centrifuged, collected and measured for hemoglobin release as above. Thirdly, to

measure RBC osmotic resistance, washed RBCs were maintained at 37°C under constant agitation for 16h. RBCs were then incubated into gradually hypotonic media at RT for 10min and pelleted by centrifugation at 200g for 2min. Supernatants and pellets were separated and assessed for hemoglobin release as above. Ratio of the supernatant to the sum of the supernatant and the pellet for each medium was expressed as percentage of the hemoglobin released upon RBC full hemolysis (*i.e.* RBCs in 0mOsm). Half-maximal effective hemolysis (EC50) was finally extrapolated using GraphPad Prism. Fourth, cryohemolysis was measured at Saint-Luc Hospital following Strechman and Gescheidt's instructions[454].

Isolation and analysis of microvesicles. Whole blood maintained for 0, 7 or 14 days at 4°C was centrifuged at 2000g for 10min. The plasma was recovered and centrifuged again at 2000g for 10min. The obtained plasma was diluted in sterile filtered PBS and centrifuged at 20.000g for 20min at 4°C. The resulting pellet was resuspended in sterile PBS before reiteration of the centrifugation step at 20.000g. The final pellet was resuspended in 1ml sterile PBS. Part of the pellet was fixed and allowed to attach for 8min onto coverslips pretreated with PLL. Coverslips were then washed, fixed on 1% glutaraldehyde in 0.1M cacodylate and processed by scanning electron microscopy as for RBCs on filters (see above). The other part of the pellet was kept at -80°C for determination of the microvesicle size and abundance using a Zetaview® from Particle Metrix.

Phosphatidylserine externalization. Washed diluted RBCs were incubated with Annexin-V Alexa 647 (Invitrogen) in calcium-containing medium upon constant agitation at RT for 15min. Labelled RBCs were then laid down on PLL-precoated coverslips, placed upside-down in labTek chambers and analyzed by confocal vital imaging, using the Zeiss LSM510 microscope, as above.

Image analysis and data quantification. RBC morphology (area, perimeter, circularity), spectrin intensity/occupation and line intensity profiles on confocal images as well as protein abundance on SDS-PAGE and western blots were determined using the Fiji software. Line intensity profiles were further analyzed for the (non)-overlapping between GPC and CD47 as follows. After threshold value determination to define the effective dynamic range, peaks were identified and classified into three categories: (i) only red, indicating non-overlapping of GPC with CD47; (ii) only green, indicating non-overlapping of CD47 with GPC; and (iii) red+green, indicating overlapping between both proteins. The abundance of peaks in each category was then expressed as percentage of total peaks. For simple and double labeling, lipid domain abundance/hemi-RBC surface was assessed by manual counting on confocal or fluorescence images and expressed by reference to the hemi-RBC projected area.

Data presentation and statistical analyses. Data are expressed as means ± SEM when the number of independent experiments was n≥3 or means ± SD if n≤2, except for RBC morphology. In the latter case, a representative experiment is presented in the figure to highlight the distribution within the sample while the statistical analysis is indicated in the legend. Statistical tests were performed only when n≥3. Two-sample t-test or one-way ANOVA followed by Bonferroni's post-hoc test were used in lipid domain abundance experiments while non-parametrical tests (Mann-Whitney test or Kruskal Wallis followed by Dunn's comparison test) were preferred in the other cases. ns, not significant; *, $p<0.05$; **, $p<0.01$; ***, $p<0.001$.

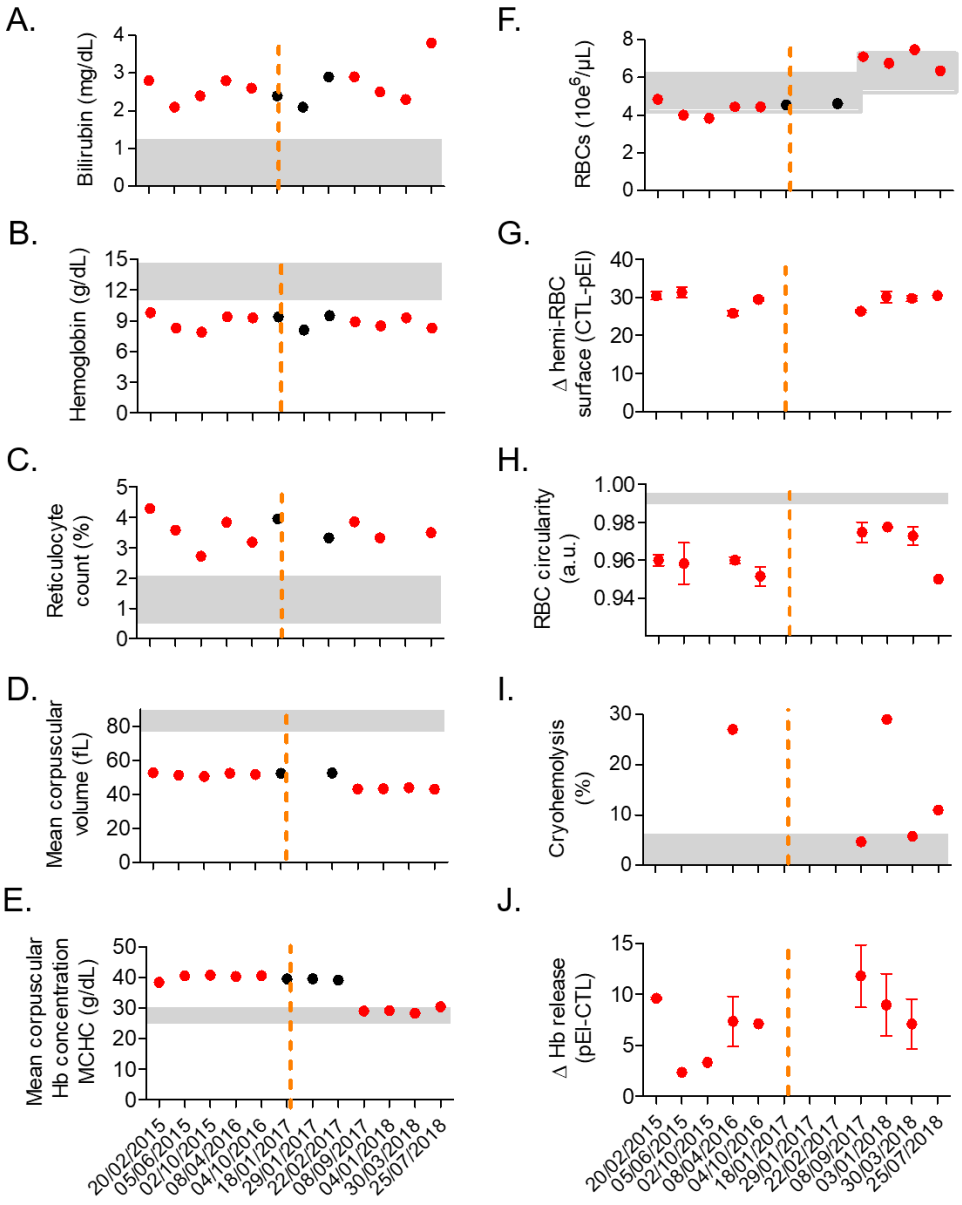

Supplemental Figure 1. Evolution of diagnostic parameters as well as RBC morphology and fragility in pEI throughout the study. (A-F) Parameters used to monitor the disease. Cholecystectomy was performed in January 2017 (orange dotted line) to avoid chronic inflammation due to gallstones. The normal range expected for pEI age is indicated by grey boxes. Red dots indicate venipunctures at which experiments have been performed. **(G-J)** Evolution of RBC surface projection (G), circularity (H) and fragility (I,J).

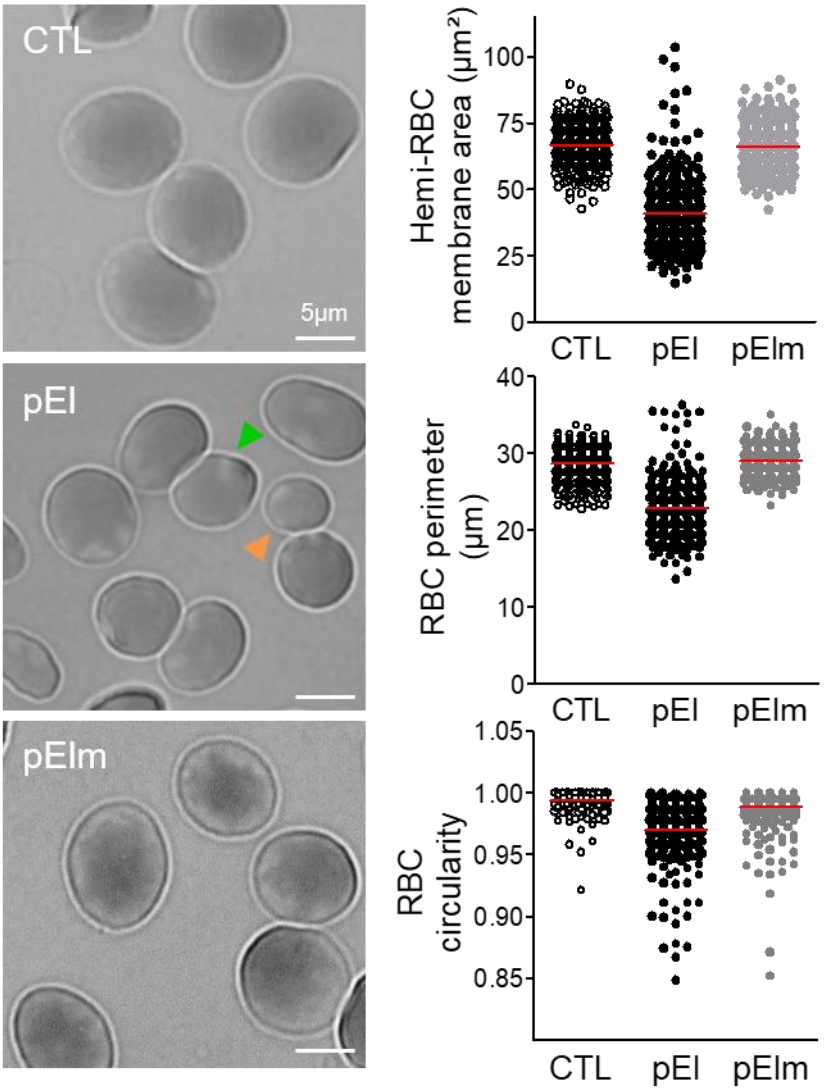

Supplemental Figure 2. Decreased membrane surface, perimeter and circularity of pEl RBCs on PLL-coated coverslips – Extension of Figure 1B. RBC hemi-surface, RBC perimeter and circularity determined on microscopy images of living RBCs laid down on PLL-precoated coverslips. Left, representative images; green arrowhead, poïkilocytotic RBC; orange arrowhead, small spherical RBC. Right, quantification shown for one representative PLL-coated coverslip per condition (n=20; area and perimeter: CTL *vs* pEl: ***, CTL *vs* pElm: ns, pEl *vs* pElm: ***; circularity: CTL *vs* pEl: ***, CTL *vs* pElm: *, pEl *vs* pElm: *).

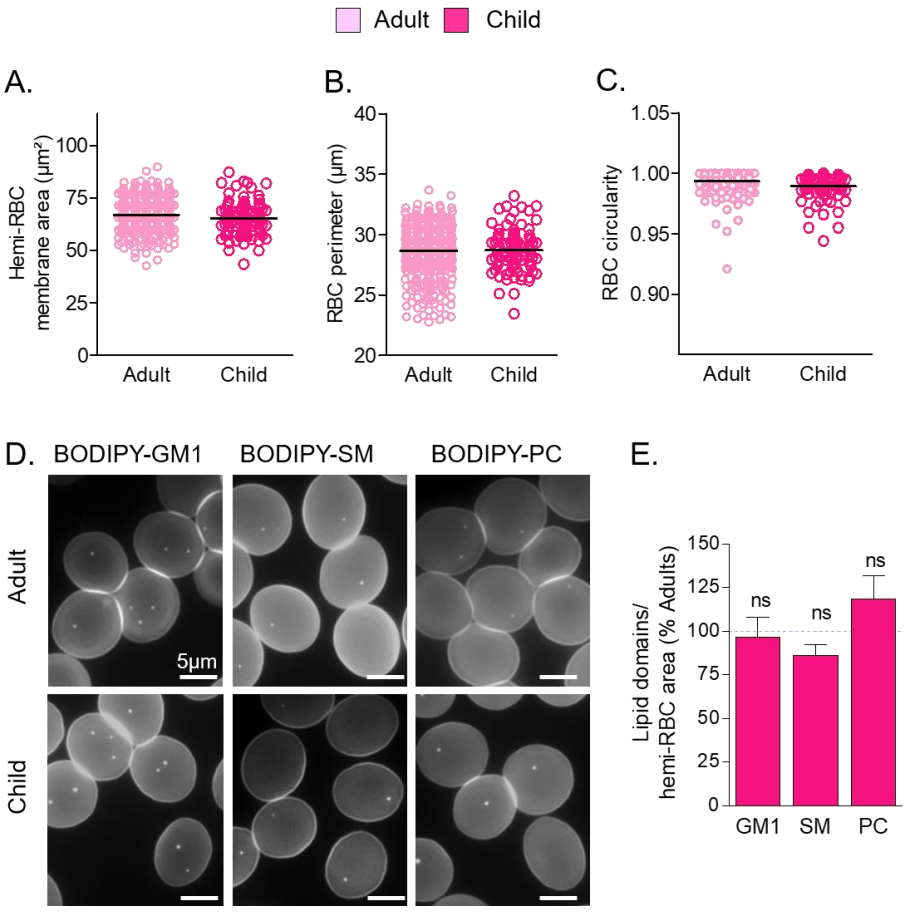

Supplemental Figure 3. Comparison of adult and child healthy donors for RBC morphology and lipid domain abundance. Washed and diluted RBCs from adults or child were spread onto PLL-coated coverslips, labeled with BODIPY-GM1, -SM or -PC and directly visualized by fluorescence microscopy. **(A-C)** Quantification of the hemi-RBC membrane area, perimeter and circularity for one representative coverslip (out of 4). **(D)** Representative images of lipid domains. **(E)** Quantification of lipid domain abundance per hemi-RBC area (means ± SEM from 3 independent experiments/lipid and 300-600 RBCs were counted per condition in each experiment).

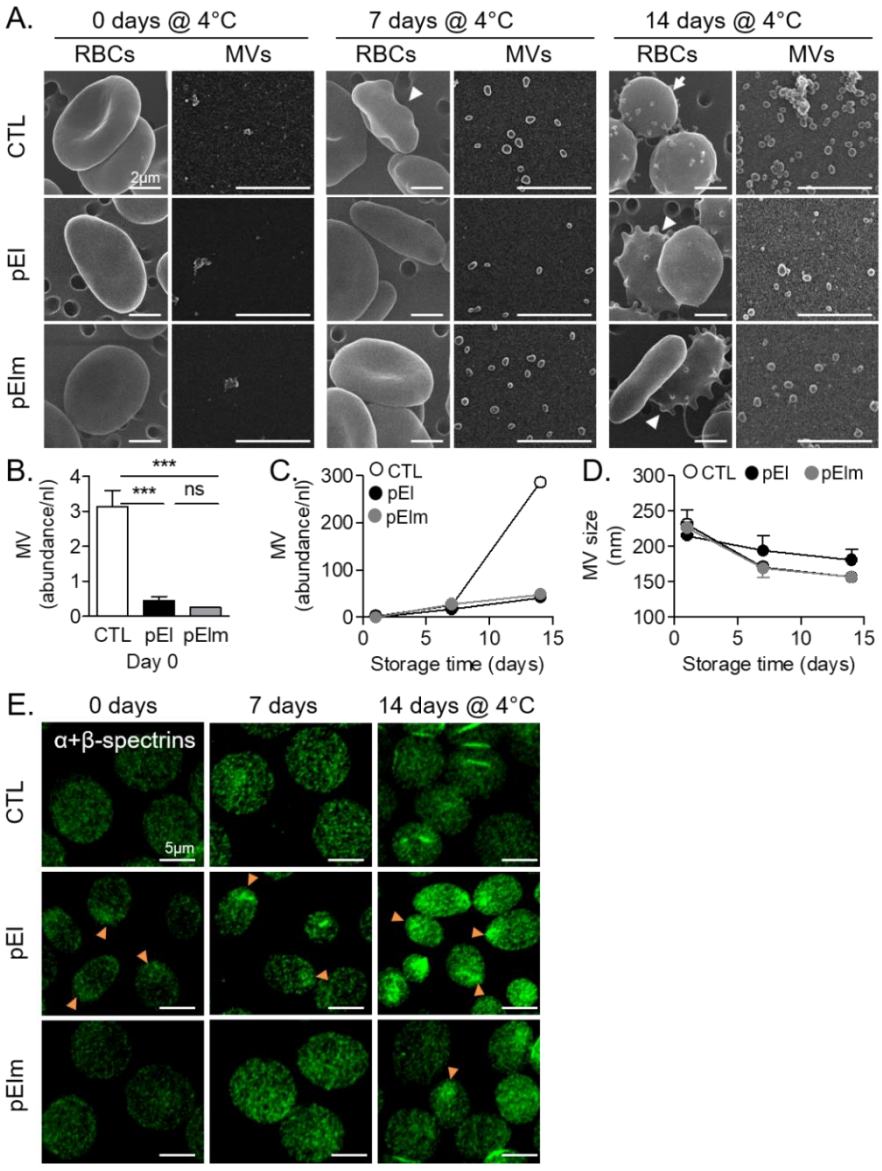

Supplemental figure 4. Evolution of the RBC morphology, microvesicles release and spectrin density during blood storage at 4°C. (A) Representative scanning electron microscopy images. RBCs maintained at 4°C for the indicated times were washed, fixed in suspension and laid down on filters (left images). MVs, isolated from the same blood samples by multiple centrifugation steps, were laid down on PLL-precoated coverslips and fixed (right images). Arrowheads, echinocytes; arrow, spherocyte. Representative images of 2 independent experiments. **(B-D)** Abundance and size of MVs, either from fresh blood (B) or upon storage (C,D) (means ± SD of 3 independent measures of the same MV preparations). **(E)** Spectrin density determined as in Figure 2A (3 experiments). Orange arrowheads point to increased spectrin density.

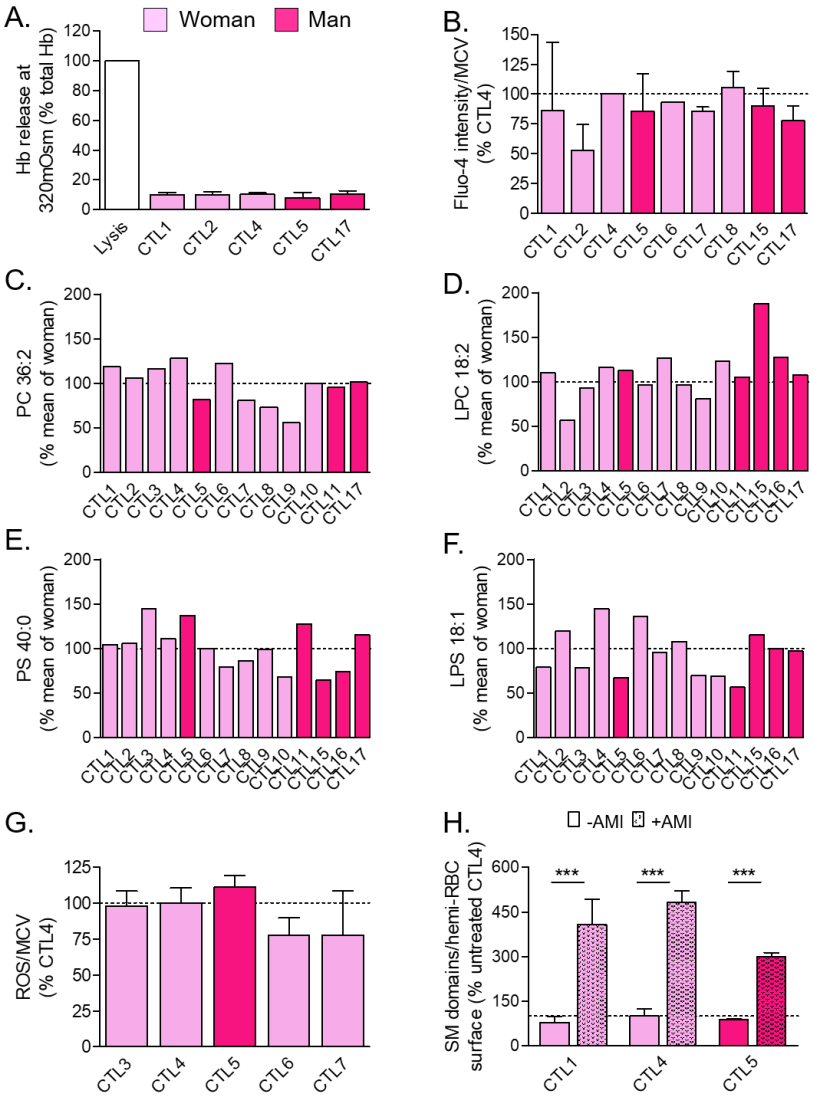

Supplemental Figure 5. Comparison of different healthy donors for RBC fragility, intracellular calcium and ROS contents, lipid content and abundance of lipid domains. (A) Hemoglobin release determined after blood incubation at 37°C for 1h (means ± SEM of 3 independent experiments). **(B,G)** Intracellular calcium and ROS contents measured as in Figures 3F and 6D and expressed as percentage of healthy donor 4 (CTL4) (means ± SD of 1 to 6 independent experiments). **(C-F)** PC 36:2, lysoPC 18:2, PS 40:0 and lysoPS 18:1 species determined by lipidomics, expressed as percentage of healthy woman and taken as examples of lipids highlighted at Figures 7 and S10. **(H)** SM-enriched domain abundance on RBCs pretreated or not with amitriptyline (AMI) (means ± SEM of 3-4 independent experiments and 200-400 RBCs were counted per condition in each experiment).

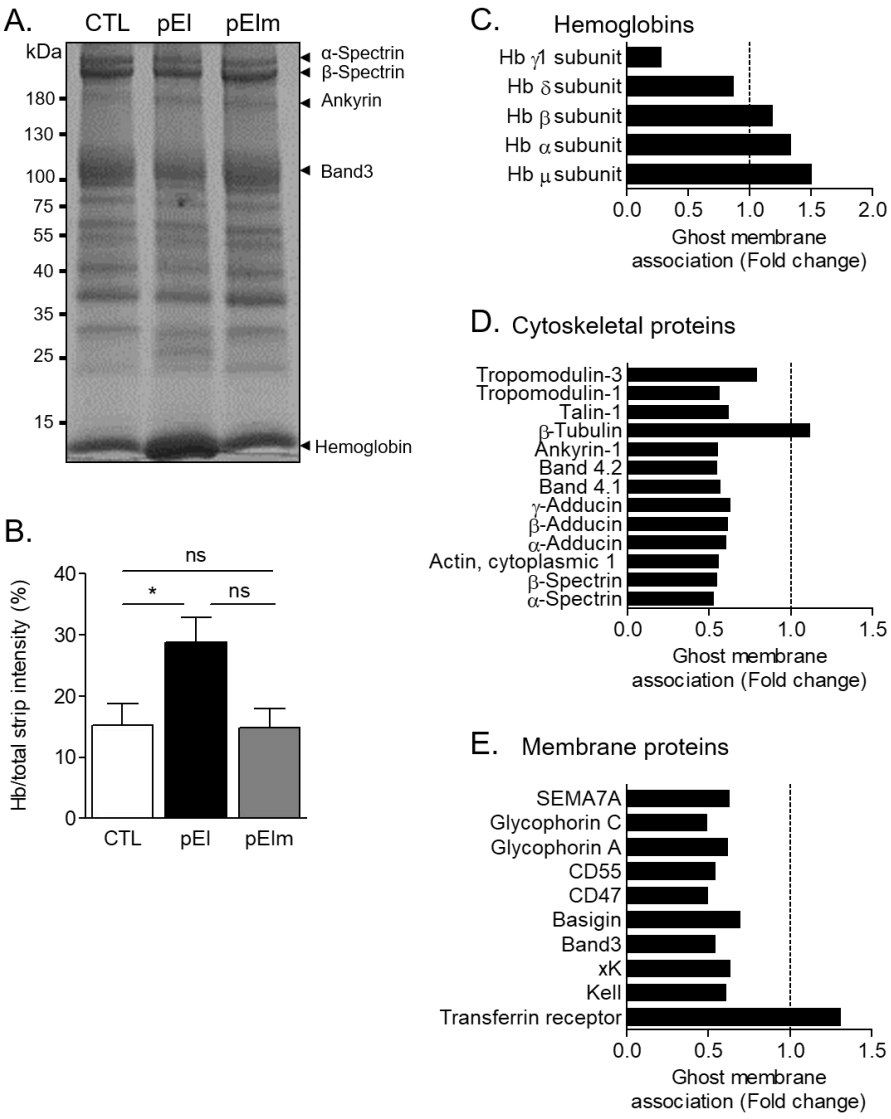

Supplemental Figure 6. Decrease of the major RBC cytoskeletal and membrane proteins contrasting with higher hemoglobin retention in the pEl ghost membrane. (A,B) Abundance of hemoglobin retained in the ghost membrane determined by SDS-PAGE. (A) Representative SDS-PAGE and Coomassie blue staining of ghost membrane proteins. (B) Quantification of hemoglobin (Hb) associated with the membrane, expressed as the percentage of the sum of all strips in the track. All data are means ± SEM of 4-8 independent experiments. **(C-E)** Abundance of hemoglobin subunits (C), major cytoskeletal proteins (D) and main membrane proteins (E) associated with the ghost membranes and determined by mass spectrometry. Data are shown for pEl and expressed by reference to healthy ghosts.

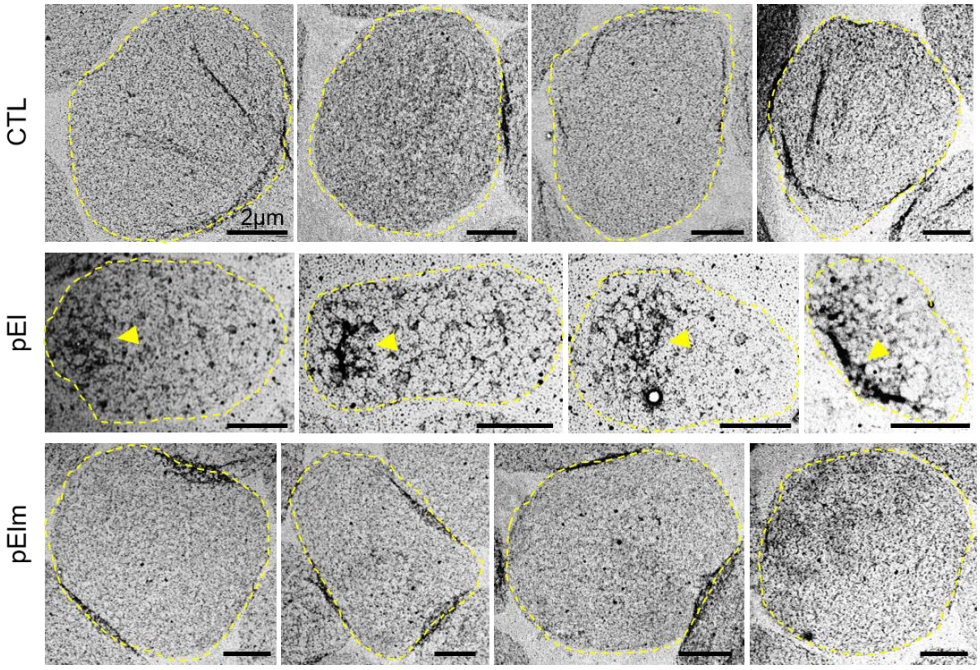

Supplemental Figure 7. Gathering of cytoskeleton proteins at one edge of pEl RBCs – Extension of Figure 2D. RBCs were laid down on PLL-precoated formvar coated grids, permeabilized with 0.5% Triton X-100, fixed and analyzed by transmission electron microscopy. Yellow lines, outlines of the RBCs. Yellow arrows, increased protein density.

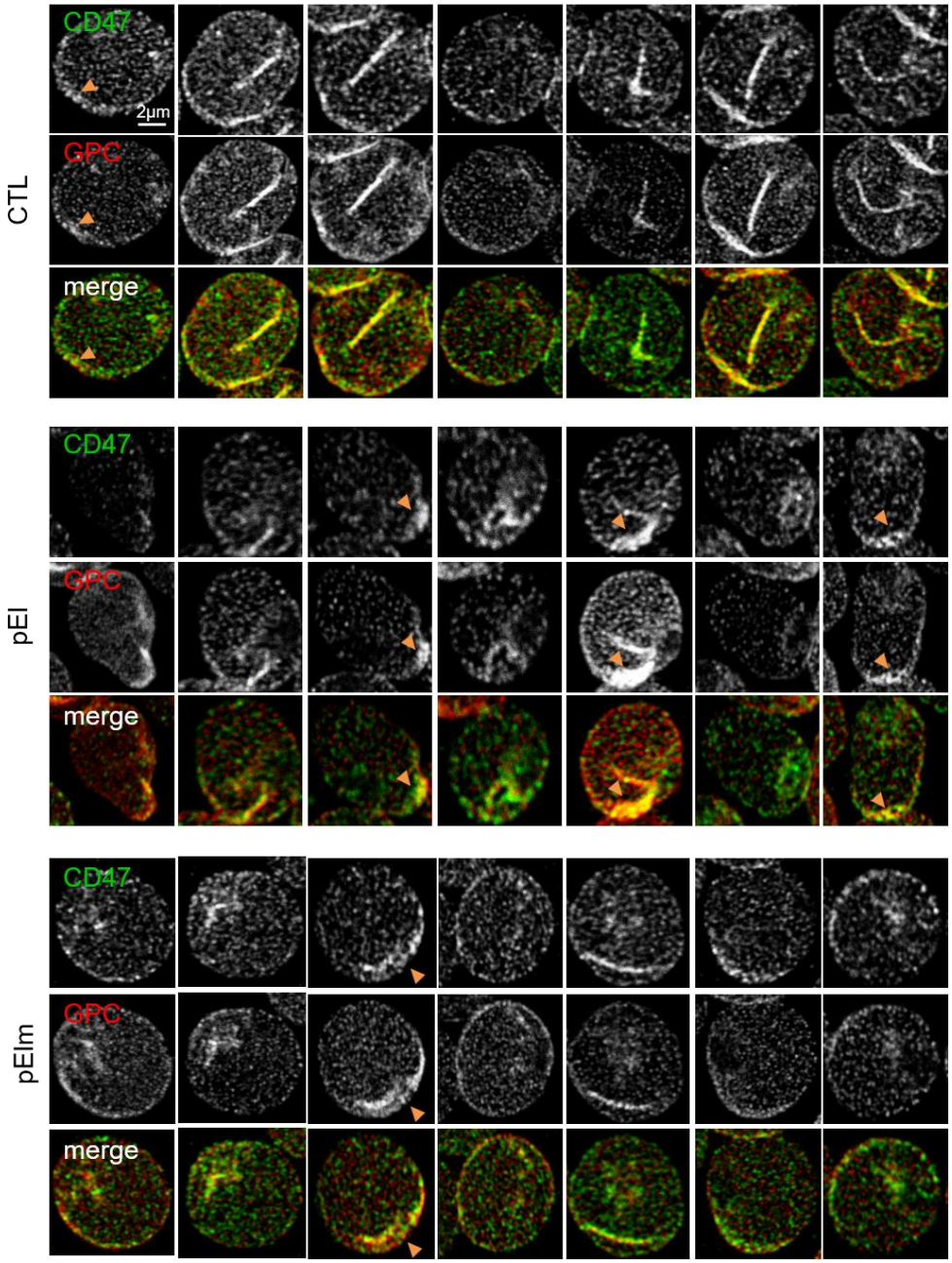

Supplemental Figure 8. Altered distribution of membrane proteins from the two anchorage complexes – Gallery of images presented at Figure 2E. RBCs were laid down on PLL-precoated coverslips, fixed and stained with antibodies against CD47 (ankyrin complexes; green) and glycophorin C (GPC; 4.1R complexes; red). Orange arrowheads point to high local protein density.

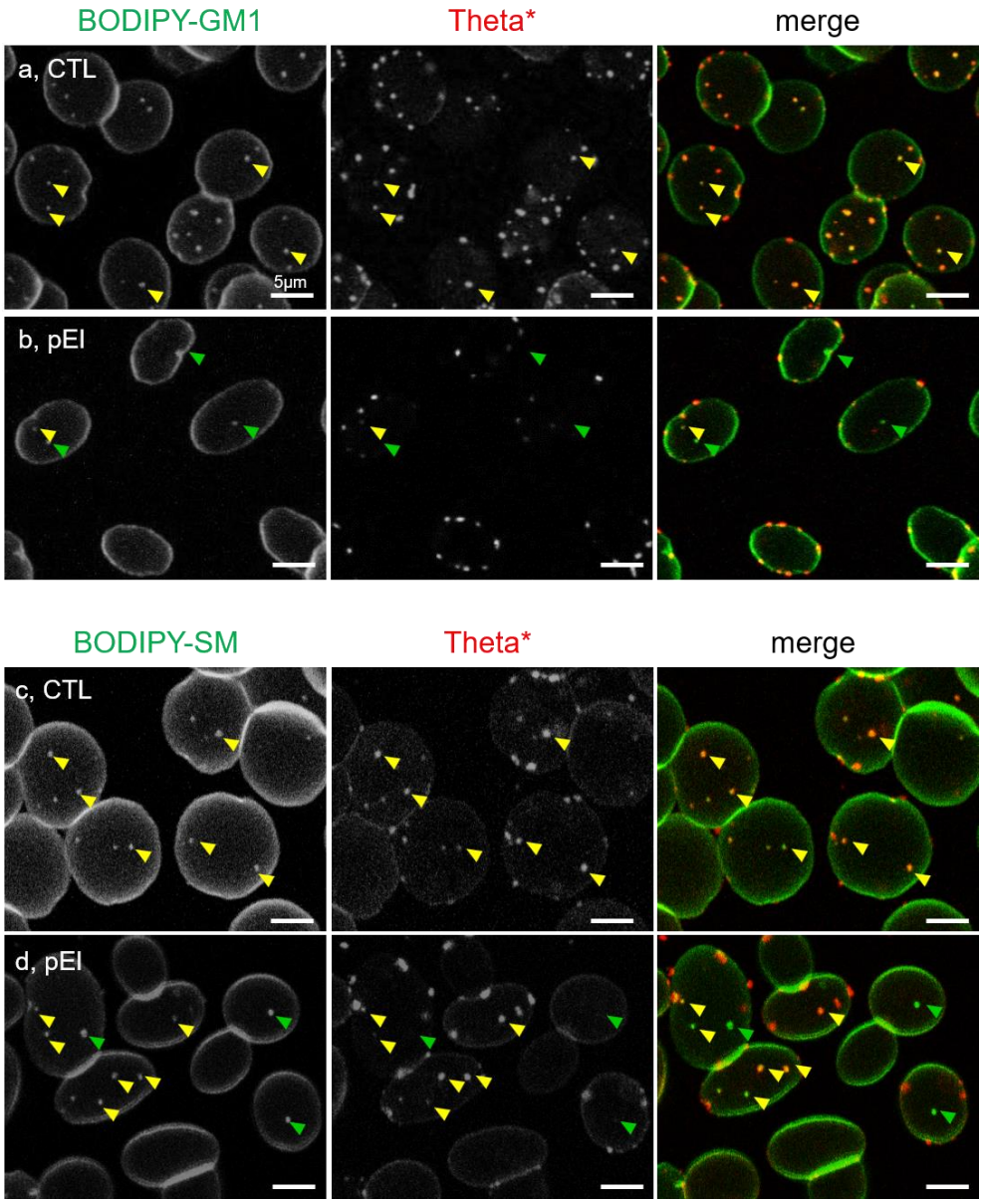

Supplemental Figure 9. Lower spatial association of GM1- and SM-enriched domains with those enriched in cholesterol (Theta*) in pEl RBCs - Illustration of quantification presented at Figure 4B. RBCs were labeled in suspension with Theta*for cholesterol, spread onto coverslips and labeled with either BODIPY-GM1 (a,b) or -SM (c,d). Green arrowheads, BODIPY-GM1 or -SM only; yellow arrowheads, BODIPY-GM1/Theta* or BODIPY-SM/Theta* co-labelled domains. Images presented at (a,b) and (c,d) are representative of 2 and 3 independent experiments, respectively.

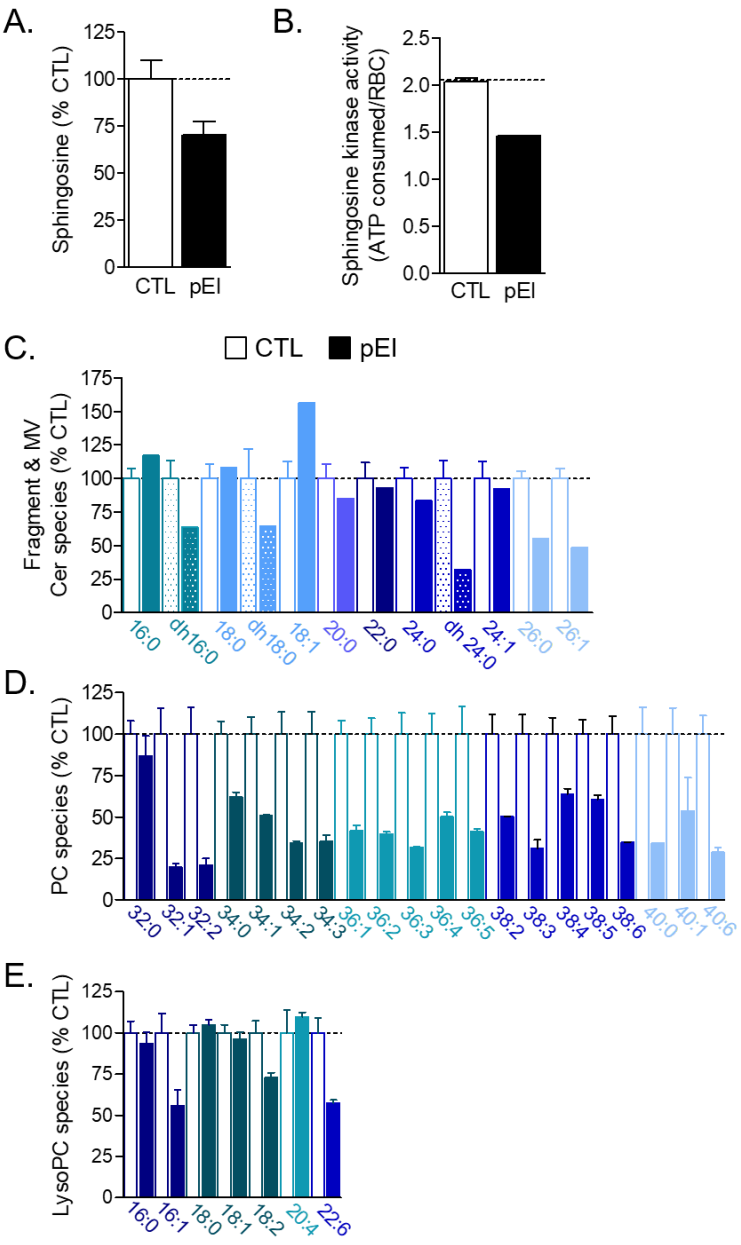

Supplemental Figure 10. Decreased sphingosine and sphingosine kinase activity as well as PC and lysoPC species in pEI RBCs – Extension of Figures 5 and 7. (A) RBC sphingosine assessed by HPLC-MS on washed, lysed and lipid-extracted RBCs. **(B)** RBC membrane sphingosine kinase activity measured by consumption of ATP added to the samples (means ± SD of quadruplicates from 1 experiment). **(C)** Fragment /microvesicle-associated Cer species. RBCs were washed, supernatants were collected, lysed and assessed by lipidomics. Cer and dihydro (dh)-Cer species are classified based on fatty acid length and insaturation number and results are expressed as percentage of results obtained in control RBCs fragments (mean of 7 healthy women). **(D,E)** RBC-associated PC and lysoPC species. RBCs were washed, lysed, extracted for lipids and assessed either for PC (D) or lysoPC (E). Species are classified based on fatty acid length and insaturation number and results are expressed as percentage of controls (mean of 9 healthy women).

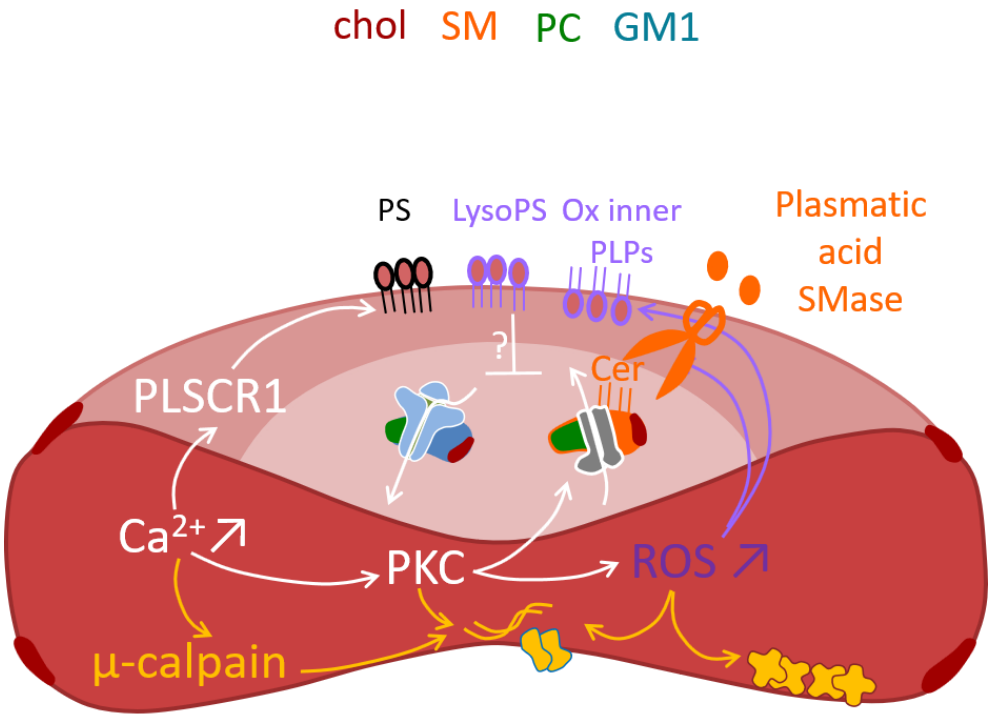

Supplemental Figure 11. Model for the molecular mechanism behind the pathogenesis of elliptocytosis. Increased of intracellular calcium levels lead to activation of calcium-dependent PKC, which in turn is responsible for activation of NADPH oxidase activity and ROS accumulation into RBCs. ROS act then on phospholipids from the inner leaflet leading to lipid peroxidation, which may be the cause for 1) alteration of membrane lipids content, 2) modifications of membrane lipid organization into lipid-enriched domains and by consequence alteration of calcium exchanges, and 3) activation of plasmatic aSMase through oxidized phospholipids [433, 434]. Enhancement of plasmatic aSMase activity lead to formation of Cer-enriched domains and modifications of the lipids content, especially into the SM-enriched domains. On the other hand, the raise of intracellular calcium and the decrease of cholesterol (chol) content lead to activation of scramblase activity (possibly PLSCR1) and abnormal exposure of PS at the membrane outer leaflet.

2. Publication 2: Calcium accumulation and alteration of membrane transversal and lateral heterogeneity correlate with the severity of hereditary spherocytosis

H. Pollet[1,*], A.S. Cloos[1,*], L. Conrard[1], A. Dumitru[2], S. Verstraeten[3], A. Stommen[1], M. Lingurski[1], P.J. Courtoy[1], C. Vermylen[4], B. Brichard[4], M. Vikkula[5,6], P. Henriet[1], P. Brouillard[5], P. Van Der Smissen[1], D. Alsteens[2] and D. Tyteca[1]

Université catholique de Louvain, 1200 Brussels, Belgium
[1] CELL Unit, de Duve Institute
[2] Louvain Institute of Biomolecular Science and Technology
[3] Pharmacologie Cellulaire et Moléculaire, Louvain Drug Research Institute
[4] PEDI Unit, Institut de Recherche Expérimentale et Clinique
[5] Human Molecular Genetics, de Duve Institute
[6] Walloon Excellence in Life Sciences and Biotechnology (WELBIO), de Duve Institute
*, co-first authors

In preparation

Keywords : red blood cell fragility, microvesicle release, spectrin network, ankyrin, young's modulus, membrane rigidity, membrane asymmetry, sphingomyelinase, calcium, lipid domains, cholesterol, phospholipids

2.1. Abstract

Hereditary spherocytosis is the most common inherited hemolytic anemia mainly resulting from mutations in the genes encoding for ankyrin (*ANK1*), Band3 (*SLC4A1*) or β-spectrin (*STPB*). It is characterized by round-shaped less deformable RBCs, possibly due to loss of membrane by microvesiculation, and by the increase of intracellular calcium. However, the etiologic relationship between cytoskeleton defect, membrane loss and calcium increase is not established. We here explored this question in ten splenectomised patients from seven families exhibiting *ANK1* or *SPTB* mutations. In all patients, the mRNA of the allele carrying the mutation was degraded by the nonsense-mediated mRNA decay mechanism. Three groups of patients were defined based on clinical parameters and RBC morphology and deformability features. Although β-spectrin and ankyrin mutations led to differential RBC morphology, cytoskeletal organization defect and rigidity, cholesterol and total phospholipid content loss as well as microvesicles release, none of those features did correlate with the disease severity. Instead, the rise in intracellular calcium and ATP represented two factors to consider upon evaluation of the disease severity. On one hand, the intracellular calcium accumulation contributed to spherocytosis through the impairment of the plasma membrane asymmetry (exposition of phosphatidylserine at the RBC surface) and potentially additional calpain-dependent cytoskeleton alteration but not through increased oxidative stress. Such calcium accumulation could result from the decreased abundance of the mechanosensitive cation channel PIEZO1 and its activity through the impaired response of the ganglioside GM1-enriched domains to calcium influx stimulation by Yoda1. On the other hand, the rise in intracellular ATP lowered the disease severity by limiting the intracellular calcium rise, possibly through direct stimulation of the calcium efflux pump PMCA activity and/or maintenance of the membrane asymmetry and the functionality of the sphingomyelin-enriched domains. Based on the integration of the intracellular calcium and ATP content modifications and the resulting alterations of membrane transversal and lateral heterogeneity in lipid domains, the ten patients were classified into three groups that perfectly matched with the disease severity score defined by clinical parameters and RBC morphology and fragility. This indicated that clinical heterogeneity in spherocytosis can be defined by the calcium-dependent membrane defects.

2.2. Introduction

Hereditary spherocytosis is the most common hereditary hemolytic anemia characterized by round-shaped less deformable RBCs. It is inherited in an autosomal dominant fashion in 75% of the cases while the 25% remnant are inherited in an autosomal recessive fashion or *de novo* mutations [295, 298, 299]. Autosomal dominant hereditary spherocytosis is often found to have primary mutations in the genes encoding for ankyrin (*ANK1*), Band3 (*SLC4A1*) or β-spectrin (*STPB*). Recessive mutations occur due to homozygous mutations in protein 4.2 gene (*EPB42*) or homozygous or compound heterozygous for α-spectrin (*SPTA1*). Most of the mutations described are "private" or of sporadic occurrences, *i.e.* they are specific to one or a few families. The only treatment is splenectomy, allowing to preserve less deformable but still functional RBCs.

In physiological contexts, RBC deformability and thereby functionality depend on several features. The first one is the RBC cytoskeleton, which is at the same time well-organized, robust and flexible. It is composed of a meshwork of spectrin tetramers linked to the lipid bilayer by two non-redundant anchorage complexes based on 4.1R and ankyrin proteins [185]. The 4.1R anchorage complexes allow for spectrin horizontal linkages whereas the ankyrin anchorage complexes ensure most of the vertical linkages between the spectrin meshwork and the lipid bilayer by creating a complex involving ankyrin, Band3 and CD47, *a.o*. [185]. Second, the RBC benefits from a finely regulated cytoplasmic viscosity controlled by the intracellular hemoglobin concentration. Third, the RBC deformation depends on a transient rise of intracellular calcium which in turn activates Gardos channels, leading to cell dehydration, and favors the local uncoupling between the membrane and the underlying spectrin cytoskeleton [148]. The RBC calcium entry is thought to be mostly operated by PIEZO1, a mechano-activated cation channel [210], while the calcium efflux is ensured by the Plasma Membrane Calcium ATPase (PMCA). Fourth, metabolic processes controlling the ATP content and the redox state also contribute to the deformability process [455-458]. The extensive antioxidant system in RBC is designed to neutralize the harmful reactive oxygen species generated through the constant exposure to variable oxygen pressures. Fifth, the RBC exhibits a very high cholesterol/phospholipid ratio as compared to other cells. Moreover, those lipids are not randomly distributed at the RBC surface but are organized into three types of submicrometric lipid domains that contribute to RBC deformation [102, 161-163, 175, 176]. The first ones, mainly enriched in cholesterol, are associated with high-curvature RBC areas and gather in highly-curved membrane areas upon RBC deformation [177]. The second ones, enriched in the ganglioside GM1, phosphatidylcholine and cholesterol, are associated with RBC low-curvature areas and increase in abundance upon activation of PIEZO1, suggesting their contribution to calcium

influx [163, 210]. The third ones, enriched in sphingomyelin, phosphatidylcholine and cholesterol, are also associated with RBC low-curvature areas and increase in abundance upon RBC shape restoration after deformation and upon calcium extrusion [163, 177].

Although the main molecular defects associated with spherocytosis are heterogeneous, the weakening of vertical linkage between the cytoskeleton and the lipid bilayer could be a common feature, leading to the lipid bilayer destabilisation and the release of microvesicles (MVs) when RBCs pass in thin capillaries or through interendothelial slits of the spleen [386]. Simulation studies have confirmed that membrane loss occurs by membrane vesiculation in spherocytosis [422], resulting in skeleton free-vesicles more diverse in size than those released in healthy RBCs [459]. Such MV release has three potential consequences for the RBC: (i) the loss of key proteins and lipids; (ii) the reduction of the surface-to-volume ratio which is determinant for the RBC passage through the spleen, potentially leading to its splenic retention and removal by the spleen resident macrophages [422, 460]; and (iii) the resulting spheric shape with a compression imposed by the underlying cytoskeleton.

However, if the primary membrane defects are well-characterized, the etiologic relationship of those defects to membrane loss is less obvious [298]. Moreover, besides cytoskeleton alterations, the disease is usually associated with an excessive increase of the intracellular calcium and sometimes with oxidative stress [424, 461] but the link between those increases and the primary defect is not established. Finally, although patients suffering from this disease with an appropriate clinical and familial history do usually not request further investigations since identification of the protein alterations and underlying genetic mutations are not likely to improve patient clinical management [462], clinical differences and evolution in the same kindred are often observed without any explanation. For those three reasons, it was crucial to elucidate whether and how the cytoskeleton and the calcium exchanges are interplayed with the plasma membrane lipid organization at the healthy RBC surface and whether this interplay could be altered in spherocytosis. To do so, we analyzed ten patients from seven families. All were splenectomized, allowing us to analyze RBCs still functional to transport oxygen but not enough deformable to pass through the splenic endothelial pores. Patients were systematically compared to a cohort of healthy donors and to RBCs upon storage at 4°C, known for microvesicles release in a process involving calcium and oxidative stress [404]. All those RBCs were analyzed for: (i) gene mutation and resulting cytoskeletal protein content, (ii) morphology, fragility and microvesicles release, (iii) cytoskeleton organization and rigidity, (iv) intracellular calcium content, exchange and signaling, including the calpain activation, the PKC-dependent NADPH oxidase-mediated reactive oxygen species (ROS) production and the

scramblase/flippase-dependent phosphatidylserine externalization, and (v) membrane lipid content and lateral distribution.

2.3. Results

The ten patients are classified into three groups based on clinical parameters, RBC morphology and RBC fragility. Ten patients from seven families suffering from spherocytosis were included in our study. They were all splenectomized (Table S1). Patients from the same kindred are highlighted with the same color code and all data are presented by year of analysis since spherocytosis is heterogeneous and features can vary from one time to another. RBCs upon storage at 4°C were systematically included in the study for comparison purpose (light blue dots).

The ten patients presented two-to-four clinical parameters indicative of hemolysis, *i.e.* increased circulating bilirubin and hemoglobin, RBC and reticulocyte count and mean corpuscular volume (MCV) and hemoglobin concentration (MCHC, Figure 1A-F). They all exhibited a decreased RBC size, similar to the one observed upon RBC storage for 2 weeks (Figure 1G). Moreover, P1 and P15 presented a significantly smaller RBC area distribution, indicating slighter RBC size variations (Figure 1H). Hence, P1, P14 and P15 exhibited a significant increase of RBC circularity, similar to RBCs stored for 2 weeks (Figure 1I). Besides clinical parameters and RBC size decrease, the RBCs of all patients were more fragile, as revealed by the increase of the medium osmolarity corresponding to 50% hemoglobin release (EC50; Figure 1K). Such increase was systematically lower than the one observed after 2 weeks at 4°C, except for P18. The later patient, like P2 and P15, also exhibited a significant increase of hemoglobin release in isosmotic medium, suggesting higher RBC fragility for those three patients (Figure 1J). All those changes did not result from healthy adult individual variations, age or splenectomy (Figure S1A-E).

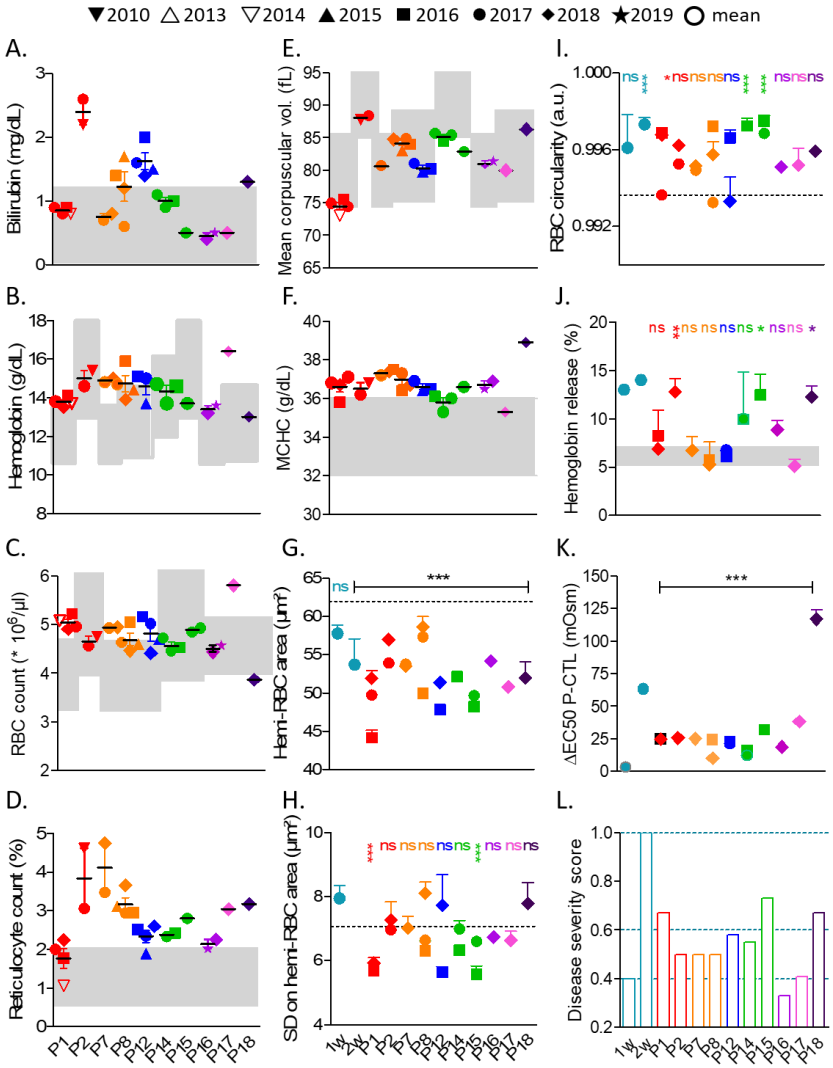

Figure 1. Differential family-unrelated clinical parameters, RBC morphology and RBC fragility and resulting disease severity scores. (A-F) Patient clinical features provided by Saint-Luc Hospital. Grey boxes, normal ranges adapted to the age of the patients. MCHC, mean corpuscular hemoglobin concentration. **(G-I)** RBC morphology. The hemi-RBC projected area (G), the standard deviation on the projected area (H) and the RBC circularity (I) were measured on RBCs laid down on poly-L-lysine-precoated coverslips. Dotted lines, healthy fresh RBCs; light blue symbols, healthy RBCs stored for 1 (1w) or 2 weeks (2w) at 4°C. The different symbols correspond to different blood venipunctures. Data are means/year ± SEM of 2-18 independent experiments with 150-400 RBCs measured/condition in each experiment. **(J,K)** RBC fragility. Hemoglobin released in isosmotic medium (J) and half-maximal effective osmolarity (EC50) determined upon RBC incubation in decreasing osmolarity media and presented as Δ patient-control values (K). Data are means/year ± SEM of 2-3 independent experiments. **(L)** Disease severity score based on clinical features and alteration of RBC morphology and deformability. The score index was determined as follows. For each clinical and laboratory feature, a score of 1 was attributed if the value was significantly different from the healthy control values vs 0 otherwise. The sum of those scores was then divided by the number of measured parameters for each patient. Based on those scores, three groups of patients were distinguished.

Increased RBC fragility is often suggested to lead to RBC vesiculation and to result into decreased RBC size and biconcavity [361]. Accordingly, P12 and P18 released 5-7-fold more microvesicles (MVs) within blood than healthy donors without any change in MV size. However, such release was quite modest as compared to the extent of MV release in stored blood (Figure S2A-C), suggesting that vesiculation was insufficient to explain the RBC surface reduction and the increased circularity observed in Figure 1G-I.

To find a quantitative way to take into account all the above RBC alterations (*i.e.* clinical parameters & RBC morphology alteration, fragility and microvesiculation), we determined a disease severity score for each patient, calculated as follows. For each clinical and laboratory feature, a score of 1 was attributed if the value was significantly different from the healthy control values *vs* 0 otherwise. The sum of these scores was then divided by the number of measured parameters for each patient. Based on this score, three groups of patients were defined: (i) P1, P15 and P18 with a score > 0.6 (*i.e.* the more severe phenotype); (ii) P2, P7, P8, P12 and P14 with a score between 0.4 and 0.6 (*i.e.* intermediate phenotype); and (iii) P16 and P17 with a score ≤ 0.4 (*i.e.* the less severe phenotype; Figure 1L). Classification of P1 and P2 as well as P14 and P15 (from the same families) in different groups suggests that the disease severity did not only depend on the primary defect.

Seven patients present echinocytes. To examine whether those three groups of patients could be discriminated based on differential loss of RBC biconcavity, RBCs of the ten patients were analyzed by high-resolution scanning electron microscopy on filters and/or vital confocal imaging on IBIDI chambers. Healthy fresh RBCs were biconcave (Figure 2 & S3; thin arrows) but vesiculated and became spherocytic upon storage (dots). In contrast, all patients presented RBCs with a large variety of morphology including discocytes, spherocytes, stomatocytes and echinocytes. Interestingly, the later were found in P1, P2, P7, P8, P14, P15, P16, although to a differential extent based on the patient and the venipuncture, but not in P12, P17 and P18 (counting ongoing). We concluded that the partial loss of RBC biconcavity at the benefit of echinocytes and/or stomatocytes cannot be related to the disease severity score. We next asked whether those two types of RBC morphology could result from differential mutation.

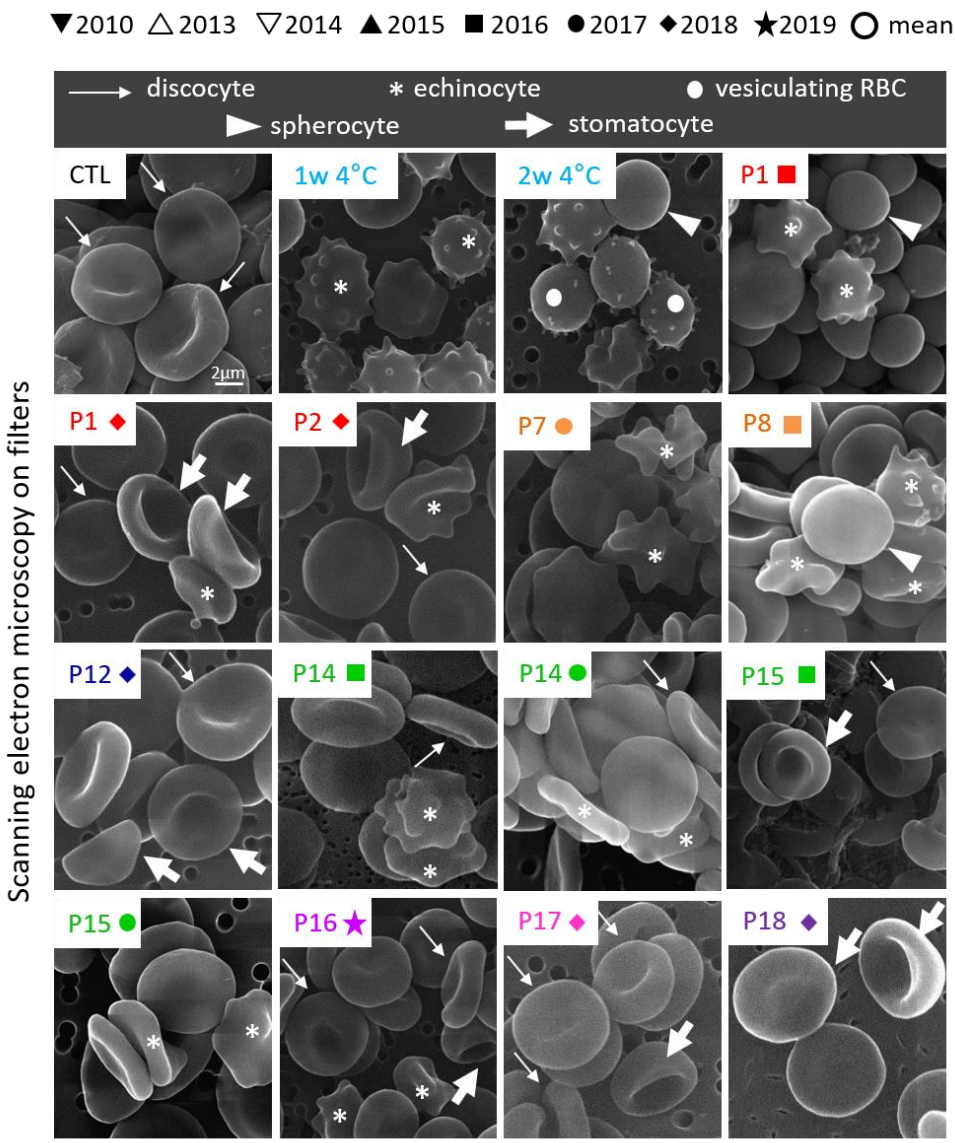

Figure 2. RBC biconcavity partial loss at the benefit of stomatocytes and/or echinocytes depending on the mutation. Healthy RBCs, either fresh (CTL) or stored at 4°C for 1 or 2 weeks, and RBCs from patients were fixed in suspension, laid down on filters and analyzed by scanning electron microscopy. Arrowheads, spherocytes; thin arrows, discocytes; thick arrows, stomatocytes; asterisks, echinocytes; dots, vesiculating RBCs. Images representative for 1-2 independent experiments.

The seven patients showing echinocytes present mutations in *SPTB* while the three others are mutated in *ANK1*. Patients were screened for mutations in genes encoding for ankyrin (*ANK1*), α-spectrin (*SPTA1*), Band3 (*SLC4A1*), protein 4.2 (*EPB42*) and β-spectrin

(*SPTB*) by NGS sequencing. Four mutations were discovered in *SPTB* (seven patients) and three others in *ANK1* (Figure 3). These include three nucleotide substitutions resulting in stop codons, as well as three deletions and one duplication leading to frame-shifts and premature stop codons. Thus, the patients showing echinocytes presented mutation in the *SPTB* gene whereas the others were mutated in the *ANK1* gene.

Patient	Gene	hgvs_dna (1)	hgvs_protein	Reads ref	Reads alt	Zygocity DNA	dbSNP id	RNA
P1	SPTB	***c.1166del***	**p.Val389Glyfs *22**	**786**	**724**	**Het**	-	mutant not seen
		c.5406C>T	p.Tyr1802Tyr	-	-	Het	*rs150709293*	T allele lost
P2	SPTB	***c.1166delT***	**p.Val389Glyfs *22**	**524**	**599**	**Het**	-	mutant not seen
		c.5406C>T	p.Tyr1802Tyr	-	-	Het	*rs150709293*	T allele lost
P7	SPTB	***c.2787_2790dup***	**p.His931Glyfs *74**	**404**	**375**	**Het**	-	*no RNA available*
P8	SPTB	***c.2787_2790dup***	**p.His931Glyfs *74**	**334**	**279**	**Het**	-	mutant not seen
		c.4476T>C	p.Leu1492Leu	-	-	Het	*rs1741487*	T allele lost
		c.4482G>A	p.Val1494Val	-	-	Het	*rs1741488*	G allele lost
P12	ANK1	***c.3771_3781del***	**p.Pro1258***	**350**	**359**	**Het**	-	mutant low
		c.4131G>A	p.Pro1377Pro	-	-	Het	*rs147536061*	A allele very low
P14	SPTB	*c.1316G>A*	p.Ser439Asn	-	-	Het	*rs229587*	G allele lost
		c.3829C>T	**p.Gln1277***	**477**	**439**	**Het**	-	mutant not seen
P15	SPTB	***c.3829C>T***	**p.Gln1277***	**670**	**638**	**Het**	-	*no RNA available*
P16	SPTB	***c.3838del***	**p.Leu1280Serfs *16**	**371**	**336**	**Het**	-	*failed*
		c.4476T>C	p.Leu1492Leu	-	-	Het	*rs1741487*	C allele lost
		c.4482G>A	p.Val1494Val	-	-	Het	*rs1741488*	A allele lost
P17	ANK1	***c.4123C>T***	**p.Arg1375***	**131**	**116**	**Het**	-	mutant not seen
P18	ANK1	*c.414C>T*	p.Asn138Asn	-	-	Het	*rs2304871*	T allele lost
		c.3613G>T	**p.Glu1205***	**682**	**689**	**Het**	-	mutant not seen

(1) ANK1: NM_001142446; SPTB: NM_001024858

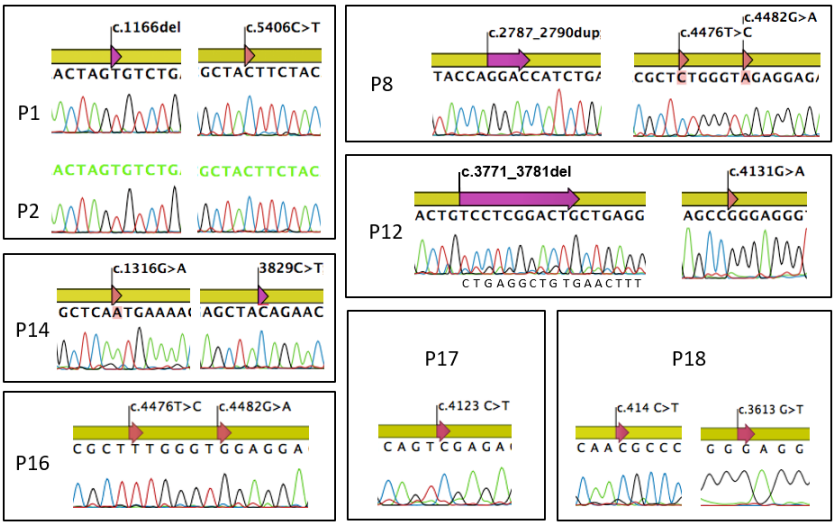

Figure 3. *ANK1* mutations in three patients *vs SPTB* in the seven other patients included in the study. (Top) Mutations (bold) and selected heterozygous polymorphisms used to assess mutant RNA stability. Patients from a same family are separated by a dashed line. Table shows gene symbol, DNA and protein changes named according to HGVS nomenclature, coverage for the mutations (reads with reference and alternative allele), zygosity in DNA, code in dbSNP, and impact of the mutations on RNA stability. (Bottom) Sequences of cDNA showing partial loss of the alleles carrying the premature Stop codons in patients.

We then assessed for mutant RNA stability by RT-PCR and sequencing. For all patients tested, we found that the mutant allele was not detectable (or barely in P12). This was likely due to degradation by nonsense-mediated mRNA decay of the RNAs carrying a premature stop codon. Loss of one allele was confirmed by sequencing heterozygous polymorphisms observed in the DNA of the patients. For P16, only the two polymorphisms produced readable sequences due to poor RNA quality. All showed that one allele was degraded (Figure 3). Thus, only 50% of β-spectrin or ankyrin should be produced.

The patients with the more severe phenotype exhibited a higher β-spectrin-to-ankyrin ratio. To check for the abundance of β-spectrin and ankyrin, western blotting was performed on ghosts using GAPDH as loading control as it was not significantly modified from one patient to another, in contrast to Band3 (Figure S4A-C). As expected from mutations and degradation by nonsense-mediated mRNA decay, the β-spectrin content was decreased in P1, P2, P8, P14, P15 and P16 while the ankyrin content was lowered in P12 and P18. More surprisingly, the β-spectrin level was increased in P12 while the ankyrin content was lowered in P16 (Figure 4A,B). In contrast, the 4.1R protein content was preserved, except in P18 (Figure 4C).

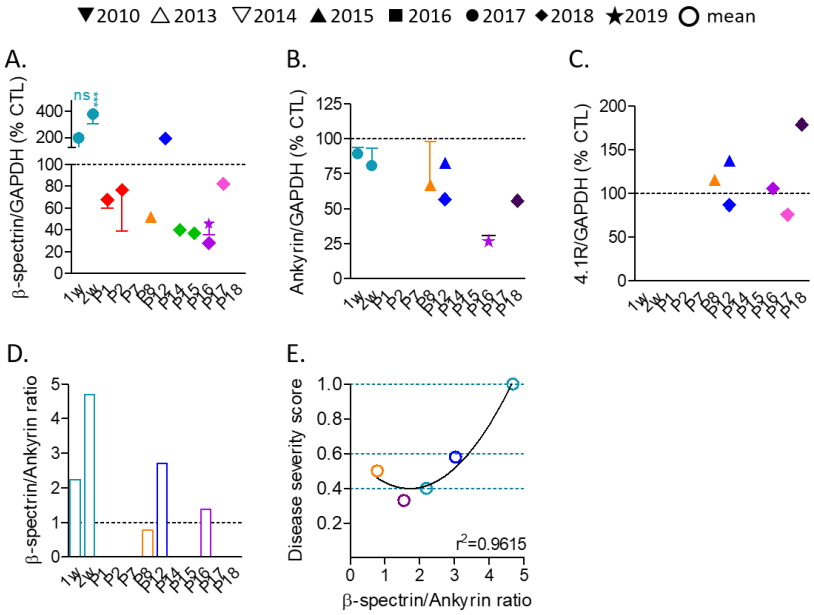

Figure 4. Differential alteration of the RBC β-spectrin-to-ankyrin content ratio. (A-C) β-spectrin, ankyrin and 4.1R contents. Healthy RBCs, either fresh (dotted line) or maintained at 4°C for 1 or 2 weeks (light blue symbols), and diseased RBCs (colored symbols) were eliminated for their hemoglobin content (ghosts) and analyzed by western blotting, quantified and normalized to GAPDH strip intensity (means/year ± SEM of 1-6 independent experiments). **(D)** β-spectrin-to-ankyrin relative abundance. **(E)** Relation between the β-spectrin-to-ankyrin ratio and the disease severity score determined in Figure 1L.

The alterations of the β-spectrin and ankyrin contents led to an increased β-spectrin-to-ankyrin ratio in P12 and stored RBCs but not in P8 and P16 (Figure 4D). Although this analysis must be extended to the entire cohort of patients and further confirmed by proteomic analysis (ongoing), this ratio seemed somehow related to the disease severity but not in a linear manner. Indeed, the disease severity only started to increase from a β-spectrin-to-ankyrin ratio of ~2.5 (Figure 4E), suggesting that the differential β-spectrin and ankyrin content observed in patients was not enough to corroborate the disease severity.

The spectrin covering depends on the β-spectrin-to-ankyrin ratio and heterogeneously distributes at the RBC surface. We therefore compared the ten patients for the organization of the spectrin cytoskeleton by confocal microscopy on RBCs immunolabeled for pan-spectrin and quantified the total spectrin covering per total RBC surface. It had the tendency to decrease in P1, P2, P15 and P16 (*SPTB* mutation) but to increase in P12 and P17 (*ANK1* mutation). One exception was P18 who presented a lower spectrin covering despite *ANK1* mutation (Figure 5B), which could result from the additional alteration of the 4.1R protein found in this patient (see Figure 4D). Spectrin covering appeared to correlate with the β-spectrin-to-ankyrin ratio, the higher the ratio, the higher the spectrin covering (Figure 5C). However, no correlation can be found with the disease severity (Figure S5A).

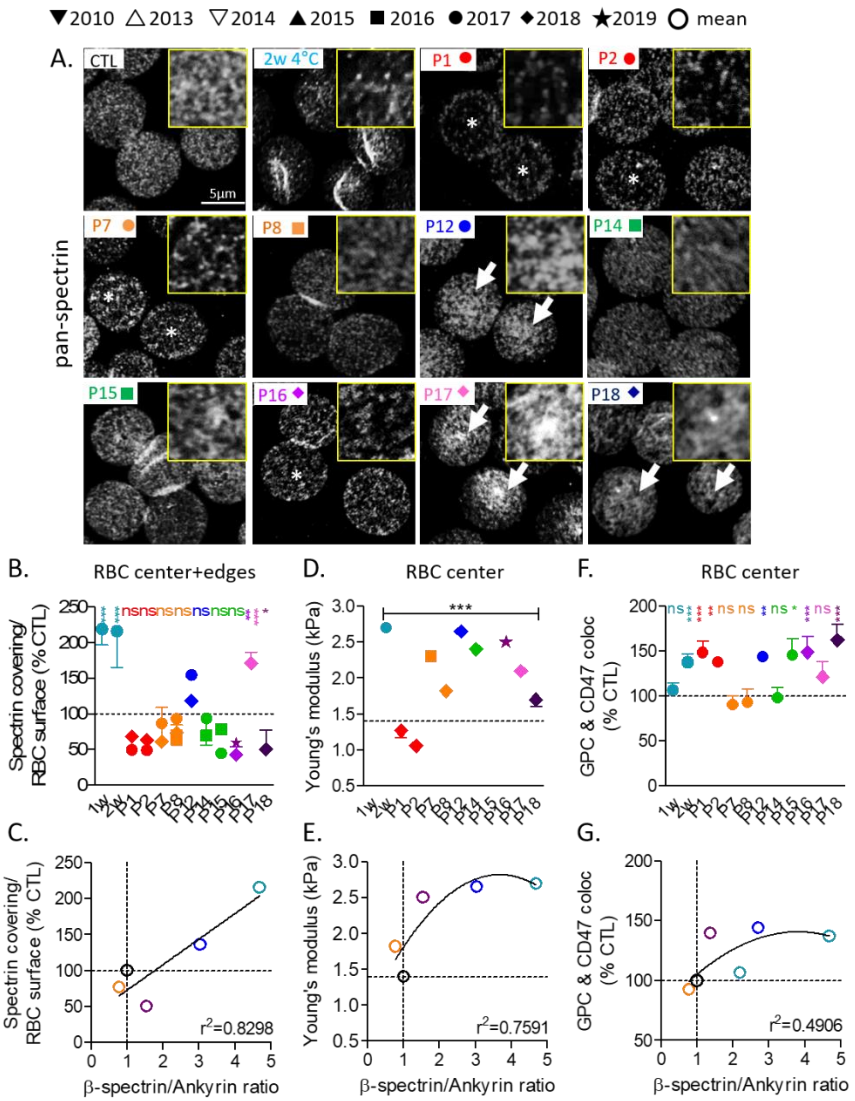

Figure 5. Differential alteration of the spectrin organization, cytoskeleton rigidity and membrane protein dissociation. (A,B,F) Fresh healthy RBCs (dotted line), healthy RBCs maintained at 4°C for 1 or 2 weeks (light blue symbols) or diseased RBCs (colored symbols) were laid down on PLL-precoated coverslips, permeabilized (A,B) or not (F) with 0.5% Triton X-100, fixed and stained with anti (αβ)-spectrin antibodies (A) or antibodies against CD47 (Ankyrin complexes) and glycophorin C (GPC; 4.1R complexes). (A) Representative confocal images of spectrin covering at the RBC surface. (B) Quantification of spectrin covering per RBC total (i.e. center+edges) surface. Data are expressed by reference to the mean of control RBCs from the same experiment and are means/year ± SEM from 3-6 independent experiments with 50-150 RBCs measured/condition. (F) Quantification of the abundance of CD47 and GPC-overlapping peaks on the RBC center determined on 18-35 profiles generated from 3-11 different images per condition (examples provided at Figure S5). Data are expressed as percentage of total peaks from all the profiles (means ± SEM). **(D)** RBC rigidity due to the cytoskeleton determined at the RBC center by atomic force microscopy at high load indentation speed. Data are means/year ± SEM of at least 10 RBCs from 3 independent experiments per condition. **(C,E,G)** Relation between the β-spectrin-to-ankyrin ratio and spectrin covering (C), Young's modulus (E) and GPC & CD47 colocalization (G).

We next determined to which extent the cytoskeletal alterations could alter the RBC elasticity by recording individual force-distance atomic force microscopy (AFM) curves on the surface of single RBCs at low indentation speeds, as in [179]. Because the indentation level reached at those speeds is ~150 nm, such measurement mainly reveals the cytoskeleton contribution to the RBC rigidity. Hence, the analysis was limited to the RBC center to avoid substrate effect. In these conditions, the Young's modulus was significantly increased for all patients, except P1 and P2 (Figure 5D). The increase of rigidity directly correlated neither with the β-spectrin-to-ankyrin ratio (Figure 5E) nor with the total spectrin covering per RBC surface (data not shown) and not at all with the disease severity score (Figure S5B).

Cytoskeleton organization and membrane elasticity alterations were accompanied by changes in membrane protein distribution. For instance, CD47 and glycophorin C (GPC), two membrane proteins respectively found in the ankyrin- and 4.1R-based complexes, appeared less punctiform than in healthy RBCs, adopting a network-like, sometimes diffuse, appearance (insets at Figure S6A). Moreover, the spatial dissociation between CD47- and GPC-enriched clusters was significantly decreased in all patients except P7, P8 and P14 (Figure 5F; see Figure S6B for quantification of colocalization based on line intensity profiles), *i.e.* whatever the spectrin covering alteration (see Figure 5B), the β-spectrin-to-ankyrin ratio (Figure 5G) and the disease severity score (Figure S5C). Again, no correlation was found with the total spectrin covering.

Since the absence of relation between spectrin covering and membrane rigidity and membrane protein distribution could result from the area of the RBC taken into account (*i.e.* total RBC surface *vs* the RBC center only), we finally compared the spectrin organization at the RBC center *vs* the edges. The spectrin appeared homogeneously distributed between the RBC center and the edges in healthy RBCs, P8, P14 and P15 (Figure 5A). P1 and P2 and to a slighter extent P7 and P16 exhibited a decrease of the spectrin covering in the RBC center with large areas devoid of spectrin labeling (asterisks and insets at Figure 5A). P12, P17 and P18 (the three patients with ankyrin defect) instead showed a spectrin enrichment in the RBC center as compared to the edges (thick arrows at Figure 5A). Except in P18, the relative spectrin distribution in the center *vs* the edges appeared somehow related to RBC morphology changes and cytoskeleton rigidity, *i.e.* the stronger the covering in RBC center, the higher the rigidity and the stomatocyte formation.

Altogether, the above data indicated that the patients with ankyrin defect presented mainly stomatocytes and a stronger spectrin covering at the RBC center. In contrast, the patients with spectrin defect who exhibited stomatocytes and echinocytes, showed lower spectrin covering at the RBC center accompanied with big holes. However, none of those

alterations could explain the differential disease severity scores, suggesting additional modifications. We therefore turned to analyze the membrane it-self, first for its cholesterol and total phospholipid contents.

Total phospholipids and cholesterol are both decreased in abundance in the three patients with *ANK1* mutation, the former decreasing in a β-spectrin-to-ankyrin-dependent manner. Both cholesterol and phospholipids were decreased in P12, P18 and, to a slighter extent for phospholipids, in P17, *i.e.* the three patients with *ANK1* mutation. Surprisingly, total phospholipids were raised in P7, P8 and P14, the three patients preserved for the total spectrin covering and the dissociation between GPC and CD47. P1, P2, P15 and P16 were modified neither for the cholesterol nor for the total phospholipid content (Figure 6A,C).

The cholesterol content decreased in a β-spectrin-to-ankyrin ratio-dependent manner (Figure 6B). The phospholipid content also showed some relation with the β-spectrin-to-ankyrin ratio but not in a linear way (Figure 6D). However, none of those parameters did correlate with the disease severity score (Figure S5D,E). Nevertheless, the two patients exhibiting increased microvesiculation (P12 and P18) were those with the lowest content of both cholesterol and phospholipids, suggesting the contribution of microvesiculation to the alteration of the plasma membrane lipid content, as supported by the relation between the MV abundance and the RBC phospholipid content (Figure S2D).

To explore whether membrane lipid content alterations could in turn affect the membrane fluidity, we performed AFM upon low indentation load to mainly consider the membrane itself while minimizing the contribution of the cytoskeleton (ongoing; Figure 6E,F).

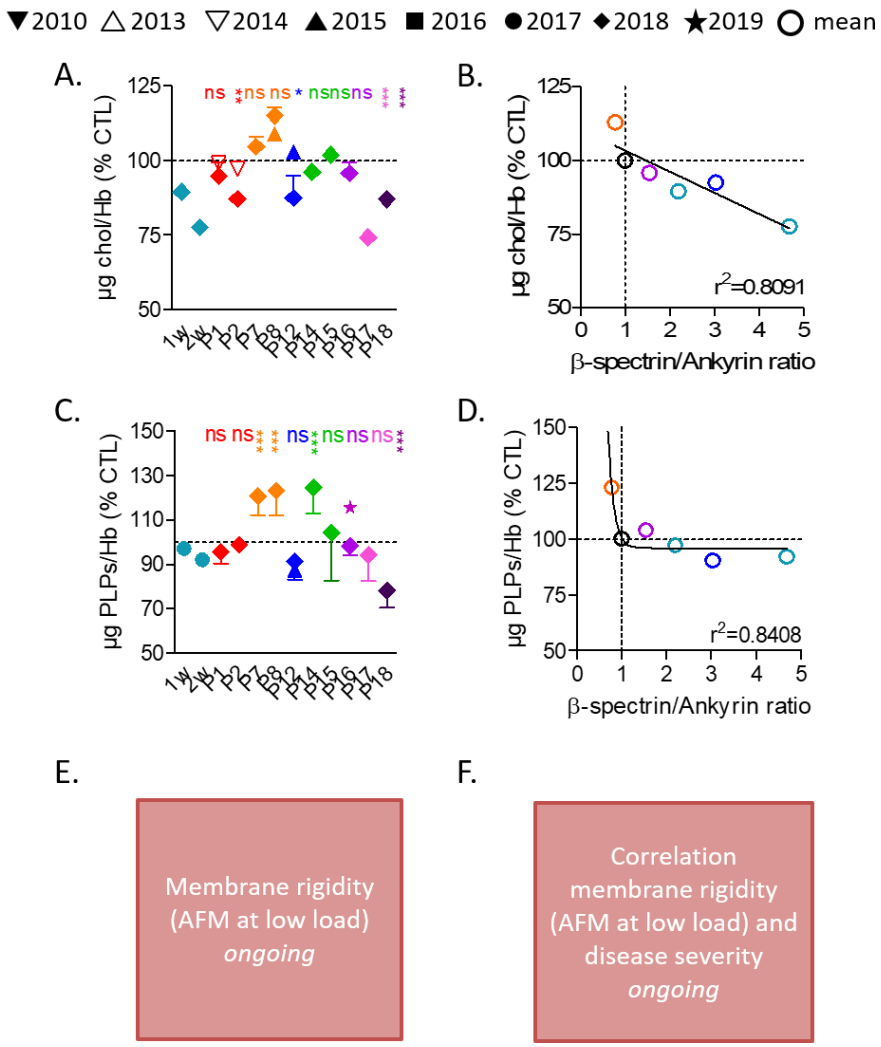

Figure 6. Preferential decrease of both the cholesterol and the total phospholipid content in the three patients with ANK1 mutation. (A,C) Healthy RBCs, either fresh (dotted line) or maintained at 4°C for 1 or 2 weeks (light blue symbols), and diseased RBCs (colored symbols) were washed, lysed, extracted (C) or not (A) and assessed either for cholesterol (A; means/year ± SEM of 3 independent experiments, except for 1 & 2w) or total phospholipids (C; means/year ± SD of 3 independent experiments, except for 1 & 2w). Data were normalized by the hemoglobin content. **(B,D)** Relation between the β-spectrin-to-anlyrin ratio and the cholesterol (B) or the phospholipid (D) content. **(E)** RBC rigidity due to the membrane determined by atomic force microscopy at low indentation speed (ongoing). **(F)** Relation between the membrane rigidity at low load and disease severity (ongoing).

The hemoglobin membrane retention preferentially increases in RBCs with the lowest β-spectrin-to-ankyrin ratio, the highest cholesterol content and the strongest disease severity. We next reasoned that such modification of the plasma membrane lipid composition should overall affect the inner plasma membrane leaflet in contact with the cytoskeleton. To test indirectly this hypothesis, we evaluated by Coomassie blue the extent of hemoglobin retention in the ghost membrane, which should be eliminated during ghost preparation. It was more retained in the membrane of P1, P2, P7, P8, P16 and P17 than in healthy donors (Figure 7A & S4A,D). This retention was maximal at the lowest β-spectrin-to-ankyrin ratio and the highest cholesterol membrane content (Figure 7B,C), suggesting alteration of the inner plasma membrane composition and/or organization. Since hemoglobin membrane retention appeared to somehow correlate with the disease severity score (Figure 7D), we further explored this possibility.

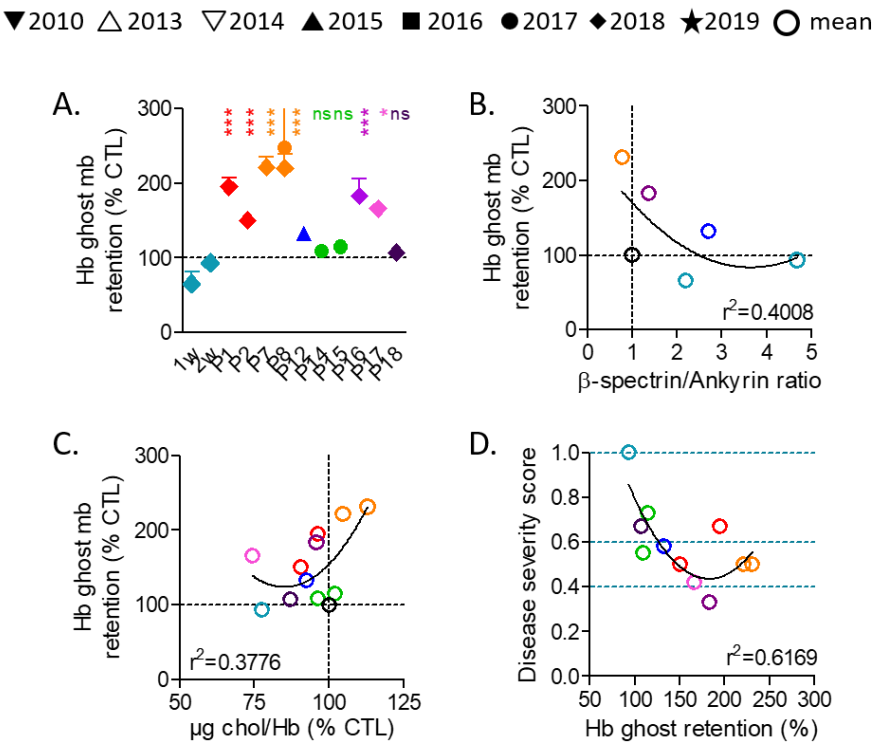

Figure 7. Preferential hemoglobin membrane retention in patients with the lowest β-spectrin-to-ankyrin ratio and disease severity score. (A) Quantification of hemoglobin (Hb) retained in ghost membrane (mb) based on SDS-PAGE stained by Coomassie blue (for representative SDS-PAGE, see Figure S4). The Hb strip is reported to the sum of all strips in the track and then on control values (means ± SEM/year of 2-7 independent experiments). **(B-D)** Relation between membrane hemoglobin retention and β-spectrin-to-ankyrin ratio (B), cholesterol content (C) and disease severity score (D).

The intracellular calcium content increases in a β-spectrin-to-ankyrin- and disease severity-dependent manner. Since the inner plasma membrane lipids are in direct contact with calcium, a key modulator of the cytoskeleton dynamics and membrane anchorage and known to be impaired in spherocytosis [424], we measured its intracellular content in RBCs of the patients at resting state. It was significantly increased in P1, P12, P15 and P18 (Figure 8A), *i.e.* those with the highest β-spectrin-to-ankyrin ratio (ongoing) and the worst disease severity score, showing good correlation between those two parameters and the calcium increase (Figure 8B,C).

The intracellular calcium increase is accompanied by a decreased PIEZO1 content and is counteracted by the rise in intracellular ATP. To explore the mechanisms behind calcium increase, we measured the content of PIEZO1 and PMCA, respectively responsible for calcium entry upon mechanical stress and its efficient extrusion [148, 210]. The PIEZO1 content was decreased in all patients tested (Figure 8D; proteomic analysis ongoing) and exhibited some relation with the intracellular calcium content and the β-spectrin abundance (Figure 8E,F). In contrast no evident modification of the PMCA level can be seen (Figure 8G; proteomic analysis ongoing).

To next test the possibility that calcium accumulation could result from ineffective extrusion due to disruption of the ATP pool fueling the PMCA, the intracellular ATP content was measured. Surprisingly and in contrast to stored RBCs which presented a drastic reduction of the ATP content already after 1 week at 4°C, a series of patients (P1, P2, P7, P8, P16 and P17) showed an increase of their intracellular ATP level (Figure 8H). Such higher ATP content could counteract the increase of the intracellular calcium content, as supported by the inverse correlation between those two parameters (Figure 8I). The highest ATP increase was found in patients with the highest hemoglobin ghost membrane retention (Figure 8J) and inversely correlated with the disease severity score (Figure 8K). The next step will be to evaluate whether those alterations could lead to calcium exchange impairment upon RBC deformation using stretchable PDMS chambers (Figure 8L).

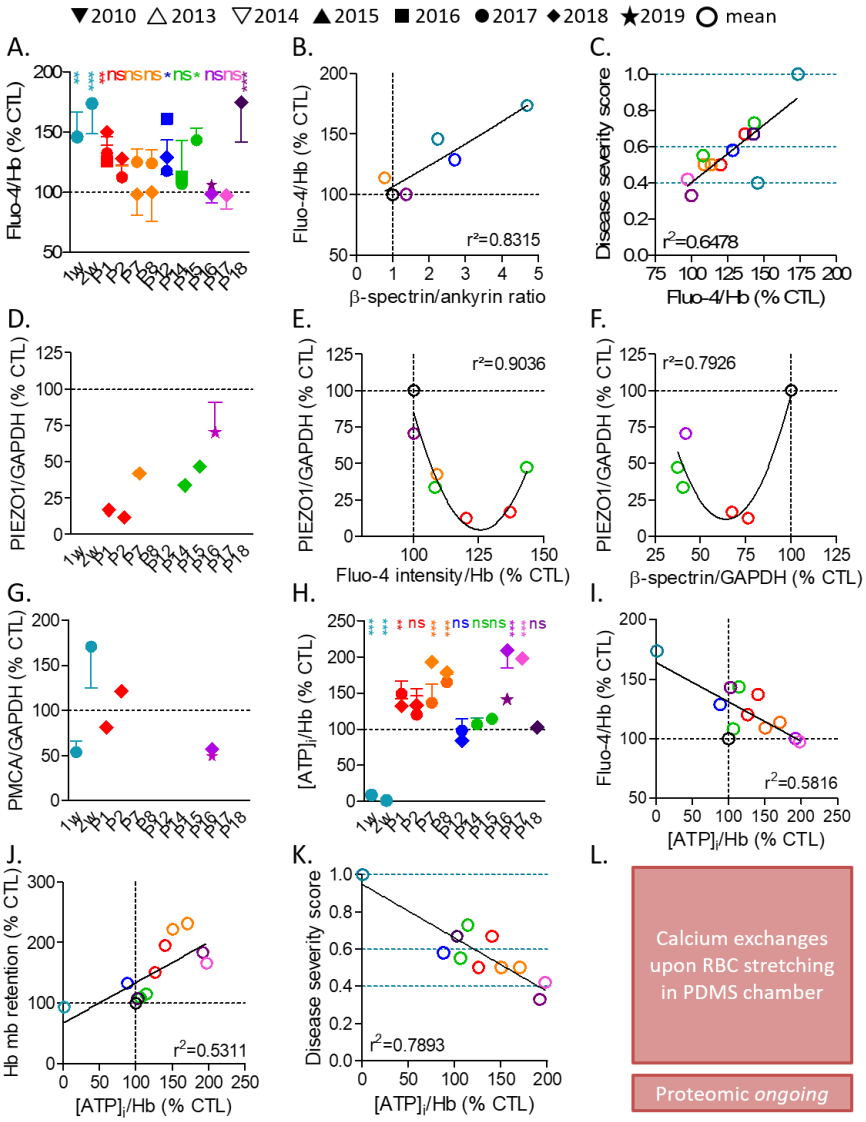

Figure 8. Disease severity-dependent increase of the intracellular calcium content counteracted by the rise in intracellular ATP. (A) Healthy RBCs, either fresh (dotted line) or maintained at 4°C for 1 or 2 weeks (light blue symbols), and diseased RBCs were probed for the intracellular calcium content, evaluated by Fluo-4 AM incubation and expressed by reference to the hemoglobin content (means/year ± SEM of 3-9 independent experiments). **(B,C)** Relation between the intracellular calcium determined in A and the β-spectrin-to-ankyrin ratio (B) or the disease severity score (C). **(D,G)** Determination of the PIEZO1 and PMCA contents by western blotting (and proteomics; ongoing) on ghosts. Data are means/year ± SEM of 1-4 independent experiments. **(E,F)** Relation between the PIEZO1 content and the intracellular calcium (E) or the β-spectrin/GAPDH content. **(H)** Intracellular ATP content measured by luminescence on RBCs incubated with luciferase and luciferin and expressed by reference to the hemoglobin content (means/year ± SEM of 3-5 independent experiments, except for P18, n=2). **(I-K)** Relation between the intracellular ATP content and the intracellular calcium content (I), the membrane hemoglobin retention (J) and the disease severity score (K). (L) Calcium exchanges upon RBC stretching in PDMS chamber.

The intracellular calcium increase contributes to the disease severity through impairment of the plasma membrane asymmetry but does not induce oxidative stress. Based on the specific calcium accumulation in the patients with the more severe spherocytosis, we then evaluated the potential contribution of this increase to the pathophysiology of the disease. The µ-calpain, a cysteine protease known to be activated by relatively low calcium concentration in RBCs [148] (Figure 9A), is currently evaluated (Figure 9B). We also measured the level of reactive oxygen species known to partly result from the activation of the calcium- and PKC-dependent NADPH oxidase in sickle cell disease [463] (Figure 9C). However, we did not find any increase (Figure 9D).

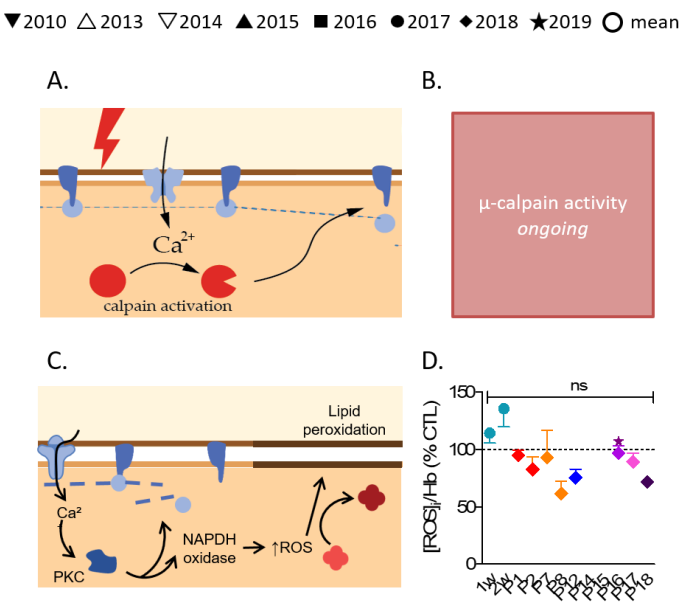

Figure 9. The intracellular calcium rise is not accompanied by increased oxidative stress. (A,C) The rise of the intracellular calcium content can lead to the activation of calcium-dependent proteases such as the µ-calpain which induces proteolysis of several cytoskeletal proteins, thereby disrupting the membrane:cytoskeleton connection (A). Calcium accumulation can also activate the PKC-dependent NADPH oxidase responsible for the production of ROS. The later can activate (i) Src tyrosine kinases, inducing phosphorylation of Band3 and its detachment from the membrane skeleton; and (ii) the oxidation of hemoglobin into hemichromes, leading to Band3 interaction and favoring its aggregation and detachment from the cytoskeleton. **(B)** Determination of the µ-calpain activity (To be done). **(D)** Measurement of the intracellular ROS content by the fluorescent probe 2',7'-dichlorodihydrofluorescein diacetate (H_2DCFDA). Data are expressed by reference to the hemoglobin content and are means/year ± SEM of 3-4 independent experiments.

In contrast, the RBC plasma membrane asymmetry, which is maintained by the ATP-dependent flippase ATP11C and abrogated by activation of the calcium- and cholesterol-dependent scramblase PLSCR1 in RBCs [80] (Figure 10A), was partially lost in P15 and to a slighter extent in P12 and P14. This was revealed by the increased abundance of RBCs showing surface phosphatidylserine (PS) exposure (Figure 10B-D; flow cytometry ongoing). This increase, which was still higher in RBCs stored for 2 weeks, very well correlated with

the disease severity score, suggesting that the loss of PS from the inner leaflet contributes to the disease.

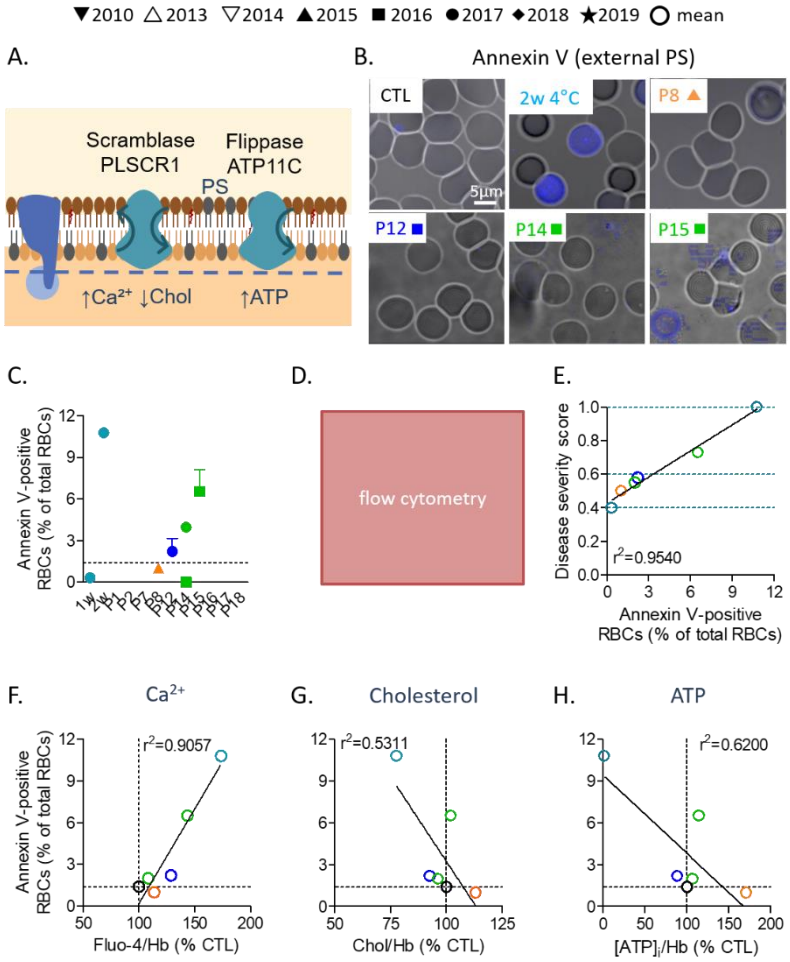

Figure 10. Contribution of the intracellular calcium increase to the disease severity through impairment of the plasma membrane asymmetry. (A) Restriction of phosphatidylserine (PS) to the RBC inner plasma membrane leaflet is insured by the ATP-dependent flippase ATP11C. Upon increase of the intracellular calcium content and decrease of the membrane cholesterol, the PLSCR1 scramblase is activated, leading to PS translocation from the inner to the outer leaflet. **(B,C)** Determination of PS exposure at the outer plasma membrane leaflet by confocal microscopy of Annexin V-Alexa 647-labelled RBCs spread on PLL-coated coverslips. (B) Representative images. (C) Quantification. Data are means/year ± SD of 1-3 independent experiments. (D) Flow cytometry on RBC labelled with Annexin V Alexa 647 (To be done). (E-H) Relation between Annexin V-positive RBCs and disease severity score (E), intracellular calcium level (F), cholesterol content (G) and intracellular ATP content (H).

The extent of PS externalization increased in a calcium content-dependent manner showing a very good correlation between those two parameters (Figure 10F), supporting the activation of the calcium-dependent scramblase and/or the inhibition of the flippase in

this process. However, since membrane asymmetry was partially lost but oxidative stress not increased at all despite the fact that the NADPH oxidase is expected to be activated at lower calcium concentration than scramblase [148], we reasoned that calcium increase should not be the only factor responsible for the loss of membrane asymmetry in spherocytotic RBCs. We therefore evaluated whether the decreased cholesterol level and the increased ATP content that we observed in some patients (see Figures 6A & 8H) could also correlate with the extent of PS externalization. This was indeed the case, as shown on Figures 10G and H.

Altogether, those data indicated that the PS partial loss from the inner plasma membrane leaflet resulted from both the calcium increase and the cholesterol decrease but was counteracted by the increase in intracellular ATP. They also revealed that membrane asymmetry impairment was a good parameter to attest for the disease severity. We finally asked whether membrane lateral heterogeneity into lipid domains, that we previously showed to contribute to calcium exchanges at the RBC surface [163, 177], could also be deregulated in spherocytosis in a disease severity-dependent manner.

GM1-enriched domains decrease in abundance in a β-spectrin-to-ankyrin ratio-dependent manner and show altered response to stimulation of calcium influx depending on the PIEZO1 content and the extent of PS externalization. We have recently provided several lines of evidence suggesting the interplay in healthy RBCs between GM1-enriched domains and calcium influx known to occur through PIEZO1 (Figure 11A) [163]. We here showed that the abundance of those domains had the tendency to decrease in all patients except P7, P8 and P12 (Figure 11B,C). This decrease did not result from age or splenectomy (Figure S1G,H). In addition, the GM1 domain response to stimulation of calcium influx by the PIEZO1 agonist Yoda1 was reduced in all patients tested except P16 (Figure 11D), as compared to the 2.5-fold in healthy RBCs (thick dotted line at Figure 11D). This analysis must be extended to RBC stretching in PDMS chambers (Figure 11I).

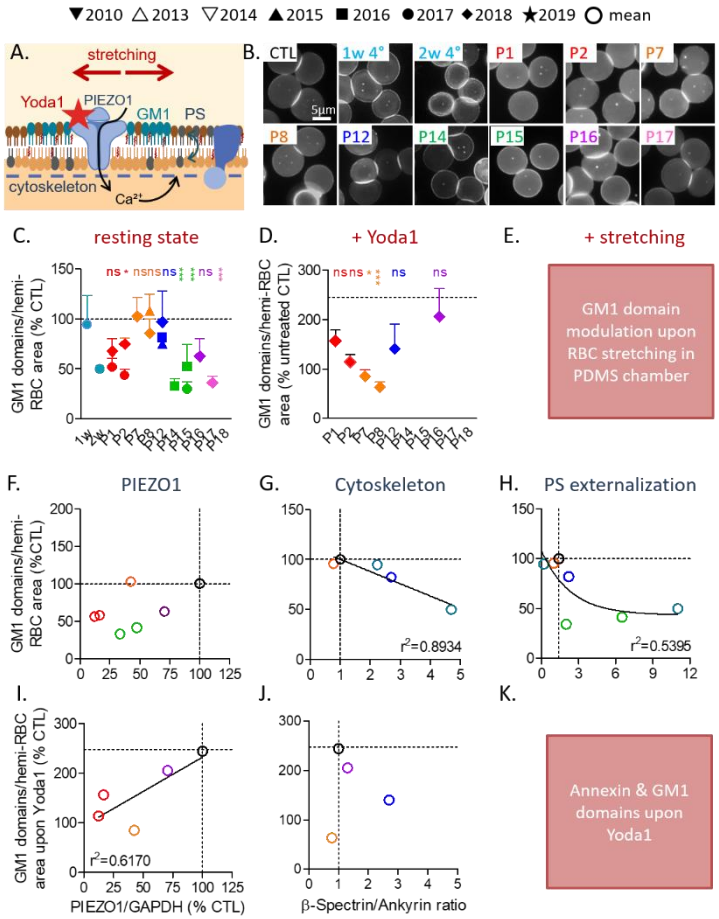

Figure 11. Differential decrease of GM1-enriched domain abundance and response to stimulation of calcium exchanges, depending on the β-spectrin-to-ankyrin ratio, the extent of PS externalization and the PIEZO1 content. (A) The interplay between GM1-enriched domains and calcium influx through PIEZO1 has been previously suggested based on domain modulation upon stimulation of calcium influx upon Yoda1 and RBC stretching in PDMS chambers (red & [163]). The PIEZO1 activity also depends on the cytoskeleton and the extent of PS surface exposure (dark blue & [429, 464]). **(B-K)** Healthy RBCs, either fresh (dotted line) or maintained at 4°C for 1 or 2 weeks (light blue symbols), and diseased RBCs were spread onto PLL-coated coverslips, labeled with BODIPY-GM1, incubated for 15 sec with Yoda1 (D, I-K) or not (B,C, F-H) and directly visualized by vital fluorescence microscopy. **(B,C)** GM1-enriched domains on RBCs at resting state. (B) Representative images. (C) Quantification of GM1 domain abundance per hemi-RBC area. Data are means/year ± SEM of 4-10 independent experiments (except for P18, n=1) in which 200-800 RBCs were counted per condition in each experiment. **(D)** GM1-enriched domain abundance upon stimulation of calcium influx by PIEZO1 activation through Yoda1. Data represent the GM1 domain abundance per hemi-RBC area expressed in percentage of healthy untreated RBCs (means/year ± SEM from 3-6 independent experiments/lipid; 300-600 RBCs were counted per condition in each experiment). **(E)** GM1 domain modulation upon RBC stretching in PDMS chamber. **(F-H)** Relation between GM1 domain abundance in resting state and the PIEZO1/GAPDH content (F), β-spectrin-to-ankyrin ratio (G) and the extent of PS externalization (H). **(I-K)** Relation between GM1-enriched domain abundance upon Yoda1 treatment and the PIEZO1/GAPDH content (I), the β-spectrin-to-ankyrin ratio (J) and the extent of PS externalization (K).

As we previously observed that patients exhibited an alteration of the PIEZO1 abundance, the cytoskeleton content and distribution as well as the extent of PS surface exposure, three known regulators of PIEZO1 activity (Figure 11A) [429, 464], we then asked whether the decreased abundance and dynamics of GM1-enriched domains could be related to those alterations. The response of GM1 domains to Yoda1, but not their abundance at resting state, decreased in a PIEZO1 content-dependent manner (Figure 11F,I), supporting the interplay between GM1-enriched domains and PIEZO1 [163] and suggesting the requirement of PIEZO1 to induce the formation of new GM1-enriched domains upon stimulation of calcium entry. In contrast, the abundance of GM1 domains in resting state, but not upon stimulation by Yoda1, decreased with the β-spectrin-to-ankyrin ratio (Figure 11G,J). Finally, the abundance of those domains appeared to decrease with the extent of PS surface exposure, but not in a linear manner (Figure 11H,K), suggesting alternative way of calcium entry and/or additional perturbation of calcium exit. To test the second hypothesis, we examined the abundance of SM-enriched domains found to contribute to calcium efflux through the calcium efflux pump PMCA [163].

SM-enriched domains increase in abundance and exhibit a decreased response to intracellular calcium depletion depending on the extent of PS exposure and hemoglobin membrane retention. In contrast to GM1-enriched domains which presented the tendency to decrease, those enriched in SM were significantly increased in all patients except P14, P15 and P17 (Figure 12B,C). Moreover, their response to intracellular calcium depletion by EGTA was reduced in five patients (Figure 12D). Those observations, which need to be confirmed upon RBC stretching in PDMS chambers (Figure 12E), suggested differential alteration of SM-enriched domain abundance and functionality in the different patients with no evident relation with disease severity.

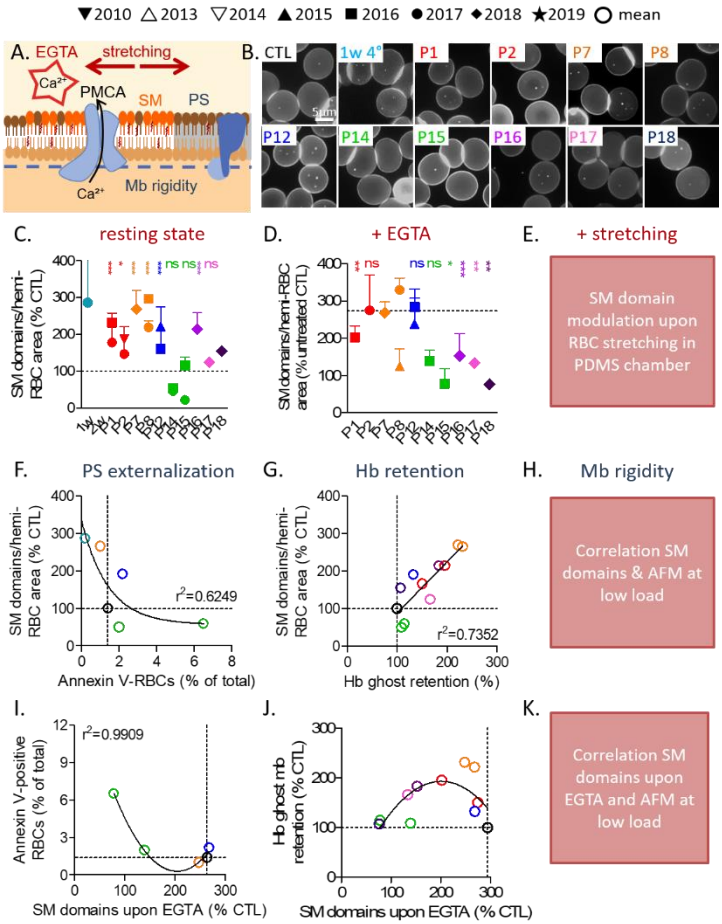

Figure 12. Differential increase of SM-enriched domain abundance and decrease of response to stimulation of calcium exchanges, depending on the extent of PS externalization and hemoglobin membrane retention. (A) The interplay between SM-enriched domains and calcium efflux through the calcium efflux pump PMCA has been previously suggested based on domain modulation through intracellular calcium depletion by EGTA and RBC stretching in PDMS chambers (red & [163]). The PMCA activity is also proposed to depend on membrane rigidity (dark blue & [58]). **(B-K)** Healthy RBCs, either fresh (dotted line) or maintained at 4°C for 1 or 2 weeks (light blue symbols), and diseased RBCs were incubated in calcium-free medium supplemented with EGTA (D, I-K) or not (B,C, F-H), spread onto PLL-coated coverslips, labeled with BODIPY-SM and directly visualized by vital fluorescence microscopy. **(B,C)** SM-enriched domain abundance on RBCs at resting state. (B) Representative images. (C) Quantification of lipid domain abundance per hemi-RBC area. Data are means/year ± SEM of 4-10 independent experiments (except for P18, n=1) in which 200-800 RBCs were counted by conditions in each experiment. **(D)** SM-enriched domain abundance upon stimulation of calcium efflux through extracellular calcium chelation with EGTA. Data represent the percentage of SM domain abundance per hemi-RBC area in healthy untreated RBCs (means/year ± SEM from 3-6 independent experiments/lipid and 300-600 RBCs were counted per condition in each experiment). **(E)** SM domain modulation upon RBC stretching in PDMS chamber. **(F-H)** Relation between SM-enriched domain abundance at resting state and the extent of PS externalization (F), hemoglobin membrane retention (G) and membrane rigidity (H). **(I-K)** Relation between SM-enriched domain abundance upon EGTA treatment and the extent of PS externalization (I), hemoglobin membrane retention (J) and membrane rigidity (K).

We next examined if SM-enriched domain differential alteration in patients could be related to the extent of cytoskeleton and inner PS impairments, as for GM1-enriched domains. The abundance of SM domains did not correlate with the β-spectrin-to-ankyrin ratio, neither in resting state nor after calcium depletion (data not shown), suggesting that membrane cytoskeleton anchorage at ankyrin complexes was not important for those domains. In contrast, as for the GM1-enriched domains, the abundance of SM-enriched domains both in resting state and after stimulation appeared to somehow correlate with the PS exposure, but not in a linear manner. Thus, at higher PS externalization than healthy RBCs, both the abundance and dynamics of SM domains decreased whereas, at lower PS externalization, the abundance of SM domains was considerably increased (Figure 12F,I). This suggested more complex impairment of SM than GM1 domains.

As the PMCA activity is proposed to depend on membrane rigidity [58], we finally asked whether the differential abundance of SM-enriched domains upon PS externalization could result from differential membrane rigidity (ongoing). In favour of this hypothesis, the abundance of SM-enriched domains at resting state increased proportionally with the extent of hemoglobin retained at the membrane. Moreover, the patients with the lowest SM domain abundance and highest PS externalization were those with the lowest hemoglobin trapped to the ghost membrane (Figure 12G,J). It remains to determine whether this resulted from alteration of the inner leaflet organization and/or membrane rigidity (Figure 12H,K).

2.4. Discussion

Major findings. The ten splenectomized patients with spherocytosis included in this study have been classified into three groups based on clinical parameters and RBC morphology alteration and fragility. Impairment of the ankyrin and/or β-spectrin content and distribution in those patients was not enough to explain the disease severity. Instead, the intracellular calcium accumulation, which highly contributed to the disease due to the decreased plasma membrane inner leaflet PS content and potentially additional cytoskeleton impairment through calpain, can be considered as a disease severity marker. Calcium accumulation could result from the decreased PIEZO1 abundance and PMCA activity in the most severe cases but was compensated by the increased intracellular ATP level and hemoglobin membrane retention. PIEZO1 abundance decrease, PS externalization and hemoglobin membrane retention in turn affected the membrane lateral heterogeneity into domains and their response to calcium exchange stimulation. Based on the integration of alteration of intracellular calcium and ATP contents, PIEZO1 and ghosts hemoglobin contents, membrane lipid asymmetry and lateral heterogeneity, the ten patients were classified into three groups that perfectly matched with the disease severity score defined by clinical parameters and RBC morphology and fragility. This indicated that clinical heterogeneity in spherocytosis can be explained by the calcium-dependent membrane defects.

β-spectrin and ankyrin mutations lead to differential RBC morphology, cytoskeletal defects, membrane lipid loss and MV release, without any correlation with the disease severity. We have identified three mutations in *ANK1* in three patients and four mutations in *SPTB* in the four other families. Those mutations resulted in haplo-insufficiency due to degradation of the mutant RNAs. No mutations in *EPB42* and *SPTA1* were found, which could be expected as *EPB42* deficiency is rare except in Japan and α-spectrin defects account for 5% of patients [361]. More surprisingly, no mutation of *SCL4A1* was found although the prevalence of Band3 deficiency is expected to be ~15-30% [295, 361]. This could be due to misdiagnosis with dehydrated hereditary stomatocytosis or cryohydrocytosis as a subset of patients with Band3 protein deficiency have features of both diseases [361]. Moreover, patients with *SCL4A1* mutations are in general milder cases of spherocytosis than the ones caused by *ANK1* and *SPTB* mutations since Band3 is only reduced by ~20-30% [465].

The patients with ankyrin defects presented stomatocytes but no echinocytes, a stronger spectrin covering at the RBC center *vs* the edges, a lower content of both phospholipids and cholesterol and a higher tendency to release MVs. In contrast, the patients with β-spectrin defects exhibited both echinocytes and stomatocytes and lower

spectrin covering at the RBC center accompanied with big holes. This indicated that mutations in a protein linking the membrane to the cytoskeleton (i.e. ankyrin) or a protein constituting the cytoskeleton (i.e. spectrin) induced differential RBC morphology transformation, spectrin organization and lipid content impairment (Figure S7).

However, none of those alterations could explain the differential disease severity scores. In contrast and as expected from previous studies [422, 466], the severity of spherocytosis was somehow related to the amount of spectrin network connectivity loss estimated here by the β-spectrin-to-ankyrin ratio, but not with the number of MVs released. All those observations suggested that additional mechanisms could take place and we provided evidence for the key contribution of calcium and downstream targets.

Calcium accumulates in a disease-dependent manner and could result from PIEZO1-independent entry pathway combined with altered calcium efflux in the most severe cases, possibly due to lipid domain alteration. In agreement with previous studies [424], the intracellular calcium content was significantly increased in four patients out of ten, in a family-independent manner. If PIEZO1 was responsible for calcium overload, it would be over-activated. Although this hypothesis remains to be tested by patch-clamp studies, several lines of evidence argued against this hypothesis and even suggested the alteration of calcium influx though PIEZO1 and GM1-enriched domains contributing to this influx. Firstly, while PIEZO1 activation can be triggered by membrane stiffening [467] and thus by the membrane cholesterol content, we rather found an increased cholesterol content in patients with normal calcium level. Secondly, even though lateral membrane tension and membrane curvature/thickness [468] can also modulate PIEZO1 activity, P1 and P2 presented a normal rigidity but the lowest PIEZO1 content. Thirdly, the GM1-enriched domain increase upon PIEZO1 activation was strongly reduced in all patients. Fourthly, a lower PIEZO1 abundance was accompanied by a higher calcium accumulation, suggesting alternative pathways of calcium entry such as $Ca_v2.1$ [206], TRPC6 [207], VDAC [208] or N-methyl D-aspartate (NMDA)-receptors [209]. To note, abundant and hyperactive NMDA receptors have been identified as the cause of abnormal calcium uptake in sickle cell disease [469].

The decreased abundance of PIEZO1 could result from membrane vesiculation or altered protein sorting during enucleation. The first possibility, which supposes that this channel is not linked to any cytoskeleton elements since spectrin or ankyrin deficiencies should lead to vesiculation in unsupported areas of the lipid bilayer [361], could be ruled out. Moreover, we did not observe increased microvesiculation in all the patients showing PIEZO1 defect. We therefore privileged the second hypothesis implying the selective sorting of proteins during erythroblast enucleation. Although the underlying mechanism is still

largely unknown, it involves association with the spectrin and/or the ankyrin cytoskeleton and could lead to abnormal loss of membrane proteins such as glycophorin A, Band3 and Rh-associated antigen, as revealed in ankyrin-deficient mice [114, 190]. The specific increase of phospholipid (but not cholesterol) content in the three less affected patients is in favor of this second hypothesis. All those observations support the importance of the interplay between cytoskeleton, lipid domains and calcium influx at the RBC surface for optimal shape and deformation. Hence, they suggest that appropriate membrane:cytoskeleton anchorage is required to maintain optimal PIEZO1 and GM1-enriched domain abundance while controlling their activity and dynamics.

This decreased PIEZO1 content directly correlated with the altered response of GM1-enriched domains to the PIEZO1 activator Yoda1, supporting the interplay between those domains and this calcium channel [163] and suggesting the requirement of PIEZO1 to induce the formation of new GM1-enriched domains upon stimulation of calcium entry. In addition, besides its consequences in terms of membrane:cytoskeleton anchorage impairment and MV release, the decrease of PS from the inner plasma membrane leaflet could also alter the PIEZO1 activity. This hypothesis, which remains to be tested in our patients, is supported by the recent observation that outer leaflet exposed PS and surface-inserted lysoPS in myoblasts suppress PIEZO1 activation, leading to impairment of myotube formation [429].

In addition to calcium entry impairments, it is also possible that the accumulation of calcium resulted from impaired PMCA activity in the more severe patients, despite normal PMCA abundance. This could not result from limited intracellular ATP content, which never decreased even in the patients with the more severe phenotype. In contrast, the SM-enriched domain abundance and functionality were impaired in the more severely affected patients. The modification of global membrane rigidity could be responsible for this effect, as fluidity has been shown to influence the pump activity [470-472]. Impairment of plasma membrane asymmetry could also play a role, as revealed by the lowest abundance and dynamics of SM-enriched domains in the patients with the highest PS loss from the inner leaflet. Those observations suggested that the maintenance of membrane transversal heterogeneity was required to preserve the lateral heterogeneity.

Calcium accumulation is counteracted by increased ATP level and hemoglobin membrane entrapment. Although calcium had the tendency to increase in eight patients out of ten, this increase was significant in only four of them and systematically lower than the level of calcium accumulated upon RBC storage at 4°C, suggesting differential mechanisms and/or compensation feature in spherocytosis. Based on similar β-spectrin-to-ankyrin ratio in RBCs upon storage and in the more severe patients, we suggest that RBCs

upon storage at 4°C would also exhibit a decreased abundance and functionality of PIEZO1. This hypothesis is currently tested. If confirmed, this would favour the second hypothesis that compensation mechanisms, such as increase of ATP, could take place in spherocytosis.

Six patients indeed showed an increased intracellular ATP level, which was not observed at all in RBCs upon storage. This level up of energy stock may be a compensation mechanism to ensure efficient calcium efflux via PMCA [184] but also to (i) preserve the phospholipid asymmetry via ATP-dependent lipid flippases [72], (ii) maintain the electrolyte gradient between the plasma and the cytoplasm through the activity of ATP-driven membrane pumps [149], and (iii) counteract the membrane rigidity due to cytoskeleton compression (Figure S7). For instance, besides calcium increase, reduced ATP level is also known to give rise to more fully connected spectrin network and higher membrane compression [456] as ATP depletion prevents the phosphorylation of 4.1R protein. In its unphosphorylated state, the 4.1R protein strongly couples the spectrin to the membrane. When bound to the membrane, the spectrin cytoskeleton acts like a network of entropic springs, imposing a tension that partially compresses the membrane. In this light, RBC needs to expend energy (in the form of ATP) to soften its cytoskeleton via spectrin dissociations [473].

The observation that patients with the greater intracellular ATP level were those exhibiting a normal intracellular calcium level suggested that the increase of ATP could have a beneficial effect on calcium overload (Figure 13B). Accordingly, normal calcium and increased intracellular ATP levels were both correlated with a lower disease severity score. Besides increased ATP levels, patients with the lowest severity score and normal calcium content also presented increased haemoglobin membrane retention (Figure 13C). Gradual accumulation of autoxidized hemoglobin in circulating RBCs is proposed to occur upon aging and to associate with the cell membrane by association with Band3 N-terminal domains [187]. Since the preservation of hemoglobin is ensured by NADPH-methemoglobin reductase activity [226, 252], we suggest that patients with increased ATP level are more prone to protect Band3:hemoglobin clusters from vesiculation [404]. The increased intracellular ATP levels and the hemoglobin retention were observed in spherocytosis but not in RBCs upon aging, providing the possibility to consider those two parameters as criteria for better prognostic.

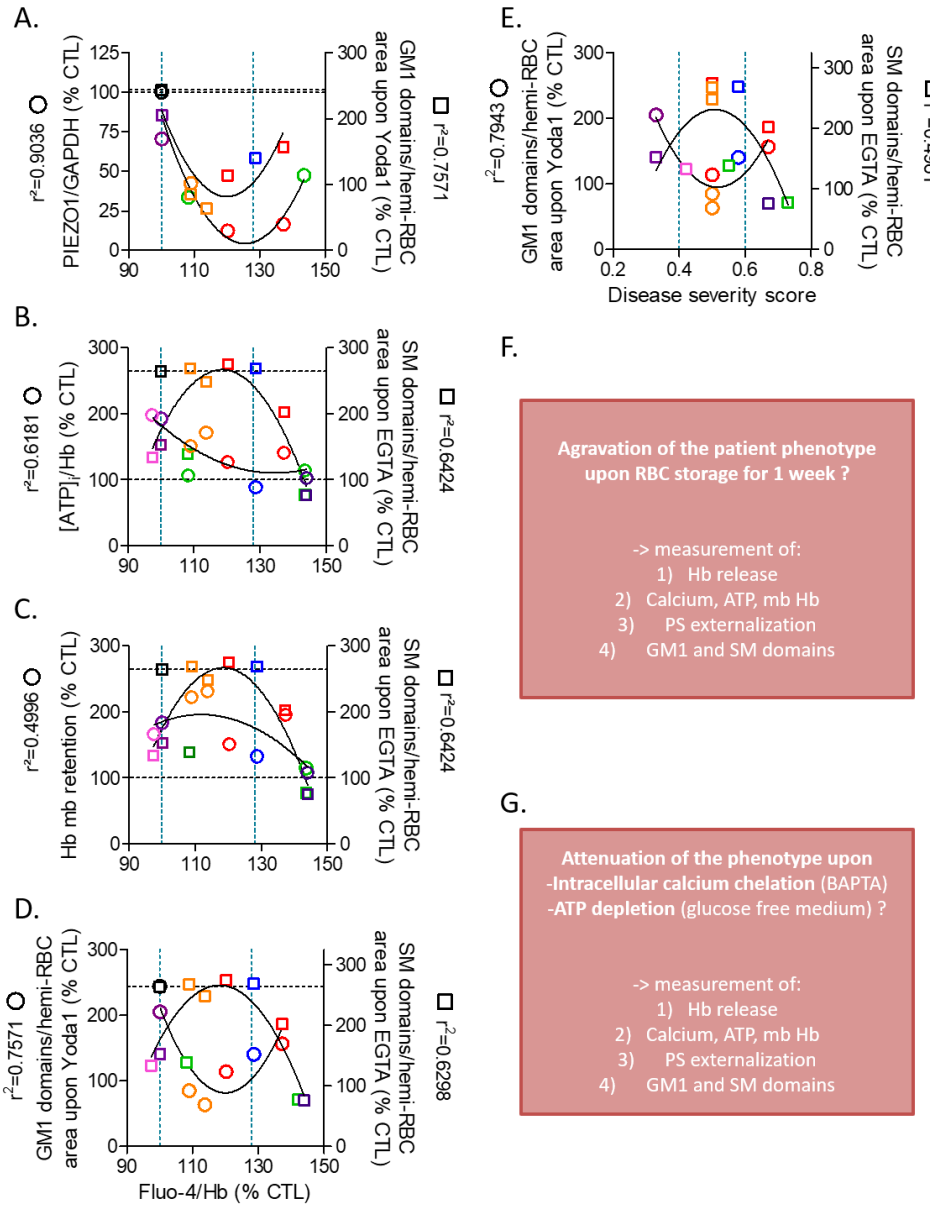

Figure 13. Relation between calcium and ATP contents, hemoglobin membrane retention, lipid domains and disease severity. (A-D) Correlations between the intracellular calcium content and PIEZO1/GAPDH relative content (A, left axis), GM1-enriched domains abundance upon Yoda1 treatment (A, right axis; D, left axis), intracellular ATP content (B, left axis), SM-enriched domain abundance upon EGTA treatment (B-D, right axis) and hemoglobin membrane retention (C, left axis). **(E)** Correlations between disease severity score and GM1-enriched domain abundance upon Yoda1 treatment (left axis) and SM-enriched domain abundance upon EGTA treatment (right axis).

Calcium accumulation is not sufficient to explain the increased MV shedding. Although increased calcium levels could activate calcium-dependent scramblases with subsequent PS externalization, one of the main features of MVs, patients exhibiting high calcium content also showed increased PS surface exposure but not always a rise of MV release. Moreover, upon RBC storage for 1 week, while the intracellular calcium and the PS externalization increased to a similar extent than in patients, the abundance of released MVs was strongly higher. It remains to test whether those differences could result from a differential activation of proteolytic enzymes such as calpains which disrupt the membrane:cytoskeleton connection, thereby favouring vesiculation [474, 475] (Figure S7, bold). Besides calcium, the cytoskeleton-induced membrane compression could also induce MV shedding (Figure S7, bold). This was indeed observed for P12, who presented the highest MV shedding and a strong increase of the young's modulus. However, such a close relation cannot be established for P18. Hence, some patients with high membrane rigidity due to the cytoskeleton compression did not show any evidence for increased vesiculation (*e.g.* P16, P17). This could be explained by the fact that these two patients did not exhibit increased calcium content. Finally, differences of lipid order between the bulk membrane and lipid domains could potentially be the trigger for membrane vesiculation, as explored in [476] and proposed by [477]. We previously suggested that the membrane exhibits a higher connectivity to the cytoskeleton, and thereby a higher lipid order, than the lipid domains [178]. The decrease of both cholesterol and phospholipid contents from P12 and P18 RBCs, and to a slighter extent from P17 but not at all from P16, represent an additional feature to take into account in the membrane lipid order alterations (Figure S7, bold).

Thus, although calcium accumulation and the resulting PS externalization, cytoskeleton-induced rigidity and membrane fluidity could all contribute to the microvesiculation process in our cohort of patients, none of those features correlated with the abundance of released MVs nor with the disease severity score. This could be because most patients, except P12, showed only one of these three triggers, minimizing the abundance of released MVs (Figure S7, bold). The increased intracellular ATP content as a compensation mechanism represented an additional explanation (Figure S7, green).

Calcium accumulation *vs* ATP rise and hemoglobin membrane retention are the main parameters to explain the disease severity. Based on the severity score, three groups of patients were defined: (i) P16 and P17 with a score ≤ 0.4 (*i.e.* the less severe phenotype); (ii) P2, P7, P8, P12 and P14 with a score between 0.4 and 0.6 (*i.e.* intermediate phenotype); and (iii) P1, P15 and P18 with a score > 0.6 (*i.e.* the more severe phenotype). Classification of P1 and P2 as well as P14 and P15 (from the same families) in different groups suggested that the disease severity did not only depend on the primary defect. Hence, classification did not correlate with the age of splenectomy, often performed soon in severe cases,

highlighting that disease severity may radically change after splenectomy and that the outcome of the procedure, in terms of RBC alteration, may be difficult to predict. Moreover, the ankyrin- or β-spectrin-deficient RBCs were altered in a family-dependent but disease severity-independent manner, again suggesting additional mechanisms.

Those additional mechanisms were calcium-dependent. For instance, calcium accumulated in RBCs in a disease severity-dependent manner and was related to the decreased abundance of PIEZO1 but compensated in the less severe patients by the rise of ATP content and hemoglobin membrane retention (Figure S7, colored rectangles delimited by grey contours). Calcium accumulation resulted into the partial loss of membrane asymmetry and thereby of PIEZO1 activity possibly through GM1-enriched domains (Figures 13A & S7). The PMCA activity will instead limit the calcium accumulation in the less severe cases, either directly through the increased intracellular ATP and/or indirectly through the increased abundance of SM-enriched domains thanks to the rise of ATP and hemoglobin membrane retention (Figures 13B,C & S7).

Based on those intracellular changes (calcium, ATP) and membrane alterations (hemoglobin membrane retention, membrane asymmetry, GM1 and SM domain abundance and functionality), we were able to separate the ten patients into three groups. The first group comprised P16 and P17 who presented a normal intracellular calcium level, a slight decrease of PIEZO1 and GM1-enriched domains and an increase of both the ATP content and hemoglobin membrane attachment. The second group included P2, P7, P8 and P14 who exhibited a slight but not significant rise of the calcium content, a strong decrease of PIEZO1 content and GM1-enriched domains but an increase of both ATP and membrane-attached haemoglobin and of SM-enriched domains. The third group was constituted by P1, P12, P15 and P18 who showed significantly increased calcium content, no compensating factors and the lowest abundance of lipid domains. This classification perfectly matched with the disease severity score defined by clinical parameters and RBC morphology and fragility, highlighting that alteration of calcium-dependent membrane transversal and lateral heterogeneity resulting from primary cytoskeletal defects could provide disease severity markers for spherocytosis.

2.5. Materials and methods

Blood collection and preparation. The study was approved by the Medical Ethics Committee of the University of Louvain, Brussels, Belgium. Blood was collected by venipuncture into K^+/EDTA-coated tubes from healthy volunteers (17 adults including one splenectomized donor and 1 child) and 10 patients who gave written informed consent. Patient blood samples were analyzed every year. Before experiments blood was diluted 10-fold in glucose- and HEPES (*N*-2-hydroxyethylpiperazine-*N*'-2-ethanesulfonic acid)-containing medium (Invitrogen) and washed twice by centrifugation at 200g for 2min and resuspension. Experiments were carried out on blood maintained for less than 5 days at 4°C, except for storage studies.

Sequencing. DNAs were extracted from whole blood using Wizard genomic DNA purification kit (Promega). *ANK1, SLC4A1, SPTA1, EPB42* and *SPTB* genes were sequenced by Ion Torrent technology using a custom-designed AmpliSeq panel (www.ampliseq.com) covering the coding exons and 5bp of flanking introns (= splice sites). DNA libraries were prepared using Ion AmpliSeq Library Kit, according to the manufacturer protocol (Life Technologies) with 10ng of DNA for each of the two primer pools. Sequencing was performed on a *Personal Genome Machine* (PGM, Life Technologies), with chip 316. The sequences were aligned to the human reference genome (hg19) with the Ion Torrent Suite Server v5 (Life Technologies) in the form of *.bam* files. These files were imported in Highlander, a software developed in the de Duve Institute of UCLouvain (http://sites.uclouvain.be/highlander/), for variant calling with the embarked Torrent variant Caller v5.2 (Life Technologies), annotation and filtering.

RNAs were extracted from whole blood using TRIzol reagent (Invitrogen) and retrotranscribed with moloney murine leukemia virus reverse transcriptase (M-MLV RT; ThermoFisher). For RT-PCR, primers were chosen in exons distant from those carrying the mutations and variants of interest. Amplicons were purified using the Wizard® SV gel and PCR clean-up system from Promega, and sequenced on an ABI3130xl sequencer with the Big Dye Terminator v3.1 chemistry (Applied Biosystems). Chromatograms were analyzed using CLCbio Main Workbench.

Scanning electron microscopy of RBCs on filters. Washed RBCs were fixed in graded concentrations (0.1% followed by 0.5% then 1.5%) of glutaraldehyde in 0.1M cacodylate buffer for 5min each. Fixed RBCs were then filtered on 0.4µm polycarbonate (it4ip) filters using a syringe and washed by cacodylate buffer pushed gently through the syringe. Post-fixation was performed on the filters in the syringe in 1% OsO_4 in 0.1M cacodylate for 2h. Filters were then washed extensively in 0.1M cacodylate and 6 times for 10min in water. Samples were dissociated from the filter capsule and covered by a second filter in order to protect the sample during further processing, *i.e.* the dehydration and the critical point

drying. Dehydration was performed in graded baths of ethanol (50, 60, 70, 80, 90, 95% for 10min each, followed by 100% 3 times for 10min) and critical point dried. Finally, samples were mounted on scanning electron microscopy stubs and sputtered with 10nm gold. All samples were observed in the CM12 electron microscope with the SED detector at 80kV.

RBC hemoglobin release measurement. Washed RBCs were maintained at 37°C under constant agitation for 16h, then incubated into gradually hypotonic media at RT for 10min and pelleted by centrifugation at 200g for 2min. Supernatants and pellets were separated and assessed for hemoglobin release. Ratio of the supernatant to the sum of the supernatant and the pellet for each medium was expressed as percentage of the hemoglobin released upon RBC full hemolysis (*i.e.* RBCs in 0mOsm). Half-maximal effective hemolysis (EC50) was extrapolated using GraphPad Prism.

Isolation and analysis of microvesicles. Whole blood maintained for 0, 7 or 14 days at 4°C was centrifuged at 2000g for 10min. The plasma was recovered and centrifuged again at 2000g for 10min. The obtained plasma was diluted in sterile filtered PBS and centrifuged at 20.000g for 20min at 4°C. The resulting pellet was resuspended in sterile PBS before reiteration of the centrifugation step at 20.000g. The final pellet was resuspended in 1ml sterile PBS. Part of the pellet was fixed and allowed to attach for 8min onto coverslips pretreated with poly-L-lysine (PLL; 70-150kDa 0.01%; Sigma-Aldrich). Coverslips were then washed, fixed on 1% glutaraldehyde in 0.1M cacodylate and processed by scanning electron microscopy as for RBCs on filters (see above). The other part of the pellet was kept at -80°C for determination of the microvesicle size and abundance using a Zetaview® from Particle Metrix.

Immunofluorescence staining of RBC membrane and cytoskeletal proteins. Diluted washed RBCs were spread onto PLL-precoated coverslips, fixed with 4% paraformaldehyde for 10min and blocked with 1% bovine serum albumin (BSA; Sigma-Aldrich) for 30min. To label membrane proteins, RBCs were then incubated for 1h with rabbit monoclonal antibodies to glycophorin C (Abcam) together with mouse monoclonal antibodies to CD47 (Invitrogen), washed 4 times in 1% BSA, incubated for 1h with the appropriate Alexa-secondary antibodies (5µg/ml) and washed 4 times with 1% BSA. Total spectrin was revealed with antibodies against α/β-spectrins (Abcam) using the same protocol as above except that a permeabilization step with 0.5% Triton X-100 for 3min was done before the fixation. All coverslips were mounted in Mowiol in the dark for 24h and examined with a Zeiss LSM 510 confocal microscope using a plan-Apochromat 63x NA 1.4 oil immersion objective.

Coomassie blue and Western blotting. RBC ghosts were prepared using a hypoosmotic hemolysis method at 4°C [452]. Ghosts were then analyzed using 4-15% sodium dodecysufalte-polyacrylamide gel electrophoresis (SDS-PAGE; Bio-rad) and

PageBlue™ Protein staining solution (ThermoFisher) following Fairbanks et al instruction [453]. Quantification of the relative abundance of proteins in PageBlue stained gels was performed using Fiji software. After migration on 8 or 10% sodium dodecysufalte-polyacrylamide gel electrophoresis prepared in home and transfer, western blotting was performed using antibodies against β-spectrin (Abcam), Ankyrin (Merck Millipore), 4.1R (Sigma), PIEZO1 (ProteIntech), PMCA (ThermoFisher) or GAPDH (Invitrogen), followed by HRP-conjugated secondary antibodies and revelation by chemiluminescence (SuperSignal® west pico/femto chemiluminescent substrate, ThermoFisher) with the Fusion Solo S from Vilber.

Atomic force microscopy measurements and data analysis. RBC were immobilized with PLL in cell culture grade phosphate buffered saline (PBS, Sigma Aldrich). Glass-bottomed Petri dishes (WillCo) were covered with PLL:DMEM (1:1, v/v) and incubated at 37°C for 30min. After a washing step with DMEM at RT for 3min, Petri dishes were dried at RT in a laminar flow hood for 2h. The RBC suspension was plated onto the PLL-coated Petri dishes at RT for 4min, then replaced by fresh DMEM and attached RBCs were further allowed to spread for another 4min. After 2 or 3 rapid washings with DMEM, the sample was used for AFM experiments performed in DMEM. AFM experiments were performed either with a Bioscope Catalyst or Resolve AFM (Bruker, Santa Barbara, USA) in Force Volume mode at ~25-30°C. Precalibrated PeakForce QNM Live Cell probes (Bruker) with spring constants between 0.08-0.1N/m and a tip radius of curvature of 65nm were used. The spring constant of the cantilevers was calibrated with a vibrometer (OFV-551, Polytec, Waldbronn) by the manufacturer. The pre-calibrated spring constant was used to determine the deflection sensitivity using the thermal noise method [478] before each experiment. Individual FD curves were recorded in contact mode on the RBC surface, specifically at the RBC center (which is the highest part) to avoid substrate effects. The force setpoint was adjusted to reach indentation levels lower than 1µm to avoid irreversible damage of the cell. We used approach and retraction velocities of 1µm s^{-1} and a 5µm ramp size. At least 300 FD curves were recorded per cell. Raw FD curves were processed offline using the NanoScope Analysis 1.80 Software (Bruker, Santa Barbara, USA). The contact part of the FD curve was fitted with the Hertz model [479, 480]:

$$F^{2/3} = \left(\frac{4}{3}\frac{E}{(1-\nu^2)}\sqrt{R}\right)^{2/3}\delta \quad (1)$$

where E is the Young's modulus, δ the indentation depth, ν the Poisson ratio, and R the contact radius. The data resulted from the analysis of individual FD curves was plotted using the Origin Lab software.

Intracellular calcium modulation and measurement. To activate PIEZO1, diluted washed RBCs were incubated with 0.5µM Yoda1 (Biotechne) for 20sec at RT. To decrease the intracellular calcium content, RBCs were preincubated at RT in a calcium-free medium

containing 1mM of the calcium-chelating agent EGTA (Sigma-Aldrich) for 10min. EGTA was maintained during the whole experiment. Intracellular calcium was measured as previously [177] by incubation of washed suspended RBCs with 5µM Fluo-4 acetoxymethyl ester (Fluo-4 AM; Invitrogen) in calcium-containing homemade medium (25mM D-glucose, 5mM HEPES, 1.8mM $CaCl_2$, 5.33mM KCl, 44mM $NaHCO_3$, 82mM NaCl, 0.9mM $NaH_2PO_4.H2O$) for 60min at 37°C under continuous agitation . RBCs were then pelleted at 200g for 2min and resuspended in homemade medium, then let for 30min at 37°C under agitation to allow the Fluo-4 AM de-esterification. RBCs were then washed by centrifugation and fluorescence intensity was measured in 96-well plates with a spectrofluorimeter (GloMax; Promega) at λexc/λem of 490nm/520nm. Data were reported on the corresponding hemoglobin content measured at 450nm.

Intracellular ATP measurement. Measurement was performed on washed RBCs thanks to a chemiluminescence assay kit (Abcam). Data were reported on the corresponding hemoglobin content measured at 450nm.

Intracellular reactive oxygen species measurement. Measurement was done on RBCs incubated in suspension with 15µM 2',7'-dichlorodihydrofluorescein diacetate (H_2DCFDA; Invitrogen) in Krebs-Ringer medium for 60min at 37°C under continuous agitation. RBCs were then pelleted as above, resuspended and measured by spectrofluorimetry (GloMax; Promega) at λexc/λem of 490nm/520nm. Data were reported on the corresponding hemoglobin content measured at 450nm.

Membrane lipid measurements. Total phospholipids were evaluated by phosphorus assay after lipid extraction [447]. Membrane cholesterol was assessed using the Amplex Red Cholesterol assay kit with omission of cholesterol esterase (Invitrogen) [102, 448]. Phospholipids and cholesterol levels were reported on the corresponding hemoglobin content in the sample, measured at 450nm by spectrophotometry (SpectraCountTM, Packard BioScience Co).

Membrane lipid vital imaging. Coverslips were coated with PLL mixed with DMEM (1:1; v:v) at 37°C for 30min, then washed at least twice with DMEM at 20°C for 5min. BODIPY-SM and -GM1 membrane insertion was performed at RT and 37°C respectively, following the procedure described in [163]. For assessing PS exposure at the outer leaflet, RBCs were labeled in suspension with Annexin V-Alexa 647 (Invitrogen) for 15 min at 20°C in a calcium-containing medium. RBCs were either spread onto PLL-coated coverslips and placed upside down in Lab-Tek chambers (ThermoFisher) or dropped to settle down in µ-Slide VI0.4 uncoated IBIDI chambers (Proxylab), both filled with medium. Samples were then observed either with a Zeiss LSM510 confocal microscope using a plan-Apochromat 63X 1.4 oil objective or a Zeiss wide-field fluorescence microscope (Observer.Z1) using a plan-Apochromat 100X 1.4 oil Ph3 objective.

Image analysis and data quantification. All confocal images into one experiment were taken with the same settings to allow (semi-)quantitative analysis of fluorescence intensity or coverage and comparison between samples. RBC morphology (area, perimeter, circularity), spectrin intensity/covering and line intensity profiles on CD47/GPC confocal images as well as protein abundance on SDS-PAGE and western blots were determined using the Fiji software. Line intensity profiles were further analyzed for the (non)-overlapping between GPC and CD47 as follows. After threshold value determination to define the effective dynamic range, peaks were identified and classified into three categories: (i) only red, indicating non-overlapping of GPC with CD47; (ii) only green, indicating non-overlapping of CD47 with GPC; and (iii) red+green, indicating overlapping between both proteins. The abundance of peaks in each category was then expressed as percentage of total peaks. Lipid domain abundance/hemi-RBC surface was assessed by manual counting on confocal or fluorescence images and expressed by reference to the hemi-RBC projected area measured into the experiment.

Statistical analyses. Results are presented in the graphs by year of analysis but statistical analysis were performed on the final mean. One-way ANOVA followed by Dunnett's or Tukey's post-hoc tests (AFM) were used (only when $n \geq 3$). ns, not significant; *, $p<0.05$; **, $p<0.01$; ***, $p<0.001$.

2.6. Supplementary material

	P1	P2	P7	P8	P12	P14	P15	P16	P17	P18
Date of birth	2007	1977	2007	2003	2003	1992	1995	2010	2003	2002
Gender	M	M	F	F	F	F	M	M	M	F
Relationship	father & son		sisters			sister & brother				
Splenectomy	2013	?	2016	2012	2014	1997	2003	2016	2008	2008
Cholecystecto-my	2013	?	?	2012	2014	?		?	?	?

Supplemental Table 1. Patient overview. M, male; F, female; ?, to be checked.

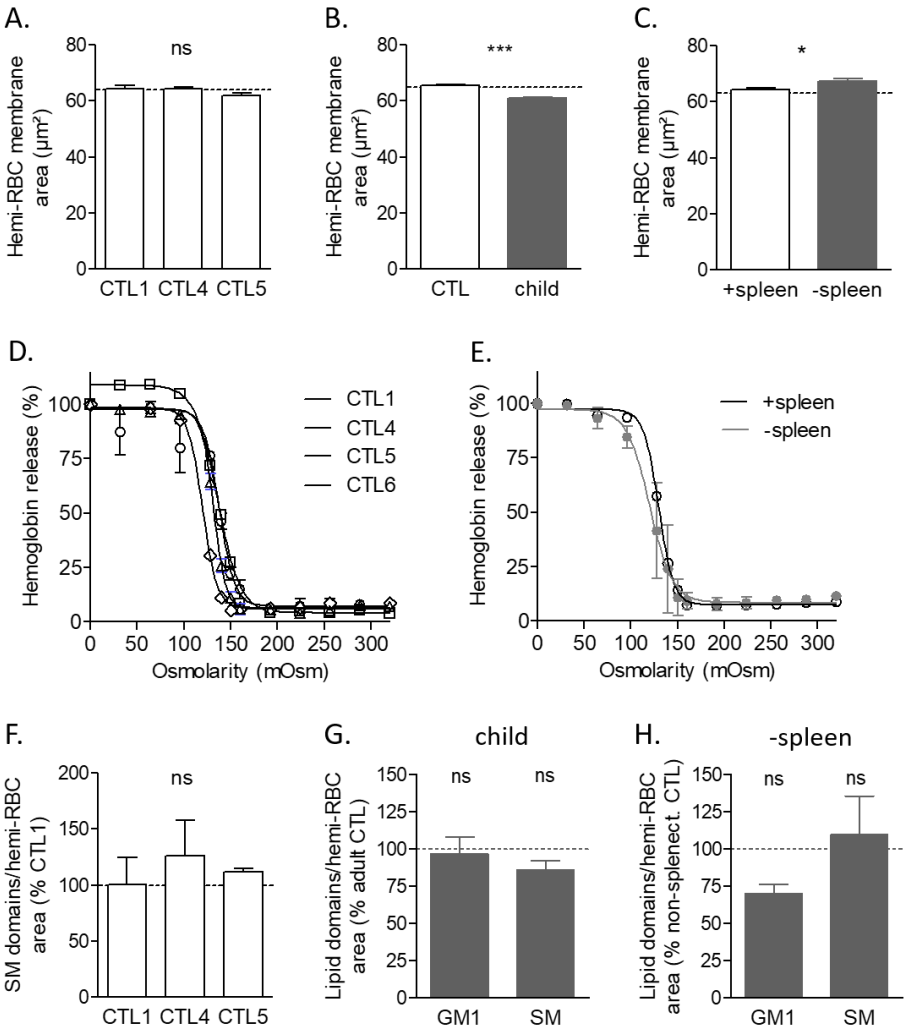

Supplemental Figure 1. Variations of healthy adult donors, donor age and splenectomy do affect neither the RBC fragility nor the lipid domain abundance but slightly modify the RBC size. (A-C) RBC projected area measured on fluorescent images of RBCs laid down on PLL-coated coverslips (means ± SEM of 4-9 independent experiments with 50-200 RBCs measured/condition in each experiment). **(D,E)** Hemoglobin release upon RBC incubation in media of decreasing osmolarity (means ± SD of 1-2 independent experiments). **(F-H)** Lipid domain abundance determined on RBCs spread onto PLL-coated coverslips, labeled with BODIPY-SM or -GM1 and visualized by fluorescence microscopy. Domain abundance is normalized by the RBC projected area. Data are mean ± SEM from 3-5 independent experiments/lipid (400-600 RBCs counted/condition in each experiment).

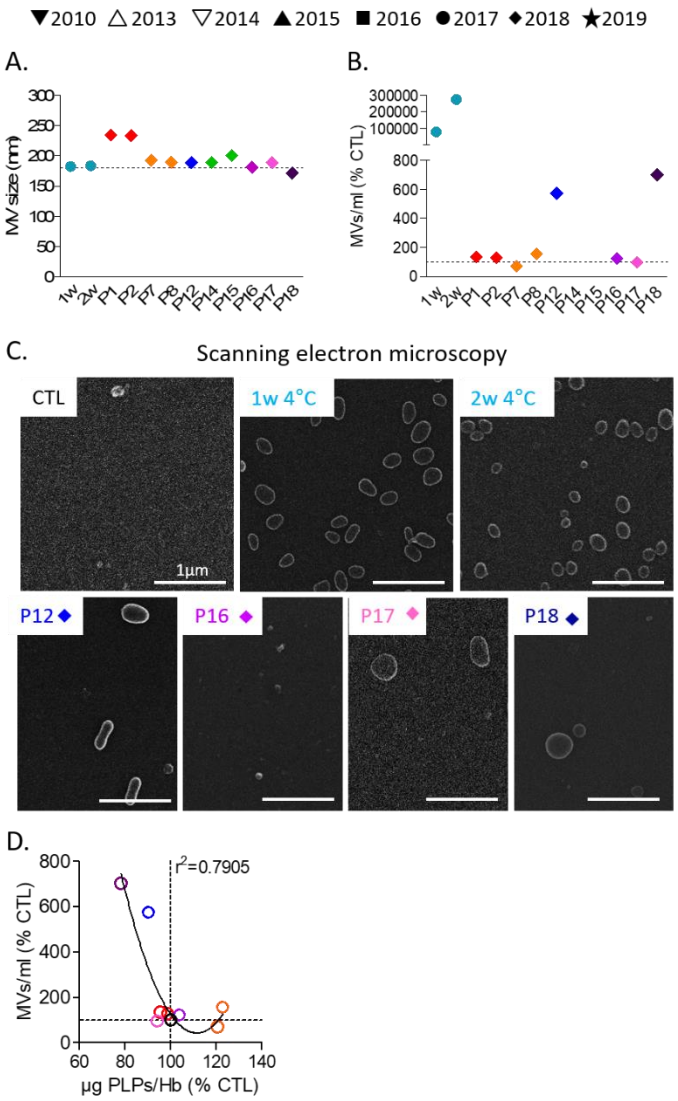

Supplemental Figure 2. Microvesicles released in the blood of patients present a similar size and morphology than those released in the blood stored at 4°C but are far less abundant. Microvesicles (MVs) isolated by multiple centrifugation steps from healthy fresh blood (dotted line), healthy blood kept at 4°C for 1 or 2 weeks (light blue symbols) or fresh blood of patients and analyzed for their size (A), abundance (B) and morphology (C). **(A,B)** Size and abundance of MVs analyzed by light scattering with Zetaview®. Data are means ± SD of 3 independent measures of the same MV preparations. Data are means/year ± SD of 3 independent measures of the same MV preparation. **(C)** Representative scanning electron microscope images of MVs laid down on PLL-coated coverslips before fixation. One image representative of 1-2 independent experiments. **(D)** Relation between MV abundance and total phospholipid content in the RBCs.

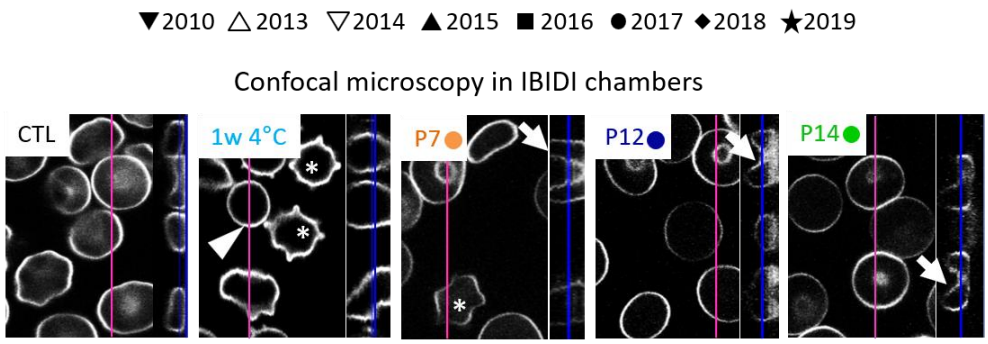

Supplemental Figure 3. Patient RBCs exhibit altered morphology. Vital confocal microscopy images of RBCs labeled with a BODIPY-lipid and laid down in IBIDI chambers. Arrowhead, spherocyte; arrows, stomatocytes; asterisks, echinocytes. One image representative of 2-3 independent experiments.

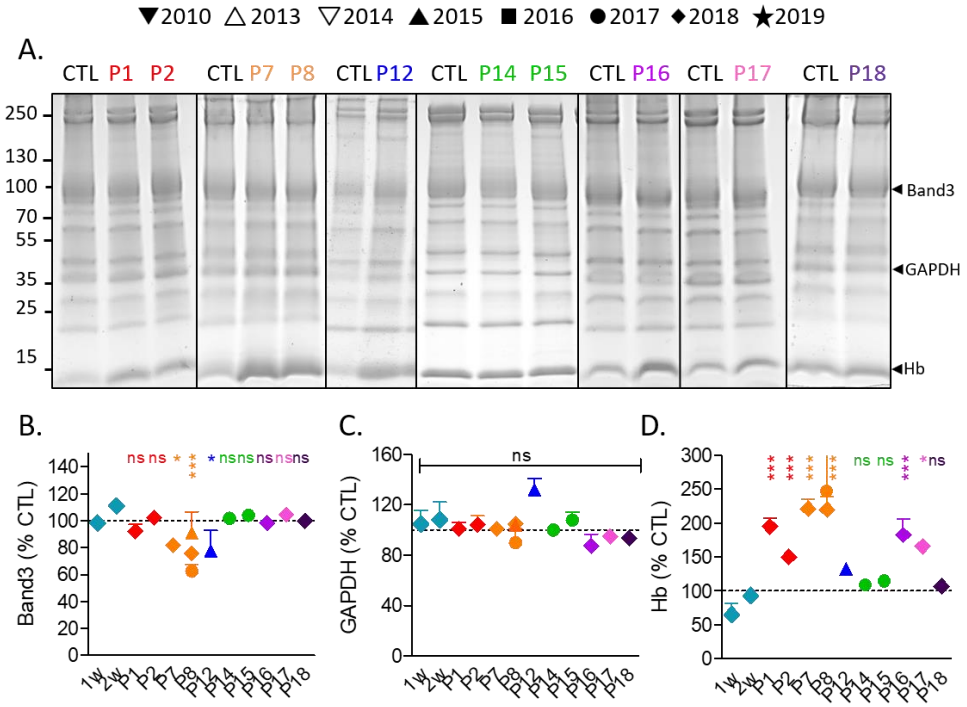

Supplemental Figure 4. Hemoglobin is differentially retained in the ghost membrane of patients but GAPDH is largely preserved – Extension of Figure 7. (A) Representative SDS-PAGE and Coomassie blue staining of ghost membrane proteins. **(B-D)** Quantification of Band3, GAPDH and hemoglobin by strip intensity reported to the sum of all strips in the track and then on control values. Data are means ± SEM/mean of 2-7 independent experiments.

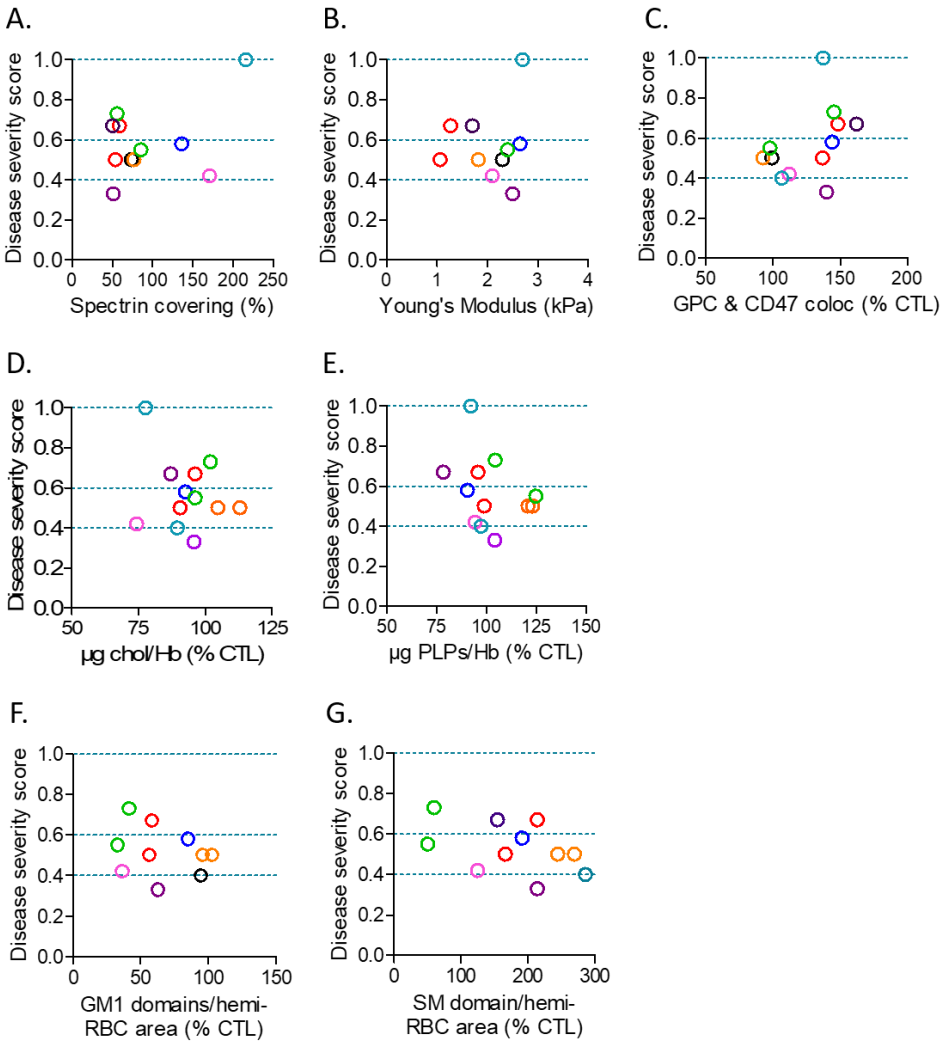

Supplemental Figure 5. Correlations between the disease severity score and cytoskeleton content and rigidity, membrane protein organization as well as membrane lipid content and organization. (A,B) Spectrin content and rigidity. **(C)** Loss of membrane protein spatial segregation. **(D,E)** Membrane cholesterol and total phospholipid contents. **(F,G)** GM1- and SM-enriched domain abundance per RBC hemi-area.

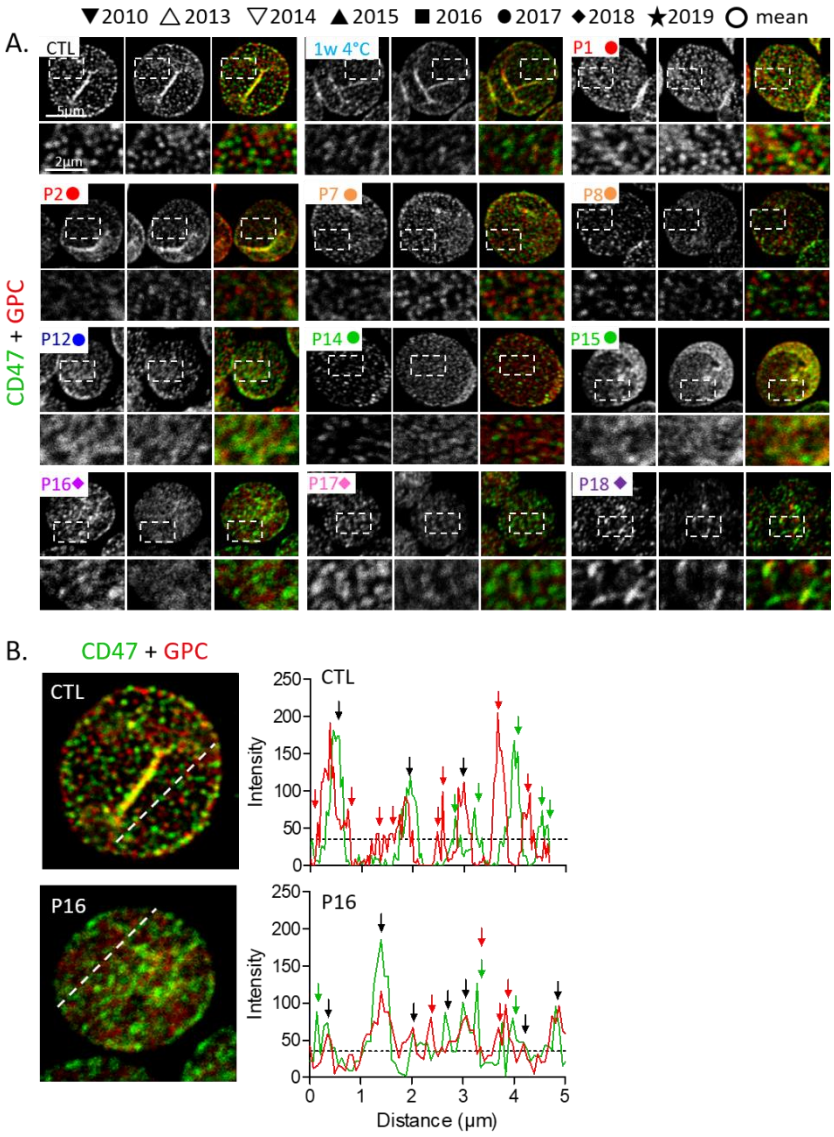

Supplemental Figure 6. Decrease of the spatial dissociation between glycophorin C and CD47 – Extension of Figure 5F. Healthy RBCs, either fresh (CTL) or stored at 4°C for 1 week, and diseased RBCs were laid down on PLL-coated coverslips, fixed and stained with antibodies against CD47 (Ankyrin complexes; green) and glycophorin C (GPC; 4.1R complexes; red). **(A)** Confocal images of representative RBCs and zooms on regions delimited by the dotted rectangles (insets). **(B)** Example of quantification on the intensity profiles along the paths indicated by white dotted lines at left. Green arrows, CD47 only; red arrows, GPC only; black arrows, CD47/GPC overlapping. Colocalization between CD47 and GPC was determined by counting the number of CD47, GPC or GPC/CD47 peaks along line intensity profiles.

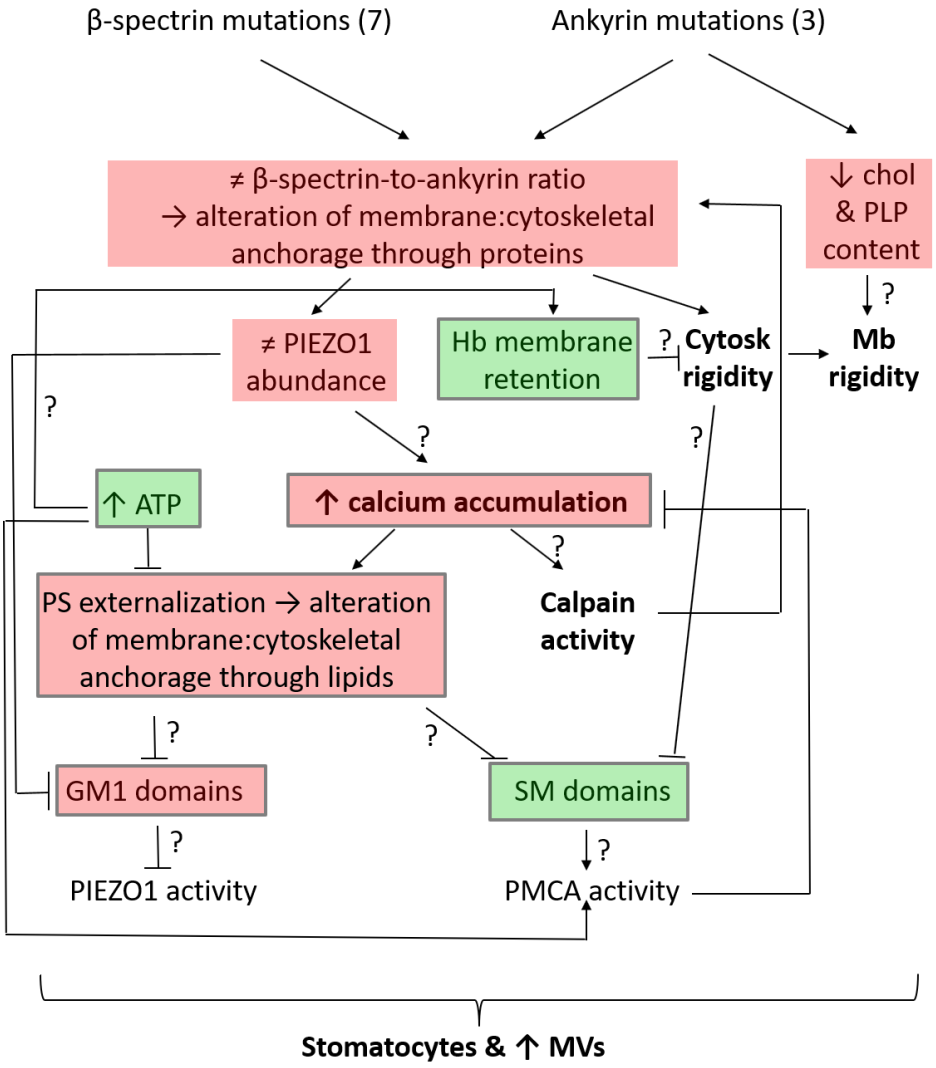

Supplemental Figure 7. Model for the interplay between cytoskeleton impairment and calcium intracellular accumulation and its consequences on plasma membrane transversal and lateral heterogeneity in spherocytosis. For explanations, see Discussion. Red, features increasing the of disease severity; green, features compensating the disease severity; grey outlines, disease severity-dependent features.

CHAPTER 4. GENERAL DISCUSSION AND PERSPECTIVES

After highlighting the major findings on hereditary elliptocytosis (HE) and spherocytosis (HS) reported in this Thesis (section 1) and evaluating the experimental strategy used (section 2), we will discuss the clinical significance of the observations (section 3) and the relevance for understanding cytoskeleton:membrane interplay (section 4). In addition, as RBC microvesiculation is a key event in chronic hemolytic diseases, their relevance in the pathophysiology of both diseases and the possibility that lipid domains could be the starting point of microvesicle (MV) shedding will be debated (section 5).

1. Summary of key findings and proposed models

To deliver oxygen to tissues, the RBC undergoes high deformations while passing through narrow capillaries. Such exceptional deformability relies on RBC intrinsic features, including (i) a biconcave shape resulting from the excess of plasma membrane surface *vs* the cytoplasmic volume, (ii) a finely regulated cytoplasmic viscosity controlled by the hemoglobin concentration, and (iii) a cytoskeleton composed of a meshwork of spectrin tetramers linked to the membrane vertically by ankyrin-based complexes and horizontally by 4.1R-based complexes.

In contrast, the importance of membrane lateral heterogeneity in lipid domains and on biophysical properties for RBC deformation was often overlooked. The current model of the laboratory highlights the coexistence at the RBC surface of three types of lipid domains playing differential roles: (i) the cholesterol-enriched domains, associated with high curvature membrane areas and able to gather in the high curvature areas formed during RBC deformation; (ii) the GM1/PC/cholesterol-enriched domains, associated with low-curvature areas and whose abundance increases with calcium entry upon RBC deformation; and (iii) the SM/PC/cholesterol-enriched domains, also associated with low-curvature areas and whose abundance increases with calcium efflux after deformation [163]. During my thesis I explored if and how lipid domains were deregulated in HE and HS to compare the importance of the horizontal and vertical membrane:cytoskeleton linkages, respectively.

RBCs of the patient suffering from HE presented spectrin tetramerization impairment due to the exclusive expression of the Leu260Pro variant of α-spectrin. We found that the intracellular calcium content was strongly increased and calcium exchanges at the RBC surface were slowed down. Mechanistically, the intracellular calcium overload induced phosphatidylserine exposure at the external plasma membrane leaflet and reactive oxygen species overproduction, resulting in lipid peroxidation. ROS accumulation could in turn trigger plasmatic acid sphingomyelinase (aSMase) activity, directly affecting SM-

enriched domains, but this remains to be shown. These membrane modifications led to slight increase of the GM1- and SM-enriched domain abundance associated with a lower cholesterol enrichment and their inability to respond to calcium exchange stimulations. These data indicate that alteration of membrane lipids and lipid domains through the plasmatic aSMase, oxidative stress and lipid scramblase activation all contribute to the pathophysiology of elliptocytosis.

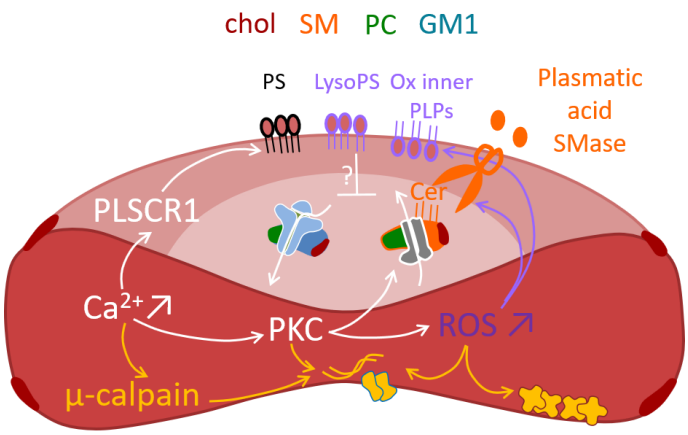

Figure 1. Model for the molecular mechanism behind the pathogenesis of elliptocytosis. Increased of intracellular calcium levels lead to activation of calcium-dependent PKC, which in turn is responsible for activation of NADPH oxidase activity and ROS accumulation into RBCs. ROS act then on phospholipids from the inner leaflet leading to lipid peroxidation, which may be the cause for 1) alteration of membrane lipids content, 2) modifications of membrane lipid organization into lipid-enriched domains and by consequence alteration of calcium exchanges, and 3) activation of plasmatic aSMase through oxidized phospholipids [433, 434]. Enhancement of plasmatic aSMase activity lead to formation of Cerarmide (cer)-enriched domains and modifications of the lipids content, especially into the SM-enriched domains. On the other hand, the raise of intracellular calcium and the decrease of cholesterol content lead to activation of scramblase activity (possibly PLSCR1) and abnormal exposure of PS at the membrane outer leaflet. ?, remains to be determined.

➔ *To validate this model, we will measure in pEl RBCs the µ-calpain activity, the spatial relationship between ceramide and SM/cholesterol-enriched domains, the effect of lysoPS accumulation of PIEZO1 activity and the oxidation state of hemoglobin and its retention to the membrane.*

The analysis of RBCs from splenectomised patients suffering from HS exhibits *ANK1* and *STPB* mutations. In all patients, RBC morphology and deformability were altered compared to healthy donors. These features together with the clinical parameters allowed to classify patients in three severity groups, which were family- and mutations-unrelated. In contrast, alterations of the cytoskeleton organization and rigidity, the morphology changes and the modification of membrane lipid contents were all disease-severity independent. The increased intracellular calcium content well correlated with the disease severity score. It contributed to membrane asymmetry impairment, lipid domain

reorganization and response to calcium exchanges stimulations and membrane microvesiculation. In contrast, increased intracellular ATP content was observed in the less affected patients with less intracellular calcium level, suggesting a possible compensatory mechanism. Altogether, our data indicate that impairment of the membrane cytoskeleton, membrane lipid content and organization in domains as well as the intracellular calcium and ATP contents all contribute to the heterogeneous pathophysiology of spherocytosis.

In section 4, I will compare our data on patients with elliptocytosis and spherocytosis for (i) the cytoskeleton protein content and organization, (ii) the membrane lipid content and organization in domains, (iii) the calcium content and exchange, (iv) the intracellular ATP, and (v) the contribution of calcium accumulation and the aSMase activation through reactive oxygen species for lipid domain alteration.

2. Experimental strategy: strengths and weaknesses

In this section, I will discuss the strengths and weaknesses of our experimental strategy while highlighting the way we tried to overcome the encountered failings.

2.1. Cell model

RBC is an ideal model to examine membrane lipid organization and its contribution to diseases due to the following features. Firstly, it is probably the best-characterized biological membrane, both for lipid and protein compositions [481, 482]. Secondly, it represents one of the best examples of cells able to endure significant and rapid deformation. Thirdly, it offers several technical advantages. For instance, RBCs are easily available, very abundant, rapidly isolated by centrifugation and highly homogenous due to the RBC quality control performed by the spleen. Moreover, their lipid metabolism is minimal as compared to nucleated cells, their plasma membrane is featureless, and they are devoid of vesicular trafficking. The two latter characteristics are very advantageous in the context of lipid organization analysis, excluding possible confusion between real domains and lipid enrichment due to membrane protrusions and endocytic pits at the cell surface.

Besides the above advantages, the RBC also presents several limitations. For instance, for optimal analysis by microscopy, they must be immobilized onto glass coverslips precoated with poly-L-lysine to avoid RBC transformation in echinocytes. However, poly-L-lysine could induce excessive RBC stretching (and the concomitant loss of the biconcavity encountered in the blood) and artificial gathering of lipids. These potential artefacts have been reasonably ruled out based on the similar evidence for lipid domains in RBCs maintained in suspension in poly-L-lysine-free systems such as IBIDI chambers or 3D-gels [175, 176]. Another limitation is that, due to the absence of nucleus in the mature RBC, it is

difficult to analyse the inner plasma membrane leaflet organization and its connection with the underlying cytoskeleton through the expression of specific fluorescent proteins.

In this study, we used RBCs of patients with genetic membrane fragility disorders such as spherocytosis and elliptocytosis. This approach also presents some difficulties. Aside from the limited number of patients diagnosed and the necessity to acquire all the data in a limited time to preserve the characteristics of "fresh" blood, the heterogeneity of mechanisms underlying these diseases complicates the interpretation. Indeed, spherocytosis and elliptocytosis are heterogeneous groups of diseases with phenotypical similarities, i.e. chronic hemolytic anaemia and to some extent RBC morphology. The responsible mutations are numerous, affecting several genes and resulting in different qualitative or quantitative defects of proteins, which all lead to the same apparent diagnosis. However, the heterogeneity of molecular alterations in different patients was not well explored and understood.

Moreover, it was long though that mature RBCs are strictly identical in the circulation and between individuals. It may be true for macroscopic elements such as morphology, size and number, but is more challenging for other types of measures such as intracellular calcium and ROS contents or membrane lipid organization in domains. For this reason, we included more than ten different healthy donors in our studies.

After analysis of RBCs upon resting state, we then extended our study to RBCs upon deformation. The major difficulty was related to the need to deform the RBC while following the dynamic of membrane lipid domains or intracellular calcium. In other words, the approach to deform RBCs must be compatible with high-resolution confocal microscopy. We therefore opted for silicon (polydimethylsiloxane, PDMS)-stretchable chambers, kindly provided by Philippe Gailly (UCLouvain, BXL), on which labelled RBCs were laid down thanks to poly-L-lysine coating. The results obtained should be confirmed by alternative approaches adapted to RBCs in suspension upon application of physiologically relevant shear stress. This could be achieved by the use of microfluidic devices coupled with automated image analysis [483].

2.2. Membrane lipid imaging

2.2.1. Lipid tools

To evidence lipid organization at the outer RBC plasma membrane leaflet, we used three main types of lipid probes compatible with vital imaging: (i) fluorescent lipid analogs inserted in the membrane; and (ii) fluorescent toxin fragments targeting endogenous lipids [102, 161, 162, 175, 176, 178].

Lipid analogs present several advantages: (i) availability for numerous lipids; (ii) efficient delivery to the membrane using defatted bovine serum albumin (BSA) as a carrier molecule; (iii) possible extraction by "back-exchange" using empty BSA; and (iv) size close to their endogenous counterparts. Although a broad variety of fluorescent lipid analogs are available and have been used in previous researches, their validity as surrogates of endogenous lipid counterparts is sometimes debated mainly because the substitution of the fatty acid chain by the fluorophore might induce differential phase partitioning as compared to the endogenous lipids [484]. Moreover, only few convincing and validated fluorescent analogs of cholesterol are available [168]. Among the different fluorophores, I chose the BODIPY [485] because : (i) it presents good quantum yield and photostability as compared to other fluorophores, allowing to reduce the concentration of analog inserted in the membrane; and (ii) BODIPY-lipids have been extensively validated by my laboratory before I started my thesis [102, 161, 162].

Toxin derivatives/fragments are of potential interest to decorate endogenous lipids. The cholera toxin, secreted by the bacteria *Vibrio cholera*, is a multi-complex protein composed of two subunits, the toxic A subunit and the non-toxic pentameric B subunit which binds GM1. The B subunit has been successfully used to bind GM1 without toxicity, but the multivalence of the probe could induce artificial clustering. To label endogenous SM, natural toxins are also available. Among these, Lysenin is produced by the worm *Eisenia Foetida*. However, after binding to membrane SM, Lysenin oligomerizes and forms pores, leading to the target cell lysis. Lysenin possesses two distinct domains, the N-terminal domain responsible for the lytic activity and the C-terminal responsible for SM binding [164]. Kobayashi and colleagues validated a minimal truncated form of Lysenin, (corresponding to the C-terminal domain) which is non-toxic (NT-Lysenin) still able to specifically bind to SM [165, 166]. Cholesterol-specific natural toxins also exist and, include the streptolysin O of *Streptococcus pyogenes*, the pneumolysin of *Streptococcus pneumoniae*, the listeriolysin O of *Listeria monocytogenes* or the perfringolysin O (or Theta toxin) of *Clostridium perfringens* [170]. In a similar approach as described above for Lysenin, the D4 domain of Theta as minimal segment able to recognize cholesterol without promoting cytolysis was isolated [172, 173]. In general, toxin fragments present several advantages as compared to fluorescent lipid analogs, allowing for (i) direct labelling of endogenous lipids, (ii) versatile coupling with fluorescent proteins or fluorophores, and (iii) possible labelling in 3D-gels. However, they also present potential disadvantages including: (i) the limitation of labelling of the outer plasma membrane leaflet in living cells, (ii) the big size of the probes in comparison to the target lipids, which restricts lipid diffusion, and (iii) the binding above a lipid target concentration threshold. For instance, the Theta toxin binds membrane cholesterol only when a ≈30% concentration is reached [172, 486-488] while Lysenin binds clustered SM [166, 489-491]. In our laboratory, we produced mCherry-

derivative of NT-Lysenin and Theta-D4. Upon living RBC labelling with those two fluorescent toxin fragments, we revealed lipid domains similar to those observed upon fluorescent lipid analog membrane insertion. Hence, the SM-enriched domains revealed by NT-Lysenin present the same characteristics as the ones observed upon BODIPY-SM insertion, i.e. (i) similar abundance, size and shape, (ii) the disappearance after moderate cholesterol depletion and (iii) the dependence to membrane tension. Moreover, sequential co-labelling of mCherry-NT-Lysenin and BODIPY-SM identified the same lipid domains, validating *a posteriori* results obtained with BODIPY-SM (Figure 2) [175]. We were not able to perform the same comparison between mCherry-Theta-D4 and a fluorescent cholesterol analog because, if analogs for sterols are available, their membrane orientation and/or distribution behaviour have been denunciated to deviate from native cholesterol [167].

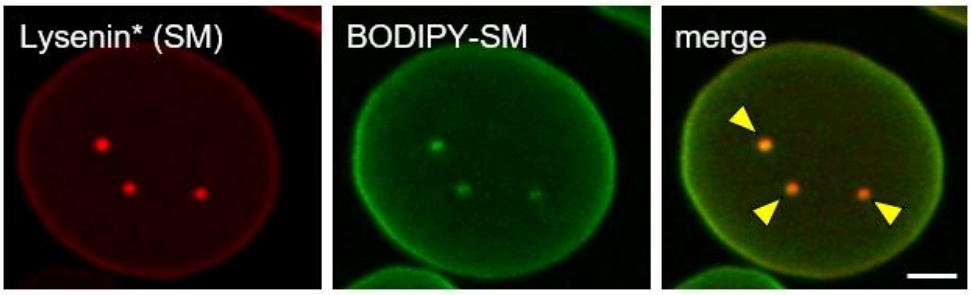

Figure 2. Colocalization between BODIPY-SM and mCherry-NT-Lysenin (Lysenin*). RBCs were labelled in suspension with mCherry-NT-Lysenin, washed, attached-spread on poly-L-Lysine-coverslips, then labelled with exogenous BODIPY-SM in the absence of mCherry-NT-Lysenin. Yellow arrows, colocalization [175].

2.2.2. Imaging methods

To study lipid domain abundance, we privileged confocal or epifluorescence imaging. Epifluorescence is fast while confocal is slower but confocal imaging allows better resolution and is needed for co-labelling. RBC spreading on poly-L-lysine allows the observation of the entire domain population in one image due to the RBC immobilization and flattening. For quantification, RBC morphology (projected area, circularity, perimeter) was measured in ImageJ by surrounding by hand each RBC for at least 400 RBCs by experiment and condition. The number of domains was manually counted on the same images. These analyses are time consuming but variability between (and even inside) a coverslip is important and is reduced by analyses of enough images and RBCs.

Super-resolution microscopy technics allow to circumvent the light diffraction limit of fluorescence microscopy, improving the resolution to ≈50 nm (*vs* ≈300 nm in confocal microscopy for instance). Their principal drawback resides in the requirement for fixation, which could reorganize the membrane lipids. Atomic force microscopy (AFM) is an

alternative technique to improve the spatial resolution while avoiding fixation. As proof-of-concept experiment, AFM was recently applied to living unlabelled RBCs by the group of David Alsteens (UCLouvain, LLN) in collaboration with the host laboratory [179, 492]. More recently, they also successfully coupled the tip of the cantilever with Theta-D4 to specifically analyse cholesterol organization in artificial membranes [493]. However, the time to process one RBC represents a major limitation, potentially leading to other artefacts.

2.3. Intracellular calcium and reactive oxygen species measurements

2.3.1. Calcium

Several probes are available to measure the intracellular calcium content, including Indo-1, Fura-2 and Fluo-4. Indo-1 and Fura-2 require excitation in the UV range while Fluo-4 can be excited at 480nm. An advantage of Fura-2 is its ratiometric property, allowing correction of artefacts due to bleaching, change in focus or variations in laser intensity. However, hemoglobin quenches the excitation/emission of these three indicators in a concentration-dependent manner. In addition, both Fura-2 and Indo-1 display dramatic spectral shifts in their emission spectra due to hemoglobin content [494]. Fluo-4 should then be privileged for measurements in RBCs.

We used Fluo-4 coupled to acetoxymethyl ester (AM). The ester group renders the molecule non-fluorescent and helps to cross the membrane. Once inside the cell, it is cleaved by intracellular esterases to Fluo-4 able to bind free calcium. Despite these advantages, Fluo-4 is not specific for calcium and can also bind other bivalent cations including magnesium. To circumvent this difficulty, we used magnesium-free home-made media.

2.3.2. Reactive oxygen species

2',7'-dichlorodihydrofluorescein diacetate (H_2DCFDA) is a reduced cell permeant form of fluorescein. Upon cleavage of the acetate groups by intracellular esterases and oxidation, the non-fluorescent H_2DCFDA is converted to the highly fluorescent 2',7'-dichlorodihydrofluorescein [495, 496]. The oxidation occurs thanks to hydrogen peroxide and hydroxyl radical, even if the specificity is still debated [497]. It is therefore recommended to use H_2DCFDA as a marker of cellular oxidative stress and not as an indicator of hydrogen peroxide formation [496]. Other problems are (i) the leakage and quenching at high concentration, (ii) the photoreduction in the presence of visible light and iii) autoxidation of the probe in complex culture media in some conditions [496]. To avoid these artefacts, RBCs were incubated in the dark and washed just before fluorescence measurements. We also opted for incubation in simple media as Krebs Ringer Hepes (KRH) medium [497].

2.4. Microvesicles isolation and analysis

Several methodologies have been developed over the years to optimize MV isolation. They are extensively described in our recent review (Annex 7, [404]). Differential ultracentrifugation is the most frequent one, even if protocols can considerably vary in terms of speed and time intervals. Increasing centrifugal forces allow to separate MVs from cell debris and intact cells thanks to their difference in size and density [498-501]. This method allows to reach a recovery of up to 80% and offers the possibility to process large volumes without the need for chemicals that could interfere with downstream analysis [500]. Among limitations one can cite MV aggregation, contamination by protein aggregates and viruses as well as MV damaging during high-speed centrifugation [498]. To avoid these drawbacks, MVs were isolated in filtered and sterile phosphate buffered saline medium and washed by centrifugation between each step.

Electron microscopy allows us to visualize MV preparations and to assess both MV size and morphology [498, 502]. Since dehydration and fixation required for traditional electron microscopy could possibly lead to MV morphology changes, these analyses were completed by dynamic light scattering measurement. Thanks to the recording of light scattering over the time and its modification due to MV Brownian motion, it is possible to determine MV size distribution [502]. To isolate MVs originating from RBCs *vs* other blood cells such as platelets, Anne-Sophie Cloos in the laboratory currently performs FACS on MVs using fluorescent antibodies against specific surface proteins of RBCs and platelets (coll. Nicolas Dauguet, UCLouvain, BXL).

3. Clinical significance

In both HE and HS, accelerated RBC clearance from the circulation is a common part of the mechanism leading to chronic anemia. In HE, we provided strong evidence that the intracellular calcium and ROS overloads and the plasmatic aSMase activity, contribute to the molecular mechanisms leading to the clearance. We therefore examined whether targeting ROS or the plasmatic aSMase activity could be beneficial fort the patient.

- ROS overload: incubation with natural scavengers as ascorbic acid (AA). Although incubation of pEl blood with AA effectively decreased the intracellular ROS content, it worsened cell circularity and did not restore RBC resistance to hemolysis. AA has been tested in various studies [503], sometimes generating conflicting results. For instance, it was beneficial in blood storage units, reducing the mechanical fragility and hemolysis over the storage period [246], and in patients with iron deficiency anemia, decreasing peroxidation and oxidation biomarkers in blood [248]. In contrast, it was inefficient in patients with sickle cell anemia, even leading to increased hemolysis biomarkers [249]. As a possible explanation for these discrepancies, pEl shares as common feature with

sickle cell disease enhanced RBC curvature, which in turn could impact plasmatic aSMase activity [446], possibly worsening hemolysis.

➔ *As results in the literature with AA are contradictory, supplementation with vitamin E could be considered as alternative possible ROS scavenger. If GSH content is reduced in pEl RBCs, supplementation with N-acetylcysteine could also be a possible promising treatment [243]. Furthermore, future drug developments in chronic hemolytic anemia should benefit from targeting calcium entry as calcium overload is a current feature observed in anemia [424]. In sickle cell disease, NMDA receptors mediate excessive calcium uptake and their inhibition by memantine administration is proposed as possible treatment [469].*

- Plasmatic aSMase overactivity: inhibition by amitriptyline treatment. We evidenced here that plasmatic aSMase inhibition by amitriptyline induced a reduction of intracellular calcium and ROS contents, an increase of RBC circularity and a decrease of hemoglobin release. Amitriptyline has already proven its effectiveness in sickle red cells, reducing RBC MV generation [426], but also on RBCs upon storage, exhibiting a reduction of hemolysis and of PS externalization [504].

  ➔ *Amitriptyline opens new avenue for treatment of elliptocytosis. To pursue this possibility, amitriptyline treatment could be tested in vivo on consenting patients.*

Our study highlights the heterogeneity of molecular modifications between patients. To help the interpretation, patients were associated with a disease severity score based on clinical parameters, RBC morphology and deformability impairments and the extent of microvesiculation. This disease severity score increases with the rise in the intracellular calcium content and instead decreases with the intracellular ATP level, suggesting that those two parameters represent aggravating and compensating mechanisms, respectively. These results show that individualized patient management should be privileged, at the expense of systematic medical care based only on classical clinical parameters.

4. Importance of the cytoskeleton:lipid domain interplay for RBC deformability

On HE and HS RBCs, we first characterized the cytoskeleton alterations (section 4.1) and then analyzed the consequences of these impairments for membrane lipid content and organization (section 4.2), calcium content and exchanges (section 4.3) and ATP level (section 4.4). We finally explored the mechanisms behind lipid domain alteration (section 4.5.).

4.1. Cytoskeletal and membrane protein content and organization

α and β spectrins associate to form dimers which can be in closed or open forms (Introduction, section 4.2.2.). Open dimers can then associate to form tetramers, representative of the principal structural units to construct the RBC cytoskeleton. There is a fine equilibrium between closed dimer, open dimer and tetramer. This equilibrium enables dynamic rearrangements of the membrane cytoskeleton when RBCs are deformed. In elliptocytosis, many mutations impair the formation of spectrin tetramers and destabilize the membrane by unknown mechanisms. Moreover, several of these mutations are distal to the tetramerization sites and, of these, several are prolines in the linkers between repeats of α-spectrin [355]. The Leu260Pro mutation found in pEl is located next to the linker between two spectrin repeats α2 and α3. Using a mini-spectrin construct incorporating the Leu260Pro mutation, Harper et al showed no significant changes in the secondary structure, suggesting that structural destabilization is relatively minor and localized. However, the mutation affects the closed-open dimer equilibrium and favors closed dimers, reducing tetramer formation [186]. Another study suggests that point mutation in a single domain results in slower folding and faster unfolding. However, this effect was not exceptionally destabilizing in the case of Leu260Pro. But when a two-domain system was used, the mutation caused a loss of the stabilizing interactions between the domains, mediated through the linker helix [356]. These effects are well compensated in patients carrying this mutation only, as we saw for the mother of pEl (pElm). The normal allele is probably taking over as α-spectrin is produced in large excess, exceeding three or four times the production of β-spectrin [430].

In elliptocytosis, any mutation affecting spectrin tetramerization should impact the horizontal linkages of the cytoskeleton and could lead to a less “connected” meshwork [422]. In pEl RBCs, the impairment of spectrin tetramerization does not appear to alter spectrin anchorage to the membrane, as no loss of spectrin content nor covering were observed. It is hypothesized that over time and deformation, elliptic RBCs tend to elongate as they are not able to restore their original shapes. In other words, the number of tetramers decrease because the equilibrium between dimers and tetramers is shifted in

favor of dimers. Based on our observations, we propose that closed spectrin dimers, useless to form the spectrin meshwork, are still attached to the membrane and tend to accumulate to one edge of the cells. The lack of spectrin tetramers could then in turn force the anchorage complexes to reorganize to ensure optimal attachment of the cytoskeleton to the membrane, leading to increased colocalization of ankyrin and 4.1R complexes.

- ➔ *Patients presenting several types of mutations in SPTA1 (in the tetramerization site, distal from it or in other α-spectrin functional domains as SH3 domain), EPB41 or SPTB should be included in the study to evaluate whether our current model is relevant to elliptocytosis in general.*
- ➔ *It remains to evaluate how spectrin tetramerization changes could impact the vertical linkages between the membrane and the cytoskeleton. Electron microscopy or super-resolution techniques should be privileged to explore this question.*
- ➔ *It would also be relevant to evaluate the role in elliptocytosis of the non-muscle myosin IIA filaments which are ≈200nm long filaments associated with short F-actin filament of the spectrin-F-actin network. Blebbistatin incubation weakens these associations, causing non-muscle myosin IIA filaments to dissociate from the spectrin-F-actin network. The resulting relaxation of the contractile forces of the network, reduces membrane tension and increases deformability. This relaxation leads to an elongation of the RBC shape, reminiscent to the RBC morphology in HE [505].*

In the ten patients suffering from spherocytosis included in our study, seven patients presented mutations in *STPB* gene (P1, P2, P7, P8, P14, P15, P16) and the other three in *ANK1* gene (P12, P17, P18). To the best of our knowledge, none of the mutations found were described before (ensembl and clinvar databases). In all patients, the alleles carrying the mutations are reduced by nonsense-mediated mRNA decay. Accordingly, a reduction of the ankyrin or the β-spectrin contents in the RBC, depending of the mutated gene, were observed. In P12 exhibiting an *ANK1* mutation, we observed a combined ankyrin content decrease with β-spectrin content increase. This observation is surprising as ankyrin deficiency is often combined with the lack of spectrin, probably by aberrant sorting during enucleation [388]. As alternative explanation, we suggest that the weakened cohesion between the cytoskeleton and the lipid bilayer could lead to MV release enriched or devoid of specific proteins. β-spectrin enrichment in P12 RBCs could then be explained by an increased release of cytoskeleton-free MVs. In agreement with this hypothesis, P12 exhibited the strongest release of MVs and increase of the RBC membrane rigidity imposed by the cytoskeleton, as old RBCs. Still more surprisingly, we observed that P16, who presents a mutation in the β-spectrin gene, shows an additional decreased abundance of ankyrin. Combined deficiency of spectrin and ankyrin are indeed often described, but secondary to mutations in *ANK1* [506].

- ➔ *To validate and extend these observations, the determination of the ankyrin and β-spectrin contents will be extended to the entire cohort of patients by proteomic analyses. It is also needed to recruit new patients, especially with SLC4A1 mutations which accounts for one third of patients affected by spherocytosis [361].*
- ➔ *To elucidate whether cytoskeletal and membrane protein impairment could occur during erythropoiesis or in the circulation, we could use the immortalized erythroid line which can be differentiated in mature functional reticulocytes [507], allowing to study protein sorting during erythroblast enucleation. Sorting impairment of membrane proteins has been already shown in 4.1R-knockout and ankyrin-deficient mice [113].*

4.2. Membrane lipid content and organization in domains

Several mechanisms behind the plasma membrane lipid reorganization detected in spherocytosis and elliptocytosis can be proposed. The first mechanism involves the direct coupling of the cytoskeleton to membrane lipids, as supported by the following observations. Firstly, it has been shown on liposomes of defined compositions that spectrin interacts with PC, PS, phosphatidylethanolamine (PE) and phosphatidylinositol (PI), which can cause enthalpic changes associated with a modification of phase transition temperature of these liposomes [508, 509]. Moreover, spectrins possess several putative lipid-binding sites. For instance, β-spectrin has a relatively high affinity towards aminophospholipid (PS and PE)-rich membrane compartments [184, 510-512]. Secondly, spectrin is present in detergent-resistant-membranes (DRM) and the probability of direct spectrin:lipid interaction has been suggested but remains to be demonstrated [184]. Thirdly, we have previously shown that membrane:cytoskeleton uncoupling at 4.1R complexes by activation of protein kinase C with phorbol-12-myristate-13-acetate (PMA, mimicking the diacylglycerol) and calyculin A (a phosphatase inhibitor) increases the abundance of BODIPY-SM and -glucosylceramide domains [161], suggesting that these lipid domains are restricted by membrane:cytoskeleton coupling at 4.1R complexes. It was then proposedthat the relaxation of this coupling leads to lipid reorganization in the inner leaflet especially PS, known to be stabilized by 4.1R complexes [513]. In the patient with elliptocytosis we observed that the increase of SM-enriched domains upon PMA/CalA treatment was abrogated, which could suggest that 4.1R-based complexes were already decoupled in the disease.

The second mechanism proposes that the link between the cytoskeleton and deformation impairment in spherocytosis and elliptocytosis could be the alteration of lipid domains involved in calcium exchanges. Several lines of evidences support this hypothesis. Firstly, all patients exhibited alteration of at least one class of lipid domains involved in calcium exchanges at the RBC surface. On the contrary, no modification of cholesterol-

enriched domains (not involved in calcium exchanges) was observed. Secondly, the GM1- and SM-enriched domain increases observed in healthy RBCs upon calcium influx and efflux were abrogated in all patients whatever the disease. It suggests a perturbation of calcium exchanges which was confirmed in elliptocytosis in PDMS chambers. Thirdly, the alteration of lipid domains by treatment with mβCD of RBCs from the patient with elliptocytosis led to calcium increase and worsened the RBC fragility. Fourthly, the increase of SM-enriched domain abundance by amitriptyline treatment led to the decrease of intracellular calcium content, supporting the importance of SM-enriched domains for calcium extrusion.

The third mechanism suggests that lipid domains may be modified in lipid composition following the increase of reactive oxygen species content and plasmatic aSMase activity, as shown in elliptocytosis.

➔ *It remains to determine whether and how lipid domains and the cytoskeleton-associated proteins are spatially related. Studying this question by confocal microscopy is challenging since labeling of proteins requires fixation, which could cause lipid redistribution. On fixed RBCs, D'auria et al showed that SM-enriched domains are spatially associated with membrane proteins of the 4.1R-based complexes [161]. To study both proteins and lipids in living cells, we could use Fab' fragments of monoclonal antibodies against specific proteins of the 4.1R- and the ankyrin-based complexes.*

4.3. Calcium intracellular content and exchanges

Calcium imbalance is a relatively common molecular mechanism in hereditary anemia such as xerocytosis, sickle cell disease or spherocytosis [264, 424, 514]. However, it remains elusive how a mutation in hemoglobin or a cytoskeletal protein could be responsible for the increased intracellular content. In contrast the entry of calcium in patients suffering of xerocytosis is easily explained when mutations are found in the gene encoding for the mechanosensitive cation channel PIEZO1 [468, 515]. For instance, some mutations in the C-terminal part of PIEZO1 are shown to be associated with a more active channel [516]. In sickle cell disease, abundant and hyperactive NMDA receptors have been identified as the cause of abnormal uptake of calcium [469]. The mechanism leading to hyperactivation of NMDA receptors is not yet elucidated, even if a clearance defect of plasma membrane receptors during the terminal RBC differentiation stages has been suggested [469]. In spherocytosis, we showed that the calcium accumulation was associated with a decreased abundance of PIEZO1. In the absence of PIEZO1, another protein involved in calcium influx could then take over, leading to calcium accumulation in RBCs at resting state. In elliptocytosis, the decreased abundance of PMCA could partially explain the accumulation of calcium inside the RBCs.

Such PIEZO1 and/or PMCA selective sorting could take place during (i) microvesiculation or fragmentation of mature RBCs, or (ii) protein sorting at the enucleation step of erythroblast maturation, which involves association with spectrin/ankyrin cytoskeleton [114]. The substantial loss of membrane in the patient with elliptocytosis could be achieved by membrane fragmentation at the end of the RBCs rather than by vesiculation, as blood MV abundance was decreased in pEl as compared to healthy RBCs [178, 477]. According to this view, it has been shown that elliptocytotic RBC precursors are round, progressively becoming more elliptical with aging after release in the circulation [345]. However, since fragmentation is often described as a form of lysis [295, 466], it is hard to conceive that a controlled mechanism of protein sorting takes place during this process. In spherocytosis, we have shown that vesiculation was increased in two patients out of 8. Nevertheless, even if selective sorting occurs by this process, it may not be sufficient to explain all our observations.

We therefore propose that the loss of PIEZO1 and PMCA in elliptocytotic RBCs and of PIEZO1 in spherocytotic RBCs would rather take place during erythroblast maturation and enucleation. Aberrant protein sorting during enucleation has already been shown to occur in elliptocytosis and spherocytosis mice models, i.e. when the cytoskeleton and the anchorages complexes are not fully functional [190]. If our hypotheses are true, this indicates that PMCA sorting depends on the horizontal linkages via spectrin tetramers and that PIEZO1 sorting depends on the ankyrin/spectrin linkages. Several literature data support the possibility that an abnormal organization of HE cytoskeleton, and particularly the 4.1R/actin-based complexes, may be responsible for the loss of PMCA during enucleation. For instance, purified F-actin (which is part of the 4.1R-based anchorage complexes in RBCs) has been shown to inhibit the activity of PMCA while incubation with short oligomers of actin stimulate the activity of the pump [517-519]. Moreover, the shape changes in activated platelets imply an increase in the F-actin-to-total actin ratio together with the redistribution of PMCA to the newly formed filopodia adjacent to F-actin rich cytoskeleton [519]. Based on this observation, we suggest that PMCA will be relocalized during cytoskeleton reorganization upon RBC deformation. The F-actin depolymerization and decoupling of the 4.1R-based complexes will then lead to PMCA activation and initiation of the calcium content restoration, as a negative feedback loop.

Besides changes of membrane protein abundance, protein activity could be altered through modifications of the membrane biophysical properties (e.g. thickness, curvature or surface tension) or of binding of specific lipids to the protein surface. Indeed, the PMCA activity is regulated by acidic phospholipids (especially PS) in the inner leaflet. Thus, upon PS externalization to the cell surface by calcium-dependent scramblases, the pump activity is decreased, and the cytosolic calcium overload is exacerbated [219, 520] and PIEZO1 is inhibited as recently revealed in myoblasts [429]. Such PS-dependent alteration of PMCA

and/or PIEZO1 activity is relevant in the HE RBCs for two reasons: (i) they present a strong decrease of the PS species; and (ii) they expose 2-fold more PS at their outer leaflet. It could also occur in the patients suffering from spherocytosis who expose a higher content of PS at the cell surface (e.g. P14, P15). Furthermore, higher plasma membrane lipid order has been shown to enhance the activity of the PMCA [471].

- ➔ *The association of PIEZO1 or PMCA with the cytoskeleton and/or anchorage complexes will be studied by confocal vital imaging on the human immortalized erythroid line (see above) transfected with fluorescent WT or mutant PIEZO1 or PMCA. This approach will be also useful to achieve genetic modifications of the target proteins while modulating lipid synthesis/contents.*
- ➔ *To estimate the protein activity, patch-clamp will be used for PIEZO1 while the extent of PMCA aggregate formation will be measured to indirectly estimate the PMCA activity [437].*

4.4. ATP intracellular content

Reduced ATP content is known to give rise to more fully connected spectrin network and higher membrane compression [14] and the availability of ATP limits the PMCA transport capacity [521]. The elliptocytotic RBCs and these from a series of patients with spherocytosis (P1, P2, P7, P8, P16 and P17) showed an increased intracellular ATP level which contrasted with the abrogation of intracellular ATP in RBCs upon aging. These patients with spherocytosis showing increased ATP also exhibited increased hemoglobin membrane retention and SM domain abundance, lower calcium content and lower disease severity, suggesting that this increase represents a compensatory mechanism. Notice that ATP pools are trapped in membrane-associated complexes involving ankyrin, Band3, GAPDH and β-spectrin [126]. Disorganization caused by the lack of one of these proteins in spherocytosis could be responsible for the disruption of the ATP-rich platforms.

- ➔ *To analyze cytoskeleton proteins and hemoglobin association with the ATP pools, the membrane-associated ATP pool can be filled with exogenous N_3-ATP or 8-azido-[α-^{32}P]-ATP in ghosts. The ghosts are then washed free of loading substrates, leaving only the ATP analogs entrapped within the membrane-associated pools. We can then analyse the pools either by western blotting or by autoradiography for the ATP analogs and other proteins of interests [126].*

4.5. Contribution of calcium accumulation and plasmatic acid sphingomyelinase to lipid domain alteration

The very high intracellular calcium content we found in the elliptocytotic RBCs as compared to those with spherocytosis led us to investigate in more details the role of this accumulation in these two diseases. To this aim, we analyzed the activity of a series of

calcium-dependent enzymes including the PKC (through PMA/calyculin treatment), the PKC-dependent NADPH oxidase [228] (through ROS measurement) and the scramblase/flippase activities (through PS externalization).

In HS, as expected from the lower calcium accumulation than in HE, ROS content was not increased, and the PS externalization was only observed in two patients out of 4. The importance of PKC activity is under evaluation. Hence, we will soon measure the activity of μ-calpain which can mediate the cleavage of the PMCA, hemoglobin, ankyrin, Band3, 4.1R, adducin and dematin [522]. These two measurements are essential to evaluate whether the intracellular calcium could indeed contribute with the cytoskeleton to increase the membrane rigidity found in all the patients, except P1 and P2.

In contrast, in HE, the three above mechanisms take place, indicating that the calcium intracellular accumulation should play a crucial role in the disease. The PKC activity and the PS externalization were discussed above. We will here focus on the oxidative stress. Upon RBC incubation with EGTA, the ROS content in HE RBCs was strongly decreased, suggesting activation of NADPH oxidase. It should be noted that NADPH oxidase is not the only mechanism of ROS generation and that plasma hemoglobin and free heme increased due to chronic hemolysis can also generate superoxide radicals via nonenzymatic mechanisms. Several consequences of ROS accumulation for the membrane lipids were observed. Firstly, membrane lipid peroxidation was considerably increased. Secondly, we observed an important increase of some lysoPS species, bioactive signaling phospholipids shown in neutrophils to be generated following activation of the NADPH oxidase [435, 436], were highly increased. Since lysolipids present an inverted conical shape which could lead to increased outward membrane curvature, they should be localized where the local curvature is maximal. Besides membrane lipids, oxidative stress could also affect the PMCA activity by direct oxidation or by binding of oxidized calmodulin [437-439], hemoglobin and spectrin [440]. The autoxidation of hemoglobin leads to formation of irreversible hemichromes which have great affinity for the cytoplasmic domain of Band3. This binding is one possible starting point of the aging process in which hemichromes binding lead to Band3 clustering and recognition by autoantibody for phagocytosis.

Based on the observation that the activity of plasmatic aSMase is increased in several hemolytic anemias [228, 426, 461, 476, 523], we also evaluated the implication of this enzyme in the two diseases. Two mechanism could explain the increased activity of plasmatic aSMase in pEl. Firstly, oxidized phospholipids accumulated in the membrane of pEl RBCs could trigger plasmatic aSMase activation [433, 434]. Secondly, the highest abundance of SM-enriched domains could favor the accessibility of the enzyme for its subtrate. We propose that lipid domains provide the crosstalk between aSMase and redox signaling. SM/PC/chol-enriched domains represent interesting candidates for this role since they (i) are enriched in SM and aSMase can act on SM present in domains, locally producing

ceramide [441], (ii) contain PCs, a major source of peroxidation if they are polyunsaturated [442-444], (iii) are increased upon aSMase inhibition, reaching a similar abundance as those enriched in ceramide.

➔ *Colabeling between ceramide- and SM-enriched domains upon amitriptyline treatment is required to check whether SM-enriched domains represent a preferential target for aSMase activity.*

5. RBC vesiculation, cytoskeleton and lipid domains

One of the major consequences of RBC calcium accumulation and membrane rigidity due to compression of the cytoskeleton to the membrane is the RBC vesiculation, leading to membrane loss and the formation of smaller and more spheric RBCs. Upon RBC storage at 4°C we observed that the high curvature-associated cholesterol-enriched domains are preferentially lost, potentially representing preferential sites for membrane microvesiculation. This observation was the starting point of our review (Pollet et al, Biomolecules 2018; Annex 7; [404]). The part of the section 5 of this review dedicated to RBCs is listed at section 5.1 of the present discussion whereas evidences for the role of lipid domains in membrane vesiculation in other cell types are provided in the full paper (Annex 7; [404]). Finally, whether the vesiculation model could account or not in elliptocytosis and spherocytosis is discussed in section 5.2.

5.1. Plasma membrane lipid domains as platforms for vesicle biogenesis and shedding in RBCs upon storage or aging?

Lutz and coll. already provided in 1976 the first indirect clue that RBCs could vesiculate from specific areas of the plasma membrane. In fact, they observed that vesicles from sheep RBCs stored at 4°C exhibit the same PLPs as the ghost membrane but a 2-fold increase of lipid-to-protein ratio and an enrichment in glycoproteins, suggesting that these proteins are mobile and can cluster in specific membrane areas, leading to vesiculation [524]. From that time, several observations have supported the potential involvement of lipid domains in RBC membrane vesiculation.

Firstly, DRMs can be prepared from MVs [525] and the MVs present raft-associated lipids and proteins. Indeed, MVs released upon calcium increase contain the raft-associated proteins GPI-anchored proteins [526] and stomatin [475, 527, 528]. Interestingly, RBCs from patients suffering from paroxysmal nocturnal hemoglobinuria do not present GPI-anchored proteins and exhibit a disturbed vesiculation capacity [529]. Moreover, in patients with stomatocytosis, which is caused by stomatin deficiency, calcium-induced MVs are more numerous and of abnormal size as compared to healthy individuals [530], suggesting that stomatin is important, but not essential, for the regulation of proper MV shedding.

Secondly, MV shedding is highly dependent on cholesterol, which is essential for both lipid rafts and submicrometric lipid domains. As a matter of fact, Santos and coll. have postulated that the total RBC membrane cholesterol content is declined by the release of cholesterol-enriched vesicles [531]. Moreover, upon strong cholesterol depletion (at high mβCD concentrations) in erythroleukemia cells, PS movement to the external leaflet upon addition of a calcium ionophore is inhibited [532], suggesting the involvement of lipid domains in transversal lipid asymmetry associated to membrane vesiculation. At low concentrations, mβCD appears to instead increase the number of MVs released [533]. These *a priori* contradictory observations could be explained by the very different mβCD concentration used and/or by the differential effects of these depletions on intracellular calcium.

Thirdly, we recently provided clues for the vesiculation of cholesterol- and SM/cholesterol-enriched domains upon RBC storage at 4 °C for <15 days [177]. Our data are, at first glance, in conflict with the observations that (i) RBCs and MVs obtained during storage in blood banks for ~40 days do not exhibit any difference in the main phospholipid classes (i.e., PC, PE, PS and SM) [534]; and (ii) RBCs and MVs from leukoreduced stored RBC units for >50 days show similar phospholipid composition, except PS [535]. Differences could be related to cholesterol enrichment (not assessed in the two latter studies), conditions of blood conservation (leukoreduction or not) and/or time of storage (<15 vs 40 and >50 days). As explained above, MVs of various lipid composition could be released upon storage time.

Finally, Dinkla and coll. showed that the formation of ceramide-enriched platforms upon RBC incubation with aSMase is accompanied by the induction of membrane irregularities enriched in the GPI-anchored protein CD59 [536]. Likewise, upon addition of ceramide at the RBC membrane, slow transformation of the biconcave RBC in echinocyte has been shown, suggesting that ceramide is responsible to form membrane spicules thanks to its conical shape [537].

We have recently proposed a hypothesis for the control of vesicle formation from lipid domains. By labeling with Laurdan, we revealed that cholesterol-enriched domains exhibit lower lipid order than the rest of the membrane in RBCs at resting state. In contrast, upon RBC vesicle release, lipid order of the domains increases, leading to lower lipid order difference between domains and the bulk [538]. We therefore speculated that lipid domains represent specific sites of MV budding by a mechanism driven by the lateral tension applied by the cytoskeleton and its impact on the line tension at phase boundary [538]. A local detachment of the cytoskeleton from the membrane and the echinocytic shape formation seem to be required for normal vesiculation in RBCs. It was already proposed in 2008 that the membrane:cytoskeleton uncoupling favours the coalescence of small rafts into large domains able to curve and to detach from the membrane [525]. Moreover, in comparison to healthy RBCs, fresh spherocytotic RBCs present higher

differential lipid order between lipid domains and the bulk membrane together with an accelerated initiation of domain vesiculation upon aging. This suggests that the cytoskeleton pressure could give the main contribution that controls the differential lipid order and drives RBC vesiculation [538].

5.2. Plasma membrane lipid domains as platforms for vesicle biogenesis and shedding in RBC membrane fragility diseases?

A recent simulation study revealed that (i) vesicles released from spherocytotic and elliptocytotic RBC membranes are more diverse in size than those released from healthy RBCs, and (ii) vesicles released from the elliptocytotic, but not from the spherocytotic, membrane may contain fragments of the cytoskeleton [459]. However, to the best of our knowledge, no comprehensive analysis of the MV abundance nor content from the blood of these patients is available in the literature. Even less information is available regarding their biogenesis and shedding. Several hypotheses have nevertheless been proposed in spherocytosis. Firstly, since proteins of the ankyrin complex are needed for the vertical anchorage of the membrane to the cytoskeleton, their simple loss could result in reduced mechanical strength and the subsequent vesiculation. Secondly, secondary loss of cytoskeleton components may create an area of weakness in the membrane. Thirdly, loss of Band3, the most abundant integral membrane protein of the RBC surface, could affect RBC membrane integrity [539]. However, the vesiculation process might differ depending on the underlying molecular defect (i.e. ankyrin, spectrin or Band3 mutation) and thus lead to MVs with different compositions [386].

In this thesis, we highlighted that the vesiculation is lower in the RBCs from patients suffering from elliptocytosis compared to healthy donors. Since calcium overload, increase of the plasmatic aSMase activity, PS exposure and oxidative stress are all features observed in eryptosis, a process involving membrane blebbing/fragmentation [540]. We instead suggest that the membrane loss in HE occurs through fragmentation.

In contrast to elliptocytosis, vesiculation was observed in spherocytosis but only significantly in two patients out of ten (P12 and P18). These two patients share the common feature to be ankyrin-deficient. However, the third patient with ankyrin-deficiency (P17) and the patient with secondary ankyrin defect (P16) showed an apparently normal MV abundance. Moreover, the vesiculation observed in our study appeared modest as compared to what is suggested in the literature. Several factors could explain these discrepancies. Firstly, all the patients tested are splenectomized. A recent study using a two-component RBC model to probe the dynamics of healthy and diseased RBCs traversing interendothelial slit reveals that the spleen might be responsible for most of the vesiculation occurring in spherocytosis [422]. Secondly, studies on mice suggest that MVs from RBCs are removed very fast from the circulation by the reticuloendothelial system

[416]. Thirdly, compensation mechanisms could allow to reduce the compression induced by the cytoskeleton on the membrane, thereby reducing membrane rigidity and therefore microvesiculation. This hypothesis could account for P16 and P17 who presented a strong increase of the intracellular ATP content. Fourth, besides the membrane rigidity imposed by the cytoskeleton, the intracellular calcium and ATP contents must be integrated while evaluating the extent of MVs released from RBCs.

- ➔ *To further study the significance of MVs released in spherocytosis, the cohort size should include both splenectomized and non-splenectomized patients. Preliminary data show that the non-splenectomized patients presented a severe decrease of the abundance of SM-enriched domains as compared to the splenectomized patients from the same families, reaching a level similar to the one observed in healthy RBCs (Figure 3). This suggests that SM-enriched domains could represent sites for vesiculation when the spleen is still present.*
- ➔ *Accelerated aging can be induced by keeping the patient blood at 4°C to expand the MV release and elucidate the respective contribution of increased calcium, membrane rigidity due to the cytoskeleton compression or ATP decrease in the microvesiculation process.*

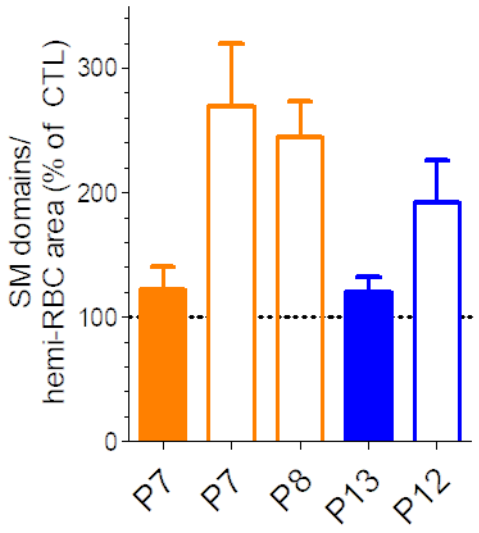

Figure 3. Sphingomyelin-enriched domain abundance at the RBC surface of non-splenectomized vs splenectomised patients suffering from spherocytosis. To note, P7 was analysed before (closed columns) and after splenectomy (open columns). Fresh healthy (dotted line) or diseased RBCs from two different families (P7,P8 vs P12,P13), splenectomized (open columns) or not (closed columns), were spread onto PLL-coated coverslips, labeled with BODIPY-SM and directly visualized by vital fluorescence microscopy. Data are means ± SEM of 4-8 independent experiments in which 200-800 RBCs were counted by condition in each experiment. Individuals from the same family are presented in the same color.

REFERENCES

1. van Meer, G., D.R. Voelker, and G.W. Feigenson, *Membrane lipids: where they are and how they behave.* Nat Rev Mol Cell Biol, 2008. **9**(2): p. 112-24.
2. Pollard, T.D., et al., *Chapter 13-Membrane structure and dynamics*, in *Cell biology*. 2017, Elsevier.
3. Carquin, M., et al., *Recent progress on lipid lateral heterogeneity in plasma membranes: From rafts to submicrometric domains.* Prog Lipid Res, 2016. **62**: p. 1-24.
4. Epand, R.M. and R.F. Epand, *Bacterial membrane lipids in the action of antimicrobial agents.* J Pept Sci, 2011. **17**(5): p. 298-305.
5. Deleu, M., et al., *Complementary biophysical tools to investigate lipid specificity in the interaction between bioactive molecules and the plasma membrane: A review.* Biochim Biophys Acta, 2014. **1838**(12): p. 3171-3190.
6. Dickson, R.C., et al., *Synthesis of mannose-(inositol-P)2-ceramide, the major sphingolipid in Saccharomyces cerevisiae, requires the IPT1 (YDR072c) gene.* J Biol Chem, 1997. **272**(47): p. 29620-5.
7. Daum, G., et al., *Systematic analysis of yeast strains with possible defects in lipid metabolism.* Yeast, 1999. **15**(7): p. 601-14.
8. Wolkers, W.F., et al., *In situ assessment of erythrocyte membrane properties during cold storage.* Mol Membr Biol, 2002. **19**(1): p. 59-65.
9. Biro, E., et al., *The phospholipid composition and cholesterol content of platelet-derived microparticles: a comparison with platelet membrane fractions.* J Thromb Haemost, 2005. **3**(12): p. 2754-63.
10. Fauvel, J., et al., *Biochemical characterization of plasma membranes and intracellular membranes isolated from human platelets using Percoll gradients.* Biochim Biophys Acta, 1986. **856**(1): p. 155-64.
11. Pankov, R., et al., *The plasma membrane lipid composition affects fusion between cells and model membranes.* Chem Biol Interact, 2006. **164**(3): p. 167-73.
12. Cezanne, L., L. Navarro, and J.F. Tocanne, *Isolation of the plasma membrane and organelles from Chinese hamster ovary cells.* Biochim Biophys Acta, 1992. **1112**(2): p. 205-14.
13. Calderon, R.O. and G.H. DeVries, *Lipid composition and phospholipid asymmetry of membranes from a Schwann cell line.* J Neurosci Res, 1997. **49**(3): p. 372-80.
14. Perkins, R.G. and R.E. Scott, *Plasma membrane phospholipid, cholesterol and fatty acyl composition of differentiated and undifferentiated L6 myoblasts.* Lipids, 1978. **13**(5): p. 334-7.
15. Sahu, S. and W.S. Lynn, *Lipid composition of human alveolar macrophages.* Inflammation, 1977. **2**(2): p. 83-91.
16. Pichler, H. and A. Emmerstorfer-Augustin, *Modification of membrane lipid compositions in single-celled organisms - From basics to applications.* Methods, 2018. **147**: p. 50-65.
17. Harayama, T. and H. Riezman, *Understanding the diversity of membrane lipid composition.* Nat Rev Mol Cell Biol, 2018. **19**(5): p. 281-296.
18. Barman, A., et al., *Phospholipases play multiple cellular roles including growth, stress tolerance, sexual development, and virulence in fungi.* Microbiol Res, 2018. **209**: p. 55-69.
19. Yang, Y., M. Lee, and G.D. Fairn, *Phospholipid subcellular localization and dynamics.* J Biol Chem, 2018. **293**(17): p. 6230-6240.
20. Ramstedt, B. and J.P. Slotte, *Membrane properties of sphingomyelins.* FEBS Lett, 2002. **531**(1): p. 33-7.

21. Singh, P. and R. Li, *Emerging roles for sphingolipids in cellular aging.* Curr Genet, 2018. **64**(4): p. 761-767.
22. D'Angelo, G., et al., *Glycosphingolipids: synthesis and functions.* FEBS J, 2013. **280**(24): p. 6338-53.
23. Yu, R.K., et al., *Structures, biosynthesis, and functions of gangliosides--an overview.* J Oleo Sci, 2011. **60**(10): p. 537-44.
24. Ogretmen, B., *Sphingolipid metabolism in cancer signalling and therapy.* Nat Rev Cancer, 2018. **18**(1): p. 33-50.
25. Bienias, K., et al., *Regulation of sphingomyelin metabolism.* Pharmacol Rep, 2016. **68**(3): p. 570-81.
26. Henry, B., et al., *Acid sphingomyelinase.* Handb Exp Pharmacol, 2013(215): p. 77-88.
27. Kornhuber, J., et al., *Secretory sphingomyelinase in health and disease.* Biol Chem, 2015. **396**(6-7): p. 707-36.
28. Goncalves, M.D., B.D. Hopkins, and L.C. Cantley, *Phosphatidylinositol 3-Kinase, Growth Disorders, and Cancer.* N Engl J Med, 2018. **379**(21): p. 2052-2062.
29. Ksiazek, M., et al., *Sources, metabolism, and regulation of circulating sphingosine-1-phosphate.* J Lipid Res, 2015. **56**(7): p. 1271-81.
30. Gorter, E. and F. Grendel, *On Bimolecular Layers of Lipoids on the Chromocytes of the Blood.* J Exp Med, 1925. **41**(4): p. 439-43.
31. Danielli, J.F. and H. Davson, *A contribution to the theory of permeability of thin films.* Journal of Cellular and Comparative Physiology, 1935. **5**: p. 495-508.
32. Robertson, J.D., *The molecular structure and contact relationships of cell membranes.* Prog Biophys Mol Biol, 1960. **10**: p. 343-418.
33. Lombard, J., *Once upon a time the cell membranes: 175 years of cell boundary research.* Biol Direct, 2014. **9**: p. 32.
34. Pinto da Silva, P. and D. Branton, *Membrane splitting in freeze-ethching. Covalently bound ferritin as a membrane marker.* J Cell Biol, 1970. **45**(3): p. 598-605.
35. Singer, S.J. and G.L. Nicolson, *The fluid mosaic model of the structure of cell membranes.* Science, 1972. **175**(4023): p. 720-31.
36. Feigenson, G.W., *Phase behavior of lipid mixtures.* Nat Chem Biol, 2006. **2**(11): p. 560-3.
37. Heberle, F.A. and G.W. Feigenson, *Phase separation in lipid membranes.* Cold Spring Harb Perspect Biol, 2011. **3**(4).
38. Sprong, H., P. van der Sluijs, and G. van Meer, *How proteins move lipids and lipids move proteins.* Nat Rev Mol Cell Biol, 2001. **2**(7): p. 504-13.
39. Ciana, A., C. Achilli, and G. Minetti, *Membrane rafts of the human red blood cell.* Mol Membr Biol, 2014. **31**(2-3): p. 47-57.
40. Heberle, F.A., et al., *Bilayer thickness mismatch controls domain size in model membranes.* J Am Chem Soc, 2013. **135**(18): p. 6853-9.
41. Samsonov, A.V., I. Mihalyov, and F.S. Cohen, *Characterization of cholesterol-sphingomyelin domains and their dynamics in bilayer membranes.* Biophys J, 2001. **81**(3): p. 1486-500.
42. Owen, D.M., et al., *Quantitative imaging of membrane lipid order in cells and organisms.* Nat Protoc, 2011. **7**(1): p. 24-35.
43. Mukherjee, R., et al., *Nanoscale Surface Characterization of Human Erythrocytes by Atomic Force Microscopy: A Critical Review.* IEEE Trans Nanobioscience, 2015. **14**(6): p. 625-33.
44. Roa, J.J., et al., *Calculation of Young's modulus value by means of AFM.* Recent Pat Nanotechnol, 2011. **5**(1): p. 27-36.
45. Alimohamadi, H. and P. Rangamani, *Modeling Membrane Curvature Generation due to Membrane(-)Protein Interactions.* Biomolecules, 2018. **8**(4).
46. McMahon, H.T. and E. Boucrot, *Membrane curvature at a glance.* J Cell Sci, 2015. **128**(6): p. 1065-1070.

47. Kapus, A. and P. Janmey, *Plasma membrane--cortical cytoskeleton interactions: a cell biology approach with biophysical considerations.* Compr Physiol, 2013. **3**(3): p. 1231-81.
48. Graham, T.R. and M.M. Kozlov, *Interplay of proteins and lipids in generating membrane curvature.* Curr Opin Cell Biol, 2010. **22**(4): p. 430-6.
49. Devaux, P.F., et al., *How lipid flippases can modulate membrane structure.* Biochim Biophys Acta, 2008. **1778**(7-8): p. 1591-600.
50. Fertuck, H.C. and M.M. Salpeter, *Localization of acetylcholine receptor by 125I-labeled alpha-bungarotoxin binding at mouse motor endplates.* Proc Natl Acad Sci U S A, 1974. **71**(4): p. 1376-8.
51. Stachowiak, J.C., et al., *Membrane bending by protein-protein crowding.* Nat Cell Biol, 2012. **14**(9): p. 944-9.
52. Aimon, S., et al., *Membrane shape modulates transmembrane protein distribution.* Dev Cell, 2014. **28**(2): p. 212-8.
53. Horvath, C.A., et al., *Epsin: inducing membrane curvature.* Int J Biochem Cell Biol, 2007. **39**(10): p. 1765-70.
54. Drin, G. and B. Antonny, *Amphipathic helices and membrane curvature.* FEBS Lett, 2010. **584**(9): p. 1840-7.
55. Parton, R.G. and M.A. del Pozo, *Caveolae as plasma membrane sensors, protectors and organizers.* Nat Rev Mol Cell Biol, 2013. **14**(2): p. 98-112.
56. Andersen, O.S. and R.E. Koeppe Ii, *Bilayer thickness and membrane protein function: An energetic perspective*, in *Annual Review of Biophysics and Biomolecular Structure*. 2007. p. 107-130.
57. Killian, J.A., *Hydrophobic mismatch between proteins and lipids in membranes.* Biochimica et Biophysica Acta - Reviews on Biomembranes, 1998. **1376**(3): p. 401-415.
58. Lee, A.G., *How lipids affect the activities of integral membrane proteins.* Biochimica et Biophysica Acta - Biomembranes, 2004. **1666**(1-2): p. 62-87.
59. van Galen, J., et al., *Sphingomyelin homeostasis is required to form functional enzymatic domains at the trans-Golgi network.* J Cell Biol, 2014. **206**(5): p. 609-18.
60. Norimatsu, Y., et al., *Protein-phospholipid interplay revealed with crystals of a calcium pump.* Nature, 2017. **545**(7653): p. 193-198.
61. Cohen, B.E., *Membrane Thickness as a Key Factor Contributing to the Activation of Osmosensors and Essential Ras Signaling Pathways.* Front Cell Dev Biol, 2018. **6**: p. 76.
62. Lee, A.G., *How lipids affect the activities of integral membrane proteins.* Biochim Biophys Acta, 2004. **1666**(1-2): p. 62-87.
63. Andersen, O.S. and R.E. Koeppe, 2nd, *Bilayer thickness and membrane protein function: an energetic perspective.* Annu Rev Biophys Biomol Struct, 2007. **36**: p. 107-30.
64. Cybulski, L.E. and D. de Mendoza, *Bilayer hydrophobic thickness and integral membrane protein function.* Curr Protein Pept Sci, 2011. **12**(8): p. 760-6.
65. Bretscher, M.S., *Asymmetrical lipid bilayer structure for biological membranes.* Nat New Biol, 1972. **236**(61): p. 11-2.
66. Op den Kamp, J.A., *Lipid asymmetry in membranes.* Annu Rev Biochem, 1979. **48**: p. 47-71.
67. Murate, M., et al., *Transbilayer distribution of lipids at nano scale.* J Cell Sci, 2015. **128**(8): p. 1627-38.
68. Zachowski, A. and P.F. Devaux, *Transmembrane movements of lipids.* Experientia, 1990. **46**(6): p. 644-56.
69. Steck, T.L. and Y. Lange, *Transverse distribution of plasma membrane bilayer cholesterol: Picking sides.* Traffic, 2018. **19**(10): p. 750-760.
70. Seigneuret, M., et al., *Asymmetric lipid fluidity in human erythrocyte membrane: new spin-label evidence.* Biochemistry, 1984. **23**(19): p. 4271-5.

71. Morrot, G., et al., *Asymmetric lateral mobility of phospholipids in the human erythrocyte membrane.* Proc Natl Acad Sci U S A, 1986. **83**(18): p. 6863-7.
72. Devaux, P.F. and R. Morris, *Transmembrane asymmetry and lateral domains in biological membranes.* Traffic, 2004. **5**(4): p. 241-6.
73. Contreras, F.X., et al., *Transbilayer (flip-flop) lipid motion and lipid scrambling in membranes.* FEBS Lett, 2010. **584**(9): p. 1779-86.
74. Gault, C.R., L.M. Obeid, and Y.A. Hannun, *An overview of sphingolipid metabolism: from synthesis to breakdown.* Adv Exp Med Biol, 2010. **688**: p. 1-23.
75. Setty, B.N., S. Kulkarni, and M.J. Stuart, *Role of erythrocyte phosphatidylserine in sickle red cell-endothelial adhesion.* Blood, 2002. **99**(5): p. 1564-71.
76. Steck, T.L., J. Ye, and Y. Lange, *Probing red cell membrane cholesterol movement with cyclodextrin.* Biophys J, 2002. **83**(4): p. 2118-25.
77. Ikonen, E., *Cellular cholesterol trafficking and compartmentalization.* Nat Rev Mol Cell Biol, 2008. **9**(2): p. 125-38.
78. Fisher, K.A., *Monolayer freeze-fracture autoradiography: quantitative analysis of the transmembrane distribution of radioiodinated concanavalin A.* J Cell Biol, 1982. **93**(1): p. 155-63.
79. Schroeder, F., et al., *Transmembrane distribution of sterol in the human erythrocyte.* Biochim Biophys Acta, 1991. **1066**(2): p. 183-92.
80. Arashiki, N., et al., *An Unrecognized Function of Cholesterol: Regulating the Mechanism Controlling Membrane Phospholipid Asymmetry.* Biochemistry, 2016. **55**(25): p. 3504-3513.
81. Takamori, S., et al., *Molecular anatomy of a trafficking organelle.* Cell, 2006. **127**(4): p. 831-46.
82. Gennis, R.B., *Biomembranes, Molecular Structure and Function*, ed. S.A.T.i. Chemistry. 1989, New York: Springer.
83. van Meer, G., et al., *Sorting of sphingolipids in epithelial (Madin-Darby canine kidney) cells.* J Cell Biol, 1987. **105**(4): p. 1623-35.
84. Lisanti, M.P., et al., *Polarized apical distribution of glycosyl-phosphatidylinositol-anchored proteins in a renal epithelial cell line.* Proc Natl Acad Sci U S A, 1988. **85**(24): p. 9557-61.
85. Yu, J., D.A. Fischman, and T.L. Steck, *Selective solubilization of proteins and phospholipids from red blood cell membranes by nonionic detergents.* J Supramol Struct, 1973. **1**(3): p. 233-48.
86. Brown, D.A. and E. London, *Structure of detergent-resistant membrane domains: does phase separation occur in biological membranes?* Biochem Biophys Res Commun, 1997. **240**(1): p. 1-7.
87. Simons, K. and E. Ikonen, *Functional rafts in cell membranes.* Nature, 1997. **387**(6633): p. 569-72.
88. Munro, S., *Lipid rafts: elusive or illusive?* Cell, 2003. **115**(4): p. 377-88.
89. Pike, L.J., *Rafts defined: a report on the Keystone Symposium on Lipid Rafts and Cell Function.* J Lipid Res, 2006. **47**(7): p. 1597-8.
90. Lingwood, D. and K. Simons, *Lipid rafts as a membrane-organizing principle.* Science, 2010. **327**(5961): p. 46-50.
91. Sezgin, E., et al., *The mystery of membrane organization: composition, regulation and roles of lipid rafts.* Nat Rev Mol Cell Biol, 2017. **18**(6): p. 361-374.
92. Bramkamp, M. and D. Lopez, *Exploring the existence of lipid rafts in bacteria.* Microbiol Mol Biol Rev, 2015. **79**(1): p. 81-100.
93. Yan, R., et al., *Spectrally Resolved and Functional Super-resolution Microscopy via Ultrahigh-Throughput Single-Molecule Spectroscopy.* Acc Chem Res, 2018. **51**(3): p. 697-705.
94. Klymchenko, A.S. and R. Kreder, *Fluorescent probes for lipid rafts: from model membranes to living cells.* Chem Biol, 2014. **21**(1): p. 97-113.

95. Klotzsch, E. and G.J. Schutz, *A critical survey of methods to detect plasma membrane rafts.* Philos Trans R Soc Lond B Biol Sci, 2013. **368**(1611): p. 20120033.
96. Yanez-Mo, M., et al., *Tetraspanin-enriched microdomains: a functional unit in cell plasma membranes.* Trends Cell Biol, 2009. **19**(9): p. 434-46.
97. Yechiel, E. and M. Edidin, *Micrometer-scale domains in fibroblast plasma membranes.* J Cell Biol, 1987. **105**(2): p. 755-60.
98. Fujiwara, T., et al., *Phospholipids undergo hop diffusion in compartmentalized cell membrane.* J Cell Biol, 2002. **157**(6): p. 1071-81.
99. Bach, J.N. and M. Bramkamp, *Flotillins functionally organize the bacterial membrane.* Mol Microbiol, 2013. **88**(6): p. 1205-17.
100. Grossmann, G., et al., *Membrane potential governs lateral segregation of plasma membrane proteins and lipids in yeast.* EMBO J, 2007. **26**(1): p. 1-8.
101. Gousset, K., et al., *Evidence for a physiological role for membrane rafts in human platelets.* J Cell Physiol, 2002. **190**(1): p. 117-28.
102. Tyteca, D., et al., *Three unrelated sphingomyelin analogs spontaneously cluster into plasma membrane micrometric domains.* Biochim Biophys Acta, 2010. **1798**(5): p. 909-27.
103. Gaus, K., et al., *Visualizing lipid structure and raft domains in living cells with two-photon microscopy.* Proc Natl Acad Sci U S A, 2003. **100**(26): p. 15554-9.
104. Travlos, G.S., *Normal structure, function, and histology of the bone marrow.* Toxicol Pathol, 2006. **34**(5): p. 548-65.
105. Chasis, J.A. and N. Mohandas, *Erythroblastic islands: niches for erythropoiesis.* Blood, 2008. **112**(3): p. 470-8.
106. Bunn, H.F. and J.C. Aster, *Pathophysiology of Blood Disorders, Second Edition*. 2017: McGraw-Hill Education.
107. Heideveld, E. and E. van den Akker, *Digesting the role of bone marrow macrophages on hematopoiesis.* Immunobiology, 2017. **222**(6): p. 814-822.
108. Palis, J., *Primitive and definitive erythropoiesis in mammals.* Front Physiol, 2014. **5**: p. 3.
109. Chiabrando, D., S. Mercurio, and E. Tolosano, *Heme and erythropoieis: more than a structural role.* Haematologica, 2014. **99**(6): p. 973-83.
110. Moras, M., S.D. Lefevre, and M.A. Ostuni, *From Erythroblasts to Mature Red Blood Cells: Organelle Clearance in Mammals.* Front Physiol, 2017. **8**: p. 1076.
111. Bell, A.J., et al., *Protein distribution during human erythroblast enucleation in vitro.* PLoS One, 2013. **8**(4): p. e60300.
112. Keerthivasan, G., A. Wickrema, and J.D. Crispino, *Erythroblast enucleation.* Stem Cells Int, 2011. **2011**: p. 139851.
113. Salomao, M., et al., *Hereditary spherocytosis and hereditary elliptocytosis: aberrant protein sorting during erythroblast enucleation.* Blood, 2010. **116**(2): p. 267-9.
114. Ovchynnikova, E., et al., *The Shape Shifting Story of Reticulocyte Maturation.* Front Physiol, 2018. **9**: p. 829.
115. Blanc, L., et al., *The water channel aquaporin-1 partitions into exosomes during reticulocyte maturation: implication for the regulation of cell volume.* Blood, 2009. **114**(18): p. 3928-34.
116. Geminard, C., A. de Gassart, and M. Vidal, *Reticulocyte maturation: mitoptosis and exosome release.* Biocell, 2002. **26**(2): p. 205-15.
117. Liu, J., et al., *Membrane remodeling during reticulocyte maturation.* Blood, 2010. **115**(10): p. 2021-7.
118. Singh, R.P., et al., *Hematopoietic Stem Cells but Not Multipotent Progenitors Drive Erythropoiesis during Chronic Erythroid Stress in EPO Transgenic Mice.* Stem Cell Reports, 2018. **10**(6): p. 1908-1919.
119. Nandakumar, S.K., J.C. Ulirsch, and V.G. Sankaran, *Advances in understanding erythropoiesis: evolving perspectives.* Br J Haematol, 2016. **173**(2): p. 206-18.

120. Hattangadi, S.M., et al., *From stem cell to red cell: regulation of erythropoiesis at multiple levels by multiple proteins, RNAs, and chromatin modifications.* Blood, 2011. **118**(24): p. 6258-68.
121. Yang, C., et al., *Sphingosine-1-phosphate signaling modulates terminal erythroid differentiation through the regulation of mitophagy.* Exp Hematol, 2019.
122. van Wijk, R. and W.W. van Solinge, *The energy-less red blood cell is lost: erythrocyte enzyme abnormalities of glycolysis.* Blood, 2005. **106**(13): p. 4034-42.
123. Montel-Hagen, A., M. Sitbon, and N. Taylor, *Erythroid glucose transporters.* Curr Opin Hematol, 2009. **16**(3): p. 165-72.
124. Hassoun, H. and J. Palek, *Hereditary spherocytosis: a review of the clinical and molecular aspects of the disease.* Blood Rev, 1996. **10**(3): p. 129-47.
125. Puchulu-Campanella, E., et al., *Identification of the components of a glycolytic enzyme metabolon on the human red blood cell membrane.* J Biol Chem, 2013. **288**(2): p. 848-58.
126. Chu, H., et al., *Identification of cytoskeletal elements enclosing the ATP pools that fuel human red blood cell membrane cation pumps.* Proc Natl Acad Sci U S A, 2012. **109**(31): p. 12794-9.
127. Lewis, I.A., et al., *Role of band 3 in regulating metabolic flux of red blood cells.* Proc Natl Acad Sci U S A, 2009. **106**(44): p. 18515-20.
128. Moraes, T.F. and R.A. Reithmeier, *Membrane transport metabolons.* Biochim Biophys Acta, 2012. **1818**(11): p. 2687-706.
129. Reece, J.B., et al., *Campbell Biology*. 2011: Pearson Education.
130. Dunn, J.-O., M. Mythen, and M. Grocott, *Physiology of oxygen transport.* BJA Education, 2016. **16**(10): p. 341-348.
131. Jensen, F.B., *The dual roles of red blood cells in tissue oxygen delivery: oxygen carriers and regulators of local blood flow.* J Exp Biol, 2009. **212**(Pt 21): p. 3387-93.
132. Novak, I., *ATP as a signaling molecule: the exocrine focus.* News Physiol Sci, 2003. **18**: p. 12-7.
133. Wan, J., A.M. Forsyth, and H.A. Stone, *Red blood cell dynamics: from cell deformation to ATP release.* Integr Biol (Camb), 2011. **3**(10): p. 972-81.
134. Wan, J., W.D. Ristenpart, and H.A. Stone, *Dynamics of shear-induced ATP release from red blood cells.* Proc Natl Acad Sci U S A, 2008. **105**(43): p. 16432-7.
135. Burnstock, G., *Blood cells: an historical account of the roles of purinergic signalling.* Purinergic Signal, 2015. **11**(4): p. 411-34.
136. Thomas, S.L., et al., *Ion channels in human red blood cell membrane: actors or relics?* Blood Cells Mol Dis, 2011. **46**(4): p. 261-5.
137. Locovei, S., J. Wang, and G. Dahl, *Activation of pannexin 1 channels by ATP through P2Y receptors and by cytoplasmic calcium.* FEBS Lett, 2006. **580**(1): p. 239-44.
138. Cinar, E., et al., *Piezo1 regulates mechanotransductive release of ATP from human RBCs.* Proc Natl Acad Sci U S A, 2015. **112**(38): p. 11783-8.
139. Lew, V.L. and T. Tiffert, *On the Mechanism of Human Red Blood Cell Longevity: Roles of Calcium, the Sodium Pump, PIEZO1, and Gardos Channels.* Front Physiol, 2017. **8**: p. 977.
140. Lim, H.W.G., M. Wortis, and R. Mukhopadhyay, *Stomatocyte-discocyte-echinocyte sequence of the human red blood cell: evidence for the bilayer- couple hypothesis from membrane mechanics.* Proc Natl Acad Sci U S A, 2002. **99**(26): p. 16766-9.
141. Sheetz, M.P. and S.J. Singer, *Biological membranes as bilayer couples. A molecular mechanism of drug-erythrocyte interactions.* Proc Natl Acad Sci U S A, 1974. **71**(11): p. 4457-61.
142. Khairy, K., J. Foo, and J. Howard, *Shapes of Red Blood Cells: Comparison of 3D Confocal Images with the Bilayer-Couple Model.* Cell Mol Bioeng, 2010. **1**(2-3): p. 173-181.

143. Svetina, S., T. Svelc Kebe, and B. Bozic, *A Model of Piezo1-Based Regulation of Red Blood Cell Volume.* Biophys J, 2019. **116**(1): p. 151-164.
144. Hoffmann, E.K., I.H. Lambert, and S.F. Pedersen, *Physiology of cell volume regulation in vertebrates.* Physiol Rev, 2009. **89**(1): p. 193-277.
145. Gallagher, P.G., *Disorders of red cell volume regulation.* Curr Opin Hematol, 2013. **20**(3): p. 201-7.
146. Huisjes, R., et al., *Squeezing for Life - Properties of Red Blood Cell Deformability.* Front Physiol, 2018. **9**: p. 656.
147. Reece, J.B., *Campbell Biology*. 2011: Benjamin Cummings / Pearson.
148. Bogdanova, A., et al., *Calcium in red blood cells-a perilous balance.* Int J Mol Sci, 2013. **14**(5): p. 9848-72.
149. Gallagher, P.G., *Disorders of erythrocyte hydration.* Blood, 2017. **130**(25): p. 2699-2708.
150. Salzer, U. and R. Prohaska, *Stomatin, flotillin-1, and flotillin-2 are major integral proteins of erythrocyte lipid rafts.* Blood, 2001. **97**(4): p. 1141-3.
151. Ciana, A., C. Balduini, and G. Minetti, *Detergent-resistant membranes in human erythrocytes and their connection to the membrane-skeleton.* J Biosci, 2005. **30**(3): p. 317-28.
152. Crepaldi Domingues, C., et al., *Resistance of human erythrocyte membranes to Triton X-100 and C12E8.* J Membr Biol, 2009. **227**(1): p. 39-48.
153. Sheetz, M.P., *Integral membrane protein interaction with Triton cytoskeletons of erythrocytes.* Biochim Biophys Acta, 1979. **557**(1): p. 122-34.
154. Ciana, A., et al., *On the association of lipid rafts to the spectrin skeleton in human erythrocytes.* Biochim Biophys Acta, 2011. **1808**(1): p. 183-90.
155. Domingues, C.C., et al., *Effect of cholesterol depletion and temperature on the isolation of detergent-resistant membranes from human erythrocytes.* J Membr Biol, 2010. **234**(3): p. 195-205.
156. Rodgers, W. and M. Glaser, *Characterization of lipid domains in erythrocyte membranes.* Proc Natl Acad Sci U S A, 1991. **88**(4): p. 1364-8.
157. Mikhalyov, I. and A. Samsonov, *Lipid raft detecting in membranes of live erythrocytes.* Biochim Biophys Acta, 2011. **1808**(7): p. 1930-9.
158. Mrowczynska, L. and H. Hagerstrand, *Patching of ganglioside(M1) in human erythrocytes - distribution of CD47 and CD59 in patched and curved membrane.* Mol Membr Biol, 2008. **25**(3): p. 258-65.
159. Montes, L.R., et al., *Ceramide-enriched membrane domains in red blood cells and the mechanism of sphingomyelinase-induced hot-cold hemolysis.* Biochemistry, 2008. **47**(43): p. 11222-30.
160. Johnson, I.D., H.C. Kang, and R.P. Haugland, *Fluorescent membrane probes incorporating dipyrromethemeboron difluoride fluorophores.* Anal Biochem, 1991. **198**(2): p. 228-37.
161. D'Auria, L., et al., *Micrometric segregation of fluorescent membrane lipids: relevance for endogenous lipids and biogenesis in erythrocytes.* J Lipid Res, 2013. **54**(4): p. 1066-76.
162. D'Auria, L., et al., *Segregation of fluorescent membrane lipids into distinct micrometric domains: evidence for phase compartmentation of natural lipids?* PLoS One, 2011. **6**(2): p. e17021.
163. Conrard, L., et al., *Spatial relationship and functional relevance of three lipid domain populations at the erythrocyte surface.* Cell Physiol Biochem, 2018(51): p. 1544-1565.
164. De Colibus, L., et al., *Structures of lysenin reveal a shared evolutionary origin for pore-forming proteins and its mode of sphingomyelin recognition.* Structure, 2012. **20**(9): p. 1498-507.
165. Kiyokawa, E., et al., *Spatial and functional heterogeneity of sphingolipid-rich membrane domains.* J Biol Chem, 2005. **280**(25): p. 24072-84.

166. Shogomori, H. and T. Kobayashi, *Lysenin: a sphingomyelin specific pore-forming toxin.* Biochim Biophys Acta, 2008. **1780**(3): p. 612-8.
167. Wustner, D., *Fluorescent sterols as tools in membrane biophysics and cell biology.* Chem Phys Lipids, 2007. **146**(1): p. 1-25.
168. McIntosh, A.L., et al., *Fluorescence techniques using dehydroergosterol to study cholesterol trafficking.* Lipids, 2008. **43**(12): p. 1185-208.
169. Hullin-Matsuda, F. and T. Kobayashi, *Monitoring the distribution and dynamics of signaling microdomains in living cells with lipid-specific probes.* Cell Mol Life Sci, 2007. **64**(19-20): p. 2492-504.
170. Hotze, E.M. and R.K. Tweten, *Membrane assembly of the cholesterol-dependent cytolysin pore complex.* Biochim Biophys Acta, 2012. **1818**(4): p. 1028-38.
171. Rossjohn, J., et al., *Structure of a cholesterol-binding, thiol-activated cytolysin and a model of its membrane form.* Cell, 1997. **89**(5): p. 685-92.
172. Ohno-Iwashita, Y., et al., *Effect of lipidic factors on membrane cholesterol topology--mode of binding of theta-toxin to cholesterol in liposomes.* Biochim Biophys Acta, 1992. **1109**(1): p. 81-90.
173. Shimada, Y., et al., *The C-terminal domain of perfringolysin O is an essential cholesterol-binding unit targeting to cholesterol-rich microdomains.* Eur J Biochem, 2002. **269**(24): p. 6195-203.
174. Mizuno, H., et al., *Fluorescent probes for superresolution imaging of lipid domains on the plasma membrane.* Chem. Sci., 2011. **2**: p. 1548-1553.
175. Carquin, M., et al., *Endogenous sphingomyelin segregates into submicrometric domains in the living erythrocyte membrane.* J Lipid Res, 2014. **55**(7): p. 1331-1342.
176. Carquin, M., et al., *Cholesterol segregates into submicrometric domains at the living erythrocyte membrane: evidence and regulation.* Cell Mol Life Sci, 2015. **72**(23): p. 4633-51.
177. Leonard, C., et al., *Contribution of plasma membrane lipid domains to red blood cell (re)shaping.* Sci Rep, 2017. **7**(1): p. 4264.
178. Leonard, C., et al., *Tuning of differential lipid order between submicrometric domains and surrounding membrane upon erythrocyte reshaping.* Cell Physiol Biochem 2018. **48**(2563-2582).
179. Dumitru, A.P., M.; Conrard, L.; Dufrêne, Y.; Tyteca, D.; Alsteens, D., *Nanoscale membrane architecture of healthy and pathological red blood cells.* Nanoscale Horizons, 2018. **3**: p. 293-304.
180. Lux, S.E., *Dissecting the red cell membrane skeleton.* Nature, 1979. **281**(5731): p. 426-9.
181. Marchesi, V.T. and E. Steers, Jr., *Selective solubilization of a protein component of the red cell membrane.* Science, 1968. **159**(3811): p. 203-4.
182. Lux, S.E., *Anatomy of the red cell membrane skeleton: unanswered questions.* Blood, 2016. **127**(2): p. 187-99.
183. Liu, S.C., L.H. Derick, and J. Palek, *Visualization of the hexagonal lattice in the erythrocyte membrane skeleton.* J Cell Biol, 1987. **104**(3): p. 527-36.
184. Boguslawska, D.M., et al., *Spectrin and phospholipids - the current picture of their fascinating interplay.* Cell Mol Biol Lett, 2014. **19**(1): p. 158-79.
185. Baines, A.J., *The spectrin-ankyrin-4.1-adducin membrane skeleton: adapting eukaryotic cells to the demands of animal life.* Protoplasma, 2010. **244**(1-4): p. 99-131.
186. Harper, S.L., et al., *The common hereditary elliptocytosis-associated alpha-spectrin L260P mutation perturbs erythrocyte membranes by stabilizing spectrin in the closed dimer conformation.* Blood, 2013. **122**(17): p. 3045-53.
187. Mohandas, N. and P.G. Gallagher, *Red cell membrane: past, present, and future.* Blood, 2008. **112**(10): p. 3939-48.

188. An, X., et al., *Phosphatidylinositol-4,5-biphosphate (PIP2) differentially regulates the interaction of human erythrocyte protein 4.1 (4.1R) with membrane proteins.* Biochemistry, 2006. **45**(18): p. 5725-32.
189. Manno, S., et al., *Modulation of erythrocyte membrane mechanical function by beta-spectrin phosphorylation and dephosphorylation.* J Biol Chem, 1995. **270**(10): p. 5659-65.
190. Salomao, M., et al., *Protein 4.1R-dependent multiprotein complex: new insights into the structural organization of the red blood cell membrane.* Proc Natl Acad Sci U S A, 2008. **105**(23): p. 8026-31.
191. Byers, T.J. and D. Branton, *Visualization of the protein associations in the erythrocyte membrane skeleton.* Proc Natl Acad Sci U S A, 1985. **82**(18): p. 6153-7.
192. Peters, L.L., et al., *Anion exchanger 1 (band 3) is required to prevent erythrocyte membrane surface loss but not to form the membrane skeleton.* Cell, 1996. **86**(6): p. 917-27.
193. Bruce, L.J., et al., *Absence of CD47 in protein 4.2-deficient hereditary spherocytosis in man: an interaction between the Rh complex and the band 3 complex.* Blood, 2002. **100**(5): p. 1878-85.
194. Manno, S., Y. Takakuwa, and N. Mohandas, *Modulation of erythrocyte membrane mechanical function by protein 4.1 phosphorylation.* J Biol Chem, 2005. **280**(9): p. 7581-7.
195. Fowler, V.M., *The human erythrocyte plasma membrane: a Rosetta Stone for decoding membrane-cytoskeleton structure.* Curr Top Membr, 2013. **72**: p. 39-88.
196. Gokhin, D.S. and V.M. Fowler, *Feisty filaments: actin dynamics in the red blood cell membrane skeleton.* Curr Opin Hematol, 2016. **23**(3): p. 206-14.
197. Peter Klinken, S., *Red blood cells.* Int J Biochem Cell Biol, 2002. **34**(12): p. 1513-8.
198. Mebius, R.E. and G. Kraal, *Structure and function of the spleen.* Nat Rev Immunol, 2005. **5**(8): p. 606-16.
199. Evans, E., N. Mohandas, and A. Leung, *Static and dynamic rigidities of normal and sickle erythrocytes. Major influence of cell hemoglobin concentration.* J Clin Invest, 1984. **73**(2): p. 477-88.
200. Sheetz, M.P., J.E. Sable, and H.G. Dobereiner, *Continuous membrane-cytoskeleton adhesion requires continuous accommodation to lipid and cytoskeleton dynamics.* Annu Rev Biophys Biomol Struct, 2006. **35**: p. 417-34.
201. Muravyov, A. and I. Tikhomirova, *Role Ca(2+) in mechanisms of the red blood cells microrheological changes.* Adv Exp Med Biol, 2012. **740**: p. 1017-38.
202. Larsen, F.L., et al., *Physiological shear stresses enhance the Ca2+ permeability of human erythrocytes.* Nature, 1981. **294**(5842): p. 667-8.
203. Johnson, R.M., *Membrane stress increases cation permeability in red cells.* Biophys J, 1994. **67**(5): p. 1876-81.
204. Brain, M.C., et al., *Evidence for a mechanosensitive calcium influx into red cells.* Blood Cells Mol Dis, 2004. **32**(3): p. 349-52.
205. Kaestner, L., et al., *The non-selective voltage-activated cation channel in the human red blood cell membrane: reconciliation between two conflicting reports and further characterisation.* Bioelectrochemistry, 2000. **52**(2): p. 117-25.
206. Andrews, D.A., L. Yang, and P.S. Low, *Phorbol ester stimulates a protein kinase C-mediated agatoxin-TK-sensitive calcium permeability pathway in human red blood cells.* Blood, 2002. **100**(9): p. 3392-9.
207. Foller, M., et al., *TRPC6 contributes to the Ca(2+) leak of human erythrocytes.* Cell Physiol Biochem, 2008. **21**(1-3): p. 183-92.
208. Bouyer, G., et al., *Erythrocyte peripheral type benzodiazepine receptor/voltage-dependent anion channels are upregulated by Plasmodium falciparum.* Blood, 2011. **118**(8): p. 2305-12.

209. Makhro, A., et al., *N-methyl-D-aspartate receptors in human erythroid precursor cells and in circulating red blood cells contribute to the intracellular calcium regulation.* Am J Physiol Cell Physiol, 2013. **305**(11): p. C1123-38.
210. Cahalan, S.M., et al., *Piezo1 links mechanical forces to red blood cell volume.* Elife, 2015. **4**.
211. Faucherre, A., et al., *Piezo1 plays a role in erythrocyte volume homeostasis.* Haematologica, 2014. **99**(1): p. 70-5.
212. Glogowska, E. and P.G. Gallagher, *Disorders of erythrocyte volume homeostasis.* Int J Lab Hematol, 2015. **37 Suppl 1**: p. 85-91.
213. Danielczok, J.G., et al., *Red Blood Cell Passage of Small Capillaries Is Associated with Transient Ca(2+)-mediated Adaptations.* Front Physiol, 2017. **8**: p. 979.
214. Murthy, S.E., A.E. Dubin, and A. Patapoutian, *Piezos thrive under pressure: mechanically activated ion channels in health and disease.* Nat Rev Mol Cell Biol, 2017. **18**(12): p. 771-783.
215. Saotome, K., et al., *Structure of the mechanically activated ion channel Piezo1.* Nature, 2018. **554**(7693): p. 481-486.
216. Kuhlman, P.A., et al., *A new function for adducin. Calcium/calmodulin-regulated capping of the barbed ends of actin filaments.* J Biol Chem, 1996. **271**(14): p. 7986-91.
217. Gauthier, E., et al., *Phosphorylation-dependent perturbations of the 4.1R-associated multiprotein complex of the erythrocyte membrane.* Biochemistry, 2011. **50**(21): p. 4561-7.
218. Mortensen, A.M. and R.F. Novak, *Dynamic changes in the distribution of the calcium-activated neutral protease in human red blood cells following cellular insult and altered Ca2+ homeostasis.* Toxicol Appl Pharmacol, 1992. **117**(2): p. 180-8.
219. Lopreiato, R., M. Giacomello, and E. Carafoli, *The plasma membrane calcium pump: new ways to look at an old enzyme.* J Biol Chem, 2014. **289**(15): p. 10261-8.
220. Zaidi, A., et al., *The plasma membrane calcium pumps-The old and the new.* Neurosci Lett, 2018. **663**: p. 12-17.
221. Sarkadi, B., et al., *Transport parameters and stoichiometry of active calcium ion extrusion in intact human red cells.* Biochim Biophys Acta, 1977. **464**(1): p. 93-107.
222. Kaestner, L. and A. Bogdanova, *Regulation of red cell life-span, erythropoiesis, senescence, and clearance.* Front Physiol, 2014. **5**: p. 269.
223. de Back, D.Z., et al., *Of macrophages and red blood cells; a complex love story.* Front Physiol, 2014. **5**: p. 9.
224. Lutz, H.U. and A. Bogdanova, *Mechanisms tagging senescent red blood cells for clearance in healthy humans.* Front Physiol, 2013. **4**: p. 387.
225. Rifkind, J.M. and E. Nagababu, *Hemoglobin redox reactions and red blood cell aging.* Antioxid Redox Signal, 2013. **18**(17): p. 2274-83.
226. Cimen, M.Y., *Free radical metabolism in human erythrocytes.* Clin Chim Acta, 2008. **390**(1-2): p. 1-11.
227. Tejero, J., S. Shiva, and M.T. Gladwin, *Sources of Vascular Nitric Oxide and Reactive Oxygen Species and Their Regulation.* Physiol Rev, 2019. **99**(1): p. 311-379.
228. George, A., et al., *Erythrocyte NADPH oxidase activity modulated by Rac GTPases, PKC, and plasma cytokines contributes to oxidative stress in sickle cell disease.* Blood, 2013. **121**(11): p. 2099-107.
229. Kim-Shapiro, D.B., A.N. Schechter, and M.T. Gladwin, *Unraveling the reactions of nitric oxide, nitrite, and hemoglobin in physiology and therapeutics.* Arterioscler Thromb Vasc Biol, 2006. **26**(4): p. 697-705.
230. Cho, C.S., et al., *Hydroxyurea-induced expression of glutathione peroxidase 1 in red blood cells of individuals with sickle cell anemia.* Antioxid Redox Signal, 2010. **13**(1): p. 1-11.
231. Rakhit, R. and A. Chakrabartty, *Structure, folding, and misfolding of Cu,Zn superoxide dismutase in amyotrophic lateral sclerosis.* Biochim Biophys Acta, 2006. **1762**(11-12): p. 1025-37.

232. Johnson, R.M., et al., *The effects of disruption of genes for peroxiredoxin-2, glutathione peroxidase-1, and catalase on erythrocyte oxidative metabolism.* Free Radic Biol Med, 2010. **48**(4): p. 519-25.
233. Agar, N.S., et al., *Erythrocyte catalase. A somatic oxidant defense?* J Clin Invest, 1986. **77**(1): p. 319-21.
234. Low, F.M., M.B. Hampton, and C.C. Winterbourn, *Peroxiredoxin 2 and peroxide metabolism in the erythrocyte.* Antioxid Redox Signal, 2008. **10**(9): p. 1621-30.
235. Ogasawara, Y., et al., *Structural and functional analysis of native peroxiredoxin 2 in human red blood cells.* Int J Biochem Cell Biol, 2012. **44**(7): p. 1072-7.
236. Lang, F., et al., *Oxidative stress and suicidal erythrocyte death.* Antioxid Redox Signal, 2014. **21**(1): p. 138-53.
237. Kuhn, V., et al., *Red Blood Cell Function and Dysfunction: Redox Regulation, Nitric Oxide Metabolism, Anemia.* Antioxid Redox Signal, 2017. **26**(13): p. 718-742.
238. Sharma, R., et al., *Antioxidant role of glutathione S-transferases: protection against oxidant toxicity and regulation of stress-mediated apoptosis.* Antioxid Redox Signal, 2004. **6**(2): p. 289-300.
239. Sharma, R., et al., *RLIP76 is the major ATP-dependent transporter of glutathione-conjugates and doxorubicin in human erythrocytes.* Arch Biochem Biophys, 2001. **391**(2): p. 171-9.
240. Bobrowska-Hagerstrand, M., et al., *Monitoring of MRP-like activity in human erythrocytes: inhibitory effect of isoflavones.* Blood Cells Mol Dis, 2001. **27**(5): p. 894-900.
241. Amen, F., et al., *N-acetylcysteine improves the quality of red blood cells stored for transfusion.* Arch Biochem Biophys, 2017. **621**: p. 31-37.
242. Berman, A.E., et al., *N-acetylcysteine prevents loss of dopaminergic neurons in the EAAC1-/- mouse.* Ann Neurol, 2011. **69**(3): p. 509-20.
243. Paschalis, V., et al., *N-acetylcysteine supplementation increases exercise performance and reduces oxidative stress only in individuals with low levels of glutathione.* Free Radic Biol Med, 2018. **115**: p. 288-297.
244. Padayatty, S.J. and M. Levine, *Vitamin C: the known and the unknown and Goldilocks.* Oral Dis, 2016. **22**(6): p. 463-93.
245. Tu, H., et al., *Low Red Blood Cell Vitamin C Concentrations Induce Red Blood Cell Fragility: A Link to Diabetes Via Glucose, Glucose Transporters, and Dehydroascorbic Acid.* EBioMedicine, 2015. **2**(11): p. 1735-50.
246. Raval, J.S., et al., *Ascorbic acid improves membrane fragility and decreases haemolysis during red blood cell storage.* Transfus Med, 2013. **23**(2): p. 87-93.
247. Sanford, K., et al., *Attenuation of Red Blood Cell Storage Lesions with Vitamin C.* Antioxidants (Basel), 2017. **6**(3).
248. Madhikarmi, N.L. and K.R. Murthy, *Antioxidant enzymes and oxidative stress in the erythrocytes of iron deficiency anemic patients supplemented with vitamins.* Iran Biomed J, 2014. **18**(2): p. 82-7.
249. Arruda, M.M., et al., *Antioxidant vitamins C and E supplementation increases markers of haemolysis in sickle cell anaemia patients: a randomized, double-blind, placebo-controlled trial.* Br J Haematol, 2013. **160**(5): p. 688-700.
250. Traber, M.G. and J.F. Stevens, *Vitamins C and E: beneficial effects from a mechanistic perspective.* Free Radic Biol Med, 2011. **51**(5): p. 1000-13.
251. Vitturi, D.A., et al., *Antioxidant functions for the hemoglobin beta93 cysteine residue in erythrocytes and in the vascular compartment in vivo.* Free Radic Biol Med, 2013. **55**: p. 119-29.
252. Kanias, T. and J.P. Acker, *Biopreservation of red blood cells--the struggle with hemoglobin oxidation.* FEBS J, 2010. **277**(2): p. 343-56.

253. Franco, R., G. Navarro, and E. Martinez-Pinilla, *Antioxidant Defense Mechanisms in Erythrocytes and in the Central Nervous System.* Antioxidants (Basel), 2019. **8**(2).
254. Pauling, L. and C.D. Coryell, *The Magnetic Properties and Structure of Hemoglobin, Oxyhemoglobin and Carbonmonoxyhemoglobin.* Proc Natl Acad Sci U S A, 1936. **22**(4): p. 210-6.
255. Yoshida, Y., et al., *Chemistry of lipid peroxidation products and their use as biomarkers in early detection of diseases.* J Oleo Sci, 2015. **64**(4): p. 347-56.
256. Niki, E., *Lipid peroxidation: physiological levels and dual biological effects.* Free Radic Biol Med, 2009. **47**(5): p. 469-84.
257. Mutemberezi, V., O. Guillemot-Legris, and G.G. Muccioli, *Oxysterols: From cholesterol metabolites to key mediators.* Prog Lipid Res, 2016. **64**: p. 152-169.
258. Kulig, W., et al., *Cholesterol under oxidative stress-How lipid membranes sense oxidation as cholesterol is being replaced by oxysterols.* Free Radic Biol Med, 2015. **84**: p. 30-41.
259. Iuliano, L., *Pathways of cholesterol oxidation via non-enzymatic mechanisms.* Chem Phys Lipids, 2011. **164**(6): p. 457-68.
260. Olkkonen, V.M. and R. Hynynen, *Interactions of oxysterols with membranes and proteins.* Mol Aspects Med, 2009. **30**(3): p. 123-33.
261. Arca, M., et al., *Increased plasma levels of oxysterols, in vivo markers of oxidative stress, in patients with familial combined hyperlipidemia: reduction during atorvastatin and fenofibrate therapy.* Free Radic Biol Med, 2007. **42**(5): p. 698-705.
262. Iuliano, L., et al., *Bioavailability of vitamin E as function of food intake in healthy subjects: effects on plasma peroxide-scavenging activity and cholesterol-oxidation products.* Arterioscler Thromb Vasc Biol, 2001. **21**(10): p. E34-7.
263. Iuliano, L., et al., *Vitamin E and enzymatic/oxidative stress-driven oxysterols in amnestic mild cognitive impairment subtypes and Alzheimer's disease.* J Alzheimers Dis, 2010. **21**(4): p. 1383-92.
264. Shalev, O., et al., *Impaired erythrocyte calcium homeostasis in beta-thalassemia.* Blood, 1984. **64**(2): p. 564-6.
265. Shalev, O., et al., *Abnormal erythrocyte calcium homeostasis in oxidant-induced hemolytic disease.* Blood, 1981. **58**(6): p. 1232-5.
266. Gorlach, A., et al., *Calcium and ROS: A mutual interplay.* Redox Biol, 2015. **6**: p. 260-71.
267. Pantaleo, A., et al., *Oxidized and poorly glycosylated band 3 is selectively phosphorylated by Syk kinase to form large membrane clusters in normal and G6PD-deficient red blood cells.* Biochem J, 2009. **418**(2): p. 359-67.
268. Ferru, E., et al., *Regulation of membrane-cytoskeletal interactions by tyrosine phosphorylation of erythrocyte band 3.* Blood, 2011. **117**(22): p. 5998-6006.
269. Bosman, G.J. and M.M. Kay, *Alterations of band 3 transport protein by cellular aging and disease: erythrocyte band 3 and glucose transporter share a functional relationship.* Biochem Cell Biol, 1990. **68**(12): p. 1419-27.
270. Samaja, M., et al., *The effect of in vitro and in vivo cellular aging on the active calcium transport in human inside-out red cell membrane vesicles.* Biochem Biophys Res Commun, 1989. **159**(2): p. 432-8.
271. Lew, V.L., et al., *Effects of age-dependent membrane transport changes on the homeostasis of senescent human red blood cells.* Blood, 2007. **110**(4): p. 1334-42.
272. Lang, F., et al., *Eryptosis, a window to systemic disease.* Cell Physiol Biochem, 2008. **22**(5-6): p. 373-80.
273. Badior, K.E. and J.R. Casey, *Molecular mechanism for the red blood cell senescence clock.* IUBMB Life, 2018. **70**(1): p. 32-40.

274. Kannan, R., J. Yuan, and P.S. Low, *Isolation and partial characterization of antibody- and globin-enriched complexes from membranes of dense human erythrocytes.* Biochem J, 1991. **278 (Pt 1)**: p. 57-62.
275. Lutz, H.U. and G. Stringaro-Wipf, *Senescent red cell-bound IgG is attached to band 3 protein.* Biomed Biochim Acta, 1983. **42**(11-12): p. S117-21.
276. Kay, M.M., et al., *Senescent cell antigen is immunologically related to band 3.* Proc Natl Acad Sci U S A, 1983. **80**(6): p. 1631-5.
277. Turrini, F., et al., *Characterization of the autologous antibodies that opsonize erythrocytes with clustered integral membrane proteins.* Blood, 1993. **81**(11): p. 3146-52.
278. Reithmeier, R.A., et al., *Band 3, the human red cell chloride/bicarbonate anion exchanger (AE1, SLC4A1), in a structural context.* Biochim Biophys Acta, 2016. **1858**(7 Pt A): p. 1507-32.
279. Waugh, S.M. and P.S. Low, *Hemichrome binding to band 3: nucleation of Heinz bodies on the erythrocyte membrane.* Biochemistry, 1985. **24**(1): p. 34-9.
280. Arashiki, N., et al., *Membrane peroxidation and methemoglobin formation are both necessary for band 3 clustering: mechanistic insights into human erythrocyte senescence.* Biochemistry, 2013. **52**(34): p. 5760-9.
281. Turrini, F., et al., *Clustering of integral membrane proteins of the human erythrocyte membrane stimulates autologous IgG binding, complement deposition, and phagocytosis.* J Biol Chem, 1991. **266**(35): p. 23611-7.
282. Hornig, R. and H.U. Lutz, *Band 3 protein clustering on human erythrocytes promotes binding of naturally occurring anti-band 3 and anti-spectrin antibodies.* Exp Gerontol, 2000. **35**(8): p. 1025-44.
283. Low, P.S., et al., *The role of hemoglobin denaturation and band 3 clustering in red blood cell aging.* Science, 1985. **227**(4686): p. 531-3.
284. Lutz, H.U., R. Flepp, and G. Stringaro-Wipf, *Naturally occurring autoantibodies to exoplasmic and cryptic regions of band 3 protein, the major integral membrane protein of human red blood cells.* J Immunol, 1984. **133**(5): p. 2610-8.
285. Lutz, H.U., P. Stammler, and S. Fasler, *How naturally occurring anti-band 3 antibodies stimulate C3b deposition to senescent and oxidatively stressed red blood cells.* Biomed Biochim Acta, 1990. **49**(2-3): p. S224-9.
286. Lutz, H.U., et al., *Opsonic potential of C3b-anti-band 3 complexes when generated on senescent and oxidatively stressed red cells or in fluid phase.* Adv Exp Med Biol, 1991. **307**: p. 367-76.
287. Lutz, H.U., P. Stammler, and S. Fasler, *Preferential formation of C3b-IgG complexes in vitro and in vivo from nascent C3b and naturally occurring anti-band 3 antibodies.* J Biol Chem, 1993. **268**(23): p. 17418-26.
288. Lutz, H.U., S. Fasler, and P. Stammler, *An affinity for complement C3 as a possible reason for the potency of naturally occurring antibodies in mediating tissue homeostasis.* Beitr Infusionsther, 1989. **24**: p. 193-9.
289. Bosman, G.J., F.L. Willekens, and J.M. Werre, *Erythrocyte aging: a more than superficial resemblance to apoptosis?* Cell Physiol Biochem, 2005. **16**(1-3): p. 1-8.
290. Kuypers, F.A. and K. de Jong, *The role of phosphatidylserine in recognition and removal of erythrocytes.* Cell Mol Biol (Noisy-le-grand), 2004. **50**(2): p. 147-58.
291. Franco, R.S., et al., *Changes in the properties of normal human red blood cells during in vivo aging.* Am J Hematol, 2013. **88**(1): p. 44-51.
292. Stewart, A., et al., *The application of a new quantitative assay for the monitoring of integrin-associated protein CD47 on red blood cells during storage and comparison with the expression of CD47 and phosphatidylserine with flow cytometry.* Transfusion, 2005. **45**(9): p. 1496-503.

293. Burger, P., et al., *CD47 functions as a molecular switch for erythrocyte phagocytosis.* Blood, 2012. **119**(23): p. 5512-21.
294. Bolton-Maggs, P.H., et al., *Guidelines for the diagnosis and management of hereditary spherocytosis--2011 update.* Br J Haematol, 2012. **156**(1): p. 37-49.
295. Da Costa, L., et al., *Hereditary spherocytosis, elliptocytosis, and other red cell membrane disorders.* Blood Rev, 2013. **27**(4): p. 167-78.
296. King, M.J. and A. Zanella, *Hereditary red cell membrane disorders and laboratory diagnostic testing.* Int J Lab Hematol, 2013. **35**(3): p. 237-43.
297. Gallagher, P.G., *Abnormalities of the erythrocyte membrane.* Pediatr Clin North Am, 2013. **60**(6): p. 1349-62.
298. Basu, A. and A. Chakrabarti, *Defects in erythrocyte membrane skeletal architecture.* Adv Exp Med Biol, 2015. **842**: p. 41-59.
299. Andolfo, I., et al., *New insights on hereditary erythrocyte membrane defects.* Haematologica, 2016. **101**(11): p. 1284-1294.
300. Gallagher, P.G., *Hereditary elliptocytosis: spectrin and protein 4.1R.* Semin Hematol, 2004. **41**(2): p. 142-64.
301. Lecomte, M.C., et al., *Molecular basis of clinical and morphological heterogeneity in hereditary elliptocytosis (HE) with spectrin alpha I variants.* Br J Haematol, 1993. **85**(3): p. 584-95.
302. Coetzer, T.L., et al., *Four different mutations in codon 28 of alpha spectrin are associated with structurally and functionally abnormal spectrin alpha I/74 in hereditary elliptocytosis.* J Clin Invest, 1991. **88**(3): p. 743-9.
303. Franck, P., et al., *Hereditary elliptocytosis: Variable clinical severity caused by 3 variants in the alpha-spectrin gene.* Int J Lab Hematol, 2018. **40**(4): p. e66-e70.
304. Garbarz, M., et al., *Hereditary pyropoikilocytosis and elliptocytosis in a white French family with the spectrin alpha I/74 variant related to a CGT to CAT codon change (Arg to His) at position 22 of the spectrin alpha I domain.* Blood, 1990. **75**(8): p. 1691-8.
305. Floyd, P.B., et al., *Heterogeneity of the molecular basis of hereditary pyropoikilocytosis and hereditary elliptocytosis associated with increased levels of the spectrin alpha I/74-kilodalton tryptic peptide.* Blood, 1991. **78**(5): p. 1364-72.
306. Lecomte, M.-C., *Spectrins in Human Diseases*, in *Cytoskeleton and Human Disease*, M. Kavallaris, Editor. 2012, Humana Press: Totowa, NJ. p. 345-374.
307. Alloisio, N., et al., *Spectrin Jendouba: an alpha II/31 spectrin variant that is associated with elliptocytosis and carries a mutation distant from the dimer self- association site.* 1992. **80**(3): p. 809-815.
308. Alloisio, N., et al., *A splice site mutation of alpha-spectrin gene causing skipping of exon 18 in hereditary elliptocytosis.* Blood, 1993. **81**(10): p. 2791-8.
309. Fournier, C.M., et al., *Spectrin St Claude, a splicing mutation of the human alpha-spectrin gene associated with severe poikilocytic anemia.* Blood, 1997. **89**(12): p. 4584-90.
310. Roux, A.F., et al., *Molecular basis of Sp alpha I/65 hereditary elliptocytosis in North Africa: insertion of a TTG triplet between codons 147 and 149 in the alpha-spectrin gene from five unrelated families.* Blood, 1989. **73**(8): p. 2196-201.
311. Risinger, M., et al., *Hereditary elliptocytosis-associated alpha-spectrin mutation p.L155dup as a modifier of sickle cell disease severity.* Pediatr Blood Cancer, 2019. **66**(2): p. e27531.
312. Hassoun, H., et al., *A novel mobile element inserted in the alpha spectrin gene: spectrin dayton. A truncated alpha spectrin associated with hereditary elliptocytosis.* J Clin Invest, 1994. **94**(2): p. 643-8.
313. Baklouti, F., et al., *Elliptocytogenic alpha I/36 spectrin Sfax lacks nine amino acids in helix 3 of repeat 4. Evidence for the activation of a cryptic 5'-splice site in exon 8 of spectrin alpha-gene.* Blood, 1992. **79**(9): p. 2464-70.

314. Marechal, J., et al., *Ethnic distribution of allele alpha LELY, a low-expression allele of red-cell spectrin alpha-gene.* Br J Haematol, 1995. **90**(3): p. 553-56.
315. Basseres, D.S., et al., *Presence of allele alphaLELY in an Amazonian Indian population.* Am J Hematol, 1998. **57**(3): p. 212-4.
316. Yawata, Y., *Cell Membrane: The Red Blood Cell as a Model*. 2006: Wiley.
317. Wilmotte, R., et al., *The exon 46-encoded sequence is essential for stability of human erythroid alpha-spectrin and heterodimer formation.* Blood, 1997. **90**(10): p. 4188-96.
318. Wilmotte, R., et al., *Low expression allele alpha LELY of red cell spectrin is associated with mutations in exon 40 (alpha V/41 polymorphism) and intron 45 and with partial skipping of exon 46.* J Clin Invest, 1993. **91**(5): p. 2091-6.
319. Delaunay, J., *Molecular basis of red cell membrane disorders.* Acta Haematol, 2002. **108**(4): p. 210-8.
320. Glele-Kakai, C., et al., *Epidemiological studies of spectrin mutations related to hereditary elliptocytosis and spectrin polymorphisms in Benin.* Br J Haematol, 1996. **95**(1): p. 57-66.
321. Dhermy, D., J. Schrevel, and M.C. Lecomte, *Spectrin-based skeleton in red blood cells and malaria.* Curr Opin Hematol, 2007. **14**(3): p. 198-202.
322. Jarolim, P., et al., *Beta spectrin PRAGUE: a truncated beta spectrin producing spectrin deficiency, defective spectrin heterodimer self-association and a phenotype of spherocytic elliptocytosis.* Br J Haematol, 1995. **91**(2): p. 502-10.
323. Basseres, D.S., et al., *Beta-spectrin Campinas: a novel shortened beta-chain variant associated with skipping of exon 30 and hereditary elliptocytosis.* Br J Haematol, 1997. **97**(3): p. 579-85.
324. Yoon, S.H., et al., *Molecular defect of truncated beta-spectrin associated with hereditary elliptocytosis. Beta-spectrin Gottingen.* J Biol Chem, 1991. **266**(13): p. 8490-4.
325. Gallagher, P.G., et al., *A splice site mutation of the beta-spectrin gene causing exon skipping in hereditary elliptocytosis associated with a truncated beta-spectrin chain.* J Biol Chem, 1991. **266**(23): p. 15154-9.
326. Sahr, K.E., et al., *Spectrin cagliari. an Ala-->Gly substitution in helix 1 of beta spectrin repeat 17 that severely disrupts the structure and self-association of the erythrocyte spectrin heterodimer.* J Biol Chem, 1993. **268**(30): p. 22656-62.
327. Gallagher, P.G., et al., *Recurrent fatal hydrops fetalis associated with a nucleotide substitution in the erythrocyte beta-spectrin gene.* J Clin Invest, 1995. **95**(3): p. 1174-82.
328. Parquet, N., et al., *Identification of three novel spectrin alpha I/74 mutations in hereditary elliptocytosis: further support for a triple-stranded folding unit model of the spectrin heterodimer contact site.* Blood, 1994. **84**(1): p. 303-8.
329. Maillet, P., et al., *Spectrin mutations in hereditary elliptocytosis and hereditary spherocytosis.* Hum Mutat, 1996. **8**(2): p. 97-107.
330. Garbarz, M., et al., *Spectrin beta Tandil, a novel shortened beta-chain variant associated with hereditary elliptocytosis is due to a deletional frameshift mutation in the beta-spectrin gene.* Blood, 1992. **80**(4): p. 1066-73.
331. Tse, W.T., et al., *An insertional frameshift mutation of the beta-spectrin gene associated with elliptocytosis in spectrin nice (beta 220/216).* Blood, 1991. **78**(2): p. 517-23.
332. Kanzaki, A., et al., *A deletional frameshift mutation of the beta-spectrin gene associated with elliptocytosis in spectrin Tokyo (beta 220/216).* Blood, 1992. **80**(8): p. 2115-21.
333. Wilmotte, R., et al., *A deletional frameshift mutation in spectrin beta-gene associated with hereditary elliptocytosis in spectrin Napoli.* Br J Haematol, 1994. **88**(2): p. 437-9.
334. Qualtieri, A., et al., *Spectrin Cosenza: a novel beta chain variant associated with Sp alphaI/74 hereditary elliptocytosis.* Br J Haematol, 1997. **97**(2): p. 273-8.
335. Maillet, P., et al., *Stop codon in exon 30 (E2069X) of beta-spectrin gene associated with hereditary elliptocytosis in spectrin Nagoya.* Hum Mutat, 1996. **8**(4): p. 366-8.

336. Garbarz, M., et al., *Spectrin Rouen (beta 220-218), a novel shortened beta-chain variant in a kindred with hereditary elliptocytosis. Characterization of the molecular defect as exon skipping due to a splice site mutation.* J Clin Invest, 1991. **88**(1): p. 76-81.
337. Conboy, J.G., et al., *An isoform-specific mutation in the protein 4.1 gene results in hereditary elliptocytosis and complete deficiency of protein 4.1 in erythrocytes but not in nonerythroid cells.* J Clin Invest, 1993. **91**(1): p. 77-82.
338. Venezia, N.D., et al., *A large deletion within the protein 4.1 gene associated with a stable truncated mRNA and an unaltered tissue-specific alternative splicing.* Blood, 1998. **91**(11): p. 4361-7.
339. Garbarz, M., et al., *Protein 4.1 Lille, a novel mutation in the downstream initiation codon of protein 4.1 gene associated with heterozygous 4,1(-) hereditary elliptocytosis.* Hum Mutat, 1995. **5**(4): p. 339-40.
340. Dalla Venezia, N., et al., *Homozygous 4.1(-) hereditary elliptocytosis associated with a point mutation in the downstream initiation codon of protein 4.1 gene.* J Clin Invest, 1992. **90**(5): p. 1713-7.
341. Garbarz, M., et al., *A variant of erythrocyte membrane skeletal protein band 4.1 associated with hereditary elliptocytosis.* Blood, 1984. **64**(5): p. 1006-15.
342. Marchesi, S.L., et al., *Molecular analysis of insertion/deletion mutations in protein 4.1 in elliptocytosis. I. Biochemical identification of rearrangements in the spectrin/actin binding domain and functional characterizations.* J Clin Invest, 1990. **86**(2): p. 516-23.
343. Conboy, J., et al., *Molecular analysis of insertion/deletion mutations in protein 4.1 in elliptocytosis. II. Determination of molecular genetic origins of rearrangements.* J Clin Invest, 1990. **86**(2): p. 524-30.
344. Lorenzo, F., et al., *Protein 4.1 deficiency associated with an altered binding to the spectrin-actin complex of the red cell membrane skeleton.* J Clin Invest, 1994. **94**(4): p. 1651-6.
345. Rebuck, J.W. and E.J. Van Slyck, *An unsuspected ultrastructural fault in human elliptocytes.* Am J Clin Pathol, 1968. **49**(1): p. 19-25.
346. Zhang, R., et al., *Spectrin: structure, function and disease.* Sci China Life Sci, 2013. **56**(12): p. 1076-85.
347. Lam, V.Q., et al., *Association studies of erythroid alpha-spectrin at the tetramerization site.* Br J Haematol, 2009. **147**(3): p. 392-5.
348. Antoniou, C., V.Q. Lam, and L.W. Fung, *Conformational changes at the tetramerization site of erythroid alpha-spectrin upon binding beta-spectrin: a spin label EPR study.* Biochemistry, 2008. **47**(40): p. 10765-72.
349. Park, S., M.E. Johnson, and L.W. Fung, *Nuclear magnetic resonance studies of mutations at the tetramerization region of human alpha spectrin.* Blood, 2002. **100**(1): p. 283-8.
350. Ipsaro, J.J., et al., *Crystal structure and functional interpretation of the erythrocyte spectrin tetramerization domain complex.* Blood, 2010. **115**(23): p. 4843-52.
351. Gaetani, M., et al., *Structural and functional effects of hereditary hemolytic anemia-associated point mutations in the alpha spectrin tetramer site.* Blood, 2008. **111**(12): p. 5712-20.
352. Swierczek, S., et al., *Novel exon 2 alpha spectrin mutation and intragenic crossover: three morphological phenotypes associated with four distinct alpha spectrin defects.* Haematologica, 2013. **98**(12): p. 1972-9.
353. Song, Y., N.H. Pipalia, and L.W. Fung, *The L49F mutation in alpha erythroid spectrin induces local disorder in the tetramer association region: Fluorescence and molecular dynamics studies of free and bound alpha spectrin.* Protein Sci, 2009. **18**(9): p. 1916-25.
354. Lecomte, M.C., et al., *Properties of normal and mutant polypeptide fragments from the dimer self-association sites of human red cell spectrin.* Eur Biophys J, 1999. **28**(3): p. 208-15.

355. Giorgi, M., et al., *Spectrin oligomerization is cooperatively coupled to membrane assembly: a linkage targeted by many hereditary hemolytic anemias?* Exp Mol Pathol, 2001. **70**(3): p. 215-30.
356. Randles, L.G., et al., *Understanding pathogenic single-nucleotide polymorphisms in multidomain proteins--studies of isolated domains are not enough.* FEBS J, 2013. **280**(4): p. 1018-27.
357. Johnson, C.P., et al., *Pathogenic proline mutation in the linker between spectrin repeats: disease caused by spectrin unfolding.* Blood, 2007. **109**(8): p. 3538-43.
358. Yawata, A., et al., *A markedly disrupted skeletal network with abnormally distributed intramembrane particles in complete protein 4.1-deficient red blood cells (allele 4.1 Madrid): implications regarding a critical role of protein 4.1 in maintenance of the integrity of the red blood cell membrane.* Blood, 1997. **90**(6): p. 2471-81.
359. Nakanishi, H., et al., *Ankyrin gene mutations in japanese patients with hereditary spherocytosis.* Int J Hematol, 2001. **73**(1): p. 54-63.
360. Bessis, M., *Red cell shapes. An illustrated classification and its rationale.* Nouv Rev Fr Hematol, 1972. **12**(6): p. 721-45.
361. Perrotta, S., P.G. Gallagher, and N. Mohandas, *Hereditary spherocytosis.* Lancet, 2008. **372**(9647): p. 1411-26.
362. Luo, Y., et al., *Spectrum of Ankyrin Mutations in Hereditary Spherocytosis: A Case Report and Review of the Literature.* Acta Haematol, 2018. **140**(2): p. 77-86.
363. Sabatino, D.E., et al., *A minimal ankyrin promoter linked to a human gamma-globin gene demonstrates erythroid specific copy number dependent expression with minimal position or enhancer dependence in transgenic mice.* J Biol Chem, 2000. **275**(37): p. 28549-54.
364. Gallagher, P.G., et al., *Erythrocyte ankyrin promoter mutations associated with recessive hereditary spherocytosis cause significant abnormalities in ankyrin expression.* J Biol Chem, 2001. **276**(45): p. 41683-9.
365. Hassoun, H., et al., *Molecular basis of spectrin deficiency in beta spectrin Durham. A deletion within beta spectrin adjacent to the ankyrin-binding site precludes spectrin attachment to the membrane in hereditary spherocytosis.* J Clin Invest, 1995. **96**(6): p. 2623-9.
366. Hassoun, H., et al., *Hereditary spherocytosis with spectrin deficiency due to an unstable truncated beta spectrin.* Blood, 1996. **87**(6): p. 2538-45.
367. Basseres, D.S., et al., *Beta-spectrin Promiss-ao: a translation initiation codon mutation of the beta-spectrin gene (ATG --> GTG) associated with hereditary spherocytosis and spectrin deficiency in a Brazilian family.* Blood, 1998. **91**(1): p. 368-9.
368. Garbarz, M., et al., *A 5' splice region G-->C mutation in exon 3 of the human beta-spectrin gene leads to decreased levels of beta-spectrin mRNA and is responsible for dominant hereditary spherocytosis (spectrin Guemene-Penfao).* Br J Haematol, 1998. **100**(1): p. 90-8.
369. Hassoun, H., et al., *Characterization of the underlying molecular defect in hereditary spherocytosis associated with spectrin deficiency.* Blood, 1997. **90**(1): p. 398-406.
370. Dhermy, D., et al., *Hereditary spherocytosis with spectrin deficiency related to null mutations of the beta-spectrin gene.* Blood Cells Mol Dis, 1998. **24**(2): p. 251-61.
371. Maciag, M., et al., *Novel beta-spectrin mutations in hereditary spherocytosis associated with decreased levels of mRNA.* Br J Haematol, 2009. **146**(3): p. 326-32.
372. Wolfe, L.C., et al., *A genetic defect in the binding of protein 4.1 to spectrin in a kindred with hereditary spherocytosis.* N Engl J Med, 1982. **307**(22): p. 1367-74.
373. Becker, P.S., J.S. Morrow, and S.E. Lux, *Abnormal oxidant sensitivity and beta-chain structure of spectrin in hereditary spherocytosis associated with defective spectrin-protein 4.1 binding.* J Clin Invest, 1987. **80**(2): p. 557-65.

374. Basseres, D.S., et al., *beta-Spectrin Sao PauloII, a novel frameshift mutation of the beta-spectrin gene associated with hereditary spherocytosis and instability of the mutant mRNA.* Braz J Med Biol Res, 2002. **35**(8): p. 921-5.
375. Wichterle, H., et al., *Combination of two mutant alpha spectrin alleles underlies a severe spherocytic hemolytic anemia.* J Clin Invest, 1996. **98**(10): p. 2300-7.
376. Dhermy, D., et al., *Coinheritance of two alpha-spectrin gene defects in a recessive spherocytosis family.* Clin Lab Haematol, 2000. **22**(6): p. 329-36.
377. Tse, W.T., et al., *Amino-acid substitution in alpha-spectrin commonly coinherited with nondominant hereditary spherocytosis.* Am J Hematol, 1997. **54**(3): p. 233-41.
378. Dhermy, D., et al., *Heterogenous band 3 deficiency in hereditary spherocytosis related to different band 3 gene defects.* Br J Haematol, 1997. **98**(1): p. 32-40.
379. Jarolim, P., et al., *Mutations of conserved arginines in the membrane domain of erythroid band 3 lead to a decrease in membrane-associated band 3 and to the phenotype of hereditary spherocytosis.* Blood, 1995. **85**(3): p. 634-40.
380. Yawata, Y., *Red cell membrane protein band 4.2: phenotypic, genetic and electron microscopic aspects.* Biochim Biophys Acta, 1994. **1204**(2): p. 131-48.
381. Kanzaki, A., et al., *Band 4.2 Shiga: 317 CGC-->TGC in compound heterozygotes with 142 GCT-->ACT results in band 4.2 deficiency and microspherocytosis.* Br J Haematol, 1995. **91**(2): p. 333-40.
382. Kanzaki, A., et al., *Band 4.2 Komatsu: 523 GAT-->TAT (175 Asp-->Tyr) in exon 4 of the band 4.2 gene associated with total deficiency of band 4.2, hemolytic anemia with ovalostomatocytosis and marked disruption of the cytoskeletal network.* Int J Hematol, 1995. **61**(4): p. 165-78.
383. Takaoka, Y., et al., *A novel mutation in the erythrocyte protein 4.2 gene of Japanese patients with hereditary spherocytosis (protein 4.2 Fukuoka).* Br J Haematol, 1994. **88**(3): p. 527-33.
384. Matsuda, M., et al., *A novel mutation causing an aberrant splicing in the protein 4.2 gene associated with hereditary spherocytosis (protein 4.2Notame).* Hum Mol Genet, 1995. **4**(7): p. 1187-91.
385. Yawata, Y., et al., *Hereditary Red Cell Membrane Disorders in Japan: Their Genotypic and Phenotypic Features in 1014 Cases Studied.* Hematology, 2001. **6**(6): p. 399-422.
386. Reliene, R., et al., *Splenectomy prolongs in vivo survival of erythrocytes differently in spectrin/ankyrin- and band 3-deficient hereditary spherocytosis.* Blood, 2002. **100**(6): p. 2208-15.
387. Da Costa, L., et al., *Temporal differences in membrane loss lead to distinct reticulocyte features in hereditary spherocytosis and in immune hemolytic anemia.* Blood, 2001. **98**(10): p. 2894-9.
388. Delaunay, J., *The molecular basis of hereditary red cell membrane disorders.* Blood Rev, 2007. **21**(1): p. 1-20.
389. Crisp, R.L., et al., *Red blood cell aquaporin-1 expression is decreased in hereditary spherocytosis.* Ann Hematol, 2016. **95**(10): p. 1595-601.
390. Vives Corrons, J.L. and I. Besson, *Red cell membrane Na+ transport systems in hereditary spherocytosis: relevance to understanding the increased Na+ permeability.* Ann Hematol, 2001. **80**(9): p. 535-9.
391. Wiley, J.S., *Red cell survival studies in hereditary spherocytosis.* J Clin Invest, 1970. **49**(4): p. 666-72.
392. Wandersee, N.J., et al., *Increased erythrocyte adhesion in mice and humans with hereditary spherocytosis and hereditary elliptocytosis.* Blood, 2004. **103**(2): p. 710-6.
393. Deatherage, B.L. and B.T. Cookson, *Membrane vesicle release in bacteria, eukaryotes, and archaea: a conserved yet underappreciated aspect of microbial life.* Infect Immun, 2012. **80**(6): p. 1948-57.

394. Robinson, D.G., Y. Ding, and L. Jiang, *Unconventional protein secretion in plants: a critical assessment.* Protoplasma, 2016. **253**(1): p. 31-43.
395. Gould, S.J. and G. Raposo, *As we wait: coping with an imperfect nomenclature for extracellular vesicles.* J Extracell Vesicles, 2013. **2**.
396. Raposo, G. and W. Stoorvogel, *Extracellular vesicles: exosomes, microvesicles, and friends.* J Cell Biol, 2013. **200**(4): p. 373-83.
397. Gyorgy, B., et al., *Membrane vesicles, current state-of-the-art: emerging role of extracellular vesicles.* Cell Mol Life Sci, 2011. **68**(16): p. 2667-88.
398. Sedgwick, A.E. and C. D'Souza-Schorey, *The biology of extracellular microvesicles.* Traffic, 2018. **19**(5): p. 319-327.
399. Turturici, G., et al., *Extracellular membrane vesicles as a mechanism of cell-to-cell communication: advantages and disadvantages.* Am J Physiol Cell Physiol, 2014. **306**(7): p. C621-33.
400. Kowal, J., et al., *Proteomic comparison defines novel markers to characterize heterogeneous populations of extracellular vesicle subtypes.* Proc Natl Acad Sci U S A, 2016. **113**(8): p. E968-77.
401. Booth, A.M., et al., *Exosomes and HIV Gag bud from endosome-like domains of the T cell plasma membrane.* J Cell Biol, 2006. **172**(6): p. 923-35.
402. Marzesco, A.M., et al., *Release of extracellular membrane particles carrying the stem cell marker prominin-1 (CD133) from neural progenitors and other epithelial cells.* J Cell Sci, 2005. **118**(Pt 13): p. 2849-58.
403. Nabhan, J.F., et al., *Formation and release of arrestin domain-containing protein 1-mediated microvesicles (ARMMs) at plasma membrane by recruitment of TSG101 protein.* Proc Natl Acad Sci U S A, 2012. **109**(11): p. 4146-51.
404. Pollet, H., et al., *Plasma Membrane Lipid Domains as Platforms for Vesicle Biogenesis and Shedding?* Biomolecules, 2018. **8**(3).
405. Ciana, A., et al., *Membrane Remodelling and Vesicle Formation During Ageing of Human Red Blood Cells.* Cell Physiol Biochem, 2017. **42**(3): p. 1127-1138.
406. Yuana, Y., A. Sturk, and R. Nieuwland, *Extracellular vesicles in physiological and pathological conditions.* Blood Rev, 2013. **27**(1): p. 31-9.
407. Gupta, A. and L. Pulliam, *Exosomes as mediators of neuroinflammation.* J Neuroinflammation, 2014. **11**: p. 68.
408. Shen, B., et al., *Biogenesis of the posterior pole is mediated by the exosome/microvesicle protein-sorting pathway.* J Biol Chem, 2011. **286**(51): p. 44162-76.
409. Muralidharan-Chari, V., et al., *Microvesicles: mediators of extracellular communication during cancer progression.* J Cell Sci, 2010. **123**(Pt 10): p. 1603-11.
410. Barteneva, N.S., N. Maltsev, and I.A. Vorobjev, *Microvesicles and intercellular communication in the context of parasitism.* Front Cell Infect Microbiol, 2013. **3**: p. 49.
411. Wu, K., et al., *Extracellular vesicles as emerging targets in cancer: Recent development from bench to bedside.* Biochim Biophys Acta, 2017. **1868**(2): p. 538-563.
412. Antonelou, M.H., A.G. Kriebardis, and I.S. Papassideri, *Aging and death signalling in mature red cells: from basic science to transfusion practice.* Blood Transfus, 2010. **8 Suppl 3**: p. s39-47.
413. Leal, J.K.F., M.J.W. Adjobo-Hermans, and G. Bosman, *Red Blood Cell Homeostasis: Mechanisms and Effects of Microvesicle Generation in Health and Disease.* Front Physiol, 2018. **9**: p. 703.
414. Antonelou, M.H. and J. Seghatchian, *Update on extracellular vesicles inside red blood cell storage units: Adjust the sails closer to the new wind.* Transfus Apher Sci, 2016. **55**(1): p. 92-104.

415. Willekens, F.L., et al., *Erythrocyte vesiculation: a self-protective mechanism?* Br J Haematol, 2008. **141**(4): p. 549-56.
416. Bocci, V., G.P. Pessina, and L. Paulesu, *Studies of factors regulating the ageing of human erythrocytes--III. Metabolism and fate of erythrocytic vesicles.* Int J Biochem, 1980. **11**(2): p. 139-42.
417. Jank, H. and U. Salzer, *Vesicles generated during storage of red blood cells enhance the generation of radical oxygen species in activated neutrophils.* ScientificWorldJournal, 2011. **11**: p. 173-85.
418. Donadee, C., et al., *Nitric oxide scavenging by red blood cell microparticles and cell-free hemoglobin as a mechanism for the red cell storage lesion.* Circulation, 2011. **124**(4): p. 465-76.
419. Kriebardis, A., et al., *Cell-derived microparticles in stored blood products: innocent-bystanders or effective mediators of post-transfusion reactions?* Blood Transfus, 2012. **10 Suppl 2**: p. s25-38.
420. Burnouf, T., et al., *An overview of the role of microparticles/microvesicles in blood components: Are they clinically beneficial or harmful?* Transfus Apher Sci, 2015. **53**(2): p. 137-45.
421. Barcellini, W., et al., *Hereditary red cell membrane defects: diagnostic and clinical aspects.* Blood Transfus, 2011. **9**(3): p. 274-7.
422. Li, H., et al., *Mechanics of diseased red blood cells in human spleen and consequences for hereditary blood disorders.* Proc Natl Acad Sci U S A, 2018. **115**(38): p. 9574-9579.
423. Sahr, K.E., et al., *Sequence and exon-intron organization of the DNA encoding the alpha I domain of human spectrin. Application to the study of mutations causing hereditary elliptocytosis.* J Clin Invest, 1989. **84**(4): p. 1243-52.
424. Hertz, L., et al., *Is Increased Intracellular Calcium in Red Blood Cells a Common Component in the Molecular Mechanism Causing Anemia?* Front Physiol, 2017. **8**: p. 673.
425. Stauffer, T.P., D. Guerini, and E. Carafoli, *Tissue distribution of the four gene products of the plasma membrane Ca2+ pump. A study using specific antibodies.* J Biol Chem, 1995. **270**(20): p. 12184-90.
426. Awojoodu, A.O., et al., *Acid sphingomyelinase is activated in sickle cell erythrocytes and contributes to inflammatory microparticle generation in SCD.* Blood, 2014. **124**(12): p. 1941-50.
427. Goni, F.M. and A. Alonso, *Effects of ceramide and other simple sphingolipids on membrane lateral structure.* Biochim Biophys Acta, 2009. **1788**(1): p. 169-77.
428. Tsikas, D., *Assessment of lipid peroxidation by measuring malondialdehyde (MDA) and relatives in biological samples: Analytical and biological challenges.* Anal Biochem, 2017. **524**: p. 13-30.
429. Tsuchiya, M., et al., *Cell surface flip-flop of phosphatidylserine is critical for PIEZO1-mediated myotube formation.* Nat Commun, 2018. **9**(1): p. 2049.
430. Chen, K., et al., *Resolving the distinct stages in erythroid differentiation based on dynamic changes in membrane protein expression during erythropoiesis.* Proc Natl Acad Sci U S A, 2009. **106**(41): p. 17413-8.
431. Fanani, M.L., et al., *Sphingomyelinase-induced domain shape relaxation driven by out-of-equilibrium changes of composition.* Biophys J, 2009. **96**(1): p. 67-76.
432. Kishimoto, Y. and N. Kawamura, *Ceramide metabolism in brain.* Mol Cell Biochem, 1979. **23**(1): p. 17-25.
433. Loidl, A., et al., *Oxidized phospholipids in minimally modified low density lipoprotein induce apoptotic signaling via activation of acid sphingomyelinase in arterial smooth muscle cells.* J Biol Chem, 2003. **278**(35): p. 32921-8.

434. Stemmer, U., et al., *Toxicity of oxidized phospholipids in cultured macrophages.* Lipids Health Dis, 2012. **11**: p. 110.
435. Frasch, S.C. and D.L. Bratton, *Emerging roles for lysophosphatidylserine in resolution of inflammation.* Prog Lipid Res, 2012. **51**(3): p. 199-207.
436. Frasch, S.C., et al., *NADPH oxidase-dependent generation of lysophosphatidylserine enhances clearance of activated and dying neutrophils via G2A.* J Biol Chem, 2008. **283**(48): p. 33736-49.
437. Zaidi, A., et al., *Oxidative inactivation of purified plasma membrane Ca2+-ATPase by hydrogen peroxide and protection by calmodulin.* Biochemistry, 2003. **42**(41): p. 12001-10.
438. Sharp, J.S. and K.B. Tomer, *Analysis of the oxidative damage-induced conformational changes of apo- and holocalmodulin by dose-dependent protein oxidative surface mapping.* Biophys J, 2007. **92**(5): p. 1682-92.
439. Zaidi, A., *Plasma membrane Ca-ATPases: Targets of oxidative stress in brain aging and neurodegeneration.* World J Biol Chem, 2010. **1**(9): p. 271-80.
440. Shinar, E., E.A. Rachmilewitz, and S.E. Lux, *Differing erythrocyte membrane skeletal protein defects in alpha and beta thalassemia.* J Clin Invest, 1989. **83**(2): p. 404-10.
441. Cremesti, A.E., F.M. Goni, and R. Kolesnick, *Role of sphingomyelinase and ceramide in modulating rafts: do biophysical properties determine biologic outcome?* FEBS Lett, 2002. **531**(1): p. 47-53.
442. Agmon, E., et al., *Modeling the effects of lipid peroxidation during ferroptosis on membrane properties.* Sci Rep, 2018. **8**(1): p. 5155.
443. Kumar, S., et al., *Insight from Molecular dynamic simulation of reactive oxygen species in oxidized skin membrane.* Sci Rep, 2018. **8**(1): p. 13271.
444. Vahaheikkila, M., et al., *How cardiolipin peroxidation alters the properties of the inner mitochondrial membrane?* Chem Phys Lipids, 2018. **214**: p. 15-23.
445. Brameshuber, M., et al., *Oxidized Phospholipids Inhibit the Formation of Cholesterol-Dependent Plasma Membrane Nanoplatforms.* Biophys J, 2016. **110**(1): p. 205-13.
446. Linke, T., et al., *Stimulation of acid sphingomyelinase activity by lysosomal lipids and sphingolipid activator proteins.* Biol Chem, 2001. **382**(2): p. 283-90.
447. Bartlett, G.R., *Phosphorus assay in column chromatography.* J Biol Chem, 1959. **234**(3): p. 466-8.
448. Grimm, M.O., et al., *Regulation of cholesterol and sphingomyelin metabolism by amyloid-beta and presenilin.* Nat Cell Biol, 2005. **7**(11): p. 1118-23.
449. Li, Q.F., et al., *Prokineticin-1/endocrine gland-derived vascular endothelial growth factor is a survival factor for human multiple myeloma cells.* Leuk Lymphoma, 2010. **51**(10): p. 1902-12.
450. Guillemot-Legris, O., et al., *High-fat diet feeding differentially affects the development of inflammation in the central nervous system.* J Neuroinflammation, 2016. **13**(1): p. 206.
451. Mutemberezi, V., et al., *Development and validation of an HPLC-MS method for the simultaneous quantification of key oxysterols, endocannabinoids, and ceramides: variations in metabolic syndrome.* Anal Bioanal Chem, 2016. **408**(3): p. 733-45.
452. Prausnitz, M.R., et al., *A quantitative study of electroporation showing a plateau in net molecular transport.* Biophys J, 1993. **65**(1): p. 414-22.
453. Fairbanks, G., T.L. Steck, and D.F. Wallach, *Electrophoretic analysis of the major polypeptides of the human erythrocyte membrane.* Biochemistry, 1971. **10**(13): p. 2606-17.
454. Streichman, S. and Y. Gescheidt, *Cryohemolysis for the detection of hereditary spherocytosis: correlation studies with osmotic fragility and autohemolysis.* Am J Hematol, 1998. **58**(3): p. 206-12.
455. Picas, L., et al., *Structural and mechanical heterogeneity of the erythrocyte membrane reveals hallmarks of membrane stability.* ACS Nano, 2013. **7**(2): p. 1054-63.

456. Betz, T., et al., *ATP-dependent mechanics of red blood cells.* Proc Natl Acad Sci U S A, 2009. **106**(36): p. 15320-5.
457. Park, Y., et al., *Metabolic remodeling of the human red blood cell membrane.* Proc Natl Acad Sci U S A, 2010. **107**(4): p. 1289-94.
458. Yoon, Y.Z., et al., *The nonlinear mechanical response of the red blood cell.* Phys Biol, 2008. **5**(3): p. 036007.
459. Li, H. and G. Lykotrafitis, *Vesiculation of healthy and defective red blood cells.* Phys Rev E Stat Nonlin Soft Matter Phys, 2015. **92**(1): p. 012715.
460. Klinken, P., *Red blood cells.* The international Journal of Biochemistry & Cell Biology, 2002. **34**(12): p. 1513-1518.
461. Ghoti, H., et al., *Oxidative stress contributes to hemolysis in patients with hereditary spherocytosis and can be ameliorated by fermented papaya preparation.* Ann Hematol, 2011. **90**(5): p. 509-13.
462. Iolascon, A., R.A. Avvisati, and C. Piscopo, *Hereditary spherocytosis.* Transfus Clin Biol, 2010. **17**(3): p. 138-42.
463. George, A., et al., *Altered phosphorylation of cytoskeleton proteins in sickle red blood cells: the role of protein kinase C, Rac GTPases, and reactive oxygen species.* Blood Cells Mol Dis, 2010. **45**(1): p. 41-5.
464. Nourse, J.L. and M.M. Pathak, *How cells channel their stress: Interplay between Piezo1 and the cytoskeleton.* Semin Cell Dev Biol, 2017. **71**: p. 3-12.
465. Bruce, L.J., *Red cell membrane transport abnormalities.* Curr Opin Hematol, 2008. **15**(3): p. 184-90.
466. Diez-Silva, M., et al., *Shape and Biomechanical Characteristics of Human Red Blood Cells in Health and Disease.* MRS Bull, 2010. **35**(5): p. 382-388.
467. Qi, Y., et al., *Membrane stiffening by STOML3 facilitates mechanosensation in sensory neurons.* Nat Commun, 2015. **6**: p. 8512.
468. Wu, J., A.H. Lewis, and J. Grandl, *Touch, Tension, and Transduction - The Function and Regulation of Piezo Ion Channels.* Trends Biochem Sci, 2017. **42**(1): p. 57-71.
469. Hanggi, P., et al., *Red blood cells of sickle cell disease patients exhibit abnormally high abundance of N-methyl D-aspartate receptors mediating excessive calcium uptake.* Br J Haematol, 2014. **167**(2): p. 252-64.
470. Pang, Y., et al., *The characterization of plasma membrane Ca2+-ATPase in rich sphingomyelin-cholesterol domains.* FEBS Lett, 2005. **579**(11): p. 2397-403.
471. Tang, D., et al., *The influence of membrane lipid structure on plasma membrane Ca2+ - ATPase activity.* Cell Calcium, 2006. **39**(3): p. 209-16.
472. Jiang, L., et al., *Partitioning of the plasma membrane Ca2+-ATPase into lipid rafts in primary neurons: effects of cholesterol depletion.* J Neurochem, 2007. **102**(2): p. 378-88.
473. Gov, N.S. and S.A. Safran, *Red blood cell membrane fluctuations and shape controlled by ATP-induced cytoskeletal defects.* Biophys J, 2005. **88**(3): p. 1859-74.
474. Morel, O., et al., *Cellular mechanisms underlying the formation of circulating microparticles.* Arterioscler Thromb Vasc Biol, 2011. **31**(1): p. 15-26.
475. Salzer, U., et al., *Ca(++)-dependent vesicle release from erythrocytes involves stomatin-specific lipid rafts, synexin (annexin VII), and sorcin.* Blood, 2002. **99**(7): p. 2569-77.
476. Pollet, H., et al., *Oxidative stress and plasmatic acid sphingomyelinase induce membrane damage and alter calcium exchange in elliptocytosis.* To be submitted.
477. Lipowsky, R., *Budding of membranes induced by intramembrane domains.* Journal de Physique II EDP Sciences, 1992. **2**(10): p. 1825-1840.
478. Hutter, J.L. and J. Bechhoefer, *Calibration of atomic-force microscope tips.* Review of Scientific Instruments, 1993. **64**(7): p. 1868-1873.

479. Schillers, H., et al., *Standardized Nanomechanical Atomic Force Microscopy Procedure (SNAP) for Measuring Soft and Biological Samples.* Scientific Reports, 2017. **7**(1): p. 5117.
480. Hertz, H., *Ueber die Berührung fester elastischer Körper.* Journal für die reine und angewandte Mathematik, 1882. **92**: p. 156-171.
481. Goodman, S.R., et al., *The proteomics and interactomics of human erythrocytes.* Exp Biol Med (Maywood), 2013. **238**(5): p. 509-18.
482. Zachowski, A., *Phospholipids in animal eukaryotic membranes: transverse asymmetry and movement.* Biochem J, 1993. **294 (Pt 1)**: p. 1-14.
483. Tomaiuolo, G., *Biomechanical properties of red blood cells in health and disease towards microfluidics.* Biomicrofluidics, 2014. **8**(5): p. 051501.
484. Wang, T.Y. and J.R. Silvius, *Different sphingolipids show differential partitioning into sphingolipid/cholesterol-rich domains in lipid bilayers.* Biophys J, 2000. **79**(3): p. 1478-89.
485. Marks, D.L., R. Bittman, and R.E. Pagano, *Use of Bodipy-labeled sphingolipid and cholesterol analogs to examine membrane microdomains in cells.* Histochem Cell Biol, 2008. **130**(5): p. 819-32.
486. Das, A., et al., *Use of mutant 125I-perfringolysin O to probe transport and organization of cholesterol in membranes of animal cells.* Proc Natl Acad Sci U S A, 2013. **110**(26): p. 10580-5.
487. Ohno-Iwashita, Y., et al., *Cholesterol-binding toxins and anti-cholesterol antibodies as structural probes for cholesterol localization.* Subcell Biochem, 2010. **51**: p. 597-621.
488. Ohno-Iwashita, Y., et al., *Perfringolysin O, a cholesterol-binding cytolysin, as a probe for lipid rafts.* Anaerobe, 2004. **10**(2): p. 125-34.
489. Abe, M. and T. Kobayashi, *Imaging local sphingomyelin-rich domains in the plasma membrane using specific probes and advanced microscopy.* Biochim Biophys Acta, 2013.
490. Ishitsuka, R., et al., *A lipid-specific toxin reveals heterogeneity of sphingomyelin-containing membranes.* Biophys J, 2004. **86**(1 Pt 1): p. 296-307.
491. Ishitsuka, R. and T. Kobayashi, *Lysenin: a new tool for investigating membrane lipid organization.* Anat Sci Int, 2004. **79**(4): p. 184-90.
492. Dumitru, A.C., et al., *Nanoscale membrane architecture of healthy and pathological red blood cells.* Nanoscale Horizons, 2018. **3**(3): p. 293-304.
493. Dumitru, A.C., et al., *High-resolution mapping and recognition of lipid domains using AFM with toxin-derivatized probes.* Chem Commun (Camb), 2018. **54**(50): p. 6903-6906.
494. Kaestner, L., et al., *Calcium imaging of individual erythrocytes: problems and approaches.* Cell Calcium, 2006. **39**(1): p. 13-9.
495. Hempel, S.L., et al., *Dihydrofluorescein diacetate is superior for detecting intracellular oxidants: comparison with 2',7'-dichlorodihydrofluorescein diacetate, 5(and 6)-carboxy-2',7'-dichlorodihydrofluorescein diacetate, and dihydrorhodamine 123.* Free Radic Biol Med, 1999. **27**(1-2): p. 146-59.
496. Gomes, A., E. Fernandes, and J.L. Lima, *Fluorescence probes used for detection of reactive oxygen species.* J Biochem Biophys Methods, 2005. **65**(2-3): p. 45-80.
497. Yazdani, M., *Concerns in the application of fluorescent probes DCDHF-DA, DHR 123 and DHE to measure reactive oxygen species in vitro.* Toxicol In Vitro, 2015. **30**(1 Pt B): p. 578-82.
498. Coumans, F.A.W., et al., *Methodological Guidelines to Study Extracellular Vesicles.* Circ Res, 2017. **120**(10): p. 1632-1648.
499. Menck, K., et al., *Isolation and Characterization of Microvesicles from Peripheral Blood.* J Vis Exp, 2017(119).
500. Konoshenko, M.Y., et al., *Isolation of Extracellular Vesicles: General Methodologies and Latest Trends.* Biomed Res Int, 2018. **2018**: p. 8545347.
501. Ramirez, M.I., et al., *Technical challenges of working with extracellular vesicles.* Nanoscale, 2018. **10**(3): p. 881-906.

502. Szatanek, R., et al., *The Methods of Choice for Extracellular Vesicles (EVs) Characterization.* Int J Mol Sci, 2017. **18**(6).
503. Lykkesfeldt, J. and H.E. Poulsen, *Is vitamin C supplementation beneficial? Lessons learned from randomised controlled trials.* Br J Nutr, 2010. **103**(9): p. 1251-9.
504. Hoehn, R.S., et al., *Acid Sphingomyelinase Inhibition Prevents Hemolysis During Erythrocyte Storage.* Cell Physiol Biochem, 2016. **39**(1): p. 331-40.
505. Smith, A.S., et al., *Myosin IIA interacts with the spectrin-actin membrane skeleton to control red blood cell membrane curvature and deformability.* Proc Natl Acad Sci U S A, 2018. **115**(19): p. E4377-E4385.
506. Eber, S.W., et al., *Ankyrin-1 mutations are a major cause of dominant and recessive hereditary spherocytosis.* Nat Genet, 1996. **13**(2): p. 214-8.
507. Trakarnsanga, K., et al., *An immortalized adult human erythroid line facilitates sustainable and scalable generation of functional red cells.* Nat Commun, 2017. **8**: p. 14750.
508. Mombers, C., et al., *Spectrin-phospholipid interaction. A monolayer study.* Biochim Biophys Acta, 1980. **603**(1): p. 52-62.
509. Grzybek, M., et al., *Spectrin-phospholipid interactions. Existence of multiple kinds of binding sites?* Chem Phys Lipids, 2006. **141**(1-2): p. 133-41.
510. An, X., et al., *Phosphatidylserine binding sites in red cell spectrin.* Blood Cells Mol Dis, 2004. **32**(3): p. 430-2.
511. An, X., et al., *Phosphatidylserine binding sites in erythroid spectrin: location and implications for membrane stability.* Biochemistry, 2004. **43**(2): p. 310-5.
512. Wolny, M., et al., *Key amino acid residues of ankyrin-sensitive phosphatidylethanolamine/phosphatidylcholine-lipid binding site of betaI-spectrin.* PLoS One, 2011. **6**(6): p. e21538.
513. Rybicki, A.C., et al., *Human erythrocyte protein 4.1 is a phosphatidylserine binding protein.* J Clin Invest, 1988. **81**(1): p. 255-60.
514. Eaton, J.W., et al., *Elevated erythrocyte calcium in sickle cell disease.* Nature, 1973. **246**(5428): p. 105-6.
515. Fermo, E., et al., *Hereditary Xerocytosis due to Mutations in PIEZO1 Gene Associated with Heterozygous Pyruvate Kinase Deficiency and Beta-Thalassemia Trait in Two Unrelated Families.* Case Rep Hematol, 2017. **2017**: p. 2769570.
516. Albuisson, J., et al., *Dehydrated hereditary stomatocytosis linked to gain-of-function mutations in mechanically activated PIEZO1 ion channels.* Nat Commun, 2013. **4**: p. 1884.
517. Dalghi, M.G., et al., *Plasma membrane calcium ATPase activity is regulated by actin oligomers through direct interaction.* J Biol Chem, 2013. **288**(32): p. 23380-93.
518. Vanagas, L., et al., *Plasma membrane calcium pump activity is affected by the membrane protein concentration: evidence for the involvement of the actin cytoskeleton.* Biochim Biophys Acta, 2007. **1768**(6): p. 1641-9.
519. Dalghi, M.G., M. Ferreira-Gomes, and J.P. Rossi, *Regulation of the Plasma Membrane Calcium ATPases by the actin cytoskeleton.* Biochem Biophys Res Commun, 2018. **506**(2): p. 347-354.
520. Cali, T., M. Brini, and E. Carafoli, *Regulation of Cell Calcium and Role of Plasma Membrane Calcium ATPases.* Int Rev Cell Mol Biol, 2017. **332**: p. 259-296.
521. Schatzmann, H.J., *ATP-dependent Ca++-extrusion from human red cells.* Experientia, 1966. **22**(6): p. 364-5.
522. Wieschhaus, A., et al., *Calpain-1 knockout reveals broad effects on erythrocyte deformability and physiology.* Biochem J, 2012. **448**(1): p. 141-52.
523. Voskou, S., et al., *Oxidative stress in beta-thalassaemia and sickle cell disease.* Redox Biol, 2015. **6**: p. 226-39.

524. Lutz, H.U., R. Barber, and R.F. McGuire, *Glycoprotein-enriched vesicles from sheep erythrocyte ghosts obtained by spontaneous vesiculation.* J Biol Chem, 1976. **251**(11): p. 3500-10.
525. Salzer, U.H., U. ; Prohaska, R., *Chapter three: insights in the organization and dynamics of erythrocyte lipid rafts*, in *Advances in Planar Lipid Bilayers and Liposomes*. 2008. p. 49-80.
526. Civenni, G., et al., *In vitro incorporation of GPI-anchored proteins into human erythrocytes and their fate in the membrane.* Blood, 1998. **91**(5): p. 1784-92.
527. Salzer, U., et al., *Vesicles generated during storage of red cells are rich in the lipid raft marker stomatin.* Transfusion, 2008. **48**(3): p. 451-62.
528. Kriebardis, A.G., et al., *RBC-derived vesicles during storage: ultrastructure, protein composition, oxidation, and signaling components.* Transfusion, 2008. **48**(9): p. 1943-53.
529. Whitlow, M., et al., *Cells lacking glycan phosphatidylinositol-linked proteins have impaired ability to vesiculate.* Blood, 1993. **81**(2): p. 510-6.
530. Wilkinson, D.K., et al., *Membrane raft actin deficiency and altered Ca2+-induced vesiculation in stomatin-deficient overhydrated hereditary stomatocytosis.* Biochim Biophys Acta, 2008. **1778**(1): p. 125-32.
531. Santos, N.C., J. Martins-Silva, and C. Saldanha, *Gramicidin D and dithiothreitol effects on erythrocyte exovesiculation.* Cell Biochem Biophys, 2005. **43**(3): p. 419-30.
532. Kunzelmann-Marche, C., J.M. Freyssinet, and M.C. Martinez, *Loss of plasma membrane phospholipid asymmetry requires raft integrity. Role of transient receptor potential channels and ERK pathway.* J Biol Chem, 2002. **277**(22): p. 19876-81.
533. Gonzalez, L.J., et al., *The influence of membrane physical properties on microvesicle release in human erythrocytes.* PMC Biophys, 2009. **2**(1): p. 7.
534. Lauren, E., et al., *Phospholipid composition of packed red blood cells and that of extracellular vesicles show a high resemblance and stability during storage.* Biochim Biophys Acta, 2018. **1863**(1): p. 1-8.
535. Bicalho, B., J.L. Holovati, and J.P. Acker, *Phospholipidomics reveals differences in glycerophosphoserine profiles of hypothermically stored red blood cells and microvesicles.* Biochim Biophys Acta, 2013. **1828**(2): p. 317-26.
536. Dinkla, S., et al., *Functional consequences of sphingomyelinase-induced changes in erythrocyte membrane structure.* Cell Death Dis, 2012. **3**: p. e410.
537. Lopez-Montero, I., et al., *Rapid transbilayer movement of ceramides in phospholipid vesicles and in human erythrocytes.* J Biol Chem, 2005. **280**(27): p. 25811-9.
538. Leonard, C., et al., *Tuning of differential lipid order between submicrometric domains and surrounding membrane upon erythrocyte reshaping.* Cell Physiol Biochem In press.
539. Alaarg, A., et al., *Red blood cell vesiculation in hereditary hemolytic anemia.* Front Physiol, 2013. **4**: p. 365.
540. Repsold, L. and A.M. Joubert, *Eryptosis: An Erythrocyte's Suicidal Type of Cell Death.* Biomed Res Int, 2018. **2018**: p. 9405617.

ANNEXES

Annex 1: Endogenous sphingomyelin segregates into submicrometric domains in the living erythrocyte membrane

M. Carquin[1], **H. Pollet[1]**, M. Veiga-da-Cunha[2], A. Cominelli[1], P. Van Der Smissen[1], F. N'kuli[1], H. Emonard[3], P. Henriet[1], H. Mizuno[4], P. J. Courtoy[1], D. Tyteca[1]

[1]CELL Unit, de Duve Institute & Université catholique de Louvain, 1200 Brussels, Belgium
[2]Laboratory of physiological chemistry, de Duve Institute & Université catholique de Louvain, 1200 Brussels, Belgium
[3]"Matrice Extracellulaire et Dynamique Cellulaire" Unit (MEDyC), CNRS UMR 7369, Université de Reims Champagne-Ardenne, Laboratoire SiRMa, 51 100 Reims, France
[4]Department of chemistry, Katholieke Universiteit Leuven, 3001 Heverlee, Belgium

Abstract
We recently reported that trace insertion of exogenous fluorescent (green BODIPY) analogs of sphingomyelin (SM) into living red blood cells (RBCs), partially spread onto coverslips, labels submicrometric domains, visible by confocal microscopy. We here extend this feature to endogenous SM, upon binding of a SM-specific nontoxic (NT) fragment of the earthworm toxin, lysenin, fused to the red monomeric fluorescent protein, mCherry [construct named His-mCherry-NT-lysenin (lysenin*)]. Specificity of lysenin* binding was verified with composition-defined liposomes and by loss of (125)I-lysenin* binding to erythrocytes upon SM depletion by SMase. The (125)I-lysenin* binding isotherm indicated saturation at 3.5 × 10(6) molecules/RBC, i.e., ∼3% of SM coverage. Nonsaturating lysenin* concentration also labeled sub-micrometric domains on the plasma membrane of partially spread erythrocytes, colocalizing with inserted green BODIPY-SM, and abrogated by SMase. Lysenin*-labeled domains were stable in time and space and were regulated by temperature and cholesterol. The abundance, size, positioning, and segregation of lysenin*-labeled domains from other lipids (BODIPY-phosphatidylcholine or -glycosphingolipids) depended on membrane tension. Similar lysenin*-labeled domains were evidenced in RBCs gently suspended in 3D-gel. Taken together, these data demonstrate submicrometric compartmentation of endogenous SM at the membrane of a living cell in vitro, and suggest it may be a genuine feature of erythrocytes in vivo.

J Lipid Res. 2014 Jul;55(7):1331-42.

DOI 10.1194/jlr.M048538

KEYWORDS

His-mCherry-NT-lysenin; cholesterol; lateral membrane heterogeneity; membrane tension; temperature; toxin; vital confocal imaging

Annex 2: Cholesterol segregates into submicrometric domains at the living erythrocyte membrane: evidence and regulation

M. Carquin[1], L. Conrard[1], **H. Pollet[1]**, P. Van Der Smissen[1], A. Cominelli[1], M. Veiga-da-Cunha[2], P.J. Courtoy[1], D. Tyteca[1]

[1]CELL Unit and [2]Laboratory of physiological chemistry, de Duve Institute & Université catholique de Louvain, 1200 Brussels, Belgium

Abstract

Although cholesterol is essential for membrane fluidity and deformability, the level of its lateral heterogeneity at the plasma membrane of living cells is poorly understood due to lack of appropriate probe. We here report on the usefulness of the D4 fragment of Clostridium perfringens toxin fused to mCherry (theta*), as specific, non-toxic, sensitive and quantitative cholesterol-labeling tool, using erythrocyte flat membrane. By confocal microscopy, theta* labels cholesterol-enriched submicrometric domains in coverslip-spread but also gel-suspended (non-stretched) fresh erythrocytes, suggesting in vivo relevance. Cholesterol domains on spread erythrocytes are stable in time and space, restricted by membrane:spectrin anchorage via 4.1R complexes, and depend on temperature and sphingomyelin, indicating combined regulation by extrinsic membrane:cytoskeleton interaction and by intrinsic lipid packing. Cholesterol domains partially co-localize with BODIPY-sphingomyelin-enriched domains. In conclusion, we show that theta* is a useful vital probe to study cholesterol organization and demonstrate that cholesterol forms submicrometric domains in living cells.

Cell Mol Life Sci. 2015 Dec;72(23):4633-51.

DOI 10.1007/s00018-015-1951-x

KEYWORDS

125I-toxin; BODIPY-sphingomyelin; C2C12 myoblasts; His-mCherry-theta-D4; Lateral membrane heterogeneity; Membrane tension; Temperature; Vital confocal imaging

Annex 3: Recent progress on lipid lateral heterogeneity in plasma membranes: from rafts to submicrometric domains

M. Carquin[1,*], L. D'Auria[2,*], **H. Pollet[1]**, E. R. Bongarzone[2], D. Tyteca[1]

[1], CELL Unit, de Duve Institute & Université Catholique de Louvain. UCL B1.75.05, Avenue Hippocrate, 75, B-1200 Brussels, Belgium.
[2], The Myelin Regeneration Group at the Dept. Anatomy & Cell Biology, College of Medicine, University of Illinois, Chicago. 808 S. Wood St. MC512. Chicago, IL. 60612. USA.
**, Co-first authors*

Abstract

The concept of transient nanometric domains known as lipid rafts has brought interest to reassess the validity of the Singer-Nicolson model of a fluid bilayer for cell membranes. However, this new view is still insufficient to explain the cellular control of surface lipid diversity or membrane deformability. During the past decades, the hypothesis that some lipids form large (submicrometric/mesoscale vs nanometric rafts) and stable (>min vs s) membrane domains has emerged, largely based on indirect methods. Morphological evidence for stable submicrometric lipid domains, well-accepted for artificial and highly specialized biological membranes, was further reported for a variety of living cells from prokaryot es to yeast and mammalian cells. However, results remained questioned based on limitations of available fluorescent tools, use of poor lipid fixatives, and imaging artifacts due to non-resolved membrane projections. In this review, we will discuss recent evidence generated using powerful and innovative approaches such as lipid-specific toxin fragments that support the existence of submicrometric domains. We will integrate documented mechanisms involved in the formation and maintenance of these domains, and provide a perspective on their relevance on membrane deformability and regulation of membrane protein distribution.

Prog Lipid Res. 2016 Apr;62:1-24.

DOI: 10.1016/j.plipres.2015.12.004.

KEYWORDS

lipid domains, lipid probes, toxin fragments, living cells, membrane lipid composition, membrane deformability

Annex 4: Contribution of plasma membrane lipid domains to red blood cell (re)shaping

C. Leonard[1,2], L. Conrard[2], M. Guthmann[2], **H. Pollet[2]**, M. Carquin[2], C. Vermylen[3], P. Gailly[4], P. Van Der Smissen[2], M-P. Mingeot-Leclercq[1], D. Tyteca[2]

[1] FACM Unit, Louvain Drug Research Institute & Université catholique de Louvain, 1200 Brussels, Belgium

[2] CELL Unit, de Duve Institute & Université catholique de Louvain, 1200 Brussels, Belgium

[3] PEDI Unit, Institut de Recherche expérimentale et clinique & Université catholique de Louvain, 1200 Brussels, Belgium

[4] CEMO Unit, Institute of Neuroscience & Université catholique de Louvain, 1200 Brussels, Belgium

Abstract

Although lipid domains have been evidenced in several living cell plasma membranes, their roles remain largely unclear. We here investigated whether they could contribute to function-associated cell (re)shaping. To address this question, we used erythrocytes as cellular model since they (i) exhibit a specific biconcave shape, allowing for reversible deformation in blood circulation, which is lost by membranevesiculation upon aging; and (ii) display at their outer plasma membrane leaflet two types of submicrometric domains differently enriched in cholesterol and sphingomyelin. We here reveal the specific association of cholesterol- and sphingomyelin-enriched domains with distinct curvature areas of the erythrocyte biconcave membrane. Upon erythrocyte deformation, cholesterol-enriched domains gathered in high curvature areas. In contrast, sphingomyelin-enriched domains increased in abundance upon calcium efflux during shape restoration. Upon erythrocyte storage at 4 °C (to mimick aging), lipid domains appeared as specific vesiculation sites. Altogether, our data indicate that lipiddomains could contribute to erythrocyte function-associated (re)shaping.

Sci Rep. 2017 Jun 27;7(1):4264.

DOI: 10.1038/s41598-017-04388-z.

KEYWORDS

His-mCherry-Theta-D4, His-mCherry-NT-Lysenin, Membrane lateral heterogeneity, Membrane curvature, Membrane stretching, Cell deformation, Red blood cell aging, Vital confocal imaging, Electron microscopy, Sphingomyelin, Cholesterol, Calcium exchanges

Annex 5: Tuning of differential lipid order between submicrometric domains and surrounding membrane upon erythrocyte reshaping.

C. Leonard[1,2], **H. Pollet[2]**, C. Vermylen[3], N. Gov[4], D. Tyteca[2], M-P. Mingeot-Leclercq[1]

[1] FACM Unit, Louvain Drug Research Institute & Université catholique de Louvain, 1200 Brussels, Belgium

[2] CELL Unit, de Duve Institute & Université catholique de Louvain, 1200 Brussels, Belgium

[3] PEDI Unit, Institut de Recherche expérimentale et clinique & Université catholique de Louvain, 1200 Brussels, Belgium

[4] Department of Chemical and Biological Physics, Weizmann Institute of Science, Rehovot, Israel

Abstract

BACKGROUND/AIMS: Transient nanometric cholesterol- and sphingolipid-enriched domains, called rafts, are characterized by higher lipid order as compared to surrounding lipids. Here, we asked whether the seminal concept of highly ordered rafts could be refined with the presence of lipid domains exhibiting different enrichment in cholesterol and sphingomyelin and association with erythrocyte curvature areas. We also investigated how differences in lipid order between domains and surrounding membrane (bulk) are regulated and whether changes in order differences could participate to erythrocyte deformation and vesiculation.

METHODS: We used the fluorescent hydration- and membrane packing-sensitive probe Laurdan to determine by imaging mode the Generalized Polarization (GP) values of lipid domains vs the surrounding membrane.

RESULTS: Laurdan revealed the majority of sphingomyelin-enriched domains associated to low erythrocyte curvature areas and part of the cholesterol-enriched domains associated with high curvature. Both lipid domains were less ordered than the surrounding lipids in erythrocytes at resting state. Upon erythrocyte deformation (elliptocytes and stimulation of calcium exchanges) or membrane vesiculation (storage at 4°C), lipid domains became more ordered than the bulk. Upon aging and in membrane fragility diseases (spherocytosis), an increase in the difference of lipid order between domains and the surrounding lipids contributed to the initiation of domain vesiculation.

CONCLUSION: The critical role of domain-bulk differential lipid order modulation for erythrocyte reshaping is discussed in relation with the pressure exerted by the cytoskeleton on the membrane.

Cell Physiol Biochem. 2018;48(6):2563-2582.

DOI: 10.1159/000492700.

KEYWORDS

Calcium exchanges; Cell deformation; Cholesterol; Cytoskeleton; His-mCherry-NT-Lysenin; His-mCherry-Theta-D4; Laurdan; Membrane curvature; Membrane lateral heterogeneity; Membrane vesiculation; Red blood cell aging; Sphingomyelin; Vital confocal imaging

Annex 6: Spatial relationship and functional relevance of three lipid domain populations at the erythrocyte surface

L. Conrard[1], A. Stommen[1], J. Steinkühler[2], R. Dimova[2], **H. Pollet[1]**, D. Tyteca[1]

[1] CELL Unit, de Duve Institute & Université catholique de Louvain, 1200 Brussels, Belgium
[2] Max Planck Institute of Colloids and Interfaces, Science Park Golm, 14424 Potsdam, Germany

Cell Physiol Biochem. 2018;51(4):1544-1565.

DOI: 10.1159/000495645.

KEYWORDS

Fluorescence microscopy, mechanical stimulation, PIEZO1, PMCA, PDMS stretching, calcium exchanges

Cellular Physiology and Biochemistry

Cell Physiol Biochem 2018;51:1544-1565
DOI: 10.1159/000495645
Published online: 29 November 2018
Accepted: 21 November 2018

Original Paper

Spatial Relationship and Functional Relevance of Three Lipid Domain Populations at the Erythrocyte Surface

Louise Conrard[a] Amaury Stommen[a] Anne-Sophie Cloos[a] Jan Steinkühler[b] Rumiana Dimova[b] Hélène Pollet[a] Donatienne Tyteca[a]

[a]CELL Unit, de Duve Institute & Université catholique de Louvain, Brussels, Belgium, [b]Theory and Bio-Systems, Max Planck Institute of Colloids and Interfaces, Science Park Golm, Potsdam, Germany

Key Words
Fluorescence microscopy • Mechanical stimulation • Piezo1 • PMCA • PDMS stretching • Calcium exchanges

Abstract
Background/Aims: Red blood cells (RBC) have been shown to exhibit stable submicrometric lipid domains enriched in cholesterol (chol), sphingomyelin (SM), phosphatidylcholine (PC) or ganglioside GM1, which represent the four main lipid classes of their outer plasma membrane leaflet. However, whether those lipid domains co-exist at the RBC surface or are spatially related and whether and how they are subjected to reorganization upon RBC deformation are not known. ***Methods:*** Using fluorescence and/or confocal microscopy and well-validated probes, we compared these four lipid-enriched domains for their abundance, curvature association, lipid order, temperature dependence, spatial dissociation and sensitivity to RBC mechanical stimulation. ***Results:*** Our data suggest that three populations of lipid domains with decreasing abundance coexist at the RBC surface: (i) chol-enriched ones, associated with RBC high curvature areas; (ii) GM1/PC/chol-enriched ones, present in low curvature areas; and (iii) SM/PC/chol-enriched ones, also found in low curvature areas. Whereas chol-enriched domains gather in increased curvature areas upon RBC deformation, low curvature-associated lipid domains increase in abundance either upon calcium influx during RBC deformation (GM1/PC/chol-enriched domains) or upon secondary calcium efflux during RBC shape restoration (SM/PC/chol-enriched domains). Hence, abrogation of these two domain populations is accompanied by a strong impairment of the intracellular calcium balance. ***Conclusion:*** Lipid domains could contribute to calcium influx and efflux by controlling the membrane distribution and/or the activity of the mechano-activated ion channel Piezo1 and the calcium pump PMCA. Whether this results from lipid domain biophysical properties, the strength of their anchorage to the underlying cytoskeleton and/or their correspondence with inner plasma membrane leaflet lipids remains to be demonstrated.

Donatienne Tyteca
CELL Unit, de Duve Institute & Université catholique de Louvain,
UCL B1.75.05, avenue Hippocrate, 75, B-1200 Brussels (Belgium)
Tel. +32-2-764.75.91, Fax +32-2-764.75.43, E-Mail donatienne.tyteca@uclouvain.be

KARGER

Introduction

Red blood cells (RBCs) are highly deformable cells that can go through capillaries 3-times narrower than their diameter to deliver oxygen throughout the body. The RBC deformation process is associated with a transient increase of the intracellular calcium [1] which plays a capital role, notably by activating Gardos channels and thus leading to cell dehydration, and by favoring a local uncoupling between the membrane and the underlying spectrin cytoskeleton [2]. RBC calcium entry is thought to be mostly operated by mechano-activated ion channels like Piezo1 [3], while calcium efflux is ensured by the RBC calcium pump, the Plasma Membrane Calcium ATPase (PMCA). This process is tightly regulated and an excessive increase of the intracellular calcium, as observed in physiological senescence or in pathological hereditary hemolytic anemias, has harmful consequences for the RBCs such as an increased vesiculation, the loss of the transverse lipid asymmetry and the consumption of the energy resources. This will lead to a decreased deformability resulting in the RBCs trapping in the spleen and their removal from the blood by the spleen resident macrophages [4].

Besides finely regulated calcium exchanges, RBC deformability has also been linked to other specific features, *i.e.* (i) the excess of plasma membrane (PM) surface in comparison with the cytoplasmic volume and the resultant biconcave shape; (ii) the tightly regulated intracellular hemoglobin concentration (32-36 g/dl); and (iii) the viscoelastic resistance of the membrane [5, 6]. The latter feature depends on the strong anchorage of the PM to a very stable cytoskeleton of spectrin thanks to two non-redundant anchorage complexes based on 4.1R and ankyrin proteins [7]. Membrane lipid composition is also suggested to regulate the membrane viscoelastic properties [8]. As a matter of fact, RBC PM exhibits a particularly high cholesterol level (~45 mol%) in comparison to other cell types (*e.g.* ~35 mol% in CHO cells or ~15 mol% in fibroblasts) [9]. Yet, this small lipid plays key roles in membrane by regulating fluidity, lipid phase separation, mechanic resistance and membrane permeability [10].

As the scientific community slowly realized the importance of membrane lipid composition for cell biological characteristics and processes, more and more evidences for lateral lipid asymmetric distribution have been provided. The first example was the well-known 'lipid rafts', defined as nanometric and transient lipid structures whose presence has been linked to several processes like lipid sorting in polarized cells and antigen presentation at the T-cell surface [11, 12]. In the last decades, advances in microscopy resolution and development of new observation techniques (*e.g.* super resolution microscopy or fluorescence lifetime spectroscopy) [13-16] and more relevant lipid probes [17, 18] have allowed to evidence bigger (submicrometric instead of nanometric) and more stable lipid domains. Those have been observed on prokaryotic cells [19], yeast [20, 21] and various eukaryotic cells like keratinocytes [22], fibroblasts [23] and RBCs [24-26]. Focus is generally made on sphingolipids and sterols as they are two major lipids of the PM external leaflet of many cells and because they are known to be enriched in rafts and associated with membrane fluidity regulation.

As a matter of fact, our group evidenced and extensively characterized cholesterol (chol)- and sphingomyelin (SM)-enriched submicrometric domains at the external PM leaflet of RBCs. These domains are stable in time and space and have been observed by fluorescence microscopy on RBCs immobilized on poly-L-lysine (PLL, *i.e.* spread), but also on RBCs in suspension in plastic chambers or in three-dimensional gels. To label the domains for fluorescence microscopy, we used fluorescent lipid analogs (*i.e.* BODIPY-SM) that get inserted at trace levels in the PM [27] and developed and carefully validated fluorescent toxin fragments specific to endogenous chol (theta*) and SM (lysenin*) [25, 26]. More recently, we also used atomic force microscopy, a high-resolution technique applicable to cells in their native state (*i.e.* without labeling), to study the biophysical properties of these domains [28]. The chol- and SM-enriched domains differ in abundance and biophysical properties (*i.e.* lipid order and association with membrane curvature areas) and differentially contribute to the

RBC deformation. For instance, chol-enriched domains gather in high-curvature membrane areas under RBC stretching and might thus increase deformability and membrane resistance under deformation; while SM-enriched domains, which increase in abundance after deformation, could be linked to RBC shape restoration after deformation [29].

Lipid domains enriched in phosphatidylcholine (PC) or glycosphingolipids like ganglioside GM1 have also been evidenced but not well-characterized [27]. Moreover, whether chol-, SM-, PC- or GM1-enriched domains coexist or are spatially related at the RBC surface and whether they are subjected to reorganization upon RBC deformation are not known. We explored the first issue on RBCs at resting state. Since multiple labeling could suffer from the use of several probes at the same time, possibly inducing toxicity and steric hindrance, we developed additional approaches aiming at comparing lipid domains for their abundance, biophysical properties (lipid order and curvature association, key properties involved in cell deformation) and ability to be modulated by temperature and controlled chol depletion. We next studied lipid domain organization through RBC deformation by mechanically stimulating RBCs (using stretchable silicon chambers) and modulating either the entry or the exit of calcium.

The present study shows the coexistence at the resting RBC PM outer leaflet of three lipid domain populations that differ in chol-, SM-, PC- and GM1-enrichment, abundance, curvature association, lipid order, temperature dependence and sensitivity to RBC spreading onto PLL. Regarding lipid domain contribution to RBC reshaping, we have previously shown that the first population of domains, *i.e.* those mostly enriched in chol, gather in increased curvature areas upon RBC deformation [29]. Here, we provide experimental evidence for the differential contribution of the two other populations of lipid domains in RBC calcium exchanges. This could occur either via the mechano-activated ion channel Piezo1 during deformation or via the calcium pump PMCA during shape restoration.

Materials and Methods

Red blood cell isolation

This study was approved by the Medical Ethics Committee of the Université Catholique de Louvain; each donor gave written informed consent. All methods were performed in accordance with the relevant guidelines and regulations. Blood was collected from 10 healthy volunteers by venopuncture into dry K^+/EDTA-coated tubes. For each experiment, blood was diluted 1:10 in Dulbecco's Modified Eagle Medium (DMEM containing 25 mM glucose, 25 mM HEPES and no phenol red, Invitrogen), then washed twice by centrifugation at 200 *g* for 2 min and resuspension. Washed RBCs were used at 5 * 10^7 cells/ml (washed RBCs:medium ratio of 1:10, *v:v*), then incubated or not with pharmacological agents or directly imaged by vital fluorescence/confocal microscopy or fluorescence correlation spectroscopy (FCS) (see below).

Pharmacological treatments

To modulate chol content, washed RBCs were preincubated in suspension at 37°C in DMEM supplemented with (i) the indicated concentrations of methyl-ß-cyclodextrin (mβCD; Sigma-Aldrich) for 30 min or (ii) 0.9 mM mβCD followed by repletion with 3.5 µg/ml mβCD:chol (Sigma-Aldrich) for 60 min. Chol content was determined as previously described [25]. SM content modulation was achieved with sphingomyelinase from *Bacillus Cereus* (Sigma-Aldrich) as described in [26]. To inhibit mechano-activated channels, labeled and immobilized RBCs were incubated with 7 µM GsMTx4 peptide (Abcam) for 15 min and observed upon treatment maintenance. To activate Piezo1 channels, labeled and immobilized RBCs were incubated with 0.5 µM Yoda1 (Biotechne) for 20 sec, washed and directly observed. To activate protein kinase C (PKC), RBCs were pre-incubated with 6 µM phorbol 12-myristate 13-acetate (PMA, Sigma-Aldrich) and 20 nM Calyculin A from Discodermia Calyx (CalA, Sigma-Aldrich) for 15 min at 37°C before labeling (upon maintenance of PMA/CalA treatment). To modulate calcium content, RBCs were pre-incubated in calcium-free homemade medium containing 1 mM calcium-chelating agent ethylene glycol-bis(β-aminoethyl ether)-N,N,N',N'-tetraacetic acid (EGTA, Sigma-Aldrich) for 10 min at RT before labeling (upon maintenance of EGTA). Residual calcium content was assessed as described below. RBCs were then possibly incubated

in 1.8 mM calcium-containing medium for 20 min to achieve calcium repletion. To modulate ATP content, RBCs were pre-incubated in glucose-free homemade medium for 2 h at 37°C before labeling. Residual ATP content was assessed by a luminescent ATP detection assay kit (Abcam). RBCs were then possibly incubated in 25 mM glucose-containing medium for 30 min to achieve glucose repletion. Treatment innocuity has been assessed by measuring the percentage of hemoglobin release (absorbance at 450 nm).

Vital fluorescence/confocal imaging

To immobilize RBCs for imaging, two complementary systems were used: RBCs spread onto poly-L-lysine (PLL, 70–150 kDa; Sigma-Aldrich)-coated coverslips and RBCs in suspension. For spread RBCs, coverslips were first coated with PLL:DMEM (1:1, *v:v*) at 37°C for 40 min, then washed with DMEM at 20°C for 5 min. Labeled RBCs were then dropped onto the coated coverslips at 20°C for exactly 4 min, the suspension was removed and replaced by fresh medium, and attached RBCs were allowed to spread for another 4 min. The coverslip was placed upside down on a Lab-Tek chamber and then observed. For the "in suspension" system, labeled RBCs were dropped to settle down in µ-Slide VI0.4 uncoated IBIDI chambers (IBIDI, Proxylab; 100 µl by channel). All preparations were examined at the labeling temperatures, either with a Zeiss LSM510 confocal/multiphoton microscope using a plan-Apochromat 63X NA 1.4 oil immersion objective or with a Zeiss wide-field fluorescence microscope (Observer.Z1) using a plan-Apochromat 100X/1.4 oil Ph3 objective.

Decoration of endogenous lipids by toxin fragments and fluorescent lipid insertion*

Washed RBCs were labeled with toxin* fragments, BODIPY-lipids (SM, PC, GM1) or TopFluor-TMR-PC. Lysenin* and theta* were produced as previously described [25, 26], dissolved in 1 mg/ml DMEM-BSA (Bovine Serum Albumin, Sigma) and cleared of aggregates before each experiment by centrifugation at 20, 000 *g* for 10 min. RBC labeling with toxins* was performed in suspension (*i.e.* before immobilization) with either 1.25 µM lysenin* or 0.55 µM theta* in DMEM/BSA at the indicated temperatures for 25 min under continuous agitation, then pelleted at 200 *g* for 2 min and resuspended in DMEM. RBC labeling with 0.6 µM BODIPY FL C5-SM, 1 µM BODIPY FL C5-GM1 or 1 µM BODIPY FL C5-HPC (Invitrogen) and 0.8 µM TopFluor-TMR-PC (Avanti polar lipids) was performed after RBC immobilization on coverslips at the indicated temperatures for 15 min. For co-labeling, RBCs were either labeled in suspension with toxin* fragments, immobilized and then labeled with fluorescent lipid analogs, or directly immobilized and co-labeled with fluorescent lipid analogs.

Lipid order

A stock solution of 2-dimethylamino-6-lauroylnaphthalene (Laurdan) was prepared in dimethyl sulfoxide (DMSO) and conserved as described in [30]. Washed RBCs were labeled at RT in suspension in DMEM/BSA containing 2.5 µM Laurdan for 60 min. 1.25 µM lysenin*, 0.55 µM theta* or 0.8 µM TopFluor-TMR-PC were added for the last 20 min. RBCs were then immobilized and examined using (i) confocal mode for lipids and (ii) multiphoton mode with acquisition at 440 nm and 490 nm and a Normaski prism for Laurdan. Lipid order determination was performed as described in [30] and in [31]. Briefly, domains and surrounding membrane ROIs and masks were obtained from the two fluorescent channels (440 nm and 490 nm) of Laurdan images. The determination of Laurdan domains co-localizing or not with the lipid domains and the following separation of the domain masks were done manually by comparing Laurdan and lipid images. A 2D GP map, where GP for each pixel were calculated from a ratio of the two fluorescence channels, was created from those masks using MATLAB (The MathWorks, Natick, MA). Briefly, each image was binned (2 × 2) and thresholded, then the GP image was calculated for each pixel using the GP equation as described in [30], and the G factor was measured as recommended in [30].

Fluorescence correlation spectroscopy

RBCs were immobilized on coverslips and labeled with 1 µM BODIPY-GM1 (as described above) and 25 nM FAST DiI (1, 1'-Dilinoleyl-3, 3,3',3'-Tetramethylindocarbocyanine, 4-Chlorobenzenesulfonate), then examined at RT on confocal microscope Leica TCS SP5 (Wetzlar, Germany) with a 63X 1.2 NA water immersion objective and 1 Airy unit. FAST DiI was excited using a 561 solid state laser and emission was collected between 607 nm and 683 nm using a filter cube. To check for bleed-through artifacts, RBCs were labeled with BODIPY-GM1 alone and in this case no significant signal was detected. The intersection

between confocal volume and RBC membrane was adjusted to the maximum photon count and positioned either on a membrane domain or a segment of the membrane exhibiting homogenous fluorescence. Photon counting was accomplished by avalanche photodiodes (Leica, Wetzlar, Germany) and time correlations were calculated at a sampling frequency of 200 kHz for a time interval of 30 sec. Each measurement point was repeated for three consecutive measurements. The obtained correlation curves were fitted using a 1-component 2D diffusion model: $G(\tau) = \frac{1}{<N>} \frac{1}{\left(1+\frac{\tau}{\tau_0^2}\right)}$

Here, τ_0 is the average residence time inside the intersection of the confocal volume and <*N*> is the average number of fluorophores in the detection volume. Only correlation traces with a satisfying fit to the model (R^2> 0.98) were considered in the analysis.

RBC (de)stretching on PDMS chambers

Deformation experiments were conducted by spreading BODIPY-SM-, GM1- or Fluo-4 (see below)-prelabeled RBCs on a 4 cm^3 polydimethylsiloxane (PDMS) stretchable chamber (Strex Inc). Briefly, PDMS chambers were coated with PLL:DMEM (1:1, *v:v*) at 37°C for 40 min, washed with DMEM at 20°C for 5 min and fixed to the stretching device (STREX, cell strain instrument, B-Bridge). Labeled RBCs were plated into the PDMS chamber for exactly 5 min, then the suspension was removed and replaced by fresh medium, and attached RBCs were allowed to spread for another 5 min. The PDMS chamber was then immediately observed at RT without stretching (unstretched) with a Zeiss wide-field fluorescence microscope (Observer. Z1) using a plan-Neofluar 63X/0.75 Ph2 objective. Stretching and destretching of the chamber were thereafter respectively performed by (i) quick (1 min) axial stretching of the right side of the PDMS chamber of 12 % of the chamber length (stretching); and (ii) return to the initial state (destretching).

Medium osmolarity modulation

CellASIC ONIX Microfluidic platform (Merck Millipore) has been used to achieve real-time imaging on living RBCs. The following media were disposed each in a well and allowed to flow successively to the central chamber: PLL (15 min, low flow), DMEM (5 min, medium flow), washed RBCs (4 min, high flow), DMEM (10 min, medium flow), toxin* or fluorescent lipid analog (15 min, low flow), DMEM (3 min, medium flow), hypo-osmolar medium (180 mOsm, 10 min, low flow). Images were acquired every 45 sec using a Zeiss LSM510 confocal microscope.

Calcium labeling and measurement

To label intracellular calcium, washed RBCs were incubated in suspension at 37°C with 3 µM Fluo-4 acetoxymethyl ester (Fluo-4 AM, Invitrogen) in 1.8 mM calcium-containing homemade medium for 60 min under continuous agitation, pelleted at 200 *g* for 2 min and resuspended in homemade medium, then let for 30 min at 37°C under agitation to allow the Fluo-4AM de-esterification. Fluo-4-labeled cells were then either immobilized, imaged with a Zeiss wide-field fluorescence microscope and analyzed as explained below; or measured in a 96-well plate with a spectrofluorimeter (SpectraCountTM, Packard BioScience Co.) at Exc/Em 490/520 nm and analyzed using hemoglobin content for normalization. As the Fluo-4 fluorescence signal is not a linear function of the calcium concentration [32], only qualitative observations could be made.

Image analysis and data quantification

Lipid domain abundance, curvature association and colocalisation were assessed by manual counting on images from confocal or epifluorescence high-resolution microscope. Measurement of RBC projected area (referred as hemi-RBC area) and Fluo-4 quantification on images was performed using ImageJ software on images where the RBC projected contours have been manually drawn on the transmission images.

Statistical analyses

*V*lues are presented as means ± SEM. Statistical significance was tested either with two-sample t-test or one-way ANOVA followed by Tukey's post-hoc test (NS, not significant; * $p < 0.05$; ** $p < 0.01$ and *** $p < 0.001$).

Results

Polar lipid- and chol-enriched domains differ in abundance, curvature association and lipid order

We have previously shown that chol- and SM-enriched domains differ in abundance [25, 26] and preferentially associate with high and low curvature areas of the biconcave RBC membrane [29]. This analysis was limited to chol and SM while not considering PC, another abundant class of outer PM leaflet lipids, or glycosphingolipids, known to play key pathophysiological roles. Here, we questioned whether PC and GM1 could also participate to the formation of domains at the outer PM leaflet and whether they differ in abundance, curvature association and lipid order as compared to chol- and SM-enriched domains. To these aims, as fluorescent probes, we used (i) theta* toxin to decorate endogenous chol [25]; (ii) lysenin* toxin or PM trace insertion of BODIPY-SM to reveal SM [26]; (iii) PM trace insertion of BODIPY-PC [27] or TopFluor-TMR-PC, two PC analogs that evidence lipid domains of comparable size, shape, localization at the center of spread RBCs (Suppl. Fig. 1A - For all supplemental material see www.karger.com/10.1159/000495645/) and abundance (Suppl. Fig. 1B) and that perfectly co-localize (Suppl. Fig. 1C); and (iv) PM trace insertion of BODIPY-GM1, as in [33].

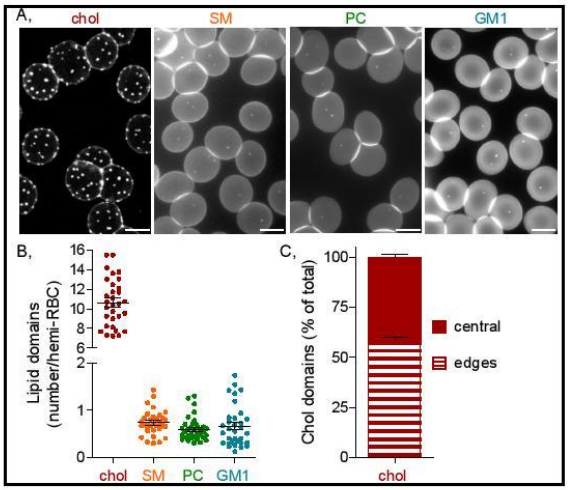

Fig. 1. Unlike polar lipid (SM, PC, GM1)-enriched domains, chol-enriched domains are abundant and equally associate with the center and the edges of spread RBCs. (A) Representative confocal/fluorescence imaging of PLL-spread RBCs labeled with theta* (chol), BODIPY-SM, -PC or –GM1 and examined at 20°C. Scale bars 5 µm. (B) Quantification of lipid domains per hemi-RBC. Means ± SEM from 31-37 experiments, each dot representing one experiment in which >100 RBCs were counted. (C) Distribution of chol-enriched domains between the edges (stripped) and the center of the membrane (full) on spread RBCs. Means ± SEM of 4 independent experiments where >70 RBCs were analyzed.

As shown in Fig. 1A, insertion of BODIPY-PC or -GM1 also revealed well-defined round lipid domains on spread RBCs. These domains exhibited similar abundance as SM-enriched domains but were quite less abundant than those enriched in chol (green and blue dots, respectively, *vs* orange or red dots, Fig. 1B). Moreover, as SM-enriched domains and ~40 % of chol-enriched domains (pictures in Fig. 1A and quantification in Fig. 1C), those enriched in PC and GM1 seemed restricted to the central area of spread RBC membrane (defined as in [29]).

Since RBC spreading can impair RBC biconcavity, we also explored lipid domain topography using plastic chambers compatible with confocal microscopy (IBIDI chambers) as an alternative imaging system in which RBCs were laid down, resulting in suspended, non-spread RBCs (Fig. 2A). This technique allowed to observe alternating regions of high curvature (HC) at the edges of the RBCs and of low curvature (LC) at the center of the cell [29]. We showed that PC- and GM1-enriched domains were preferentially associated with the LC areas of the RBC, like SM-enriched domains (green, blue and orange arrowheads, Fig. 2A), while chol-enriched domains were preferentially located in HC areas (red arrows, Fig. 2A, [29]).

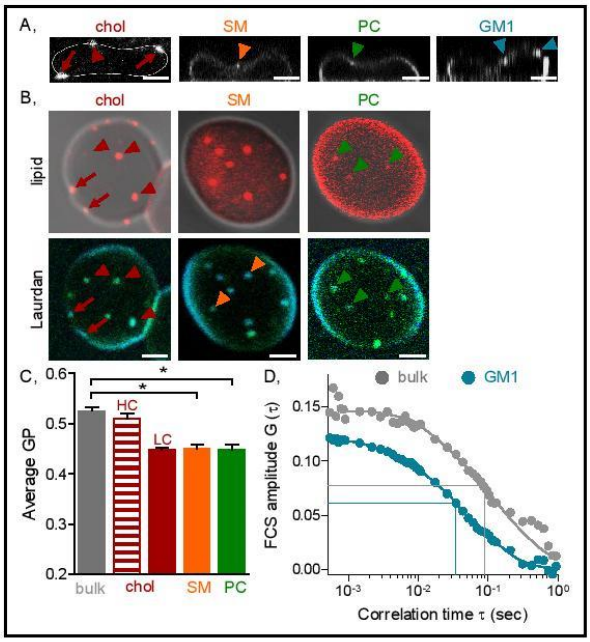

Fig. 2. Unlike polar lipid-enriched domains, chol-enriched domains associate with both low and high curvature areas of suspended RBCs and present differential lipid order. (A) Representative imaging of chol-, SM-, PC- and GM1-enriched domains on RBCs in suspension. RBCs were labeled at 20°C, put in IBIDI chambers and analyzed by confocal imaging. Images shown are reconstruction of Z-stacks and are representative of >2 experiments. (B, C) Membrane lipid order of chol-, SM- and PC-enriched domains determined by Laurdan. (B) RBCs double-labeled at 20°C with theta*, lysenin* or Top-Fluor-TMR-PC (top images) and the fluidity-sensitive probe Laurdan (bottom images) were spread and observed in confocal/biphoton microscopy. Red arrows point to high-curvature chol/Laurdan-enriched domains while red, orange and green arrowheads point to low-curvature lipid/Laurdan-enriched domains. (C) Generalized polarization (GP; proportional to membrane lipid order) of membrane without domains (bulk, grey bar) vs chol-enriched domains sorted according to their curvature localization (HC: high-curvature domains, stripped bar; LC: low-curvature domains, full bar) and polar lipid-enriched domains (orange and green bars). Means ± SEM of 2-3 independent experiments where >100 RBCs have been analyzed. Red and orange bars were reproduced from [31] to facilitate comparison with PC-enriched domains (green bar). (D) Diffusion in GM1-enriched domains determined by FCS. Example of a FCS curve of diffusion in GM1-enriched domains (blue dots) or in the surrounding membrane (grey dots) at 20°C. Time required to decrease the correlation amplitude by half in the studied spot is inversely proportional to the lipid diffusivity. Representative graph of 9 RBCs. All scale bars 2 µm.

Next, we examined whether these different lipid domains could exhibit a differential lipid order by using Laurdan (2-dimethylamino-6-lauroylnaphthalene), an artificial fluorescent probe known for its spectroscopic properties influenced by both the composition and dynamics of its local surrounding [34, 35]. Laurdan allowed us to reveal both the surrounding membrane and submicrometric domains. Hence, each class of lipid domains was recognized by co-labeling between a specific red fluorescent probe and Laurdan. We observed that the vast majority of chol-, SM- and PC-enriched domains in LC areas was marked by Laurdan (red, orange and green arrowheads, Fig. 2B) while only a part of chol-enriched domains in HC was labeled (red arrows, Fig. 2B), in agreement with our previous study [31]. Thanks to the Laurdan fluorescence emission at two wavelengths, we next calculated the Generalized Polarization (GP, see material and methods; proportional to the membrane lipid order) of the chol-, SM- and PC-enriched domains. As previously observed, chol-enriched domains located in HC exhibited a higher lipid order than those present in LC areas (compare stripped to full red columns, Fig. 2C) [31]. On the other hand, all the polar lipid-enriched domains in LC, including those enriched in PC, exhibited a lower lipid order than the surrounding membrane (compare colored columns to the grey column, Fig. 2C). These results indicate that, while lipid domains presented a differential lipid order based on their curvature area association,

those associated with LC cannot be discriminated by this criteria. As the only commercially-available, vital imaging-compatible, monomeric probe for GM1 has an emission wavelength similar to Laurdan, it was impossible to study GM1-enriched domain lipid order by this method. We therefore used Fluorescence Correlation Spectroscopy (FCS) to circumvent this difficulty and explored the diffusion properties of the dye FAST DiI in GM1-enriched domains or in the surrounding membrane (blue dots *vs* grey dots, Fig. 2D). Over 11 analyzed RBCs, 9 had a mean ratio between the diffusion time of GM1-enriched domains and the surrounding membrane of 0.53±0.12, indicating that the dye diffused twice faster in GM1-enriched domains than in the surrounding membrane. The other 2 RBCs had a mean ratio of 2.49±1.09 and exhibited thus domains in which the dye diffused more than twice slower than in the rest of the membrane. This opposite behavior might be explained by the co-existence of two distinct GM1-enriched domain populations or by the presence of lipid domains starting to vesiculate. Even if FCS does not measure the exact same membrane properties as Laurdan, these results seemed in agreement with the hypothesis that most submicrometric polar lipid domains exhibit a lower lipid order than the surrounding membrane. Such observation is in opposition with the general idea that lipid domains are more ordered than the membrane bulk. This could result from the high chol content and the strong membrane:cytoskeleton anchorage found in RBCs.

Altogether, these data suggest that at least two distinct lipid domain populations coexist at the outer PM leaflet of RBCs: those located in HC areas, exhibiting a similar lipid order than the surrounding membrane and mainly enriched in chol, *vs* those located in LC areas with a lower lipid order and enriched in polar lipids and/or chol.

Polar lipid-enriched domains depend on chol for their formation and maintenance

To next explore whether LC domains were co-enriched in polar lipids and chol, we performed double labeling with BODIPY-polar lipids and theta* on spread RBCs (Fig. 3). ~25 % of chol-enriched domains colocalized with polar lipids (yellow arrowheads in Fig. 3A and yellow portions of red columns, Fig. 3B). Considering that RBCs without any polar lipid-enriched domain were excluded from this quantification, this proportion and the lipid domain distribution in LC *vs* HC were in agreement with the simple labeling presented in Fig. 1, excluding artefactual redistribution upon double labeling. In addition, most polar lipid domains were also enriched in chol: ~65 % for SM- and ~85 % for PC- and GM1-enriched domains (yellow portions of

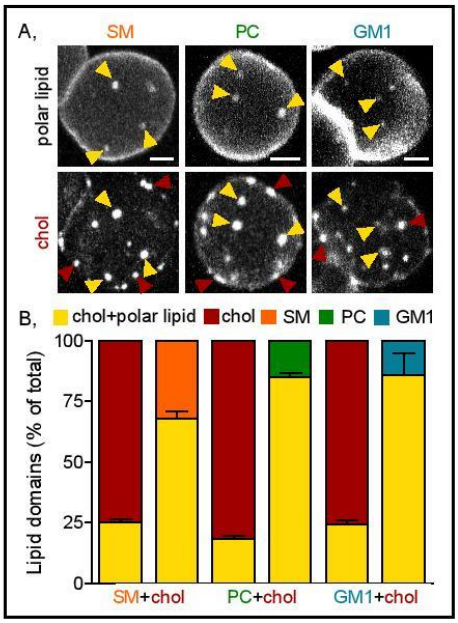

Fig. 3. The majority of lipid domains in low curvature areas are co-enriched in chol and polar lipids. (A) Representative images of PLL-spread RBCs double-labeled at 20°C for polar lipids (top images) and chol (bottom images). Yellow arrowheads point to lipid domains co-enriched in chol and polar lipid, while red arrowheads show domains mainly enriched in chol. Scale bars 2 µm. (B) Quantification. Percentages of chol-enriched domains that colocalize with polar lipid-enriched domains are shown as yellow portions of the red columns. Percentages of polar lipid-enriched domains that colocalize with chol-enriched domains are shown as yellow portions of orange, green or blue columns. Means ± SEM of 2 independent experiments where 24-38 RBCs were analyzed.

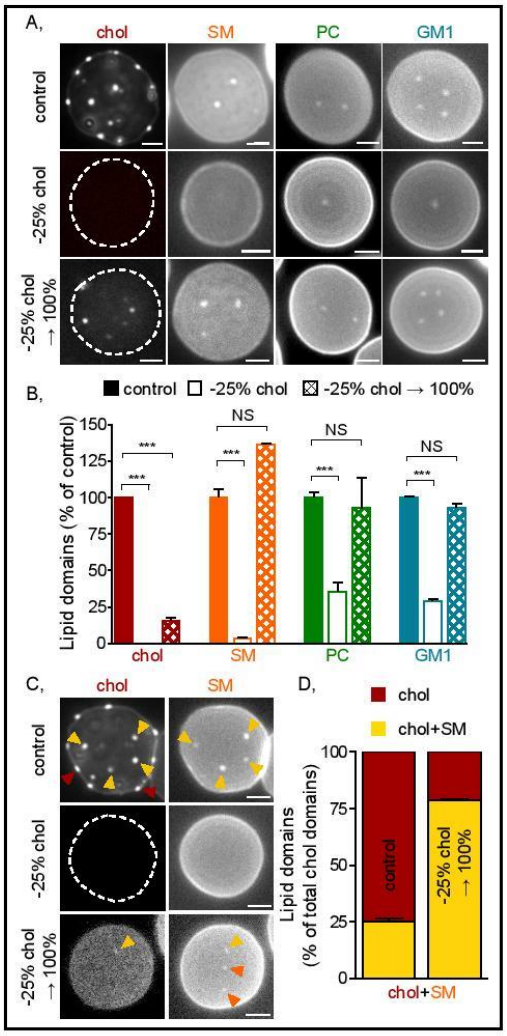

Fig. 4. All lipid domains vanish upon chol depletion and only those in low curvature areas can be restored after chol repletion. RBCs were either kept untreated (control) or chol-depleted by mβCD (0.9 mM; -25 % chol), followed or not by chol repletion (-25 % chol → 100 %) with encapsulated chol. RBCs were then either mono-labeled for chol, SM, PC or GM1 as in Fig. 1. (A, B) or double-labeled for chol and SM (C, D), spread on PLL and observed in fluorescence microscopy, all at 20°C. (A) Representative single-labeling images of different RBCs from 3 independent experiments. (B) Quantification of lipid domains in control (full bars), chol depletion (empty bars) and repletion (squared bars) conditions, expressed as percentage of the control values. Means ± SEM of 3 independent experiments where >300 RBCs were analyzed. (C) Representative double-labeling images of 2 independent experiments. Yellow arrows point to lipid domains co-enriched in chol and SM, while red and orange arrows show domains mainly enriched in chol or SM, respectively. (D) Quantification of chol- and SM-co-enriched domains (yellow portions of the bars), expressed as a percentage of the total chol-enriched domains. Means ± SEM of 2 independent experiments where >200 RBCs were analyzed. All scale bars 2 µm.

orange, green or blue columns, respectively, Fig. 3B). These results suggest that while chol-enriched domains in HC were not co-enriched in polar lipids, the majority of those located in LC was enriched in polar lipids.

To further evaluate the importance of chol for the formation and/or the maintenance of LC-associated lipid domains, we partially depleted membrane chol with methyl-β-cyclodextrin (mβCD), a cage-compound whose use on RBC membrane has been previously validated (-25 % of total membrane chol after a 0.9 mM treatment; open columns, Fig. 4B) [25]. As expected, chol-enriched domains completely disappeared under this treatment and theta* labeling was no more visible (red, Fig. 4A and B). Polar lipid domains were also affected, but to a differential extent: SM-enriched domains were almost completely abrogated while PC- and GM1-enriched domains decreased by ~65 % (orange, green and blue open columns, respectively, Fig. 4B). Hence, upon restoration of the chol content thanks to mβCD cages saturated with chol (squared columns, Fig. 4B), all polar lipid domains could be recovered.

Chol content is thus not only essential for maintenance, but also for the formation of LC-associated domains. In contrast, only a small percentage of chol-enriched domains (~15 %, red squared column, Fig. 4B) could reform upon chol repletion. As those domains were mainly located at the center of spread RBC membrane (*i.e.* in LC areas) and highly colocalized with SM-enriched domains (>75 % *vs* ~25 % in control conditions, yellow arrowheads in Fig. 4C and yellow portions of the columns in Fig. 4D), we suggest that chol-enriched domains associated with HC areas are biophysically less stable and thus require longer time or specific conditions to reform after this treatment.

We thus conclude that lipid domains associated with both HC and LC areas of the RBC outer leaflet are enriched in chol and depend on this lipid content.

GM1/PC-enriched domains are prevalent in resting RBCs at physiological temperature

To further investigate whether lipid domains associated with LC were co-enriched or not in all polar lipids, *i.e.* SM, PC and GM1, we analyzed polar lipid domain behavior upon temperature increase between 20 and 37°C. Indeed, temperature modulates membrane fluidity and thus phase separation and lipid domain organization [36]. Two opposite behaviors could be evidenced: (i) SM-enriched domains whose number decreased by ~30 % when temperature raised from 20°C to 37°C (orange circles, Fig. 5A) in agreement with [25], *vs* (ii) PC- and GM1-enriched domains whose number doubled in the same range of temperatures (green and blue circles, Fig. 5A). By performing double labeling of polar lipids at 20°C and 37°C (Fig. 5B), we evidenced a nearly perfect colocalisation between PC- and GM1-enriched domains whatever the temperature (columns 1 and 2, Fig. 5B), while the percentages of PC- or GM1-enriched domains also enriched in SM decreased between 20°C and 37°C (columns 3 and 5 *vs* 4 and 6, Fig. 5B). Those results suggest that domains co-enriched in PC and GM1 are dominant at physiological temperature while a drop in temperature induces their co-enrichment in SM. This observation also suggests that SM-, PC- and GM1-enriched domains can be either associated or dissociated based on RBC physiological needs.

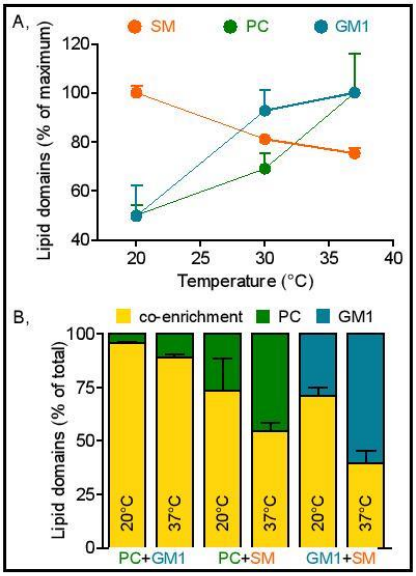

Fig. 5. In contrast to SM-enriched domains, PC- and GM1-enriched domains prevail in resting RBCs at physiological temperature. (A) Abundance of polar lipid-enriched domains at various temperatures, expressed as percentage of maximal abundance. RBCs were mono-labeled, spread and observed at the indicated temperatures. Means ± SEM of 2 independent experiments where >400 RBCs were analyzed. (B) Extent of polar lipid co-enrichment at 20°C and 37°C. Percentage of domains co-enriched in PC and GM1, PC and SM or GM1 and SM are shown as yellow portions of total PC (green)- or GM1 (blue)-enriched domains. Means ± SEM of 2 independent experiments where >200 RBCs were analyzed.

GM1-enriched domains increase in abundance upon RBC mechanical stimulation while SM-enriched domains increase thereafter upon RBC shape restoration

To further test this hypothesis, we analyzed domain abundance upon different approaches of mechanical stimulations: differential RBC spreading on PLL (Fig. 6A), hypo-osmotic swelling (Suppl. Fig. 2) and RBC (de)stretching on silicon (polydimethylsiloxane, PDMS) chambers (Fig. 6B).

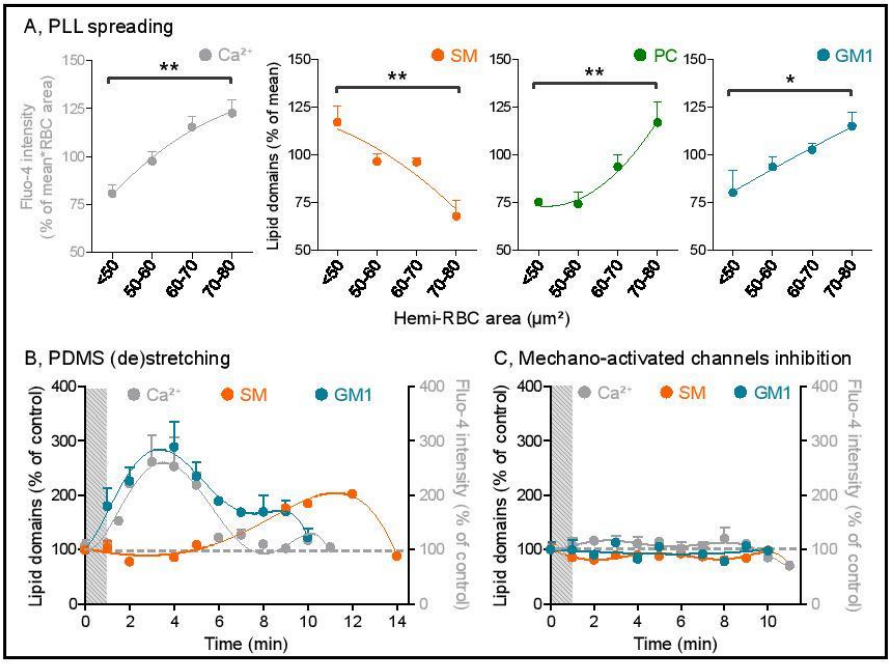

Fig. 6. PC- and GM1-enriched domains increase in abundance upon mechanical stimulation. (A) Differential spreading of RBCs on PLL. Morphometry of cell calcium content (grey dots) and domain abundance (SM, orange; PC, green; GM1, blue) under increasing projected areas of spread RBCs. RBCs were labeled at 37°C, immobilized on PLL for 4 min, washed and then let to spread for another 4 min, resulting in differential spreading (represented by different projected hemi-RBC areas). Means ± SEM of 3 independent experiments where >500 RBCs were counted. (B) (De)stretching of RBCs on silicon (PDMS) chambers. RBCs were labeled at 37°C for SM (orange dots), GM1 (blue dots) or calcium (grey dots). Lipid domains were counted and Fluo-4 intensity was measured before (t = 0 min) and after RBCs were stretched for 1 min (grey stripped zone) in PDMS chambers. Means ± SEM of 3 independent experiments where >200 RBCs were analyzed at each time. (C) (De)stretching of RBCs on PDMS chambers under inhibition of mechano-activated channels. RBCs were labeled as in (B), treated with 7 µM GsMTx4 for 15 min, stretched for 1 min (grey stripped zone) in PDMS chambers and analyzed during the indicated times upon destretching. Means ± SEM of 3 independent experiments where >100 RBCs were analyzed at each time.

We first took advantage of the differential spreading of RBCs on PLL that results from variations in the local PLL concentration, the RBC density and the adhesion duration. This heterogeneity, which was reflected in a 50 to 80 µm^2 range of immobilized RBC projected area (Fig. 6A) and a spreading-dependent accumulation of intracellular calcium (grey dots, Fig. 6A), differentially impacted lipid domains. Indeed, while PC- and GM1-enriched domains increased in abundance under RBC area increase (green and blue dots, Fig. 6A), SM-enriched domains tended to disappear (orange dots, Fig. 6A). In contrast, the abundance of chol-enriched was only slightly modified (red dots, Suppl. Fig. 3A). These observations point to the specific potential involvement of PC- and GM1-, but not SM-, enriched domains in RBC deformation upon mechanical stimulation.

We then checked whether basic mechanical stimulation by osmotic swelling could also lead to a differential modulation of lipid domains. Real-time imaging revealed the *de novo* formation of SM- and PC-enriched domains (orange and green arrowheads, Suppl. Fig. 2) shortly after the application of a hypo-osmolar medium, whereas GM1-enriched domains

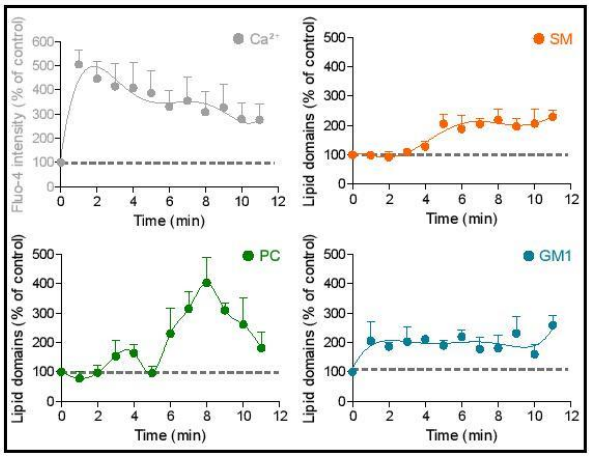

Fig. 7. PC- and GM1-enriched domains rapidly increase in abundance upon Piezo1 chemical activation while the increase in SM-enriched domains is delayed. RBCs were labeled for calcium (grey dots) or polar lipids (orange, green or blue dots) at 37°C, immobilized on PLL, treated with 0.5 µM Yoda1 for 20 sec to activate Piezo1 and immediately observed during the indicated times. Means ± SEM of 3 independent experiments for each panel where >300 RBCs were analyzed at each time.

disappeared (blue arrowhead, Suppl. Fig. 2) and chol-enriched domains remained unaffected.

Finally, we simulated RBC deformation using stretchable PDMS chambers that previously allowed us to evidence the gathering of chol-enriched domains in high-curvature membranes (Suppl. Fig. 3 B,C) and the increase of SM-enriched domains during shape restoration after deformation [29]. Immobilized RBCs were stretched for one min (grey stripped bar, Fig. 6B) and then let to recover for an additional 14 min time interval. As expected [1, 2, 29], RBC mechanical stress application occurred concomitantly with a transient intracellular calcium increase, which reached a maximal accumulation 3 min after stretching (grey dots, Fig. 6B). GM1-enriched domains showed a similar (~3fold) and transient increase (blue dots, Fig. 6B), thus perfectly coinciding with the transient calcium entry. After that, intracellular calcium decreased back to its initial concentration 6 min after stretching. From that time, the SM-enriched domain abundance started to increase (orange dots, Fig. 6B) [29].

Altogether, these results suggest that GM1-enriched domains could be linked to calcium influx during deformation whereas SM-enriched domains are linked to calcium efflux and shape restoration. This represents an additional line of evidence for the segregation between GM1- and SM-enriched domains at the RBC PM upon physiological conditions.

To further test the potential link between lipid domains and calcium exchange kinetics upon RBC deformation, we used the peptide GsMTx4, a validated inhibitor of the mechano-activated ion channels [37] which are mostly responsible for the calcium entry upon RBC deformation [1]. We showed that this treatment abolished calcium entry as well as GM1- and SM-enriched domain increase without inducing detectable toxicity (Suppl. Fig. 4). These results support our hypothesis of the correlation between GM1-enriched domain abundance and the calcium influx. Moreover, they suggest that the delayed SM-enriched domain increase is dependent on a primary calcium entry.

GM1-enriched domains are linked to Piezo1-mediated calcium influx

As GM1-enriched domains seemed to be involved into the deformation-dependent calcium influx, we explored the potential link between those domains and Piezo1. This non-selective mechano-activated cation channel plays a key role in the RBC deformation-dependent calcium influx and the following cellular volume regulation [3]. To test this hypothesis, RBCs were treated for 20 sec with Yoda1, a small agonist of this channel [38]. As expected, an immediate strong increase of the intracellular calcium concentration was observed (grey dots, Fig. 7) without detectable signs of toxicity (Suppl. Fig. 4). Intracellular calcium concentration then slowly decreased, suggesting the activation of the calcium efflux mechanisms and/or a possible slow desorption of Yoda1. The immediate increase

of intracellular calcium was concomitant with a 2-fold increase of GM1-enriched domains (blue dots, Fig. 7), while the SM-enriched domain increase was delayed and only appeared 5 min after the treatment (orange dots, Fig. 7). PC-enriched domains showed an intermediate behavior, with a first slight increase 3 min after the treatment followed by a second, more important, increase after 6 min (green dots, Fig. 7).

From all these data, we concluded that GM1-enriched domains, but not those enriched in SM, are closely linked to the Piezo1-mediated calcium entry into RBC upon deformation.

SM/PC-enriched domain abundance is closely related to the secondary calcium efflux and/or the extent of the membrane:cytoskeleton anchorage

The delayed increase of SM-enriched domains and the intermediate behavior of PC-enriched domains under Yoda1 activation suggested that not only SM- but also PC-enriched domains might contribute to secondary calcium efflux. In RBCs, this efflux is exclusively operated by the energy-dependent PMCA. This pump is regulated by calmodulin binding (and thus intracellular calcium concentration) but also by calpain cleavage, intracellular domain modifications and even acidic lipids from the inner leaflet [39].

To test an eventual link between SM- and PC-enriched domains and PMCA activation, secondary calcium efflux was stimulated without activating the Piezo1-mediated influx. In 2002, Andrews and collaborators reported that the treatment of RBCs with a phorbol ester stimulates a protein kinase C (PKC) mediated $Ca_v2.1$-like calcium permeability pathway [40]. As this calcium entry is Piezo1-independent, we speculated that SM- and PC-, but not GM1-enriched domains, would be increased by this treatment. We thus used phorbol myristate acetate (PMA, a diacylglycerol analog) and calyculin A (CalA, a phosphatase inhibitor) to activate PKC. As expected, we observed a slight increase of intracellular calcium (data not shown) as well as a ~2-fold increase of SM- and PC-enriched domains that contrasted with the decrease of GM1-enriched domains (images in Fig. 8A and quantification in Fig. 8B).

We then stimulated calcium efflux in a more direct approach. To this aim, we used the calcium chelator EGTA to remove all traces of calcium in the extracellular medium (Fig. 8A, C) [29]. This treatment induced an important decrease of intracellular calcium (-95 % of control fluorescence, data not shown) and led to a ~2.5 fold increase of SM-enriched domains, as previously reported [29], but also a ~1.8 fold increase of PC-enriched domains (empty bars, Fig. 8C). The GM1-enriched domains were, on the other hand, decreased by this treatment, supporting the hypothesis of their involvement in calcium influx but not in its efflux. This treatment seemed not toxic since RBC re-incubation in 1.8 mM calcium-containing medium fully restored domain abundance (squared bars, Fig. 8C) and since hemoglobin release remained unchanged as compared to untreated RBCs (Suppl. Fig. 4).

We next aimed to target the PMCA pump by depleting the RBC energy content by incubation in a glucose-free medium for 2 h (Fig. 8D). This treatment, which led to a 75% decrease of the RBC ATP content (from ~2-3 mM in control cells to ~500-750 µM in depleted cells, data not shown), was not sufficient to directly inhibit the PMCA (K_M for ATP, ~3 µM). Nevertheless and in agreement with [41] and [42], it was able to indirectly impair the PMCA. Indeed, while calcium initial content was fully restored 6 min after stretching in control RBCs (see Fig. 6B and full grey points in Fig. 8E), it could not be restored even after 12 min in energy-deprived RBCs (empty grey points in Fig. 8E). Surprisingly, this PMCA inhibition also induced a high increase of SM- and PC-enriched domains, while GM1-enriched domains were not affected (empty bars, Fig. 8D). We can reasonably exclude toxicity to explain this observation, as revealed by the reversibility of the ATP depletion effect (squared bars, Fig. 8D) and the low hemoglobin release (Suppl. Fig. 4). Those results could be related to the increase of reactive oxygen species (ROS) upon energy privation through the inhibition of the anti-oxidant enzymes like the glutathione synthase (K_M for ATP, ~400 µM, [43]). Produced ROS might in turn disturb the PMCA, but also the membrane:cytoskeleton anchorage. This hypothesis is discussed in the last section of the Discussion but remains to be tested.

Our results suggest that while SM- and PC-enriched domains increase in abundance upon calcium efflux and/or cytoskeleton modulation, those enriched in GM1 are instead

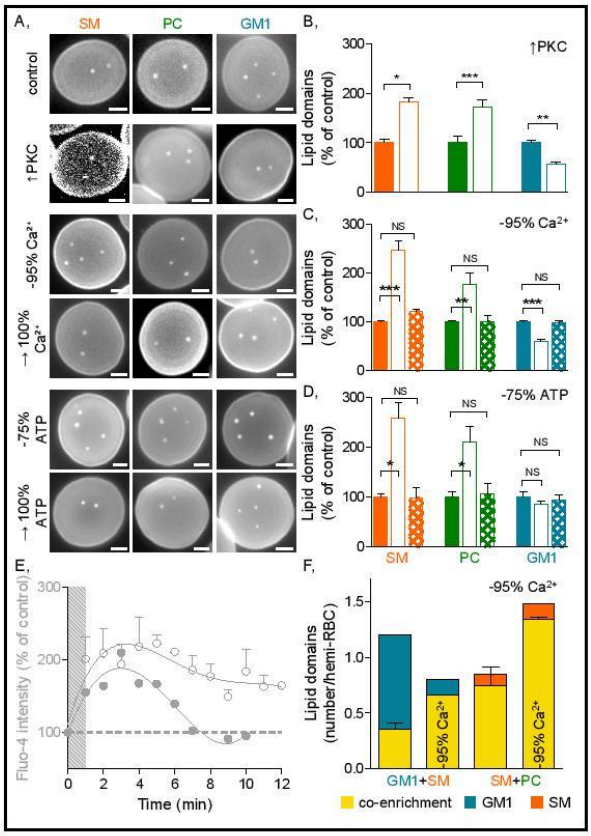

Fig. 8. Unlike GM1-enriched domains, SM- and PC-enriched domains increase upon secondary calcium efflux and/or membrane:cytoskeleton impairment. RBCs were either (i) kept untreated (control); (ii) treated with a phorbol ester (PMA, 6 µM) and a phosphatase inhibitor (CalA, 20 nM; ↑ PKC); (iii) incubated in a calcium-free medium containing 1 mM EGTA (-95 % Ca^{2+}), followed or not by reincubation in calcium-containing medium (→ 100 % Ca^{2+}); or (iv) incubated in a glucose-free medium for 2 h (-75 % ATP), followed or not by reincubation in a glucose-containing medium (→ 100 % ATP). All RBCs were then spread and labeled for polar lipids at 37°C. (A) Representative images. Scale bars 2 µm. (B-D) Quantification of lipid domains in control RBCs (plain bars), under treatment (empty bars) and in repletion conditions (squared bars). Means ± SEM of 3 independent experiments where >300 RBCs were analyzed. (E) Control (plain dots) and ATP-depleted (empty dots) RBCs were labeled for calcium at 37°C, stretched for 1 min (grey stripped zone) in PDMS chambers and analyzed during the indicated times upon destretching. (F) Double labeling between GM1 and SM or SM and PC on RBCs upon intracellular calcium depletion at 37°C. Percentage of domains double-enriched in GM1 and SM or in SM and PC are shown as yellow portions of total GM1 (blue)- or SM (orange)-enriched domains.

unaffected or even decreased. Hence, they suggest the association between SM- and PC-enriched domains upon calcium efflux, at the detriment of GM1-enriched domains. This was confirmed by double-labeling of RBCs upon EGTA treatment. Indeed, GM1-enriched domains that were not co-enriched in SM decreased (blue columns, Fig. 8F) as new lipid domains co-enriched in SM and PC, but not in GM1, were formed (orange columns, Fig. 8F).

Polar lipid domain integrity is needed for calcium exchanges at the RBC surface

Finally, we questioned whether polar lipid-enriched domains were only modulated through, or needed for, calcium exchanges at the RBC PM by abrogating lipid domains. We first used mβCD, which disrupted all lipid domains at moderate concentration (0.9-1 mM, -25 % chol, see Fig. 4B). Under this concentration, calcium entry upon RBC stretching in silicon chambers was completely inhibited (from a 2.7-fold increase of fluorescence in untreated RBCs to no increase in mβCD-treated RBCs, grey dot at 1 mM, Fig. 9A). At a lower mβCD concentration (0.5 mM, -15 % chol, empty dot, Fig. 9A), chol- and SM-enriched domains were already disrupted (red and orange dots at 0.5 mM, Fig. 9A), while PC and GM1-enriched domains were not affected (green and blue dots at 0.5 mM). At this concentration, calcium

entry was non-significantly decreased (from a 2.7-fold increase of fluorescence in untreated RBCs to a 2.4-fold increase upon mβCD treatment, grey dot at 0.5 mM, Fig. 9A), indicating that RBCs were still able to respond to stretching by a calcium entry. The abolition of the stretching-induced calcium increase at 1 mM could result from the absence of resting-state GM1/PC-enriched domains for the primary Piezo1 activation or from the impossibility for these domains to get formed around Piezo1 under activation to sustain an efficient calcium entry. However, we cannot discard the possibility that this effect only resulted from the slight (~8 %) decrease of the chol content between 0.5 mM and 1 mM mβCD.

Finally, we used sphingomyelinase (SMase), a hydrolase catalyzing the breakdown of SM and allowing to decrease the PM SM content by up to 60 % (empty dots, Fig. 9B) without detectable cell toxicity [26]. We showed that a moderate SM depletion (-30 % at 3 mU/ml) led to the nearly complete disappearance of SM-enriched domains (-90 %, orange dots, Fig. 9B) and a ~2-fold increase of intracellular calcium (grey dots, Fig. 9B). As a matter of fact, the decrease of SM domains upon SMase treatment was proportional (R^2=0.9553) to the intracellular calcium increase. These data suggest that SM-enriched domains are not only a marker of active calcium extrusion, but are also required to maintain a low intracellular calcium concentration.

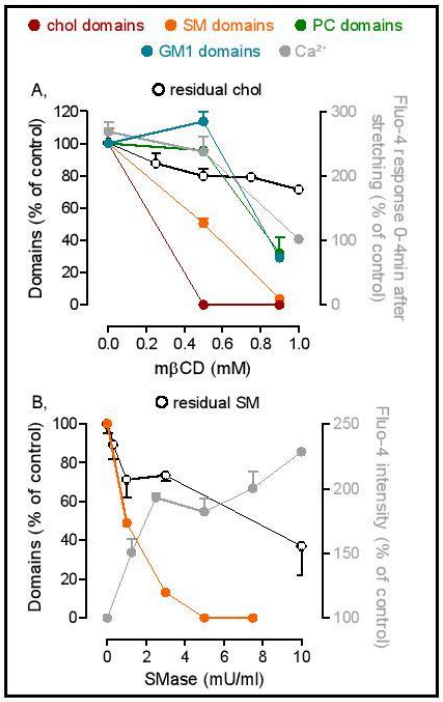

Fig. 9. Intracellular calcium content is altered upon lipid domain abrogation. (A) RBCs were treated in suspension with the indicated concentrations of mβCD and either (i) directly analyzed for chol residual content (empty dots); or (ii) spread onto PLL-coverslips for analysis of lipid domain abundance (red, orange, green or blue dots) at 37°C; or (iii) laid down on PDMS chambers and analyzed 2 min after stretching for intracellular calcium (expressed as the percentage of calcium content in unstretched RBCs; grey symbols). (B) RBCs were treated in suspension with the indicated concentrations of sphingomyelinase (SMase) and (i) directly analyzed for SM residual content (open dots) and intracellular calcium content (grey dots) at 37°C; or (ii) spread onto PLL-coated coverslips for SM-enriched domain abundance at 37°C counting (orange dots). Means ± SEM of 2-3 independent experiments where >200 RBCs were analyzed.

Discussion

In the last decades, evidence for lipid domains of various composition at the surface of several cells has emerged. First transient nanometric domains enriched in sphingolipids and chol [11] and then more stable and larger domains that could exhibit a differential lipid composition than rafts. In the last few years, we evidenced and characterized two types of submicrometric lipid domains at the RBC surface, mainly enriched in chol and/or SM [25, 26, 29]. We here extended this study to PC and GM1, two other main lipids of the outer PM leaflet, and mapped their relationship and functional relevance.

Lipid domain diversity at resting state

Based on previous results on chol- and SM-enriched domains and on the new data we acquired on PC- and GM1-enriched domains, we suggest the coexistence of three populations of lipid domains in RBCs at resting state at physiological temperature: (i) mostly chol-enriched ones, abundant (~8/hemi-RBC), HC-associated and exhibiting high lipid order; (ii) GM1/PC/chol-enriched ones, less abundant (~1.5/hemi-RBC), LC-located and presenting lower ordering; and (iii) SM/PC/chol-enriched ones, rare (~0.6/hemi-RBC), also LC-located and with low ordering. Considering the wide range of domain features that lipid-lipid interactions can generate in molecular simulations of simple and complex bilayers, it is not so surprising to unveil such a diversity of lipid domains in living cell membranes. As a matter of fact, lipid clusters in simulated membranes show various (i) composition, as they are not only enriched in SM and chol, but also in gangliosides (GM1 and GM3) and in PC analogs [44, 45]; (ii) lipid order; and (iii) topography, as some GM3 nano-clusters have been shown to preferentially associate with concave (when viewed from the extracellular medium) membranes [46]. Such lipid domain diversity is also supported by several experimental data on simple lipid mixtures [47-49].

Direct lipid:lipid interactions could be able to induce lipid clusters in systems devoid of proteins and certainly help to understand some of the lipid domain behaviors that we evidenced on RBCs. For example, differential temperature dependence between GM1- and PC-enriched domains *vs* those enriched in SM is partly explainable by individual lipid intrinsic properties (*e.g.* head group, acyl chain length and saturation [50]). Moreover, lipid domain biogenesis and/or maintenance also depend on the chol content, as chol is a key regulator of membrane fluidity (and thus space between phospholipids for optimal head group interactions) and is able to directly interact with SM or GM1 [45, 51].

In a complex active system including lipids and proteins like living cell membranes, it is however unlikely that such lipid:lipid interactions are the only key regulators of lipid domains. We previously proposed several regulators for chol-enriched domains located in RBC HC areas [29]. We will here focus on the LC-associated lipid domains. The maintenance of GM1/PC/chol- and SM/PC/chol-enriched domains at a low level in LC areas of RBCs at resting state could involve membrane:cytoskeleton anchorage and/or charge-mediated interactions. Lipid domain stability in time and space at resting state supports the hypothesis of their restriction by anchorage of the membrane to the spectrin cytoskeleton, either via direct interactions with anchorage complex proteins or via an inner PM leaflet coupling. The strong dependence of SM/PC/chol-enriched domains to the intracellular calcium increase (either after stretching in PDMS chambers or under pharmacological treatments) suggests their restriction through the 4.1R anchorage complex. Indeed, anchorage through 4.1R complex is strongly decreased following calcium increase, as the binding of calmodulin/calcium to the proteins of this complex decreases their affinity for each other [2]. PKC activation and ATP depletion also led to the modulation of the anchorage through 4.1R, and SM/PC-enriched domains were also highly sensitive to those two treatments. GM1/PC/chol-enriched domains seemed on the other hand closely linked to the ankyrin-based anchorage complexes (our unpublished data).

Lipid domain modulation upon stretching and calcium exchanges

The three domain populations did not exhibit the same response to stimuli applied to the RBCs. Chol-enriched domains gather in increased curvature areas upon RBC deformation but do not increase in abundance. They could be involved in creating/maintaining HC areas needed for RBC deformation (red domains, Fig. 10) [29]. In contrast, both GM1/PC/chol- and SM/PC/chol-enriched domains were strongly increased during calcium exchanges accompanying RBC (re)shaping process, but in different kinetics. To the best of our knowledge, this is the first time that lipid domains of the external PM leaflet are proposed to contribute to calcium exchanges, crucial for the RBC to gain in flexibility when it is subjected to mechanical stress (*e.g.* in small capillaries or in the spleen). Indeed, a transient calcium influx will lead to the Gardos channel activation and a consequent cell dehydration, increasing the surface/volume

ratio and favoring cell deformation (Fig. 10) [1]. The importance of calcium for RBC mechanical stability and deformation is further illustrated by the demonstration that permanent calcium upregulation, linked to uncontrolled impairment of cytoskeletal density and/or anchorage (*e.g.* in RBCs of patients with haemolytic anemia), compromises mechanical stability of the RBC membrane [52].

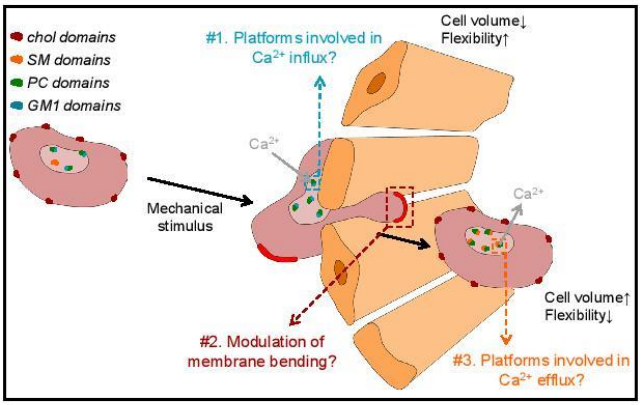

Fig. 10. Evidence-based hypothetical model of the contribution of lipid domains to RBC deformation. Under mechanical stress (e.g. in the spleen sinusoids), GM1/PC-enriched domains (blue/green) increase to favor calcium influx while chol-enriched domains (red) gather in the high-curvature membrane and modulate membrane bending. At the same time, cell volume decreases via activation of the Gardos channels and the RBC flexibility increases via uncoupling between membrane and the cytoskeleton at the 4.1R complexes. The cell volume is restored after the end of the stress application by calcium efflux thanks to the contribution of SM/PC-enriched domains (orange/green).

Calcium influx can occur through several channels like Piezo1, Cav2.1 and TRPC (*i.e.* transient receptor potential cation channel). Piezo1, a mechanically-activated cation channel, has been evidenced to play the major role in RBC deformation-induced calcium increase [3]. Moreover, mutations in Piezo1 causing an increased cation permeability have been linked to hereditary xerocytosis where RBCs are dehydrated [53]. Here, we show a close relation between the number of GM1/PC/chol-enriched domains at the RBC surface and the activation state of Piezo1 (blue/green, domains, Fig. 10), based on three lines of evidence: (i) the strong increase of lipid domain abundance under RBC stretching, which is inhibited by a mechano-activated channel inhibitor; (ii) the same increase under the chemical Piezo1 activation; and (iii) the concomitant inhibition of the stretching-mediated calcium entry and abrogation of domains under chol depletion.

SM/PC/chol-enriched domains seem also to be related to calcium exchanges, not during its influx but instead during its efflux (orange/green domains, Fig. 10). Calcium efflux is as important as influx since a prolonged calcium increase will lead to the RBC senescence and removal from the blood [2]. The involvement of SM/PC/chol-enriched domains in calcium efflux is based on the following evidences. First, they exhibit a delayed increase in abundance upon calcium entry (either by stretching or chemical activation). Second, they specifically increase in abundance when secondary calcium efflux is activated (either via PMA/CalA or EGTA treatment).

Lipid domains as modulators of Piezo1 and PMCA membrane localization and/or activity?

Sorting and activation of membrane proteins is the most studied function of lipid domains [54-57]. These effects can be attributed either to the modification of bilayer properties (thickness, curvature or surface tension) or to the binding of specific lipids to the protein surface. It is easily imaginable that mechanically-activated channels like Piezo could be affected by the surrounding membrane properties. Their activity have already been shown to be highly dependent on the membrane stiffening [58] and thus the membrane chol

content, but also on the level of fatty acid saturation [59]. Moreover, new insights in Piezo1 structure evidenced a bend in its transmembrane section [60], whose stabilization energy might be partly compensated by the surrounding lipids.

Based on the results presented in this article, we suggest that GM1/PC/chol-enriched domains could contribute to the regulation of Piezo1 by modulating its environment biophysical properties to allow an efficient and transient calcium influx. This is based on the three following facts. First, GM1 are inverted cone shaped lipids and the bend evidenced in the structure of Piezo1 at resting state supports the possibility that Piezo1 rests in a locally curved lipid bilayer environment, while upon rising membrane tension, the reduction of curvature could open the pore. Second, domains co-enriched in GM1 and chol should present a higher thickness than other domains, which could favor the recruitment/stabilization of Piezo1 transmembrane domains [61]. Indeed, a mechanically-activated protein has recently been shown to have a more expanded constriction pore in the presence of a positive mismatch (thicker lipids) than in negative mismatch (thinner lipids) [62]. Third, GM1-enriched domains appear dependent on the anchorage through ankyrin (our unpublished data) and the cytoskeleton is known to modulate Piezo1 activity [63].

While the sequence of events linking lipid domains to Piezo1 remains to be elucidated, several hypotheses can be suggested. First, GM1/PC/chol domains could be formed following the calcium ion influx and represent a secondary event. However, the fact that a Piezo1-independent calcium influx, as achieved through PKC activation [40], instead induced a decrease of GM1-enriched domains does not support this hypothesis. Second Piezo1 could modulate its surrounding environment upon activation by recruiting specific lipids such as GM1 and chol, forming domains which might modify Piezo1 dynamic properties and allow an efficient and transient calcium influx. Third, Piezo1 could be preferentially localized in GM1/PC/chol-enriched domains in RBCs at resting state, an association necessary for the primary activation of the channel. Simulation studies and localization experiments are needed to investigate these hypotheses.

While the results we present in this article suggest a correlation between calcium efflux and SM/PC/chol-enriched domain abundance, their specific role in PMCA regulation remains to be elucidated. We here propose two non-mutually exclusive hypotheses. On one hand, as for Piezo1, SM/PC/chol-enriched domains could represent a favorable environment for the protein activity. This could be linked to (i) the domain specific biophysical properties (*e.g.* lipid order); (ii) the strength of their cytoskeleton anchorage; and/or (iii) their correspondence with specific lipids in the inner leaflet, *a.o.*. The membrane lipid order hypothesis is supported by (i) our present observation that SM/PC/chol-enriched domains were more disordered than the rest of the membrane; (ii) our previous observation that lipid domain order increases to a bigger extent than the bulk membrane order upon stimulation of calcium efflux by treatment of RBCs with EGTA [31]; and (iii) several studies in model membranes, although with sometimes conflicting information. For instance, PMCA activity is decreased in highly-ordered areas of liposomes made of PC/SM/chol [64] but is favored in highly ordered lens fiber lipids in comparison with disordered DOPC liposomes [65]. Besides membrane fluidity, SM/PC/chol-enriched domains could contribute to the regulation of PMCA activity through the reversible and controlled modulation of membrane:cytoskeleton anchorage upon deformation-induced calcium entry. As a matter of fact, the protein 4.1R has been shown to directly interact with PMCA1 and to be essential for its activity in enterocytes [66]. The close relationship between the membrane:cytoskeleton anchorage, the PMCA activity and the SM/PC/chol-enriched domains could partly explain the *a priori* contradictory results we obtained by stimulating the PMCA through PKC activation *vs* impairing the pump through ATP depletion. Indeed, both treatments could induce the uncoupling of the membrane:cytoskeleton anchorage (by phosphorylation of the 4.1R complexes *vs* potential increase of ROS damages) and the increase of calcium (by stimulating a Piezo1-independent calcium influx *vs* indirectly impairing the PMCA) together with a secondary membrane:cytoskeleton uncoupling (by calmodulin binding). One hypothesis is that the reversibility of lipid domain abundance increase depends on the transient

membrane:cytoskeleton uncoupling, which became permanent under the two treatments, resulting into an incapacity to de-form the domains. Finally, SM/PC/chol-enriched domains at the external PM leaflet could contribute to the regulation of PMCA activity through their potential coupling with specific lipids in the inner PM leaflet, known to regulate PMCA activity [67, 68]. For example, electrostatic interactions and subsequent clustering of PIP_2 at the inner leaflet have been shown to be induced by a local calcium increase [69]. This could in turn induce a transbilayer clustering in superposition in the outer leaflet resulting into SM-enriched domain formation, as shown by super-resolution microscopy [70].

On the other hand, SM/PC/chol-enriched domains might modulate the PM distribution of PMCA to protect the pump from the reactions with ROS. Indeed, PMCA activity has been shown to be decreased by direct oxidation [71] or by binding of oxidized calmodulin [72]. This oxidation leads to conformational changes and the formation of aggregates that cannot recover their activity [73]. SM, on the other hand, is proposed to be a natural antioxidant that inhibits the peroxidation of unsaturated phospholipids and chol [74].

Altogether, our study opens new avenue to explore the importance of PM lipid domains in cell deformation associated to other physiological processes, such as the phagocytic cup, the immunological synapse, cell division or migration and invasion.

Abbreviations

BODIPY (*N*-(4,4-Difluoro-5,7-Dimethyl-4-Bora-3a,4a-Diaza-*s*-Indacene-3- Pentanoyl)); BSA (bovine serum albumin); CalA (calyculin A); Chol (cholesterol); FASTDil (1,1'-Dilinoleyl-3,3,3',3'-Tetramethylindocarbocyanine, 4-Chlorobenzenesulfonate); DMEM (Dulbecco's Modified Eagle Medium); EGTA (ethylene glycol-bis(β-aminoethyl ether)-N,N,N',N'-tetraacetic acid); FCS (fluorescence correlation spectroscopy); GM1 (monosialotetrahexosylganglioside); GP (generalized polarization); HC (high curvature); Laurdan (2-dimethylamino-6-lauroylnaphthalene); LC (low curvature); mβCD (methyl-β-cyclodextrin); PC (phosphatidylcholine); PDMS (polydimethylsiloxane); PKC (protein kinase C); PLL (poly-L-lysine); PM (plasma membrane); PMA (phorbol myristate acetate); PMCA (plasma membrane calcium ATPase); RBC (red blood cell); ROS (reactive oxygen species); SM (sphingomyelin); SMase (sphingomyelinase)

Acknowledgements

We thank Drs. A. Miyawaki, M. Abe and T. Kobayashi (Riken Brain Science Institute, Saitama, Japan & University of Strasbourg, France) as well as H. Mizuno (KU Leuven, Belgium) for generously supplying the Dronpa-NT-Lysenin and Dronpa-theta-D4 plasmids. We thank Pr. P. Gailly (Institute of Neuroscience, Université catholique de Louvain, Belgium) for providing us a mechanical cell strain instrument for PDMS chambers. J. Steinkühler was supported by the MaxSynBio consortium, which is jointly funded by the Federal Ministry of Education and Research (BMBF) of Germany (FKZ 031A359L) and the Max Planck Society (MPG). This work was supported by belgian grants from UCLouvain (FSR and Actions de Recherches concertées, ARC), F.R.S-FNRS and Salus Sanguinis foundation.

Disclosure Statement

The authors declare they have no conflict of interest.

References

1 Danielczok JG, Terriac E, Hertz L, Petkova-Kirova P, Lautenschlager F, Laschke MW, Kaestner L: Red Blood Cell Passage of Small Capillaries Is Associated with Transient Ca(2+)-mediated Adaptations. Front Physiol 2017;8:979-990.
2 Bogdanova A, Makhro A, Wang J, Lipp P, Kaestner L: Calcium in red blood cells-a perilous balance. Int J Mol Sci 2013;14:9848-9872.
3 Cahalan SM, Lukacs V, Ranade SS, Chien S, Bandell M, Patapoutian A: Piezo1 links mechanical forces to red blood cell volume. Elife 2015;4:e07370.
4 Klinken P: Red blood cells. Int J Biochem Cell Biol 2002;34:1513-1518.
5 Mohandas N, Gallagher PG: Red cell membrane: past, present, and future. Blood 2008;112:3939-3948.
6 Viallat A, Abkarian M: Red blood cell: from its mechanics to its motion in shear flow. Int J Lab Hematol 2014;36:237-243.
7 Byers TJ, Branton D: Visualization of the protein associations in the erythrocyte membrane skeleton. Proc Natl Acad Sci U S A 1985;82:6153-6157.
8 Uyuklu M, Meiselman HJ, Baskurt OK: Effect of decreased plasma cholesterol by atorvastatin treatment on erythrocyte mechanical properties. Clin Hemorheol Microcirc 2007;36:25-33.
9 Carquin M, D'Auria L, Pollet H, Bongarzone ER, Tyteca D: Recent progress on lipid lateral heterogeneity in plasma membranes: From rafts to submicrometric domains. Prog Lipid Res 2016;62:1-24.
10 Simons K, Vaz WL: Model systems, lipid rafts, and cell membranes. Annu Rev Biophys Biomol Struct 2004;33:269-295.
11 Lingwood D, Simons K: Lipid rafts as a membrane-organizing principle. Science 2010;327:46-50.
12 Janes PW, Ley SC, Magee AI, Kabouridis PS: The role of lipid rafts in T cell antigen receptor (TCR) signalling. Semin Immunol 2000;12:23-34.
13 Sydor AM, Czymmek KJ, Puchner EM, Mennella V: Super-Resolution Microscopy: From Single Molecules to Supramolecular Assemblies. Trends Cell Biol 2015;25:730-748.
14 Godin AG, Lounis B, Cognet L: Super-resolution microscopy approaches for live cell imaging. Biophys J 2014;107:1777-1784.
15 Hell SW, Sahl SJ, Bates M, Zhuang X, Heintzmann R, Booth MJ, Bewersdorf J, Shtengel G, Hess H, Tinnefeld P: The 2015 super-resolution microscopy roadmap. J Phys D Appl Phys 2015;48:443001-443002.
16 de Almeida RF, Loura LM, Prieto M: Membrane lipid domains and rafts: current applications of fluorescence lifetime spectroscopy and imaging. Chem Phys Lipids 2009;157:61-77.
17 Abe M, Kobayashi T: Imaging local sphingomyelin-rich domains in the plasma membrane using specific probes and advanced microscopy. Biochim Biophys Acta 2013;1841:720-726.
18 Mizuno H, Abe M, Dedecker P, Makino A, Rocha S, Ohno-Iwashita Y, Hofkens J, Kobayashi T, Miyawaki A: Fluorescent probes for superresolution imaging of lipid domains on the plasma membrane. Chem Sci 2011;2:1548-1553.
19 Barak I, Muchova K: The role of lipid domains in bacterial cell processes. Int J Mol Sci 2013;14:4050-4065.
20 Toulmay A, Prinz WA: Direct imaging reveals stable, micrometer-scale lipid domains that segregate proteins in live cells. J Cell Biol 2013;202:35-44.
21 Malinsky J, Opekarova M, Tanner W: The lateral compartmentation of the yeast plasma membrane. Yeast 2010;27:473-478.
22 Mound A, Lozanova V, Warnon C, Hermant M, Robic J, Guere C, Vie K, Lambert de Rouvroit C, Tyteca D, Debacq-Chainiaux F, Poumay Y: Non-senescent keratinocytes organize in plasma membrane submicrometric lipid domains enriched in sphingomyelin and involved in re-epithelialization. Biochim Biophys Acta 2017;1862:958-971.
23 Frisz JF, Lou K, Klitzing HA, Hanafin WP, Lizunov V, Wilson RL, Carpenter KJ, Kim R, Hutcheon ID, Zimmerberg J, Weber PK, Kraft ML: Direct chemical evidence for sphingolipid domains in the plasma membranes of fibroblasts. Proc Natl Acad Sci U S A 2013;110:613-622.
24 Tyteca D, D'Auria L, Van Der Smissen P, Medts T, Carpentier S, Monbaliu JC, de Diesbach P, Courtoy PJ: Three unrelated sphingomyelin analogs spontaneously cluster into plasma membrane micrometric domains. Biochim Biophys Acta 2010;1798:909-927.
25 Carquin M, Conrard L, Pollet H, Van Der Smissen P, Cominelli A, Veiga-da-Cunha M, Courtoy PJ, Tyteca D: Cholesterol segregates into submicrometric domains at the living erythrocyte membrane: evidence and regulation. Cell Mol Life Sci 2015;72:4633-4651.

26 Carquin M, Pollet H, Veiga-da-Cunha M, Cominelli A, Van Der Smissen P, N'Kuli F, Emonard H, Henriet P, Mizuno H, Courtoy PJ, Tyteca D: Endogenous sphingomyelin segregates into submicrometric domains in the living erythrocyte membrane. J Lipid Res 2014;55:1331-1342.
27 D'Auria L, Van Der Smissen P, Bruyneel F, Courtoy PJ, Tyteca D: Segregation of fluorescent membrane lipids into distinct micrometric domains: evidence for phase compartmentation of natural lipids? PLoS One 2011;6:e17021.
28 Dumitru A, Poncin M, Conrard L, Dufrêne Y, Tyteca D, Alsteens D: Nanoscale membrane architecture of healthy and pathological red blood cells. Nanoscale Horizons 2018;3:293-304.
29 Leonard C, Conrard L, Guthmann M, Pollet H, Carquin M, Vermylen C, Gailly P, Van Der Smissen P, Mingeot-Leclercq MP, Tyteca D: Contribution of plasma membrane lipid domains to red blood cell (re)shaping. Sci Rep 2017;7:4264-4281.
30 Owen DM, Rentero C, Magenau A, Abu-Siniyeh A, Gaus K: Quantitative imaging of membrane lipid order in cells and organisms. Nat Protoc 2011;7:24-35.
31 Leonard C, Pollet H, Vermylen C, Gov N, Tyteca D, Mingeot-Leclercq MP: Tuning of Differential Lipid Order Between Submicrometric Domains and Surrounding Membrane Upon Erythrocyte Reshaping. Cell Physiol Biochem 2018;48:2563-2582.
32 Kaestner L, Tabellion W, Weiss E, Bernhardt I, Lipp P: Calcium imaging of individual erythrocytes: problems and approaches. Cell Calcium 2006;39:13-19.
33 D'Auria L, Fenaux M, Aleksandrowicz P, Van Der Smissen P, Chantrain C, Vermylen C, Vikkula M, Courtoy PJ, Tyteca D: Micrometric segregation of fluorescent membrane lipids: relevance for endogenous lipids and biogenesis in erythrocytes. J Lipid Res 2013;54:1066-1076.
34 Parasassi T, Gratton E: Membrane lipid domains and dynamics as detected by Laurdan fluorescence. J Fluoresc 1995;5:59-69.
35 Sanchez SA, Tricerri MA, Gratton E: Laurdan generalized polarization fluctuations measures membrane packing micro-heterogeneity *in vivo*. Proc Natl Acad Sci U S A 2012;109:7314-7319.
36 van Meer G, Voelker DR, Feigenson GW: Membrane lipids: where they are and how they behave. Nat Rev Mol Cell Biol 2008;9:112-124.
37 Gnanasambandam R, Ghatak C, Yasmann A, Nishizawa K, Sachs F, Ladokhin AS, Sukharev SI, Suchyna TM: GsMTx4: Mechanism of Inhibiting Mechanosensitive Ion Channels. Biophys J 2017;112:31-45.
38 Syeda R, Xu J, Dubin AE, Coste B, Mathur J, Huynh T, Matzen J, Lao J, Tully DC, Engels IH, Petrassi HM, Schumacher AM, Montal M, Bandell M, Patapoutian A: Chemical activation of the mechanotransduction channel Piezo1. Elife 2015;4:e07369.
39 Lopreiato R, Giacomello M, Carafoli E: The plasma membrane calcium pump: new ways to look at an old enzyme. J Biol Chem 2014;289:10261-10268.
40 Andrews DA, Yang L, Low PS: Phorbol ester stimulates a protein kinase C-mediated agatoxin-TK-sensitive calcium permeability pathway in human red blood cells. Blood 2002;100:3392-3399.
41 Bruce J: Plasma membrane calcium pump regulation by metabolic stress. World J Biol Chem 2010;1:221-228.
42 Barrow SL, Voronina SG, da Silva Xavier G, Chvanov MA, Longbottom RE, Gerasimenko OV, Petersen OH, Rutter GA, Tepikin AV: ATP depletion inhibits Ca2+ release, influx and extrusion in pancreatic acinar cells but not pathological Ca2+ responses induced by bile. Pflugers Arch 2008;455:1025-1039.
43 Raftos JE, Whillier S, Kuchel PW: Glutathione synthesis and turnover in the human erythrocyte: alignment of a model based on detailed enzyme kinetics with experimental data. J Biol Chem 2010;285:23557-23567.
44 Ackerman DG, Feigenson GW: Multiscale modeling of four-component lipid mixtures: domain composition, size, alignment, and properties of the phase interface. J Phys Chem B 2015;119:4240-4250.
45 Gu RX, Ingolfsson HI, de Vries AH, Marrink SJ, Tieleman DP: Ganglioside-Lipid and Ganglioside-Protein Interactions Revealed by Coarse-Grained and Atomistic Molecular Dynamics Simulations. J Phys Chem B 2017;121:3262-3275.
46 Koldso H, Shorthouse D, Helie J, Sansom MS: Lipid clustering correlates with membrane curvature as revealed by molecular simulations of complex lipid bilayers. PLoS Comput Biol 2014;10:e1003911.
47 Veatch SL, Keller SL: Seeing spots: complex phase behavior in simple membranes. Biochim Biophys Acta 2005;1746:172-185.
48 Kahya N, Schwille P: Fluorescence correlation studies of lipid domains in model membranes. Mol Membr Biol 2006;23:29-39.
49 Sezgin E, Gutmann T, Buhl T, Dirkx R, Grzybek M, Coskun U, Solimena M, Simons K, Levental I, Schwille P: Adaptive lipid packing and bioactivity in membrane domains. PLoS One 2015;10:e0123930.

50 Chapman D: Phase transitions and fluidity characteristics of lipids and cell membranes. Q Rev Biophys 1975;8:185-235.
51 Garcia-Arribas AB, Alonso A, Goni FM: Cholesterol interactions with ceramide and sphingomyelin. Chem Phys Lipids 2016;199:26-34.
52 Manno S, Takakuwa Y, Mohandas N: Modulation of erythrocyte membrane mechanical function by protein 4.1 phosphorylation. J Biol Chem 2005;280:7581-7587.
53 Glogowska E, Schneider ER, Maksimova Y, Schulz VP, Lezon-Geyda K, Wu J, Radhakrishnan K, Keel SB, Mahoney D, Freidmann AM, Altura RA, Gracheva EO, Bagriantsev SN, Kalfa TA, Gallagher PG: Novel mechanisms of PIEZO1 dysfunction in hereditary xerocytosis. Blood 2017;130:1845-1856.
54 Koshy C, Ziegler C: Structural insights into functional lipid-protein interactions in secondary transporters. Biochim Biophys Acta 2015;1850:476-487.
55 Bhatia T, Cornelius F, Brewer J, Bagatolli LA, Simonsen AC, Ipsen JH, Mouritsen OG: Spatial distribution and activity of Na(+)/K(+)-ATPase in lipid bilayer membranes with phase boundaries. Biochim Biophys Acta 2016;1858:1390-1399.
56 Dawaliby R, Trubbia C, Delporte C, Masureel M, Van Antwerpen P, Kobilka BK, Govaerts C: Allosteric regulation of G protein-coupled receptor activity by phospholipids. Nat Chem Biol 2016;12:35-39.
57 Posada IM, Fantini J, Contreras FX, Barrantes F, Alonso A, Goni FM: A cholesterol recognition motif in human phospholipid scramblase 1. Biophys J 2014;107:1383-1392.
58 Qi Y, Andolfi L, Frattini F, Mayer F, Lazzarino M, Hu J: Membrane stiffening by STOML3 facilitates mechanosensation in sensory neurons. Nat Commun 2015;6:8512-8525.
59 Ridone P, Grage SL, Patkunarajah A, Battle AR, Ulrich AS, Martinac B: "Force-from-lipids" gating of mechanosensitive channels modulated by PUFAs. J Mech Behav Biomed Mater 2018;79:158-167.
60 Saotome K, Murthy SE, Kefauver JM, Whitwam T, Patapoutian A, Ward AB: Structure of the mechanically activated ion channel Piezo1. Nature 2017;554:481-486.
61 Wu J, Lewis AH, Grandl J: Touch, Tension, and Transduction - The Function and Regulation of Piezo Ion Channels. Trends Biochem Sci 2017;42:57-71.
62 Bavi O, Vossoughi M, Naghdabadi R, Jamali Y: The Combined Effect of Hydrophobic Mismatch and Bilayer Local Bending on the Regulation of Mechanosensitive Ion Channels. PLoS One 2016;11:e0150578.
63 Nourse JL, Pathak MM: How cells channel their stress: Interplay between Piezo1 and the cytoskeleton. Semin Cell Dev Biol 2017;71:3-12.
64 Pang Y, Zhu H, Wu P, Chen J: The characterization of plasma membrane Ca2+-ATPase in rich sphingomyelin-cholesterol domains. FEBS Lett 2005;579:2397-2403.
65 Tang D, Dean WL, Borchman D, Paterson CA: The influence of membrane lipid structure on plasma membrane Ca2+ -ATPase activity. Cell Calcium 2006;39:209-216.
66 Liu C, Weng H, Chen L, Yang S, Wang H, Debnath G, Guo X, Wu L, Mohandas N, An X: Impaired intestinal calcium absorption in protein 4.1R-deficient mice due to altered expression of plasma membrane calcium ATPase 1b (PMCA1b). J Biol Chem 2013;288:11407-11415.
67 Di Leva F, Domi T, Fedrizzi L, Lim D, Carafoli E: The plasma membrane Ca2+ ATPase of animal cells: structure, function and regulation. Arch Biochem Biophys 2008;476:65-74.
68 Pignataro MF, Dodes-Traian MM, Gonzalez-Flecha FL, Sica M, Mangialavori IC, Rossi JP: Modulation of plasma membrane Ca2+-ATPase by neutral phospholipids: effect of the micelle-vesicle transition and the bilayer thickness. J Biol Chem 2015;290:6179-6190.
69 Wang YH, Collins A, Guo L, Smith-Dupont KB, Gai F, Svitkina T, Janmey PA: Divalent cation-induced cluster formation by polyphosphoinositides in model membranes. J Am Chem Soc 2012;134:3387-3395.
70 Abe M, Makino A, Hullin-Matsuda F, Kamijo K, Ohno-Iwashita Y, Hanada K, Mizuno H, Miyawaki A, Kobayashi T: A role for sphingomyelin-rich lipid domains in the accumulation of phosphatidylinositol-4, 5-bisphosphate to the cleavage furrow during cytokinesis. Mol Cell Biol 2012;32:1396-1407.
71 Zaidi A, Barron L, Sharov VS, Schoneich C, Michaelis EK, Michaelis ML: Oxidative inactivation of purified plasma membrane Ca2+-ATPase by hydrogen peroxide and protection by calmodulin. Biochemistry 2003;42:12001-12010.
72 Sharp JS, Tomer KB: Analysis of the oxidative damage-induced conformational changes of apo- and holocalmodulin by dose-dependent protein oxidative surface mapping. Biophys J 2007;92:1682-1692.
73 Zaidi A: Plasma membrane Ca-ATPases: Targets of oxidative stress in brain aging and neurodegeneration. World J Biol Chem 2010;1:271-280.
74 Subbaiah PV, Sircar D, Lankalapalli RS, Bittman R: Effect of double bond geometry in sphingosine base on the antioxidant function of sphingomyelin. Arch Biochem Biophys 2009;481:72-79.

Annex 7: Plasma Membrane Lipid Domains as Platforms for Vesicle Biogenesis and Shedding?

H. Pollet, L. Conrard, A-S. Cloos and D. Tyteca

CELL Unit, de Duve Institute & Université Catholique de Louvain, UCL B1.75.05, Avenue Hippocrate, 75, B-1200 Brussels, Belgium;

Biomolecules. 2018 Sep 14;8(3). pii: E94.

DOI: 10.3390/biom8030094.

KEYWORDS

calcium; ceramide; cholesterol; cytoskeleton; lipid domains; microvesicle; oxidative stress; raft; red blood cell; sphingomyelinase

biomolecules

MDPI

Review

Plasma Membrane Lipid Domains as Platforms for Vesicle Biogenesis and Shedding?

Hélène Pollet, Louise Conrard, Anne-Sophie Cloos and Donatienne Tyteca *

CELL Unit, de Duve Institute & Université Catholique de Louvain, UCL B1.75.05, Avenue Hippocrate, 75, B-1200 Brussels, Belgium; helene.pollet@uclouvain.be (H.P.); louise.conrard@uclouvain.be (L.C.); anne-sophie.cloos@student.uclouvain.be (A.-S.C.)

* Correspondence: donatienne.tyteca@uclouvain.be; Tel.: +32-2-764-7591; Fax: +32-2-764-7543

Received: 5 August 2018; Accepted: 4 September 2018; Published: 14 September 2018

Abstract: Extracellular vesicles (EVs) contribute to several pathophysiological processes and appear as emerging targets for disease diagnosis and therapy. However, successful translation from bench to bedside requires deeper understanding of EVs, in particular their diversity, composition, biogenesis and shedding mechanisms. In this review, we focus on plasma membrane-derived microvesicles (MVs), far less appreciated than exosomes. We integrate documented mechanisms involved in MV biogenesis and shedding, focusing on the red blood cell as a model. We then provide a perspective for the relevance of plasma membrane lipid composition and biophysical properties in microvesiculation on red blood cells but also platelets, immune and nervous cells as well as tumor cells. Although only a few data are available in this respect, most of them appear to converge to the idea that modulation of plasma membrane lipid content, transversal asymmetry and lateral heterogeneity in lipid domains may play a significant role in the vesiculation process. We suggest that lipid domains may represent platforms for inclusion/exclusion of membrane lipids and proteins into MVs and that MVs could originate from distinct domains during physiological processes and disease evolution.

Keywords: microvesicle; cytoskeleton; cholesterol; ceramide; sphingomyelinase; raft; lipid domains; calcium; oxidative stress; red blood cell

1. Introduction

In recent decades, the field of transcellular signaling has been revolutionized by the emerging concept of signal transmission through extracellular vesicles (EVs). For a long time, vesicles seen in intercellular spaces by electron microscopy were thought to be artifacts or inert cellular fragments resulting from damaged cells in the vicinity. Nonetheless, all cells, from bacteria to plants and animal cells, seem to have the ability to produce EVs [1,2]. However, there is still no real consensus regarding EV classification and nomenclature [3], probably due to the variety of EV size, composition, origin and targets, but also due to difficulties related to their isolation and analysis (see Section 2). Most reviews classify EVs into three groups: exosomes, microvesicles (MVs) and apoptotic bodies (Figure 1) [4–7]. Exosomes are the smallest EVs (50–150 nm in diameter) and are released upon multivesicular bodies exocytosis. MVs are produced by direct local deformation and budding of the plasma membrane (PM) leading to vesicles of more heterogeneous and bigger size (100 nm–1 µm in diameter). It should be noted that these vesicles are often given other names, including ectosomes, microparticles, shedding vesicles or oncosomes (in the particular case of cancer cells). Apoptotic bodies (1–5 µm in diameter) are generated by blebbing of cells undergoing apoptosis. However, this classification should be taken with caution as most of the currently used techniques only make it possible to separate small EVs enriched in exosomes from large EVs enriched in MVs (see Section 2) [8]. Yet, other studies have

evidenced by imaging the budding from the PM of vesicles with size closer to that of exosomes [9–11]. In this review, we will focus on PM-derived vesicles whatever their size.

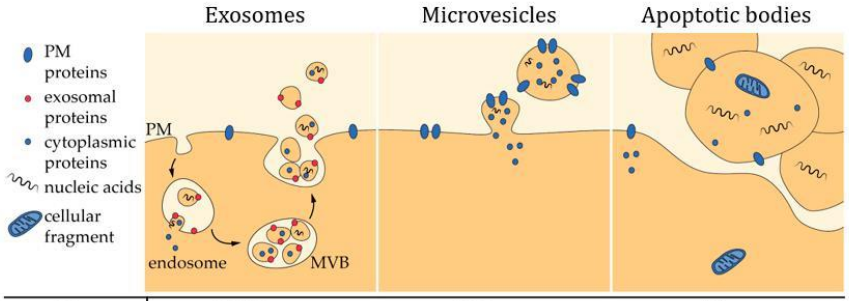

Size	50-150nm	0.1-1µm	1-5µm
Origin	endosome	plasma membrane	plasma membrane of apoptotic cells
Isolation	• differential ultracentrifugation • density gradient • size-exclusion chromatography • immune-capture		differential ultracentrifugation (standard protocol needed)
Other names	prostasomes	ectosomes microparticles shedding vesicles	

Figure 1. Characteristics of the three main classes of extracellular vesicles. MVB, multivesicular body; PM, plasma membrane.

Extracellular vesicles have been shown to contribute to a large variety of pathophysiological processes including red blood cell (RBC) senescence [12], coagulation [13], inflammation [13,14], migration [15], tumorigenesis [16] and infection [17]. As they are found in body fluids (e.g., blood, urine, cerebrospinal fluid, milk), they are easily accessible and might represent useful diagnostic biomarkers and/or targets for therapeutic applications (reviewed in [18]). In this review, we will focus on vesicles derived from the PM of RBCs, platelets, immune cells, nervous cells and tumor cells. Before providing detailed information regarding their biogenesis, we present below a short non-exhaustive overview of their pathophysiological effects.

Erythrocytes undergo multiple changes during their 120-day lifespan in the circulation, including the decreased activity of multiple enzymes, the gradual accumulation of oxidative damage, the redistribution of ions, the loss of membrane by vesiculation as well as cell volume, density and deformability alterations (for reviews, see [19–21]). Microvesicle generation constitutes a central mechanism in the RBC homeostasis and is responsible for the loss of ~20% of the PM while the hemoglobin concentration increases by ~14% [22,23]. Microvesicles have been proposed to contribute to RBC senescence by two opposite mechanisms. On one hand, they protect RBCs from premature elimination via transport of molecules that could induce recognition by the reticuloendothelial system such as non-functional hemoglobin, oxidized and aggregated Band3 and oxidized proteins [23] (Figure 2a). On the other hand, they appear to contain CD47, a self-marker that prevents the recognition and clearance of RBCs by macrophages. Elimination of CD47 from the RBC membrane through selective shedding could then promote the removal of old RBCs [24] (Figure 2b). Studies on mice suggest that MVs from RBCs are removed very fast from the circulation by the reticuloendothelial system [25] because they can have deleterious effects on other cells. For instance, MVs bear at their external leaflet phosphatidylserine (PS), which acts as an "eat me" signal for macrophages but also promotes coagulation, as PS enhances prothrombinase activity and other coagulation factors (Figure 2a,c). Moreover, RBC-derived MVs induce an excessive production of reactive oxygen species

(ROS) in neutrophils and could be responsible for exhortation of the respiratory burst, i.e., the rapid release of ROS necessary to answer to an infection [26] (Figure 2d). Finally, they contain hemoglobin, which allows them to bind nitric oxide modifying thereby bioavailability of the latter for vascular homeostasis regulation [27] (Figure 2e). However, these effects have been shown with MVs isolated from blood storage. Although the biological content should reflect the functional properties of circulating MVs, further investigations in vivo are needed to confirm these hypotheses. Nevertheless, the properties described above could partly explain reduced post-transfusion efficacy and increased risk of adverse reactions in patients after transfusion [28,29].

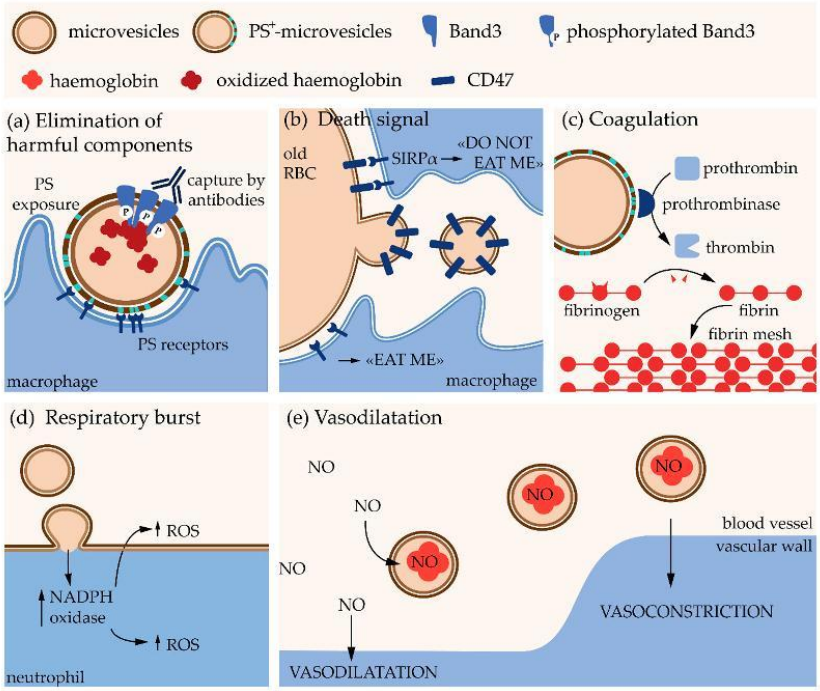

Figure 2. Pathophysiological effects of erythrocyte-derived microvesicles. PS, phosphatidylserine; RBC, red blood cell; SIRPα, signal regulatory protein α; NADPH; reduced form of nicotinamide adenine dinucleotide phosphate; ROS, reactive oxygen species; NO, nitric oxide.

Platelet is another blood cell type able to release a high quantity of EVs. Platelet EVs represent ~30% of the blood EVs [30] and, in contrast to RBCs, these include MVs as well as exosomes. Platelet-derived vesicles are essential for the regulation of the hemostasis, as revealed by the bleeding disorders caused by the decreased formation of platelet-derived MVs in patients with Scott Syndrome [31]. Their pro-coagulant activity is due to the exposition on their surface of pro-coagulant molecules, such as PS and tissue factor (TF), one initiator of the coagulation cascade [30]. Additionally, platelet-derived MVs promote cell proliferation, survival and migration, which are essential for endothelial repair and wound healing [32]. They are also effectors of the immune response by increasing monocyte adhesion, promoting inflammatory pathways and cytokine release in monocytes and endothelial cells (ECs) [33], stimulating antigen-specific IgG production [34] and upregulating neutrophil aggregation, activation and phagocytic activity [35].

Monocytes and neutrophils themselves are also able to release MVs and exosomes, producing autocrine effects or serving as mediators to communicate with other cells (reviewed in [36,37]). They can have either pro-inflammatory or anti-inflammatory effects [38]. They also

promote blood coagulation through exposure of PS and TF in monocyte MVs and through direct interaction between neutrophil MVs and platelets, which promotes platelet activation [39] and TF expression [36].

In the central nervous system, only exosome-like EVs have been described in neurons, oligodendrocytes and Schwann cells in physiological conditions [40]. On the other side, microglia cells (i.e., the macrophage resident cells) and astrocytes (i.e., support cells, also involved in the blood brain barrier) have been shown to release both exosomes and MV-like EVs [41]. The major MVs described are released by microglia cells and astrocytes upon ATP activation of P_2X_7 receptors and contain the interleukin-1β which is released at the site of tissue damage to initiate an acute inflammatory response [42]. Extracellular vesicles also appear to play critical role in neurodegenerative diseases. For example, in Alzheimer disease, MVs released by microglia promote the amyloid-β pathogenesis by increasing the solubility of the misfolded protein (i.e., the soluble form is more neurotoxic than the aggregated one) [43]. Moreover, as microglia-derived MVs regulate the inflammatory response, they have been shown to be increased and to play major role in multiple sclerosis, a form of neuroinflammation [44]. Those MVs carry inflammation factors that promote the degradation of the extracellular matrix and tight and adherens junctions, leading to the disruption of the blood brain barrier [45].

Cancer cell-associated vesicles were reported for the first time in 1978 in patients suffering from Hodgkin disease. Since then, evidence has been accumulating that tumor-derived MVs constitute important players in cancer initiation and progression through communications between cancer cells. Microvesicles also facilitate intercellular communication between cancer cells and microenvironmental cells (e.g., stromal, immune and vascular cells), either located directly in the primary tumor-environment or at distance, promoting pre-metastatic niche formation. Microvesicles are implicated in several stages of tumorigenesis and metastasis by increasing angiogenesis and extracellular matrix remodeling, promoting escape from the immune system, inducing resistance to therapy and triggering blood coagulation (reviewed in [16,18,46,47]). Because of the multiple roles of MVs in cancer, they could be seen as prognostic and/or diagnostic biomarkers. Hence, they could represent emerging targets for cancer therapy (reviewed in [18]).

2. Microvesicle Isolation and Characterization

Several methodologies have been developed over the years to optimize EV isolation. Differential ultracentrifugation is the most frequent one, even if protocols can considerably vary in terms of speed and time intervals. Increasing centrifugal forces allow to separate EVs from cell debris and intact cells thanks to their difference in size and density [48–51]. This method makes it possible to reach a recovery of up to 80% and offers the possibility to process large volumes without the need for chemicals that could interfere with downstream analysis [50]. Among limitations, one can cite EV aggregation, contamination by protein aggregates and viruses as well as EV damaging during high-speed centrifugation [48]. Moreover, since it is moderately time-consuming and the equipment is expensive, it is not considered to be a clinically applicable isolation technique. Another method based on centrifugation is the density gradient centrifugation, which presents a lower recovery of 10–50% but avoids protein contamination of samples thanks to density differences [48,52]. Nevertheless, co-isolation of lipoproteins cannot be excluded. For the same reasons as for differential ultracentrifugation, this methodology finds no clinical application [48]. Filtration represents an alternative method that can be applied alone or in combination with ultracentrifugation. However mechanical damage due to the pressure applied for passing EVs through the filter can affect their properties [50]. According to the size cut-off of the column, size-exclusion chromatography allows EV separation from non-aggregated proteins and high density lipoproteins (HDL) but contamination with material of similar size, such as aggregated proteins and viruses, cannot be excluded. The excellent recovery rate (up to 90%), the absence of EV damaging, the low cost and the quickness make this methodology interesting for clinical applications. However, this method is

not suitable for large volumes and requires a pre-concentration step by ultracentrifugation [48]. Finally, the affinity-based methods (better known as immune-capturing methods) are based on the interaction of EV surface molecules with antibodies, lectins or lipid-binding proteins, either biotinylated or coupled to magnetic beads. These techniques are fast and simple and contamination of purified sample is minimal. However, it is cost-effective and not adapted to processing large-volume samples [50]. In the face of the large diversity of isolation methods, the quantity and the quality of the starting material must guide the researcher.

Another criterion to consider is the type of analysis downstream of EV purification, including their structural characterization. Here also several techniques exist. Electron microscopy makes it possible to assess EV size and morphology and to identify their cellular origin [48,53]. Since dehydration and fixation required for traditional electron microscopy could possibly lead to EV morphology changes, cryo-electron microscopy is widely recommended. Atomic force microscopy (AFM) also makes it possible to determine EV structural properties via the interaction of a probing tip (cantilever) with the surface of the sample, which generates a 3D-image of the surface topography. However, as for electron microscopy, changes in EV morphology can occur due to the necessity of immobilizing the material [53]. Additionally, one can cite the dynamic light scattering and nanoparticle tracking, which are both based on the same principle. Thanks to the recording of light scattering over time and its modification due to EV Brownian motion, it is possible to determine their size and size distribution. This approach is more reliable when the sample size is homogenous and not polydispersed [53]. For larger EVs, flow cytometry is an alternative technique combining light scattering and fluorescence. The labeling of EVs with fluorescent antibodies/probes allows the specific recognition of surface markers [48,53]. In addition to structural characterization, it is also possible to biochemically characterize the EVs. This is beyond the scope of the manuscript and we invite the reader to refer to the review by Ramirez et al. for more insights regarding techniques for biochemical and in vivo characterization [51].

3. Microvesicle Molecular Properties

The abundance and properties of MVs appear to fluctuate depending on the cell origin, the pathophysiological context and also the subject tested (e.g., age, gender, fasting state, medication exposure, physical activities, pregnancy and diseases) [54–58]. Moreover, variations in isolation techniques, culture conditions and methods to stimulate the shedding (e.g., calcium [Ca^{2+}] ionophores, lipopolysaccharide, hypoxia, tumor necrosis factor TNFα, ATP) could lead to conflicting data [59]. Finally, most studies related to MV content are based on "MV pellets" obtained by differential ultracentrifugation, which most of the time contain mixed populations (especially when extracted from body fluids) [8]. It is then difficult to provide a digest of the MV content and even more to erect rigid rules. Nevertheless, efforts have been made to collect datasets from many EV studies and put them online (Vesiclepedia; EVpedia) [60,61] and to carefully characterize co-isolated mixed EV populations from "traditional" isolation procedures to refine and determine new optimized protocols [8].

Microvesicles are limited by a lipid bilayer (Section 3.3) and can carry a diversity of proteins (Section 3.1) and nucleic acids (Section 3.2). Although they are expected to exhibit a similar content as the PM from which they derive, accumulated evidence highlights that the MV composition is the outcome of a regulated sorting mechanism at the PM, leading to enrichment or despoliation of some chosen components.

3.1. Protein Content

Proteins associated with MV biogenesis are generally found in these vesicles. For instance, the MVs produced by the tumoral LOX cell line are positive for the small GTPase ARF6 known to regulate their release [62]. Likewise, Rab GTPases suspected to play a role in MVs released by neuroblastoma cells associate with these vesicles [63]. Regarding cytoskeleton proteins, actin has been detected in neutrophil- [64] and RBC-derived MVs while spectrin, the structural basis of RBC cytoskeleton, is lacking [65,66]. Proteins known to localize in lipids rafts appear also enriched in

some MVs [39,66,67], but it is not a common rule (see Section 5.3). Some MVs, in particular those released by ECs, neutrophils and tumor cells, are charged with proteolytic enzymes, allowing tissue microenvironment remodeling which is essential for angiogenesis, tissue repair or cancer cell invasion. For instance, matrix metalloproteinases are found in large oncosomes from prostate cancer tissues and cells [68,69] and in MVs from human breast carcinoma cells, neutrophils [64] and ECs [70]. For a complete review on metalloproteinases in EVs, see [71]. Adhesion molecules are also commonly found in MVs as they can mediate direct stimulation of the recipient cells or initiate MV internalization. Thus, different classes of integrins are associated with MVs from monocytes/macrophages, neutrophils, platelets, endothelial progenitor cells and tumoral cells [39,72–76]. For example, P-selectin is found in platelet-derived MVs [73] and the P-selectin glycoprotein ligand-1 (PSGL-1) is detected in monocyte/macrophage-derived MVs able to fusion with platelets [39]. Finally, MVs could contribute to the propagation of oncoproteins among the tumoral cells, as it was shown for the oncogenic form of the epidermal growth factor receptor (EGFRvIII) present in aggressive human brain tumors [77].

3.2. Nucleic Acid Content

The study of RNA in EV samples represents a growing field of research thanks to technical advances in the detection of scarce and complex RNA samples. Using high-throughput RNA sequencing, various mRNAs and many types of non-coding RNAs have been found in EVs [78]. For instance, MVs from endothelial progenitor cells are loaded with mRNAs associated with the PI3K/Akt signaling pathway, which triggers angiogenesis in ECs and promotes cell survival, proliferation and organization in capillary-like structures [76]. Another example is the transfer of mRNA for growth factors from tumoral-derived MVs to monocytes. This enhances monocyte survival in vitro [79]. Non-coding RNAs might also be present in MVs [80]. For instance, miRNA has been detected in embryonic stem cell MVs [81] and human adult liver stem cell-derived MVs [82]. The presence of far more types of non-coding RNAs has been assessed in mixed EV populations or non-defined EVs [78,80]. However, several investigations have pointed out that, when comparing MVs with exosomes, the latter is the richest reservoir for almost all RNAs [83,84]. Even if that does not mean the RNA transfer through MVs is inefficient, it suggests that transcellular transfer of genetic material is less important in MVs than in exosomes. To the best of our knowledge there is no indication that DNA is present in MVs, but it was already found in apoptotic bodies, exosomes, "exosome-like" vesicles (i.e., unknown origin) and mixed EV populations [85]. However, it is possible to artificially load MVs with plasmid DNA with effective transfer to the recipient [86].

3.3. Lipid Content

Lipids are the basic structural constituents of EVs but are the least-studied components and the least-appreciated topic in dedicated reviews. Although EVs have for a long time been mainly distinguished based on their size, origin and protein content, protein-to-lipid ratio has recently been proposed as an alternative criterion, at least until selective markers become available. For instance, apoptotic bodies exhibit the highest protein-to-lipid ratio, followed by MVs and then by exosomes, as revealed by a comprehensive analysis of EV preparations from various myeloid and lymphoid cells lines as well as blood plasma [87]. As lipids present a density of approximately $\approx$1 g cm^{-3} and proteins of >1.3 g cm^{-3}, density gradients (see above Section 2) could therefore be used to separate subpopulations of EVs with differential protein-to-lipid ratios [52].

Focusing on MV lipid content, only a few reliable data can be found in the literature, with sometimes conflicting information (Table 1). Although ceramide (Cer) and sphingomyelin (SM) are enriched in the MVs originating from some tumor cells (namely U87 glioblastoma and Huh7 hepatocellular carcinoma cells) and from human bone marrow-derived mesenchymal stem cells [88], these two sphingolipids (SLs) are less enriched in MVs from platelets and not at all in MVs isolated from plasma or RBCs upon storage. Regarding phospholipid (PLP) content, while PS and phosphatidylethanolamine (PE) appear to be depleted from MVs, phosphatidylcholine

(PC) seems to present a similar content as in the PM. No reliable information can be found on cholesterol (chol) content, except in two studies showing no spectacular enrichment. To summarize, some studies reveal that MVs exhibit a similar lipid composition as the PM, while others show specific enrichment/depletion, leading to the suggestion that MVs can shed from specific PM locations. Discrepancies between studies could be related to the cell origin and the pathophysiological context, but also to the MV isolation, purification and characterization conditions.

Table 1. Lipid content in microvesicles and enrichment as compared to the originating cells. Data are expressed as percent of total lipid quantified and as MV/cell ratios (brackets), except when specified. Percentages or ratios were calculated from raw data when furnished or estimated on graphs. MS, mass spectrometry; TLC, thin layer chromatography; PM, plasma membrane; -, not determined; SM, sphingomyelin; Cer, ceramide; PC, phosphatidylcholine; PS, phosphatidylserine; PE, phosphatidylethanolamine; chol, cholesterol; PLPs, phospholipids.

Cell Type/Body Fluid	Lipid Analysis	MV Size (nm)	% of Total Lipid Content (MV/Cell Ratio)						Ref.
			SM	Cer	PC	PS	PE	Chol/PLPs	
U87 glioblastoma cells	MS	50–600	15% (2)	0.7% (2.4)	25% (0.9)	17% (1)	9.6% (0.9)	-	[88]
Huh7 hepatocellular carcinoma cells	MS	50–600	15% (3.6)	0.3% (1.5)	27% (1.3)	7.4% (0.6)	6.8% (0.7)	-	[88]
Bone marrow derived stem cells	MS	50–600	8.6% (1.6)	0.5% (1.9)	25% (1.2)	8% (0.7)	3.7% (0.5)	-	[88]
Placenta	MS	-	37%	1%	15%	17%	2%	-	[89]
Plasma EVs (ratio on platelets)	TLC	-	21% (1)	-	59% (1.8)	3.6% (0.3)	9.4% (0.3)	-	[90]
Stored RBCs (53 ± 4 days)	MS	-	(1)	-	(1)	(7)	(0.8)	-	[91]
Stored RBCs (35–42 days)	MS	100–300	33% (1)	-	26% (1)	10% (1)	30% (1)	-	[92]
ATP-depleted RBCs	Enzymatic	~200	26% (0.9)	-	27% (0.9)	-	25% (0.8)	(0.9)	[93]
Platelets	MS	-	14% (1.3)	0.7% (1.3)	27% (0.7)	17% (1)	37% (1)	-	[94]
Platelets (ratio on PM platelets)	TLC	-	25% (1.1)	-	31% (1.1)	14% (0.8)	30% (1)	(1.5)	[95]

Remodeling of membrane asymmetry in MVs appears at first glance less debated. Accordingly, PS exposure at the outer leaflet is the most widespread tool to identify EVs. However, it should be noted that Annexin V, a specific tool for outer PM leaflet PS, seems not able to unveil the entire EV population. For instance, by cryo-electron microscopy, Arraud et al. revealed that a large amount of EVs from plasma does not expose PS [30]. Whether this population refers to exosomes remains to be determined. Moreover, Annexin V appears to bind only 20% of unstimulated platelet-derived MVs and its binding on activated platelets depends on the agonist used for platelet activation [96]. Furthermore, severe disruption of protein-protein interactions associated with RBC morphology changes can induce increased MV production without increased PS exposure [97]. Finally, MVs induced upon RBC treatment with sphingomyelinase (SMase) are much more heterogeneous in PS exposure than those generated by spontaneous vesiculation, suggesting distinct mechanisms for biogenesis [98]. Therefore, one should be careful not to discard relevant MV population(s) when using Annexin V as a MV marker. Hence, these observations could suggest that different MV types can be generated by the same cell population depending on its activation state, suggesting distinct mechanisms of biogenesis (see Sections 4 and 5).

Lipids present in MVs could also act as messengers (for a complete review [99]). For instance, diacylglycerol and PLPs of MVs released from platelets, RBCs, ECs and thymocytes can be hydrolyzed by phospholipases A_2 to release a polyunsaturated fatty acid that is necessary for eicosanoids

(i.e., lipophilic hormones) production [100]. In vivo, phospholipases A_2 could trigger the incorporation of the target MVs to the recipient cells with the help of the produced eicosanoids. For instance, in rheumatoid arthritis, the concerted action of secreted phospholipase A_2 enriched in inflamed joint fluid and platelet-type 12-lipoxygenase present in platelet-derived MVs produces an eicosanoid (the 12(S)-hydroxyeicosatetranoic acid) which triggers the fusion of MVs with the neutrophil membrane [101].

4. Microvesicle Biogenesis and Shedding—General Mechanisms

In this section, we describe in detail the mechanisms involved in RBC microvesiculation. We then provide some clues on nucleated cells.

4.1. Red Blood Cells

4.1.1. Main Determinants of Red Blood Cell Integrity Maintenance

Through its life span, alterations of one or several factors that regulate RBC deformability will rapidly affect the RBC integrity and therefore initiate MV shedding from the membrane. Four major factors regulating the RBC deformability have been described: (i) the cytoskeleton structural properties and its vertical interactions with the membrane; (ii) the cytoplasmic viscosity; (iii) ion balance and subsequent volume regulation; and (iv) metabolic processes controlling ATP levels and redox state.

First, the RBC cytoskeleton strengthens the lipid bilayer and endows the membrane with durability and flexibility to survive in the circulation [102]. It is made of a pseudohexagonal meshwork of spectrins linked to the membrane by two multiprotein anchorage complexes: the ankyrin and the 4.1R complexes (Figure 3a). Ankyrin links the spectrin tetramers to the membrane through association with the membrane channel Band3. This complex is completed by association with the "marker of self" CD47, among others. 4.1R forms the second anchorage complex with actin and Band3, *inter alia* (for a complete review see [102]). The modulation of the interactions between cytoskeleton and membrane is tightly regulated by protein phosphorylation [103–105], association with PLPs [106,107] and Ca^{2+} [108], among others.

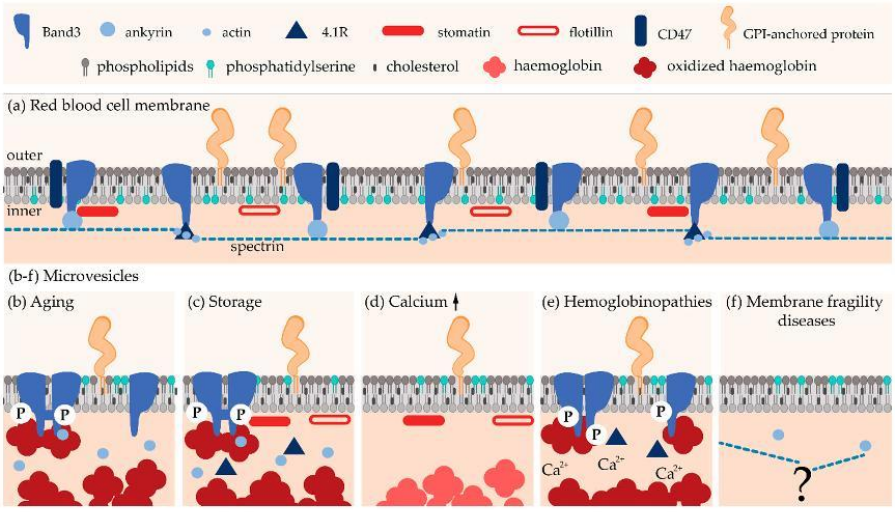

Figure 3. Schematic representation of lipid and protein composition of red blood cell-derived microvesicles. (**a**) RBC plasma membrane. (**b**–**f**) RBC-derived microvesicles in (**b**,**c**) physiological processes (senescence in vivo and storage at 4 °C), (**d**) pharmacological Ca^{2+} boost, and (**e**,**f**) pathological situations (hemoglobinopathies and membrane fragility diseases).

Second, RBC cytoplasmic viscosity, determined by hemoglobin concentration (comprised between 32 and 36 g/dL [109]) and state (i.e., polymerization, crystallization, degradation and oxidation [110]), is finely regulated.

Third, RBC ion balance and subsequent volume control is regulated by ion channels, symporters, antiporters and pumps. Among ion channels, one can cite Piezo1, a mechanosensitive non-selective cation channel recently identified as the link between mechanical forces, Ca^{2+} influx and RBC volume homeostasis. The Ca^{2+}-activated K^+ channel (named Gardos), the $Cl^-/HCO_3{}^-$ antiporter Band3 and the plasma membrane Ca^{2+} ATPase pump (PMCA) are also essential for the RBC homeostasis. For additional information regarding the regulation of RBC hydration and volume, please refer to [110,111].

Fourth, deformability of RBCs is affected by metabolic processes controlling ATP content and redox state. Intracellular ATP represents an energy source needed for (i) ion pumps like Na^+/K^+- and Ca^{2+}-ATPases, ATP-dependent glucose transporters, flippases and floppases; (ii) modulation of the compliance of the membrane with the cytoskeleton; and (iii) de novo synthesis of glutathione that is essential for the antioxidant system [104,112–114]. The extensive antioxidant system in RBC is designed to neutralize the harmful ROS generated through the constant exposure to variable oxygen pressures. Indeed, the major source of RBC oxidative stress is hemoglobin redox reactions. The reactive free radical species generated by hemoglobin reactions and the interactions of hemoglobin with membrane and cytoskeleton proteins both induce oxidative stresses and are involved in RBC aging. In addition, exogenous oxidants enter the RBC and react with hemoglobin [115]. The main antioxidant protein is the glutathione which presents two forms: the reduced GSH and oxidized GSSG. GSH scavenges ROS and reacts with another glutathione to form the inoffensive GSSG. The GSH pool is then restored by the action of the glutathione reductase and the reduced form of nicotinamide adenine dinucleotide phosphate (NADPH) [19].

4.1.2. Microvesicles upon Red Blood Cell Senescence, Blood Storage and Intracellular Calcium Boost

In plasma, RBC-derived MVs are a homogeneous population of ~150 nm in diameter [116]. Regarding composition, RBC-derived MVs from the plasma of healthy individuals (i) exhibit a very high content of Band3 and actin, contrasting with a lack of spectrin and ankyrin, (ii) are enriched in enzymes involved in redox homeostasis and in irreversibly modified hemoglobin, (iii) present PS at their outer lipid leaflet, and (iv) contain the glycosylphosphatidylinositol (GPI)-anchored proteins CD55 and CD59 (Figure 3b; reviewed in [21]).

During blood storage, remodeling of the RBC membrane is associated with the oxidative cross-linking and subsequent loss of Band3, lipid raft rearrangement and loss, as well as caspases activation [117]. Accordingly, RBC storage-derived MVs (i) accumulate oxidized and clustered Band3 and actin but lack spectrin, (ii) contain aggregated hemoglobin, (iii) expose PS at the surface, and (iv) contain the GPI-anchored proteins acetylcholinesterase and CD55 as well as stomatin and flotillins [65,66].

As the features of MVs stored in vitro are reminiscent of those of aging-released MVs, one can suggest a similar if not identical mechanism of shedding, even though some aspects of RBC aging in vivo may be more pronounced in blood bank RBC concentrates [118]. However, the loss of Band3 and several raft proteins from the RBC membrane upon storage seems to occur with distinct kinetics [117], suggesting several distinct vesiculation processes during storage. In agreement with this hypothesis, RBC-derived MVs upon storage present size and total protein content that increase over time. Moreover, the oxidation index of the MVs is very high before 3 weeks of storage, then abruptly decreases. Finally, while the vesicles contain apoptosis-related signaling molecules after day 10 of storage, the presence of CD47 is only visible from day 17 [65]. Our unpublished data also suggest multiple vesiculation processes during RBC storage.

Two non-mutually exclusive mechanisms have been proposed in the literature to explain MV release from RBCs:

- Band3 Model

Accumulation of Band3 and actin, which contrasts with the absence of spectrin in MVs generated upon RBC aging and blood storage, supports the hypothesis that partial membrane:cytoskeleton uncoupling, due to the breakage of ankyrin:Band3 binding, could contribute to the vesiculation process [21]. Accordingly, a simulation study highlighted that a significant reduction of the local anchorage density is required for vesiculation [119]. Furthermore, it has been shown that cytoskeleton stiffness and density both increase upon RBC senescence, leading to larger compressive forces on the cell membrane. These cytoskeleton modifications have been hypothesized to result from the vesicle detachment from the membrane and the subsequent increased membrane curvature [120–122].

However, cytoskeleton instability is probably not the primary event leading to vesiculation. Indeed, MV enrichment in enzymes involved in redox homeostasis and in irreversibly modified hemoglobin suggests that oxidative damage also contribute to the vesiculation process. Bosman et al. even suggested that this constitutes the primary trigger for vesiculation [21]. The increase in oxidative stress during RBC senescence results from a decrease in the anti-oxidative defense due to a lower activity of superoxide dismutase, catalase, glucose-6-phosphate dehydrogenase and aspartate aminotransferase. These latter two enzymes are involved in the formation of anti-oxidant glutathione (GSH) and NADPH molecules [123–125]. Oxidative stress appears to lead to the clustering of Band3 thanks to two mechanisms (Figure 4a). First, ROS activate Src tyrosine kinases, which in turn induce phosphorylation of Band3. Accordingly, hyper-phosphorylation of Band3 has been evidenced upon RBC aging and storage [126]. This phosphorylation in turn induces Band3 detachment from membrane skeleton, most probably by disruption from ankyrin, increasing its mobility and its clustering [126]. Second, ROS induce oxidation of hemoglobin into hemichromes, which are unable to bind O_2. The hemichromes interact with the Band3 cytoplasmic tail, also favoring its aggregation and its detachment from the cytoskeleton. The key role of hemoglobin in Band3 clustering is supported by two recent observations: (i) in the early phase of RBC storage, a significant amount of hemoglobin is associated with the lipid bilayer in MVs [127]; (ii) accumulation of oxidized hemoglobin during storage occurs together with its enrichment into MVs [128]. It should be noted that membrane peroxidation also seems to be required for Band3 clustering and termination of the RBC life [129]. Once Band3 is aggregated, it will both (i) promote the binding of autologous immunoglobulin G and initiates the removal of senescent RBCs from the bloodstream [19,130], and (ii) initiate the membrane budding and the subsequent MV release. This vesicle release is most probably due to the membrane:cytoskeleton anchorage destabilization. This involvement of oxidative stresses in vesicle release is supported by the fact that a treatment with antioxidants decreases the formation of MVs from RBCs [131].

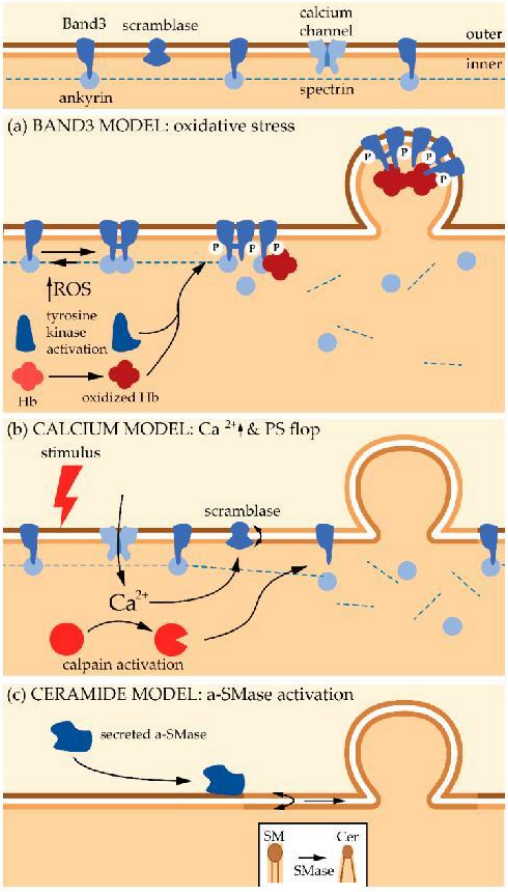

Figure 4. Models described in the literature for the biogenesis and shedding of red blood cell-derived microvesicles. Hb: haemoglobin; P: phosphorylation; a-SMase: acid sphingomyelinase.

- Calcium Accumulation Model

An alternative model to Band3 aggregation relies on the increase of intracellular Ca^{2+} concentration. This increase is observed during RBC physiological senescence [132], which could partly result from the decreased efficiency of Ca^{2+} extrusion due to the accumulation of oxidative stresses. This increase is also seen in eryptosis (i.e., apoptosis of anucleated cells) which is triggered by a variety of stimuli including hyperosmolarity, oxidative stress and exposure to xenobiotics [133].

To induce Ca^{2+} accumulation inside the RBCs, Ca^{2+} ionophores like A23187 are often used. The sudden increase in Ca^{2+} is known to trigger biochemical and morphological changes that finally result into the release of vesicles. Vesicles collected under this treatment (i) are free of cytoskeleton components, (ii) contain hemoglobin, and (iii) are enriched in GPI-anchored proteins (e.g., acetylcholinesterase and CD55) and raft lipids (Figure 3d). Two types of vesicles differing in size have been described: on one hand MVs with a diameter of ~150 nm and on the other hand nanovesicles (NVs) with a diameter of ~60 nm [67,134,135]. These two types of vesicles can be further distinguished based on biochemical contents. For instance, synexin and sorcin are the most abundant proteins after hemoglobin in NVs, while stomatin is highly enriched in MVs [67]. Two populations of Ca^{2+}-induced vesicles differing in size (~200 vs. ~120 nm in diameter) have further been confirmed by another

group [136]. The correspondence between the NVs described in [67] with the smallest MV population observed in [136] remains to be determined. Anyway, all these data suggest that different types of vesicles exist [136], which is an additional argument in favor of their formation and shedding from PM specific regions (see Section 5).

Mechanistically, budding and release of MVs under Ca^{2+} increase correlate with the production of diacylglycerol on the inner leaflet and its flop to the outer one [137]. Moreover, altered Ca^{2+} levels induce the recruitment and activation of Ca^{2+}-dependent enzymes such as scramblases with subsequent PS externalization, which appears to be one of the main features of MVs, even if PS-negative MVs have been reported [138]. Last but not least, increased Ca^{2+} level activates proteolytic enzymes such as calpains which disrupt the membrane:cytoskeleton connection, favoring vesiculation [67,139] (Figure 4b).

Since Ca^{2+} ionophore-induced MVs and those generated upon senescence and storage differ in protein composition, Bosman et al. suggested that alteration in intracellular Ca^{2+} concentration is not the primary factor in RBC MV generation in vivo nor in the blood banks [21]. We propose the alternative hypothesis that different types of MVs are produced by the same cell, either simultaneously or sequentially, generating MVs with differential lipid and protein compositions. In favor of this hypothesis, Le Van Kim et al. postulated that, only from day 35 of storage, RBCs become very old and exhibit a clustered form of Band3 and membrane microvesiculation [126], which could suggest that another process is responsible for MV release before day 35.

4.1.3. Microvesicles in Red Blood Cell Hemoglobinopathies

The concentration of RBC-derived MVs is increased in the blood of patients with hemoglobinopathies like thalassemia or sickle cell disease [140]. In α- and β-thalassemia, one of the globin chains is mutated leading to an insufficient quantity of hemoglobin heterotetramers and to the formation of hemoglobin precipitates within the erythroid precursors [141]. Blood MVs of those patients contain high concentrations of oxidized denatured globin chains, as well as catalase and peroxiredoxin-2, two enzymes involved in the control of the redox status (Figure 3e). Mechanistically, hemichromes (i.e., oxidized hemoglobin) bind to Band3, inducing the formation of Band3 dimers that are subsequently phosphorylated by tyrosine kinases. According to the Band3 vesiculation model (see Section 4.1.2), this phosphorylation leads to the weakening of the binding between the membrane and the cytoskeleton, as well as the clustering of Band3, finally leading to the membrane instability and the release of MVs [142].

Sickle cell disease is associated with the formation of hemoglobin S (HbS) polymers of deoxygenated hemoglobin. Sickle RBCs were the first pathologic cells described as a source of MVs [140]. Oxidative stress is nowadays recognized as a key component of the chronic inflammatory state associated with sickle cell disease. Reactive oxygen species-mediated damage to sickle RBC membrane proteins and lipids contribute to their rigidity and fragility [143]. It leads to membrane destabilization, poor deformability, changes of the hydration status, increase in intracellular Ca^{2+} and tyrosine phosphorylation of Band3 [110]. One of the consequence is the production of MVs which (i) contain Band3, glycophorin A and protein 4.1 but lack spectrin, (ii) exhibit increased Ca^{2+} level, (iii) contain, but are not enriched in, SM, PC, PS, PE nor in chol, (iv) present a similar acetylcholinesterase activity as in the parental cell membrane, and (vi) contain heme [140,144]. Thus, in haemoglobinopathies, oxidative damage inducing Band3 clustering appears as the initial key step in the microvesiculation process.

4.1.4. Microvesicles in Red Blood Cell Membrane Fragility Diseases

Besides haemoglobinopathies, some membrane fragility diseases like hereditary spherocytosis are associated with an increased vesicle release. This disease is caused by defects in proteins of the ankyrin complexes that vertically connect the membrane to the cytoskeleton [145]. When these interactions are compromised, membrane:cytoskeleton cohesion is lost, leading to membrane destabilization,

decrease of the RBC surface area-to-volume ratio with the formation of spherocytes that are trapped and destroyed in the spleen, resulting into hemolysis [146]. Elliptocytosis is another RBC membrane fragility disease that is linked to disruptions of horizontal cytoskeleton interactions, resulting into an alteration of the spectrin tetramer self-association. The RBCs are characterized by an elliptical or elongated shape and by a decreased deformability [147]. Shear-stress induced vesiculation could contribute to membrane loss in this disease but this is not supported by sound evidence.

A recent simulation study nevertheless revealed that (i) vesicles released from spherocytotic and elliptocytotic RBC membranes are more diverse in size than those released from healthy RBCs, and (ii) vesicles released from the elliptocytotic, but not from the spherocytotic, membrane may contain fragments of the cytoskeleton [148] (Figure 3f). However, to the best of our knowledge, no comprehensive analysis of the MV content from the blood of these patients is available in the literature. Even less information is available regarding their biogenesis and shedding from the PM. Several hypotheses have nevertheless been proposed to provide a link between cytoskeleton alteration and vesiculation in spherocytosis. First, since proteins of the ankyrin complex are needed for the vertical anchorage of the membrane to the cytoskeleton, their simple loss could result in reduced mechanical strength and the subsequent vesiculation. Second, secondary loss of cytoskeleton components may create an area of weakness in the membrane. Third, loss of Band3, the most abundant integral membrane protein of the RBC surface, could affect RBC membrane integrity [149]. However, the vesiculation process might differ depending on the underlying molecular defect (i.e., ankyrin, spectrin or Band3 mutation) and thus lead to MVs with different compositions [150]. Accordingly, Band3 has been found in MVs from spherocytotic RBCs with a defect in ankyrin or spectrin, but not from spherocytotic RBCs with a mutation in Band3 [150,151]. A comprehensive study on vesicle composition and shedding mechanisms in spherocytosis and elliptocytosis is therefore required.

4.2. Nucleated Cells

Most of the knowledge regarding the mechanism of MV biogenesis in nucleated cells comes from studies on cancerous cells [152,153]. Following cell stimulation, the shedding mechanism seems to start with the influx of Ca^{2+}, resulting in the activation of Ca^{2+}-dependent proteases, such as calpains. This in turn disrupts the membrane cytoskeleton with formation of membrane protrusions. At the same time, the Ca^{2+}-dependent scramblase is activated, leading to PS exposition to the external leaflet [154,155].

To start outward-budding vesiculation at the PM, membrane curvature is required and can be induced by several mechanisms (reviewed in [156]), including changes in lipid composition and asymmetry (see Section 5) and clustering of integral membrane proteins with an inherent curvature. However, little is known about the involvement of these processes in membrane vesiculation and only assumptions can be made. For example, while tetraspanins (integral membrane proteins known to gather together to form PM microdomains [157]) are often proposed as exosomal markers, specialized tetraspanins can also induce PM curvature [158], and their presence in shedding vesicles has been reported [83]. The establishment of a membrane bud could then participate in the sorting of proteins into the shedding MVs. Assisting proteins could also actively help sorting other proteins into MVs. For example, some matrix metalloproteases are delivered to nascent MVs through the association of vesicle-associated membrane protein 3 (VAMP3) with tetraspanin CD9 [159]. Other studies suggest that proteins can be sorted through the endosomal recycling pathway regulated by the GTPase ARF6. This idea arises from the observation that MHC class I, β1-integrin and VAMP3 are contained within MVs and known to be trafficked via ARF6 pathway [16,160].

The mechanisms underlying MV production involve multiple partners, depending on cell type and stimulation. However, Ras superfamily GTPases are postulated to be major mediators of MV formation. Indeed, activated RhoA promotes actin-myosin contraction that is required for MV formation through the downstream signaling of ROCK (Rho-associated coiled-coil containing kinases) and ERK (extracellular signal-regulated kinases) [161]. In cancerous cells in hypoxic conditions,

the small GTPase RAB22A colocalizes with budding MVs. Moreover, MV release under hypoxic conditions is completely abrogated upon RAB22A knockdown while it is modestly preserved under non-hypoxic conditions, suggesting that alternative mechanisms exist depending on the hypoxia state of the cell [162]. Muralidharan-Chari et al. showed that ARF6 is responsible for the regulation of MV release in tumor cells. Indeed, once ARF6 is activated, it promotes the recruitment of ERK to the PM. ERK then phosphorylates myosin light-chain kinase which in turn phosphorylates myosin light-chain. This allows the contraction of actomyosin at the necks of MVs and thus MV release [62]. Another pathway implies the endosomal sorting complexes required for transport (ESCRT). This complex was initially thought to only play critical role into exosome biogenesis from the endosomal membrane, but it was later described that some proteins from the ESCRT (named TSG101 and VPS4 ATPase) can be relocated from the endosomal membrane to the PM where they mediate the release of MVs [11]. Accordingly, Booth et al. visualized the budding of domains enriched in proteins from the ESCRT at the lymphocyte PM [9].

5. Microvesicle Biogenesis and Shedding—Role of Plasma Membrane Composition and Biophysical Properties

As highlighted above, data available for RBC microvesiculation upon aging in vivo and in vitro and upon Ca^{2+} intracellular boost are rapidly increasing. Accordingly, two models for MV shedding have been proposed (Figure 4a,b). On the other hand, it is not known whether there are different types of EVs that are simultaneously or sequentially released by cells and that could have different roles. Last but not least, the above models do not include the contribution of PM lipids in the vesiculation process. For instance, it is not known whether the budding of MVs could occur from specific regions of the PM and if some specific lipid domains could represent the starting point of the vesiculation process. Although only limited data are available in this respect, most of them appear to converge to the idea that (modulation of) PM lipid content (Section 5.1), transversal asymmetry (Section 5.2) and lateral heterogeneity (Section 5.3) may play a significant role in the vesiculation process.

5.1. Plasma Membrane Lipid Composition

As highlighted in Section 3.3, MVs and the PM from which they derive can differ in terms of lipid composition, suggesting a selective sorting into MVs. In this section, we summarize current knowledge of the role of specific SLs and chol in the formation and release of MVs. Comparison to exosome formation is sometimes provided. However, for extended information regarding the role of SLs and chol in the biogenesis of exosomes, please refer to [163,164], respectively.

5.1.1. Sphingolipids and Sphingomyelinases

SLs exhibit both structural and signaling roles. Among SLs, Cer not only serve of structural roles in biomembranes through its conical shape (see below), but also have a variety of effects on signal transduction and the regulation of cell function, particularly the potentiation of signaling pathway leading to cell death. On the other hand, sphingosine 1-phosphate is an important signaling lipid, controlling cell growth, adhesion, migration, survival and inflammatory response, highlighting the importance to maintain an adequate Cer/sphingosine 1-phosphate balance [165]. Among other ways, Cer can be generated upon hydrolysis of SM through the action of SMases. Neutral SMases (n-SMases) are found in the Golgi and the endoplasmic reticulum or in the Golgi and the nucleus but also at the PM [166]. Although n-SMases have been shown to facilitate exosome biogenesis (reviewed in [163]), their role in MV biogenesis has been less explored. One recent study shows that n-SMase inhibition increases the basal release of MVs from epithelial cells while decreasing secretion of exosomes, suggesting that n-SMase differentially controls the release of exosomes and MVs in these cells [167]. This contrasts with the observation by Bianco et al. that n-SMase activity is not required for MV shedding from the cell surface of primary microglia under stimulation with ATP, a very efficient way to promote EV release [168]. Besides n-SMase, acid SMase (a-SMase) is able to generate Cer in

lysosomes, but also at other subcellular places. Indeed, an acidic environment also exists outside of lysosomes and the membrane lipid composition could alter the Km of the enzyme, thus allowing a-SMase activity at higher pH [169]. Thus, after certain stimuli, a-SMase can reach the outer PM leaflet by fusion of secretory lysosomes with the PM [170]. Moreover, the enzyme can also be secreted by myeloid cells and the vascular endothelium. The molecular mechanisms behind regulation of a-SMase are only partially characterized (for a review, see [169]). The role of a-SMase in MV shedding has been evidenced in a large diversity of cells under stress membrane conditions (e.g., sickle cell disease, RBCs upon storage) or danger signals (e.g., ATP). For instance, RBC membrane alteration in sickle cell disease enhances SMase activation, resulting in strong increase of production and storage of sphingosine and sphingosine 1-phosphate as well as MV generation. Treatment with amitryptiline, a functional inhibitor of a-SMase, reduces MV generation both in vitro and in vivo. As suggested by the authors, this mechanism could be applicable to other RBC disorders [171]. Acid sphingomyelinase is also implicated in the biogenesis of MVs from RBCs during storage [172] (Figure 4c). Moreover, Bianco et al. have demonstrated that ATP-induced MV shedding by glial cells upon ATP activation of the P_2X_7 receptor is associated with the rapid activation and PM translocation of a-SMase [168]. The contribution of a-SMase in MV shedding has been recently confirmed in macrophages upon ATP stimulation [173].

Although the above examples support a role for SMase in MV shedding, the link between Cer production and membrane blebbing is still unclear. Alterations of the PM biophysical properties due to Cer generation could partly provide this link, based on the following features. First, Cer has a cone-shaped structure that can give a spontaneous curvature to the membrane. This property, combined with the fact that Cer synthesized in the external leaflet may be redistributed to the inner one, could lead to membrane evagination [163,174]. Second, hydrolysis of SM, which has a high affinity for chol in membranes, results in increased chol efflux from the PM to intracellular membrane [175] and increased fluidity. Third, several studies report the capacity of Cer to form domains. For instance, real time fluorescence imaging on lipid monolayers treated with SMase has revealed Cer-enriched domains with shape and long-range organization controlled by line tension and dipolar electrostatic repulsion [176]. Hence, hydrophobic Cer molecules separate from other lipids in membranes and self-associate into small Cer-enriched domains which have the tendency to spontaneously fuse into large Cer-enriched platforms easily detectable by fluorescence microscopy (reviewed in [169]). Moreover, although chol- and Cer-enriched domains are dissociated, they are largely interplayed [177] and Cer competes with chol for the formation of domains with SM [178]. Finally, substantial amount of n-SMase PM activity in human skin fibroblasts has been shown to reside at the cytosolic leaflet of SM/Cer-enriched caveolae, suggesting that metabolism of these lipids might occur locally ([166]; see also below).

Besides Cer and sphingosine 1-phosphate, psychosine (also called galactosylsphingosine) has been shown to play a role in MV shedding. This inverted cone-shaped SL progressively accumulates in brain membrane of Krabbe disease (a genetic leukodystrophy due to mutations in the galactosylceramidase gene) and causes demyelination by the killing of oligodendrocytes. Using Twitcher mouse as a model for Krabbe disease, the group of Bongarzone showed ten years ago that psychosine specifically accumulates in lipid rafts. This accumulation occurs together with an increase in chol in these domains, as well as changes in the distribution of the raft markers flotillin-2 and caveolin-1. Altogether, these alterations lead to the deregulation of raft-associated signaling [179]. More recently, the group established a link between raft disruption, membrane microvesiculation and demyelination. For instance, using RBCs and oligodendrocytes, they showed that psychosine disrupts SM-enriched domains and increases the rigidity of local PM areas while promoting the shedding of MVs. Areas of higher rigidity have been confirmed in Twitcher myelin and correlate with higher contents in psychosine and myelin microvesiculation [180] (see also Section 5.3.5).

5.1.2. Cholesterol

As highlighted in Section 3.3, reliable information regarding chol enrichment in MVs as compared to the PM is still lacking. In the same way, only a few studies have been dedicated to the importance of chol to MV biogenesis and shedding, a role that has been proposed for exosome release (reviewed in [164]). Using flow cytometry and EVs stained with anti-chol antibody, Osteikoetxea et al. have shown stronger staining for exosomes than MVs whereas the two populations are enriched in GM1 [87]. Moreover, living keratinocytes labeled by the liquid-disordered (L_d) marker DiIC18 and the liquid-ordered (L_o) GM1 marker cholera toxin B subunit reveal submicrometric lipid domain separation together with spontaneous vesiculation of the L_d domains and cortical cytoskeleton detachment from the membrane, phenomena enhanced by chol depletion by methyl-β-cyclodextrin (mβCD) [181]. In contrast, depletion of chol from the PM of THP-1 monocytes leads to impaired membrane shedding and reduction of MV abundance [39] while loading of the same cells with chol stimulates MV release [182]. Besides the possibility that high mβCD concentration could affect PM integrity and extract other molecules than chol, one hypothesis to reconcile these observations is the differential chol PM level and PM:cytoskeleton anchorage strength which could strongly vary from one cell to another [183].

Chol could contribute to the microvesiculation process through its ability to modulate PM lipid order and/or via its capacity to cluster into lipid domains. We indeed specifically found that chol-enriched domains are lost by vesiculation upon RBC storage at 4°C, suggesting they could represent sites for vesiculation upon aging. While additional work is needed to demonstrate the contribution of chol in the MV process, our data are supported by theoretical work [184] and biophysical experiments on model membranes [185,186] that have proposed the line tension associated with the domain boundary as driving force for specific lipid domain vesiculation.

5.2. Plasma Membrane Transversal Asymmetry

Cell membranes exhibit transbilayer asymmetry, first hypothesized in the 70′s by Bretscher [187]. This asymmetry contributes to PM complexity and diversity by the differential repartition between the two leaflets of lipid molecular shapes, lipid order as well as lipid charge and dipole, thereby leading to optimal physiological output. SM, glycosphingolipids (GSLs) and PC are preferentially found in the outer PM leaflet of mammalian cells whereas PE, PS and phosphatidylinositol-4,5-biphosphate (PIP_2) are mostly located in the inner leaflet.

Lipid asymmetry participates in several cellular functions involving the formation of high local membrane curvature. For example, inner PIP_2 contributes to phagocytosis [188]. Moreover, translocation to the outer leaflet of PLPs normally restricted to the inner one (e.g., PE and PS) has been proposed to play a role in a large variety of cell events. First, it participates in hemostasis by regulation of thrombin production [189,190] (see Section 1). Second, appearance of PS and PE at the cell surface often accompanies RBC microvesiculation during storage, resulting into RBC removal [191]. However, as explained at Section 3.3, this is not always the case. Third, PS surface exposure contributes to the clearance of apoptotic cell bodies [192], viewed as a cellular response contributing to the shedding of intracellular Ca^{2+} excess allowing the cell to recover after stress and apoptotic triggers [193]. In parallel to PS externalization, SM flips to the inner leaflet, where it is hydrolyzed to Cer by an intracellular n-SMase. SM hydrolysis disturbs its tight interaction with chol, resulting in chol redistribution from the PM towards the cell interior. Reduced SM and chol contents in turn alter PM biophysical properties, allowing for membrane blebbing and vesicle shedding [194].

5.3. Plasma Membrane Lateral Heterogeneity

5.3.1. General Features

Although membrane transversal asymmetry is well accepted, lateral distribution within the same leaflet in lipid domains has been subjected for a long time to intense debates. Limited

availability of reliable fluorescent probes, poor lipid fixation, imaging artifacts due to membrane protrusions/projections and utilization of highly disruptive methods of isolation have been often denounced. Moreover, lipid domains have sometimes been reported under non-physiological conditions, potentially explaining the discrepancies between the results obtained by different research groups (reviewed in [183]). Nevertheless, membrane lateral heterogeneity has been shown at different scales, times, compositions and regulations, resulting in a wide diversity of domains in cell membranes. The concept of lipid rafts, introduced in the 90′s by Simons et al. is used to describe unstable (seconds) nanoscale assemblies (<100 nm) enriched in SLs, chol and GPI-anchored proteins [195,196]. Besides rafts, various types of membrane domains are characterized by their enrichment in specific proteins, such as caveolae [197] and tetraspanin-enriched domains [157]. Rafts can sometimes be stabilized to form larger platforms through protein:protein and protein:lipid interactions [198]. In the past decades, owing to the development of new probes and imaging methods, morphological evidence for stable (min vs. sec for rafts) submicrometric domains (>200 nm in diameter vs. <100 nm for rafts) has been reported in artificial models [199–201], highly specialized biological membranes [200,202] and a variety of cells from prokaryotes to yeast and mammalian cells [203–209]. A substantial, albeit non-exhaustive, list of examples is presented in [183] and [210]. Finally, lipid domains could be not stably present but transiently generated by the hydrolysis of specific lipids. An example is the SM degradation by SMase that can form Cer-rich domains with diameters of ~200 nm up to several micrometers [211,212] (see also Section 5.1.1).

It is generally admitted that lipid domains present a different lipid order from the surrounding membrane. This was first suggested in the 90′s by the lipid raft hypothesis, which proposed that sterols and SLs, due to their favorable interactions, can self-aggregate into domains of higher lipid order as compared to the surrounding lipids (bulk membrane). Later, evidence was provided in membrane models. First, sterol-containing biomimetic model membranes, including planar supported lipid layers and giant unilamellar vesicles (GUVs), exhibit the coexistence of two liquid phases, the L_o phase enriched in chol and SLs and the L_d phase enriched in unsaturated lipids [213,214]. Second, giant PM vesicles (GPMVs) derived from living cells [199] reveal that L_o and L_d phases in natural PM can assume a wide range of lipid order states [215]. Finally, regions of different lipid order than the bulk have been shown at the surface of several cells including RBCs, platelets and monocytes [216–220] (see below).

Using a combination of mechanical modeling and GUV experiments, Phillips et al. showed that lipid domains can adopt a flat or dimpled morphology, depending on domain spontaneous curvature, boundary line tension and size [221]. Hence, several studies support the possibility that molecule inclusion/exclusion in lipid domains of differential lipid order could provide a way for their sorting into MVs. First, L_d phases tend to spontaneously reside in curved membrane regions of GUVs whereas L_o phases are preferentially localized in flat regions [185]. Second, modification of the outer PM leaflet by a chol/SM-binding protein (Ostreolysin A) promotes formation of MVs from Madin-Darby canine kidney (MDCK) cells. These MVs exhibit a significant enrichment in lysophosphatidylcholine and chol and could result from the Ostreolysin-binding to chol/SM membrane domains, suggesting that Ostreolysin-induced vesiculation is accompanied by specific lipid sorting into membrane patches that bud from the PM to create vesicles and tubules [222]. Third, submicrometric lipid domain separation together with spontaneous vesiculation of the L_d domains has been provided in living keratinocytes labeled by the L_d marker DiIC18 and the L_o GM1 marker cholera toxin B subunit. Such vesiculation is increased by chol depletion, which further enhances L_o/L_d domain separation and detachment of the cortical cytoskeleton from the membrane [181]. Finally, evidence for lipid domains and their possible role in membrane vesiculation are provided here below for RBCs (Section 5.3.2), platelets (Section 5.3.3), immune cells (Section 5.3.4), nervous cells (Section 5.3.5) and tumor cells (Section 5.3.6). In all these sections, we started by summarizing the state of the art regarding evidence for lipid domains and thereafter provided some clues for their possible involvement in membrane vesiculation.

5.3.2. Red Blood Cells

Stable lipid domains at the RBC surface have been evidenced and characterized by our group. They were first revealed by vital fluorescence and/or confocal imaging thanks to the trace insertion at the external PM leaflet of fluorescent analogs of SM, PC, GM1 and Cer (Figure 5a) [204,207,223]. They were later confirmed using fluorescent toxin derivatives specific to endogenous SM [203] and chol (illustrated at Figure 5a for chol) [206], validating a posteriori the use of fluorescent SM analogs to study the behavior of endogenous SM. Those domains are differentially dependent on the chol content, the membrane:cytoskeleton anchorage and the membrane tension. They also differentially associate to high and low RBC membrane curvature areas and exhibit a different response to RBC mechanical stimulation [224]. Altogether, our data suggest the coexistence at the RBC surface of at least three types of domains (i) those mostly enriched in chol, which gather in high-curvature membranes during the RBC deformation, (ii) those mostly enriched in GM1 which might be associated with the Ca^{2+} entry regulation during deformation, and (iii) those mostly enriched in SM and chol, which might regulate the Ca^{2+} efflux during the shape restoration after deformation [183,203,206,210,220,224,225]. Using other probes (e.g., cholera toxin B subunit conjugates, antibodies or treatment with PlcHR2, a phospholipase C/SMase from *Pseudomonas aeruginosa*) and techniques (e.g., SDS-digested freeze-fracture replica labeling), other groups have evidenced stable domains enriched in GM1 [226], GM3 [227] or Cer [228].

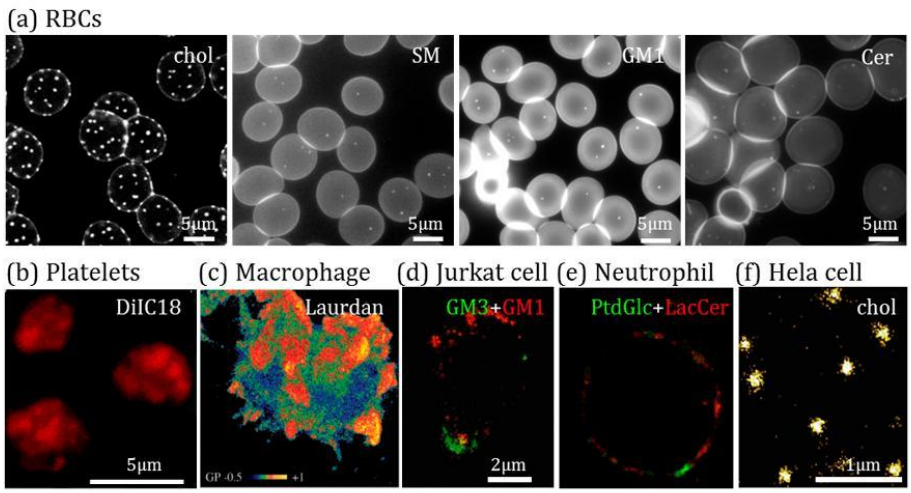

Figure 5. Visualization of plasma membrane lipid domains. (**a**) RBCs labeled for chol with Theta-D4-mCherry or with boron-dipyrromethene-sphingomyelin (BODIPY-SM), -GM1 (BODIPY-GM1) or –ceramide (BODIPY-Cer) and analyzed by fluorescence or confocal microscopy. (**b**) Platelets labeled with DilC18 and analyzed by fluorescence microscopy. (**c**) Macrophage labeled with Laurdan and vizualized by two-photon microscopy. (**d**) Jurkat cell labeled for GM3 and GM1 using anti-GM3 serum and cholera toxin B subunit, respectively, and visualized by confocal imaging. (**e**) Human neutrophil stained for phosphatidylglucoside (PtdGlc) and lactosylceramide (LacCer) and examined by stimulated emission depletion microscopy (STED). (**f**) HeLa cell labeled for chol with Theta-D4-DRONPA and processed by photoactivated localization microscopy (PALM). Adapted from (**a**) [225]; (**b**) [229]; (**c**) [230]; (**d**) [231]; (**e**) [232]; (**f**) [233].

Besides those domains, detergent-resistant membranes (DRMs) enriched in stomatin, flotillins, Glut-1, aquaporin-1 and Band3 have been evidenced [234,235]. Those raft-like domains have been linked to the *Plasmodium falciparum* infection [236] and to vesicle release upon Ca^{2+} influx [66,67].

Additional lines of evidence for the existence of lipid domains at the RBC surface are based on multiphoton microscopy of Laurdan-labeled RBCs and AFM imaging of unlabeled RBCs. Domains of

various sizes and lipid order have been shown [104,205,220,237,238], suggesting that a large variety of lipid domains might exist at the RBC membrane.

Lutz et al. already provided in 1976 the first indirect clue that RBCs could vesiculate from specific areas of the PM. In fact, they observed that vesicles from sheep RBCs stored at 4°C exhibit the same PLPs as the ghost membrane but a 2-fold increase of lipid-to-protein ratio and an enrichment in glycoproteins, suggesting that those proteins are mobile and can cluster in specific membrane areas, leading to vesiculation [239]. From that time, several observations have supported the potential involvement of lipid domains in RBC membrane vesiculation.

First, DRMs can be prepared from MVs [240] and the MVs present raft-associated lipids and proteins. Indeed, MVs released upon Ca^{2+} increase contain GPI-anchored proteins [241] and stomatin [65–67]. Interestingly, RBCs from patients suffering from paroxysmal nocturnal hemoglobinuria do not present GPI-anchored proteins and exhibit a disturbed vesiculation capacity [242]. Moreover, in patients with stomatocytosis associated with stomatin deficiency, Ca^{2+}-induced MVs are more numerous and of abnormal size as compared to healthy individuals [243], suggesting that stomatin is important, but not essential, for the regulation of proper MV shedding.

Second, MV shedding is highly dependent on chol, which is essential for both lipid rafts and submicrometric lipid domains. As a matter of fact, Santos et al. have postulated that the total RBC membrane chol content is declined by the release of chol-enriched vesicles [244]. Moreover, upon strong chol depletion (at high mβCD concentrations) in erythroleukemia cells, PS movement to the external leaflet upon addition of a Ca^{2+} ionophore is inhibited [245], suggesting the involvement of lipid domains in transversal lipid asymmetry associated with membrane vesiculation. At low concentrations, mβCD appears to instead increase the number of MVs released [246]. These a priori contradictory observations could partly be explained by the very different mβCD concentration used.

Third, we recently provided clues for the vesiculation of chol- and SM/chol-enriched domains upon RBC storage at 4 °C for <15 days [224]. Our data are, at first glance, in conflict with the observations that (i) RBCs and MVs obtained during storage in blood banks for ~40 days do not exhibit any difference in the main PLP classes (i.e., PC, PE, PS and SM) [92], and (ii) RBCs and MVs from leukoreduced stored RBC units for >50 days show similar PLP composition, except PS [91]. Differences could be related to chol enrichment (not assessed in the two latter studies, to the best of our knowledge), conditions of blood conservation (leukoreduction or not) and/or time of storage (<15 vs. 40 and >50 days).

Finally, Dinkla et al. showed that the formation of Cer-enriched platforms upon RBC incubation with a-SMase is accompanied by the induction of membrane irregularities enriched in the GPI-anchored protein CD59 [98]. Likewise, upon addition of Cer at the RBC membrane, slow transformation of the biconcave RBC in echinocyte has been shown, suggesting that Cer is responsible for forming membrane spicules thanks to its conical shape [174].

We recently proposed a hypothesis for the control of vesicle formation from lipid domains. By labeling with Laurdan, we revealed that chol-enriched domains exhibit lower lipid order than the rest of the membrane in RBCs at resting state. In contrast, upon RBC vesicle release, the lipid order of the domains increases, leading to a lower lipid order difference between domains and the bulk [220]. We therefore speculated that lipid domains represent specific sites of MV budding by a mechanism driven by the lateral tension applied by the cytoskeleton and its impact on the line tension at phase boundary [220]. A local detachment of the cytoskeleton from the membrane and the echinocytic shape formation seem to be required for normal vesiculation in RBCs. It was already proposed in 2008 that the membrane:cytoskeleton uncoupling favors the coalescence of small rafts into large domains able to curve and to detach from the membrane [240]. Moreover, in comparison to healthy RBCs, fresh spherocytotic RBCs present higher differential lipid order between lipid domains and the bulk membrane together with an accelerated initiation of domain vesiculation upon aging. This suggests that the cytoskeleton pressure could give the main contribution that controls the differential lipid order and drives RBC vesiculation [220].

5.3.3. Platelets

The first proof for lateral lipid heterogeneity at the PM of activated platelets occurred in 1996 when Dorahy et al. isolated at 4°C DRMs enriched in GSLs, chol and GM1 [247]. A few years later, Gousset et al. used fluorescence microscopy and Fourier transform infrared spectroscopy to show that, under platelet activation (either by chilling or thanks to thrombin or collagen), a reversible phase separation in large domains takes place (Figure 5b) [229]. This phase separation, as well as the platelet activation, is highly dependent on the membrane chol content, as both are abrogated by mβCD [248,249]. Those domains have been thought to be involved into platelet early activation by recruiting key receptors like GpVI (a collagen receptor) or FcγRIIa (a low affinity receptor for immune complexes), thus allowing the recruitment and the spatio-temporal activation of tyrosine kinase-dependent pathways [249]. On the other side, chol-enriched domains also appear as sites where the phosphoinositide (PI) metabolism is highly active [250]. The presence of PIP_2 induces interactions with the actin cytoskeletal elements through their plekstrin homology (PH) domains [251]. Thereby, an artificial enrichment of PIP_2 in membrane increases the membrane:cytoskeleton energy (and decrease the vesicle release upon activation) while the artificial expression of a PH domain, which sequestrates PIP_2, results in a reduction of the cytoskeleton membrane adhesion energy [252].

As first evidence for the importance of lipid domains in platelet vesiculation, their activation by thrombin leads to translocation of intracellular stomatin to the PM. Moreover, stomatin is selectively sorted into released MVs while flotillin, another raft marker which exposes different subcellular localization in resting platelets, is excluded [253]. This supports the existence of different types of platelet rafts and maybe vesiculation mechanisms. Several years later, it has been shown that alteration of chol content and/or distribution using mβCD and filipin reduces the release of PS-bearing MVs upon Ca^{2+} activation. While the MVs and the resting platelets present the raft-associated GM1 on their surface, the stimulated platelets from which the MVs originate lose the GM1 signal, suggesting its loss by vesiculation [254].

Lipid rafts in platelets are also connected to platelet membrane deformation. The addition of a low amount of short-chain PLP analogs (1–2% of endogenous PLPs) into the outer leaflet of human resting platelets induces the formation of cell membrane extensions enriched in GM1. Chol depletion impedes formation of these PM extensions, GM1 enrichment and actin polymerization [255]. The same observation has been obtained on thrombin-activated platelets [255]. These data are consistent with the previous observation that chol accumulates in the tips of filopodia and the leading edges of spreading cells [256]. Moreover, PIP kinases are particularly active in lipid domains. After platelet activation and subsequent increase of the intracellular Ca_{2+} concentration and filopodia extension, they are shown to be cleaved by calpain [250]. This would in turn decrease the PIP_2 levels in domains and *in fine* the adhesion between the membrane and the cytoskeleton at those places, favouring vesicle release [257]. This reinforces the idea that lipid rafts could actively participate to membrane dynamic and actin reorganization.

5.3.4. Immune Cells

Stable lipid domains have been shown on resting macrophages at physiological temperature by two-photon microscopy [230]. Those domains are highly ordered, chol-dependent and grouped at protrusions (filopodia), adhesion points and cell-cell contacts (Figure 5c).

Lipid domains are also relevant to immune cells upon activation. First, in response to chemoattractants, T lymphocytes and neutrophils polarize and migrate, and this is accompanied by lipid coalescence to form domains with different properties at the front and rear of the cell [231,258] (Figure 5d). Although differences have been shown according to cell type and mode of migration (transmigration or migration in a two-dimensional system), domains located at the uropod (rear) are generally (i) resistant to Triton X-100 extraction (and thus highly ordered), (ii) enriched in GM1 and GPI-anchored proteins, and (iii) associated with receptors and signaling molecules involved in cell adhesion [259–261]. Regarding domains at the leading edge, they are (i) sensitive to Triton

X-100 extraction, as they are not as ordered as uropod domains, (ii) enriched in GM3 and PIP_2, and (iii) associated with the machinery that induces localized actin polymerization and that senses the environment (G-coupled receptors, PI3kinase, among others) [259,261]. Domains at both cell edges depend on the membrane chol content, and their reversible disappearance inhibits the cell polarization as well as the chemoattractant-stimulated actin polymerization [261].

A second example for the implication of lipid domains in immune cells upon activation occurs in phagocytes once at the site of infection. Nakayama et al. showed that neutrophil phagocytosis signaling through the CD11b/CD18 integrins is dependent on Lyn-coupled lactosylceramide (LacCer)-enriched domains. Those domains colocalize with integrins in actin-enriched phagocytotic cup regions [262]. Moreover, as shown by stimulated emission depletion microscopy (STED), those domains are distinct from phosphatidylglucoside (PtdGlc)-enriched domains, which might on their side mediate the differentiation of neutrophils as well as their apoptosis (Figure 5e) [232].

Chol is not only essential for monocyte deformation [263] but seems also to be involved in their vesiculation, as revealed by the fact that chol depletion decreases MV abundance [39] whereas chol loading stimulates their release [182]. These MVs contain TF and PSGL-1, which are both found in DRMs. Moreover, disruption of rafts by mβCD leads to relocalization of these proteins in non-raft fractions [39].

In ATP-activated macrophages, an elegant study has demonstrated the involvement of lipid rafts in the regulation of membrane receptor trafficking onto filopodia in the course of MV generation. Macrophages release MVs enriched in TF, integrin β1 and PSGL-1 at the tip of filopodia. When filipin is added to perturb raft dynamics, TF translocation onto filopodia and enrichment in MVs are lost, whereas production of PS^+-MVs and the associated prothrombinase activity are unaltered, suggesting that different mechanisms of sorting and/or MV production also exist in those cells [264]. Another recent study postulates that TF is maintained in a noncoagulant/cryptic state through SM at the PM of macrophages until vesiculation. Accordingly, when macrophages are stimulated with ATP, the a-SMase is translocated to the PM and the hydrolysis of SM increases both TF activity at the cell surface and the release of TF^+-MVs, without changing the PS externalization. It has been suggested by the authors that inactive TF is associated with rafts and is activated by disruption of these structures [173]. Although at first glance in contradiction with the idea that MVs are shed from lipid domains, this observation could once again be related to the fact that PM exhibits different types of lipid domains with different potential to vesiculate.

5.3.5. Nervous Cells

DRMs have been evidenced on neurons as well as glial cells. Their composition varies depending on the cell type, the activation state and the pathological conditions. In agreement with observations acquired via the DRM technique, nanometric domains with specific biophysical properties (i.e., stiffer than the surrounding membrane) have been revealed by AFM on hippocampal neurons. Those domains are enriched in GPI-anchored proteins and increase in size without changing in stiffness upon actin depolymerization [265]. In oligodendrocytes, signaling domains enriched in galactosylceramide and sulfatide have also been shown to coalesce in submicrometric domains under activation by apposed membranes in wrapped myelin. This process implies actin filament depolymerization and regulates the lateral diffusion of myelin proteins [266,267]. In microglial cells, the ATP receptor P_2X_7 is localized in raft domains [268].

Those lipid domains have been shown to depend on membrane chol, gangliosides and Cer contents [269,270]. Their integrity is essential for major neuronal and glial functions like the neurotransmitter signaling [271], the survival and proliferation signaling in oligodendrocytes [272] and pro-inflammatory response in microglia [270]. As a consequence, they are often associated with neurodegenerative diseases. For example, resulting from a defective SL metabolism, their composition and biophysical properties are altered in the brain cortex from patients suffering from Alzheimer disease. This disruption has been linked to an impaired generation and degradation of amyloid-β

peptide [273,274]. In Parkinson's disease, the mutation of the protein DJ-1, which is associated with rafts in astrocytes, results in raft disruption and consequent glutamatergic signaling disruption [275]. Lipid domains are also affected in lipid-related diseases (e.g., Krabbe disease), where a defective enzymatic activity leads to altered lipid raft signaling pathways [179,276].

In microglial cells, activation of the raft-associated ATP receptor P_2X_7 leads to the release of MVs [268] in an a-SMase-dependent manner [168]. In brain tumors, an oncogenic factor is released in MVs containing flotillin-1 [277]. Diseases where the membrane lipid content is altered are also associated with an abnormal vesicle release. For example, in Krabbe disease, the abnormal accumulation of psychosine in the oligodendrocyte membrane disrupts lipid rafts [179]. This leads to the disruption of several signaling pathways but also to an increased rigidity of localized areas promoting the shedding of MVs [180], thought to be essential in the demyelination observed in this disease (see also Section 5.1).

5.3.6. Cancer Cells

Lipid domains have also been observed at the surface of various cancerous cells. First, AFM imaging of purified membranes from human breast cancer cells has revealed the presence of submicrometric domains which contain chol, SM and flotillin 1 [278]. Second, super-resolution fluorescence microscopy of HeLa cells has demonstrated two types of lipid domains of ~250 nm in diameter that are differentially enriched in chol and SM [279] (Figure 5f). Third, electron microscopy of Jurkat T-cells indicates the coexistence of SM- and GM1-enriched domains [280].

Moreover, the lipid domain composition is suggested to be different in the cancerous cells *vs* healthy cells. For example, the carcinoembryogenic antigen (CEA) is not only localized at the apical surface of some colon cancer cells, as in healthy colon epithelial cells, but also at their basolateral side. This observation has been explained by the increased pH within the Golgi which apparently affects GPI-anchorage of CEA in rafts [233]. As another example, Apaf-1 (Apoptotic peptidase activating factor 1, a protein involved in the apoptosome) is abnormally located in rafts instead of in the cytosol in diffuse B cell lymphoma. Upon raft perturbation by mβCD, cytosol location of Apaf-1 is restored and the apoptosome can be correctly assembled [281]. Finally, in multidrug-resistant tumor cells, caveolae-associated caveolin-1, phospholipase D, chol and SM are upregulated, supporting the hypothesis that multidrug-resistance of tumor cells could partially result from lipid domain modifications [282].

As lipid domain modification seems to actively participate to the phenotype of cancerous cells, they could represent interesting targets for anti-cancer treatments. Actually, edelfosine, a synthetic alkyl-lysoPLP with anti-tumor activity, has been shown to destabilize synthetic membranes composed of POPC (palmitoyloleoylphosphatidylcholine)/SM/chol or SM/chol [283]. It preferentially localizes in rafts in lymphoma cells, where it inhibits the PI3K/Akt proliferation signaling pathway and promotes the recruitment of the death receptor Fas [283,284]. Likewise, saponins are widely used in medicine for their anti-cancerous activity [285]. One steroid saponin, ginsenoside Rh2, has been reported to disrupt rafts and to consequently lead to apoptosis, either via the inactivation of the PI3K/Akt pathway [286] or via the activation of the Fas pathway [287]. We recently showed that the activity of ginsenoside Rh2 is decreased by membrane chol, renewing the idea that saponin cytotoxicity is only ascribed to an interaction with membrane chol [288].

Significant evidence supports a role for lipid domains in cancerous MV biogenesis and shedding. For instance, murine leukemia cells release MVs specifically enriched in mammary tumor virus-induced antigens and in chol and SM, suggesting a lipid raft origin [289]. Another example is that the heat shock protein HSP-70-1A, which is located at low concentrations in the cytosol of healthy cells, is upregulated and found at the PM of tumor cells and is associated with increased resistance to radiotherapy and poor survival chances. Biophysical studies on supported lipid bilayers indicate that its membrane location results from interaction with the anionic lipid PS and is enhanced

by saturation of the lipid chains as found in dipalmitoylphosphatidylserine (DPPS). Upon addition of chol in the lipid bilayers made of DPPS/DPPC, membrane blebbing occurs [290].

6. Future Challenges

As EVs appear to be emerging as targets for disease diagnosis and therapy, a deeper understanding of their composition, biogenesis and shedding mechanisms as well as their pathophysiological roles is required. Whereas EV pathophysiological effects and composition have been extensively studied, biogenesis and shedding mechanisms are still poorly understood. As already stressed by many other reviews, the inherent complications of working with EVs are the extreme versatility of cells to produce different EV subpopulations with distinct sizes, cargoes, morphologies and probably distinct biogenesis mechanisms. This is in addition to the already complicated mixture of EVs in body fluids which contain EVs from different cell origins. In this context, there is a great need to improve the standardization of isolation and analysis of EVs, including identification of specific markers. Hence, once isolated, it is essential to determine MV diversity in a specific physiological process or disease, while providing a comprehensive proteomic and lipidomic analysis in comparison with the PM from which they originate. MVs derived from a same cell type should also be compared in different pathophysiological contexts.

Concerning MV biogenesis, it is still unclear whether a cell is able to simultaneously release distinct populations that contain specific types of molecules or if the content is determined by distinct stimuli, for instance the stage of the disease. Answering these questions will require to determine whether MVs originate from distinct PM areas differentially enriched in specific molecules along physiological processes and disease evolution. The hypothesis behind this is that sorting of proteins or lipids into MVs may rely on their accumulation or exclusion in lipid domains. Several lines of evidence provided in this review support the implication of those domains in membrane vesiculation. First, the lipid raft as MV origin hypothesis is supported by several studies. However, one should remain cautious, since the depletion of membrane chol content to explore the implication of lipid rafts in this process is not sufficient to draw sound conclusions. Second, the biophysical properties of the lipid domains are in accordance with theoretical models and imply the importance of the line tension on domain edge due to differential lipid organization/composition between domains and the bulk membrane. Third, upon membrane:cytoskeleton uncoupling, small rafts are able to coalesce into larger domains able to curve and detach from the membrane, suggesting the interplay between lipid domains and the cytoskeleton in the vesiculation process. Confirming these hypotheses will depend on the development of live cell imaging methods and reliable probes to define the diversity of MVs and to follow the dynamics of lipid domain conversion into MVs.

Author Contributions: All authors contributed to the writing of the review. Illustrations, H.P.

Acknowledgments: We acknowledge funding from UCL (Fonds Spéciaux de Recherche, FSR and Actions de Recherche Concertées, ARC), the F.R.S-FNRS and the Salus Sanguinis foundation. We apologize to all colleagues whose work was not cited due to space constriction.

Conflicts of Interest: The authors declare no conflict of interest.

References

1. Deatherage, B.L.; Cookson, B.T. Membrane vesicle release in bacteria, eukaryotes, and archaea: A conserved yet underappreciated aspect of microbial life. *Infect. Immun.* **2012**, *80*, 1948–1957. [CrossRef] [PubMed]
2. Robinson, D.G.; Ding, Y.; Jiang, L. Unconventional protein secretion in plants: A critical assessment. *Protoplasma* **2016**, *253*, 31–43. [CrossRef] [PubMed]
3. Gould, S.J.; Raposo, G. As we wait: Coping with an imperfect nomenclature for extracellular vesicles. *J. Extracell. Vesicles* **2013**, *2*. [CrossRef] [PubMed]
4. Raposo, G.; Stoorvogel, W. Extracellular vesicles: Exosomes, microvesicles, and friends. *J. Cell Biol.* **2013**, *200*, 373–383. [CrossRef] [PubMed]

5. Gyorgy, B.; Szabo, T.G.; Pasztoi, M.; Pal, Z.; Misjak, P.; Aradi, B.; Laszlo, V.; Pallinger, E.; Pap, E.; Kittel, A.; et al. Membrane vesicles, current state-of-the-art: Emerging role of extracellular vesicles. *Cell. Mol. Life Sci.* **2011**, *68*, 2667–2688. [CrossRef] [PubMed]
6. Sedgwick, A.E.; D'Souza-Schorey, C. The biology of extracellular microvesicles. *Traffic* **2018**, *19*, 319–327. [CrossRef] [PubMed]
7. Turturici, G.; Tinnirello, R.; Sconzo, G.; Geraci, F. Extracellular membrane vesicles as a mechanism of cell-to-cell communication: Advantages and disadvantages. *Am. J. Physiol. Cell Physiol.* **2014**, *306*, C621–C633. [CrossRef] [PubMed]
8. Kowal, J.; Arras, G.; Colombo, M.; Jouve, M.; Morath, J.P.; Primdal-Bengtson, B.; Dingli, F.; Loew, D.; Tkach, M.; Thery, C. Proteomic comparison defines novel markers to characterize heterogeneous populations of extracellular vesicle subtypes. *Proc. Natl. Acad. Sci. USA* **2016**, *113*, E968–E977. [CrossRef] [PubMed]
9. Booth, A.M.; Fang, Y.; Fallon, J.K.; Yang, J.M.; Hildreth, J.E.; Gould, S.J. Exosomes and HIV Gag bud from endosome-like domains of the T cell plasma membrane. *J. Cell Biol.* **2006**, *172*, 923–935. [CrossRef] [PubMed]
10. Marzesco, A.M.; Janich, P.; Wilsch-Brauninger, M.; Dubreuil, V.; Langenfeld, K.; Corbeil, D.; Huttner, W.B. Release of extracellular membrane particles carrying the stem cell marker prominin-1 (CD133) from neural progenitors and other epithelial cells. *J. Cell Sci.* **2005**, *118*, 2849–2858. [CrossRef] [PubMed]
11. Nabhan, J.F.; Hu, R.; Oh, R.S.; Cohen, S.N.; Lu, Q. Formation and release of arrestin domain-containing protein 1-mediated microvesicles (ARMMs) at plasma membrane by recruitment of TSG101 protein. *Proc. Natl. Acad. Sci. USA* **2012**, *109*, 4146–4151. [CrossRef] [PubMed]
12. Ciana, A.; Achilli, C.; Gaur, A.; Minetti, G. Membrane Remodelling and Vesicle Formation During Ageing of Human Red Blood Cells. *Cell. Physiol. Biochem.* **2017**, *42*, 1127–1138. [CrossRef] [PubMed]
13. Yuana, Y.; Sturk, A.; Nieuwland, R. Extracellular vesicles in physiological and pathological conditions. *Blood Rev.* **2013**, *27*, 31–39. [CrossRef] [PubMed]
14. Gupta, A.; Pulliam, L. Exosomes as mediators of neuroinflammation. *J. Neuroinflamm.* **2014**, *11*, 68. [CrossRef] [PubMed]
15. Shen, B.; Fang, Y.; Wu, N.; Gould, S.J. Biogenesis of the posterior pole is mediated by the exosome/microvesicle protein-sorting pathway. *J. Biol. Chem.* **2011**, *286*, 44162–44176. [CrossRef] [PubMed]
16. Muralidharan-Chari, V.; Clancy, J.W.; Sedgwick, A.; D'Souza-Schorey, C. Microvesicles: Mediators of extracellular communication during cancer progression. *J. Cell Sci.* **2010**, *123*, 1603–1611. [CrossRef] [PubMed]
17. Barteneva, N.S.; Maltsev, N.; Vorobjev, I.A. Microvesicles and intercellular communication in the context of parasitism. *Front. Cell. Infect. Microbiol.* **2013**, *3*, 49. [CrossRef] [PubMed]
18. Wu, K.; Xing, F.; Wu, S.Y.; Watabe, K. Extracellular vesicles as emerging targets in cancer: Recent development from bench to bedside. *Biochim. Biophys. Acta* **2017**, *1868*, 538–563. [CrossRef] [PubMed]
19. Lutz, H.U.; Bogdanova, A. Mechanisms tagging senescent red blood cells for clearance in healthy humans. *Front. Physiol.* **2013**, *4*, 387. [CrossRef] [PubMed]
20. Antonelou, M.H.; Kriebardis, A.G.; Papassideri, I.S. Aging and death signalling in mature red cells: From basic science to transfusion practice. *Blood Transfus.* **2010**, *8* (Suppl. 3), S39–S47.
21. Leal, J.K.F.; Adjobo-Hermans, M.J.W.; Bosman, G. Red Blood Cell Homeostasis: Mechanisms and Effects of Microvesicle Generation in Health and Disease. *Front. Physiol.* **2018**, *9*, 703. [CrossRef] [PubMed]
22. Antonelou, M.H.; Seghatchian, J. Update on extracellular vesicles inside red blood cell storage units: Adjust the sails closer to the new wind. *Transfus. Apher. Sci.* **2016**, *55*, 92–104. [CrossRef] [PubMed]
23. Willekens, F.L.; Werre, J.M.; Groenen-Dopp, Y.A.; Roerdinkholder-Stoelwinder, B.; de Pauw, B.; Bosman, G.J. Erythrocyte vesiculation: A self-protective mechanism? *Br. J. Haematol.* **2008**, *141*, 549–556. [CrossRef] [PubMed]
24. Stewart, A.; Urbaniak, S.; Turner, M.; Bessos, H. The application of a new quantitative assay for the monitoring of integrin-associated protein CD47 on red blood cells during storage and comparison with the expression of CD47 and phosphatidylserine with flow cytometry. *Transfusion* **2005**, *45*, 1496–1503. [CrossRef] [PubMed]
25. Bocci, V.; Pessina, G.P.; Paulesu, L. Studies of factors regulating the ageing of human erythrocytes—III. Metabolism and fate of erythrocytic vesicles. *Int. J. Biochem.* **1980**, *11*, 139–142. [CrossRef]
26. Jank, H.; Salzer, U. Vesicles generated during storage of red blood cells enhance the generation of radical oxygen species in activated neutrophils. *Sci. World J.* **2011**, *11*, 173–185. [CrossRef] [PubMed]

27. Donadee, C.; Raat, N.J.; Kanias, T.; Tejero, J.; Lee, J.S.; Kelley, E.E.; Zhao, X.; Liu, C.; Reynolds, H.; Azarov, I.; et al. Nitric oxide scavenging by red blood cell microparticles and cell-free hemoglobin as a mechanism for the red cell storage lesion. *Circulation* **2011**, *124*, 465–476. [CrossRef] [PubMed]
28. Kriebardis, A.; Antonelou, M.; Stamoulis, K.; Papassideri, I. Cell-derived microparticles in stored blood products: Innocent-bystanders or effective mediators of post-transfusion reactions? *Blood Transfus.* **2012**, *10* (Suppl. 2), S25–S38.
29. Burnouf, T.; Chou, M.L.; Goubran, H.; Cognasse, F.; Garraud, O.; Seghatchian, J. An overview of the role of microparticles/microvesicles in blood components: Are they clinically beneficial or harmful? *Transfus. Apher. Sci.* **2015**, *53*, 137–145. [CrossRef] [PubMed]
30. Arraud, N.; Linares, R.; Tan, S.; Gounou, C.; Pasquet, J.M.; Mornet, S.; Brisson, A.R. Extracellular vesicles from blood plasma: Determination of their morphology, size, phenotype and concentration. *J. Thromb. Haemost.* **2014**, *12*, 614–627. [CrossRef] [PubMed]
31. Zwaal, R.F.; Comfurius, P.; Bevers, E.M. Scott syndrome, a bleeding disorder caused by defective scrambling of membrane phospholipids. *Biochim. Biophys. Acta* **2004**, *1636*, 119–128. [CrossRef] [PubMed]
32. Tao, S.C.; Guo, S.C.; Zhang, C.Q. Platelet-derived Extracellular Vesicles: An Emerging Therapeutic Approach. *Int. J. Biol. Sci.* **2017**, *13*, 828–834. [CrossRef] [PubMed]
33. Vajen, T.; Benedikter, B.J.; Heinzmann, A.C.A.; Vasina, E.M.; Henskens, Y.; Parsons, M.; Maguire, P.B.; Stassen, F.R.; Heemskerk, J.W.M.; Schurgers, L.J.; et al. Platelet extracellular vesicles induce a pro-inflammatory smooth muscle cell phenotype. *J. Extracell. Vesicles* **2017**, *6*, 1322454. [CrossRef] [PubMed]
34. Sprague, D.L.; Elzey, B.D.; Crist, S.A.; Waldschmidt, T.J.; Jensen, R.J.; Ratliff, T.L. Platelet-mediated modulation of adaptive immunity: Unique delivery of CD154 signal by platelet-derived membrane vesicles. *Blood* **2008**, *111*, 5028–5036. [CrossRef] [PubMed]
35. Edelstein, L.C. The role of platelet microvesicles in intercellular communication. *Platelets* **2017**, *28*, 222–227. [CrossRef] [PubMed]
36. Johnson, B.L., III; Kuethe, J.W.; Caldwell, C.C. Neutrophil derived microvesicles: Emerging role of a key mediator to the immune response. *Endocr. Metab. Immune Disord. Drug Targets* **2014**, *14*, 210–217. [CrossRef] [PubMed]
37. Halim, A.T.; Ariffin, N.A.; Azlan, M. Review: The Multiple Roles of Monocytic Microparticles. *Inflammation* **2016**, *39*, 1277–1284. [CrossRef] [PubMed]
38. Angelillo-Scherrer, A. Leukocyte-derived microparticles in vascular homeostasis. *Circ. Res.* **2012**, *110*, 356–369. [CrossRef] [PubMed]
39. Del Conde, I.; Shrimpton, C.N.; Thiagarajan, P.; Lopez, J.A. Tissue-factor-bearing microvesicles arise from lipid rafts and fuse with activated platelets to initiate coagulation. *Blood* **2005**, *106*, 1604–1611. [CrossRef] [PubMed]
40. Budnik, V.; Ruiz-Canada, C.; Wendler, F. Extracellular vesicles round off communication in the nervous system. *Nat. Rev. Neurosci.* **2016**, *17*, 160–172. [CrossRef] [PubMed]
41. Paolicelli, R.C.; Bergamini, G.; Rajendran, L. Cell-to-cell Communication by Extracellular Vesicles: Focus on Microglia. *Neuroscience* **2018**. [CrossRef] [PubMed]
42. Bianco, F.; Pravettoni, E.; Colombo, A.; Schenk, U.; Moller, T.; Matteoli, M.; Verderio, C. Astrocyte-derived ATP induces vesicle shedding and IL-1 beta release from microglia. *J. Immunol.* **2005**, *174*, 7268–7277. [CrossRef] [PubMed]
43. Joshi, P.; Turola, E.; Ruiz, A.; Bergami, A.; Libera, D.D.; Benussi, L.; Giussani, P.; Magnani, G.; Comi, G.; Legname, G.; et al. Microglia convert aggregated amyloid-beta into neurotoxic forms through the shedding of microvesicles. *Cell Death Differ.* **2014**, *21*, 582–593. [CrossRef] [PubMed]
44. Carandini, T.; Colombo, F.; Finardi, A.; Casella, G.; Garzetti, L.; Verderio, C.; Furlan, R. Microvesicles: What is the Role in Multiple Sclerosis? *Front. Neurol.* **2015**, *6*, 111. [CrossRef] [PubMed]
45. Minagar, A.; Alexander, J.S. Blood-brain barrier disruption in multiple sclerosis. *Mult. Scler.* **2003**, *9*, 540–549. [CrossRef] [PubMed]
46. Raimondo, S.; Corrado, C.; Raimondi, L.; De Leo, G.; Alessandro, R. Role of Extracellular Vesicles in Hematological Malignancies. *Biomed. Res. Int.* **2015**, *2015*, 821613. [CrossRef] [PubMed]
47. Gopal, S.K.; Greening, D.W.; Rai, A.; Chen, M.; Xu, R.; Shafiq, A.; Mathias, R.A.; Zhu, H.J.; Simpson, R.J. Extracellular vesicles: Their role in cancer biology and epithelial-mesenchymal transition. *Biochem. J.* **2017**, *474*, 21–45. [CrossRef] [PubMed]

48. Coumans, F.A.W.; Brisson, A.R.; Buzas, E.I.; Dignat-George, F.; Drees, E.E.E.; El-Andaloussi, S.; Emanueli, C.; Gasecka, A.; Hendrix, A.; Hill, A.F.; et al. Methodological Guidelines to Study Extracellular Vesicles. *Circ. Res.* **2017**, *120*, 1632–1648. [CrossRef] [PubMed]
49. Menck, K.; Bleckmann, A.; Schulz, M.; Ries, L.; Binder, C. Isolation and Characterization of Microvesicles from Peripheral Blood. *J. Vis. Exp.* **2017**. [CrossRef] [PubMed]
50. Konoshenko, M.Y.; Lekchnov, E.A.; Vlassov, A.V.; Laktionov, P.P. Isolation of Extracellular Vesicles: General Methodologies and Latest Trends. *Biomed. Res. Int.* **2018**, *2018*, 8545347. [CrossRef] [PubMed]
51. Ramirez, M.I.; Amorim, M.G.; Gadelha, C.; Milic, I.; Welsh, J.A.; Freitas, V.M.; Nawaz, M.; Akbar, N.; Couch, Y.; Makin, L.; et al. Technical challenges of working with extracellular vesicles. *Nanoscale* **2018**, *10*, 881–906. [CrossRef] [PubMed]
52. Mateescu, B.; Kowal, E.J.; van Balkom, B.W.; Bartel, S.; Bhattacharyya, S.N.; Buzas, E.I.; Buck, A.H.; de Candia, P.; Chow, F.W.; Das, S.; et al. Obstacles and opportunities in the functional analysis of extracellular vesicle RNA—An ISEV position paper. *J. Extracell. Vesicles* **2017**, *6*, 1286095. [CrossRef] [PubMed]
53. Szatanek, R.; Baj-Krzyworzeka, M.; Zimoch, J.; Lekka, M.; Siedlar, M.; Baran, J. The Methods of Choice for Extracellular Vesicles (EVs) Characterization. *Int. J. Mol. Sci.* **2017**, *18*. [CrossRef] [PubMed]
54. Aharon, A.; Brenner, B. Microparticles and pregnancy complications. *Thromb. Res.* **2011**, *127* (Suppl. 3), S67–S71. [CrossRef]
55. Wilhelm, E.N.; Mourot, L.; Rakobowchuk, M. Exercise-Derived Microvesicles: A Review of the Literature. *Sports Med.* **2018**. [CrossRef] [PubMed]
56. Strohacker, K.; Breslin, W.L.; Carpenter, K.C.; Davidson, T.R.; Agha, N.H.; McFarlin, B.K. Moderate-intensity, premeal cycling blunts postprandial increases in monocyte cell surface CD18 and CD11a and endothelial microparticles following a high-fat meal in young adults. *Appl. Physiol. Nutr. Metab.* **2012**, *37*, 530–539. [CrossRef] [PubMed]
57. Alijotas-Reig, J.; Palacio-Garcia, C.; Llurba, E.; Vilardell-Tarres, M. Cell-derived microparticles and vascular pregnancy complications: A systematic and comprehensive review. *Fertil. Steril.* **2013**, *99*, 441–449. [CrossRef] [PubMed]
58. Gustafson, C.M.; Shepherd, A.J.; Miller, V.M.; Jayachandran, M. Age- and sex-specific differences in blood-borne microvesicles from apparently healthy humans. *Biol. Sex Differ.* **2015**, *6*, 10. [CrossRef] [PubMed]
59. Bernimoulin, M.; Waters, E.K.; Foy, M.; Steele, B.M.; Sullivan, M.; Falet, H.; Walsh, M.T.; Barteneva, N.; Geng, J.G.; Hartwig, J.H.; et al. Differential stimulation of monocytic cells results in distinct populations of microparticles. *J. Thromb. Haemost.* **2009**, *7*, 1019–1028. [CrossRef] [PubMed]
60. Kalra, H.; Simpson, R.J.; Ji, H.; Aikawa, E.; Altevogt, P.; Askenase, P.; Bond, V.C.; Borras, F.E.; Breakefield, X.; Budnik, V.; et al. Vesiclepedia: A compendium for extracellular vesicles with continuous community annotation. *PLoS Biol.* **2012**, *10*, e1001450. [CrossRef] [PubMed]
61. Kim, D.K.; Kang, B.; Kim, O.Y.; Choi, D.S.; Lee, J.; Kim, S.R.; Go, G.; Yoon, Y.J.; Kim, J.H.; Jang, S.C.; et al. EVpedia: An integrated database of high-throughput data for systemic analyses of extracellular vesicles. *J. Extracell. Vesicles* **2013**, *2*. [CrossRef] [PubMed]
62. Muralidharan-Chari, V.; Clancy, J.; Plou, C.; Romao, M.; Chavrier, P.; Raposo, G.; D'Souza-Schorey, C. ARF6-regulated shedding of tumor cell-derived plasma membrane microvesicles. *Curr. Biol.* **2009**, *19*, 1875–1885. [CrossRef] [PubMed]
63. Keerthikumar, S.; Gangoda, L.; Liem, M.; Fonseka, P.; Atukorala, I.; Ozcitti, C.; Mechler, A.; Adda, C.G.; Ang, C.S.; Mathivanan, S. Proteogenomic analysis reveals exosomes are more oncogenic than ectosomes. *Oncotarget* **2015**, *6*, 15375–15396. [CrossRef] [PubMed]
64. Gasser, O.; Hess, C.; Miot, S.; Deon, C.; Sanchez, J.C.; Schifferli, J.A. Characterisation and properties of ectosomes released by human polymorphonuclear neutrophils. *Exp. Cell Res.* **2003**, *285*, 243–257. [CrossRef]
65. Kriebardis, A.G.; Antonelou, M.H.; Stamoulis, K.E.; Economou-Petersen, E.; Margaritis, L.H.; Papassideri, I.S. RBC-derived vesicles during storage: Ultrastructure, protein composition, oxidation, and signaling components. *Transfusion* **2008**, *48*, 1943–1953. [CrossRef] [PubMed]
66. Salzer, U.; Zhu, R.; Luten, M.; Isobe, H.; Pastushenko, V.; Perkmann, T.; Hinterdorfer, P.; Bosman, G.J. Vesicles generated during storage of red cells are rich in the lipid raft marker stomatin. *Transfusion* **2008**, *48*, 451–462. [CrossRef] [PubMed]

67. Salzer, U.; Hinterdorfer, P.; Hunger, U.; Borken, C.; Prohaska, R. Ca^{++}-dependent vesicle release from erythrocytes involves stomatin-specific lipid rafts, synexin (annexin VII), and sorcin. *Blood* **2002**, *99*, 2569–2577. [CrossRef] [PubMed]
68. Di Vizio, D.; Morello, M.; Dudley, A.C.; Schow, P.W.; Adam, R.M.; Morley, S.; Mulholland, D.; Rotinen, M.; Hager, M.H.; Insabato, L.; et al. Large oncosomes in human prostate cancer tissues and in the circulation of mice with metastatic disease. *Am. J. Pathol.* **2012**, *181*, 1573–1584. [CrossRef] [PubMed]
69. Millimaggi, D.; Festuccia, C.; Angelucci, A.; D'Ascenzo, S.; Rucci, N.; Flati, S.; Bologna, M.; Teti, A.; Pavan, A.; Dolo, V. Osteoblast-conditioned media stimulate membrane vesicle shedding in prostate cancer cells. *Int. J. Oncol.* **2006**, *28*, 909–914. [CrossRef] [PubMed]
70. Taraboletti, G.; D'Ascenzo, S.; Borsotti, P.; Giavazzi, R.; Pavan, A.; Dolo, V. Shedding of the matrix metalloproteinases MMP-2, MMP-9, and MT1-MMP as membrane vesicle-associated components by endothelial cells. *Am. J. Pathol.* **2002**, *160*, 673–680. [CrossRef]
71. Shimoda, M.; Khokha, R. Metalloproteinases in extracellular vesicles. *Biochim. Biophys. Acta* **2017**, *1864*, 1989–2000. [CrossRef] [PubMed]
72. Dolo, V.; Ginestra, A.; Cassara, D.; Violini, S.; Lucania, G.; Torrisi, M.R.; Nagase, H.; Canevari, S.; Pavan, A.; Vittorelli, M.L. Selective localization of matrix metalloproteinase 9, beta1 integrins, and human lymphocyte antigen class I molecules on membrane vesicles shed by 8701-BC breast carcinoma cells. *Cancer Res.* **1998**, *58*, 4468–4474. [PubMed]
73. Heijnen, H.F.; Schiel, A.E.; Fijnheer, R.; Geuze, H.J.; Sixma, J.J. Activated platelets release two types of membrane vesicles: Microvesicles by surface shedding and exosomes derived from exocytosis of multivesicular bodies and alpha-granules. *Blood* **1999**, *94*, 3791–3799. [PubMed]
74. Pluskota, E.; Woody, N.M.; Szpak, D.; Ballantyne, C.M.; Soloviev, D.A.; Simon, D.I.; Plow, E.F. Expression, activation, and function of integrin alphaMbeta2 (Mac-1) on neutrophil-derived microparticles. *Blood* **2008**, *112*, 2327–2335. [CrossRef] [PubMed]
75. Mezouar, S.; Darbousset, R.; Dignat-George, F.; Panicot-Dubois, L.; Dubois, C. Inhibition of platelet activation prevents the P-selectin and integrin-dependent accumulation of cancer cell microparticles and reduces tumor growth and metastasis in vivo. *Int. J. Cancer* **2015**, *136*, 462–475. [CrossRef] [PubMed]
76. Deregibus, M.C.; Cantaluppi, V.; Calogero, R.; Lo Iacono, M.; Tetta, C.; Biancone, L.; Bruno, S.; Bussolati, B.; Camussi, G. Endothelial progenitor cell derived microvesicles activate an angiogenic program in endothelial cells by a horizontal transfer of mRNA. *Blood* **2007**, *110*, 2440–2448. [CrossRef] [PubMed]
77. Al-Nedawi, K.; Meehan, B.; Micallef, J.; Lhotak, V.; May, L.; Guha, A.; Rak, J. Intercellular transfer of the oncogenic receptor EGFRvIII by microvesicles derived from tumour cells. *Nat. Cell Biol.* **2008**, *10*, 619–624. [CrossRef] [PubMed]
78. Kim, K.M.; Abdelmohsen, K.; Mustapic, M.; Kapogiannis, D.; Gorospe, M. RNA in extracellular vesicles. *Wiley Interdiscip. Rev. RNA* **2017**, *8*. [CrossRef] [PubMed]
79. Baj-Krzyworzeka, M.; Szatanek, R.; Weglarczyk, K.; Baran, J.; Urbanowicz, B.; Branski, P.; Ratajczak, M.Z.; Zembala, M. Tumour-derived microvesicles carry several surface determinants and mRNA of tumour cells and transfer some of these determinants to monocytes. *Cancer Immunol. Immunother.* **2006**, *55*, 808–818. [CrossRef] [PubMed]
80. Fatima, F.; Nawaz, M. Vesiculated Long Non-Coding RNAs: Offshore Packages Deciphering Trans-Regulation between Cells, Cancer Progression and Resistance to Therapies. *Non-Coding RNA* **2017**, *3*, 10. [CrossRef] [PubMed]
81. Yuan, A.; Farber, E.L.; Rapoport, A.L.; Tejada, D.; Deniskin, R.; Akhmedov, N.B.; Farber, D.B. Transfer of microRNAs by embryonic stem cell microvesicles. *PLoS ONE* **2009**, *4*, e4722. [CrossRef] [PubMed]
82. Fonsato, V.; Collino, F.; Herrera, M.B.; Cavallari, C.; Deregibus, M.C.; Cisterna, B.; Bruno, S.; Romagnoli, R.; Salizzoni, M.; Tetta, C.; et al. Human liver stem cell-derived microvesicles inhibit hepatoma growth in SCID mice by delivering antitumor microRNAs. *Stem Cells* **2012**, *30*, 1985–1998. [CrossRef] [PubMed]
83. Crescitelli, R.; Lasser, C.; Szabo, T.G.; Kittel, A.; Eldh, M.; Dianzani, I.; Buzas, E.I.; Lotvall, J. Distinct RNA profiles in subpopulations of extracellular vesicles: Apoptotic bodies, microvesicles and exosomes. *J. Extracell. Vesicles* **2013**, *2*. [CrossRef] [PubMed]
84. Dong, L.; Lin, W.; Qi, P.; Xu, M.D.; Wu, X.; Ni, S.; Huang, D.; Weng, W.W.; Tan, C.; Sheng, W.; et al. Circulating Long RNAs in Serum Extracellular Vesicles: Their Characterization and Potential Application as Biomarkers for Diagnosis of Colorectal Cancer. *Cancer Epidemiol. Biomark. Prev.* **2016**, *25*, 1158–1166. [CrossRef] [PubMed]

85. Kawamura, Y.; Yamamoto, Y.; Sato, T.A.; Ochiya, T. Extracellular vesicles as trans-genomic agents: Emerging roles in disease and evolution. *Cancer Sci.* **2017**, *108*, 824–830. [CrossRef] [PubMed]
86. Kanada, M.; Bachmann, M.H.; Hardy, J.W.; Frimannson, D.O.; Bronsart, L.; Wang, A.; Sylvester, M.D.; Schmidt, T.L.; Kaspar, R.L.; Butte, M.J.; et al. Differential fates of biomolecules delivered to target cells via extracellular vesicles. *Proc. Natl. Acad. Sci. USA* **2015**, *112*, E1433–E1442. [CrossRef] [PubMed]
87. Osteikoetxea, X.; Balogh, A.; Szabo-Taylor, K.; Nemeth, A.; Szabo, T.G.; Paloczi, K.; Sodar, B.; Kittel, A.; Gyorgy, B.; Pallinger, E.; et al. Improved characterization of EV preparations based on protein to lipid ratio and lipid properties. *PLoS ONE* **2015**, *10*, e0121184. [CrossRef] [PubMed]
88. Haraszti, R.A.; Didiot, M.C.; Sapp, E.; Leszyk, J.; Shaffer, S.A.; Rockwell, H.E.; Gao, F.; Narain, N.R.; DiFiglia, M.; Kiebish, M.A.; et al. High-resolution proteomic and lipidomic analysis of exosomes and microvesicles from different cell sources. *J. Extracell. Vesicles* **2016**, *5*, 32570. [CrossRef] [PubMed]
89. Baig, S.; Lim, J.Y.; Fernandis, A.Z.; Wenk, M.R.; Kale, A.; Su, L.L.; Biswas, A.; Vasoo, S.; Shui, G.; Choolani, M. Lipidomic analysis of human placental syncytiotrophoblast microvesicles in adverse pregnancy outcomes. *Placenta* **2013**, *34*, 436–442. [CrossRef] [PubMed]
90. Weerheim, A.M.; Kolb, A.M.; Sturk, A.; Nieuwland, R. Phospholipid composition of cell-derived microparticles determined by one-dimensional high-performance thin-layer chromatography. *Anal. Biochem.* **2002**, *302*, 191–198. [CrossRef] [PubMed]
91. Bicalho, B.; Holovati, J.L.; Acker, J.P. Phospholipidomics reveals differences in glycerophosphoserine profiles of hypothermically stored red blood cells and microvesicles. *Biochim. Biophys. Acta* **2013**, *1828*, 317–326. [CrossRef] [PubMed]
92. Lauren, E.; Tigistu-Sahle, F.; Valkonen, S.; Westberg, M.; Valkeajarvi, A.; Eronen, J.; Siljander, P.; Pettila, V.; Kakela, R.; Laitinen, S.; et al. Phospholipid composition of packed red blood cells and that of extracellular vesicles show a high resemblance and stability during storage. *Biochim. Biophys. Acta* **2018**, *1863*, 1–8. [CrossRef] [PubMed]
93. Lutz, H.U.; Liu, S.C.; Palek, J. Release of spectrin-free vesicles from human erythrocytes during ATP depletion. I. Characterization of spectrin-free vesicles. *J. Cell Biol.* **1977**, *73*, 548–560. [CrossRef] [PubMed]
94. Hu, Q.; Wang, M.; Cho, M.S.; Wang, C.; Nick, A.M.; Thiagarajan, P.; Aung, F.M.; Han, X.; Sood, A.K.; Afshar-Kharghan, V. Lipid profile of platelets and platelet-derived microparticles in ovarian cancer. *BBA Clin.* **2016**, *6*, 76–81. [CrossRef] [PubMed]
95. Biro, E.; Akkerman, J.W.; Hoek, F.J.; Gorter, G.; Pronk, L.M.; Sturk, A.; Nieuwland, R. The phospholipid composition and cholesterol content of platelet-derived microparticles: A comparison with platelet membrane fractions. *J. Thromb. Haemost.* **2005**, *3*, 2754–2763. [CrossRef] [PubMed]
96. Connor, D.E.; Exner, T.; Ma, D.D.; Joseph, J.E. The majority of circulating platelet-derived microparticles fail to bind annexin V, lack phospholipid-dependent procoagulant activity and demonstrate greater expression of glycoprotein Ib. *Thromb. Haemost.* **2010**, *103*, 1044–1052. [PubMed]
97. Cluitmans, J.C.; Gevi, F.; Siciliano, A.; Matte, A.; Leal, J.K.; De Franceschi, L.; Zolla, L.; Brock, R.; Adjobo-Hermans, M.J.; Bosman, G.J. Red Blood Cell Homeostasis: Pharmacological Interventions to Explore Biochemical, Morphological and Mechanical Properties. *Front. Mol. Biosci.* **2016**, *3*, 10. [CrossRef] [PubMed]
98. Dinkla, S.; Wessels, K.; Verdurmen, W.P.; Tomelleri, C.; Cluitmans, J.C.; Fransen, J.; Fuchs, B.; Schiller, J.; Joosten, I.; Brock, R.; et al. Functional consequences of sphingomyelinase-induced changes in erythrocyte membrane structure. *Cell Death Dis.* **2012**, *3*, e410. [CrossRef] [PubMed]
99. Boilard, E. Extracellular vesicles and their content in bioactive lipid mediators: More than a sack of microRNA. *J. Lipid Res.* **2018**. [CrossRef] [PubMed]
100. Rousseau, M.; Belleannee, C.; Duchez, A.C.; Cloutier, N.; Levesque, T.; Jacques, F.; Perron, J.; Nigrovic, P.A.; Dieude, M.; Hebert, M.J.; et al. Detection and quantification of microparticles from different cellular lineages using flow cytometry. Evaluation of the impact of secreted phospholipase A2 on microparticle assessment. *PLoS ONE* **2015**, *10*, e0116812. [CrossRef] [PubMed]
101. Duchez, A.C.; Boudreau, L.H.; Naika, G.S.; Bollinger, J.; Belleannee, C.; Cloutier, N.; Laffont, B.; Mendoza-Villarroel, R.E.; Levesque, T.; Rollet-Labelle, E.; et al. Platelet microparticles are internalized in neutrophils via the concerted activity of 12-lipoxygenase and secreted phospholipase A2-IIA. *Proc. Natl. Acad. Sci. USA* **2015**, *112*, E3564–E3573. [CrossRef] [PubMed]
102. Lux, S.E.T. Anatomy of the red cell membrane skeleton: Unanswered questions. *Blood* **2016**, *127*, 187–199. [CrossRef] [PubMed]

103. Manno, S.; Takakuwa, Y.; Mohandas, N. Modulation of erythrocyte membrane mechanical function by protein 4.1 phosphorylation. *J. Biol. Chem.* **2005**, *280*, 7581–7587. [CrossRef] [PubMed]
104. Picas, L.; Rico, F.; Deforet, M.; Scheuring, S. Structural and mechanical heterogeneity of the erythrocyte membrane reveals hallmarks of membrane stability. *ACS Nano* **2013**, *7*, 1054–1063. [CrossRef] [PubMed]
105. Muravyov, A.V.; Tikhomirova, I.A. Role molecular signaling pathways in changes of red blood cell deformability. *Clin. Hemorheol. Microcirc.* **2013**, *53*, 45–59. [PubMed]
106. An, X.; Zhang, X.; Debnath, G.; Baines, A.J.; Mohandas, N. Phosphatidylinositol-4,5-biphosphate (PIP2) differentially regulates the interaction of human erythrocyte protein 4.1 (4.1R) with membrane proteins. *Biochemistry* **2006**, *45*, 5725–5732. [CrossRef] [PubMed]
107. Kapus, A.; Janmey, P. Plasma membrane—Cortical cytoskeleton interactions: A cell biology approach with biophysical considerations. *Compr. Physiol.* **2013**, *3*, 1231–1281. [PubMed]
108. Bogdanova, A.; Makhro, A.; Wang, J.; Lipp, P.; Kaestner, L. Calcium in red blood cells-a perilous balance. *Int. J. Mol. Sci.* **2013**, *14*, 9848–9872. [CrossRef] [PubMed]
109. Huisjes, R.; Bogdanova, A.; van Solinge, W.W.; Schiffelers, R.M.; Kaestner, L.; van Wijk, R. Squeezing for Life—Properties of Red Blood Cell Deformability. *Front. Physiol.* **2018**, *9*, 656. [CrossRef] [PubMed]
110. Evans, E.; Mohandas, N.; Leung, A. Static and dynamic rigidities of normal and sickle erythrocytes. Major influence of cell hemoglobin concentration. *J. Clin. Investig.* **1984**, *73*, 477–488. [CrossRef] [PubMed]
111. Lew, V.L.; Tiffert, T. On the Mechanism of Human Red Blood Cell Longevity: Roles of Calcium, the Sodium Pump, PIEZO1, and Gardos Channels. *Front. Physiol.* **2017**, *8*, 977. [CrossRef] [PubMed]
112. Betz, T.; Lenz, M.; Joanny, J.F.; Sykes, C. ATP-dependent mechanics of red blood cells. *Proc. Natl. Acad. Sci. USA* **2009**, *106*, 15320–15325. [CrossRef] [PubMed]
113. Park, Y.; Best, C.A.; Auth, T.; Gov, N.S.; Safran, S.A.; Popescu, G.; Suresh, S.; Feld, M.S. Metabolic remodeling of the human red blood cell membrane. *Proc. Natl. Acad. Sci. USA* **2010**, *107*, 1289–1294. [CrossRef] [PubMed]
114. Yoon, Y.Z.; Kotar, J.; Yoon, G.; Cicuta, P. The nonlinear mechanical response of the red blood cell. *Phys. Biol.* **2008**, *5*, 036007. [CrossRef] [PubMed]
115. Rifkind, J.M.; Nagababu, E. Hemoglobin redox reactions and red blood cell aging. *Antioxid. Redox Signal.* **2013**, *18*, 2274–2283. [CrossRef] [PubMed]
116. Rubin, O.; Crettaz, D.; Canellini, G.; Tissot, J.D.; Lion, N. Microparticles in stored red blood cells: An approach using flow cytometry and proteomic tools. *Vox Sang.* **2008**, *95*, 288–297. [CrossRef] [PubMed]
117. Kriebardis, A.G.; Antonelou, M.H.; Stamoulis, K.E.; Economou-Petersen, E.; Margaritis, L.H.; Papassideri, I.S. Storage-dependent remodeling of the red blood cell membrane is associated with increased immunoglobulin G binding, lipid raft rearrangement, and caspase activation. *Transfusion* **2007**, *47*, 1212–1220. [CrossRef] [PubMed]
118. Bosman, G.J.; Lasonder, E.; Groenen-Dopp, Y.A.; Willekens, F.L.; Werre, J.M.; Novotny, V.M. Comparative proteomics of erythrocyte aging in vivo and in vitro. *J. Proteom.* **2010**, *73*, 396–402. [CrossRef] [PubMed]
119. Zhu, Q.; Salehyar, S.; Cabrales, P.; Asaro, R.J. Prospects for Human Erythrocyte Skeleton-Bilayer Dissociation during Splenic Flow. *Biophys. J.* **2017**, *113*, 900–912. [CrossRef] [PubMed]
120. Fricke, K.; Sackmann, E. Variation of frequency spectrum of the erythrocyte flickering caused by aging, osmolarity, temperature and pathological changes. *Biochim. Biophys. Acta* **1984**, *803*, 145–152. [CrossRef]
121. Gov, N.S.; Safran, S.A. Red blood cell membrane fluctuations and shape controlled by ATP-induced cytoskeletal defects. *Biophys. J.* **2005**, *88*, 1859–1874. [CrossRef] [PubMed]
122. Edwards, C.L.; Scales, M.T.; Loughlin, C.; Bennett, G.G.; Harris-Peterson, S.; De Castro, L.M.; Whitworth, E.; Abrams, M.; Feliu, M.; Johnson, S.; et al. A brief review of the pathophysiology, associated pain, and psychosocial issues in sickle cell disease. *Int. J. Behav. Med.* **2005**, *12*, 171–179. [CrossRef] [PubMed]
123. Bartosz, G.; Gaczynska, M.; Grzelinska, E.; Soszynski, M.; Michalak, W.; Gondko, R. Aged erythrocytes exhibit decreased anion exchange. *Mech. Ageing Dev.* **1987**, *39*, 245–250. [CrossRef]
124. Bartosz, G.; Tannert, C.; Fried, R.; Leyko, W. Superoxide dismutase activity decreases during erythrocyte aging. *Experientia* **1978**, *34*, 1464. [CrossRef] [PubMed]
125. Fornaini, G.; Magnani, M.; Fazi, A.; Accorsi, A.; Stocchi, V.; Dacha, M. Regulatory properties of human erythrocyte hexokinase during cell ageing. *Arch. Biochem. Biophys.* **1985**, *239*, 352–358. [CrossRef]
126. Azouzi, S.; Romana, M.; Arashiki, N.; Takakuwa, Y.; El Nemer, W.; Peyrard, T.; Colin, Y.; Amireault, P.; Le Van Kim, C. Band 3 phosphorylation induces irreversible alterations of stored red blood cells. *Am. J. Hematol.* **2018**, *93*, E110–E112. [CrossRef] [PubMed]

127. Szigyarto, I.C.; Deak, R.; Mihaly, J.; Rocha, S.; Zsila, F.; Varga, Z.; Beke-Somfai, T. Flow Alignment of Extracellular Vesicles: Structure and Orientation of Membrane-Associated Bio-macromolecules Studied with Polarized Light. *ChemBioChem* **2018**, *19*, 545–551. [CrossRef] [PubMed]
128. Wither, M.; Dzieciatkowska, M.; Nemkov, T.; Strop, P.; D'Alessandro, A.; Hansen, K.C. Hemoglobin oxidation at functional amino acid residues during routine storage of red blood cells. *Transfusion* **2016**, *56*, 421–426. [CrossRef] [PubMed]
129. Arashiki, N.; Kimata, N.; Manno, S.; Mohandas, N.; Takakuwa, Y. Membrane peroxidation and methemoglobin formation are both necessary for band 3 clustering: Mechanistic insights into human erythrocyte senescence. *Biochemistry* **2013**, *52*, 5760–5769. [CrossRef] [PubMed]
130. Lutz, H.U.; Flepp, R.; Stringaro-Wipf, G. Naturally occurring autoantibodies to exoplasmic and cryptic regions of band 3 protein, the major integral membrane protein of human red blood cells. *J. Immunol.* **1984**, *133*, 2610–2618. [PubMed]
131. Stowell, S.R.; Smith, N.H.; Zimring, J.C.; Fu, X.; Palmer, A.F.; Fontes, J.; Banerjee, U.; Yazer, M.H. Addition of ascorbic acid solution to stored murine red blood cells increases posttransfusion recovery and decreases microparticles and alloimmunization. *Transfusion* **2013**, *53*, 2248–2257. [CrossRef] [PubMed]
132. Freikman, I.; Fibach, E. Distribution and shedding of the membrane phosphatidylserine during maturation and aging of erythroid cells. *Biochim. Biophys. Acta* **2011**, *1808*, 2773–2780. [CrossRef] [PubMed]
133. Repsold, L.; Joubert, A.M. Eryptosis: An Erythrocyte's Suicidal Type of Cell Death. *Biomed. Res. Int.* **2018**, *2018*, 9405617. [CrossRef] [PubMed]
134. Allan, D.; Thomas, P.; Limbrick, A.R. The isolation and characterization of 60 nm vesicles ('nanovesicles') produced during ionophore A23187-induced budding of human erythrocytes. *Biochem. J.* **1980**, *188*, 881–887. [CrossRef] [PubMed]
135. Butikofer, P.; Kuypers, F.A.; Xu, C.M.; Chiu, D.T.; Lubin, B. Enrichment of two glycosyl-phosphatidylinositol-anchored proteins, acetylcholinesterase and decay accelerating factor, in vesicles released from human red blood cells. *Blood* **1989**, *74*, 1481–1485. [PubMed]
136. Nguyen, D.B.; Ly, T.B.; Wesseling, M.C.; Hittinger, M.; Torge, A.; Devitt, A.; Perrie, Y.; Bernhardt, I. Characterization of Microvesicles Released from Human Red Blood Cells. *Cell. Physiol. Biochem.* **2016**, *38*, 1085–1099. [CrossRef] [PubMed]
137. Allan, D.; Michell, R.H. Calcium ion-dependent diacylglycerol accumulation in erythrocytes is associated with microvesiculation but not with efflux of potassium ions. *Biochem. J.* **1977**, *166*, 495–499. [CrossRef] [PubMed]
138. Nguyen, D.B.; Wagner-Britz, L.; Maia, S.; Steffen, P.; Wagner, C.; Kaestner, L.; Bernhardt, I. Regulation of phosphatidylserine exposure in red blood cells. *Cell. Physiol. Biochem.* **2011**, *28*, 847–856. [CrossRef] [PubMed]
139. Morel, O.; Jesel, L.; Freyssinet, J.M.; Toti, F. Cellular mechanisms underlying the formation of circulating microparticles. *Arterioscler. Thromb. Vasc. Biol.* **2011**, *31*, 15–26. [CrossRef] [PubMed]
140. Westerman, M.; Porter, J.B. Red blood cell-derived microparticles: An overview. *Blood Cells Mol. Dis.* **2016**, *59*, 134–139. [CrossRef] [PubMed]
141. Rachmilewitz, E.A.; Thorell, B. Hemichromes in single inclusion bodies in red cells of beta thalassemia. *Blood* **1972**, *39*, 794–800. [PubMed]
142. Ferru, E.; Pantaleo, A.; Carta, F.; Mannu, F.; Khadjavi, A.; Gallo, V.; Ronzoni, L.; Graziadei, G.; Cappellini, M.D.; Turrini, F. Thalassemic erythrocytes release microparticles loaded with hemichromes by redox activation of p72Syk kinase. *Haematologica* **2014**, *99*, 570–578. [CrossRef] [PubMed]
143. George, A.; Pushkaran, S.; Konstantinidis, D.G.; Koochaki, S.; Malik, P.; Mohandas, N.; Zheng, Y.; Joiner, C.H.; Kalfa, T.A. Erythrocyte NADPH oxidase activity modulated by Rac GTPases, PKC, and plasma cytokines contributes to oxidative stress in sickle cell disease. *Blood* **2013**, *121*, 2099–2107. [CrossRef] [PubMed]
144. Camus, S.M.; De Moraes, J.A.; Bonnin, P.; Abbyad, P.; Le Jeune, S.; Lionnet, F.; Loufrani, L.; Grimaud, L.; Lambry, J.C.; Charue, D.; et al. Circulating cell membrane microparticles transfer heme to endothelial cells and trigger vasoocclusions in sickle cell disease. *Blood* **2015**, *125*, 3805–3814. [CrossRef] [PubMed]
145. Eber, S.; Lux, S.E. Hereditary spherocytosis—Defects in proteins that connect the membrane skeleton to the lipid bilayer. *Semin. Hematol.* **2004**, *41*, 118–141. [CrossRef] [PubMed]
146. Perrotta, S.; Gallagher, P.G.; Mohandas, N. Hereditary spherocytosis. *Lancet* **2008**, *372*, 1411–1426. [CrossRef]

147. Diez-Silva, M.; Dao, M.; Han, J.; Lim, C.T.; Suresh, S. Shape and Biomechanical Characteristics of Human Red Blood Cells in Health and Disease. *MRS Bull.* **2010**, *35*, 382–388. [CrossRef] [PubMed]
148. Li, H.; Lykotrafitis, G. Vesiculation of healthy and defective red blood cells. *Phys. Rev. E Stat. Nonlin. Soft Matter Phys.* **2015**, *92*, 012715. [CrossRef] [PubMed]
149. Alaarg, A.; Schiffelers, R.M.; van Solinge, W.W.; van Wijk, R. Red blood cell vesiculation in hereditary hemolytic anemia. *Front. Physiol.* **2013**, *4*, 365. [CrossRef] [PubMed]
150. Reliene, R.; Mariani, M.; Zanella, A.; Reinhart, W.H.; Ribeiro, M.L.; del Giudice, E.M.; Perrotta, S.; Iolascon, A.; Eber, S.; Lutz, H.U. Splenectomy prolongs in vivo survival of erythrocytes differently in spectrin/ankyrin- and band 3-deficient hereditary spherocytosis. *Blood* **2002**, *100*, 2208–2215. [PubMed]
151. Peters, L.L.; Shivdasani, R.A.; Liu, S.C.; Hanspal, M.; John, K.M.; Gonzalez, J.M.; Brugnara, C.; Gwynn, B.; Mohandas, N.; Alper, S.L.; et al. Anion exchanger 1 (band 3) is required to prevent erythrocyte membrane surface loss but not to form the membrane skeleton. *Cell* **1996**, *86*, 917–927. [CrossRef]
152. Tricarico, C.; Clancy, J.; D'Souza-Schorey, C. Biology and biogenesis of shed microvesicles. *Small GTPases* **2017**, *8*, 220–232. [CrossRef] [PubMed]
153. Nawaz, M.; Camussi, G.; Valadi, H.; Nazarenko, I.; Ekstrom, K.; Wang, X.; Principe, S.; Shah, N.; Ashraf, N.M.; Fatima, F.; et al. The emerging role of extracellular vesicles as biomarkers for urogenital cancers. *Nat. Rev. Urol.* **2014**, *11*, 688–701. [CrossRef] [PubMed]
154. Hugel, B.; Martinez, M.C.; Kunzelmann, C.; Freyssinet, J.M. Membrane microparticles: Two sides of the coin. *Physiology* **2005**, *20*, 22–27. [CrossRef] [PubMed]
155. Muhsin-Sharafaldine, M.R.; McLellan, A.D. Tumor-Derived Apoptotic Vesicles: With Death They Do Part. *Front. Immunol.* **2018**, *9*, 957. [CrossRef] [PubMed]
156. McMahon, H.T.; Boucrot, E. Membrane curvature at a glance. *J. Cell Sci.* **2015**, *128*, 1065–1070. [CrossRef] [PubMed]
157. Yanez-Mo, M.; Barreiro, O.; Gordon-Alonso, M.; Sala-Valdes, M.; Sanchez-Madrid, F. Tetraspanin-enriched microdomains: A functional unit in cell plasma membranes. *Trends Cell Biol.* **2009**, *19*, 434–446. [CrossRef] [PubMed]
158. Bari, R.; Guo, Q.; Xia, B.; Zhang, Y.H.; Giesert, E.E.; Levy, S.; Zheng, J.J.; Zhang, X.A. Tetraspanins regulate the protrusive activities of cell membrane. *Biochem. Biophys. Res. Commun.* **2011**, *415*, 619–626. [CrossRef] [PubMed]
159. Clancy, J.W.; Sedgwick, A.; Rosse, C.; Muralidharan-Chari, V.; Raposo, G.; Method, M.; Chavrier, P.; D'Souza-Schorey, C. Regulated delivery of molecular cargo to invasive tumour-derived microvesicles. *Nat. Commun.* **2015**, *6*, 6919. [CrossRef] [PubMed]
160. D'Souza-Schorey, C.; Chavrier, P. ARF proteins: Roles in membrane traffic and beyond. *Nat. Rev. Mol. Cell Biol.* **2006**, *7*, 347–358. [CrossRef] [PubMed]
161. Li, B.; Antonyak, M.A.; Zhang, J.; Cerione, R.A. RhoA triggers a specific signaling pathway that generates transforming microvesicles in cancer cells. *Oncogene* **2012**, *31*, 4740–4749. [CrossRef] [PubMed]
162. Wang, T.; Gilkes, D.M.; Takano, N.; Xiang, L.; Luo, W.; Bishop, C.J.; Chaturvedi, P.; Green, J.J.; Semenza, G.L. Hypoxia-inducible factors and RAB22A mediate formation of microvesicles that stimulate breast cancer invasion and metastasis. *Proc. Natl. Acad. Sci. USA* **2014**, *111*, E3234–E3242. [CrossRef] [PubMed]
163. Verderio, C.; Gabrielli, M.; Giussani, P. Role of sphingolipids in the biogenesis and biological activity of extracellular vesicles. *J. Lipid Res.* **2018**. [CrossRef] [PubMed]
164. Pfrieger, F.W.; Vitale, N. Cholesterol and the journey of extracellular vesicles. *J. Lipid Res.* **2018**. [CrossRef] [PubMed]
165. Morad, S.A.; Cabot, M.C. Ceramide-orchestrated signalling in cancer cells. *Nat. Rev. Cancer* **2013**, *13*, 51–65. [CrossRef] [PubMed]
166. Veldman, R.J.; Maestre, N.; Aduib, O.M.; Medin, J.A.; Salvayre, R.; Levade, T. A neutral sphingomyelinase resides in sphingolipid-enriched microdomains and is inhibited by the caveolin-scaffolding domain: Potential implications in tumour necrosis factor signalling. *Biochem. J.* **2001**, *355*, 859–868. [CrossRef] [PubMed]
167. Menck, K.; Sonmezer, C.; Worst, T.S.; Schulz, M.; Dihazi, G.H.; Streit, F.; Erdmann, G.; Kling, S.; Boutros, M.; Binder, C.; et al. Neutral sphingomyelinases control extracellular vesicles budding from the plasma membrane. *J. Extracell. Vesicles* **2017**, *6*, 1378056. [CrossRef] [PubMed]

168. Bianco, F.; Perrotta, C.; Novellino, L.; Francolini, M.; Riganti, L.; Menna, E.; Saglietti, L.; Schuchman, E.H.; Furlan, R.; Clementi, E.; et al. Acid sphingomyelinase activity triggers microparticle release from glial cells. *EMBO J.* **2009**, *28*, 1043–1054. [CrossRef] [PubMed]
169. Henry, B.; Ziobro, R.; Becker, K.A.; Kolesnick, R.; Gulbins, E. Acid sphingomyelinase. *Handb. Exp. Pharmacol.* **2013**, 77–88. [CrossRef]
170. Xu, M.; Xia, M.; Li, X.X.; Han, W.Q.; Boini, K.M.; Zhang, F.; Zhang, Y.; Ritter, J.K.; Li, P.L. Requirement of translocated lysosomal V1 H^+-ATPase for activation of membrane acid sphingomyelinase and raft clustering in coronary endothelial cells. *Mol. Biol. Cell* **2012**, *23*, 1546–1557. [CrossRef] [PubMed]
171. Awojoodu, A.O.; Keegan, P.M.; Lane, A.R.; Zhang, Y.; Lynch, K.R.; Platt, M.O.; Botchwey, E.A. Acid sphingomyelinase is activated in sickle cell erythrocytes and contributes to inflammatory microparticle generation in SCD. *Blood* **2014**, *124*, 1941–1950. [CrossRef] [PubMed]
172. Hoehn, R.S.; Jernigan, P.L.; Japtok, L.; Chang, A.L.; Midura, E.F.; Caldwell, C.C.; Kleuser, B.; Lentsch, A.B.; Edwards, M.J.; Gulbins, E.; et al. Acid Sphingomyelinase Inhibition in Stored Erythrocytes Reduces Transfusion-Associated Lung Inflammation. *Ann. Surg.* **2017**, *265*, 218–226. [CrossRef] [PubMed]
173. Wang, J.; Pendurthi, U.R.; Rao, L.V.M. Sphingomyelin encrypts tissue factor: ATP-induced activation of A-SMase leads to tissue factor decryption and microvesicle shedding. *Blood Adv.* **2017**, *1*, 849–862. [CrossRef] [PubMed]
174. Lopez-Montero, I.; Rodriguez, N.; Cribier, S.; Pohl, A.; Velez, M.; Devaux, P.F. Rapid transbilayer movement of ceramides in phospholipid vesicles and in human erythrocytes. *J. Biol. Chem.* **2005**, *280*, 25811–25819. [CrossRef] [PubMed]
175. Slotte, J.P.; Hedstrom, G.; Rannstrom, S.; Ekman, S. Effects of sphingomyelin degradation on cell cholesterol oxidizability and steady-state distribution between the cell surface and the cell interior. *Biochim. Biophys. Acta* **1989**, *985*, 90–96. [CrossRef]
176. Fanani, M.L.; De Tullio, L.; Hartel, S.; Jara, J.; Maggio, B. Sphingomyelinase-induced domain shape relaxation driven by out-of-equilibrium changes of composition. *Biophys. J.* **2009**, *96*, 67–76. [CrossRef] [PubMed]
177. Castro, B.M.; Prieto, M.; Silva, L.C. Ceramide: A simple sphingolipid with unique biophysical properties. *Prog. Lipid Res.* **2014**, *54*, 53–67. [CrossRef] [PubMed]
178. Goni, F.M.; Alonso, A. Effects of ceramide and other simple sphingolipids on membrane lateral structure. *Biochim. Biophys. Acta* **2009**, *1788*, 169–177. [CrossRef] [PubMed]
179. White, A.B.; Givogri, M.I.; Lopez-Rosas, A.; Cao, H.; van Breemen, R.; Thinakaran, G.; Bongarzone, E.R. Psychosine accumulates in membrane microdomains in the brain of krabbe patients, disrupting the raft architecture. *J. Neurosci.* **2009**, *29*, 6068–6077. [CrossRef] [PubMed]
180. D'Auria, L.; Reiter, C.; Ward, E.; Moyano, A.L.; Marshall, M.S.; Nguyen, D.; Scesa, G.; Hauck, Z.; van Breemen, R.; Givogri, M.I.; et al. Psychosine enhances the shedding of membrane microvesicles: Implications in demyelination in Krabbe's disease. *PLoS ONE* **2017**, *12*, e0178103. [CrossRef] [PubMed]
181. Vind-Kezunovic, D.; Nielsen, C.H.; Wojewodzka, U.; Gniadecki, R. Line tension at lipid phase boundaries regulates formation of membrane vesicles in living cells. *Biochim. Biophys. Acta* **2008**, *1778*, 2480–2486. [CrossRef] [PubMed]
182. Liu, M.L.; Reilly, M.P.; Casasanto, P.; McKenzie, S.E.; Williams, K.J. Cholesterol enrichment of human monocyte/macrophages induces surface exposure of phosphatidylserine and the release of biologically-active tissue factor-positive microvesicles. *Arterioscler. Thromb. Vasc. Biol.* **2007**, *27*, 430–435. [CrossRef] [PubMed]
183. Carquin, M.; D'Auria, L.; Pollet, H.; Bongarzone, E.R.; Tyteca, D. Recent progress on lipid lateral heterogeneity in plasma membranes: From rafts to submicrometric domains. *Prog. Lipid Res.* **2016**, *62*, 1–24. [CrossRef] [PubMed]
184. Lipowsky, R. Budding of membranes induced by intramembrane domains. *J. Phys. II EDP Sci.* **1992**, *2*, 1825–1840. [CrossRef]
185. Baumgart, T.; Hess, S.T.; Webb, W.W. Imaging coexisting fluid domains in biomembrane models coupling curvature and line tension. *Nature* **2003**, *425*, 821–824. [CrossRef] [PubMed]
186. Yang, S.-T.; Kiessling, V.; Tamm, L.K. Line tension at lipid phase boundaries as driving force for HIV fusion peptide-mediated fusion. *Nat. Commun.* **2016**, *7*, 11401. [CrossRef] [PubMed]
187. Bretscher, M.S. Phosphatidyl-ethanolamine: Differential labelling in intact cells and cell ghosts of human erythrocytes by a membrane-impermeable reagent. *J. Mol. Biol.* **1972**, *71*, 523–528. [CrossRef]

188. Yeung, T.; Grinstein, S. Lipid signaling and the modulation of surface charge during phagocytosis. *Immunol. Rev.* **2007**, *219*, 17–36. [CrossRef] [PubMed]
189. Bevers, E.M.; Comfurius, P.; van Rijn, J.L.; Hemker, H.C.; Zwaal, R.F. Generation of prothrombin-converting activity and the exposure of phosphatidylserine at the outer surface of platelets. *Eur. J. Biochem. FEBS* **1982**, *122*, 429–436. [CrossRef]
190. Lentz, B.R. Exposure of platelet membrane phosphatidylserine regulates blood coagulation. *Prog. Lipid Res.* **2003**, *42*, 423–438. [CrossRef]
191. Larson, M.C.; Karafin, M.S.; Hillery, C.A.; Hogg, N. Phosphatidylethanolamine is progressively exposed in RBCs during storage. *Transfus. Med.* **2017**, *27*, 136–141. [CrossRef] [PubMed]
192. Nagata, S.; Suzuki, J.; Segawa, K.; Fujii, T. Exposure of phosphatidylserine on the cell surface. *Cell Death Differ.* **2016**, *23*, 952–961. [CrossRef] [PubMed]
193. Stratton, D.; Moore, C.; Zheng, L.; Lange, S.; Inal, J. Prostate cancer cells stimulated by calcium-mediated activation of protein kinase C undergo a refractory period before re-releasing calcium-bearing microvesicles. *Biochem. Biophys. Res. Commun.* **2015**, *460*, 511–517. [CrossRef] [PubMed]
194. Tepper, A.D.; Ruurs, P.; Wiedmer, T.; Sims, P.J.; Borst, J.; van Blitterswijk, W.J. Sphingomyelin hydrolysis to ceramide during the execution phase of apoptosis results from phospholipid scrambling and alters cell-surface morphology. *J. Cell Biol.* **2000**, *150*, 155–164. [CrossRef] [PubMed]
195. Simons, K.; Ikonen, E. Functional rafts in cell membranes. *Nature* **1997**, *387*, 569–572. [CrossRef] [PubMed]
196. Lingwood, D.; Simons, K. Lipid rafts as a membrane-organizing principle. *Science* **2010**, *327*, 46–50. [CrossRef] [PubMed]
197. Parton, R.G.; del Pozo, M.A. Caveolae as plasma membrane sensors, protectors and organizers. *Nat. Rev. Mol. Cell Biol.* **2013**, *14*, 98–112. [CrossRef] [PubMed]
198. Pike, L.J. Rafts defined: A report on the Keystone Symposium on Lipid Rafts and Cell Function. *J. Lipid Res.* **2006**, *47*, 1597–1598. [CrossRef] [PubMed]
199. Baumgart, T.; Hammond, A.T.; Sengupta, P.; Hess, S.T.; Holowka, D.A.; Baird, B.A.; Webb, W.W. Large-scale fluid/fluid phase separation of proteins and lipids in giant plasma membrane vesicles. *Proc. Natl. Acad. Sci. USA* **2007**, *104*, 3165–3170. [CrossRef] [PubMed]
200. Bernardino de la Serna, J.; Perez-Gil, J.; Simonsen, A.C.; Bagatolli, L.A. Cholesterol rules: Direct observation of the coexistence of two fluid phases in native pulmonary surfactant membranes at physiological temperatures. *J. Biol. Chem.* **2004**, *279*, 40715–40722. [CrossRef] [PubMed]
201. Kahya, N.; Scherfeld, D.; Bacia, K.; Poolman, B.; Schwille, P. Probing lipid mobility of raft-exhibiting model membranes by fluorescence correlation spectroscopy. *J. Biol. Chem.* **2003**, *278*, 28109–28115. [CrossRef] [PubMed]
202. Plasencia, I.; Norlen, L.; Bagatolli, L.A. Direct visualization of lipid domains in human skin stratum corneum's lipid membranes: Effect of pH and temperature. *Biophys. J.* **2007**, *93*, 3142–3155. [CrossRef] [PubMed]
203. Carquin, M.; Pollet, H.; Veiga-da-Cunha, M.; Cominelli, A.; Van Der Smissen, P.; N'Kuli, F.; Emonard, H.; Henriet, P.; Mizuno, H.; Courtoy, P.J.; et al. Endogenous sphingomyelin segregates into submicrometric domains in the living erythrocyte membrane. *J. Lipid Res.* **2014**, *55*, 1331–1342. [CrossRef] [PubMed]
204. D'Auria, L.; Fenaux, M.; Aleksandrowicz, P.; Van Der Smissen, P.; Chantrain, C.; Vermylen, C.; Vikkula, M.; Courtoy, P.J.; Tyteca, D. Micrometric segregation of fluorescent membrane lipids: Relevance for endogenous lipids and biogenesis in erythrocytes. *J. Lipid Res.* **2013**, *54*, 1066–1076. [CrossRef] [PubMed]
205. Sanchez, S.A.; Tricerri, M.A.; Gratton, E. Laurdan generalized polarization fluctuations measures membrane packing micro-heterogeneity in vivo. *Proc. Natl. Acad. Sci. USA* **2012**, *109*, 7314–7319. [CrossRef] [PubMed]
206. Carquin, M.; Conrard, L.; Pollet, H.; Van Der Smissen, P.; Cominelli, A.; Veiga-da-Cunha, M.; Courtoy, P.J.; Tyteca, D. Cholesterol segregates into submicrometric domains at the living erythrocyte membrane: Evidence and regulation. *Cell. Mol. Life Sci.* **2015**, *72*, 4633–4651. [CrossRef] [PubMed]
207. Tyteca, D.; D'Auria, L.; Van Der Smissen, P.; Medts, T.; Carpentier, S.; Monbaliu, J.C.; de Diesbach, P.; Courtoy, P.J. Three unrelated sphingomyelin analogs spontaneously cluster into plasma membrane micrometric domains. *Biochim. Biophys. Acta* **2010**, *1798*, 909–927. [CrossRef] [PubMed]
208. Bach, J.N.; Bramkamp, M. Flotillins functionally organize the bacterial membrane. *Mol. Microbiol.* **2013**, *88*, 1205–1217. [CrossRef] [PubMed]
209. Grossmann, G.; Opekarova, M.; Malinsky, J.; Weig-Meckl, I.; Tanner, W. Membrane potential governs lateral segregation of plasma membrane proteins and lipids in yeast. *EMBO J.* **2007**, *26*, 1–8. [CrossRef] [PubMed]

210. Leonard, C.; Alsteens, D.; Dumitru, A.; Mingeot-Leclercq, M.; Tyteca, D. Lipid domains and membrane (re)shaping: From biophysics to biology. In *The Role of the Physical Properties of Membranes in Influencing Biological Phenomena*; Ruysschaert, J., Epand, R., Eds.; Springer Series in Biophysics: Basel, Switzerland, 2017; Volume 19, pp. 121–175.
211. Grassme, H.; Jendrossek, V.; Riehle, A.; von Kurthy, G.; Berger, J.; Schwarz, H.; Weller, M.; Kolesnick, R.; Gulbins, E. Host defense against Pseudomonas aeruginosa requires ceramide-rich membrane rafts. *Nat. Med.* **2003**, *9*, 322–330. [CrossRef] [PubMed]
212. Stancevic, B.; Kolesnick, R. Ceramide-rich platforms in transmembrane signaling. *FEBS Lett.* **2010**, *584*, 1728–1740. [CrossRef] [PubMed]
213. Dietrich, C.; Bagatolli, L.A.; Volovyk, Z.N.; Thompson, N.L.; Levi, M.; Jacobson, K.; Gratton, E. Lipid Rafts Reconstituted in Model Membranes. *Biophys. J.* **2001**, *80*, 1417–1428. [CrossRef]
214. Jacobson, K.; Mouritsen, O.G.; Anderson, R.G.W. Lipid rafts: At a crossroad between cell biology and physics. *Nat. Cell Biol.* **2007**, *9*, 7–14. [CrossRef] [PubMed]
215. Sezgin, E.; Gutmann, T.; Buhl, T.; Dirkx, R.; Grzybek, M.; Coskun, Ü.; Solimena, M.; Simons, K.; Levental, I.; Schwille, P. Adaptive lipid packing and bioactivity in membrane domains. *PLoS ONE* **2015**, *10*, e0123930. [CrossRef] [PubMed]
216. Stone, M.B.; Shelby, S.A.; Núñez, M.F.; Wisser, K.; Veatch, S.L. Protein sorting by lipid phase-like domains supports emergent signaling function in B lymphocyte plasma membranes. *eLife* **2017**, *6*, e19891. [CrossRef] [PubMed]
217. Owen, D.M.; Oddos, S.; Kumar, S.; Davis, D.M.; Neil, M.A.A.; French, P.M.W.; Dustin, M.L.; Magee, A.I.; Cebecauer, M. High plasma membrane lipid order imaged at the immunological synapse periphery in live T cells. *Mol. Membr. Biol.* **2010**, *27*, 178–189. [CrossRef] [PubMed]
218. Rentero, C.; Zech, T.; Quinn, C.M.; Engelhardt, K.; Williamson, D.; Grewal, T.; Jessup, W.; Harder, T.; Gaus, K. Functional Implications of Plasma Membrane Condensation for T Cell Activation. *PLoS ONE* **2008**, *3*, e2262. [CrossRef] [PubMed]
219. Gaus, K.; Chklovskaia, E.; Fazekas de St Groth, B.; Jessup, W.; Harder, T. Condensation of the plasma membrane at the site of T lymphocyte activation. *J. Cell Biol.* **2005**, *171*, 121–131. [CrossRef] [PubMed]
220. Leonard, C.; Pollet, H.; Vermylen, C.; Gov, N.S.; Tyteca, D.; Mingeot-Leclercq, M.-P. Tuning of differential lipid order between submicrometric domains and surrounding membrane upon erythrocyte reshaping. *Cell. Physiol. Biochem.* **2018**, *48*, 2563–2582. [CrossRef] [PubMed]
221. Ursell, T.S.; Klug, W.S.; Phillips, R. Morphology and interaction between lipid domains. *Proc. Natl. Acad. Sci. USA* **2009**, *106*, 13301–13306. [CrossRef] [PubMed]
222. Skocaj, M.; Yu, Y.; Grundner, M.; Resnik, N.; Bedina Zavec, A.; Leonardi, A.; Krizaj, I.; Guella, G.; Macek, P.; Kreft, M.E.; et al. Characterisation of plasmalemmal shedding of vesicles induced by the cholesterol/sphingomyelin binding protein, ostreolysin A-mCherry. *Biochim. Biophys. Acta* **2016**, *1858*, 2882–2893. [CrossRef] [PubMed]
223. D'Auria, L.; Van der Smissen, P.; Bruyneel, F.; Courtoy, P.J.; Tyteca, D. Segregation of fluorescent membrane lipids into distinct micrometric domains: Evidence for phase compartmentation of natural lipids? *PLoS ONE* **2011**, *6*, e17021. [CrossRef] [PubMed]
224. Leonard, C.; Conrard, L.; Guthmann, M.; Pollet, H.; Carquin, M.; Vermylen, C.; Gailly, P.; Van Der Smissen, P.; Mingeot-Leclercq, M.P.; Tyteca, D. Contribution of plasma membrane lipid domains to red blood cell (re)shaping. *Sci. Rep.* **2017**, *7*, 4264. [CrossRef] [PubMed]
225. Conrard, L.; Stommen, A.; Steinkhühler, J.; Dimova, R.; Pollet, H.; Tyteca, D. Spatial relationship and functional relevance of three lipid domain populations at the erythrocyte surface. Submitted.
226. Mikhalyov, I.; Samsonov, A. Lipid raft detecting in membranes of live erythrocytes. *Biochim. Biophys. Acta* **2011**, *1808*, 1930–1939. [CrossRef] [PubMed]
227. Murate, M.; Abe, M.; Kasahara, K.; Iwabuchi, K.; Umeda, M.; Kobayashi, T. Transbilayer distribution of lipids at nano scale. *J. Cell Sci.* **2015**, *128*, 1627–1638. [CrossRef] [PubMed]
228. Montes, L.R.; Lopez, D.J.; Sot, J.; Bagatolli, L.A.; Stonehouse, M.J.; Vasil, M.L.; Wu, B.X.; Hannun, Y.A.; Goni, F.M.; Alonso, A. Ceramide-enriched membrane domains in red blood cells and the mechanism of sphingomyelinase-induced hot-cold hemolysis. *Biochemistry* **2008**, *47*, 11222–11230. [CrossRef] [PubMed]

229. Gousset, K.; Wolkers, W.F.; Tsvetkova, N.M.; Oliver, A.E.; Field, C.L.; Walker, N.J.; Crowe, J.H.; Tablin, F. Evidence for a physiological role for membrane rafts in human platelets. *J. Cell Physiol.* **2002**, *190*, 117–128. [CrossRef] [PubMed]
230. Gaus, K.; Gratton, E.; Kable, E.P.; Jones, A.S.; Gelissen, I.; Kritharides, L.; Jessup, W. Visualizing lipid structure and raft domains in living cells with two-photon microscopy. *Proc. Natl. Acad. Sci. USA* **2003**, *100*, 15554–15559. [CrossRef] [PubMed]
231. Gomez-Mouton, C.; Abad, J.L.; Mira, E.; Lacalle, R.A.; Gallardo, E.; Jimenez-Baranda, S.; Illa, I.; Bernad, A.; Manes, S.; Martinez, A.C. Segregation of leading-edge and uropod components into specific lipid rafts during T cell polarization. *Proc. Natl. Acad. Sci. USA* **2001**, *98*, 9642–9647. [CrossRef] [PubMed]
232. Ekyalongo, R.C.; Nakayama, H.; Kina, K.; Kaga, N.; Iwabuchi, K. Organization and functions of glycolipid-enriched microdomains in phagocytes. *Biochim. Biophys. Acta* **2015**, *1851*, 90–97. [CrossRef] [PubMed]
233. Mizuno, H.; Abe, M.; Dedecker, P.; Makino, A.; Rocha, S.; Ohno-Iwashita, Y.; Hofkens, J.; Kobayashi, T.; Miyawaki, A. Fluorescent probes for superresolution imaging of lipid domains on the plasma membrane. *Chem. Sci.* **2011**, *2*, 1548–1553. [CrossRef]
234. Rungaldier, S.; Oberwagner, W.; Salzer, U.; Csaszar, E.; Prohaska, R. Stomatin interacts with GLUT1/SLC2A1, band 3/SLC4A1, and aquaporin-1 in human erythrocyte membrane domains. *Biochim. Biophys. Acta* **2013**, *1828*, 956–966. [CrossRef] [PubMed]
235. Salzer, U.; Prohaska, R. Stomatin, flotillin-1, and flotillin-2 are major integral proteins of erythrocyte lipid rafts. *Blood* **2001**, *97*, 1141–1143. [CrossRef] [PubMed]
236. Murphy, S.C.; Samuel, B.U.; Harrison, T.; Speicher, K.D.; Speicher, D.W.; Reid, M.E.; Prohaska, R.; Low, P.S.; Tanner, M.J.; Mohandas, N.; et al. Erythrocyte detergent-resistant membrane proteins: Their characterization and selective uptake during malarial infection. *Blood* **2004**, *103*, 1920–1928. [CrossRef] [PubMed]
237. Cai, M.; Zhao, W.; Shang, X.; Jiang, J.; Ji, H.; Tang, Z.; Wang, H. Direct evidence of lipid rafts by in situ atomic force microscopy. *Small* **2012**, *8*, 1243–1250. [CrossRef] [PubMed]
238. Dumitru, A.C.; Poncin, M.A.; Conrard, L.; Dufrêne, Y.; Tyteca, D.; Alsteens, D. Nanoscale membrane architecture of healthy and pathological red blood cells. *Nanoscale Horiz.* **2018**, *3*, 293–304. [CrossRef]
239. Lutz, H.U.; Barber, R.; McGuire, R.F. Glycoprotein-enriched vesicles from sheep erythrocyte ghosts obtained by spontaneous vesiculation. *J. Biol. Chem.* **1976**, *251*, 3500–3510. [PubMed]
240. Salzer, U.H.; Hunger, U.; Prohaska, R. Chapter three: Insights in the organization and dynamics of erythrocyte lipid rafts. *Adv. Planar Lipid Bilayers Liposomes* **2008**, *6*, 49–80.
241. Civenni, G.; Test, S.T.; Brodbeck, U.; Butikofer, P. In vitro incorporation of GPI-anchored proteins into human erythrocytes and their fate in the membrane. *Blood* **1998**, *91*, 1784–1792. [PubMed]
242. Whitlow, M.; Iida, K.; Marshall, P.; Silber, R.; Nussenzweig, V. Cells lacking glycan phosphatidylinositol-linked proteins have impaired ability to vesiculate. *Blood* **1993**, *81*, 510–516. [PubMed]
243. Wilkinson, D.K.; Turner, E.J.; Parkin, E.T.; Garner, A.E.; Harrison, P.J.; Crawford, M.; Stewart, G.W.; Hooper, N.M. Membrane raft actin deficiency and altered Ca^{2+}-induced vesiculation in stomatin-deficient overhydrated hereditary stomatocytosis. *Biochim. Biophys. Acta* **2008**, *1778*, 125–132. [CrossRef] [PubMed]
244. Santos, N.C.; Martins-Silva, J.; Saldanha, C. Gramicidin D and dithiothreitol effects on erythrocyte exovesiculation. *Cell Biochem. Biophys.* **2005**, *43*, 419–430. [CrossRef]
245. Kunzelmann-Marche, C.; Freyssinet, J.M.; Martinez, M.C. Loss of plasma membrane phospholipid asymmetry requires raft integrity. Role of transient receptor potential channels and ERK pathway. *J. Biol. Chem.* **2002**, *277*, 19876–19881. [CrossRef] [PubMed]
246. Gonzalez, L.J.; Gibbons, E.; Bailey, R.W.; Fairbourn, J.; Nguyen, T.; Smith, S.K.; Best, K.B.; Nelson, J.; Judd, A.M.; Bell, J.D. The influence of membrane physical properties on microvesicle release in human erythrocytes. *PMC Biophys.* **2009**, *2*, 7. [CrossRef] [PubMed]
247. Dorahy, D.J.; Lincz, L.F.; Meldrum, C.J.; Burns, G.F. Biochemical isolation of a membrane microdomain from resting platelets highly enriched in the plasma membrane glycoprotein CD36. *Biochem. J.* **1996**, *319*, 67–72. [CrossRef] [PubMed]
248. Bali, R.; Savino, L.; Ramirez, D.A.; Tsvetkova, N.M.; Bagatolli, L.; Tablin, F.; Crowe, J.H.; Leidy, C. Macroscopic domain formation during cooling in the platelet plasma membrane: An issue of low cholesterol content. *Biochim. Biophys. Acta* **2009**, *1788*, 1229–1237. [CrossRef] [PubMed]

249. Bodin, S.; Tronchere, H.; Payrastre, B. Lipid rafts are critical membrane domains in blood platelet activation processes. *Biochim. Biophys. Acta* **2003**, *1610*, 247–257. [CrossRef]
250. Bodin, S.; Giuriato, S.; Ragab, J.; Humbel, B.M.; Viala, C.; Vieu, C.; Chap, H.; Payrastre, B. Production of phosphatidylinositol 3,4,5-trisphosphate and phosphatidic acid in platelet rafts: Evidence for a critical role of cholesterol-enriched domains in human platelet activation. *Biochemistry* **2001**, *40*, 15290–15299. [CrossRef] [PubMed]
251. Caroni, P. New EMBO members' review: Actin cytoskeleton regulation through modulation of PI(4,5)P(2) rafts. *EMBO J.* **2001**, *20*, 4332–4336. [CrossRef] [PubMed]
252. Flaumenhaft, R. Formation and fate of platelet microparticles. *Blood Cells Mol. Dis.* **2006**, *36*, 182–187. [CrossRef] [PubMed]
253. Mairhofer, M.; Steiner, M.; Mosgoeller, W.; Prohaska, R.; Salzer, U. Stomatin is a major lipid-raft component of platelet alpha granules. *Blood* **2002**, *100*, 897–904. [CrossRef] [PubMed]
254. Wei, H.; Malcor, J.M.; Harper, M.T. Lipid rafts are essential for release of phosphatidylserine-exposing extracellular vesicles from platelets. *Sci. Rep.* **2018**, *8*, 9987. [CrossRef] [PubMed]
255. Larive, R.M.; Baisamy, L.; Urbach, S.; Coopman, P.; Bettache, N. Cell membrane extensions, generated by mechanical constraint, are associated with a sustained lipid raft patching and an increased cell signaling. *Biochim. Biophys. Acta* **2010**, *1798*, 389–400. [CrossRef] [PubMed]
256. Heijnen, H.F.; Van Lier, M.; Waaijenborg, S.; Ohno-Iwashita, Y.; Waheed, A.A.; Inomata, M.; Gorter, G.; Mobius, W.; Akkerman, J.W.; Slot, J.W. Concentration of rafts in platelet filopodia correlates with recruitment of c-Src and CD63 to these domains. *J. Thromb. Haemost.* **2003**, *1*, 1161–1173. [CrossRef] [PubMed]
257. O'Connell, D.J.; Rozenvayn, N.; Flaumenhaft, R. Phosphatidylinositol 4,5-bisphosphate regulates activation-induced platelet microparticle formation. *Biochemistry* **2005**, *44*, 6361–6370. [CrossRef] [PubMed]
258. Gomez-Mouton, C.; Lacalle, R.A.; Mira, E.; Jimenez-Baranda, S.; Barber, D.F.; Carrera, A.C.; Martinez, A.C.; Manes, S. Dynamic redistribution of raft domains as an organizing platform for signaling during cell chemotaxis. *J. Cell Biol.* **2004**, *164*, 759–768. [CrossRef] [PubMed]
259. Seveau, S.; Eddy, R.J.; Maxfield, F.R.; Pierini, L.M. Cytoskeleton-dependent membrane domain segregation during neutrophil polarization. *Mol. Biol. Cell* **2001**, *12*, 3550–3562. [CrossRef] [PubMed]
260. Millan, J.; Montoya, M.C.; Sancho, D.; Sanchez-Madrid, F.; Alonso, M.A. Lipid rafts mediate biosynthetic transport to the T lymphocyte uropod subdomain and are necessary for uropod integrity and function. *Blood* **2002**, *99*, 978–984. [CrossRef] [PubMed]
261. Pierini, L.M.; Eddy, R.J.; Fuortes, M.; Seveau, S.; Casulo, C.; Maxfield, F.R. Membrane lipid organization is critical for human neutrophil polarization. *J. Biol. Chem.* **2003**, *278*, 10831–10841. [CrossRef] [PubMed]
262. Nakayama, H.; Yoshizaki, F.; Prinetti, A.; Sonnino, S.; Mauri, L.; Takamori, K.; Ogawa, H.; Iwabuchi, K. Lyn-coupled LacCer-enriched lipid rafts are required for CD11b/CD18-mediated neutrophil phagocytosis of nonopsonized microorganisms. *J. Leukoc. Biol.* **2008**, *83*, 728–741. [CrossRef] [PubMed]
263. Saha, A.K.; Dallo, S.F.; Detmar, A.L.; Osmulski, P.; Gaczynska, M.; Huang, T.H.; Ramasubramanian, A.K. Cellular cholesterol regulates monocyte deformation. *J. Biomech.* **2017**, *52*, 83–88. [CrossRef] [PubMed]
264. Rothmeier, A.S.; Marchese, P.; Petrich, B.G.; Furlan-Freguia, C.; Ginsberg, M.H.; Ruggeri, Z.M.; Ruf, W. Caspase-1-mediated pathway promotes generation of thromboinflammatory microparticles. *J. Clin. Investig.* **2015**, *125*, 1471–1484. [CrossRef] [PubMed]
265. Roduit, C.; van der Goot, F.G.; De Los Rios, P.; Yersin, A.; Steiner, P.; Dietler, G.; Catsicas, S.; Lafont, F.; Kasas, S. Elastic membrane heterogeneity of living cells revealed by stiff nanoscale membrane domains. *Biophys. J.* **2008**, *94*, 1521–1532. [CrossRef] [PubMed]
266. Boggs, J.M.; Wang, H. Co-clustering of galactosylceramide and membrane proteins in oligodendrocyte membranes on interaction with polyvalent carbohydrate and prevention by an intact cytoskeleton. *J. Neurosci. Res.* **2004**, *76*, 342–355. [CrossRef] [PubMed]
267. Boggs, J.M.; Gao, W.; Zhao, J.; Park, H.J.; Liu, Y.; Basu, A. Participation of galactosylceramide and sulfatide in glycosynapses between oligodendrocyte or myelin membranes. *FEBS Lett.* **2010**, *584*, 1771–1778. [CrossRef] [PubMed]
268. Gonnord, P.; Delarasse, C.; Auger, R.; Benihoud, K.; Prigent, M.; Cuif, M.H.; Lamaze, C.; Kanellopoulos, J.M. Palmitoylation of the P2X7 receptor, an ATP-gated channel, controls its expression and association with lipid rafts. *FASEB J.* **2009**, *23*, 795–805. [CrossRef] [PubMed]

269. Ohmi, Y.; Ohkawa, Y.; Yamauchi, Y.; Tajima, O.; Furukawa, K.; Furukawa, K. Essential roles of gangliosides in the formation and maintenance of membrane microdomains in brain tissues. *Neurochem. Res.* **2012**, *37*, 1185–1191. [CrossRef] [PubMed]
270. Schilling, T.; Eder, C. Importance of lipid rafts for lysophosphatidylcholine-induced caspase-1 activation and reactive oxygen species generation. *Cell. Immunol.* **2010**, *265*, 87–90. [CrossRef] [PubMed]
271. Allen, J.A.; Halverson-Tamboli, R.A.; Rasenick, M.M. Lipid raft microdomains and neurotransmitter signalling. *Nat. Rev. Neurosci.* **2007**, *8*, 128–140. [CrossRef] [PubMed]
272. Decker, L.; ffrench-Constant, C. Lipid rafts and integrin activation regulate oligodendrocyte survival. *J. Neurosci.* **2004**, *24*, 3816–3825. [CrossRef] [PubMed]
273. Martin, V.; Fabelo, N.; Santpere, G.; Puig, B.; Marin, R.; Ferrer, I.; Diaz, M. Lipid alterations in lipid rafts from Alzheimer's disease human brain cortex. *J. Alzheimers Dis.* **2010**, *19*, 489–502. [CrossRef] [PubMed]
274. Yuyama, K.; Mitsutake, S.; Igarashi, Y. Pathological roles of ceramide and its metabolites in metabolic syndrome and Alzheimer's disease. *Biochim. Biophys. Acta* **2014**, *1841*, 793–798. [CrossRef] [PubMed]
275. Booth, H.D.E.; Hirst, W.D.; Wade-Martins, R. The Role of Astrocyte Dysfunction in Parkinson's Disease Pathogenesis. *Trends Neurosci.* **2017**, *40*, 358–370. [CrossRef] [PubMed]
276. Hein, L.K.; Rozaklis, T.; Adams, M.K.; Hopwood, J.J.; Karageorgos, L. Lipid composition of microdomains is altered in neuronopathic Gaucher disease sheep brain and spleen. *Mol. Genet. Metab.* **2017**, *121*, 259–270. [CrossRef] [PubMed]
277. Al-Nedawi, K.; Meehan, B.; Kerbel, R.S.; Allison, A.C.; Rak, J. Endothelial expression of autocrine VEGF upon the uptake of tumor-derived microvesicles containing oncogenic EGFR. *Proc. Natl. Acad. Sci. USA* **2009**, *106*, 3794–3799. [CrossRef] [PubMed]
278. Orsini, F.; Cremona, A.; Arosio, P.; Corsetto, P.A.; Montorfano, G.; Lascialfari, A.; Rizzo, A.M. Atomic force microscopy imaging of lipid rafts of human breast cancer cells. *Biochim. Biophys. Acta* **2012**, *1818*, 2943–2949. [CrossRef] [PubMed]
279. Kiyokawa, E.; Baba, T.; Otsuka, N.; Makino, A.; Ohno, S.; Kobayashi, T. Spatial and functional heterogeneity of sphingolipid-rich membrane domains. *J. Biol. Chem.* **2005**, *280*, 24072–24084. [CrossRef] [PubMed]
280. Kokkonen, N.; Khosrowabadi, E.; Hassinen, A.; Harrus, D.; Glumoff, T.; Kietzmann, T.; Kellokumpu, S. Abnormal Golgi pH Homeostasis in Cancer Cells Impairs Apical Targeting of Carcinoembryonic Antigen by Inhibiting Its Glycosyl-Phosphatidylinositol Anchor-Mediated Association with Lipid Rafts. *Antioxid. Redox Signal.* **2018**. [CrossRef] [PubMed]
281. Hirpara, J.L.; Loh, T.; Ng, S.B.; Chng, W.J.; Pervaiz, S. Aberrant localization of apoptosis protease activating factor-1 in lipid raft sub-domains of diffuse large B cell lymphomas. *Oncotarget* **2016**, *7*, 83964–83975. [CrossRef] [PubMed]
282. Lavie, Y.; Fiucci, G.; Czarny, M.; Liscovitch, M. Changes in membrane microdomains and caveolae constituents in multidrug-resistant cancer cells. *Lipids* **1999**, *34*, S57–S63. [CrossRef] [PubMed]
283. Ausili, A.; Martinez-Valera, P.; Torrecillas, A.; Gomez-Murcia, V.; de Godos, A.M.; Corbalan-Garcia, S.; Teruel, J.A.; Gomez Fernandez, J.C. Anticancer Agent Edelfosine Exhibits a High Affinity for Cholesterol and Disorganizes Liquid-Ordered Membrane Structures. *Langmuir* **2018**, *34*, 8333–8346. [CrossRef] [PubMed]
284. Mollinedo, F.; Gajate, C. Lipid rafts as major platforms for signaling regulation in cancer. *Adv. Biol. Regul.* **2015**, *57*, 130–146. [CrossRef] [PubMed]
285. Lorent, J.H.; Quetin-Leclercq, J.; Mingeot-Leclercq, M.P. The amphiphilic nature of saponins and their effects on artificial and biological membranes and potential consequences for red blood and cancer cells. *Org. Biomol. Chem.* **2014**, *12*, 8803–8822. [CrossRef] [PubMed]
286. Park, E.K.; Lee, E.J.; Lee, S.H.; Koo, K.H.; Sung, J.Y.; Hwang, E.H.; Park, J.H.; Kim, C.W.; Jeong, K.C.; Park, B.K.; et al. Induction of apoptosis by the ginsenoside Rh2 by internalization of lipid rafts and caveolae and inactivation of Akt. *Br. J. Pharmacol.* **2010**, *160*, 1212–1223. [CrossRef] [PubMed]
287. Yi, J.S.; Choo, H.J.; Cho, B.R.; Kim, H.M.; Kim, Y.N.; Ham, Y.M.; Ko, Y.G. Ginsenoside Rh2 induces ligand-independent Fas activation via lipid raft disruption. *Biochem. Biophys. Res. Commun.* **2009**, *385*, 154–159. [CrossRef] [PubMed]
288. Verstraeten, S.L.; Albert, M.; Paquot, A.; Muccioli, G.G.; Tyteca, D.; Mingeot-Leclercq, M.P. Membrane cholesterol delays cellular apoptosis induced by ginsenoside Rh2, a steroid saponin. *Toxicol. Appl. Pharmacol.* **2018**, *352*, 59–67. [CrossRef] [PubMed]

289. Van Blitterswijk, W.J.; Emmelot, P.; Hilkmann, H.A.; Hilgers, J.; Feltkamp, C.A. Rigid plasma-membrane-derived vesicles, enriched in tumour-associated surface antigens (MLr), occurring in the ascites fluid of a murine leukaemia (GRSL). *Int. J. Cancer* **1979**, *23*, 62–70. [CrossRef] [PubMed]
290. Lamprecht, C.; Gehrmann, M.; Madl, J.; Romer, W.; Multhoff, G.; Ebner, A. Molecular AFM imaging of Hsp70-1A association with dipalmitoyl phosphatidylserine reveals membrane blebbing in the presence of cholesterol. *Cell Stress Chaperones* **2018**, *23*, 673–683. [CrossRef] [PubMed]